

THE UNIVERSITY OF ADELAIDE

DEPARTMENT OF MECHANICAL ENGINEERING



**The Effects of Internal Flow Disturbances
on the Vibration Response of
and the Acoustic Radiation from Pipes**

by

Michael Peter Norton, B.E.(Hons)

Thesis for the Degree of Doctor of Philosophy

March, 1979

THE EFFECTS OF INTERNAL FLOW DISTURBANCES ON THE VIBRATIONAL RESPONSE OF AND
THE ACOUSTIC RADIATION FROM PIPES

by

Michael Peter Norton

E R R A T A

- Page 43 Equation [2.18] Replace $12\beta^2$ by $6\beta^2$.
- Page 59 Line 9 Insert a comma after "changed".
- Page 153 Line 5 Replace "external acoustic radiation" by
"external acoustic radiation (see Figures
4.45(a) and (b))".
- Page 213 Line 15 Replace "acoustic energy flux is reflected,
and consequently almost all of the" by
"acoustic energy flux is reflected since $2ka_1 \geq 1.0$
for the frequency ranges of interest. Consequently
almost all of the".
- Page 293 Line 6 Replace "equation [2.17]" by "equation [2.18]".
- Page 293 Equation [7.1] Replace $12\beta^2$ by $6\beta^2$.
- Page 307 Equation [7.9] Replace $12\beta^2$ by $6\beta^2$.
- Page 369 Equation [B.5] Replace 4 by 8.
- Page 369 Equation [B.6] Replace $12\beta^2$ by $6\beta^2$.
- Page 370 Equation [B.9] Replace $12\beta^2$ by $6\beta^2$.

A D D E N D A

- Page xvi 4.45(a) σ for various M_0 (steel pipe, $\beta = 0.0070$) 152(a).
- Page xvi 4.45(b) Effect of ka_m on σ for various n 152(b).
- Page 152(a) Figure 4.45(a) σ for various M_0 (steel pipe, $\beta = 0.0070$).
- Page 152(b) Figure 4.45(b) Effect of ka_m on σ for various n .

TABLE OF CONTENTS

SUMMARY	i
STATEMENT OF ORIGINALITY	iv
ACKNOWLEDGEMENTS	v
NOMENCLATURE	vii
LIST OF FIGURES	xiv
1 INTRODUCTION	
1.1 General Introduction	1
1.2 Review of Previous Work	3
1.3 Objectives of the Present Investigation	15
2 THEORETICAL CONSIDERATIONS	
2.1 Introduction	19
2.2 Internal Acoustic Modes	22
2.3 Resonant Structural Vibration Modes	26
2.4 The Joint Acceptance	27
2.5 Coincidence and its Effects on the Pipe Wall Response	29
2.6 Summary	44
3 DESCRIPTION OF THE EXPERIMENTAL FACILITIES	
3.1 Introduction	45
3.2 Devices Tested	46
3.3 Experimental Flow Facility	50
3.4 Flow Facility Performance	62
3.5 Instrumentation and its Calibration	64
3.5.1 The Wall Pressure Transducers	73
3.5.2 Pipe Wall Vibration and Acoustic Radiation Measurement Procedures	80
3.5.3 The Data Acquisition System	86
3.6 Summary	87

4	EXPERIMENTS WITH A 90° MITRED BEND	
4.1	Introduction	89
4.2	Detailed Investigation of Flow in the Region of the Bend	90
4.2.1	Experimental Arrangement	90
4.2.2	Character of the Flow Associated with the 90° Mitred Bend	92
4.2.3	The Wall Pressure Field	99
4.3	Vibrational and Acoustic Effects Downstream of the Bend	133
4.3.1	Spectra of the Wall Pressure Fluctuations	133
4.3.2	Acceleration Response of and Acoustic Radiation from the Test Section	140
4.4	The Flow Dependence of the Internal Wall Pressure Field	153
4.5	General Discussion	157
5	EXPERIMENTS WITH OTHER INTERNAL FLOW DISTURBANCES	
5.1	Introduction	160
5.2	Spectra of Wall Pressure Fluctuations	161
5.3	Acceleration Response of and Acoustic Radiation from the Test Section	173
5.4	The Flow Dependence of the Internal Wall Pressure Field	205
5.5	General Discussion	214
5.5.1	90° Radiused Bends	214
5.5.2	45° Mitred Bend	216
5.5.3	Butterfly Valve	217
5.5.4	Gate Valve	219
5.5.5	Summary	225
6	WALL PRESSURE FLUCTUATION CROSS CORRELATIONS	
6.1	Introduction	227
6.2	Theoretical Background	230
6.3	Digital Techniques	245

6.3.1	Statistical Considerations	247
6.3.2	Linear Phase Digital Filters	251
6.4	Cross Correlations Associated with a 90° Mitred Bend	256
6.5	General Discussion	290
7	THEORETICAL ESTIMATION OF THE ACOUSTIC RADIATION DUE TO VARIOUS INTERNAL FLOW DISTURBANCES	
7.1	Introduction	292
7.2	Estimation of the Acceleration Response and Acoustic Radiation	293
7.3	Comparison with Various Experimental Measurements	305
7.4	Thick Walled Cylinders	317
7.4.1	Acceleration Response of and Acoustic Radiation from the Test Section	318
7.4.2	Comparison between prediction for thick and thin walled cylinders	325
7.5	General Discussion	333
7.5.1	Practical Applications and Limitations	338
7.5.2	Summary of the Theoretical Estimation Procedure	340
8	CONCLUSIONS AND RECOMMENDATIONS	
8.1	Conclusions	342
8.2	Recommendations	350
	REFERENCES	353
	APPENDIX A - Estimation of Acoustic Coincidence for Higher Order Modes	361
	APPENDIX B - General Formalism of the Pipe Response and Acoustic Radiation	367
	APPENDIX C - Various Experimental Results for Orifice Plates	371

SUMMARY

The effects of internal flow disturbances due to pipe fittings - specifically radiused bends, mitred bends, valves and orifice plates - have been investigated in considerable detail to determine the character of the disturbance due to the pipe fittings; to determine what effects various geometries of pipe fitting have on the vibrational response of, and the acoustic radiation from, a pipe carrying a flowing fluid; to investigate the mechanism by which the pipe is excited as a result of the flow disturbances produced by these devices; to establish methods of estimating acoustic radiation due to various pipe fittings; and, to provide basic data on which the design of pipe work for low noise could be based.

It has been shown experimentally that the various internal flow disturbances generate internal sound fields. These range from mild internal sound fields (due to the radiused bends, the 45° mitred bend, the gate valve and the orifice plate with an orifice to internal pipe radius ratio of 0.90), to intense internal sound fields (due to the 90° mitred bend, the butterfly valve and the orifice plate with an orifice to internal pipe radius ratio of 0.76). The power spectral density and the overall mean square pressure of the wall pressure fluctuations associated with the radiused bends, the 45° mitred bend, the gate valve and the 0.90 radius ratio orifice plate scale essentially as the third and fourth powers of the flow speed respectively, for all Strouhal numbers, at positions sufficiently far away from the flow disturbance, such that a fully-developed turbulent pipe flow has been re-established. For the 90° mitred bend, the butterfly valve and the 0.76 radius ratio orifice plate, they scale as the third and fourth powers of the flow speed for Strouhal numbers below the cut off frequency of the first higher order acoustic mode, and as the fifth and

sixth powers of the flow speed for Strouhal numbers above it.

The experimentally observed increases in pipe wall acceleration and acoustic power radiation (over those for straight pipe flow) are associated with the internal sound fields generated by the flow disturbances, and are greatest at $\beta = 1$, and are essentially confined to frequencies close to the cut off frequencies of the various higher order modes. This is because (i) the joint acceptance of structural and acoustic modes peak very sharply at wave number coincidence; (ii) wave number coincidence occurs at the resonance frequency of a structural mode (exact coincidence) or very close to it, so that the modal receptance is also at or close to its maximum value at coincidence; and (iii) by the nature of the dispersion (wave number - frequency) relations of the acoustic and structural modes, coincidence occurs at a frequency very close to the cut off frequency of the acoustic mode. Thus, as a result of coincidence, the higher order acoustic modes select and enhance the vibration of those resonant pipe modes which radiate most efficiently into the external fluid.

Longitudinal space-time correlations of the wall pressure fluctuations downstream of an internal flow disturbance, allow the internal acoustic field to be separated from the turbulent pressure field in various filter bands. Because of their dispersive nature, the wall pressure fluctuations associated with the higher order modes have to be estimated by subtracting the turbulent and plane wave components from the total wall pressure fluctuations, but, in this way, the field can be resolved into turbulent, plane wave and higher order mode components. Such measurements have been made for the 90° mitred bend.

Procedures have been developed for theoretically estimating the vibration response of and the acoustic radiation from cylindrical pipes downstream of the flow disturbances, at positions where a fully-

developed turbulent pipe flow has been re-established. These procedures take into account the coincidence phenomenon and the relative proportions of the various components in the total wall pressure fluctuations in any given frequency band where higher order modes are propagational. The agreement between the theoretical and experimental results is good and in particular for the severe flow disturbances where the higher order modes dominate the wall pressure field over contributions from plane waves and turbulent pressure fluctuations.

STATEMENT OF ORIGINALITY

This thesis contains no material which has been accepted for the award of any other degree or diploma in any University. To the best of the author's knowledge and belief, this thesis contains no material previously published or written by another person, except where due reference is made in the text.

MICHAEL PETER NORTON

March 1979

ACKNOWLEDGEMENTS

The work described in this thesis has been carried out in the Department of Mechanical Engineering of the University of Adelaide under the aegis of Professor R.E. Luxton, to whom the author is indebted for the opportunity to conduct this research. The author acknowledges the personal interest taken by Professor Luxton in his work.

To Dr. M.K. Bull, who supervised this work, the author is deeply indebted and wishes to express his sincere appreciation. His dedication to this work, and the unselfish giving of his time throughout the course of the research and during the preparation of this thesis will not be forgotten. His help was invaluable to say the least.

The author acknowledges the keen interest taken by Dr. J.M. Pickles in part of this work and during the preparation of this thesis, and appreciates his guidance and advice.

A very special thanks goes to Dr. D.C. Rennison for his unselfish devotion in time and effort to assist and advise on the experimental work in the early part of this research.

The assistance of the workshop staff, under Mr. D. Kerr, is gratefully acknowledged, particularly the invaluable help provided by Mr. D. Kerr himself, Mr. D. Morrison, Mr. H. Bode, Mr. G. Osborne and Mr. M. Bethune in the construction of the experimental pipe flow rig and the electronic equipment.

The author is indebted to his wife, Cecilia, and to his parents for their encouragement and support without which the completion of this thesis would certainly have been in doubt.

Another very special thanks goes to Fiona McLeod for the typing of the manuscript. Her cheerful nature and her dedication to her work eased the burden of the actual compilation of this text, and

ensured that the inevitable deadline in the presentation of this thesis was met.

Acknowledgement is made of the help given by Mr. M. Scutter and Dr. C. Abell over the years, particularly in computing and data acquisition techniques.

Finally, acknowledgement is made of the financial support provided by the Australian Research Grants Committee, without which this work would not have been possible.

NOMENCLATURE

a_i	Internal pipe radius
a_m	Mean pipe radius
B_e	Equivalent resolution bandwidth
c_e	Speed of sound in acoustic medium outside the pipe
c_g	Group velocity of internal acoustic mode
c_i	Speed of sound in acoustic medium inside the pipe
c_{LP}	Compressional wavespeed in plate = $(E/\rho_s \psi^2)^{1/2}$
c_p	Phase velocity of internal acoustic mode
C_p	Static pressure coefficient = $[p_{s1} - p_{s0}] / \frac{1}{2} \rho_f U_o^2$
c_x	Empirical decay constant for the axial narrow band correlation coefficient of a turbulent pressure field
c_y	Empirical decay constant for the circumferential narrow band correlation coefficient of a turbulent pressure field
d	Internal pipe diameter
E	Modulus of elasticity
$E\{ \}$	Expected (mean) value = η' for turbulent pressure fluctuations, and = $\tilde{\eta}$ for acoustic pressure fluctuations (Chapter 6 only)
f	Frequency
$f()$	Probability density function
f_H	Highpass filter frequency breakpoint
f_L	Lowpass filter frequency breakpoint
f_N	Nyquist folding frequency
f_r	Ring frequency of pipe = $\omega_r / 2\pi$
G	= c_g / c_i
h	Pipe wall thickness
h	Sampling or digitizing interval (Chapter 6 only)
$H(z)$	Digital filter transfer function
I	Nett acoustic energy flux

$j_{\alpha\alpha}^2(\omega)$	Joint acceptance of the α^{th} structural mode $= j_{\text{mmmm}}^2(\omega) = j_{\text{mm}}^2(\omega) \cdot j_{\text{nn}}^2(\omega)$
$j_{\alpha\alpha}^2(v)$	Joint acceptance of the α^{th} structural mode as a function of non-dimensional frequency
J	Bessel function
k	Order of digital filter (Chapter 6 only)
k	$= (\kappa_{\text{pq}}^2 + k_{\text{x}}^2)^{\frac{1}{2}}$
k_{m}	Axial component of structural wavenumber $= m\pi/\ell$
k_{n}	Circumferential component of structural wavenumber $= n/a_{\text{m}}$
k_{x}	Axial acoustic wavenumber
K	$= (K_{\text{m}}^2 + K_{\text{n}}^2)^{\frac{1}{2}}$
K_{m}	$= k_{\text{m}} a_{\text{m}} = m\pi a_{\text{m}}/\ell$
K_{n}	$= k_{\text{n}} a_{\text{m}} = n$
K_{x}	$= k_{\text{x}} a_{\text{m}}$
ℓ	Pipe length
m	Maximum number of correlation lag values (Chapter 6 only) $= \tau_{\text{max}}/h$
m	Axial structural mode order (integer number of half waves in the length ℓ)
M_{LP}	$= c_{\text{LP}}/c_{\text{e}}$
M_{o}	Mean centre-line flow Mach number $= U_{\text{o}}/c_{\text{e}}$ (immediately before test section)
M_{α}	Generalised mass of α^{th} mode
n	Number of applications of digital filter (Chapter 6 only)
n	Circumferential structural mode order (integer number of full waves around the circumference)
N	Sample size (Chapter 6 only)
$N(v)$	Modal density of pipe
p	Radial acoustic mode order (number of plane diametral nodal surfaces)
p	Pressure fluctuations (Chapter 6 only)

p_1	Static pressure ahead of shock wave
p_2	Static pressure behind shock wave
p_4	Initial pressure in high pressure chamber of shock tube
$\overline{p^2}$	Overall mean square wall pressure fluctuations
p'	Overall root mean square wall pressure fluctuations = $(\overline{p^2})^{1/2}$
p'	Turbulent pressure fluctuations (Chapter 6 only)
p_{s_1}	Local static pressure
p_{s_0}	Static pressure immediately before test section
\tilde{p}	Acoustic pressure fluctuations
\tilde{p}_+	Incident acoustic pressure fluctuations
\tilde{p}_-	Reflected acoustic pressure fluctuations
$\tilde{p}_{H.O.}$	Acoustic pressure fluctuations associated with higher order acoustic modes
$\tilde{p}_{P.W.}$	Acoustic pressure fluctuations associated with plane waves
$\langle p^2 \rangle$	Time averaged mean square filtered fluctuating pressure = $R_{pp}(0,0)$
$p(\underline{x};t)$	Instantaneous wall pressure fluctuations at a point x and time $t = p'(\underline{x};t) + \tilde{p}(\underline{x};t)$
$P_{r.m.s.}$	Root mean square amplitude of incident pressure wave at pipe outlet
q	Circumferential acoustic mode order (number of cylindrical nodal surfaces concentric with the cylinder axis)
q_0	Flow dynamic pressure = $\frac{1}{2}\rho_f U_0^2$
Q_i	Internal quality factor associated with material damping
Q_j	Quality factor associated with the dissipation at structural joints
Q_{rad}	Modal quality factor associated with radiation damping = $\omega M_\alpha / R_{rad}$
Q_α	Overall modal quality factor of the α th structural mode
r	Radial co-ordinate

r	Reflection coefficient (Chapter 6 only)
\tilde{r}	Co-ordinate on pipe surface (Equation [2.9])
R	Characteristic gas constant
R	Reflection coefficient (Equation [5.2])
R/a_m	Ratio of bend radius to mean pipe radius
R_{rad}	Radiation resistance = $\rho_e c_e S \sigma_\alpha$
$R_{xy}(\xi, \tau)$	Longitudinal space-time cross-correlation of two arbitrary random processes, real or complex
S	Pipe surface area = $2\pi a_m \ell$
S_o	Peak strouhal number associated with vortex shedding
t	Time
t_c	Characteristic length associated with vortex shedding
T	Time period
T_o	Reservoir (stagnation) temperature
T_r	Sample length = Nh
U	Mean flow velocity
U_c	Convection velocity of a turbulent pressure field
U_o	Mean centre-line flow velocity immediately before test section
U_*	Friction velocity
x	Co-ordinate in pipe axial direction (x-direction)
x	Digital input to difference equation (Chapter 6 only)
x'	Quantized digital signal = $x + \epsilon_x$
X	Non-dimensional streamwise co-ordinate = x/d
y	Co-ordinate in pipe axial direction (y-direction)
y	Digital output from difference equation (Chapter 6 only)
y'	Quantised digital signal = $y + \epsilon_y$
Y	Non-dimensional streamwise co-ordinate = y/d
z	z Transform = $e^{j\omega T}$

$Z_{\alpha}(\omega)$	Obstructance function of the α^{th} pipe vibrational mode
$\frac{1}{\alpha}$	Absorption coefficient (Chapter 6 only)
α	Structural mode order = (m,n)
α_p	Proportion of Φ_p associated with higher order acoustic modes
α_{pq}	Characteristic numbers for Bessel function
β	Pipe wall thickness parameter = $h/\sqrt{12} a_m$
γ	Ratio of specific heat of a gas at constant pressure to the specific heat at constant temperature
δ	Maxima associated with well behaved and damped $\cos(\tau - \tau_p)$ correlation functions (Equation [6.20])
Δv_1	$= n^2/2\psi M_{LP}^2$
$\Delta\omega$	Bandwidth = $\omega_1 - \omega_2$
Δf	Bandpass filtered array = $f_L - f_H$ (Chapter 6 only)
ϵ_r	Normalised standard error = $\sqrt{1/B_e T_r}$
ϵ_x	Aperture time error
ϵ_y	Aperture time error
η	Circumferential spatial separation
η'	Expected value of turbulent pressure fluctuations
$\tilde{\eta}$	Expected value of acoustic pressure fluctuations
θ	Angle around pipe circumference ($\theta = 180^\circ$ is on the inner wall)
I_p	Non-dimensional mean square wall pressure fluctuations
I_{ζ}	Non-dimensional mean square pipe wall acceleration response
I_{π}	Non-dimensional mean square acoustic power radiated
κ_{pq}	$= \pi\alpha_{pq}/a_i = (\omega_{co})_{pq}/c_i$
Λ	$= \ell/a_m$
μ	Poisson's ratio
ν	Non-dimensional frequency = $\omega/\omega_r = \nu/\psi$

\bar{v}	$= v/\psi$
v_{ac}	Acoustic coincidence frequency of a flat plate with the same thickness as the pipe wall $= c_e^2/\beta c_{LP}^2$
v_c	Coincidence frequency $= \omega_c/\omega_r$
$(v_{co})_{pq}$	Non-dimensional cut off frequency of (p,q) th internal acoustic mode
\bar{v}_{co}	$= v_{co}/\psi$
v_f	Fluid kinematic viscosity
v_{mn}	Non-dimensional frequency of (m,n) th pipe mode
ξ	Axial spatial separation
ξ_T	Distance from downstream transducer to anechoic termination
ρ_e	Density of external fluid medium surrounding the pipe
ρ_f	Density of fluid inside the pipe
ρ_{fs}	$= \rho_f/\rho_s$
ρ_s	Density of pipe material
ρ_{xy}	Correlation coefficient of two arbitrary random processes, x and y
σ	Radiation ratio $= R_{rad}/S\rho_e c_e$
σ_o	Radiation ratio associated with straight pipe flow
σ_α	Radiation ratio of α^{th} pipe vibration mode
τ	Time delay $= t_2 - t_1$
$\tau_{\sim P.H.O.}$	Time delay associated with higher order mode propagation
$\tau_{P'}$	Time delay associated with turbulent pressure fluctuations
$\tau_{\sim P.W.}$	Time delay associated with plane wave propagation
ϕ	Angular co-ordinate
$\phi_p(\omega)$	Power spectral density of wall pressure fluctuations
$\phi_{\zeta}(\omega)$	Power spectral density of pipe wall acceleration
$[[\phi_{\zeta}(\omega)]]$	Space averaged power spectral density of pipe wall acceleration

ϕ_{π}	Power spectral density of acoustic power radiation
$\phi_p(\omega)$	Non-dimensional power spectral density of wall pressure fluctuations = $\phi_p(\omega)U_o/q_o^2a_i$
$\phi_{\zeta}(\omega)$	Non-dimensional power spectral density of pipe wall acceleration = $\phi_{\zeta}(\omega)/\omega^3a_m^2$
Φ_{π}	Non-dimensional power spectral density of acoustic power radiation = $\phi_{\pi}/\rho_e c_e^2 S a_m$
Φ_{p_o}	Non-dimensional power spectral density of wall pressure fluctuations associated with straight pipe flow
$(\Phi_{\zeta})_o$	Non-dimensional power spectral density of pipe wall acceleration associated with straight pipe flow
$(\Phi_{\pi})_o$	Non-dimensional power spectral density of acoustic power radiation associated with straight pipe flow
ψ	= $(1 - \mu^2)^{1/2}$
$\psi_{mn}(x)$	Mode shape of (m,n)th structural mode
ω	Radian (angular) frequency
$(\omega_{co})_{pq}$	Cut off radian frequency of (p,q)th acoustic mode
ω_{mn}	Radian frequency of (m,n)th pipe mode
ω_r	Pipe ring frequency = c_{LP}/a_m
Ω	Strouhal number = $\omega a_i/U_o$
$\Omega\Phi'_p$	= $\omega\phi_p/\bar{p}^2$

LIST OF FIGURES

<u>Figure Number</u>	<u>Title</u>	<u>Page</u>
2.1	A model of bend excitation with flow	20
2.2	Internal acoustic modes	25
2.3(a)-(g)	Axial joint acceptance	30-36
2.4	Schematic illustration of coincidence	38
2.5-2.7	Coincidence of acoustic and structural modes	40-42
3.1	Inlet piping and 90° mitred bend	48
3.2	Radiused bend ($R/a_m = 6.4$)	48
3.3	Nominal valve dimensions	49
3.4	Gate valve	51
3.5	Butterfly valve	51
3.6	Details of test rig and various pipe fittings	52
3.7	Rotatable instrumentation section	54
3.8	Instrumented 90° mitred bend	54
3.9	Flow control equipment	56
3.10	Vibration isolator	56
3.11	Non-dimensional pipe wall acceleration (at $X = 12.0$)	58
3.12	Test pipe in anechoic chamber	60
3.13	Instrumentation	60
3.14	Pilot probe traverse	63
3.15	Wall pressure transducers	63
3.16-3.22	Universal velocity profiles	65-71
3.23	Details of piezo-electric transducer	74
3.24	Circuit diagram of transducer preamplifier	74
3.25	Instrumentation	76
3.26	Oscilloscope traces of the response of a piezo-electric transducer to the passage of a shock wave	77

<u>Figure Number</u>	<u>Title</u>	<u>Page</u>
3.27	Shock tube calibration of transducers	79
3.28	Calibration acoustic coupler	81
3.29	Frequency response of a piezo-electric transducer as measured with an acoustic coupler	82
3.30	Mass loading effects of a B & K 8307, 0.5g accelerometer	84
4.1	Location of measurement ports	91
4.2	Mean velocity profiles	93
4.3	Oscillation of the separation bubble	95
4.4(a)-(c)	Time history of velocity variation	96-98
4.5	Axial variation of static pressure along the inner wall	100
4.6	Axial and circumferential static pressure variation	101
4.7-4.18	Spectral density of wall pressure field	103-114
4.19	Variation of p'/q_0 with reynolds number	116
4.20	Root mean square wall pressure fluctuations	117
4.21	Circumferential variation of p'/q_0 before bend	119
4.22	Circumferential variation of p'/q_0 after bend	120
4.23	Frequency weighted power spectral density of Φ_p	122
4.24-4.26	Wall pressure fluctuations before bend (100 Hz bandwidth)	125-127
4.27-4.29	Wall pressure fluctuations after bend (100 Hz bandwidth)	128-130
4.30	Flow disturbance in the region of the bend	132
4.31	Spectral density of wall pressure field	134
4.32	Spectral density of wall pressure field (mean values)	135
4.33-4.35	Wall pressure fluctuations (100 Hz bandwidth)	137-139
4.36	Non-dimensional pipe wall acceleration	141
4.37	Non-dimensional acoustic power radiation	142

<u>Figure Number</u>	<u>Title</u>	<u>Page</u>
4.38-4.40	Pipe wall acceleration (100 Hz bandwidth)	144-146
4.41-4.43	Acoustic power radiation (100 Hz bandwidth)	147-149
4.44	Spectral densities of Φ_{ζ} and Φ_{π} relative to straight pipe flow and corresponding radiation ratio σ/σ_{α}	151
4.45	Modal density of experimental test pipe	152
4.46	Flow dependence of Φ_p for straight pipe	154
4.47	Flow dependence of Φ_p for 90° mitred bend	156
5.1-5.4	Spectral density of wall pressure field	162-165
5.5	Spectral density of wall pressure field (mean values)	166
5.6-5.8	Spectral density of wall pressure field	168-170
5.9	Spectral density of wall pressure field (mean values)	171
5.10	Sound field in bellmouth inlet	172
5.11-5.15	Non-dimensional pipe wall acceleration	174-178
5.16-5.20	Non-dimensional acoustic power radiation	179-183
5.21-5.26	Pipe wall acceleration (100 Hz bandwidth)	185-190
5.27-5.32	Acoustic power radiation (100 Hz bandwidth)	191-196
5.33-5.37	Spectral densities of Φ_{ζ} and Φ_{π} relative to straight pipe flow and the corresponding radiation ratio σ/σ_0	200-204
5.38	Flow dependence of Φ_p for 45° mitred bend	207
5.39	Flow dependence of Φ_p for gate valve	208
5.40	Flow dependence of Φ_p for butterfly valve	210
5.41	Butterfly valve "fully open" - sound field in bellmouth inlet	218
5.42	Gate valve "fully open" - sound field in bellmouth inlet	220
5.43	Pipe wall acceleration (100 Hz bandwidth)	222
5.44	Acoustic power radiation (100 Hz bandwidth)	223

<u>Figure Number</u>	<u>Title</u>	<u>Page</u>
5.45	Spectral densities of Φ_r and Φ_π relative to straight pipe flow and the corresponding radiation ratio σ/σ_0	224
6.1(a)-(c)	Correlation coefficients of incident and reflected waves	238-239
6.2(a)-(c)	Correlation coefficients of incident and reflected waves	241-242
6.3	Key steps in the wall pressure cross correlations	246
6.4	Pressure transducer voltage output	249
6.5	Digital filter flowchart	253
6.6	Response of a digital filter to a step input	254
6.7	Frequency response of a typical digital filter used	254
6.8	Correlation of a bandpass filtered signal with an unfiltered signal	257
6.9	Autocorrelation of a square wave	258
6.10-6.12	Correlations for $\xi = 0.036\text{m}$	260-261
6.13-6.15	Correlations for $\xi = 0.187\text{m}$	263-264
6.16-6.18	Correlations for $\xi = 0.187\text{m}$	265-266
6.19-6.21	Correlations for $\xi = 0.187\text{m}$	267-268
6.22-6.24	Correlations for $\xi = 0.187\text{m}$	269-270
6.25-6.27	Correlations for $\xi = 5.186\text{m}$	272-273
6.28-6.33	Correlations for $\xi = 3.182\text{m}$	274-276
6.34-6.44	Correlations for $\xi = 3.182\text{m}$	278-283
6.45-6.50	Correlations for $\xi = 5.186\text{m}$	284-286
6.51-6.52	Correlation coefficient associated with $\tau_{P.P.W.}$	288
7.1-7.3	Coincidence of acoustic and structural modes	296-298
7.4	Schematic illustration of the estimation of I_p in a $\frac{1}{3}$ -octave band	303
7.5	Illustration of estimation of v_{mn}/v_c using (a) Heckl's, and (b) Arnold and Warburton's equations	306

<u>Figure Number</u>	<u>Title</u>	<u>Page</u>
7.6	Axial joint acceptance (estimation of half power bandwidth)	308
7.7-7.9	I_{ζ}/I_p - Comparison of theoretical estimates and experimental results.	310-312
7.10-7.12	I_{π}/I_p - Comparison of theoretical estimates and experimental results	313-315
7.13-7.14	Thick wall pipe non-dimensional acceleration spectra	319-320
7.15-7.16	Thick wall pipe non-dimensional acoustic power radiation	321-322
7.17(a)-(b)	90° Mitred bend - a comparison between thick and thin wall cylinders	327-328
7.18(a)-(b)	Butterfly valve open - a comparison between thick and thin wall cylinders	329-330
7.19(a)-(b)	Gate valve open - a comparison between thick and thin wall cylinders	331-332
7.20-7.21	I_{ζ}/I_p for thick wall pipe	334-335
7.22-7.23	I_{π}/I_p for thick wall pipe	336-337
C1	Orifice plate	372
C2	R.M.S. Pressure fluctuations	373
C3-C4	Non-dimensional spectra of wall pressure fluctuations	374-375
C5	Frequency weighted power spectral density	376
C6-C10	Non-dimensional spectra of acoustic power radiated	377-381
C11-C12	Narrow band analysis of acoustic power radiated	382-383
C13-C14	Non-dimensional spectra of acoustic power radiated	384-385
C15-C19	Non-dimensional acceleration spectra	386-390
C20-C21	Narrow band analysis of acceleration spectra	391-392
C22-C23	Non-dimensional acceleration spectra	393-394
C24-C25	Spectral densities of wall acceleration, acoustic radiation, and radiation ratios relative to straight pipe flow	395-396



CHAPTER 1

INTRODUCTION

1.1 GENERAL INTRODUCTION

There is an increasing public awareness of the environmental, psychological and physiological hazards of excessively high noise and vibration levels. The advent of industrial noise legislation and hearing conservation regulations in various countries has brought about a flurry of activity to bring about quick solutions. If a new plant is being designed, and there is a noise requirement to be met, or if an existing plant is giving trouble, with complaints being made by various bodies, long term economic solutions to the problem can be achieved only by obtaining fundamental solutions, as opposed to trial and error methods. The latter are generally inefficient, time consuming and ultimately expensive. To date, adequate solutions are hampered by the lack of a fundamental understanding of various noise and vibration sources and paths.

In particular, from the process industries to space shuttle builders there is a keen interest in the problem of controlling the vibration of, and the noise radiation from, pipes or ducts carrying a flowing fluid. It has long been recognised that pipe fittings (pipe bends, valves, orifice plates, tee-junctions, etc.) can be major noise sources in piping systems, in that they may provide either an intense local or distributed flow disturbance which may excite the pipe wall, which in turn may radiate appreciable acoustic energy into the surroundings. There is a need for a better understanding of the mechanisms of this energy transfer so that designers of piping systems can estimate the noise levels to be

expected from a particular piping geometry and can avoid designs likely to be excessively noisy.

In a fully-developed turbulent pipe flow through a straight length of pipe with no flow discontinuities or pipe fittings, the radiation of sound due to the vibration of the pipe walls is due to the random fluctuating pressures associated with the turbulent flow. This random wall pressure field extends over complete piping lengths and cannot be removed from the flow: it represents a minimum excitation level always present within the pipe. The situation is somewhat more complex when internal flow disturbances associated with pipe fittings are present in the system. They generate intense internal acoustic pressure fluctuations which propagate essentially unattenuated through the piping system. It is necessary to determine the extent to which the acoustic waves generated by the flow disturbance and the local effects of the disturbance itself (e.g. flow separation and increased turbulence levels) contribute to the pipe wall excitation and the external acoustic radiation. Clearly, satisfactory models of the excitation produced by bends and other pipe fittings need to be developed.

Previous work in the department of Mechanical Engineering, at the University of Adelaide has been directed towards a better understanding of the basic mechanism of the energy transfer from a fully-developed turbulent pipe flow. The next obvious stage is to apply and extend this understanding to the more common practical case of a pipe containing bends and other flow discontinuities. This investigation is concerned with studying the effects of flow disturbances due to pipe fittings - specifically bends, valves and orifice plates - in order:

- (i) to determine the character of the disturbance due to the pipe fittings;

- (ii) to determine what effects various geometries of pipe fittings have on the vibrational response of, and acoustic radiation from, a pipe carrying a fluid flow;
- (iii) to investigate the mechanism by which the pipe is excited as a result of the flow disturbances produced by those devices; and
- (iv) to provide guidance for pipe work designers on the acoustic radiation to be expected from various pipe fittings, and advice on design of pipe work for low noise.

1.2 REVIEW OF PREVIOUS WORK

In the main, pipe fittings such as pipe bends, valves and orifice plates have been recognised extensively in the literature as major noise sources. However, little fundamental understanding of the mechanism by which the pipe is excited as a result of the flow disturbances produced by these devices exists. Much of the literature on noise due to pipe discontinuities has been based on empirical studies of valve noise and in particular on the measurement of noise characteristics of the discontinuities. There are considerable discrepancies between existing experimental results and theoretical predictions of acoustic transmission loss from a pipe for the simple case of a plane acoustic wave propagating in a pipe. Rennison (1976) rectified this and proposed a "lower bound" to the acoustic power radiation from pipes excited by acoustic plane waves. However little work has been attempted on predicting the pipe wall response and the external acoustic radiation in the more complex situation involving multi-modal acoustic propagation inside a pipe with a fully-developed turbulent pipe flow.

General investigations of the vibrational response of

structures excited by random pressure environments have been based on idealised structures such as strings, beams, flat plates and cylinders, with simple excitations such as progressive acoustic waves and boundary layer pressure fluctuations. Lyon (1956) initiated theoretical developments by considering the response of a string to excitation by different noise fields. In particular, he studied the excitation of strings to flowing turbulence, and the response of an infinite string to a turbulent pressure field convected along its length was compared with the response of a finite string.

Powell (1958 a,b) developed the method of normal mode analysis in which he represented the response of a finite structure in terms of its normal modes of vibration. In this approach the boundary conditions determine the natural modes and generalised harmonic analysis is used to determine the response. The power spectrum and hence the r.m.s. value of the spatially averaged response was derived; it involves the joint acceptance (a function expressing the efficiency of the exciting forces) between the spatial structure of the pressure field and the geometry of the modes of vibration. Powell's techniques have been used extensively over the years by numerous researchers; they are also the basis for a statistical model used in this investigation to predict the pipe wall response downstream of various internal flow disturbances, the total response of the pipe structure being represented by the summed response of its resonant modes.

Dyer (1959) investigated the response of plates to a decaying convected random pressure field using Powell's (1958) normal mode analysis and an analytical approach similar to that of Lyon (1956). He extended Lyon's treatment of one-dimensional transverse vibrations of strings to the two-dimensional flexural vibrations of plates. A

general solution for the plate vibration in terms of the impulse response of the plate was derived, together with a solution for the response to a decaying convected small scale random pressure field.

Several subsequent experimental studies have been made of the statistical properties of the fluctuating wall pressure field associated with a turbulent boundary layer and fully-developed turbulent pipe flow, for example Willmarth and Woolridge (1962), Corcos (1962, 1963), Bakewell (1964), Bull (1963, 1967) and Cockburn and Robertson (1974). In general, these indicate that the cross spectral density of the wall pressure field, for both types of flow can be fairly well represented by Corcos's model. There are significant shortcomings in the Corcos model at wavenumbers lower than the convection wavenumber in that the model overestimates the measured spectral levels. Rennison (1976) used the Corcos model in theoretical predictions of the pipe wall response to a turbulent boundary layer field and he discusses the shortcomings in considerable detail.

Further comprehensive theoretical and experimental studies of the vibration response of panels excited by boundary layer pressure fields have been performed by Maestrello (1965 a, 1965 b, 1967). Wilby (1967) also investigated the response of panels to turbulent boundary layer excitation and plane acoustic waves. Maestrello reported on the vibration response of and the sound power radiated from panels excited by a turbulent boundary layer for various subsonic flow speeds. Panels of different thicknesses were investigated. Wilby compared his experimental results with theoretical predictions based on simply supported mode shapes. He assumed that the structural vibrations were represented by their normal modes of vibration and that the vibrations were dominated by standing waves. Maestrello on the other hand considered both the standing and the running wave cases.

Strawderman and Christman (1972) also investigated turbulence induced plate vibration. They were concerned with fluid loading on finite and infinite plates, particularly heavy fluid loading (e.g. water), and its effects on the turbulence induced vibration statistics. They concluded that while the fluid-loaded plates exhibit modal behaviour, the fluid-loaded modes are not, in general, identical to the natural modes, since the inertial component of the fluid-loading is several orders of magnitude greater than the resistive component.

Rattaya and Junger (1964) used Powell's normal mode analysis to investigate the turbulent flow excitation of cylindrical shells. Amplification of the pipe wall response by coincidence effects in pipes conducting high speed air or steam flow was examined, and it was concluded that hydrodynamic coincidence would occur only for supersonic flow.

Clinch (1970) also considered simply supported thin cylindrical shells which he analysed using Powell's normal mode and joint acceptance method. He derived an expression for the root mean square displacement essentially as a function of frequency bandwidth and compared his theoretical results with turbulent water flow. His measured results and theoretical predictions show close agreement, but are limited to the response of thin-walled pipes to the turbulent wall pressure field at high mode orders and frequencies.

As has been illustrated in the preceding paragraphs, extensive work has been done on the vibration response of and the acoustic radiation from various structures, due to turbulent boundary layer pressure fluctuations. There has been no comprehensive assessment of the various parameters involved e.g. detailed investigation on structural damping, the dependence of the vibration response and acoustic radiation on flow speed and experimental verification of

theoretically predicted radiation ratios. Rennison (1976), undertook an extensive experimental and theoretical investigation of the vibrational response of and the acoustic radiation from thin-walled pipes, due to turbulent boundary layer flow. His work was performed in the department of Mechanical Engineering at the University of Adelaide, and was directed towards a better understanding of the basic mechanism of the energy transfer from a fully-developed turbulence in the contained flow to the surroundings through the wall of a straight pipe. The work reported in this investigation is indeed an extension of his work. Rennison was primarily concerned with two different excitations: (i) a random wall pressure field associated with fully-developed turbulent pipe flow, and (ii) acoustic plane waves propagating inside the pipe. Many of the gaps and shortcomings of previous works related to (i) above were made good in his work; his procedure for calculating the dynamic response of a thin-walled cylindrical shell to the random pressure field generated by a fully-developed pipe flow is modified in this investigation for a multi-modal acoustic pressure field, superimposed on a fully-developed turbulent pipe flow.

Theoretical studies of acoustic plane wave and multi-mode transmission in cylindrical pipes with no flow have been made by Cremer (1955), Heckl (1958) and summarised by Morfey (1971). Cremer's approach is based on ray statistics and Heckl's on mode statistics, and equations are developed to predict the transmission loss. Both theories are limited to frequencies below the ring frequency of the pipe. For the acoustic multi-mode sound transmission case, it is assumed that the internal sound field is equally distributed over the propagating acoustic modes. Heckl's experimental results are in reasonable agreement with the theoretical predictions at frequencies where the higher order modes could propagate. However, his theoretical

results do not take into account damping of the pipe walls. His theoretical predictions are based on a forced stiffness - controlled response i.e. the relevant pipe responses are forced by the various internal acoustic pressure distributions. Hence no account is taken of the various resonant structural modes that would couple to the higher order acoustic modes propagating inside the pipe. At low frequencies where the internal sound field comprises plane acoustic waves, experimentally measured values of transmission loss are some 30 dB less than those predicted. Neither Cremer nor Heckl investigated; (a) the modal content of the structural response, (b) the assumption that there was equi-partition of acoustic energy at frequencies where higher order modes could propagate, or (c) the effects of damping for both acoustic plane wave and multi-modal transmission through the pipe wall.

Rennison (1976) investigated transmission losses for acoustic plane waves propagating inside a pipe (with no flow). He concluded that the resonant response of the pipe determined the acoustic radiation instead of the forced stiffness-controlled response as postulated by Cremer and Heckl. From his experiments and supporting theoretical analysis, the resonant response and the associated acoustic radiation result primarily from intrinsic inhomogeneties in the pipe. These inhomogeneties in the pipe structure and end conditions give rise to coupling between plane wave excitation and resonant modes of the pipe; so that the vibrational response will in general be greater than the forced response which would be expected in the ideal case. From these findings, Rennison proposed a "lower bound" concept to the acoustic radiation from pipes excited by internally propagating acoustic plane waves, based on a peristaltic wave motion in the wall of a pipe of finite length. Good agreement is found between theory

and experiment, for pipes of high material damping. The resonant contribution to the pipe wall vibrational response and the acoustic radiation increases as the material damping decreases, and the lower bound underestimates both the response and the radiation by up to 30 dB.

Kuhn (1974), and Kuhn and Morfey (1976 a) also investigated the transmission loss of sound through pipe walls. They were primarily concerned with low frequency sound i.e. frequencies at which only plane acoustic waves could propagate. They also recognised that the transmitted sound power as measured by Heckl was up to 30 dB higher than would be estimated from his model. They accounted for this increased sound power by pipe bending waves. By careful isolation (de-coupling the mechanical and acoustical effects of the near field of the speaker source from the test-pipe) they suppressed the bending waves and achieved reductions of 20 dB. However as pointed out by Rennison (1976) they did not state whether the SPL in the far field of the source was maintained constant and no actual measurements were made of the effects on the measured pipe transmission loss of de-coupling the source near field from the test pipe. Their inclusion of a 90° mitred bend (with no flow) was found to cause significant increases in $\frac{1}{3}$ octave radiated sound power. Forced response predicted values were exceeded by up to 20 dB even with the source decoupled. They concluded that the mitred bend caused significant bending wave excitation when plane waves are incident on the bend (speaker generated plane waves). While bending waves may indeed account for some proportion of the discrepancies, even for their straight pipe (and source decoupled) case, there are discrepancies of up to 12 dB at low frequency values between theory and experiment. Kuhn (1974) concluded that the non-propagating (1,0) higher order mode was responsible for those discrepancies. No attempt was made in the calculation of the

transmission loss or in the explanation of the discrepancies to take account of the possible coupling of the acoustic modes to the resonant vibrational modes of the pipe.

The literature review up to this point has been confined to (a) the excitation of structures by random pressure fields (mainly turbulent pressure fluctuations), and (b) the acoustic excitation of cylindrical shells for the no flow situation. Kuhn and Morfey (1976 b) investigated the noise due to fully-developed turbulent flow exhausting from straight and bent pipes. They were concerned in this case with the velocity dependence of the acoustic power radiating from the exit region of a circular pipe at subsonic speeds. The 90° mitred bend they used generated high intensity internal plane waves and the acoustic power radiated from the pipe exit was found to grow approximately as U^6 (where U is the flow velocity at the pipe exit). They also concluded that the mitred bend could generate not only locally fluctuating aerodynamic forces (which force the pipe into bending modes) but also distributed and propagating acoustic pressures. No attempt was made to decouple the bend from the test section to investigate the effects of the bending modes downstream, or to investigate the effects of the propagating acoustic waves generated by the bend on the pipe wall response.

Numerous authors have reported that control valves are the primary source of noise in pipe flow systems and in particular in high pressure gas and steam systems. As a result, much of the literature on noise due to pipe discontinuities has been limited to empirical studies of valve noise. Seebold (1971) presented field data for a fuel gas piping system. He reports that measured noise levels were significantly higher than those obtained by available prediction methods; but no mention whatsoever is given of which specific prediction

method was used although he reviews several empirical noise prediction schemes. He attributes the differences to the coincidence of like pipe and gas modes although no attempt is made to theoretically justify his conclusion.

Boger (1971) discusses several procedures for reducing valve noise but does not attempt to develop a fundamental understanding of the source of the problem. His paper includes discussion of the possibility of; (a) increasing the pipe wall thickness, (b) using acoustical insulation downstream of the device, (c) using downstream in-line silencers, and (d) using expansion plates downstream of the valve to absorb some of the pressure reduction over the whole system.

Allen (1971) also discusses the prediction and abatement of control valve noise. He favoured techniques for predicting valve noise based on empiricism and recommended that the noise characteristics for each valve type and adjacent piping configuration be established by actual test. His arguments are based on a view that very little, either qualitatively or quantitatively, is known concerning the turbulence level of a bounded fluid stream. Once again, as in the cases of Seebold and Boger, no attempt was made to develop an analytical model which accurately describes the mechanism of noise generation and propagation in a piping system. A fundamental knowledge of the coupling of the energy propagating from the source between the fluid and the pipe wall is important to achieve economical noise control.

White and Sawley (1972) have considered several factors which are important in the proper description of the energy interaction and propagation in fluid-filled piping systems. In particular, they discuss bending waves in the pipe and acoustic propagation in the fluid. The emphasis in their work is on attempting to define the ways in which acoustical and vibrational energy can propagate in

pipng systems, but no work was actually done on developing representative theoretical models of the pipe wall vibration and external acoustic radiation.

Karvelis (1975) reported on an experimental investigation of the wall pressure fluctuations in piping containing simple control devices. He was only concerned with the internal acoustic field and does not report on the pipe wall response or the external acoustic radiation. His efforts were concentrated on orifice plates and valves; he found that the wall pressure fields at downstream distances greater than 10 pipe diameters are completely dominated by the acoustic component. Strong peaks in the acoustic wall pressure field were found at the cut-off frequencies of the various higher order internal acoustic modes. Karvelis also attempted to separate the various components of the overall wall pressure fluctuations using space-time cross-correlation techniques. He succeeded in separating the turbulent and plane wave components for low frequencies (frequencies at which only plane waves can propagate). At higher frequencies he was not able to separate the turbulent and the acoustic components because of the dispersive nature of the higher order modes. This was a significant shortcoming of his work and one that is largely overcome in the present investigation. Karvelis's wall pressure spectral data were presented only in a qualitative manner and no attempt was made to quantify the results in terms of non-dimensional spectra for comparison of different internal flow disturbances and results from other investigations.

Bull and Norton (1976) also demonstrated that various bends, and in particular, mitred bends generate strong internal acoustic fields which propagate both upstream and downstream away from the source. Spectral measurements of the acceleration response of and

the acoustic power radiated from a thin walled test section downstream of the disturbance are presented. The increases at low frequencies were found to be due to internal plane acoustic waves, but the more pronounced increases at higher frequencies were found to be associated with the higher order internal acoustic modes. Further to their earlier work, Bull and Norton (1977 a) established experimentally and analytically that this enhanced vibrational response and external acoustic radiation (compared with results for a straight pipe) is confined to frequencies close to the cut-off frequencies of the various higher order internal acoustic modes. As will be seen later, this is because:

- (i) the joint acceptance of structural and acoustic modes peaks very sharply at coincidence;
- (ii) coincidence occurs at a frequency which is very close to the cut-off frequency of the acoustic mode; and
- (iii) coincidence occurs at the resonance frequency of a structural mode or very close to it, so that the modal receptance is also at or close to its maximum value at coincidence.

This early work laid the foundations for this thesis.

Walter, McDaniel and Reethof (1977, 1978) observed the same phenomenon and they demonstrated the role of coincidence in a similar manner to Bull and Norton. As a result of the shell equations they used, they were unable to obtain analytical expressions for the coincidence frequency. Such expressions were obtained by Bull and Norton (1977 a) by using approximate relationships for the resonance frequencies of a pipe (based on Heckl's (1962) work on the vibrations of point driven cylindrical shells).

The internal characteristics of the flow in the region of a

cylindrical 90° mitred bend have been investigated by Tunstall and Harvey (1968). They established that the mitred bend produces a downstream secondary circulation which does not conform to the twin-circulatory flow usually found in radiused pipe bends. The secondary flow was dominated by a single circulation about the axis that switched at low, random frequencies between the clockwise and anti-clockwise states. They explained the phenomenon in terms of the asymmetry of the inner wall separation bubble leading to its oscillation in sympathy with the switching of direction of the spiral flow.

Heskestad (1971) measured the mean flow through a two-dimensional, constant width, 90° mitred bend and compared the results with predictions of free-streamline theories. From the static pressure and mean velocity distribution in the vicinity of the bend he determined the shape and extent of the flow separation on the inner wall.

Fricke and Stevenson (1968, 1970) and Fricke (1971) have reported pressure fluctuations in separated flows. For their configuration they showed that the wall pressure fluctuations beneath a region of separated flow could be associated with convected turbulence in the shear layer, and that there was no significant contribution from acoustic waves. Their pressure cross-correlations showed no radiation of pressure fluctuations upstream or downstream from the reattachment position. They assumed that if there were such a radiation, it would show up in the cross-correlation measurements as a maximum at delay times equal to ξ/a_0 (where ξ is the spatial separation and a_0 is the local speed of sound). They overlooked the possibility of higher order acoustic modes being present and masking their results - since these higher order modes are dispersive no one delay time can be associated with any particular mode - hence their conclusions.

Mabey (1972) summarised numerous measurements of wall pressure fluctuations in separated flows. By presenting the spectra in terms of a frequency parameter based on the separation bubble length he obtained similar spectra for forward facing steps, cavities, leading-edge separation on wings, sudden enlargements in pipes etc. The local pressure fluctuations caused by the bubble increase gradually from the separation line, reach a maximum near the reattachment line and then decrease gradually downstream of the reattachment line.

In summary, this literature review has concentrated on

- (i) reviewing the major investigations into the vibrational response of structures excited by random pressure environments;
- (ii) reviewing the major theoretical and experimental studies of acoustic plane wave and multi-mode transmission in cylindrical pipes with no flow;
- (iii) demonstrating the lack of research of a fundamental nature into pipe flow noise associated with internal flow disturbances; and
- (iv) reviewing some of the investigations into the pressure fluctuation characteristics in a separated region of flow.

1.3 OBJECTIVES OF THE PRESENT INVESTIGATION

As illustrated in the review of previous work in the last section, several important theoretical and experimental studies relating to the vibration response of simple structures to boundary layer pressure fluctuations have been carried out. In these early works, analytical techniques have been developed for the prediction of the vibration response of and the acoustic radiation from thin walled cylindrical pipes, excited by an internal fully-developed turbulent flow. Major theoretical and experimental studies of

acoustic plane wave and multi-mode transmission in cylindrical pipes, with no flow are also available.

Pipe fittings in a pipe flow system, produce internal flow disturbances, and are an acoustic source. They generate both a non-propagating "near field" and a propagating "far field". The pressure fluctuations associated with the "near field" are attenuated rapidly with distance away from the disturbance and the "far field" comprises a propagating internal acoustic field superimposed on a fully-developed turbulent wall pressure field. Virtually all the available literature on noise due to internal flow disturbances has been based on empirical studies of control valve noise. Some works have been published on the internal acoustic fields generated at, and propagating from these disturbances, but there has been no attempt to relate these internal fluctuating pressure fields (comprising turbulent and acoustic pressure fluctuations) to the pipe wall dynamics. Hence, no comprehensive theoretical and experimental work is available to date on the vibrational and acoustic effects of various internal flow disturbances in pipes with an internal fully-developed turbulent flow. The general aims of this investigation have been discussed in section 1.1. These aims are now defined in somewhat more detail.

The first part of the investigation is a largely experimental study of the effects of various internal flow disturbances on the vibrational response of, and the acoustic radiation from, a pipe carrying a flowing fluid. The particular internal flow disturbances selected are 90° radiused bends, a 45° mitred bend, a 90° mitred bend, a globe valve, a butterfly valve and several orifice plates. Spectral measurements of the vibration response of, the acoustic power radiated from, and the internal wall pressure field in a steel pipe with a re-established fully-developed internal turbulent air flow downstream of individual internal flow disturbances are presented. Comparisons

are made with similar data for straight pipe fully-developed turbulent flow which can be considered as a datum for flow generated piping noise. Theoretical explanations for the increased spectral density measurements (compared with results for a straight pipe) are presented.

The second part of the investigation is an experimental study of the internal flow characteristics upstream and downstream, in the immediate vicinity of a 90° mitred bend. The 90° mitred bend produces an asymmetric flow disturbance that is a strong generator of both plane acoustic waves and higher order modes. Of primary concern are; (i) the relationship between the pressure fluctuations in the vicinity of the bend and the characteristics of the flow separation caused by the bend; and (ii) the relationship between the pressure fluctuations in the vicinity of the bend and those downstream of the bend where local non-propagating disturbances have become attenuated.

The third part of the investigation is concerned with a detailed study of the mechanisms involved in the energy transfer from a pipe downstream of an internal flow disturbance (where local non-propagating effects have been attenuated and the internal pressure field comprises an acoustic plane wave field and an acoustic higher order mode field superimposed on a fully-developed turbulent pressure field). Space-time longitudinal cross-correlation techniques are used to separate the three components of the internal pressure field, and to associate energy levels with each of them. This part of the investigation is confined to the particular case of the 90° mitred bend.

The fourth part of the investigation involves the development of analytical techniques for the prediction of acoustic radiation from and the vibration response of pipes downstream of individual internal flow disturbances.

As is evident from the preceding objectives, this investigation represents an extensive theoretical and experimental study into pipe flow noise associated with internal flow disturbances. It is, as such, the first comprehensive fundamental study of the effects of internal flow disturbances on the vibration response of and the acoustic radiation from pipes with a fully-developed turbulent flow. Even so it cannot be completely comprehensive and many more significant questions need to be answered. Some of these will be raised in the concluding chapters of this thesis.

CHAPTER 2THEORETICAL CONSIDERATIONS2.1 INTRODUCTION

Internal disturbances to the flow through a pipe are responsible for the generation of an intense internal sound field and, compared with undisturbed fully-developed turbulent flow, produce an enhanced vibrational response of the pipe wall and external acoustic radiation. To estimate the vibrational response of the pipe wall and the external acoustic radiation, the nature of the internal acoustic field has to be known and in particular the various components of the overall wall pressure fluctuations.

The vibration of the pipe wall at any point in a system can be associated with the wall pressure fluctuations due to one, some or all of the following excitations

- (i) non-propagating local fluid dynamic and acoustic wall pressure fluctuations, associated with the internal flow disturbance.
- (ii) fully-developed turbulent pipe flow wall pressure fluctuations, associated with undisturbed "straight pipe" flow.
- (iii) the propagating internal acoustic field, associated with the internal flow disturbance.

Figure 2.1 illustrates the above forms of pipe wall excitation for the particular case of a 90° mitred bend. The vibration of the pipe wall can also be associated with the mechanical transmission of vibration excited by pipe fittings at other points in the piping system.

In this chapter, we are concerned with the effects of various internal flow disturbances on the vibration of and the acoustic radiation from sections of the piping system at some distance downstream

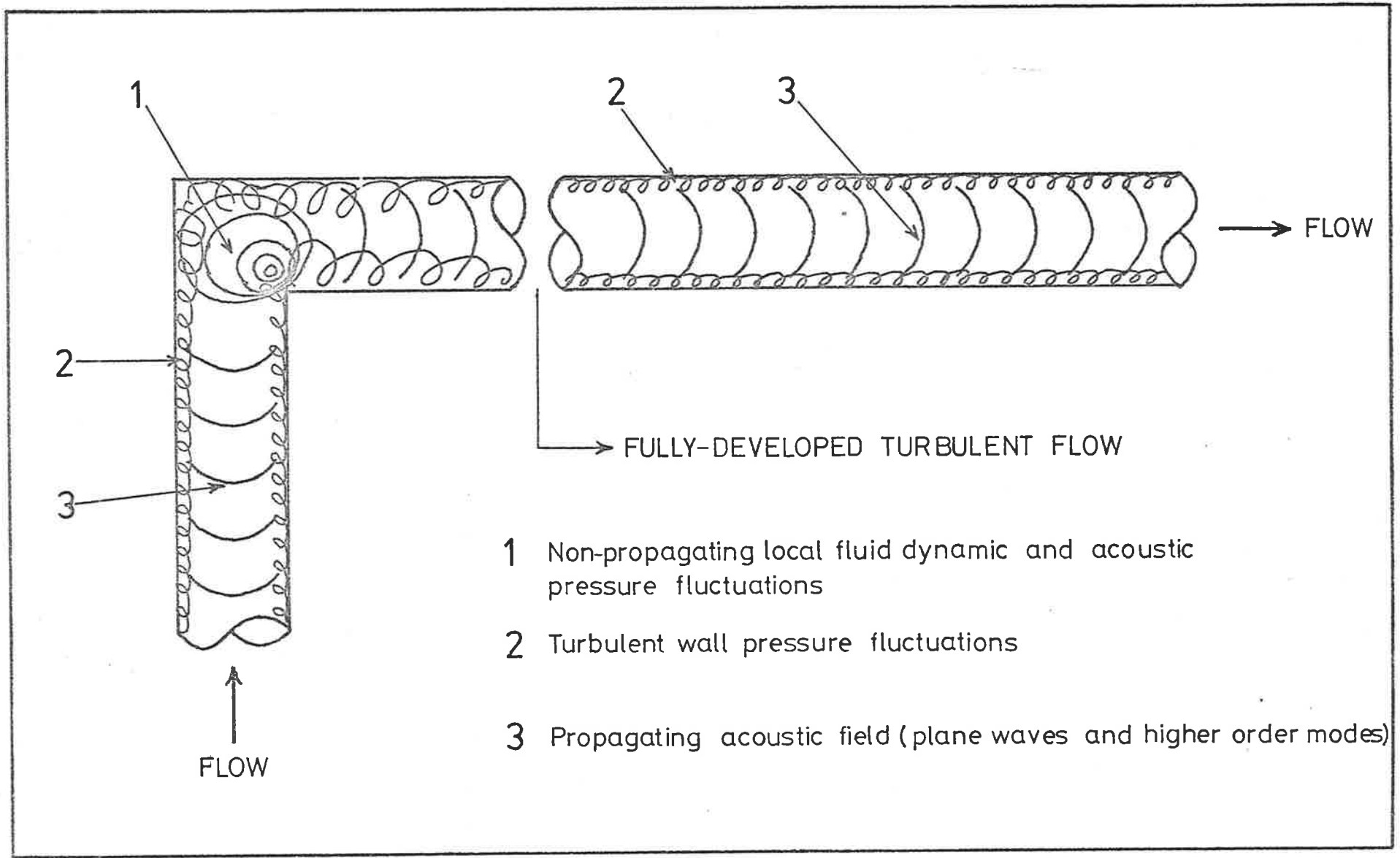


FIGURE 2.1 A MODEL OF BEND EXCITATION WITH FLOW

of the disturbance sufficient for the re-establishment of an undisturbed mean-flow velocity profile (or in similar conditions upstream). At these points, non-propagating disturbances due to the fittings have died out, and the only excitation that the pipe wall is subjected to are those reaching it by acoustic or mechanical transmission superimposed on a turbulent wall pressure field. For the particular experimental set up that has been used, disturbances due to mechanical transmission are negligible because of the impedance mismatch between the general pipework and the thin-walled test section in the anechoic chamber where the measurements were made. This is discussed in detail in Chapter 3.

An internal flow disturbance can be considered to be an acoustic source which can excite a large number of internal acoustic modes. The propagating internal acoustic field consists of plane waves and higher order modes which carry a mean energy flow away from the source. The propagation of internal acoustic modes in a duct is extensively treated in the literature (e.g. Morse and Ingard, 1968, p.467) and is summarised briefly in this chapter. These acoustic modes couple to various resonant structural vibration modes and produce enhanced pipe wall vibration and external acoustic power radiation; this is illustrated in subsequent chapters. This enhanced pipe wall vibration and external acoustic power radiation is most pronounced at frequencies close to the cut-off frequencies of the propagating higher order internal acoustic modes; this is because

- (i) the joint acceptance of structural and acoustic modes peak very sharply at a frequency corresponding to the condition of coincidence (defined in section 2.5);
- (ii) coincidence occurs at the resonance frequency of a

structural mode (exact coincidence) or very close to it, so that the modal receptance is also at or close to its maximum value at coincidence; and

- (iii) by the nature of the dispersion (wavenumber-frequency) relations of the acoustic and structural modes, coincidence occurs at a frequency very close to the cut-off frequency of the acoustic mode.

Expressions are developed in this chapter for the prediction of the coincidence frequency for the various internal higher order acoustic modes. Bull and Rennison (1974,a) have developed a procedure for calculating the dynamic response of a thin-walled cylindrical shell to the random pressure field generated by a fully-developed turbulent pipe flow, and this procedure is modified here to apply to an acoustic pressure field. For the purposes of analysis, the pipe is modelled as a thin cylindrical shell with simply supported ends, and the calculation of the statistical properties of the vibration response is based on the normal mode method of generalised harmonic analysis, where the total response of the pipe structure is represented as the sum of the responses in its resonant structural modes.

2.2 INTERNAL ACOUSTIC MODES

For a cylinder with radial, angular and axial coordinates r , ϕ , and x , the solution to the wave equation for the pressure associated with acoustic propagation in a stationary internal fluid has, for propagation in the positive x -direction, the well known form (Morse and Ingard, 1968, p.509)

$$p(r, \phi, x) = \sum_p \sum_q (A_{pq} \cos p\phi + B_{pq} \sin p\phi) J_p(\kappa_{pq} r) e^{j(k_x x - \omega t)}, \quad [2.1]$$

where
$$\kappa_{pq}^2 + k_x^2 = \left(\frac{\omega}{c_i}\right)^2 = k^2, \quad [2.2]$$

ω is the radian frequency, k_x is the axial acoustic wavenumber and c_i is the speed of sound in the internal fluid. The (p,q) th wave or mode has p plane diametral nodal surfaces and q cylindrical nodal surfaces concentric with the cylinder axis and it can propagate only at frequencies above its cut-off frequency $(\omega_{co})_{pq}$, where $(\omega_{co})_{pq} = \kappa_{pq} c_i$ and $k = \kappa_{pq}$. Now $\kappa_{pq} = (\omega_{co})_{pq} / c_i = \pi \alpha_{pq} / a_i$ where a_i is the internal pipe radius and the α_{pq} 's are determined by the boundary condition $J'_m(\pi\alpha) = 0$ for a rigid wall, where J_m is a Bessel function of the first kind of order m . The α_{pq} 's for a rigid duct are well documented in the literature (Morse and Ingard, 1968, p.511). For the first higher order mode $\alpha_{10} = 0.5861$, which implies that sound can propagate in a pipe only as plane waves ($p=q=0$) if $ka_i < 1.84$, but as both plane waves and higher order modes if $ka_i \geq 1.84$. Expressed in terms of the ring frequency of a pipe the cut-off frequency is

$$(v_{co})_{pq} = \frac{(\omega_{co})_{pq}}{\omega_r} = \frac{\kappa_{pq} c_i}{\omega_r}, \quad [2.3]$$

where $\omega_r = c_{LP} / a_m$, and a_m is the mean pipe radius. Hence, equation [2.2] can be rewritten in non-dimensional form as

$$v^2 = (v_{co})_{pq}^2 + \left(\frac{K_x c_i}{M_{LP} c_e}\right)^2, \quad [2.4]$$

where $K_x = k_x a_m$, $M_{LP} = c_{LP} / c_e$ and c_e is the external speed of sound.

The internal acoustic modes can be classified as plane waves ($p=q=0$), symmetric higher order modes ($p=0, q \geq 1$) or asymmetric higher order "spinning" modes ($p \geq 1, q \geq 0$). The form of the first ten modes and their non-dimensional cut-off frequencies for the steel

test section used, taking $c_i \approx c_e$ and $M_{LP} = 15.4$, are illustrated in Figure 2.2. The phase velocity c_p of an internal acoustic mode in a duct with rigid walls is

$$c_p = \frac{\omega}{k_x} = \frac{c_i}{\left[1 - \left[\frac{c_i k_{pq}}{\omega} \right]^2 \right]^{1/2}}, \quad [2.5]$$

and it is the velocity at which points of constant phase propagate in the axial direction. The group velocity c_g is

$$c_g = \frac{\partial \omega}{\partial k_x} = \frac{c_i^2}{c_p}, \quad [2.6]$$

and it is the velocity of progress of the "center of gravity" of a group of waves that differ somewhat in frequency. It is always less than c_i for $ka_i \geq 1.84$. Morfey (1964, 1968) has shown that from a group velocity or energy transfer viewpoint, the cut-off frequencies of the higher order modes are reduced by a factor of $(1 - M_o^2)^{1/2}$, where M_o is the mean flow Mach number. Mason (1969) verified Morfey's work experimentally and concluded that the cut-off frequencies decreased in frequency with increasing flow speed for sound propagation both up and down stream from the source. Hence for internal acoustic waves propagating in a pipe with a mean flow M_o , induced from a reservoir, as in this investigation, equation [2.3] becomes

$$(v_{co})_{pq} = \frac{k_{pq} c_i}{\omega_r} \left[\frac{1 - M_o^2}{1 + \frac{\gamma-1}{2} M_o^2} \right]^{1/2}, \quad [2.7]$$

where $\frac{c_e}{c_i} = \left[1 + \frac{\gamma-1}{2} M_o^2 \right]^{1/2}$, and $c_e = \gamma RT_o$.

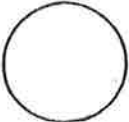
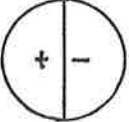
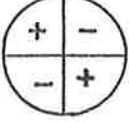
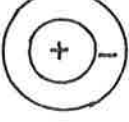
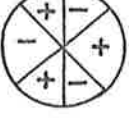
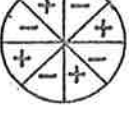
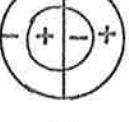
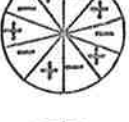

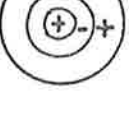
(p, q)	Mode	$(\nu_{co})_{pq}$
(0, 0)		0.000 plane waves
(1, 0)		0.122 higher order modes
(2, 0)		0.203
(0, 1)		0.254
(3, 0)		0.279
(4, 0)		0.353
(1, 1)		0.354
(5, 0)		0.425
(2, 1)		0.445
(0, 2)		0.465

FIGURE 2.2 INTERNAL ACOUSTIC MODES

Since Morfey's result is for comparison of cut-off frequencies in two states at the same static temperature and that when, as here, they are not the same, the additional function $[1 + \frac{\gamma-1}{2} M_o^2]^{\frac{1}{2}}$ comes into account for the temperature difference.

2.3 RESONANT STRUCTURAL VIBRATION MODES

The resonance frequency of the (m,n)th structural mode of a pipe with wall thickness h is given approximately by

$$v_{mn}^2 = \beta^2 K^4 + \frac{\psi^2 K_m^4}{K^4} \quad [2.8]$$

This is a modified form of Heckl's (1962) result. Here $K^2 = K_m^2 + K_n^2$; and $K_m = k_{m m} a_m = m\pi a_m / l$; and $K_n = k_{n m} a_m = n$, are the axial and circumferential wavenumber components of the structural wave respectively. Equation [2.8] is applicable to a thin cylindrical shell with simply supported ends and its limitations are discussed in Rennison (1976) and Rennison and Bull (1977). Resonant structural vibration frequencies can be calculated accurately from the analysis of Arnold and Warburton (1953) which is based on thin shell theory, and their experimental comparisons show excellent agreement with exact strain energy theory. A comparison of Arnold and Warburton's (1953) results with equation [2.8] indicates that the latter produces underestimates of the resonance structural frequencies by approximately 50% for low K_m values for the $n=1$ and $n=2$ modes ($k_{n m} a_m > v_{mn}$). For all other values, equation [2.8] gives a good approximation (Heckl, 1962 and Szechenyi, 1971). But, the modal density, which is the frequency rate of change of modes is estimated better as frequency increases (Rennison, 1976 and Miller and Hart, 1967) and for statistical estimates of the pipe wall response and hence the acoustic radiation from a cylindrical pipe this is quite acceptable. This is discussed in detail in Chapter 7 in relation

to a theoretical estimation of the pipe wall response to several resonant structural modes which are coincident with particular higher order acoustic modes. Comparisons are also made with Arnold and Warburton's (1953) theory.

2.4 THE JOINT ACCEPTANCE

The vibrational response of the pipe wall in any one of its natural modes of vibration, to excitation by a particular wall pressure field, is determined by the joint acceptance function which expresses the degree of spatial coupling that exists between the pressure excitation and the structural mode, and by the receptance of the structural mode. The receptance function is the inverse of the obstructance function, $Z_{\alpha}(\omega)$, and is well known (see Appendix B, equation [B.2]). It has a sharp maximum at the resonance frequency for any given structural mode, and the response function is proportional to the product of the joint acceptance and the receptance (see equation [2.18]). When the wall pressure excitation is an acoustic one, the joint acceptance expresses the degree of spatial coupling between the $(m,n)^{\text{th}}$ structural mode and the $(p,q)^{\text{th}}$ acoustic mode.

The joint acceptance is defined, generally, as

$$j_{mmmn}^2(\omega) = \frac{1}{\phi_p S^2} \int_S dS(\underline{r}) \psi_{mn}(\underline{r}) \int_S dS(\underline{r}') \psi_{mn}(\underline{r}') \phi_p(\xi, \omega), \quad [2.9]$$

where the vector \underline{r} represents a point on the internal surface of the pipe, $\xi = (\underline{r}' - \underline{r})$ (with components ξ and η in the axial and circumferential direction respectively), $\psi_{mn}(\underline{r})$ is the mode shape of the $(m,n)^{\text{th}}$ structural mode, and $\phi_p(\xi, \omega)$ is the cross-spectral density of the wall pressure field where $\phi_p(0, \omega) = \phi_p$.

The cross-spectral density of the wall pressure field of the $(p,q)^{\text{th}}$ propagating acoustic mode is given by

$$\phi_{pq}(\xi, \omega) = \phi(\omega) e^{jk_x \xi} \cos\left(\frac{p\eta}{a_i}\right), \quad [2.10]$$

where the suffix p is replaced by pq to designate the particular acoustic mode.

The natural modes of vibration depend on the end conditions and for the purposes of analysis, the structural mode shapes are taken to be those for a pipe with simply supported ends, so that

$$\psi_{mn}(\underline{r}) = \sin \frac{m\pi x}{\ell} \begin{Bmatrix} \sin ny/a_m \\ \cos ny/a_m \end{Bmatrix}, \quad [2.11]$$

where y is a circumferential coordinate along the mean pipe surface, m is the integer number of half-waves in the length ℓ and n is the integer number of full-waves around the circumference.

Since, the cross-spectral density and the mode shapes can each be expressed as the product of a function of ξ only and a function of η only, the joint acceptance can be expressed as

$$j_{mnmn}^2(\omega) = j_{mm}^2(\omega) \cdot j_{nn}^2(\omega), \quad [2.12]$$

where j_{mm}^2 and j_{nn}^2 depend on axial and circumferential parameters respectively. Equations [2.9], [2.10] and [2.11] give, for the joint acceptance of the (m,n)th structural mode excited by the (p,q)th acoustic mode,

$$j_{mm}^2(\omega) = \frac{2K_m^2 (1 - \cos \Lambda K_m \cos \Lambda K_x)}{\Lambda^2 (K_m^2 - K_x^2)^2}, \quad [2.13]$$

$$\text{and } j_{nn}^2(\omega) = \begin{cases} \frac{1}{4} & \text{for } n = p \\ 0 & \text{for } n \neq p \end{cases}, \quad [2.14]$$

where $\Lambda = \ell/a_m$. The maximum value of $j_{mm}^2(\omega)$ occurs when $K_m = K_x$, except for very low m values ($m=1$ and $m=2$), and this maximum value is $\frac{1}{4}$.

The joint acceptance function in the axial direction ($j_{mm}^2(\omega)$), is illustrated in Figure 2.3 for several (integer) values of the mode order m . From these Figures, it can be seen that (j_{mm}^2) maximum occurs at $K_x = K_m$ for $m \geq 3$ and that the secondary peaks are at least 12 dB less than the primary peak for $m \geq 3$. All the Figures are plotted on separate diagrams, each with identical scales, to illustrate the preceding points.

2.5 COINCIDENCE AND ITS EFFECTS ON THE PIPE WALL RESPONSE

Coincidence between a resonant structural mode and an internal acoustic mode, is the condition in which the circumferential distance along the pipe surface between diametral nodes of the (p,q) th acoustic mode is equal to half the wavelength of the (m,n) th structural mode in the same direction ($n=p$), and also in which the structural and acoustic wavenumber components in the axial direction are equal ($K_x = K_m$). In the ideal case, the coincidence frequency would be the resonance frequency of the (m,n) th structural mode and this would then imply matching of phase velocities ($v/K_m = v/K_x$). These conditions could be simultaneously satisfied in the ideal case of an infinite pipe: then structural standing waves could occur only in the circumferential direction but K_m could vary continuously. This matching of wavenumbers and frequencies could be termed exact coincidence. However, for a finite pipe of length ℓ , only discrete (standing wave)

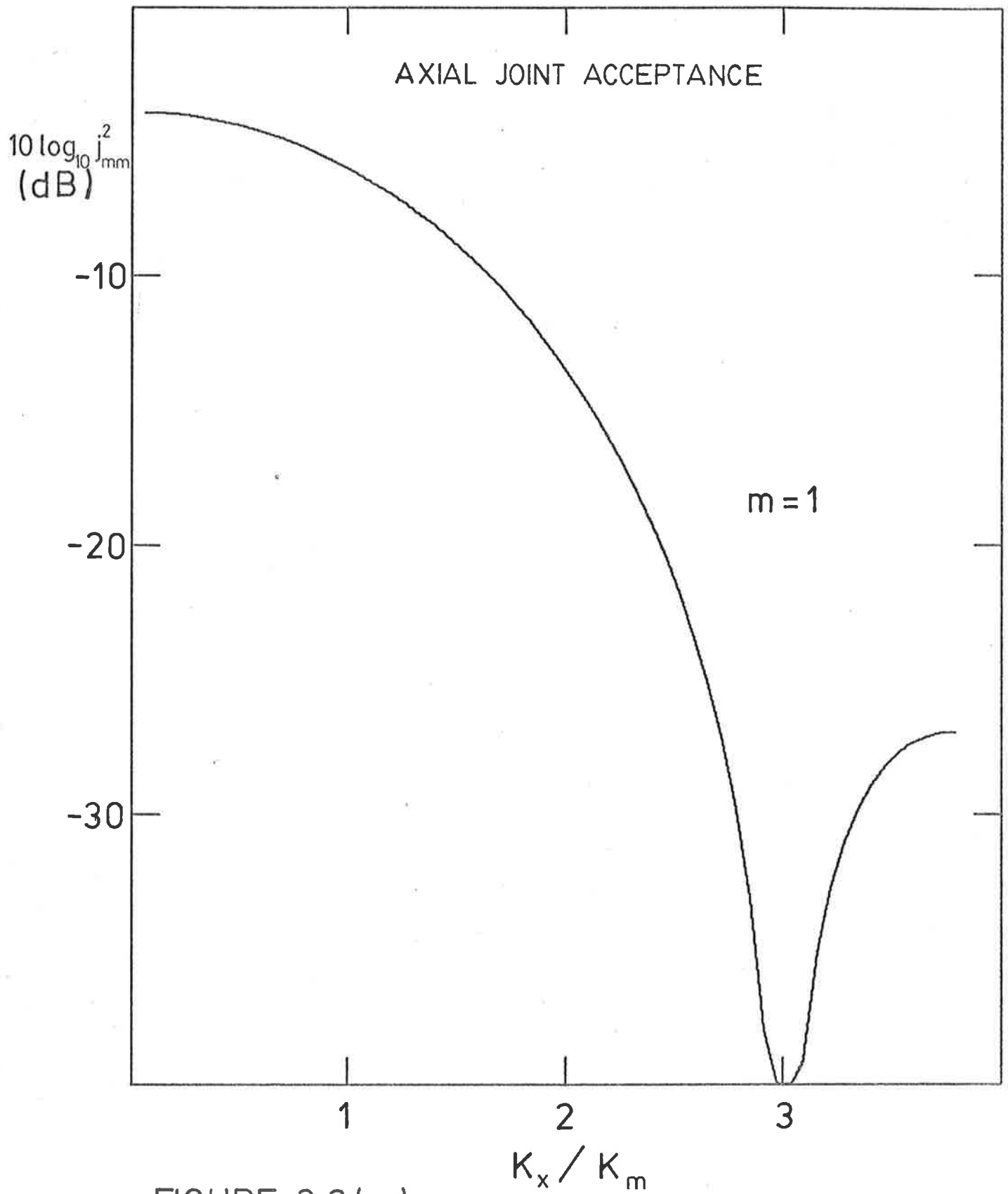


FIGURE 2.3(a)

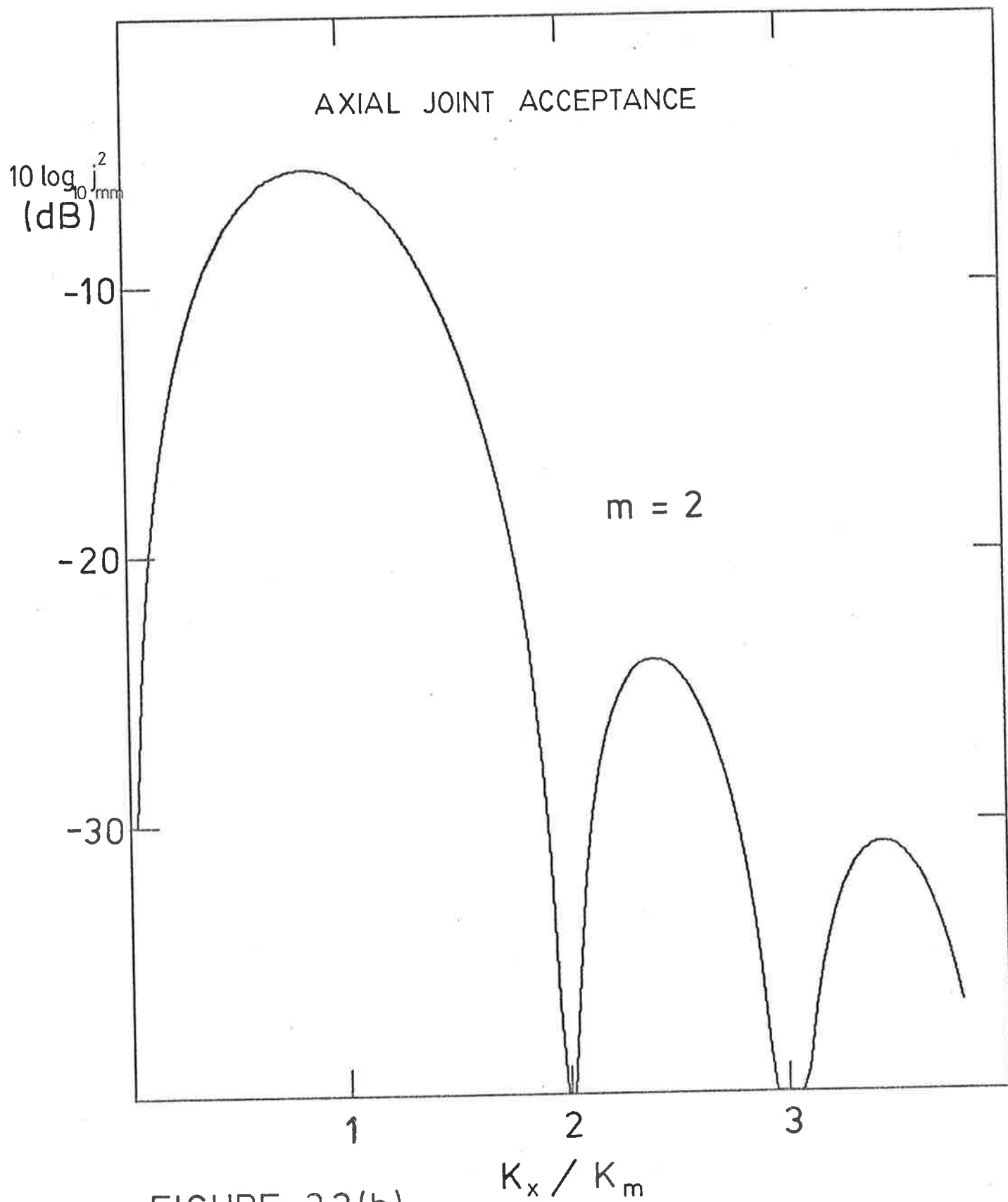
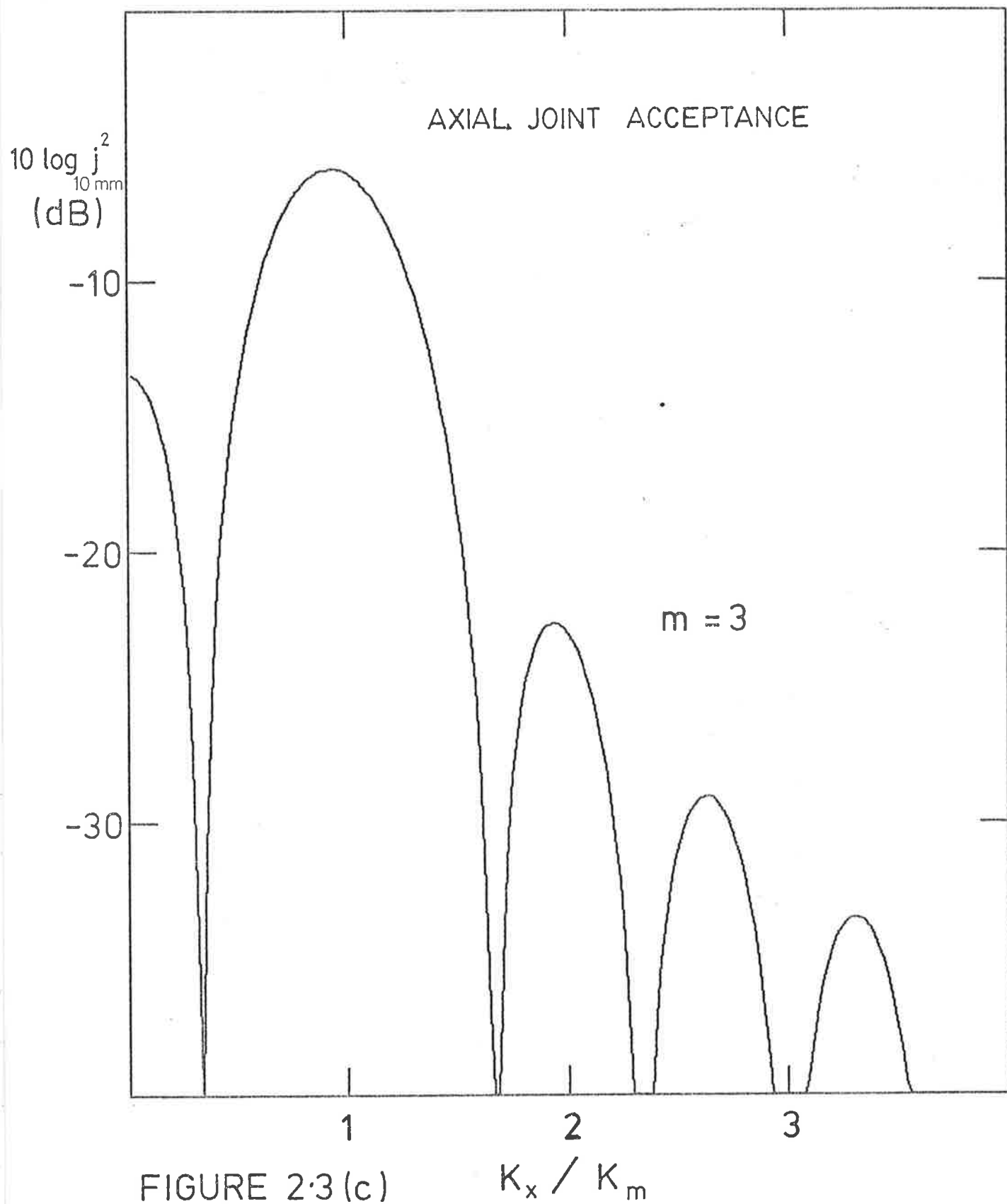


FIGURE 2.3(b)



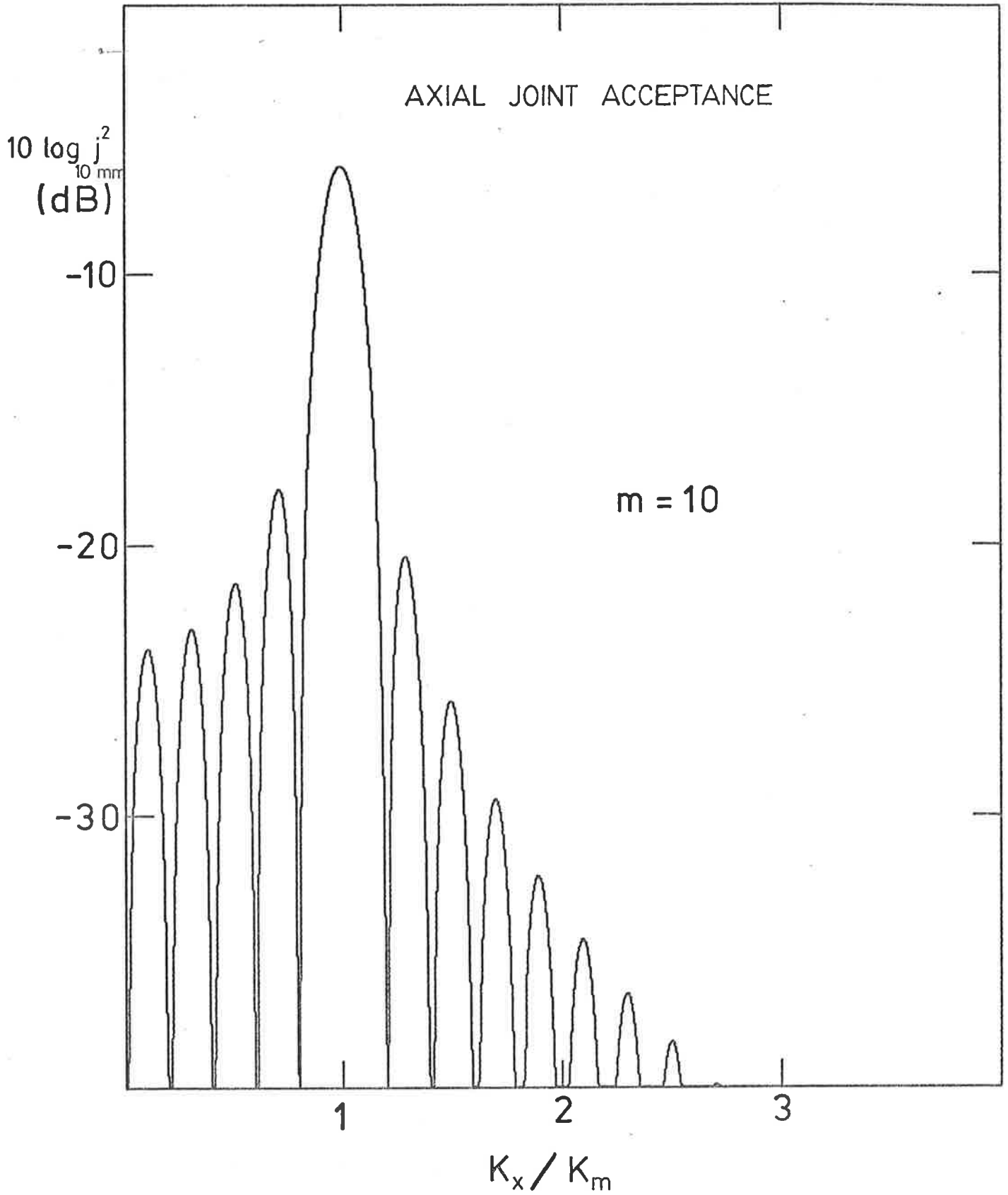


FIGURE 2.3(d)

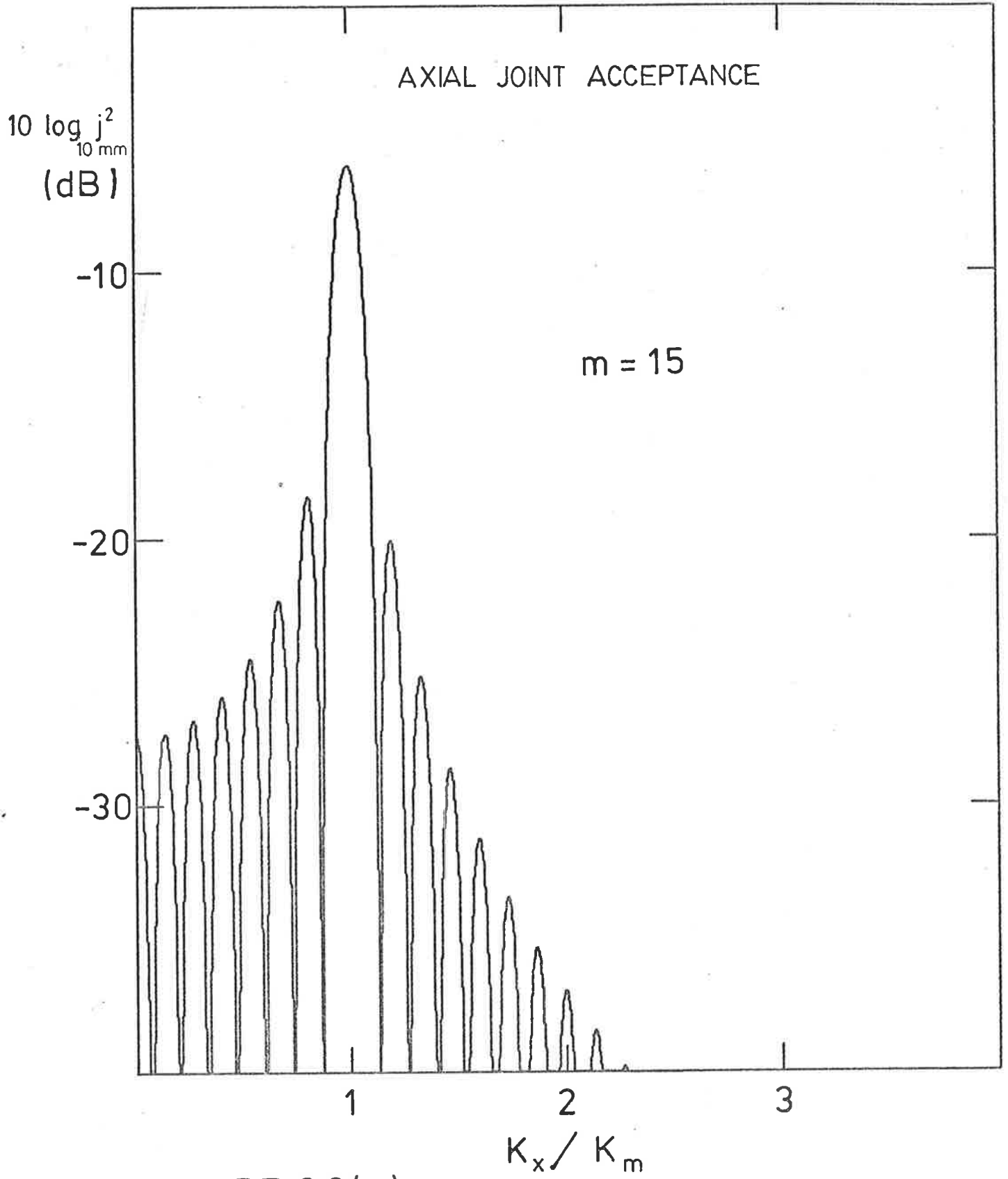


FIGURE 2.3(e)

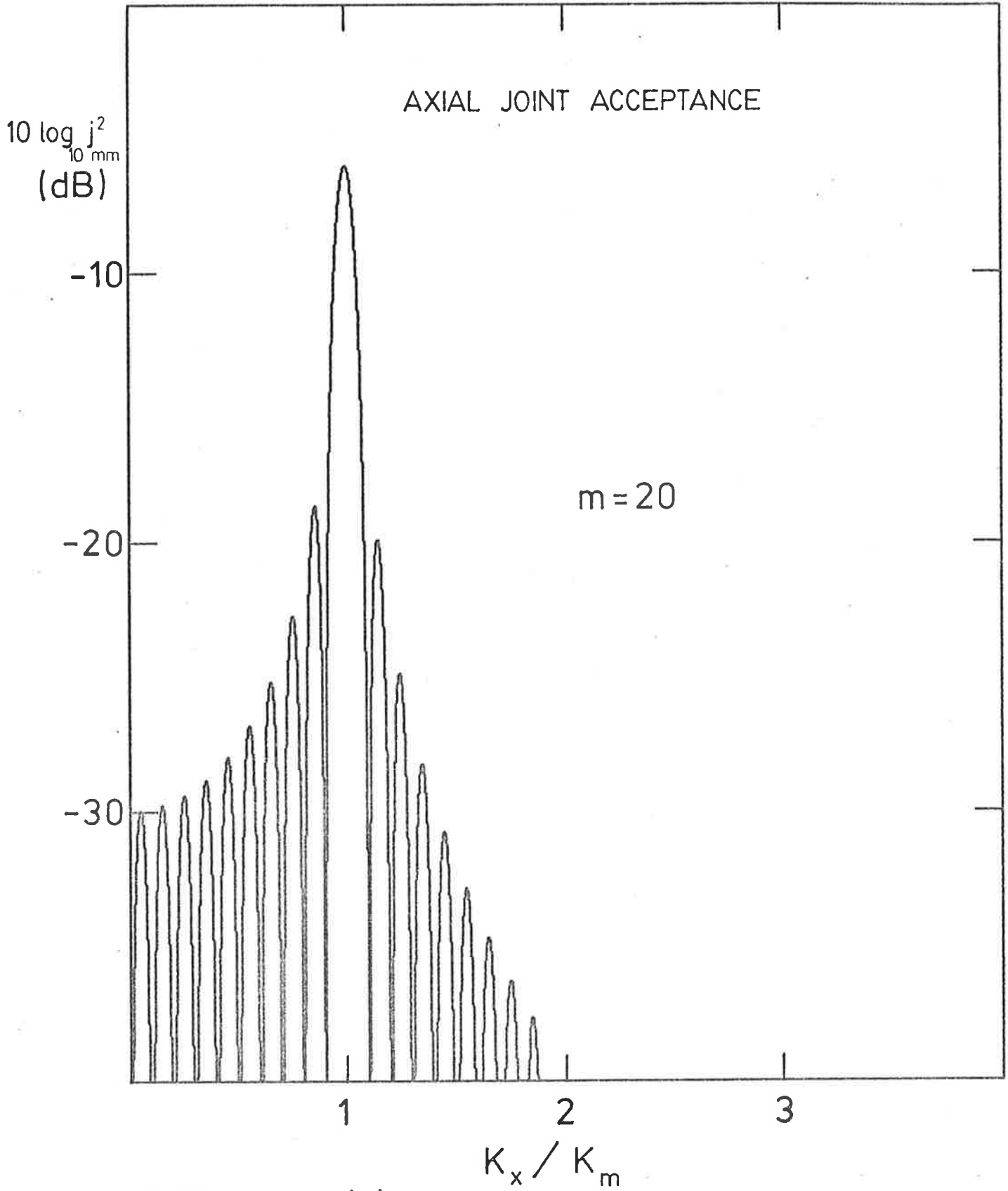


FIGURE 2.3 (f)

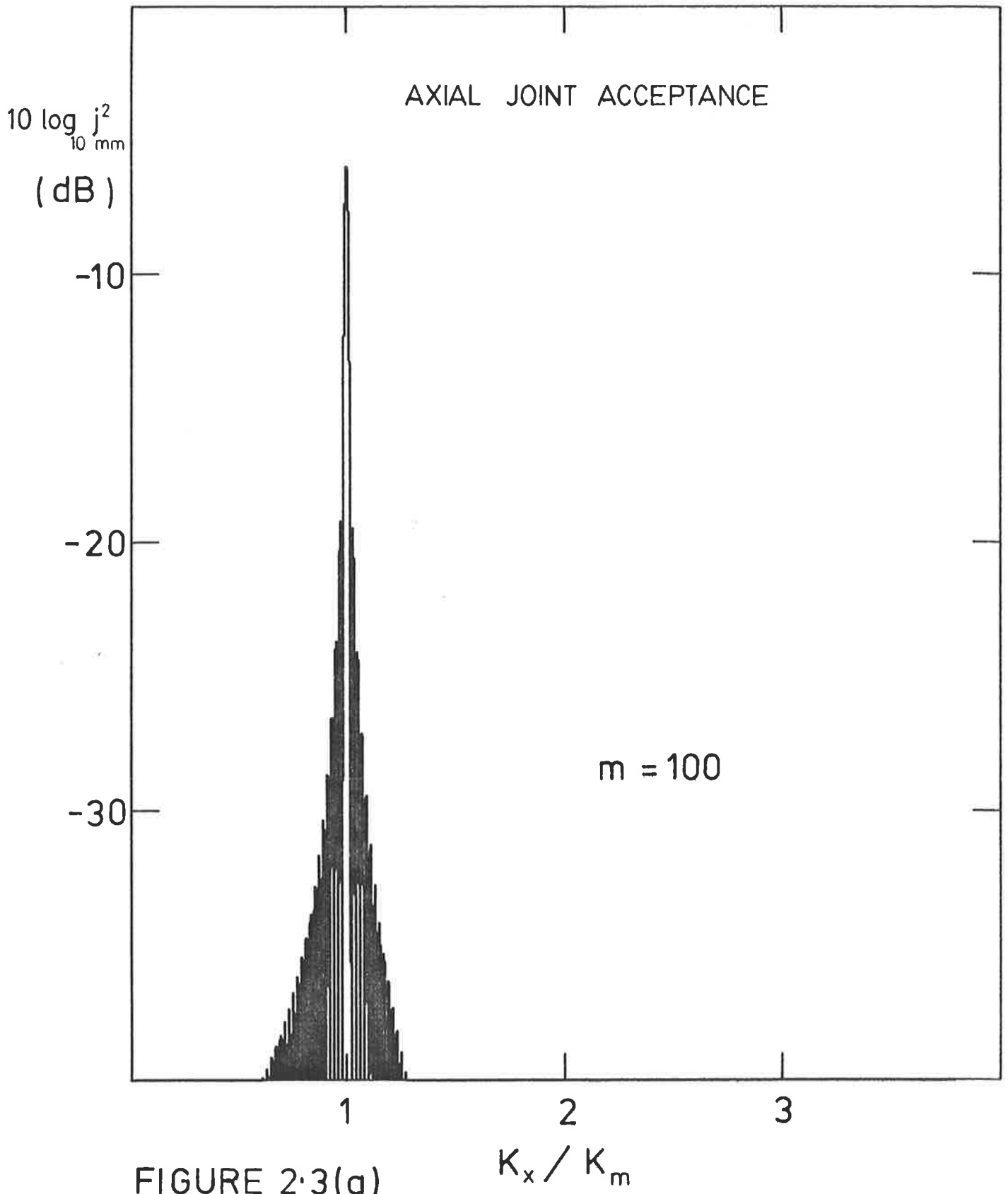


FIGURE 2·3(g)

values of K_m are possible, and in this case the two conditions cannot in general be simultaneously satisfied. In this case, the acoustic mode couples most efficiently to the structural mode(s) closest to exact coincidence. Thus, this matching of wavenumbers only might be termed wavenumber coincidence. Now only the spatial coincidence conditions can be exactly satisfied - that is circumferential matching and $K_x = K_m$. The joint acceptance function peaks sharply ($j_{mm}^2 = j_{nn}^2 = \frac{1}{4}$ and j_{mnmn}^2 has its maximum value of $[\frac{1}{4}]^2$) at the frequency for which the acoustic mode has a longitudinal wavenumber equal to the structural wavenumber of the resonant mode, and this frequency is now different from the structural resonance frequency. The receptance function however still has its maximum at the structural resonance frequency. In principle this implies two peaks close together in the response (see Figure 2.4,b), but in practice because the joint acceptance function varies very much more rapidly with frequency (even for metal pipes where damping is light) than the receptance function, the peak associated with the joint acceptance is dominant (see Figure 2.4,c). There is a narrow frequency band associated with the primary peak of the joint acceptance function, and secondary peaks are at least 12 dB less. The modal receptance is also at its maximum value (in the case of exact coincidence) or close to it (in the case of wavenumber coincidence only), but because of its less rapid variation with frequency the effects of coincidence are in general confined essentially to the narrow frequency band associated with the primary peak of the joint acceptance function. This situation is schematically illustrated in Figure 2.4. Because the effects of coincidence are confined to this narrow frequency band, a sharp peak in structural response to excitation by higher order acoustic modes is therefore to be expected. This is illustrated in considerable detail in Chapters 4 and 5 and, for metal pipes in particular

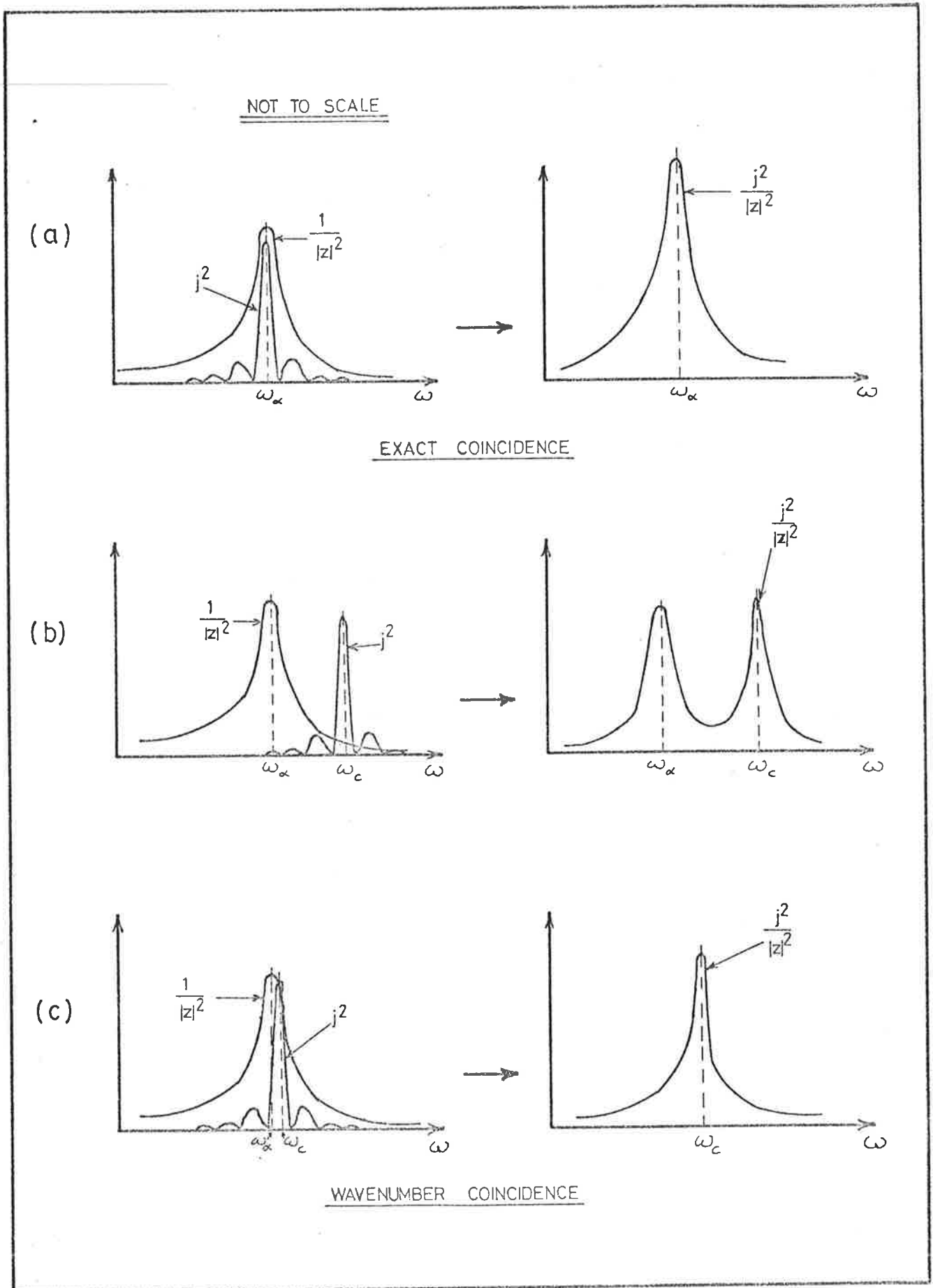


FIGURE 2.4 SCHEMATIC ILLUSTRATION OF COINCIDENCE

($M_{LP} \gg 1$), coincidence occurs very close to the cut-off frequencies of the higher order acoustic modes. Figures 2.5, 2.6 and 2.7 are plots of acoustic and structural axial wavenumbers against non-dimensional frequencies as given by equations 2.4 and 2.8, for several structural and acoustic modes. It should be pointed out that the acoustic modes presented are those for propagation in a stationary internal fluid in the pipe and that flow would reduce the cut-off frequency by a factor of $(1 - M_0^2)^{1/2}$ and hence shift the acoustic wavenumber plots to the left, in relation to the corresponding structural wavenumber plots.

The simultaneous solution of equation [2.4] and [2.8] (see Appendix A), with $v = v_{mn} = v_c$, $n = p$, and $K_x = K_m$, yields the exact coincidence frequency v_c and the corresponding value of K_m as in Bull and Norton (1977,a). If it is assumed that $c_i \approx c_e$, an approximate solution for low circumferential mode order n , and thin pipes, is

$$v_c \approx v_{co} + \frac{n^2}{2\psi M_{LP}^2}, \quad [2.15]$$

with
$$K_x = K_m \approx n \sqrt{v_{co}/\psi}. \quad [2.16]$$

Values calculated from the preceding approximations for several higher order modes propagating in a cylindrical pipe are presented in Appendix A and comparisons made with values obtained graphically from plots of equation [2.4] and [2.8].

Equation [2.15] is an approximation and the $n^2/2\psi M_{LP}^2$ term does not take into account the effects of β (pipe wall thickness) and the axial mode order m . An improved approximation of equation [2.15] was obtained by using Newton's method of successive approximations (Bull, 1978), and is

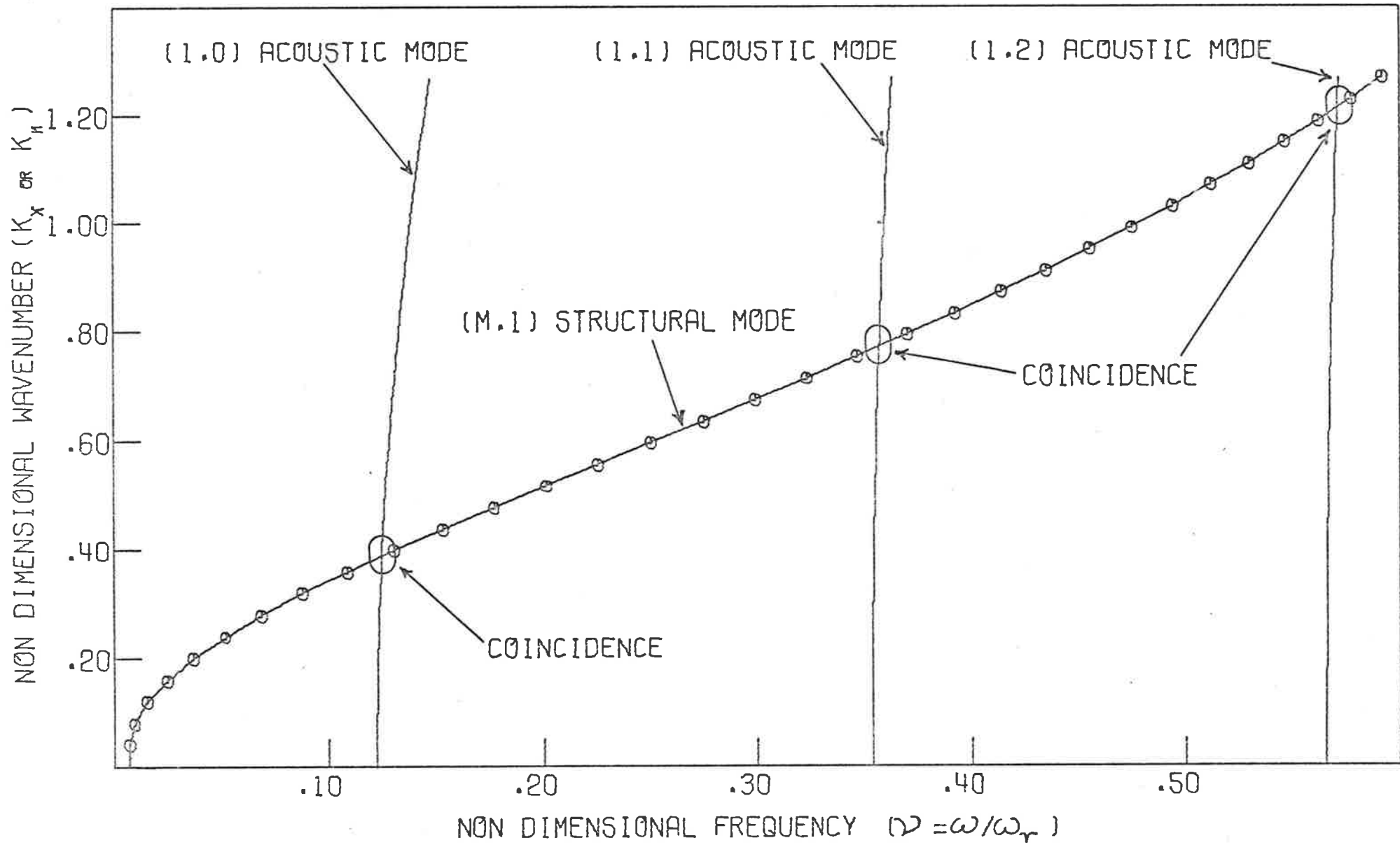


FIGURE 2.5 COINCIDENCE OF ACOUSTIC AND STRUCTURAL MODES.

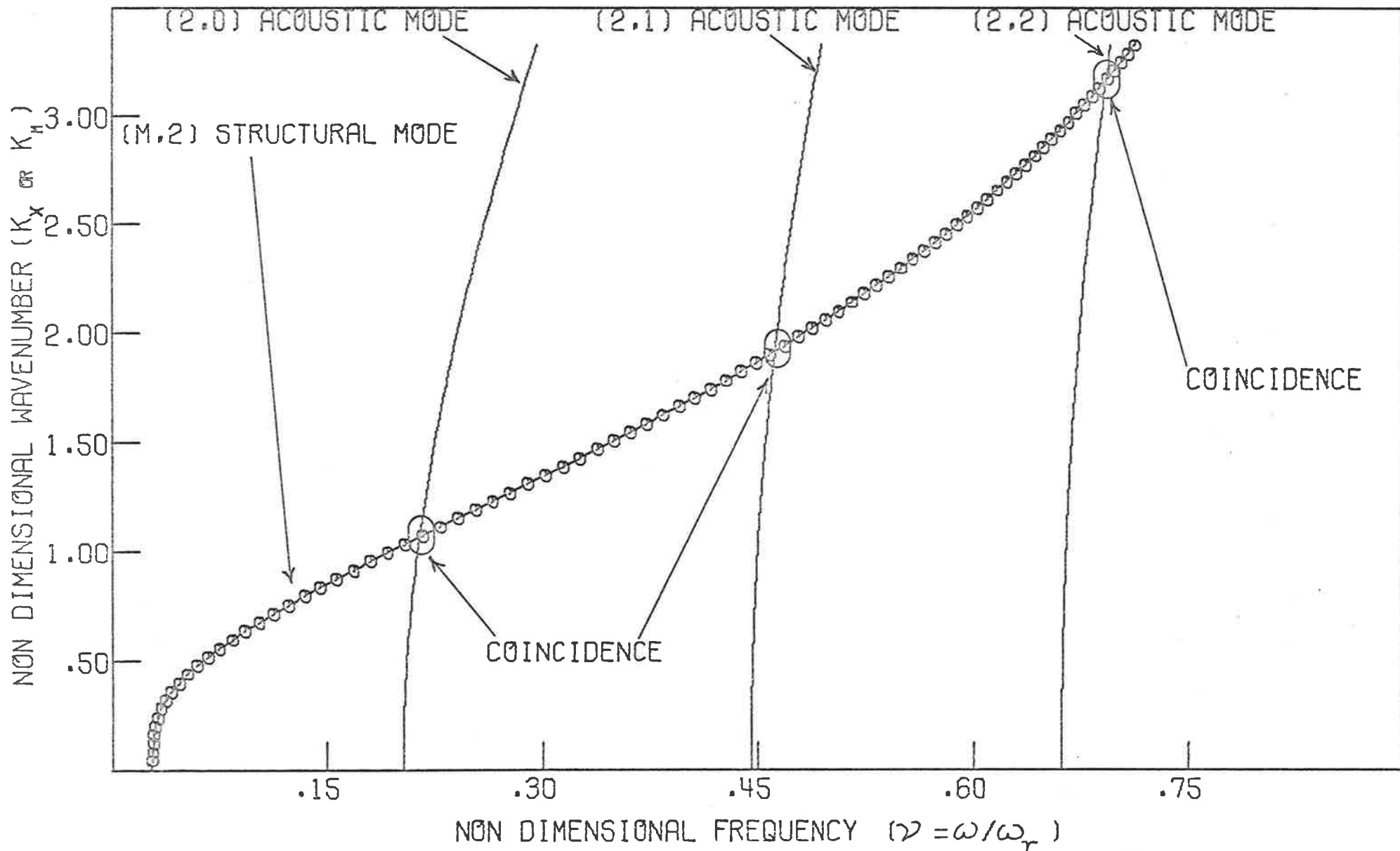


FIGURE 2.6 COINCIDENCE OF ACOUSTIC AND STRUCTURAL MODES.

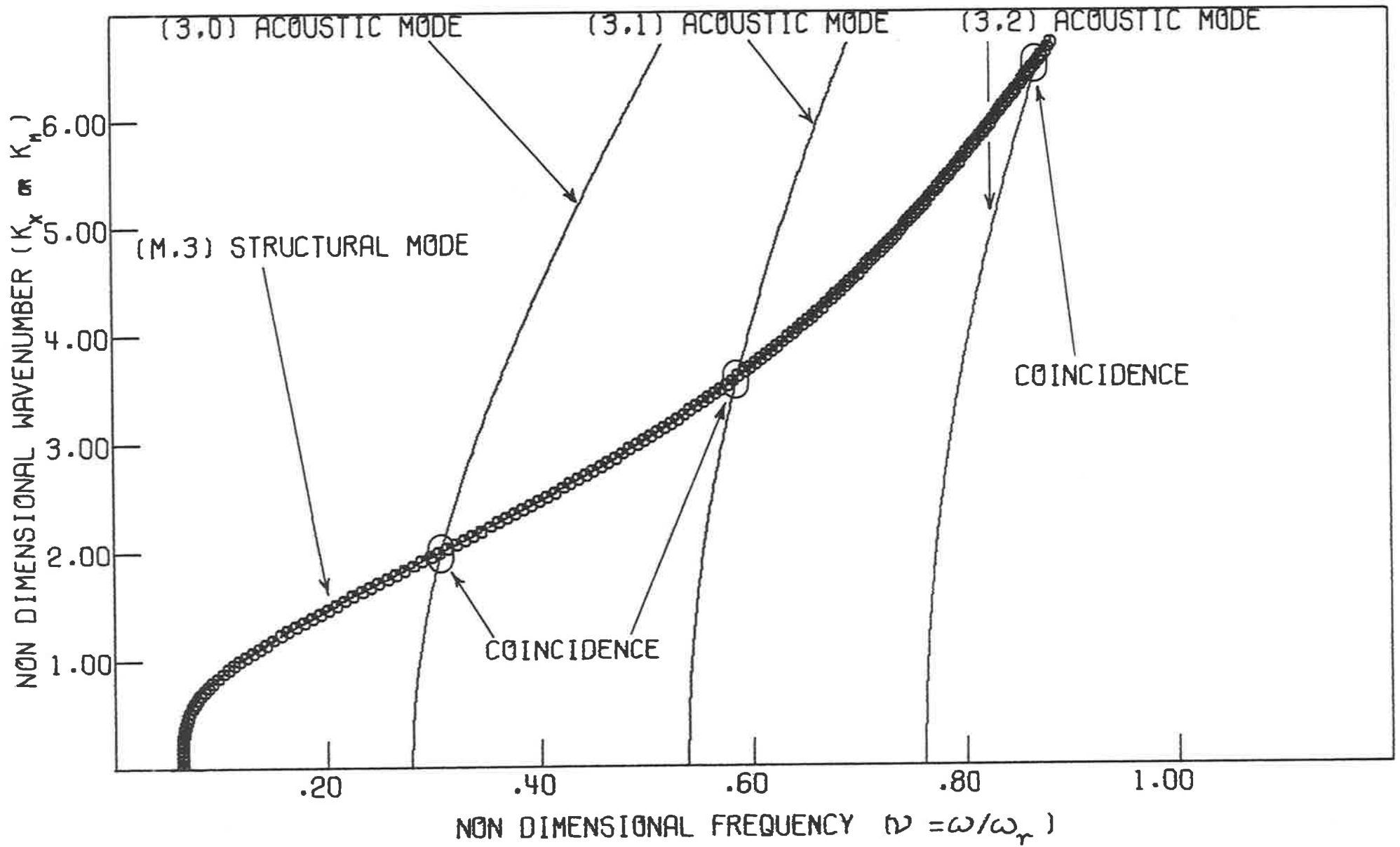


FIGURE 2.7 COINCIDENCE OF ACOUSTIC AND STRUCTURAL MODES.

$$v_c = v_{co} + \frac{1}{2}\Delta v_1 (1 + [1 + \bar{v}_{co}]^3 [\Delta v_1 / v_{co}]) ([1 - \bar{v}_{co}] + [1 + \bar{v}_{co}]^3 - [\beta^2 n^4 / v_{co}^2] [1 + \bar{v}_{co}]^5) \quad , \quad [2.17]$$

where $\Delta v_1 = n^2 / 2\psi M_{LP}^2$ and $\bar{v}_{co} = v_{co} / \psi$. Numerical comparisons between equation [2.15] and [2.17] for several higher order modes are presented in Appendix A. For metal pipes, $M_{LP} \gg 1$, and equations [2.15] and [2.17] then indicate that for low order modes in such pipes the exact coincidence frequency is very close to (typically within a few percent of) the cut-off frequency of the acoustic mode. This is borne out by the plots of the acoustic and structural resonance frequencies against axial wavenumber in Figures 2.5 to 2.7.

The calculation of the statistical properties of the vibration response of the pipe wall is based on the normal mode method of generalised harmonic analysis (Powell, 1958), and the total response of the pipe structure is represented by the sum of the responses in its resonant structural modes. The space-averaged spectral density of the non-dimensional acceleration response as derived by Bull and Rennison (1974,a) is

$$\frac{\Phi_{\zeta}(\omega)}{\Phi_p(\omega)} = \frac{\rho_{fs}^2 M_o^3 a_i}{12\beta^2 M_{LP}^3 a_m} \sum_{\alpha} \frac{j_{\alpha\alpha}^2(\omega)}{\left[1 - \left(\frac{\omega}{\omega_{\alpha}}\right)^2\right]^2 + \left[\frac{\omega}{\omega Q_{\alpha}}\right]^2} \quad , \quad [2.18]$$

where $\Phi_p(\omega)$ is the non-dimensional power spectral density of the wall pressure fluctuations, ρ_{fs} is the ratio of the fluid density to the density of the pipe material, α represents the α^{th} structural mode where $\alpha = (m,n)$ and Q_{α} is the overall modal quality factor. The general formalism for equation [2.18] and the corresponding equation for the non-dimensional spectral density of the acoustic power radiation is

presented in Appendix B.

Thus, by means of the phenomenon of coincidence, the higher order acoustic modes select and enhance the vibration of a number of resonant structural modes which in turn radiate most efficiently into the fluid outside the pipe. With a detailed understanding of the particular higher order modes that are excited by various types of internal flow disturbances and the degree to which they contribute to the overall excitation of the pipe wall, suitable approximations to the dynamic response (equation [2.18]) can be made and the pipe wall acceleration levels and consequently the acoustic power radiation levels can be estimated. This is dealt with in detail in several subsequent chapters.

2.6 SUMMARY

A brief theoretical introduction to the propagation of internal acoustic modes in a cylindrical pipe and their coupling to particular resonant structural vibration modes of the pipe has been presented in this chapter. The pipe wall response function is proportional to the product of the joint acceptance and the receptance (see equation [2.18]) and the behaviour of these functions is discussed. An approximate solution for the estimation of the coincidence frequency for thin pipes for the various higher order acoustic modes has been obtained. Some slight modification to this is necessary for the effect of flow which reduces the cut-off frequency by a factor of $(1 - M_0^2)^{\frac{1}{2}}$. For metal pipes, by equations [2.15] and [2.17], the coincidence frequency is very close to the cut-off frequency of the acoustic mode. Wavenumber diagrams have been presented to illustrate this phenomenon. The concepts presented in this chapter are the basis for theoretical estimates of the pipe wall vibration and acoustic power radiation which are discussed in subsequent chapters.

CHAPTER 3

DESCRIPTION OF THE EXPERIMENTAL FACILITIES

3.1 INTRODUCTION

In this chapter, the various internal flow disturbances investigated, the layout of the experimental flow facility and its performance, and the various measurement and data acquisition procedures used during the investigation are discussed.

The overall aim of the investigation was to obtain measurements of the vibration response of and the acoustic radiation from a cylindrical pipe, excited by both a fully-developed turbulent flow and a variety of internal flow disturbances. The high speed, intermittent, induced flow pipe facility used by Rennison (1976) was also used for the present investigation. The rig, originally designed for the study of acoustic radiation from a straight pipe carrying undisturbed fully-developed turbulent flow, is similar to a blow down wind tunnel. The rig has been modified by interposing a straight entry length and the pipe fitting to be investigated between the existing bell mouth inlet and the test section. The pipe fitting is located outside an anechoic chamber, while the radiation from the straight test section and its wall acceleration are measured in the anechoic chamber downstream of the pipe fitting.

In addition to the spectral measurements of the pipe wall response and the external acoustic radiation, extensive internal wall pressure fluctuation measurements were obtained for a wide range of flow speeds using piezo-electric crystal transducers. In the case of one of the internal flow disturbances (a 90° mitred bend) the wall pressure fluctuations were acquired digitally using a high speed data acquisition system. This was done to obtain the data simultaneously

at various axial positions along the test section in order to obtain longitudinal space-time cross-correlations of the wall pressure fluctuations.

The mean flow parameters were obtained from total pressure measurements inside the pipe (in a plane normal to the flow) and the corresponding static pressure measurements along the pipe wall. An automatic pitot probe traverse mechanism was used for the total pressure measurements.

3.2 DEVICES TESTED

Several internal flow disturbances were selected for the investigation for comparison with fully-developed turbulent pipe flow. The internal flow disturbances investigated were;

- (1) A 90° radiused bend with a radius ratio, R/a_m , of 6.4,
- (2) A 90° radiused bend with a radius ratio, R/a_m , of 3.0,
- (3) A 45° mitred bend,
- (4) A 90° mitred bend,
- (5) A gate valve,
- (6) A butterfly valve.

In addition some results are presented for;

- (7) A 55 mm diameter orifice plate,
- (8) A 65 mm diameter orifice plate.

Of the orifice plate results some were obtained by the author in conjunction with Hyland (1979), while others are those obtained by Hyland (1979). Hyland was specifically concerned with an experimental investigation of the noise generation due to orifices in pipework with flow. His work was initiated by, and is an experimental extension of, preliminary results obtained by Bull and Norton (1976, 1977a, 1977b) and was carried out in parallel with later stages of the present investigation.

The initial intention was to use commercially produced cold

drawn bends of various radii, but those obtainable were not of suitable quality for a laboratory investigation. Hence a procedure for fabricating them from moulded epoxy resin was developed. A toroidal wooden mould was made up and layers of the epoxy resin (mixed with fibreglass to strengthen it) were coated on. The radiused bend was then cut out of the finished product. Two sets of 90° radiused bends with ratios of bend radius to mean pipe radius R/a_m of 6.4 and 3.0 were made. Techniques were also developed for producing accurate mitred bends: two lengths of steel pipe selected for uniformity of internal bore were mitred in special jigs and then joined either by welding or by clamping. A 90° mitred bend and a 45° mitred bend were made using the welding technique. An additional instrumented 90° mitred bend was made using the clamping technique and this will be discussed later in this chapter. Figures 3.1 and 3.2 show the 90° welded mitred bend and the fabricated $R/a_m = 6.4, 90^\circ$ radiused bend that were used.

Two commercial 3 inch valves, namely a gate valve and a butterfly valve were purchased. As the piping used in the experimental work was of non-standard dimensions (72.54 mm I.D. or 2.856 in I.D.), it was necessary to design tapered mating pieces for each of the valves to match the experimental pipe work. The overall lengths for each valve plus its mating pieces were made to be the same for interchangeability. The gate valve obtained, had flanged ends and the bore had to be machined to match the mating pieces. The butterfly valve did not require any machining of the bore. Both valves were sandwiched between adjacent flanges of the mating pieces. The nominal valve dimensions are illustrated in Figure 3.3. The mating pieces were constructed from a hollow steel bar of 60 mm I.D. and 100 mm O.D., cut to the required length. Standard 3 inch drop-forged steel flanges were welded on at the ends and the whole assembly was machined down to



FIGURE 3.1 INLET PIPING AND 90° MITRED BEND

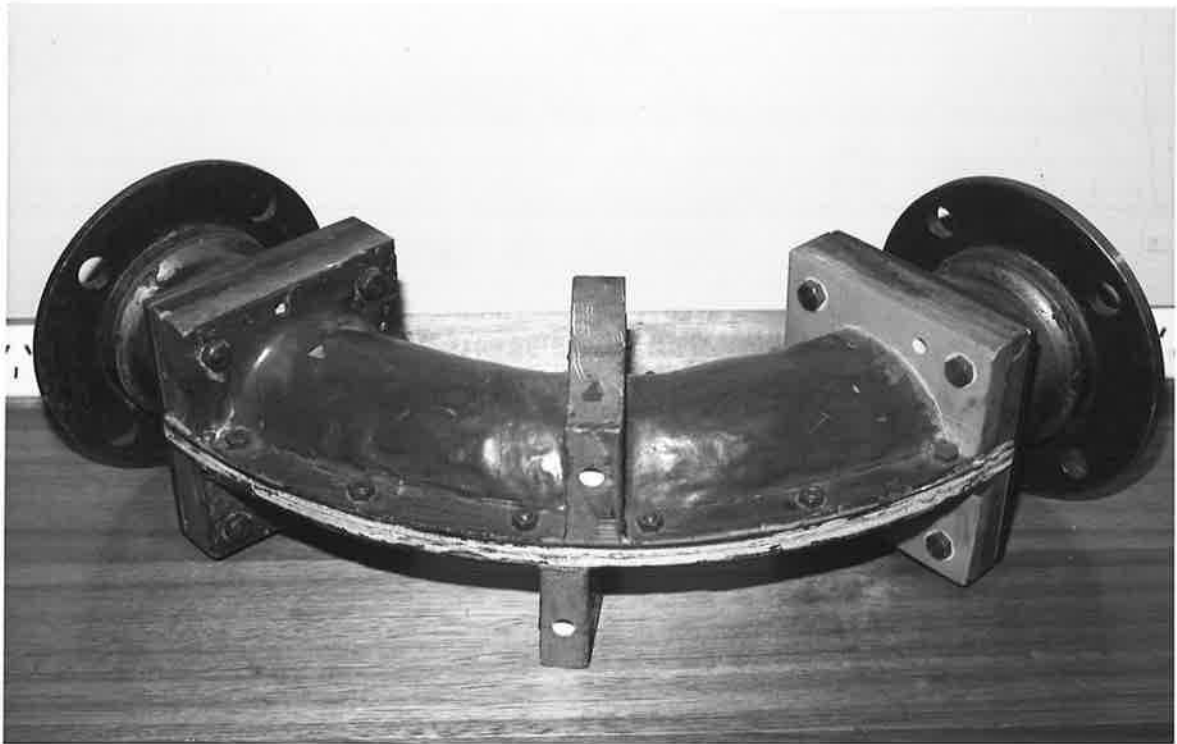
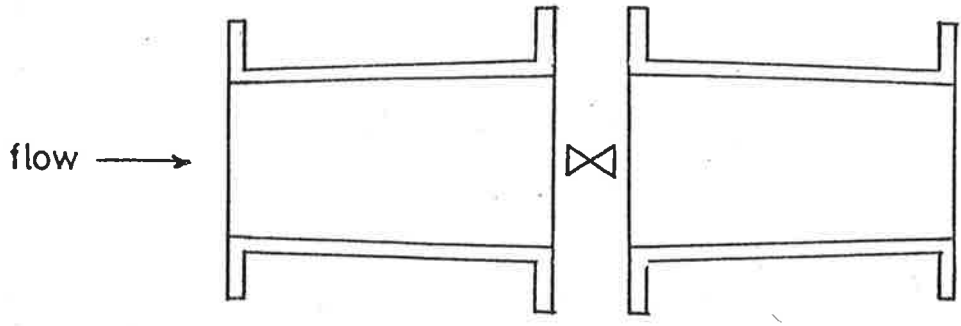
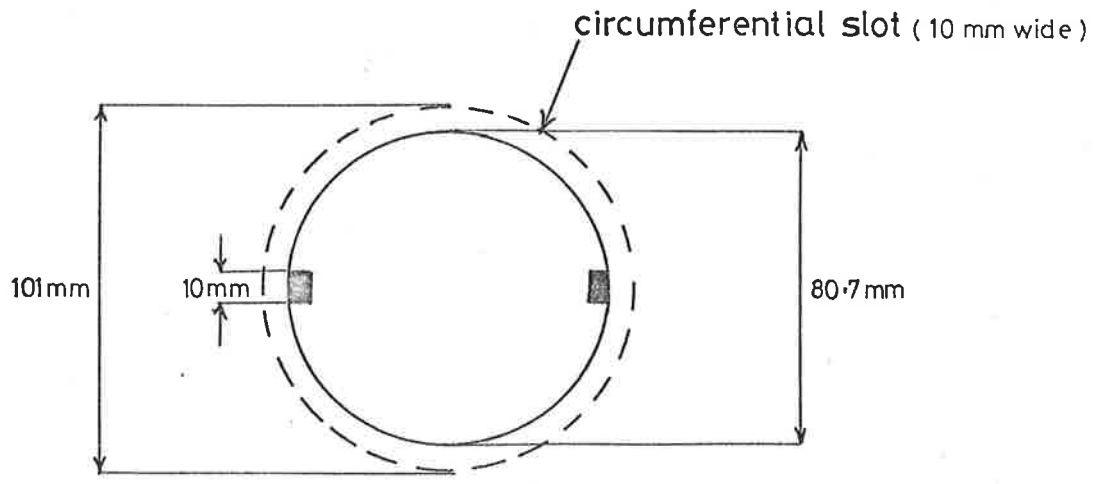


FIGURE 3.2 RADIUSED BEND ($R/a_m = 6.4$)

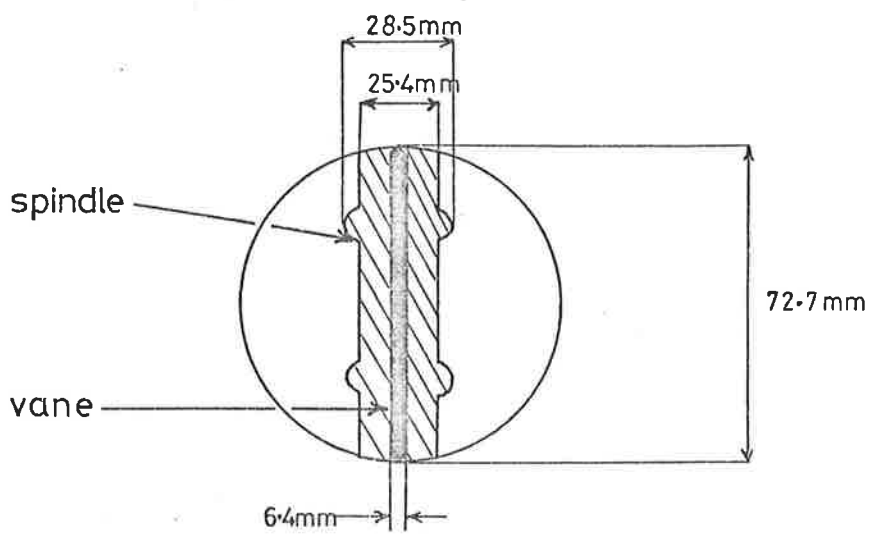


Mating piece arrangement for gate and butterfly valves



Gate valve fully open
(cross section)

NOT TO SCALE



Butterfly valve fully open
(cross section)

FIGURE 3-3 NOMINAL VALVE DIMENSIONS

specified dimensions. O-rings were mounted in grooves on the flanges to seal the joints. The two valves tested are shown in Figures 3.4 and 3.5.

The two orifice plates investigated in conjunction with Hyland (1979), have radius ratios (orifice radius to internal pipe radius) of 0.76 and 0.90 respectively. The orifice plates are 7 mm thick and are chamfered around the outlet side leaving only a thin edge, while the inlet face of the plate remained flat with a 90° corner at the edge of the hole (in accordance with British Standard Specifications). Additional relevant experimental results for the orifice plates, obtained by Hyland (1979), are presented in Appendix C, for comparison in later chapters with the results obtained for the various other pipe fittings used in this investigation.

3.3 EXPERIMENTAL FLOW FACILITY

The general arrangement of the experimental apparatus, the coordinate system used, and the details of the various pipe fitting are illustrated in Figure 3.6. X is a non-dimensional streamwise coordinate, expressed in terms of the pipe diameter, with its origin at the geometrical centre of the pipe fitting producing the flow disturbance; it is therefore negative at locations upstream of the fitting and positive downstream. All pipe sections have been made from cold-drawn steel tubing. The internal diameter is 72.54 mm throughout and the wall thickness is 6.35 mm, with the exception of the thin-walled test section, which has a wall thickness of 0.89 mm.

All mating pipe sections are flanged and located by spigots. At all joints the pipe bores are accurately matched, so that no extraneous disturbances due to discontinuities in the pipe are introduced.

Upstream of the flow disturbance there is an inlet bellmouth (extending over $-59.2 \leq X \leq -49.2$) and a straight section of pipe about 45 diameters long, (beginning at $X = -49.2$); downstream of the



FIGURE 3.4 GATE VALVE



FIGURE 3.5 BUTTERFLY VALVE

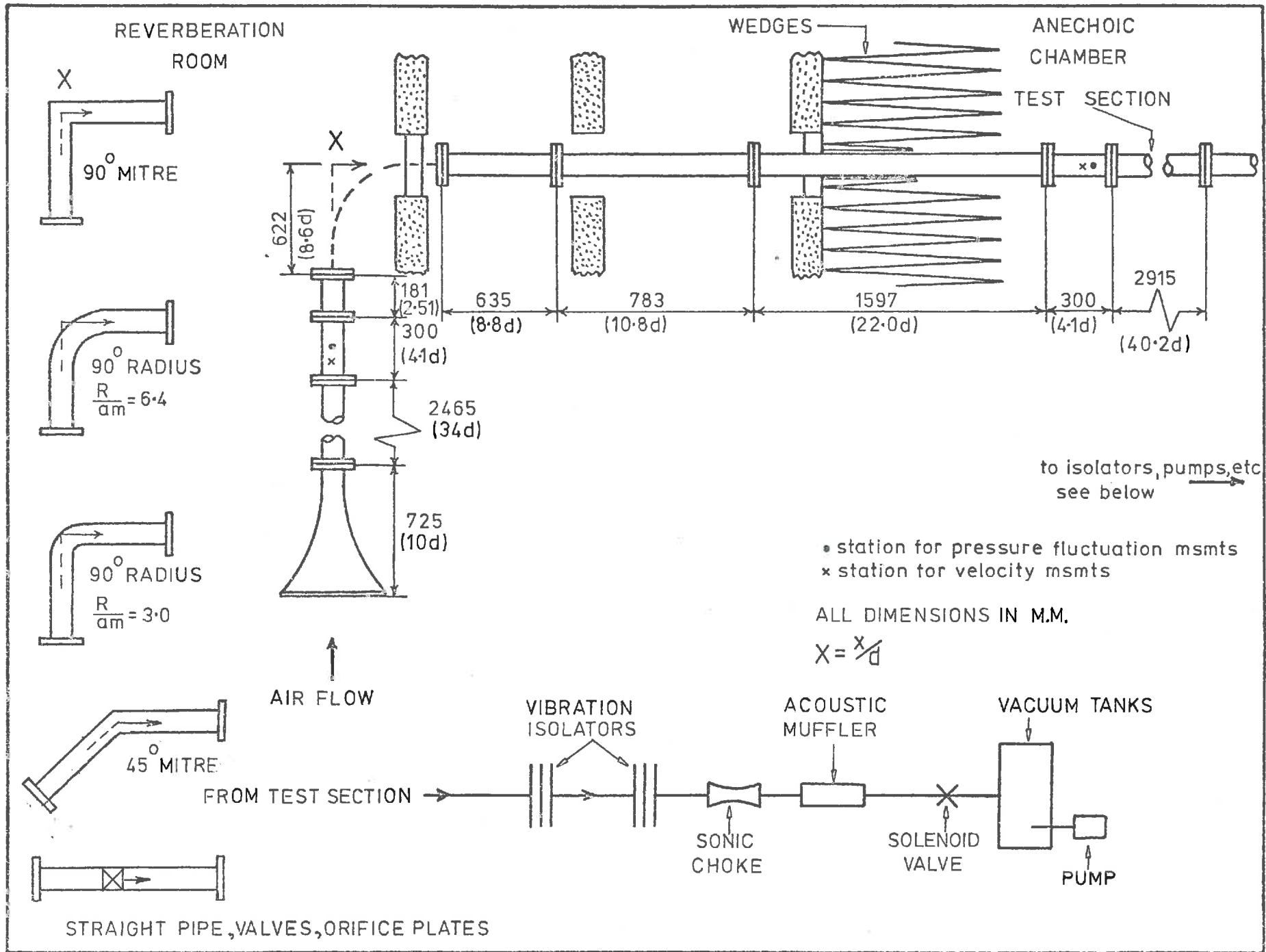


FIG 3.6 DETAILS OF TEST RIG AND VARIOUS PIPE FITTINGS

bend there is a further length of straight pipe, extending to the start of the test section at $X = 54.3$. The test section is 40.2 diameters long ($54.3 \leq X \leq 94.5$). The downstream end of the test section is connected through two mechanical filters, a sonic choke, an acoustic filter, and a remotely controlled quick acting valve to two large air receivers which can be evacuated to a pressure of about 15 kPa. This arrangement effectively isolates the test section from both vibrational and acoustic disturbances occurring downstream of it when the flow is on.

When the quick-acting valve is opened, air flows from atmosphere through the piping system to the vacuum vessels. The mass-flow rate and flow velocity are controlled by the throat area of the sonic choke. A series of nozzles allows flows with centre-line velocities in the range 65 to 180 m/s, and corresponding running times ranging from about 15 to 5 seconds, to be obtained. Five nozzles are available; these give mean centreline flow Mach numbers of $M_0 \sim 0.22, 0.35, 0.40, 0.45$ and 0.50 , at $X = 52.4$. The precise values depend on frictional effects in the piping system and vary slightly from one disturbance to another.

The pipe fitting and inlet piping are located in a reverberant chamber and the test section spans an anechoic chamber. An instrumentation section, in which measurements of mean flow velocity and wall pressure spectra can be made by means of pitot tubes and piezoelectric pressure transducers respectively, can be located at various points in the system. This is shown in Figure 3.7. Static pressure measurements are also obtainable from the instrumentation section. The section is rotatable, hence circumferential variations, in the various flow parameters monitored, can be detected at positions upstream, in the vicinity and downstream of the flow disturbances. As mentioned in section 3.2, a 90° mitred instrumented bend was made, in which

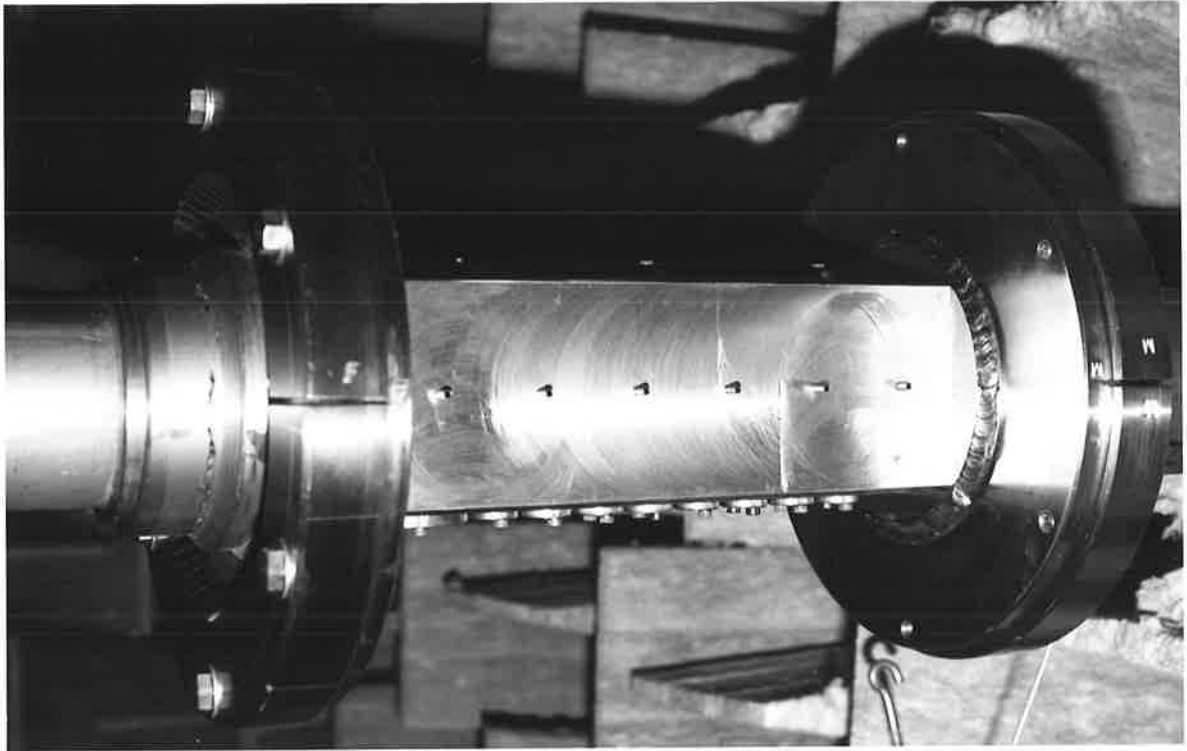


FIGURE 3.7 ROTATABLE INSTRUMENTATION SECTION

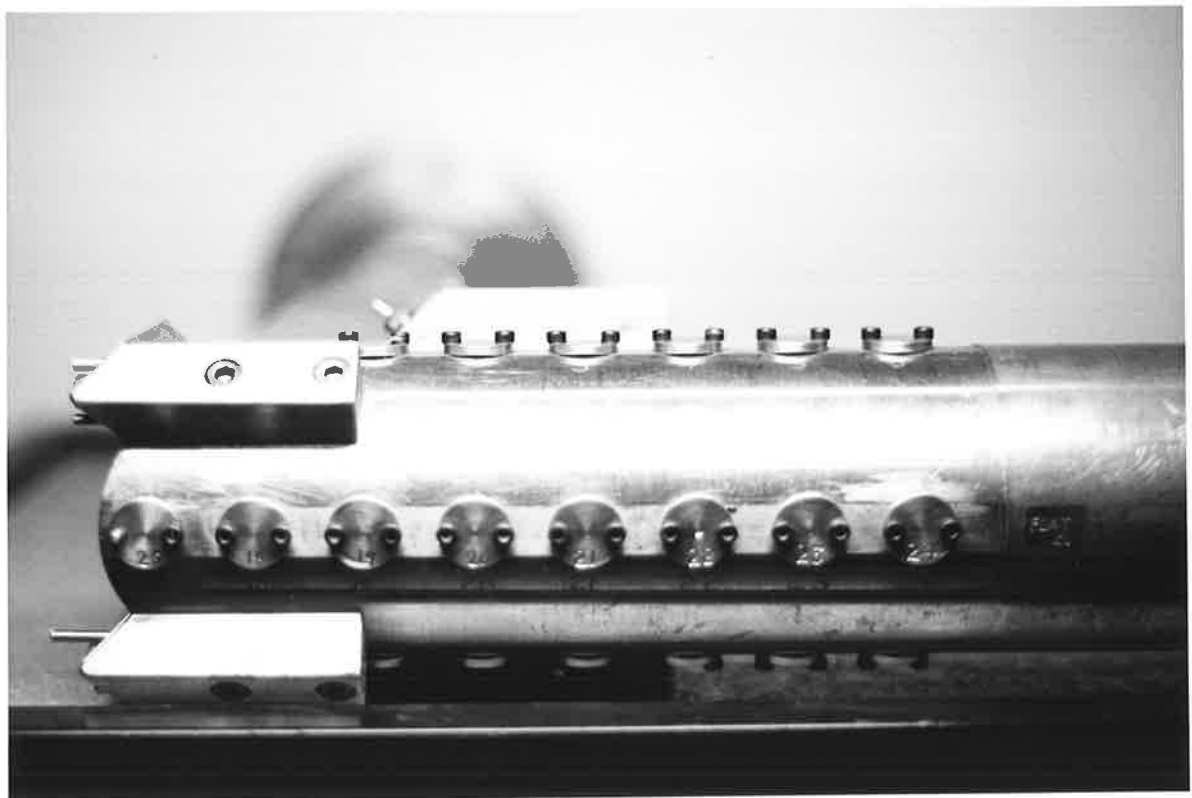


FIGURE 3.8 INSTRUMENTED 90° MITRED BEND

circumferential and axial variation of static pressure and wall pressure fluctuation measurements can be made immediately upstream or downstream of the bend. This is shown in Figure 3.8.

The induced flow rig flow control equipment is shown in Figure 3.9, and Figure 3.10 gives a close up view of one of the mechanical vibration isolators. The flow control equipment comprised two vibration isolators (only one is visible in Figure 3.9), the sonic choke, an acoustic filter and a remotely controlled quick acting valve. The acoustic filter comprises glass wool packing wrapped around a cylindrical perforated sheet metal liner inside a 150 mm diameter steel pipe. This filter attenuates flow noise downstream of the sonic choke. The vibration isolators act as low pass mechanical filters for vibrations generated downstream of the system and there are two of them in the system. Each isolator consists of a series of three steel plates (6.5 mm thick and 250 mm square) separated from each other and the flanges by soft rubber gaskets, 6 mm thick. The rubber gaskets are of the same internal diameter as the pipe and are cast from moulding rubber. The insertion loss of each vibration isolator is greater than 40 dB over the frequency range from 200 Hz to 20 kHz (Rennison, 1976). Thus the test section is effectively isolated from any mechanical or acoustic disturbances generated by the sonic choke or by the flow downstream of it.

As mentioned in Chapter 2, the vibration of the test section pipe wall can also be associated with the mechanical transmission of vibration excited by the pipe fittings in their own vicinity. Vibration isolation of the test section from the internal flow disturbance was considered unnecessary for this particular experimental set up, because of the impedance mismatch between the general pipework and the thin-walled test section. In addition, the instrumentation section (Figure 3.7) was positioned immediately upstream of the thin-walled test section

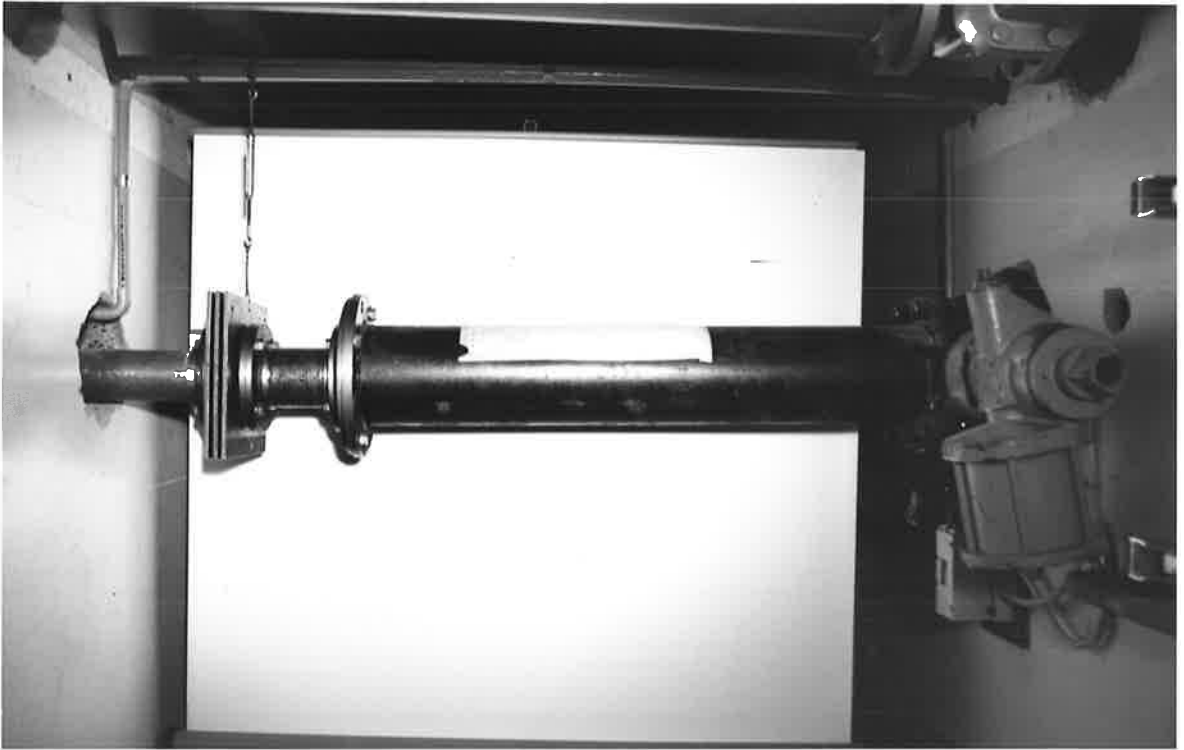


FIGURE 3-9 FLOW CONTROL EQUIPMENT

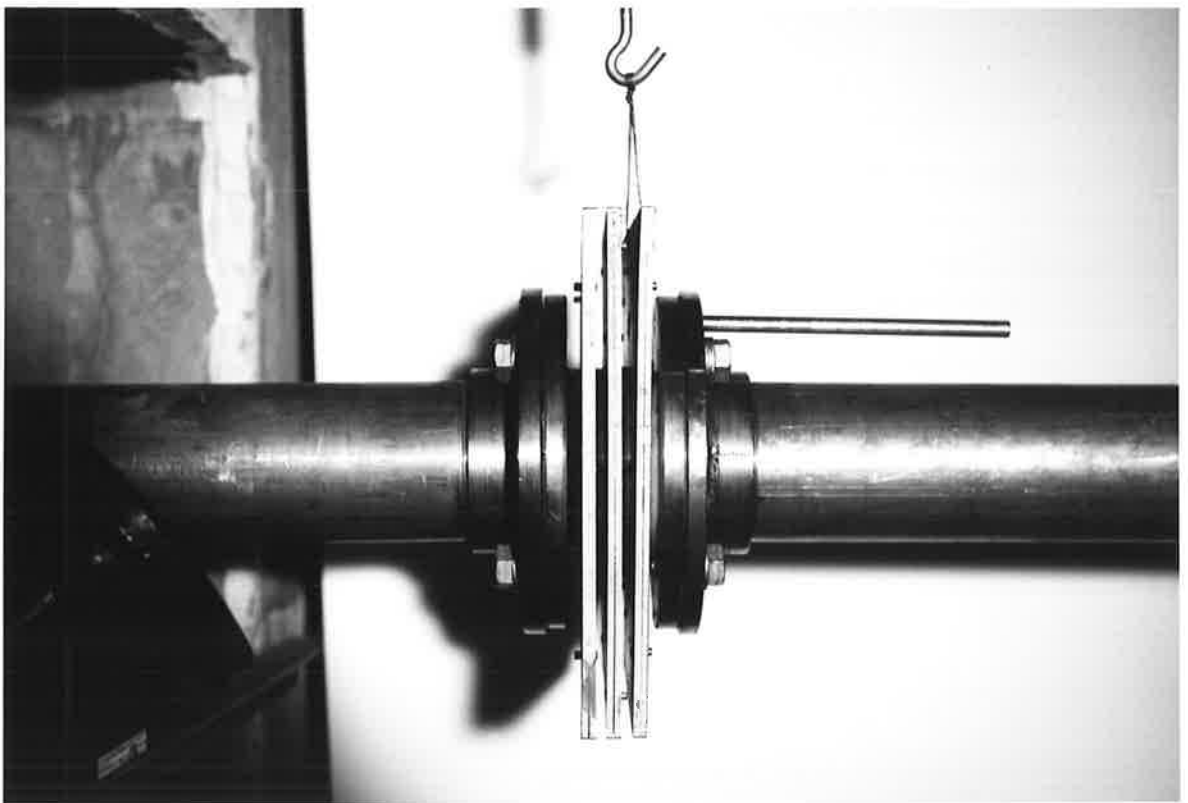


FIGURE 3-10 VIBRATION ISOLATOR

when acoustic radiation and pipe wall vibrational measurements were being obtained in the anechoic chamber. It represents a further impedance mismatch because of its substantial mass and wall thickness in comparison to both the piping and the test section (the instrumentation section was bored out of a solid cylindrical steel bar).

An experiment was performed with the 90° mitred bend to substantiate the above discussion. Acceleration measurements were made with the flow system rearranged so that the test section was located immediately downstream of the bend (by interchanging it with the pipe run which was previously between it and the bend). With the new arrangement the thin-walled test section was positioned at $5.1 \leq X \leq 45.3$, with the instrumentation section between the test section and the bend. A 90° mitred bend with a shortened arm after the bend was used, where the distance from the geometrical centre of the bend to the tip of the flange on the arm was $X = 1.0$. Pipe wall acceleration measurements were obtained at $X \approx 12.0$. At this axial position, the mean flow velocity profile was symmetrical but not fully-developed (see Figure 4.2). The wall pressure fluctuations were also circumferentially uniform, but were slightly higher than in a region further downstream where a fully-developed velocity profile had been re-established (see Figure 4.7). As will be seen in Chapter 4, at this axial position ($X \approx 12.0$), most of the effects of the local non-propagating disturbances had disappeared. Hence, any measurements of the pipe wall response would represent a total response due to (a) a propagating internal wall pressure field and (b) mechanical vibrations due to the bend. The results obtained for the pipe wall acceleration response at $X \approx 12.0$ are presented in Figure 3.11 for several flow speeds. Because of frictional effects in the pipe, the flow velocity is lower close to the bend than further downstream (by a maximum amount of about 14% at the highest flow speed). Bearing in

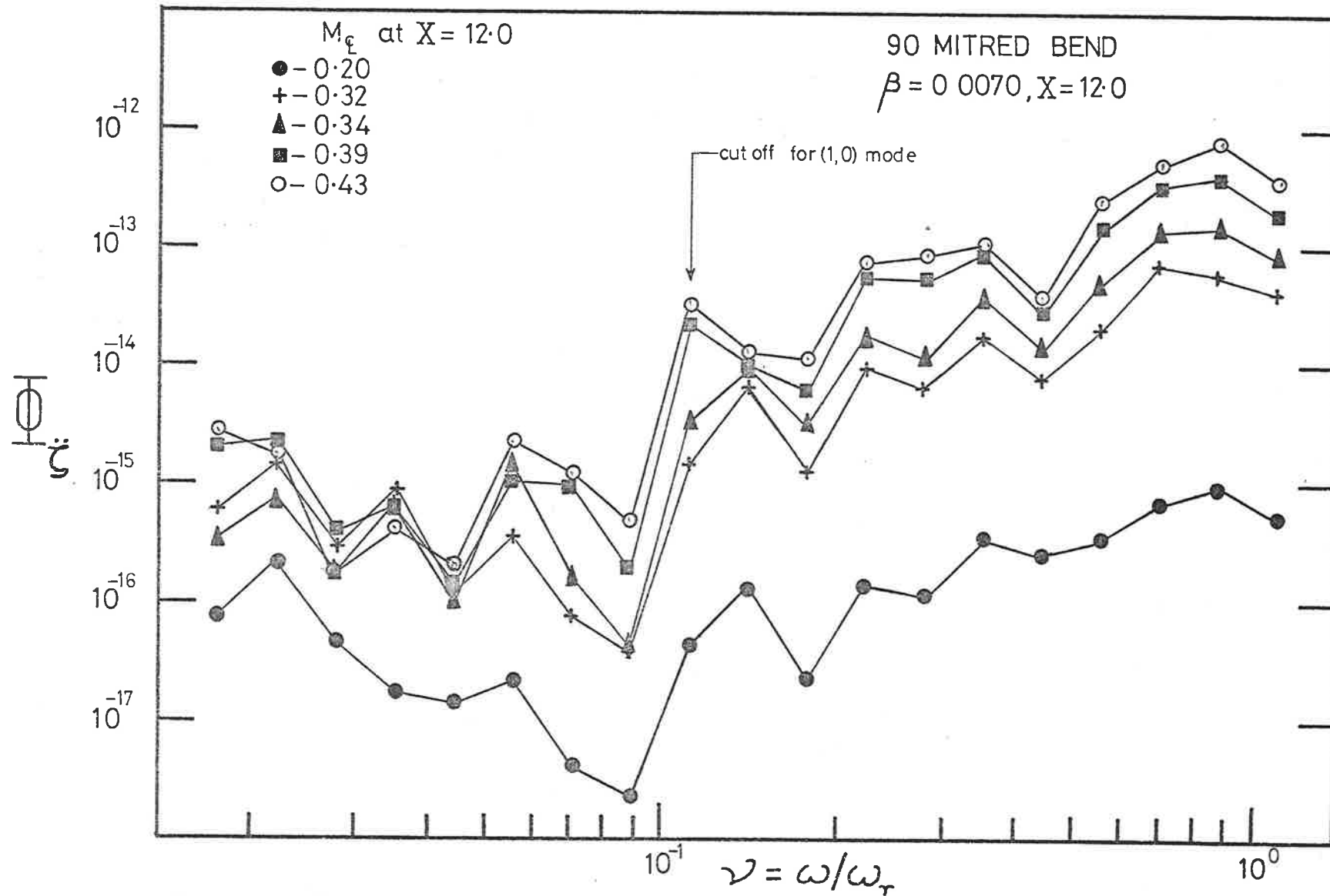


FIGURE 3.11 NON-DIMENSIONAL PIPE WALL ACCELERATION (at $X=12.0$)

mind that internal wall pressure fluctuation levels are higher than in the anechoic chamber ($X > 50.0$), the pipe wall acceleration levels in Figure 3.11 are comparable with those at $X = 74.4$ (mid-point of test section when in the anechoic chamber, Figure 4.36). More importantly, the general shape of the spectra are the same in both sets of results, indicating that the pipe wall is being excited by similar mechanisms in both cases. Any mechanical vibrations generated by the bend would decay with axial distance from the bend and in addition the character of the excitation would be changed due to the impedance mismatch that would occur at the several flanged joints. Hence, one would expect the character of the vibration response to be somewhat different at $X \approx 12.0$ and $X = 74.4$ if mechanical transmission were the dominant source of pipe wall vibration. Hence the conclusion that the test section is effectively isolated from any mechanical disturbances generated at the bend.

The thin-walled test section was 40.2 diameters long and spanned the anechoic chamber. It was drawn to the same internal diameter as the thick-walled pipe and the instrumentation section. A thick-walled pipe (6.35 mm) of approximately the same length was also used for comparison of acoustic radiation and pipe wall acceleration with corresponding data for the thin-walled test section, and this is discussed in Chapter 7. The details of the two experimental test section pipes are presented in Table 3.1 and, Figure 3.12 shows the thin-walled steel pipe in the flow rig inside the anechoic chamber. Figure 3.13 shows some of the instrumentation used in the experimental programme; this is discussed in detail in section 3.5.

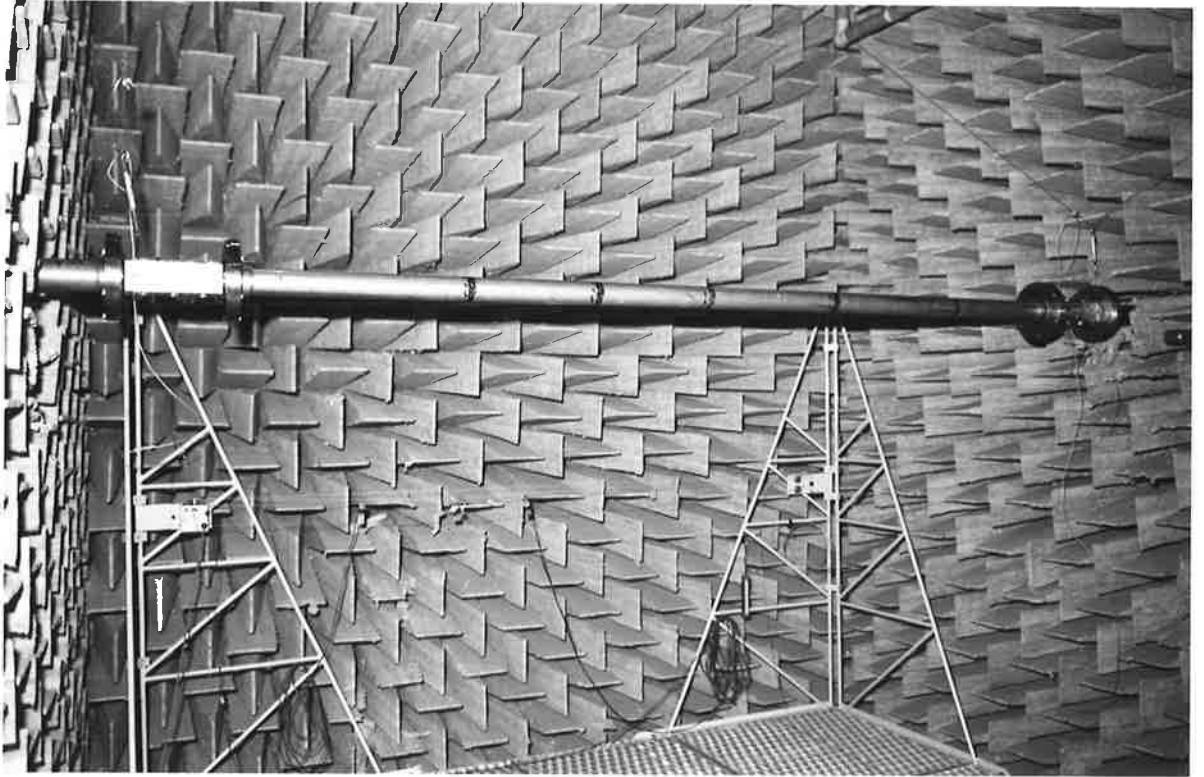


FIGURE 3-12 TEST PIPE IN ANECHOIC CHAMBER



FIGURE 3-13 INSTRUMENTATION

TABLE 3.1

DETAILS OF EXPERIMENTAL TEST SECTION PIPES

Test Pipe	"Thin-Walled"	"Thick-Walled"
Material	Cold drawn seamless steel	Cold drawn seamless steel
E (GPa)	196	196
μ	0.28	0.28
$\psi = (1 - \mu^2)^{\frac{1}{2}}$	0.960	0.960
ρ_s (Kg/m ³)	7800	7800
c_{LP} (m/s)	5222	5222
l (m)	2.92	2.99
a_i (mm)	36.27	36.27
a_e (mm)	37.16	42.62
a_m (mm)	36.72	39.45
h (mm)	0.89	6.35
β	0.0070	0.04648
Λ	79.4	75.7
f_r (kHz)	22.6	21.1
M_{LP}	15.3	15.3
v_{ac}	0.62	0.09

3.4 FLOW FACILITY PERFORMANCE

Mean velocity profiles have been obtained at all five flow speeds for each disturbance just upstream of the test section ($X = 52.4$). Additional measurements were obtained, in the case of the 90° mitred bend, at a measuring point upstream of the bend ($X = -12.9$). The measurements show in all cases, that there is a fully-developed turbulent flow at entry to the disturbance and that at entry to the test section an undisturbed fully-developed turbulent flow profile has been re-established.

The mean velocity profiles were obtained from total pressure measurements inside the pipe (in a plane normal to the pipe axis) and the corresponding static pressure measurements on the pipe wall. Total pressures were measured by means of a pitot probe mounted on a rig which automatically traverses the inside of the pipe at a constant speed. The nose of the pitot tube was flattened to an internal thickness of 0.50 mm and an external thickness of 1.00 mm; it projected 57 mm upstream of the probe support. A resistance potentiometer in the traverse rig produces a voltage proportional to the probe position. The rig is shown in Figure 3.14. Figure 3.15 shows the piezo-electric crystal transducers used which are discussed in the next section. The static pressure ports on the instrumentation section wall consist of 0.50 mm diameter holes, connected to brass tubing outlets. Both the static and total pressures were measured with an electronic manometer and a barocell.

The variations in circumferential static pressure were found to be negligible, implying axi-symmetric flow at both axial positions. The axial variations in static pressure are very small over the instrumentation section span (4.1 diameters) and there is an almost linear decrease in static pressure with distance in the flow direction. Static pressure measurements were always obtained without the pitot probe



FIGURE 3-14 PITOT PROBE TRAVERSE

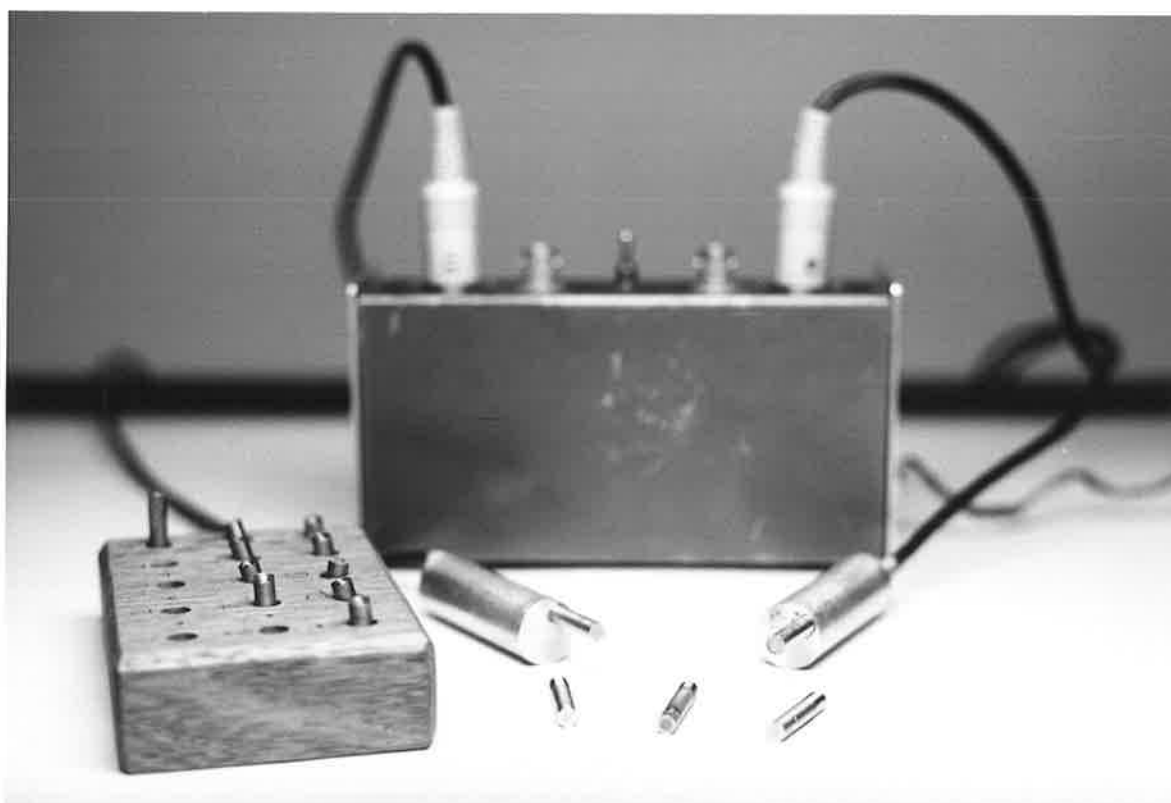


FIGURE 3-15 WALL PRESSURE TRANSDUCERS

immersed in the pipe. Standard compressible flow relations have been used to obtain the mean velocity profiles from the static and total pressure measurements.

The velocity profiles are presented in the universal form (the universal velocity distribution law for smooth pipes) in Figures 3.16 to 3.22. They compare well with the $1/7$ th power velocity distribution derived from Blasius's resistance formula, and the Universal velocity-distribution law for very large Reynolds numbers as presented by Schlichting (pp 560-592, 1968). Friction velocities have been calculated both from measurements of the pressure drop along the pipe and from the velocity profiles, using the Clauser (1954) method - good agreement is found. The results for both radiused bends were similar and so only those for the $R/a_m = 3.0$ are presented (Figure 3.19). From Figure 3.17, it can be seen that fully-developed turbulent pipe flow is established before the 90° mitred bend i.e. the entry length is sufficient to ensure fully-developed turbulent pipe flow at entry to the disturbance.

Hence the conclusion that there is essentially a fully-developed turbulent flow at entry to all the disturbances and at entry to the test section downstream of the disturbances. The mean centreline flow Mach numbers before the test section ($X = 52.4$) are presented in Table 3.2.

3.5 INSTRUMENTATION AND ITS CALIBRATION

In this section the various measurement and data acquisition techniques used during the investigation are described. For each flow disturbance, spectral measurements of (i) the fluctuating internal wall pressure field; (ii) the wall accelerations of the test section; and (iii) the acoustic power radiated from the test section, have been obtained in $1/3$ -octave bands and in 100 Hz constant bandwidth.

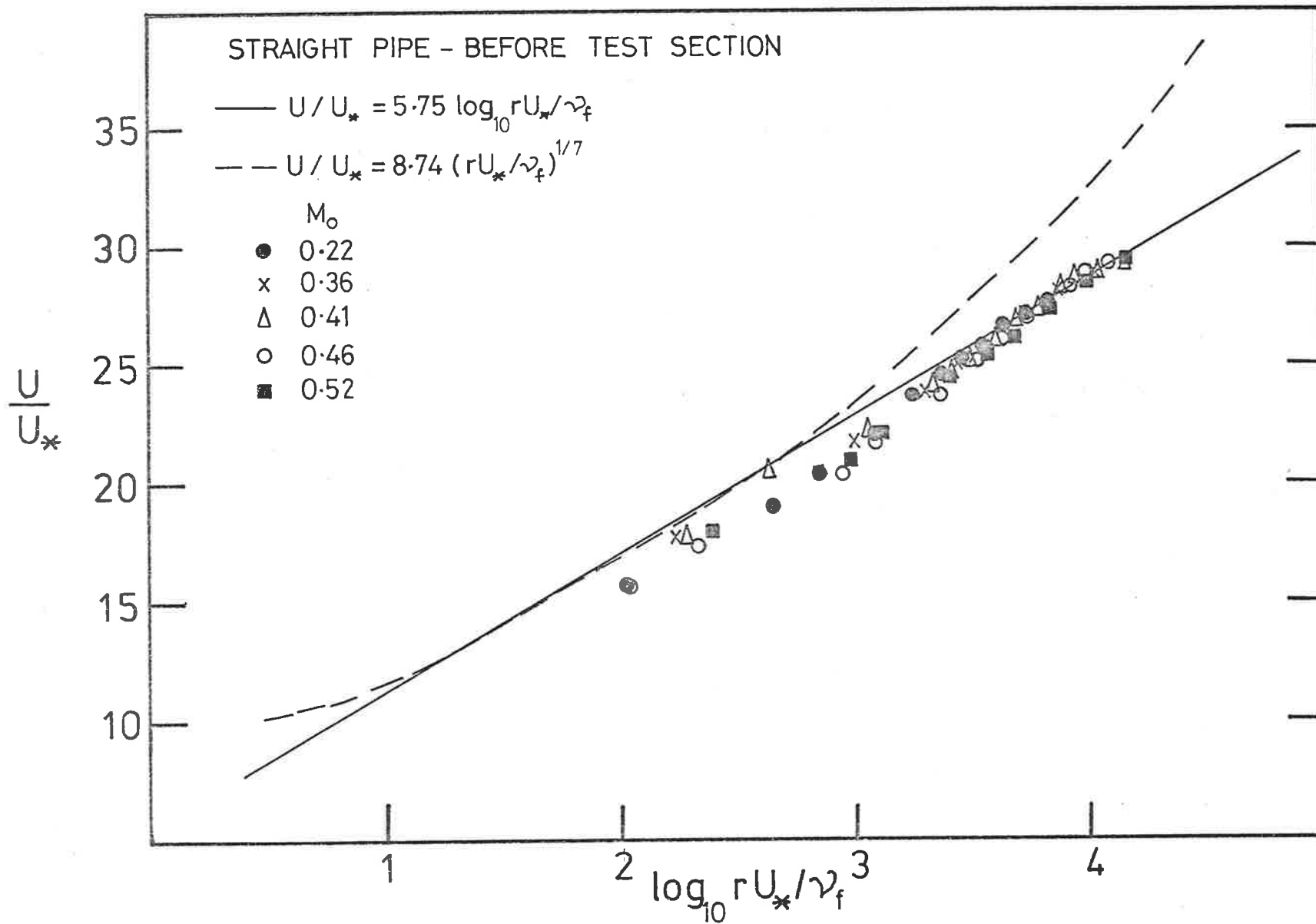


FIGURE 3.16 UNIVERSAL VELOCITY PROFILES

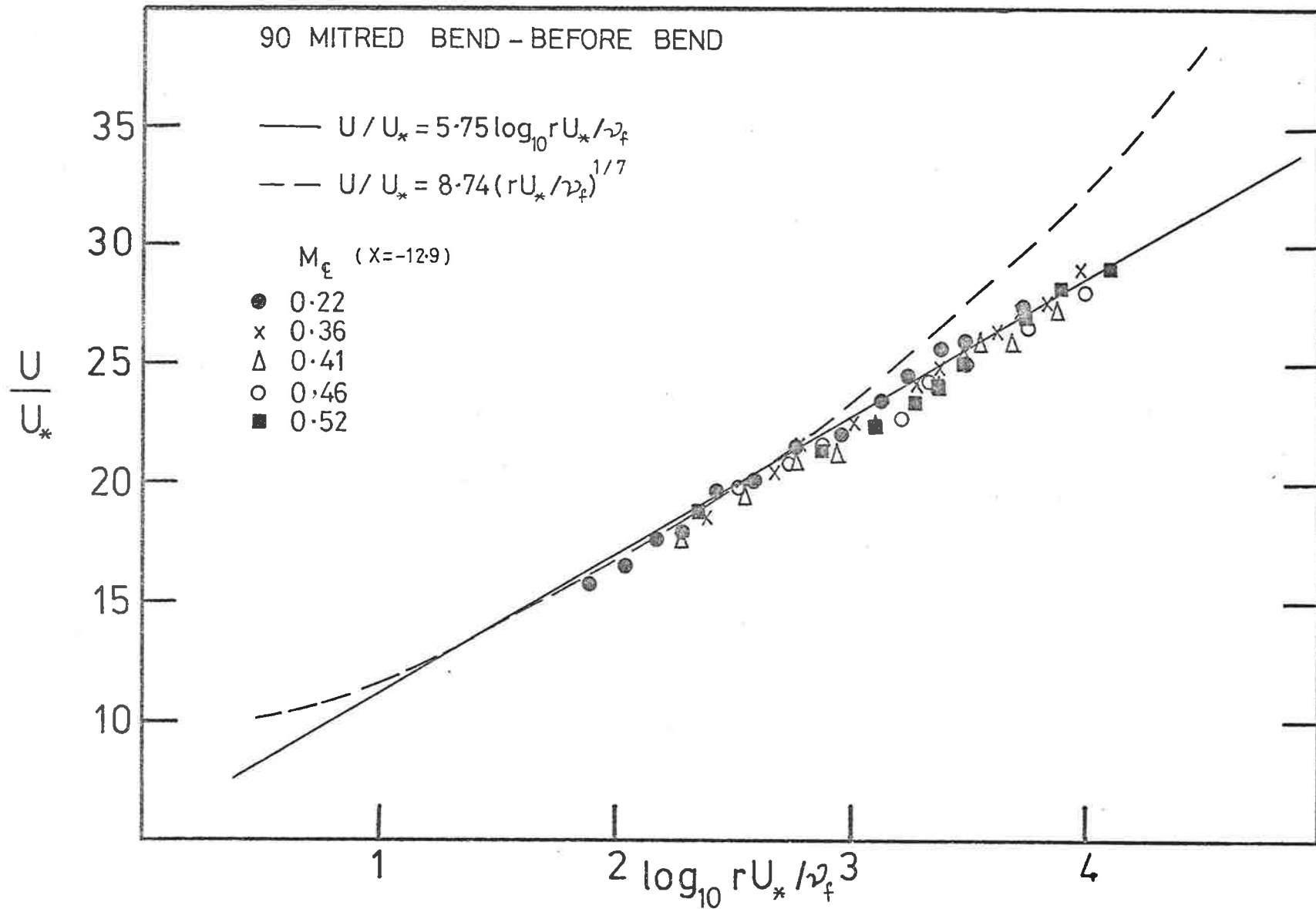


FIGURE 3.17 UNIVERSAL VELOCITY PROFILES

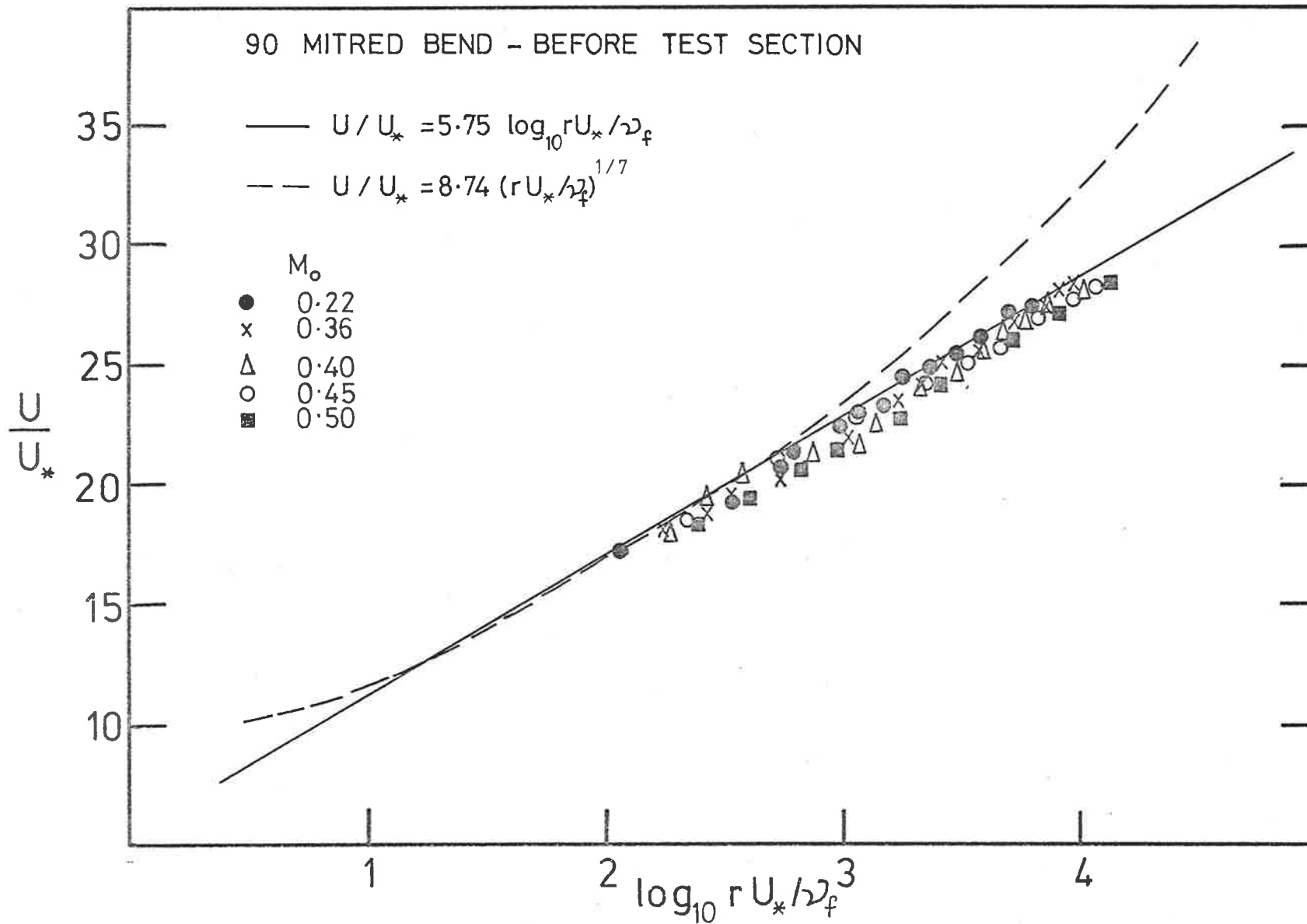


FIGURE 3-18 UNIVERSAL VELOCITY PROFILES

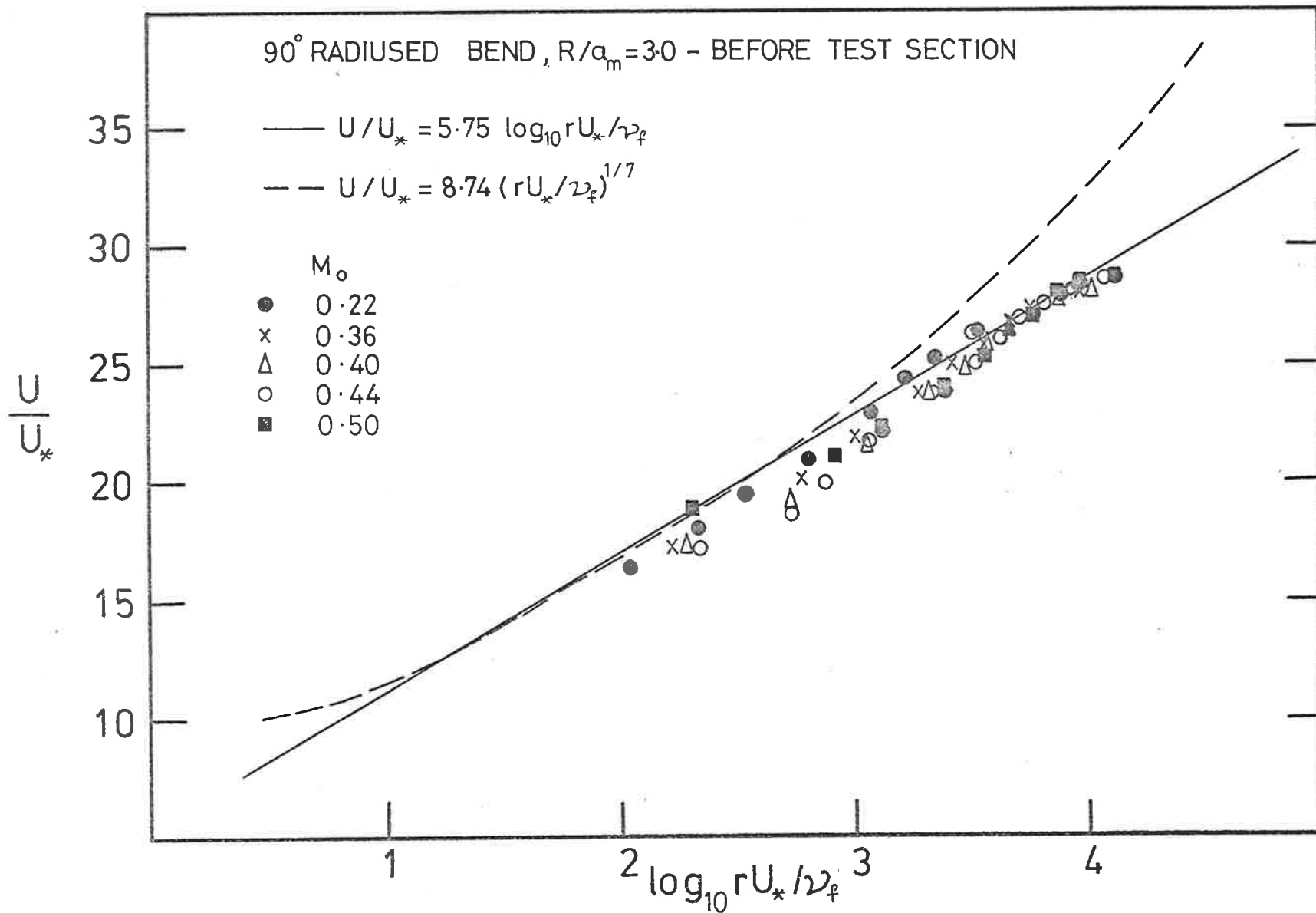


FIGURE 3-19 UNIVERSAL VELOCITY PROFILES

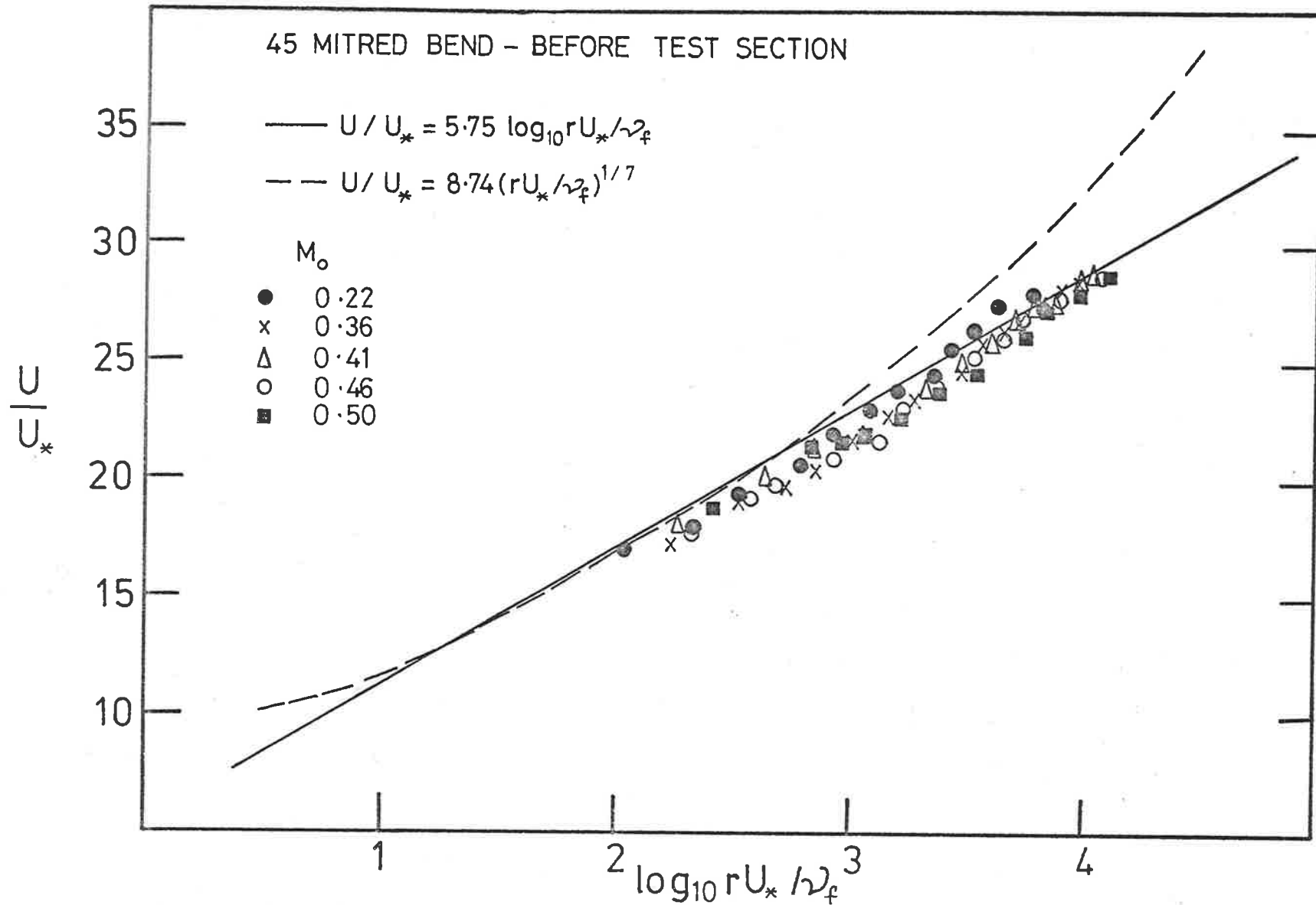


FIGURE 3.20 UNIVERSAL VELOCITY PROFILES

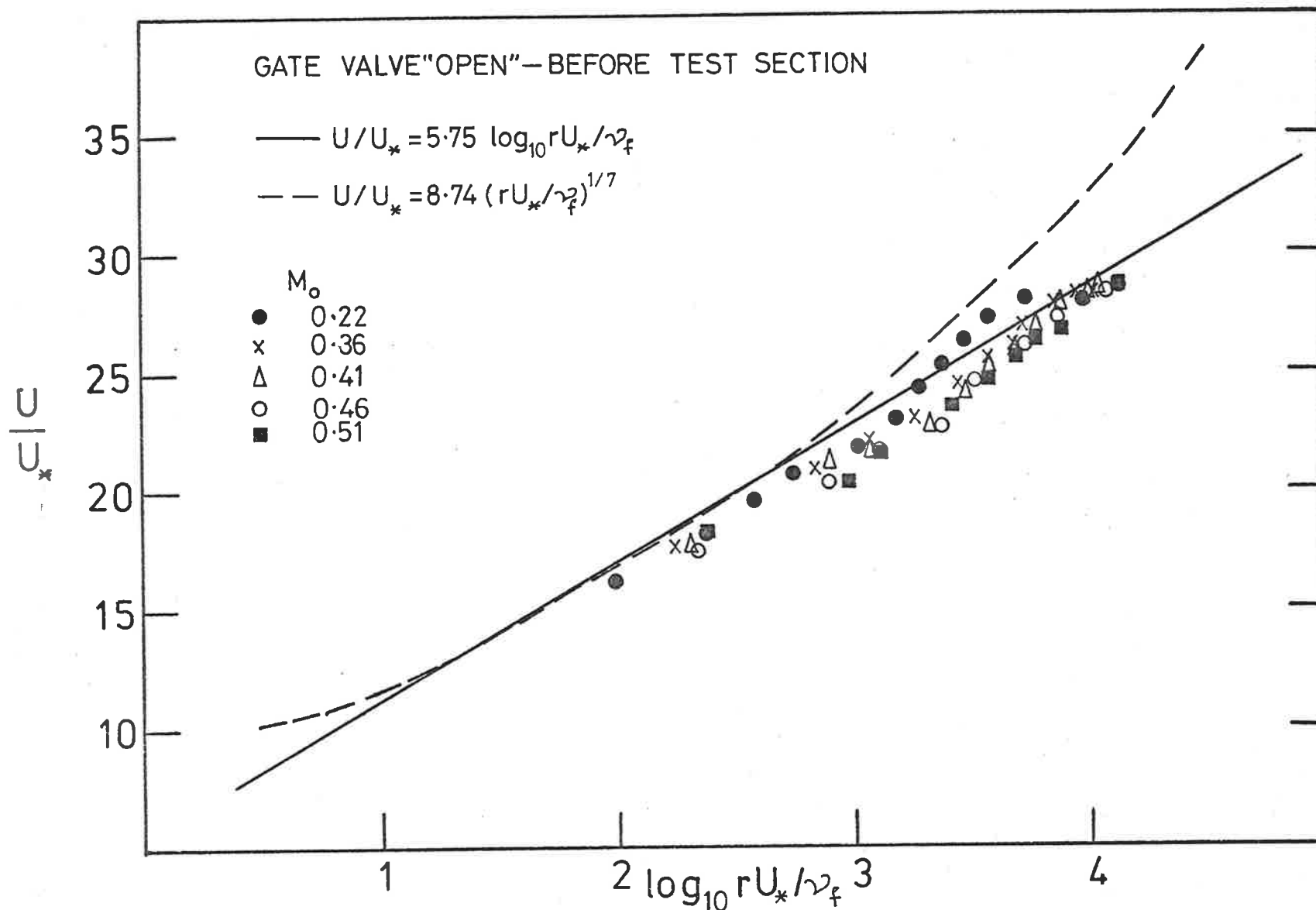


FIGURE 3.21 UNIVERSAL VELOCITY PROFILES

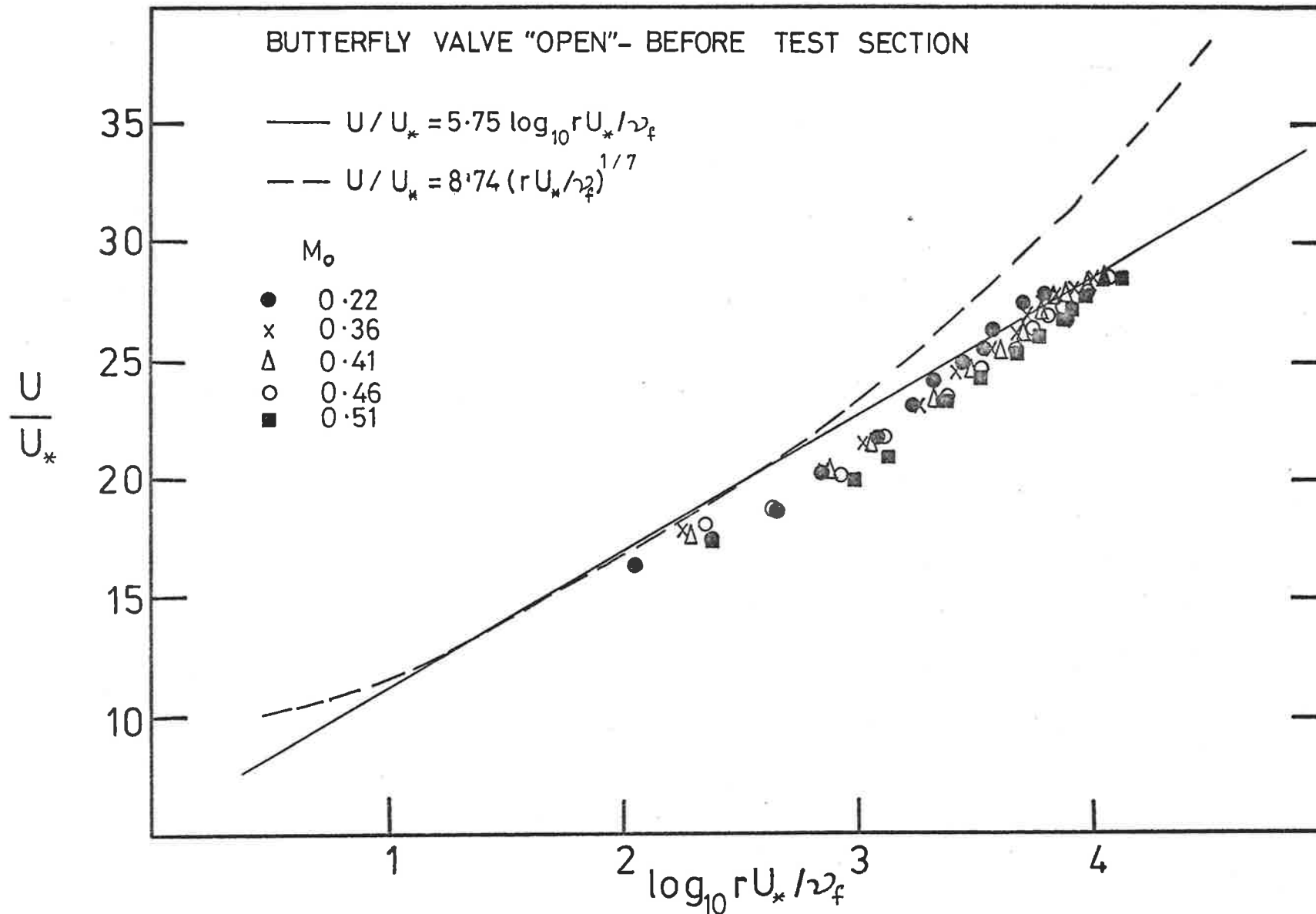


FIGURE 3.22 UNIVERSAL VELOCITY PROFILES

TABLE 3-2MEAN CENTRLINE FLOW MACH NUMBERS (before the test section at X = 52.4)

NOMINAL MACH NUMBER	0.20	0.35	0.40	0.45	0.50
Straight Pipe	0.220	0.361	0.410	0.462	0.520
90° Radiused Bend ($R/a_m = 6.4$)	0.219	0.359	0.400	0.460	0.500
90° Radiused Bend ($R/a_m = 3.0$)	0.219	0.357	0.397	0.443	0.496
Gate Valve	0.220	0.360	0.406	0.461	0.512
45° Mitred Bend	0.220	0.360	0.407	0.460	0.503
90° Mitred Band	0.219	0.356	0.395	0.448	0.495
Butterfly Valve	0.218	0.357	0.408	0.460	0.505

In the particular case of the 90° mitred bend the wall pressure fluctuations were acquired digitally at several axial positions downstream of the disturbance. The remaining wall pressure spectral data were analysed in analogue form using standard Brüel and Kjaer noise and vibration equipment.

3.5.1 The Wall Pressure Transducers

Piezo-electric transducers were used to measure the wall pressure fluctuations. The transducers used in the present investigation are similar to those used by Lim (1971), Rennison (1976) and Thomas (1977). The piezo-electric transducer was used rather than a condenser microphone because of its higher attainable frequency response characteristics, the smaller overall size, and the stability of its calibration with variations in the mean ambient pressure.

The transducer consists of a small lead zirconate-titanate piezo-electric crystal of both diameter and thickness of 0.75 mm, mounted on a brass stem. The stem is set in a brass plug of 5 mm external diameter and the stem is insulated from the plug with silicon loaded ebonite. The designation for the piezo-electric material is PZT-5H and it is manufactured by the Brush Clevite Company of Southampton, England. The small gap between the transducer crystal and the surrounding body is filled with silicone moulding rubber. An electrical contact (conducting silver paint) is placed on the top surface of the crystal. A thin diaphragm of epoxy cement is applied to the transducer top face to offer some degree of protection and to ensure a surface free of discontinuities. The details of the piezo-electric transducer are presented in Figure 3.23. A detailed description of the various stages in the assembly of the transducers is given by Thomas (1977).

The piezo-electric transducers are very high impedance

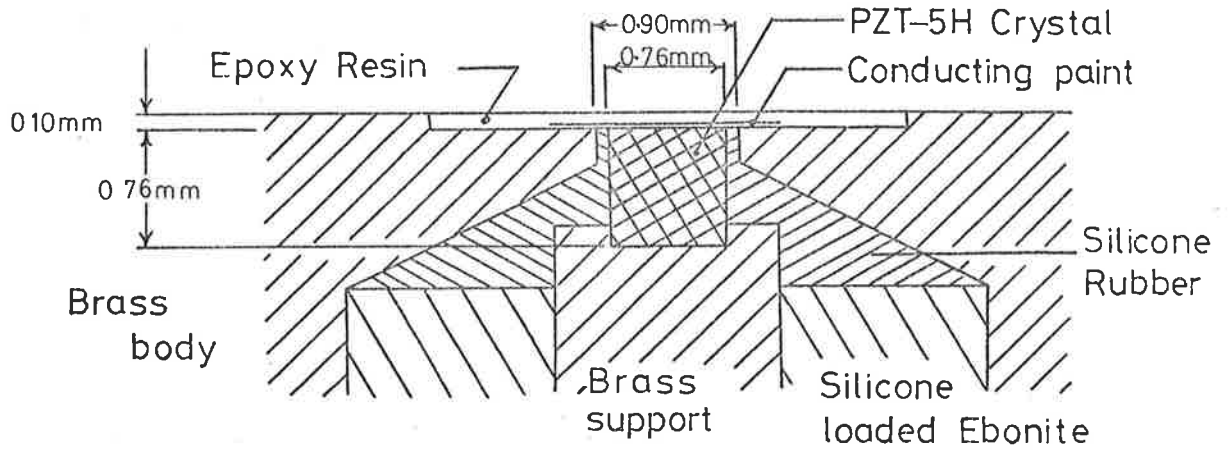


FIGURE 3.23 DETAILS OF PIEZO-ELECTRIC TRANSDUCER
(FROM THOMAS, 1977)

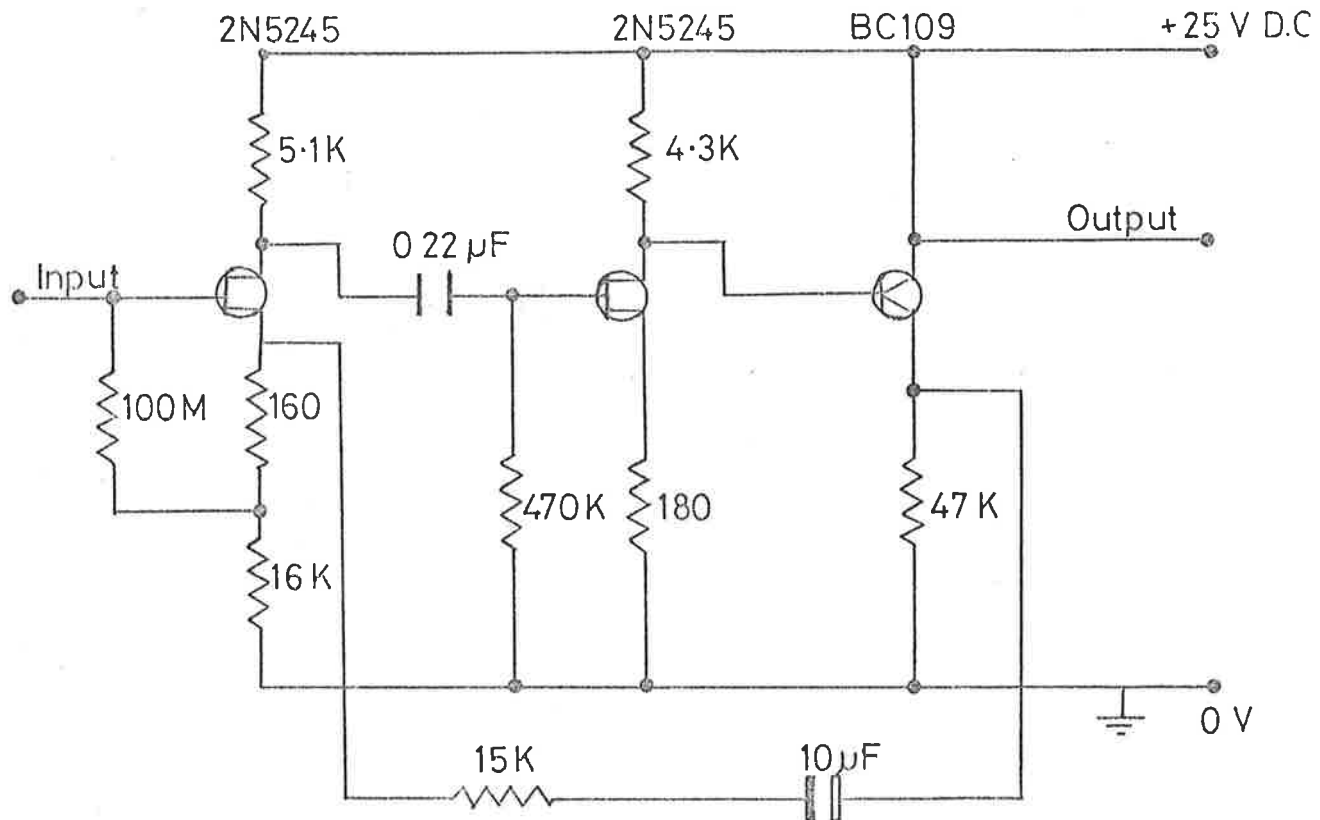


FIGURE 3.24 CIRCUIT DIAGRAM OF TRANSDUCER PREAMPLIFIER
(FROM LIM, 1971)

devices and therefore, a pre-amplifier is required for impedance matching. For this purpose, the pre-amplifier described by Lim (1971) was used. This is illustrated in Figure 3.24. The transducer, mounted in the brass plug was mounted on the pre-amplifier and connected to a D.C. supply. Figure 3.15 shows two of the transducers mounted on their respective pre-amplifiers, together with several other transducers. The output from the transducer pre-amplifier was passed to a Brüel and Kjaer 2114 Microphone amplifier/spectrometer, and then fed to both a Nagra IVL tape recorder and a B & K 3347 Real Time Analyser. The schematic arrangement of the apparatus is shown in Figure 3.25.

Two methods were used to calibrate the transducers: (i) a method based on the propagation of a shock wave of known strength across the transducer face, and (ii) a method based on comparing the response of the transducer with that of a calibrated microphone in an acoustic coupler.

In the first method, shocks of various strengths were passed down a 40 mm x 65 mm rectangular shock tube over the face of the in-situ transducer to determine its sensitivity, linearity and frequency response. Measurement of the voltage rise at the transducer output, for various shock strengths allows a calibration curve to be obtained. Oscilloscope traces of typical transducer shock wave responses are shown in Figure 3.26. The progressive fall off in output voltage with time, after the initial rise due to the passage of the pressure step is attributed to the lack of low frequency response of the transducer/pre-amplifier combination. The high frequency oscillations seen on the trace are associated with the fundamental longitudinal resonance of the brass stem upon which the crystal is mounted. These oscillations were dampened by covering the transducer/pre-amplifier with plasticine.

The magnitude of the pressure rise across the shock may be

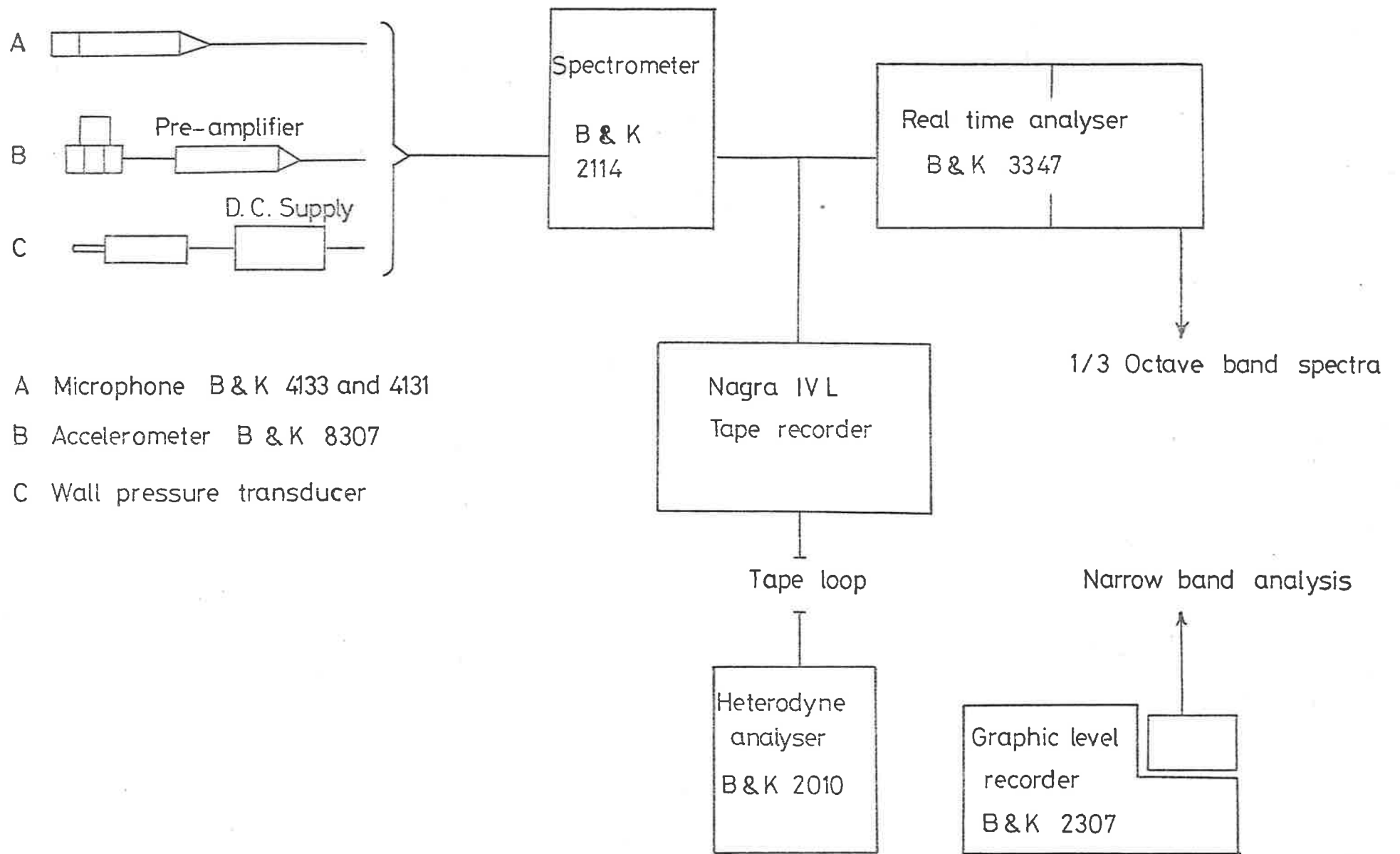
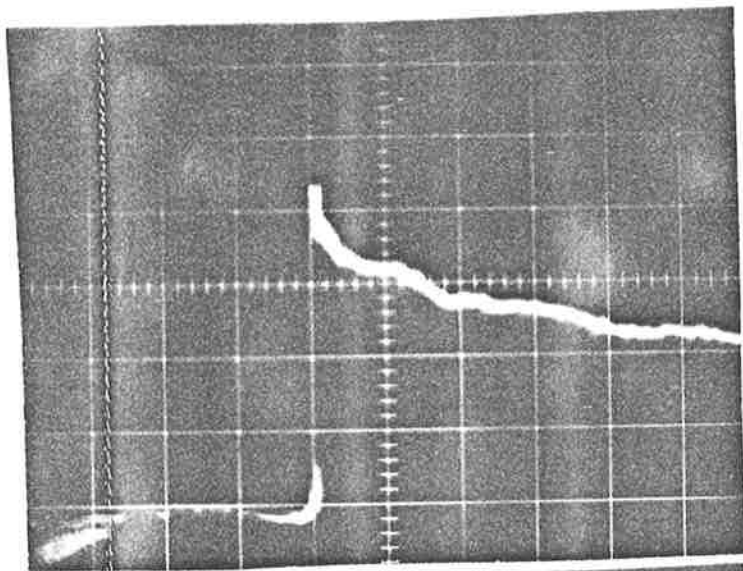
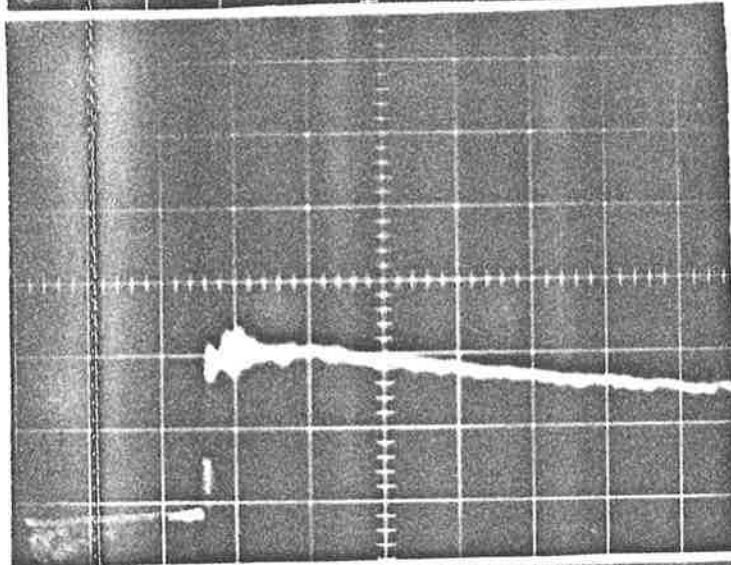


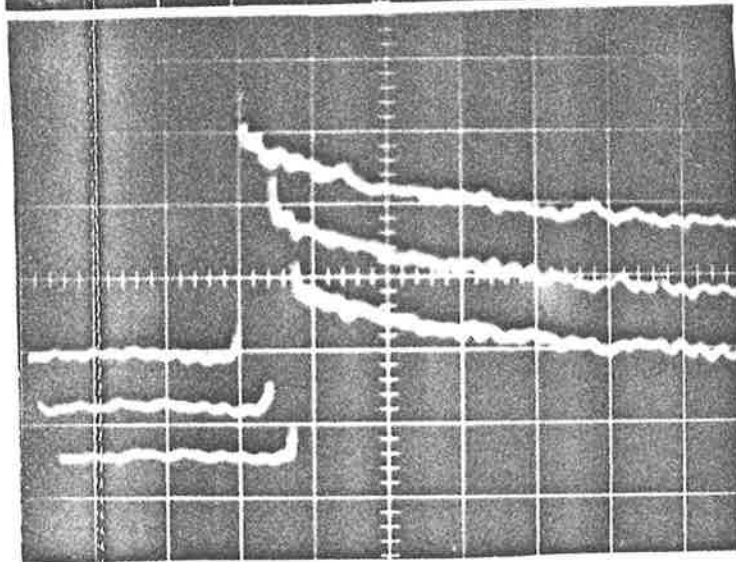
FIGURE 3-25 INSTRUMENTATION



1 V / division



1 V / division



1 V / division

100 μ s / division

FIGURE 3-26 OSCILLOSCOPE TRACES OF THE RESPONSE OF A PIEZO-ELECTRIC TRANSDUCER TO THE PASSAGE OF A SHOCK WAVE

estimated using the approximate shock tube relation

$$\left[\frac{p_1}{p_2} \right]^{1/7} = \frac{2}{1 + \left[\frac{p_1}{p_4} \right]^{1/7}}, \quad [3.1]$$

where p_1 is the static pressure ahead of the shock (this is atmospheric pressure in an open ended shock tube),
 p_2 is the static pressure behind the shock,
 p_4 is the initial pressure in the high pressure chamber of the shock tube.

The magnitude of the pressure step across the shock front is

$$\Delta p = (p_2 - p_1).$$

Typical calibration curves that result from these procedures are presented in Figure 3.27 for three of the transducers used. The curves are well defined straight lines. The sensitivity of the transducers (including pre-amplifier) varied from about 0.10 mV/Pa to 0.30 mV/Pa, and was linear over a range of shock strengths from 8 to 34 kPa, with a flat frequency response from 100 Hz to 100 kHz.

The second method, based on comparing the response of the transducer with that of a calibrated microphone in an acoustic coupler, was used to provide an easier alternative to the shock tube calibration technique during the numerous experimental runs on the induced flow rig. Furthermore, the acoustic coupler calibration procedure was designed such that the transducer did not have to be removed from the instrumentation plug during calibration. It thus remained flush with the plug surface throughout the experiments. The output of the transducer was calibrated against that of a calibrated B & K $\frac{1}{4}$ inch 4136 condenser microphone, using a small coupler into which they both face and in which cyclic pressure variations are created. This is

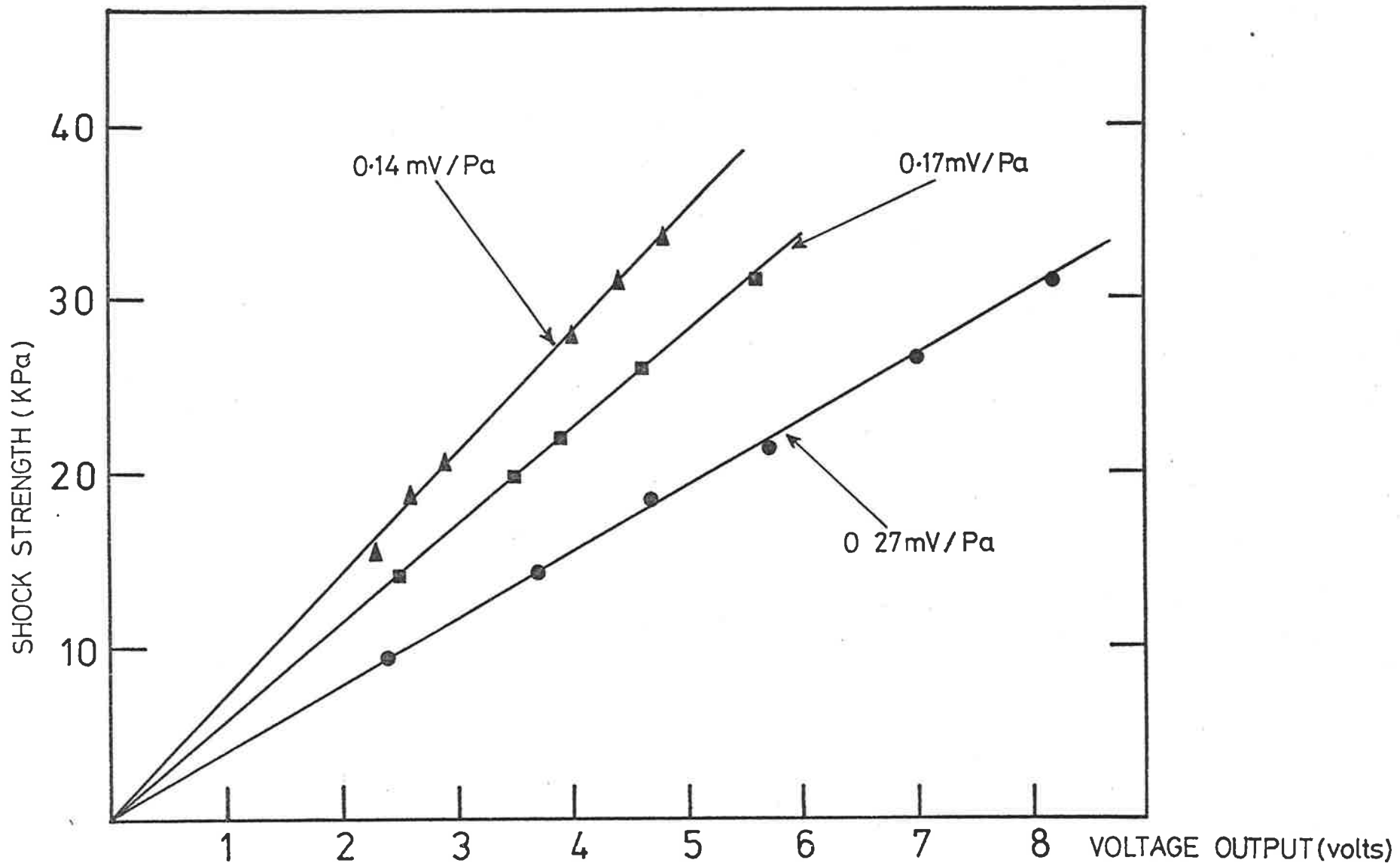


FIGURE 3.27 SHOCK TUBE CALIBRATION OF TRANSDUCERS

illustrated in Figure 3.28. The pressure oscillations are provided by means of a small ear piece speaker which is driven by a signal generator. Silicone grease is used to ensure that no air leaks are present. Using this technique, the calibration was verified for frequencies up to 2 kHz. Above 2 kHz, the pressure generated in the cavity is not uniform due to wave effects; this limits the calibration to 2 kHz. A typical frequency response of a piezo-electric transducer as measured with the acoustic coupler is presented in Figure 3.29. The response of the transducer is flat to 2 kHz with deviations occurring at higher frequencies.

Piezo-electric crystal transducers are sensitive to any vibrations of the instrumentation plug. This together with pre-amplifier electrical noise could contaminate the true wall pressure fluctuation signal. The spectral density of the electronic noise was 40 dB less than the measured pressure fluctuations associated with straight pipe flow and up to 80 dB less than that associated with the severe flow disturbances. The vibrational response of the transducer/pre-amplifier was investigated by blanking off the mounted transducer from the flow. The spectral density of the vibrational signal obtained with the transducer blanked off from the flow was always less than 1% of the signal with the transducer flush with the internal pipe wall and exposed to the flow. Furthermore, the transducer/pre-amplifier was always dampened with plasticine to reduce vibrational effects.

3.5.2 Pipe Wall Vibration and Acoustic Radiation Measurement Procedures

Since the flow rig used is an intermittent induced air flow rig, steady state conditions prevail for a finite time which is shorter than the running time. Experimental measurements were obtained only during the steady state period. Both the pipe wall acceleration and

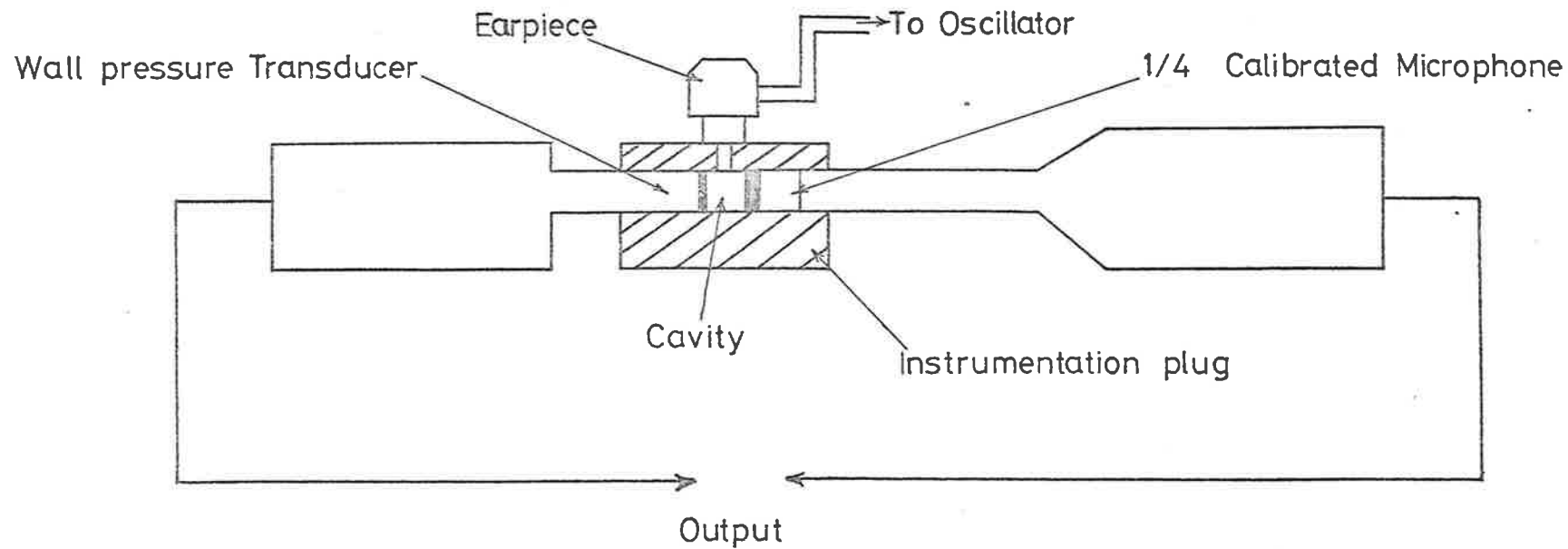


FIGURE 3-28 CALIBRATION ACOUSTIC COUPLER

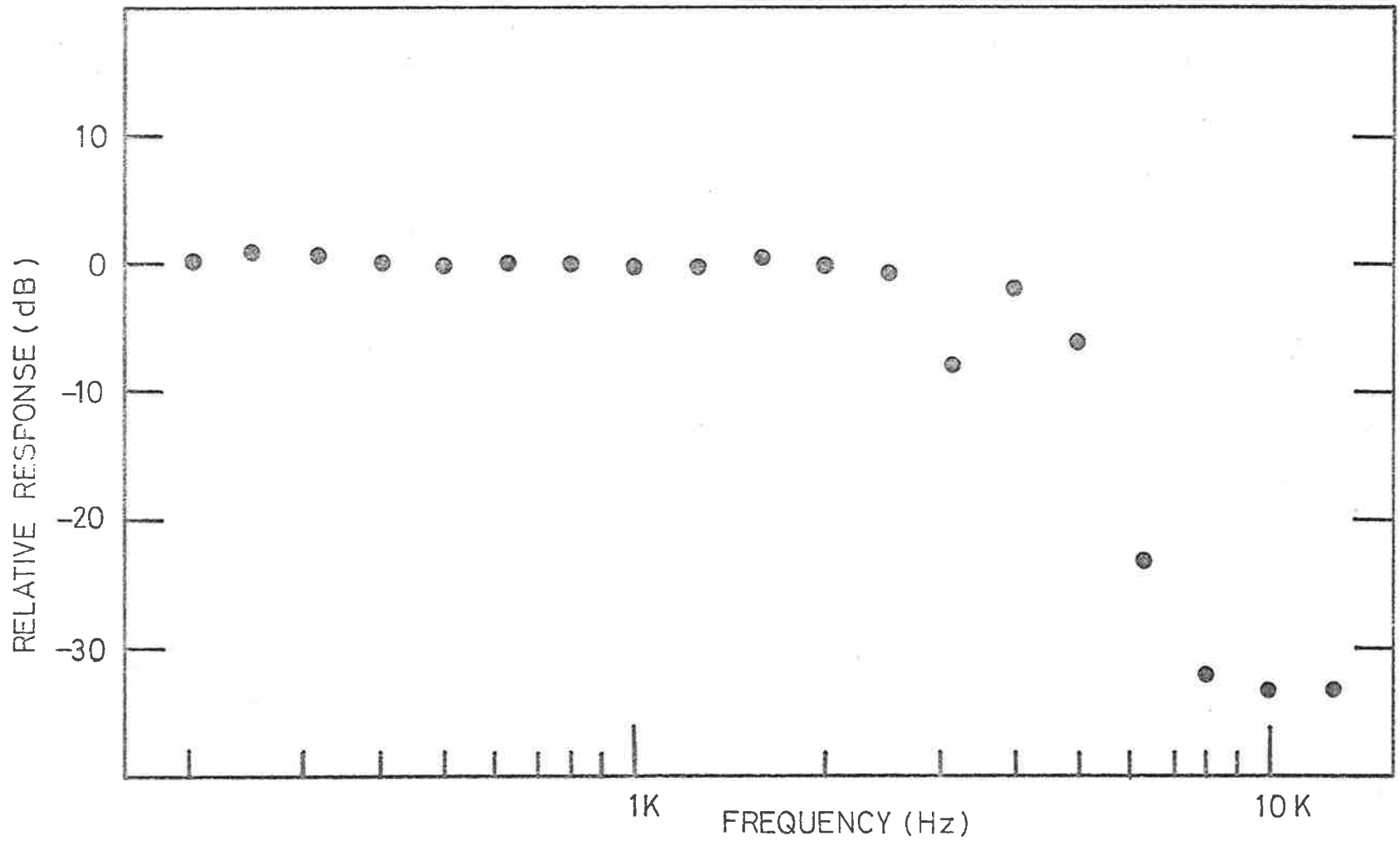


FIGURE 3-29 FREQUENCY RESPONSE OF A PIEZO-ELECTRIC TRANSDUCER AS MEASURED WITH AN ACOUSTIC COUPLER

the acoustic power radiated were monitored with a Real Time Analyser and it was found that the steady state period was only fractionally shorter than the running time for each flow speed.

The $\frac{1}{3}$ -octave band acceleration response of the pipe wall was measured with a B & K 8307 0.5 g accelerometer. The accelerometer was calibrated with a B & K accelerometer calibrator type 4291. The 8307 accelerometer has a nominally flat frequency response to frequencies in excess of 40 kHz. The accelerometer was fastened to the pipe surface with a thin layer of beeswax, which does not affect its frequency response. At high frequencies, however, the mass of the accelerometer causes a reduction in the response for light structures. Rennison (1976) made an assessment of this "mass-loading" by measuring the reductions in the pipe acceleration response following the addition of several small masses to the 8307 (0.5 g) accelerometer attached to the thin-walled test pipe, for a constant electromagnetic excitation power input. The measurements were extrapolated back to the case of zero mass-loading to give estimates of the necessary correction to be applied to the 0.5 g accelerometer. Rennison's (1976) results are used in this investigation and are presented in Figure 3.30.

Background "electronic" noise levels were found to be well below the acceleration response levels and no corrections were necessary. As for the wall pressure fluctuations the spectral data were tape recorded and analysed on a narrow band analyser. This is illustrated schematically in Figure 3.25.

The particular anechoic chamber used in this investigation is a free field environment for $\frac{1}{3}$ -octave band acoustic measurements from 200 Hz to above 40 kHz. For a finite pipe of length ℓ , the far field directivity pattern of acoustic radiation from the pipe will correspond to that of an infinite line source composed of incoherent

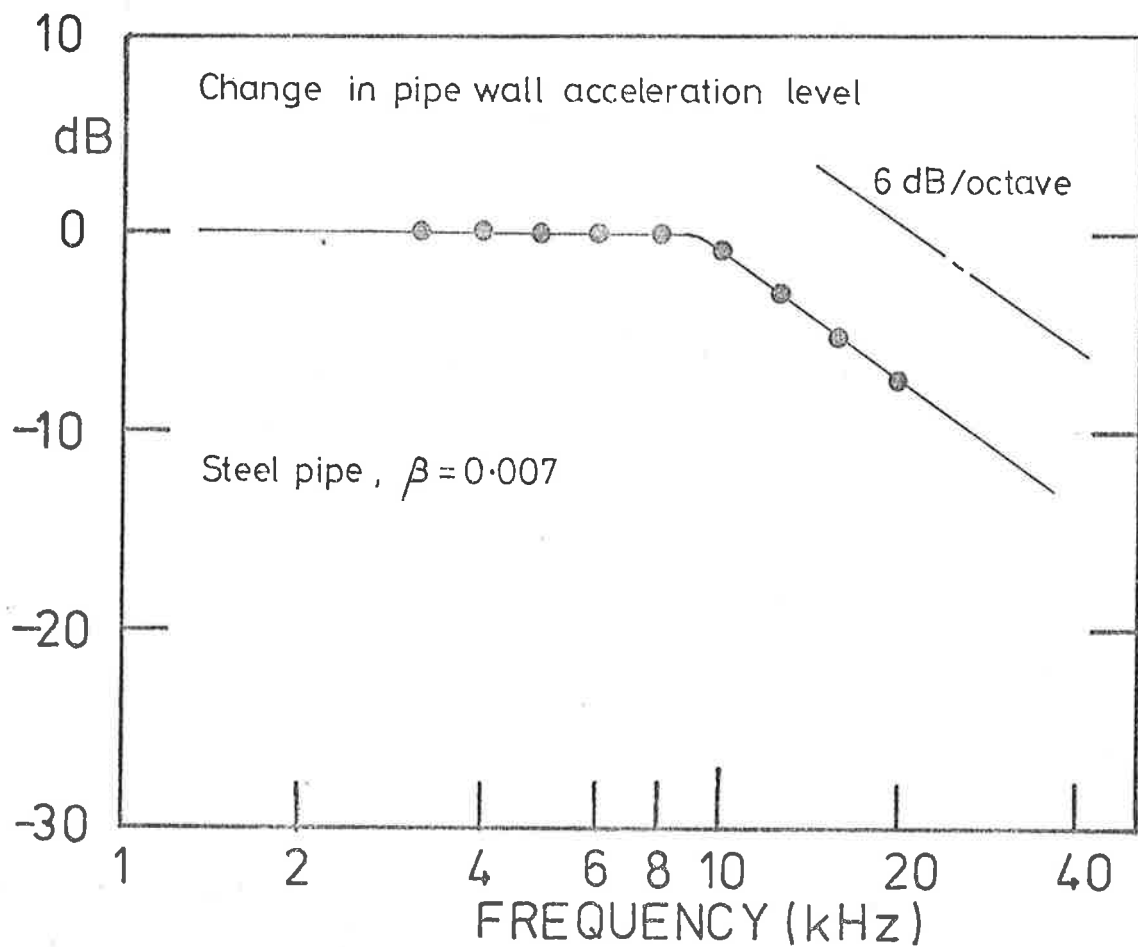


FIGURE 3.30 MASS LOADING EFFECTS OF A B & K 8307 (0.5g) ACCELEROMETER (FROM RENNISON, 1976)

sources if the observer is positioned within an imaginary cylindrical volume (i) whose length is equal to the pipe length ℓ ; (ii) whose radius is $< \ell/2$, and; (iii) which is axi-symmetric with the pipe centreline. Rennison (1976) investigated the far field directivity pattern of acoustic radiation from a cylindrical pipe during flow excitation. The radial dependence of the far field was determined by measuring the decreases in radiated sound pressure levels (in $1/3$ octave bands) as the radial distance from the pipe axis was successively doubled from 0.125 m to 1.0 m. In this range of radial distances, but not significantly beyond, Rennison found that there were exactly 3 dB decreases in radiated sound pressure levels between each successive radial positions for all frequencies ≥ 800 Hz. At frequencies between 250 Hz and 800 Hz there were approximate free field conditions. To satisfy both criteria (i.e. a free field condition and a line source) such that a single measurement of the radiated intensity will enable an accurate estimate of the total acoustic power radiated, subsequent far field acoustic measurements obtained by Rennison (1976) were made at a radial distance of 0.25 m.

The acoustic power radiated from the test section in the present investigation was measured over the frequency range 250 Hz to 40 kHz. Measurements were obtained in the anechoic chamber with the microphone 0.25 m from the pipe centreline, resulting in free field conditions - a doubling of distance from the pipe produces a decrease in sound pressure level of 3 dB - being achieved. The $1/3$ -octave band measurements were obtained using a B & K 4133 ($1/2$ inch) condenser microphone. This microphone has a flat frequency response over the desired range (250 Hz to 40 kHz). However, at low flow speeds (where the signal levels are low), the background "electronic" noise is significant. Measurements were obtained using a B & K 4131 (1" microphone) for these low flow speeds ($M_0 \sim 0.20$). This particular

condenser microphone has a lower background "electronic" noise level. As for the wall pressure fluctuations and the pipe wall response, output signals were recorded on magnetic tape and narrow band analysed (Figure 3.25).

3.5.3 The Data Acquisition System

All the data used in Chapter 6 on the wall pressure fluctuation cross correlations were recorded on computer tape using a multiple input channel data acquisition system designed by and built in the Department of Mechanical Engineering at the University of Adelaide. The cross correlations themselves were performed on the Control Data Corporation CYBER 173 computer of the University of Adelaide.

The data acquisition system is capable of making measurements at rates up to four million per second. The system is programmed from the front panel or from magnetic tape. Measurements can be made on any number of channels up to 12 analogue channels and 4 digital channels. These measurements, each of eight bit precision, are written onto a 16 K shift register memory that is hard wired within the system. Different quantities of the memory can be allocated independently to each of the 16 channels according to requirements. The sampling rate on each channel can be independently varied up to a maximum of 0.5 MHz.

Once the memory has been allocated to each channel, the whole of the contents of the memory is written on a standard IBM 9 track computer tape as a continuous block with a preamble on each record providing information such as sampling rates, and memory block sizes. The system then repeats this process, acquiring and writing data, for any selectable number of times.

The sampling rate used was 50 kHz and two channels were used for acquiring the relevant data for cross correlation of the wall pressure fluctuations. Hence each record consisted of 8192 (2^{13}) words

of memory. The memory is arranged in modules of 256 words and there are 64 modules of memory - i.e. 32 modules of memory per channel for this particular experimental set up.

The analogue to digital converters were set for a bipolar operating mode with an input range of ± 5 volts. Since the transducer output voltages were of the order of a few hundred milli-volts in amplitude (turbulent pressure fluctuations and acoustic pressure fluctuations), amplification of the signals before digitization was essential. Digital techniques relating to the acquiring of the data are discussed in detail in Chapter 6 (section 6.3).

3.6 SUMMARY

In this chapter are presented details of the various internal flow disturbances investigated and their construction, together with the details of the induced air flow rig that accommodated the various disturbances. The flow facility performance was investigated with and without the various disturbances. A discussion has also been presented on the design of the piezo-electric wall pressure transducer and its calibration using both shock tube and acoustic coupler techniques. Measurement procedures for obtaining the pipe wall acceleration response and the acoustic radiation have been briefly discussed. Finally a description of the high speed data acquisition system has been presented.

Five flow nozzle configurations were used, corresponding to nominal mean centreline Mach numbers (M_0) of 0.20, 0.35, 0.40, 0.45 and 0.50. Steady state conditions vary from 5 seconds for the largest Mach number to 14 seconds for the smallest Mach number. Fully-developed turbulent pipe flow is established before the flow disturbance and it is re-established before the test section. Vibration isolation of the test section from the flow disturbance was unnecessary because of

the large impedance mismatch between the test section and the instrumentation section and between the instrumentation section and the general pipe work.

Piezo-electric crystal transducers were used for the measurement of the wall pressure fluctuations because of the higher frequency response attainable, the smaller overall size, and the stability of their calibration with changes in mean ambient pressure and their robustness in comparison with the diaphragm of a condenser microphone.

Conventional B & K equipment allowed for satisfactory collection of experimental data of the pipe wall response and the external acoustic radiation over a broad frequency range from 250 Hz to 40 KHz for the five flow speeds. The data were tape recorded on an analogue tape recorder and processed.

The data for the wall pressure fluctuation cross-correlations were processed digitally on a high speed data acquisition system and the Cyber 173 Computer.

CHAPTER 4

EXPERIMENTS WITH A 90° MITRED BEND

4.1 INTRODUCTION

The work reported in this chapter is part of a systematic investigation of the pipe-wall vibrational response and the resulting acoustic radiation, caused by either an undisturbed fully-developed turbulent pipe flow or a disturbed flow due to the presence of various pipe fittings. Results of the study of the vibration and acoustic radiation due to undisturbed fully-developed internal turbulent flows have been reported previously by Bull and Rennison (1974, 1977), Bull, Pickles and Rennison (1976) and by Rennison (1976). These results form a datum against which the measured effects of various flow disturbances can be judged. Some results for radiused and mitred bends have been reported previously by Bull and Norton (1976, 1977). The bends are responsible for the generation of an internal sound field, and enhanced vibrational response and external acoustic radiation (compared with results for a straight pipe) are observed. This chapter is concerned, in the main, with a 90° mitred bend and with its effects on fully-developed turbulent pipe flow. Wall pressure fluctuations and other flow parameters have been measured at various positions upstream, in the immediate vicinity, and downstream of the bend, and of primary concern are (a) the characteristics of the flow separation caused by the bend, (b) the relation between the characteristics of the flow separation and the wall pressure fluctuations, and (c) the vibrational and acoustic effects at a downstream position where a fully-developed turbulent velocity profile has been re-established.

The 90° mitred bend was chosen because it represents a severe,

asymmetric internal flow disturbance which generates an intense internal sound field. Hence, in this chapter, extensive experimental results are presented for (a) a detailed investigation of flow in the region of the bend and (b) the vibrational and acoustic effects.

All the experimental results of the vibration response and the acoustic radiation presented in this chapter relate to the thin-walled cylindrical test-section that spans the anechoic chamber where $\beta = 0.0070$, $\psi = 0.960$, $\Lambda = 79.4$ and $M_{LP} = 15.37$.

4.2 DETAILED INVESTIGATION OF FLOW IN THE REGION OF THE BEND

This section is concerned with wall pressure fluctuations and other flow parameters to develop a better understanding of the character of the flow in the vicinity of a 90° mitred bend. Extensive wall pressure fluctuation, static pressure and total pressure measurements were made at numerous circumferential and axial positions, both upstream and downstream of the mitred bend. The work presented in this section is an extension of earlier work by Bull and Norton (1977, b).

4.2.1 Experimental Arrangement

The general arrangement of the experimental apparatus, an intermittent induced air-flow rig, is described in detail in Chapter 3. This rig has been used to investigate the effects of the 90° mitred bend for various flow speeds with centre-line velocities in the range 65 to 170 m/s.

Measurement positions for static pressures, total pressure traverses, wall pressure spectra and root mean square wall pressure fluctuations in the vicinity of the bend are shown in Figure 4.1. Referred to the coordinate system defined in the figure, these cover the ranges $0 < X < 4$ and (by reversal of the bend) $-4 < Y < 0$. X and

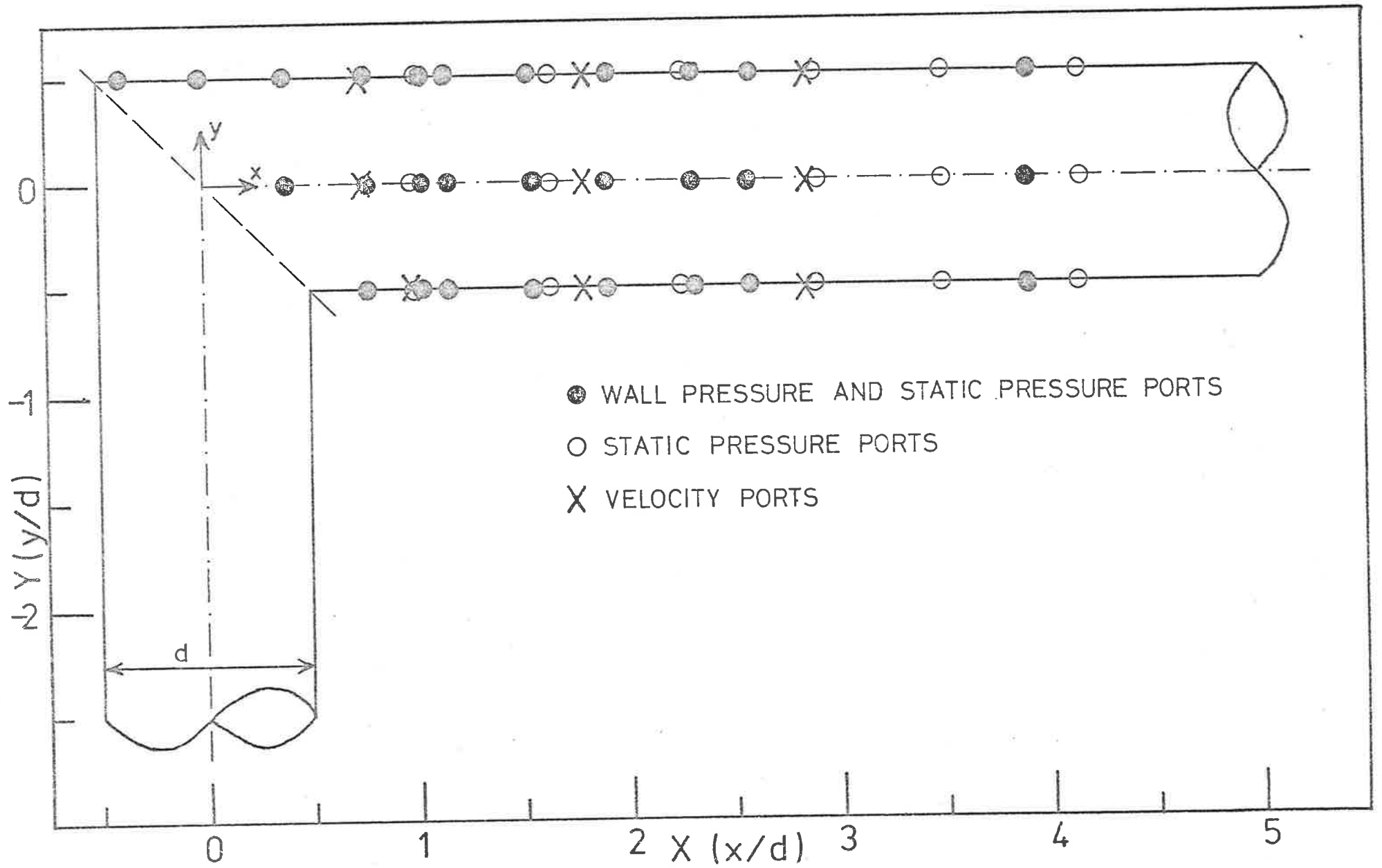


FIGURE 4.1 LOCATION OF MEASUREMENT PORTS

Y coordinates are used here to enable location of ports along the inner and outer wall of the bend. This is different from the $\pm X$ coordinates (along the centreline) that are used for the location of measurement positions not in the vicinity of the bend. The latter system is also used in the next chapter for the various other pipe fittings investigated. Measurements have been made, for the 90° mitred bend, at points in the range $9 < X < 14$, $X \geq 52.4$, and Y (or X) ≤ -12.9 .

4.2.2 Character of the flow associated with the 90° Mitred Bend

Mean velocity profiles over cross-sections normal to the pipe axis have been obtained for three flow speeds corresponding to centre-line Mach numbers at $X = 52.4$ of $M_0 \sim 0.20$, 0.40 and 0.50 , at various streamwise positions both upstream and downstream of the bend. In all cases, fully-developed turbulent pipe flow is established before the bend ($Y = -12.9$) and has been re-established at the downstream measuring point at $X = 52.4$. At points $9 < X < 14$, the mean velocity profile is axisymmetric but not fully-developed. Typical results are shown in Figure 4.2 for $M_0 \sim 0.40$. Immediately downstream of the bend, the flow is asymmetric in the plane of symmetry of the bend. In the plane perpendicular to the bend, the mean flow is symmetrical about the pipe axis.

By flow visualisation, Tunstall and Harvey (1968) have previously established that flow separation occurs both at the inner edge and in the vicinity of the outer edge of the bend. This is reflected in the mean velocity profiles in the plane of symmetry of the bend and immediately downstream of it. Tunstall and Harvey (1968) also established that over a distance of about three diameters downstream of the bend, the fluid has a spiral motion which switches randomly between a clockwise and an anticlockwise direction of rotation

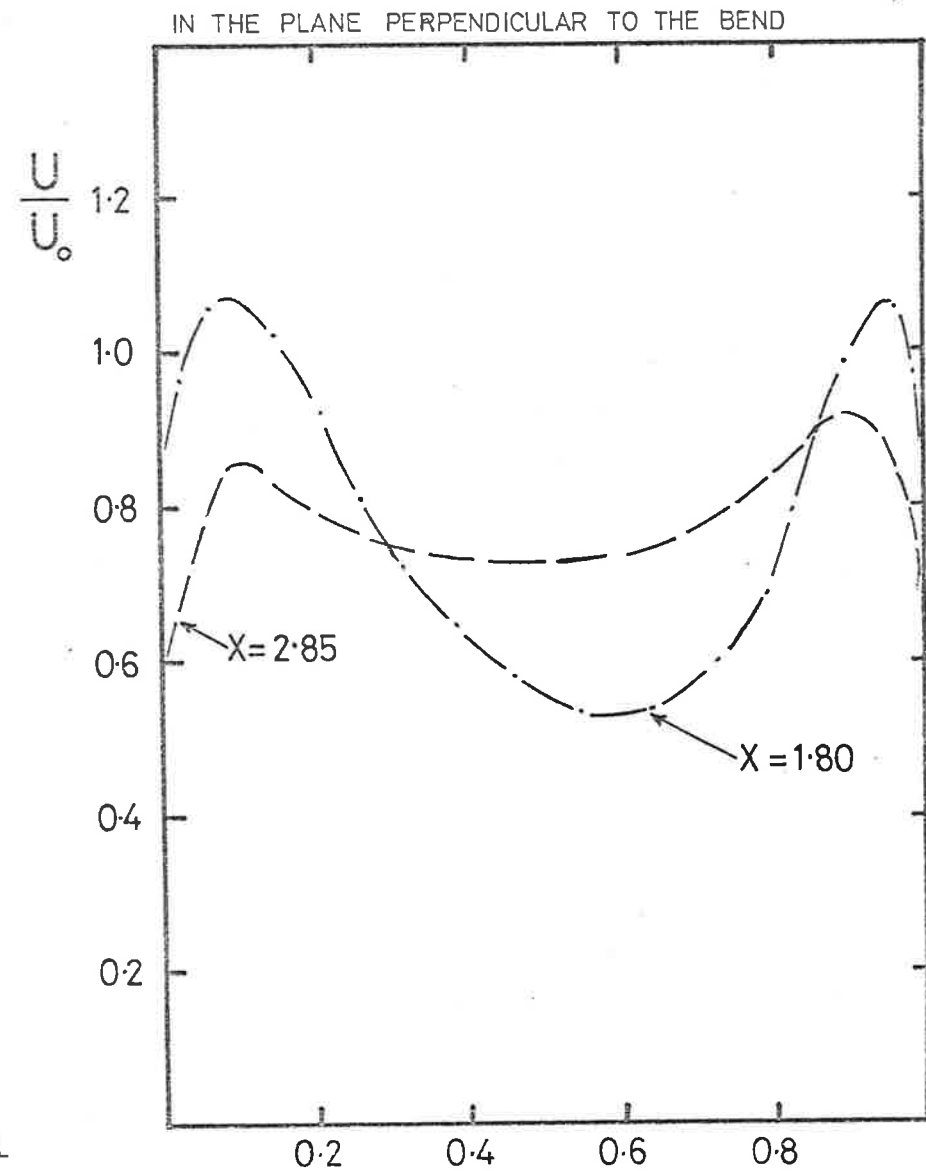
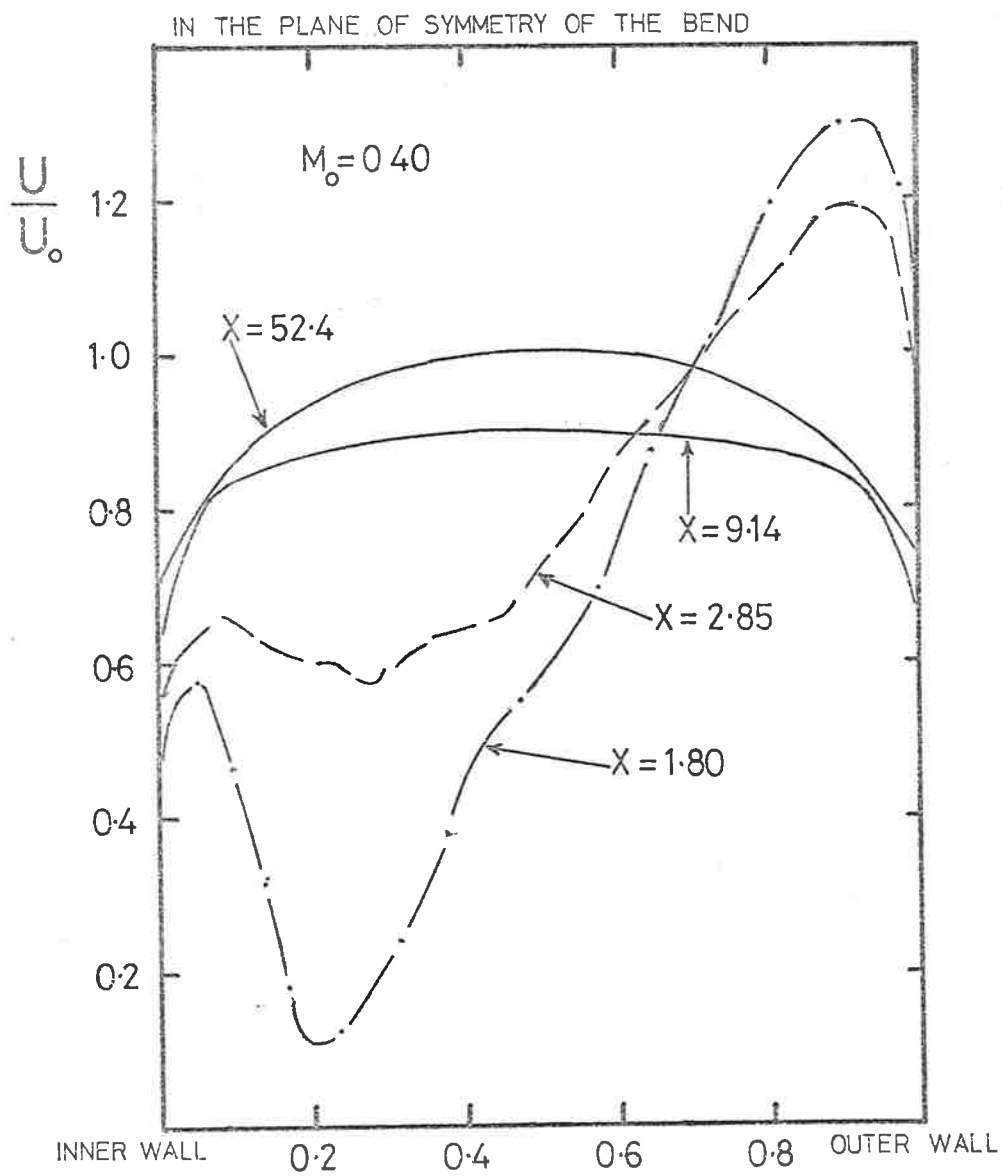


FIGURE 4.2 MEAN VELOCITY PROFILES

at frequencies in the Strouhal number range $0.001 < \Omega < 0.02$. This contrasts with the twin-circulatory flow usually associated with radiused bends. They also found that the separation bubbles, at both the inner and outer corners of the bend, are displaced to one side or other of the plane of the bend and oscillate between these two positions in sympathy with the switching of direction of the spiralling flow. This is illustrated in Figure 4.3. Mean velocity profiles measured in the present work are in agreement with those of Tunstall and Harvey, and the presence of the switching phenomenon was confirmed by time histories of velocity variations detected by both pitot tubes and hot wire anemometers, at points both in and out of the plane of the bend. This is illustrated in Figure 4.4. At points in the plane of the bend, the switching is between states with the same mean velocity, while at points out of the plane of the bend it is between states with different mean velocities. This is consistent with oscillations of the separation bubble in sympathy with the switching. Switching was observed at $X = 0.75, 1.80$ (where it was strongest), and 2.85 , but was not detectable at the downstream position $X = 9.14$. Tunstall and Harvey restricted themselves to a maximum flow speed of 30 m/s ; the present experiments confirm these observations for flow speeds of up to 170 m/s . It can thus be concluded that the switching phenomenon always accompanies separation and lasts as long as the mean velocity profiles in the plane of the bend are asymmetric (i.e. as long as the effects of separation are present).

Heskestad (1971) measured the static pressure and velocity distributions in the vicinity of a two-dimensional 90° mitred bend, and from them determined the shape and extent of the flow separation originating at the inner edge of the bend. The separation was found to extend downstream a distance of about 2.95 diameters (that is from

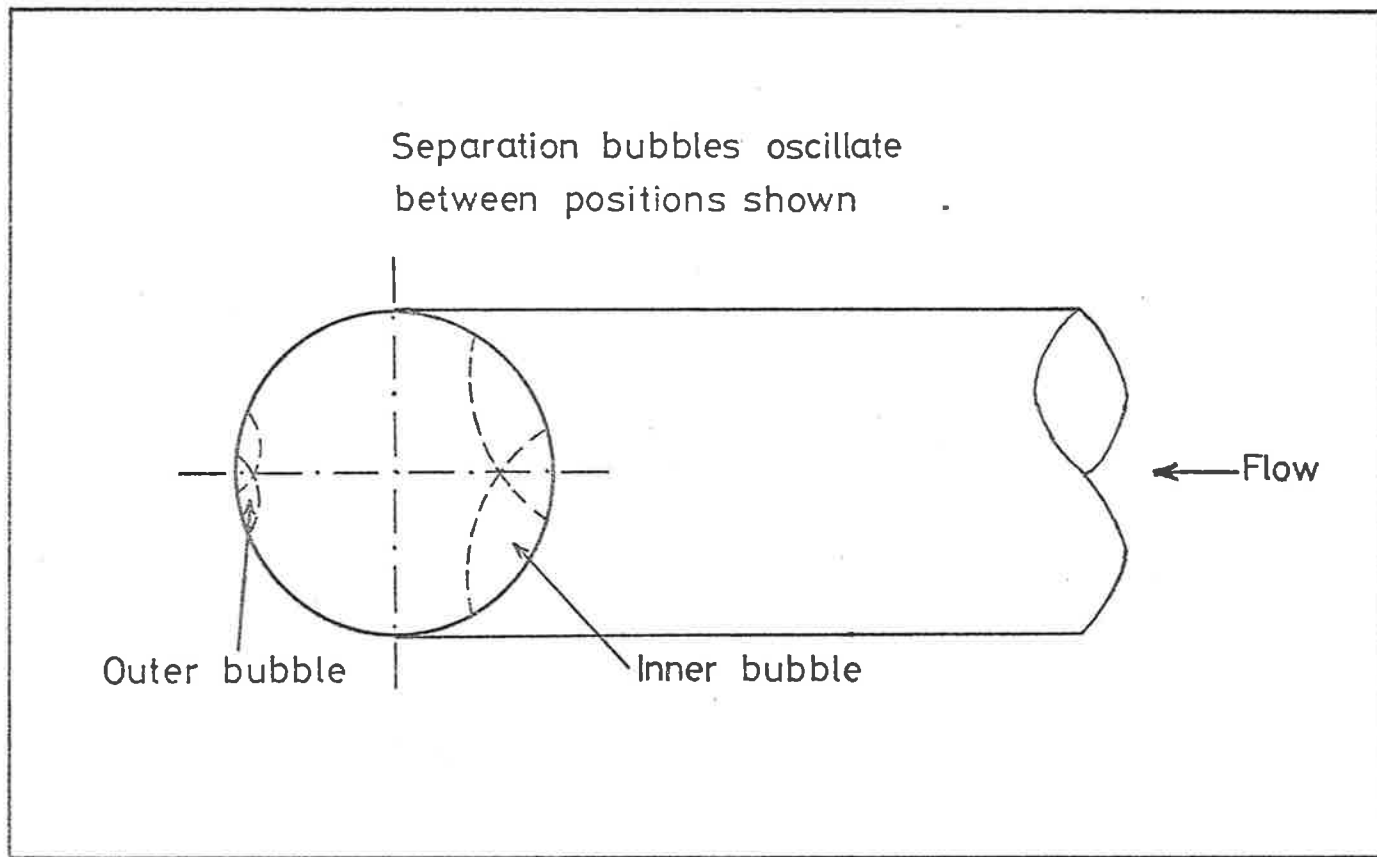
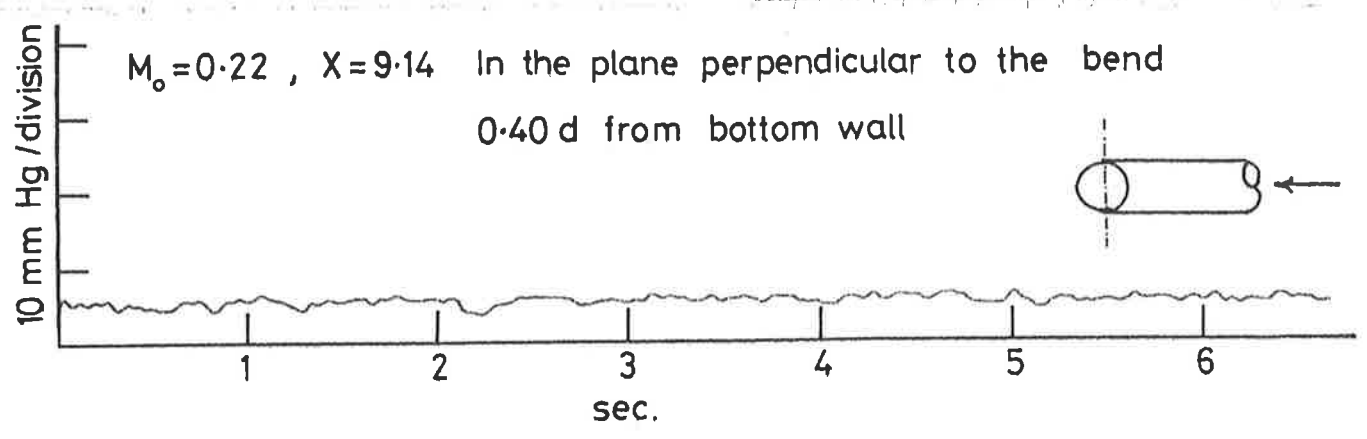


FIGURE 4.3 OSCILLATION OF THE SEPARATION BUBBLE

Note Y Axis represents relative total pressure scale



NO SWITCHING DETECTED AT $X = 9.14$

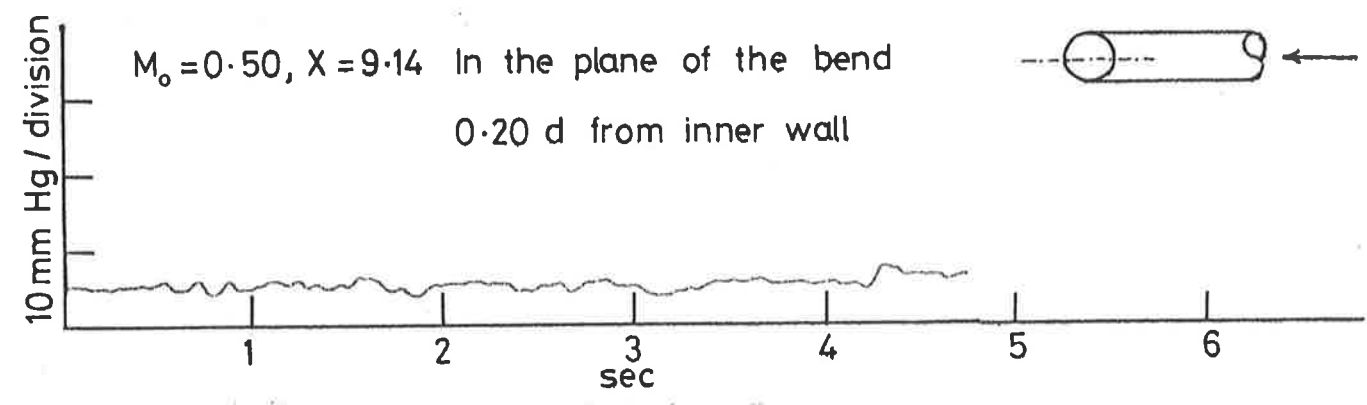
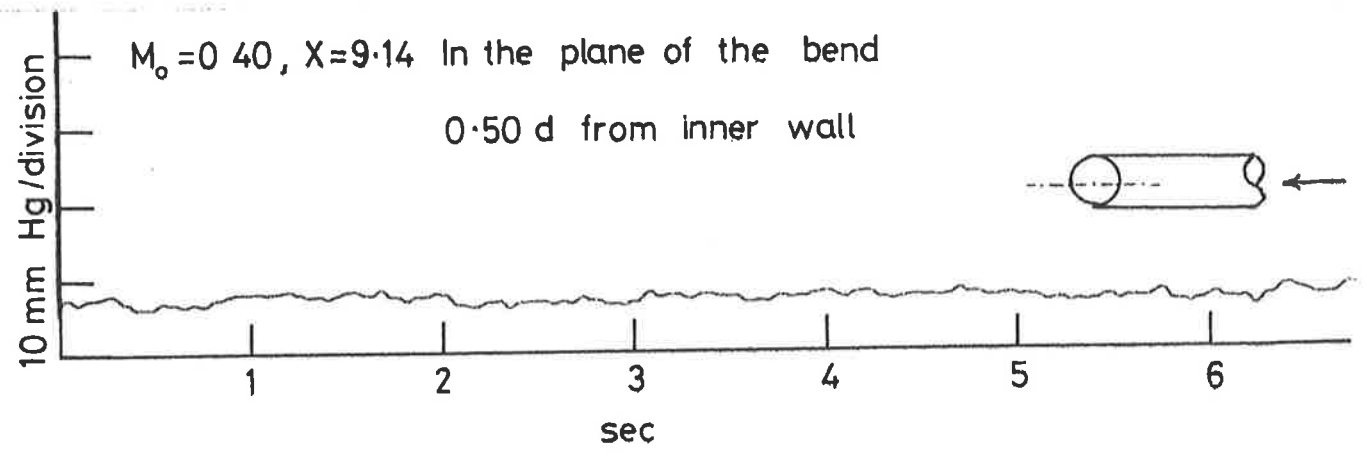


FIGURE 4.4(a) TIME HISTORY OF VELOCITY VARIATION

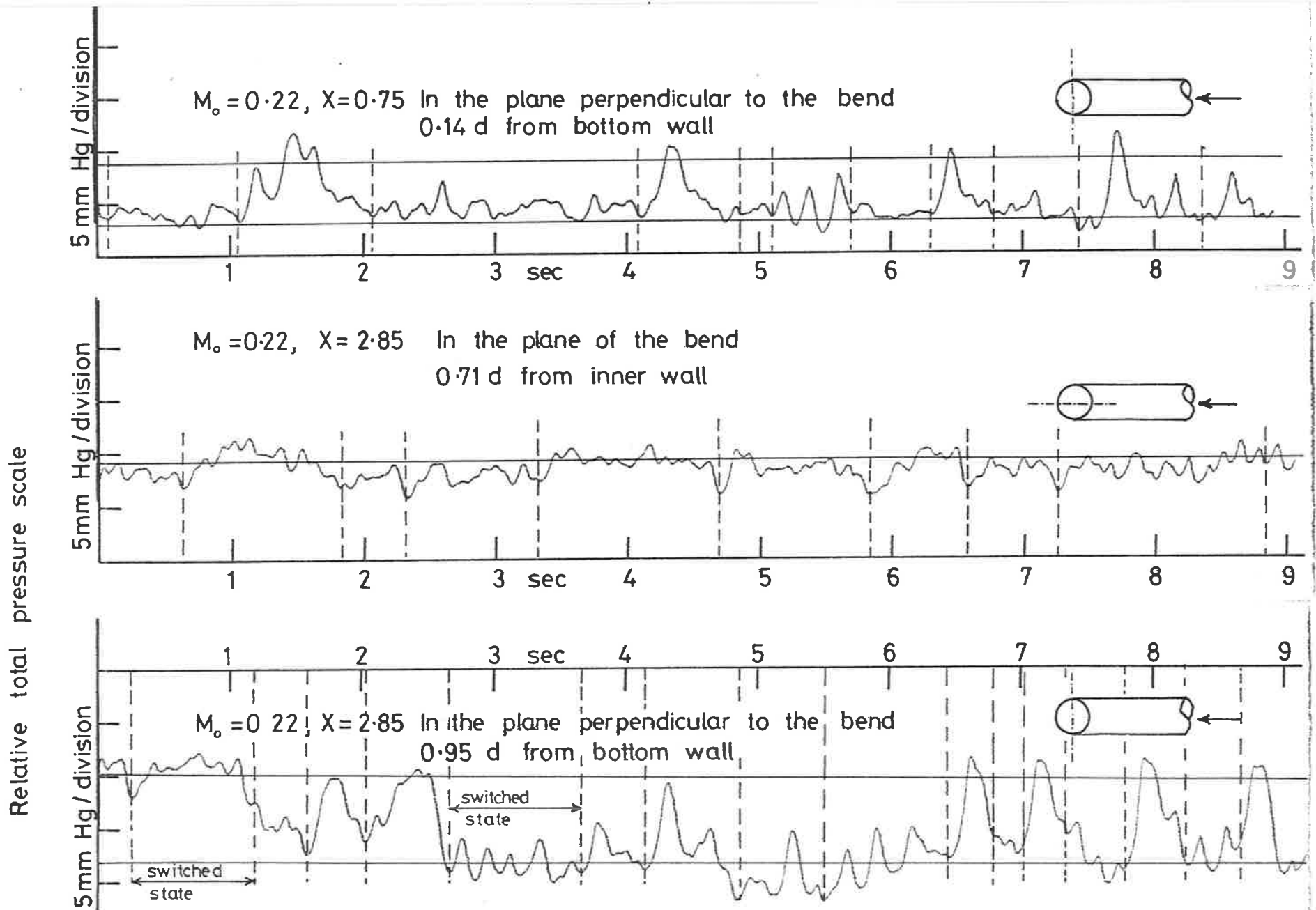
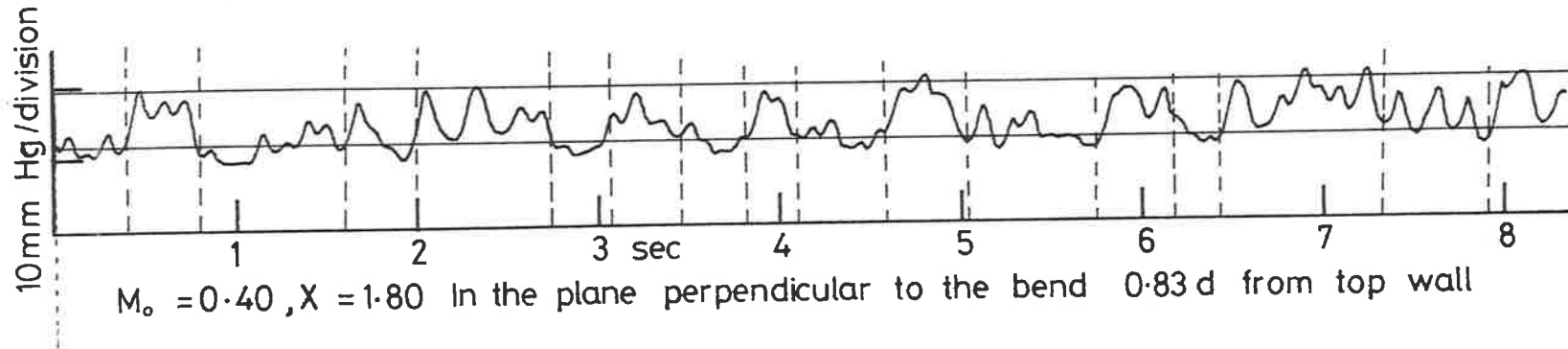


FIGURE 4.4(b) TIME HISTORY OF VELOCITY VARIATION



Relative total pressure scale

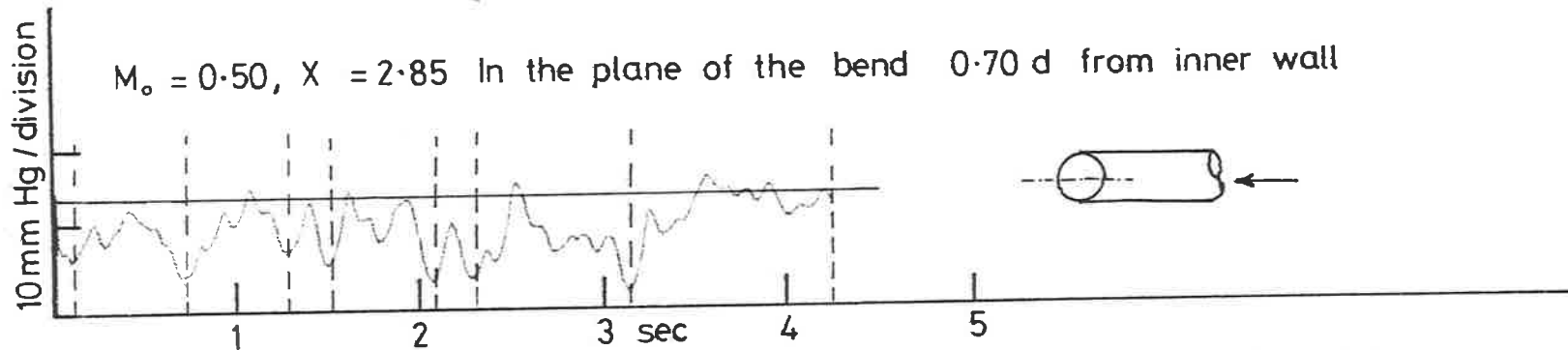
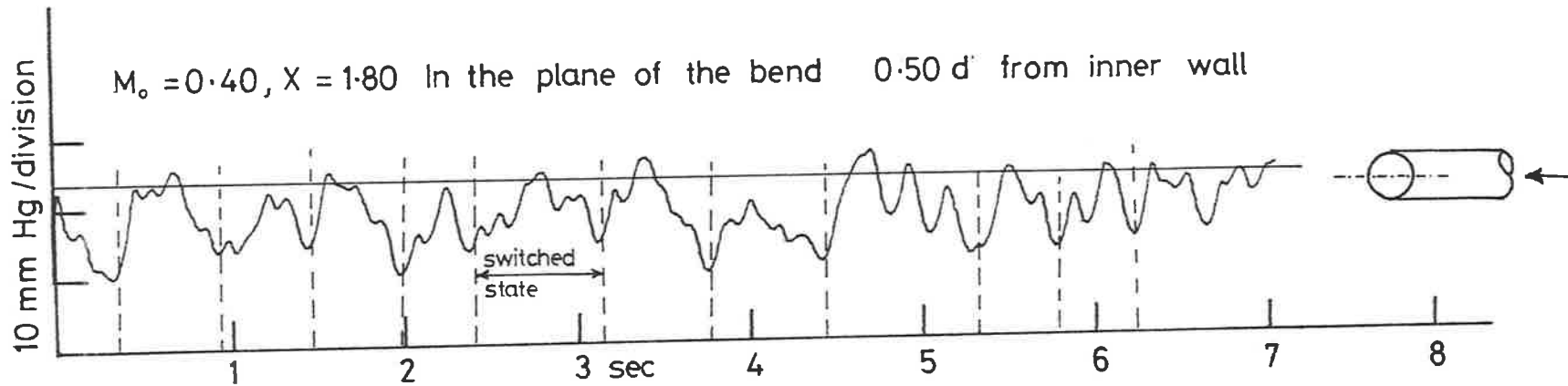


FIGURE 4.4(c) TIME HISTORY OF VELOCITY VARIATION

$X = 0.50$ to $X = 3.45$ in the coordinate system used here).

For the two-dimensional mitred bend, the static pressure drops sharply near the separation point (the inner edge of the bend), is roughly constant along the length of the separated region, reaches its minimum value upstream of the reattachment point and rises steeply to a maximum value downstream of reattachment. At the reattachment point itself the static pressure has increased above the minimum by about 71% of the overall rise. Heskestad's data and the measured axial variation of static pressure on the inner wall of the bend in the present work are shown in Figure 4.5. Assumption of similar behaviour in the two cases leads to an estimate for the location of the reattachment point for the circular pipe of $X \approx 1.3$.

Tunstall and Harvey's (1968) investigation indicates reattachment on the inside of their 90° mitred bend in a pipe of circular cross-section at $X \sim 1.25$. It can therefore be concluded that in the present experiments the separation on the inside of the bend extends from $X = 0.50$ to $X = 1.25 - 1.30$. It will be seen later that this conclusion is supported by the pressure fluctuation measurements.

The axial variation of static pressure, in the present experiments, along lines on the inside and outside walls of the bend and along lines in the plane normal to the bend are shown in Figure 4.6. As far as the separation in the outer corner is concerned, these data do not give any clear indication of the positions of the separation and reattachment points.

4.2.3 The Wall Pressure Field

The power spectral density ϕ_p of the wall pressure fluctuations has been measured at various flow speeds, at various axial and circumferential positions upstream and downstream of the bend. The data are presented in the form of the non-dimensional power spectral

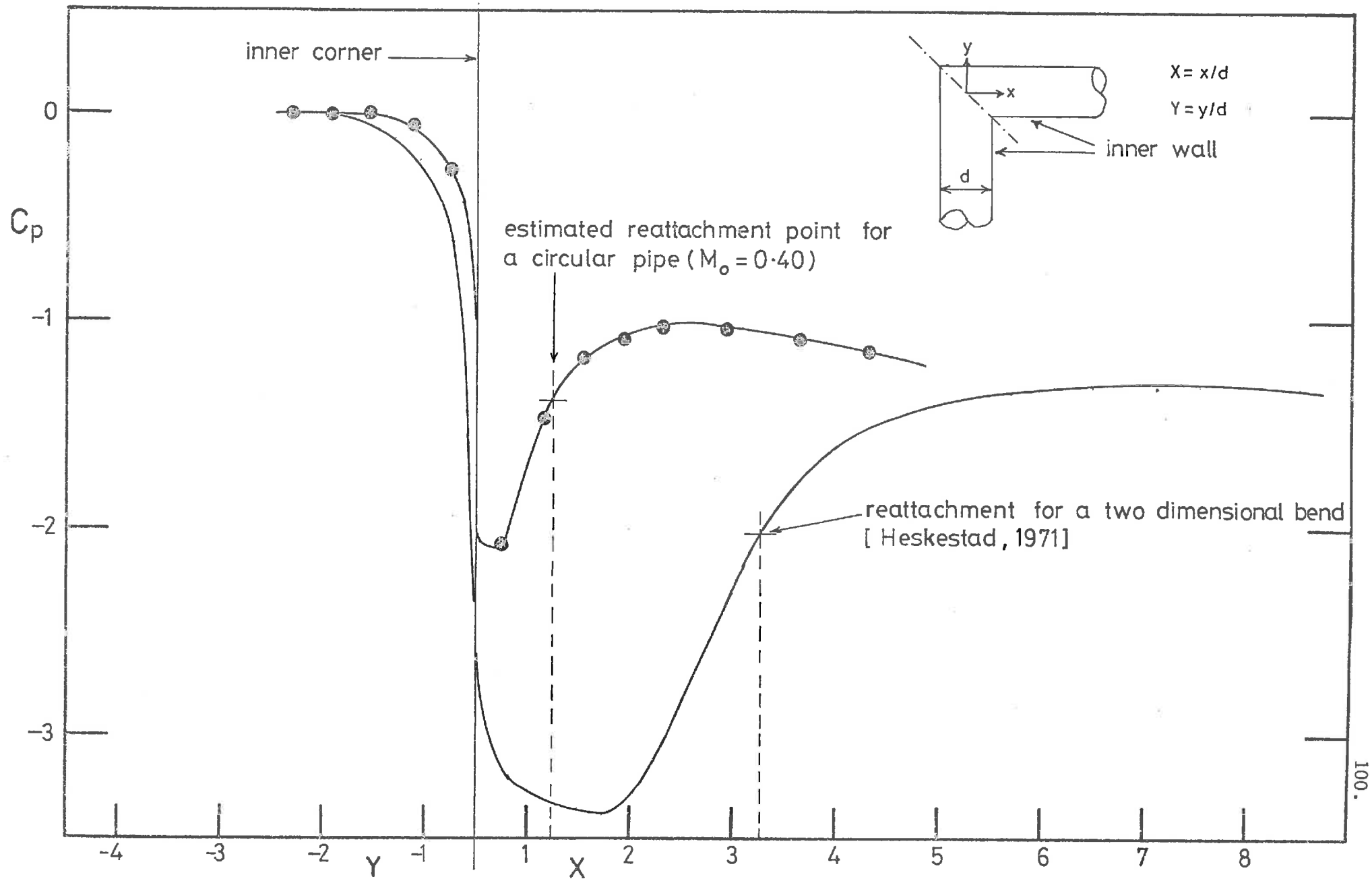


FIGURE 4.5 AXIAL VARIATION OF STATIC PRESSURE ALONG THE INNER WALL

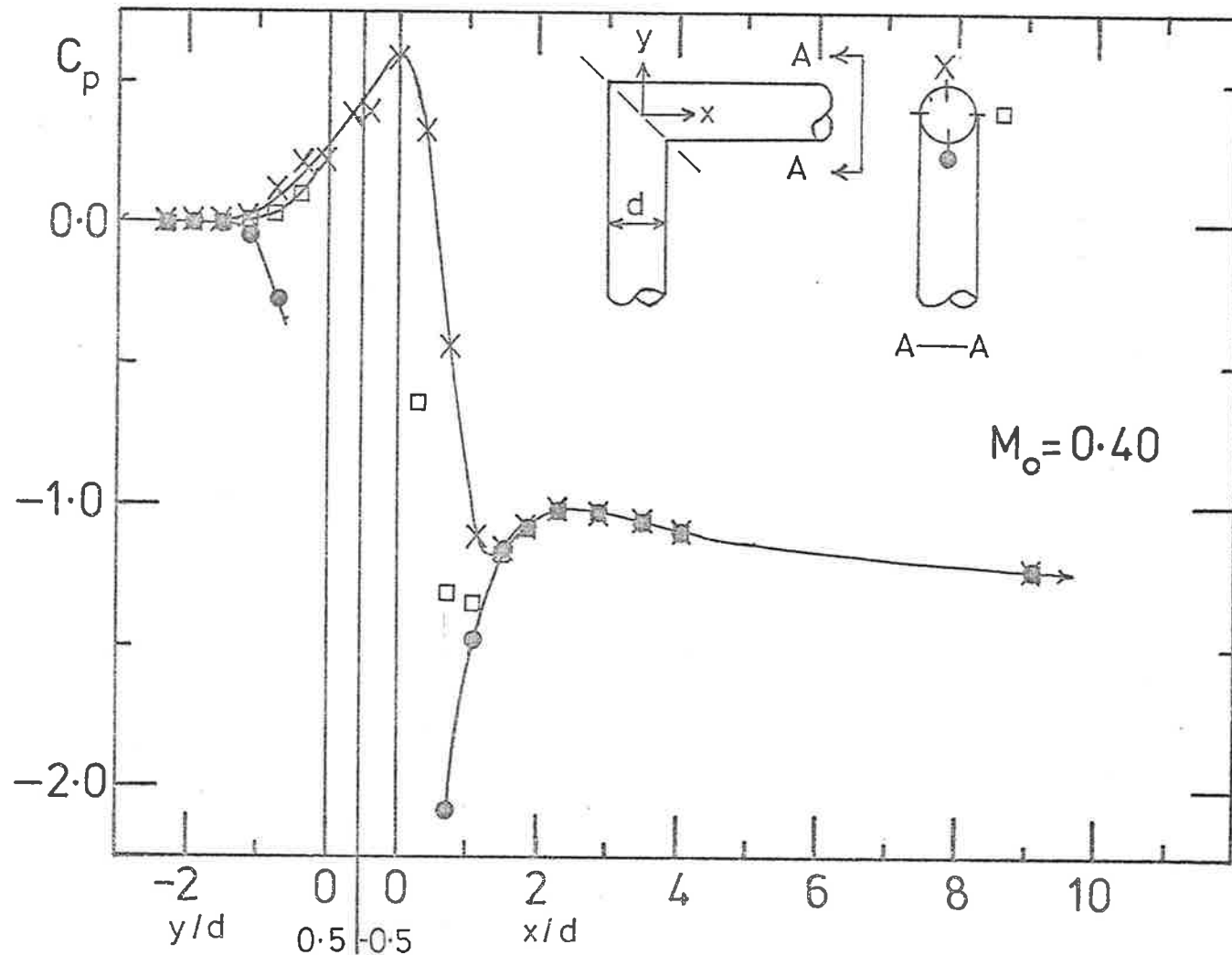


FIGURE 4.6 AXIAL AND CIRCUMFERENTIAL STATIC PRESSURE VARIATION

density $\phi_p = \phi_p U_o / q_o^2 a_i$, as a function of Strouhal number, $\Omega = \omega a_i / U_o$, where $q_o^2 = \frac{1}{2} \rho_f U_o^2$, ρ_f is the density of fluid in the pipe, ω is the circular (radian) frequency, and U_o is the mean centre-line flow velocity at positions where the flow is fully-developed (away from the disturbance).

Typical results, for $M_o \sim 0.40$, are presented in Figure 4.7 for the non-dimensional spectra of the wall pressure fluctuations on the inner wall. At the downstream positions $9 < X < 14$ (where the flow is axisymmetric, but an undisturbed mean flow profile has not been re-established) and $X = 52.8$ (where an undisturbed profile has been re-established) the spectral densities of the wall pressures are circumferentially uniform but are still in excess of those of undisturbed turbulent pipe flow. The spectra of wall pressure fluctuations in the test section ($X \geq 52.8$) are discussed in detail in the next section. The excess there can be attributed to acoustic waves generated by the flow disturbance in the vicinity of the bend itself. This is discussed in Chapter 6. Close to the bend, $0 < X < 4$, where the flow is strongly influenced by the separation bubble on the inner wall, there are large circumferential variations in spectral density, typically by one order of magnitude. The spectral density values generally in this region are greater than those for undisturbed pipe flow by a factor of the order of 10^4 . This is illustrated by the spectral data in Figures 4.8 to 4.12, for various axial and circumferential positions close to the bend. There is negligible circumferential and axial variation before the bend and the spectral density values in this region are also greater than those for undisturbed pipe flow. This is illustrated in Figures 4.13 and 4.14. This behaviour of the wall pressure spectra is typical of all the flow speeds investigated. Figures 4.15 and 4.16 illustrate axial variation along the inner wall after the bend for $M_o \sim 0.20$ and $M_o \sim 0.50$;

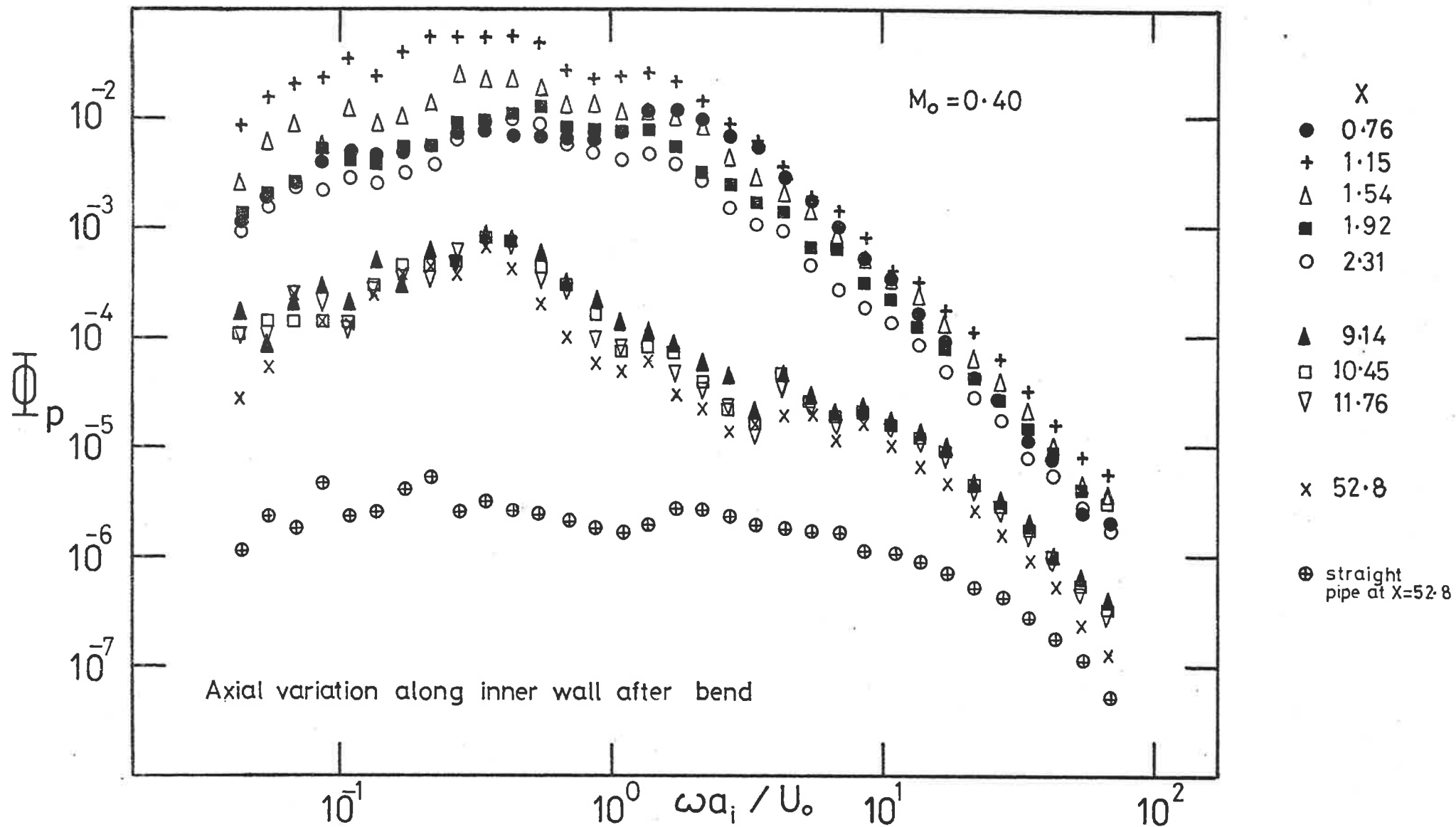


FIGURE 4.7 SPECTRAL DENSITY OF WALL PRESSURE FIELD

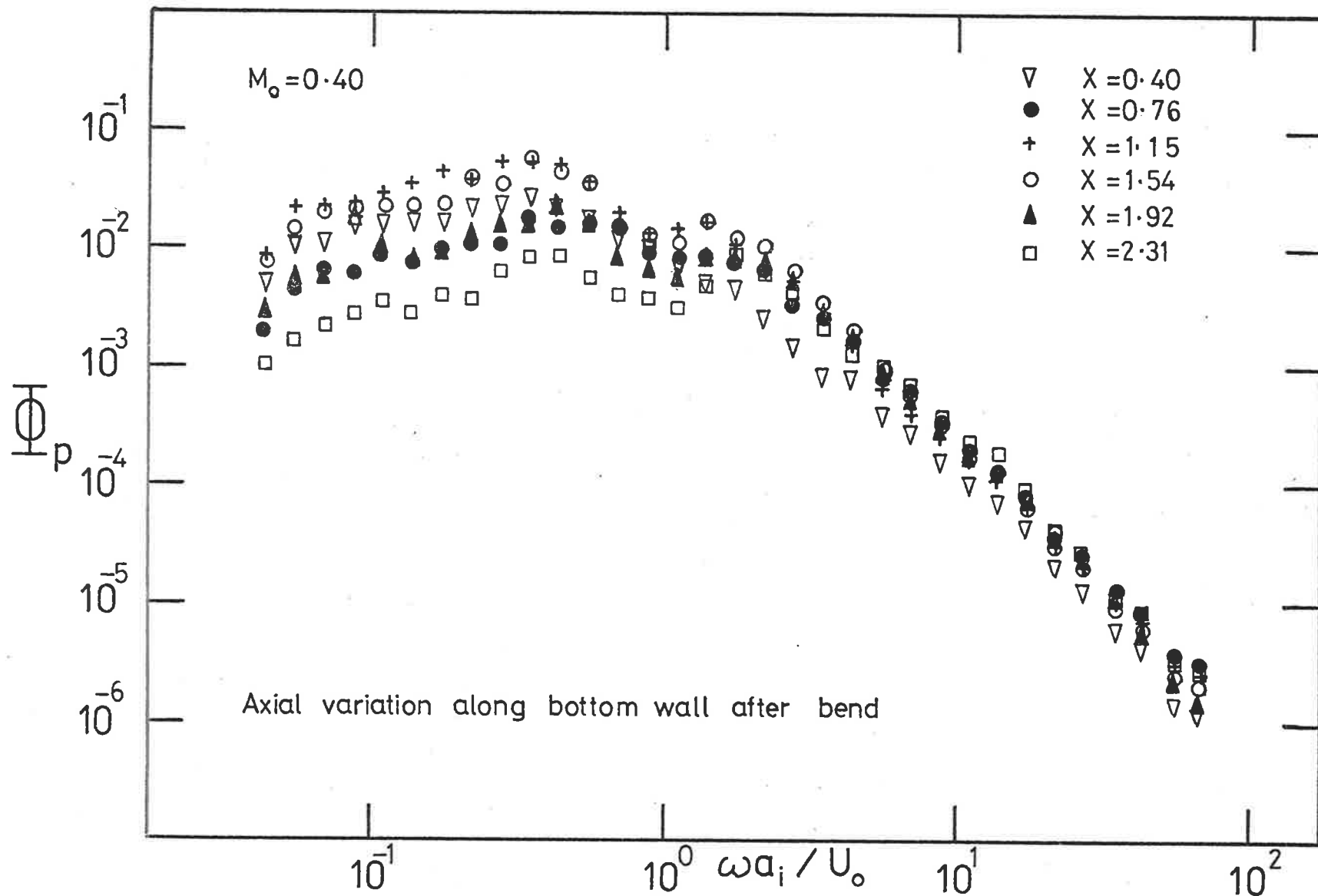


FIGURE 4.8 SPECTRAL DENSITY OF WALL PRESSURE FIELD

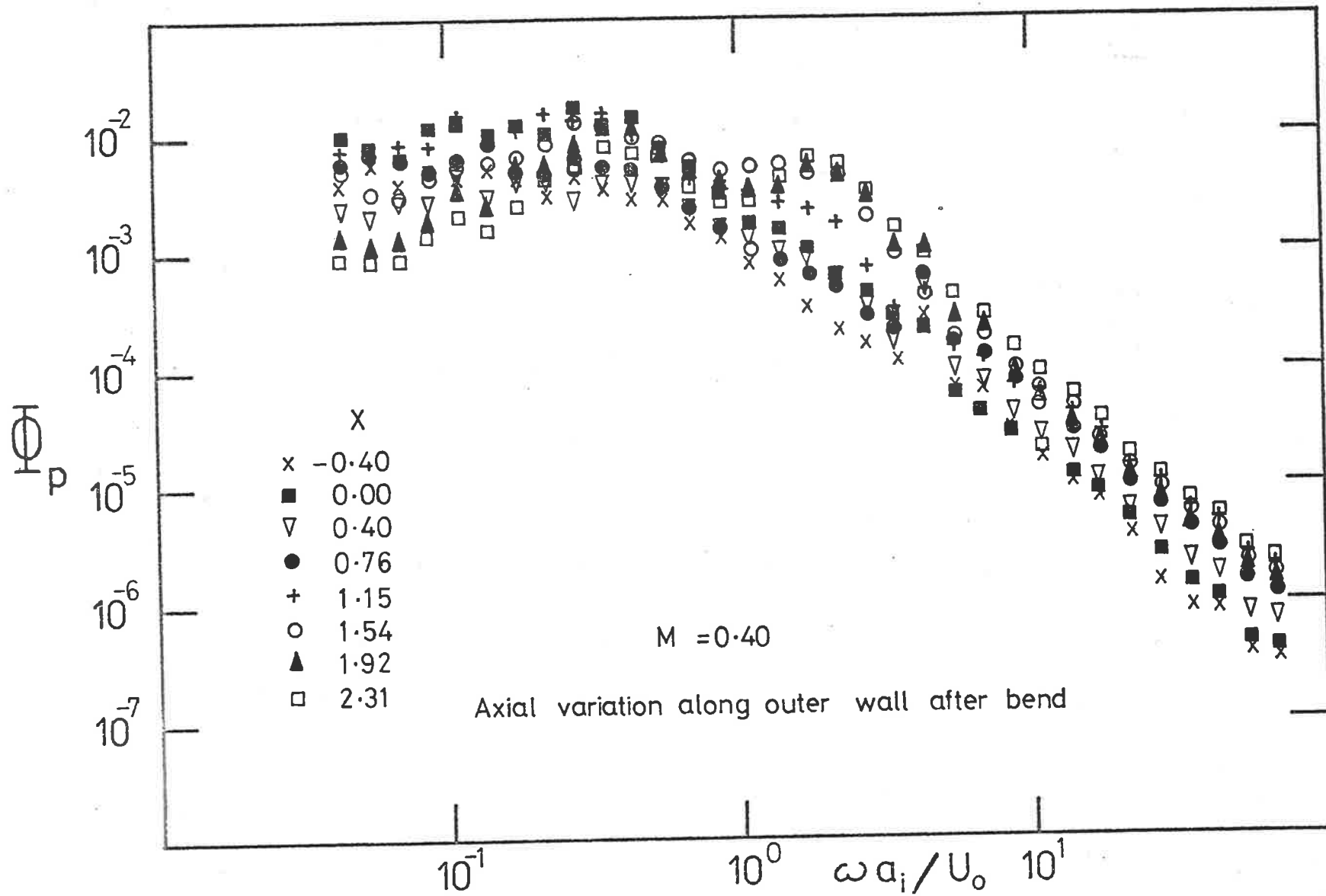


FIGURE 4.9 SPECTRAL DENSITY OF WALL PRESSURE FIELD

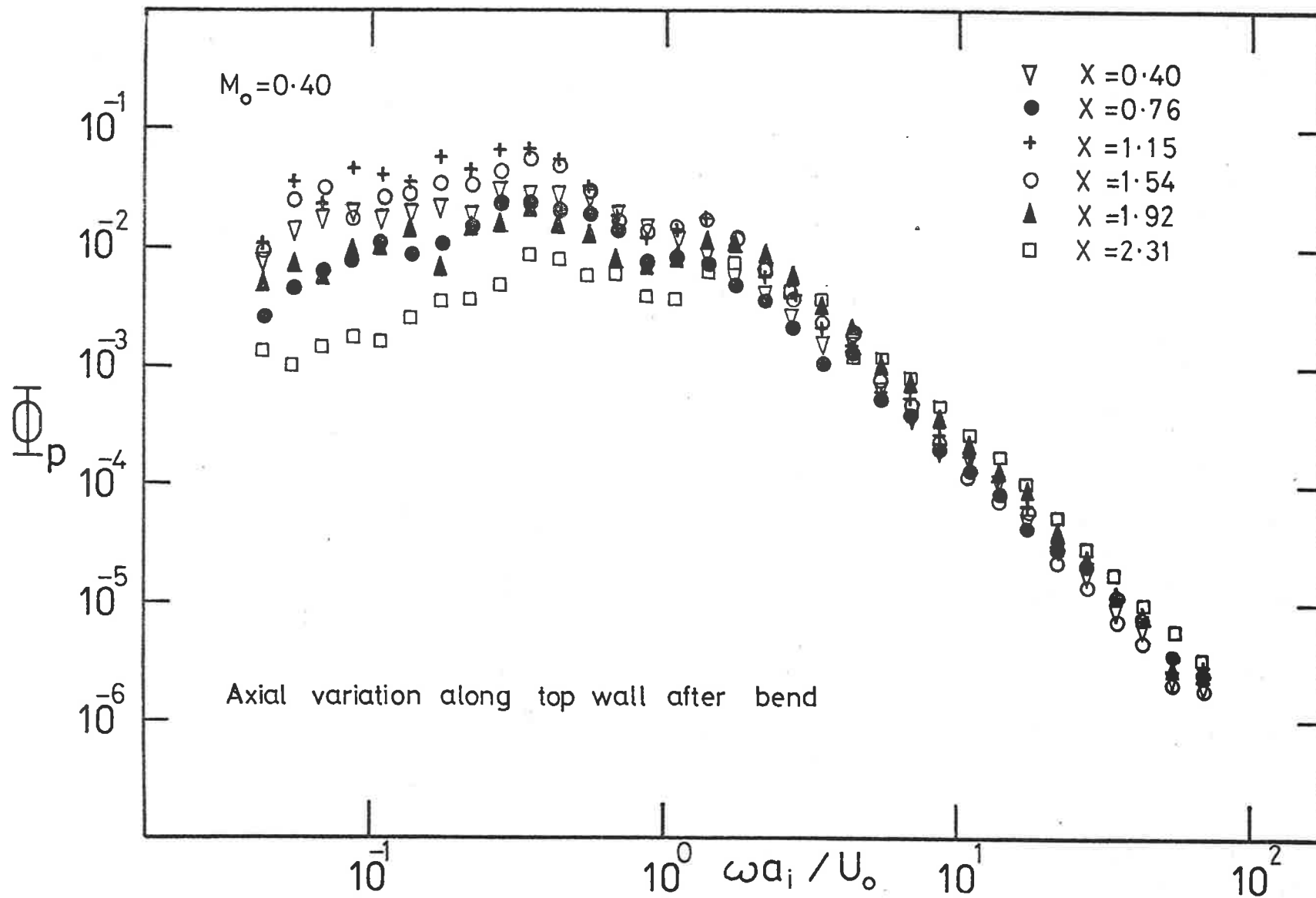


FIGURE 4.10 SPECTRAL DENSITY OF WALL PRESSURE FIELD

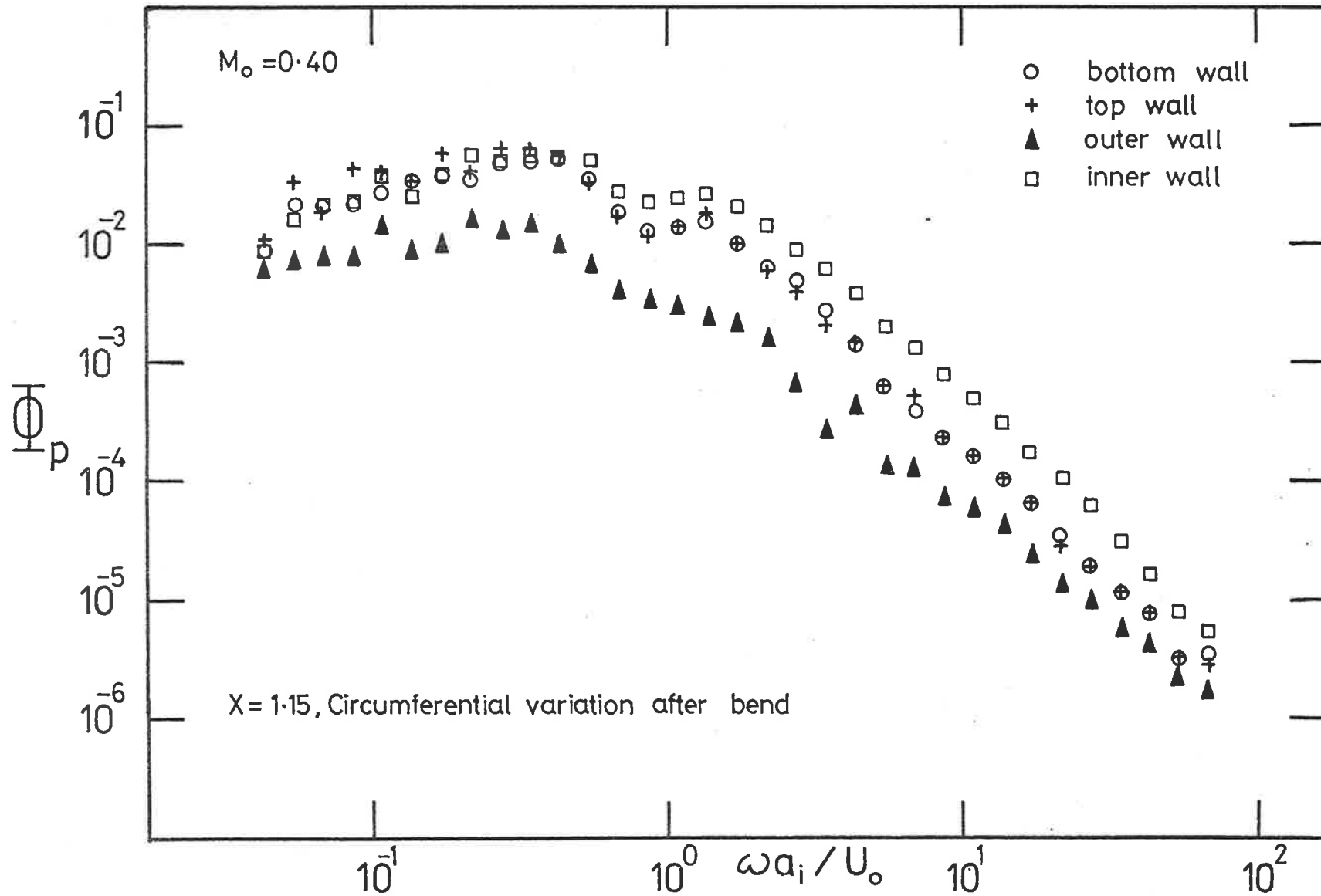


FIGURE 4.11 SPECTRAL DENSITY OF WALL PRESSURE FIELD

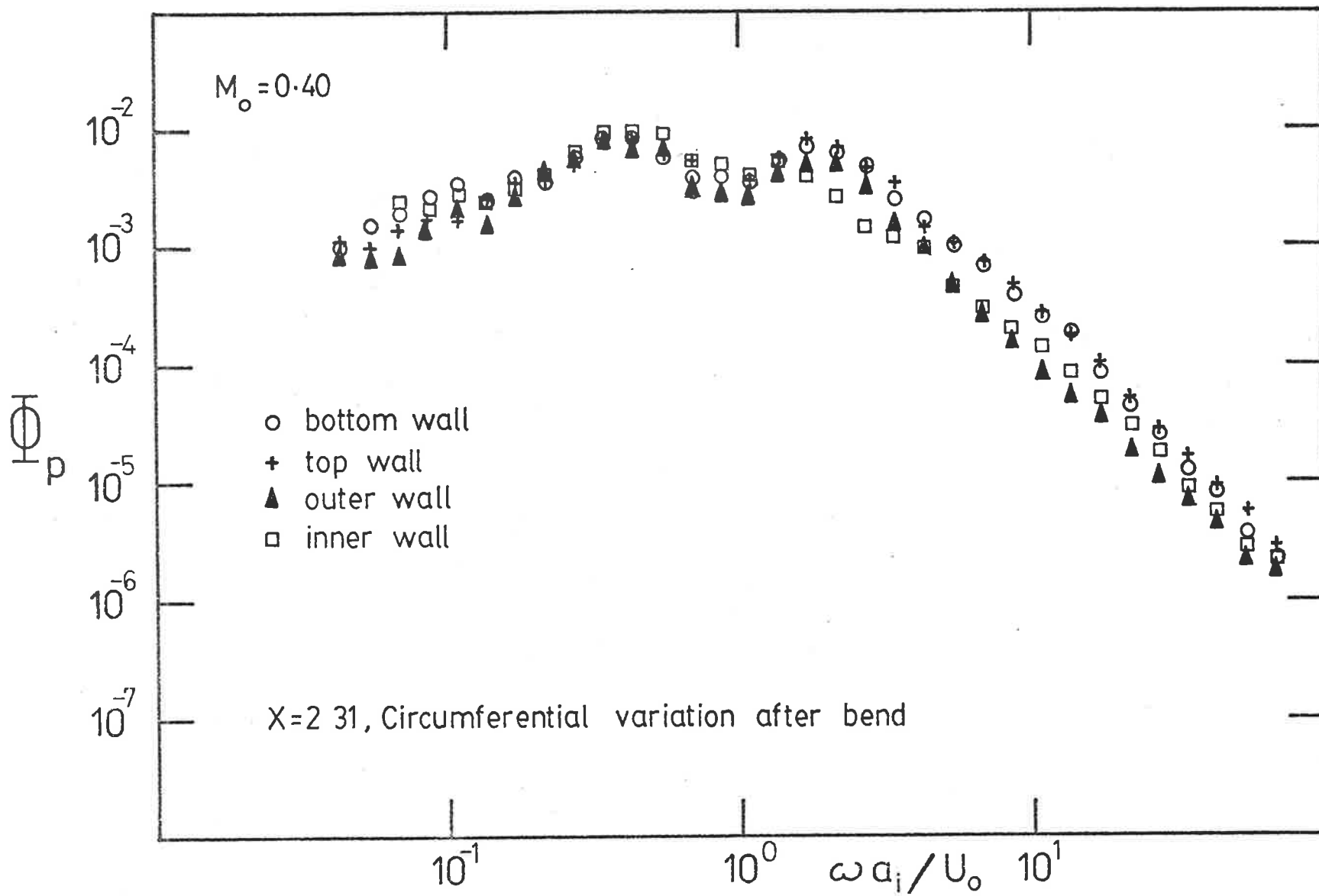


FIGURE 4.12 SPECTRAL DENSITY OF WALL PRESSURE FIELD

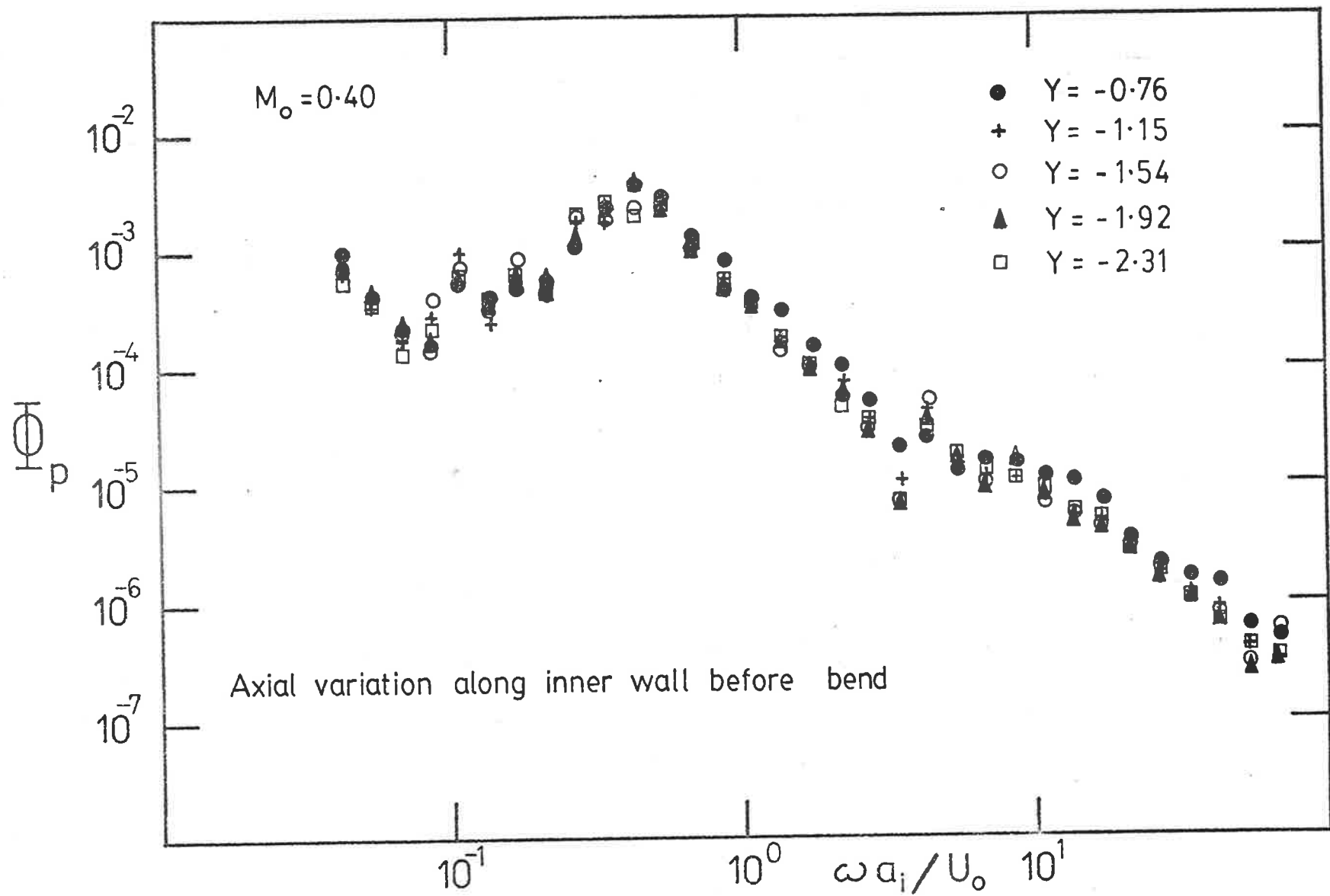


FIGURE 4.13 SPECTRAL DENSITY OF WALL PRESSURE FIELD

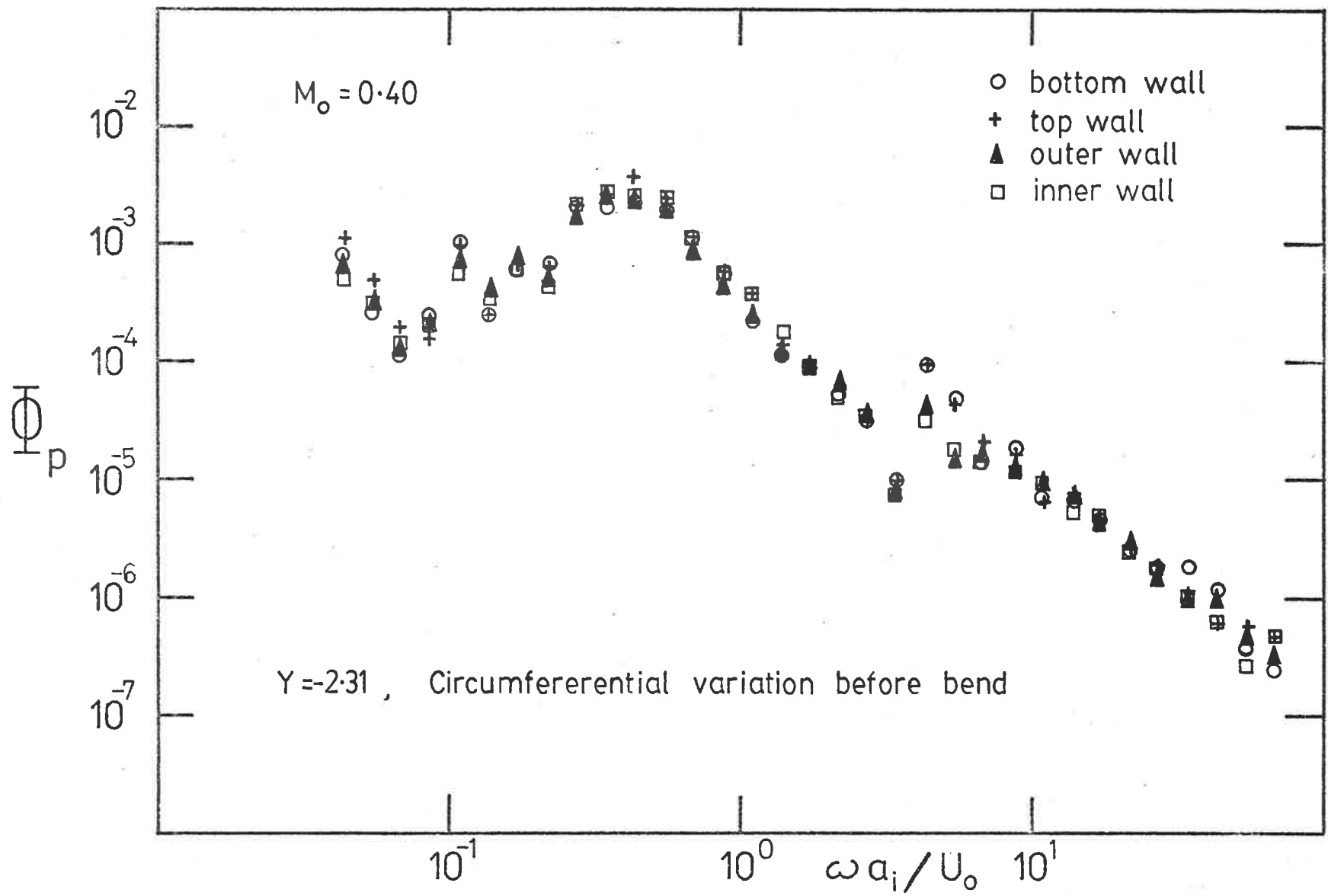


FIGURE 4.14 SPECTRAL DENSITY OF WALL PRESSURE FIELD

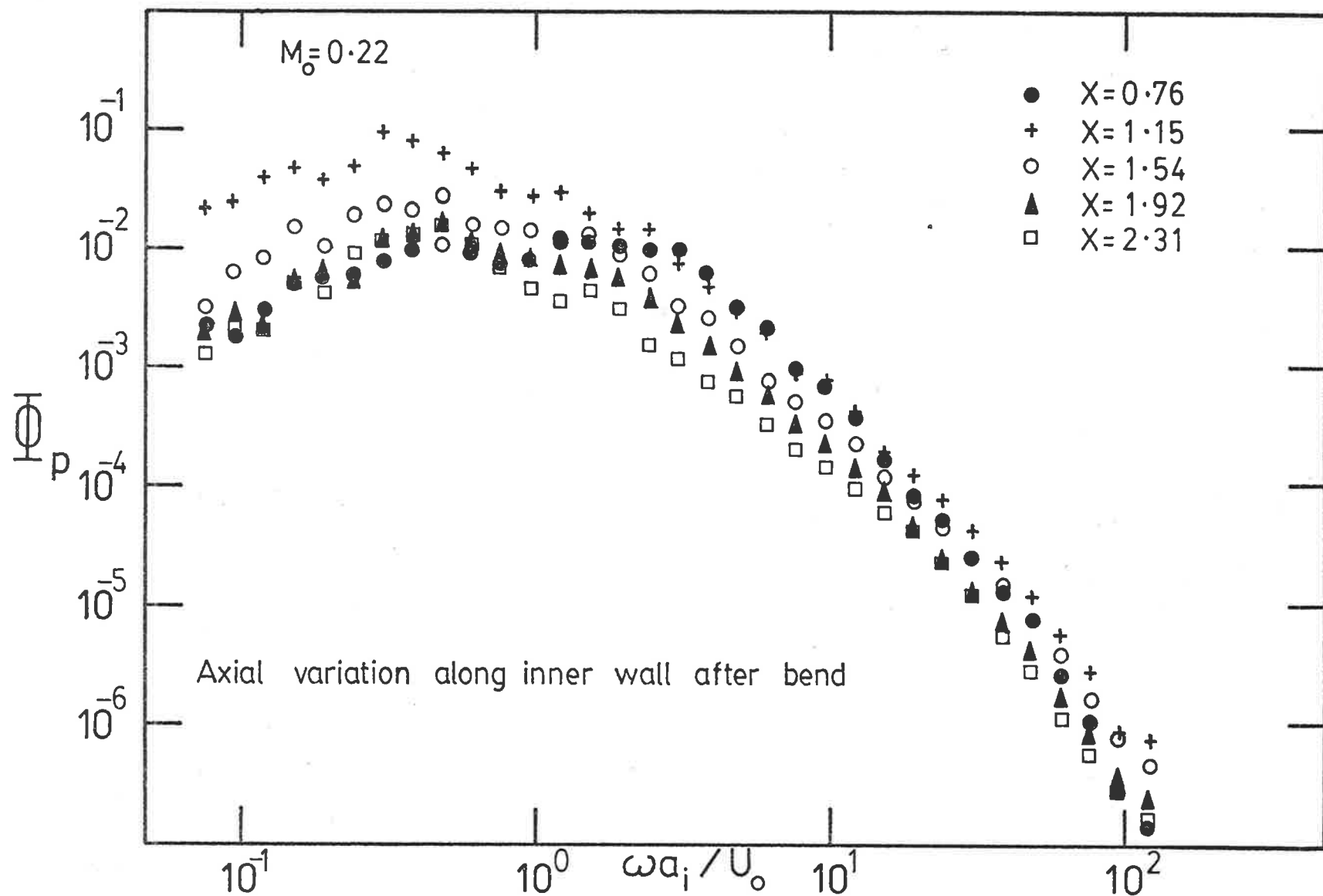


FIGURE 4.15 SPECTRAL DENSITY OF WALL PRESSURE FIELD

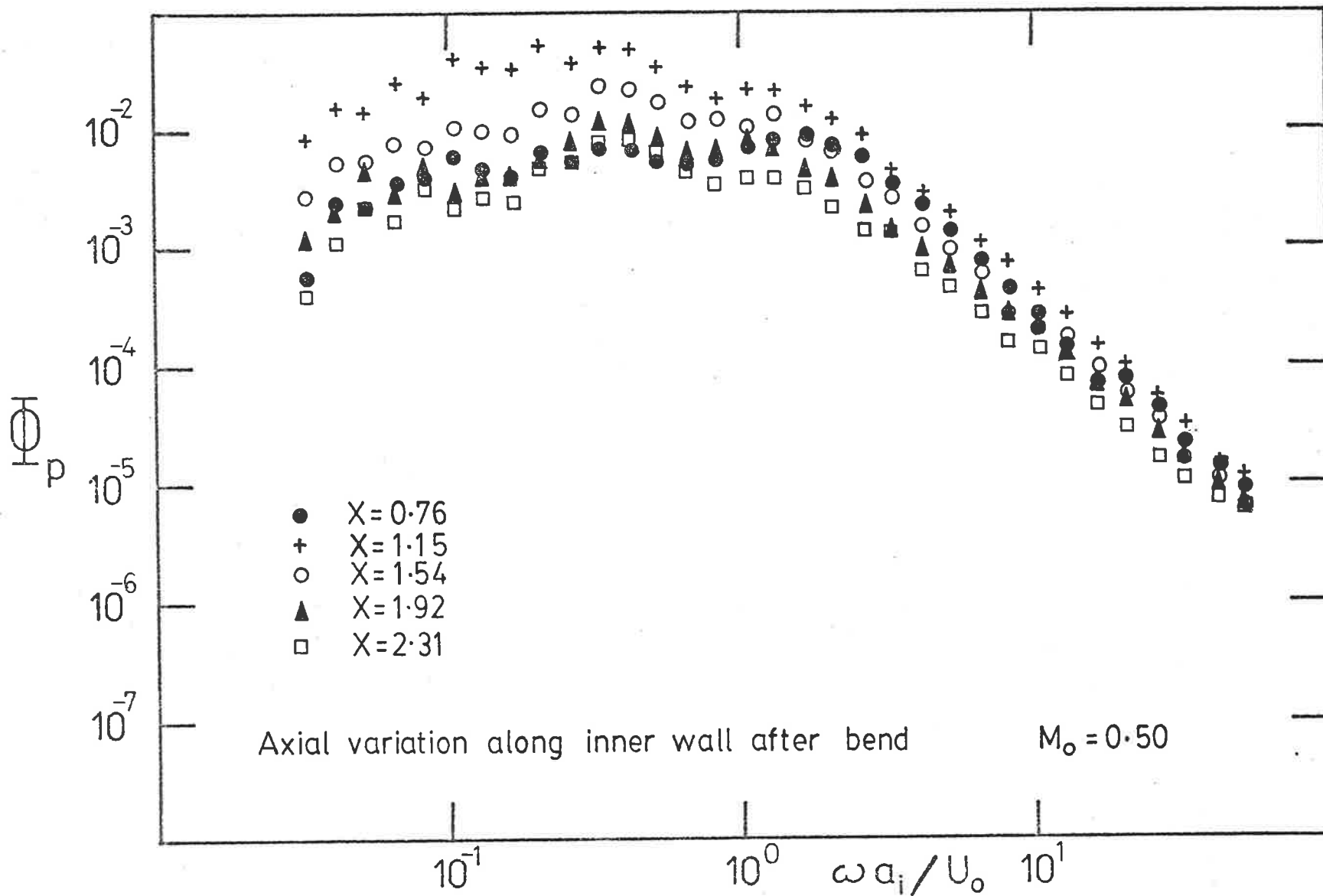


FIGURE 4.16 SPECTRAL DENSITY OF WALL PRESSURE FIELD

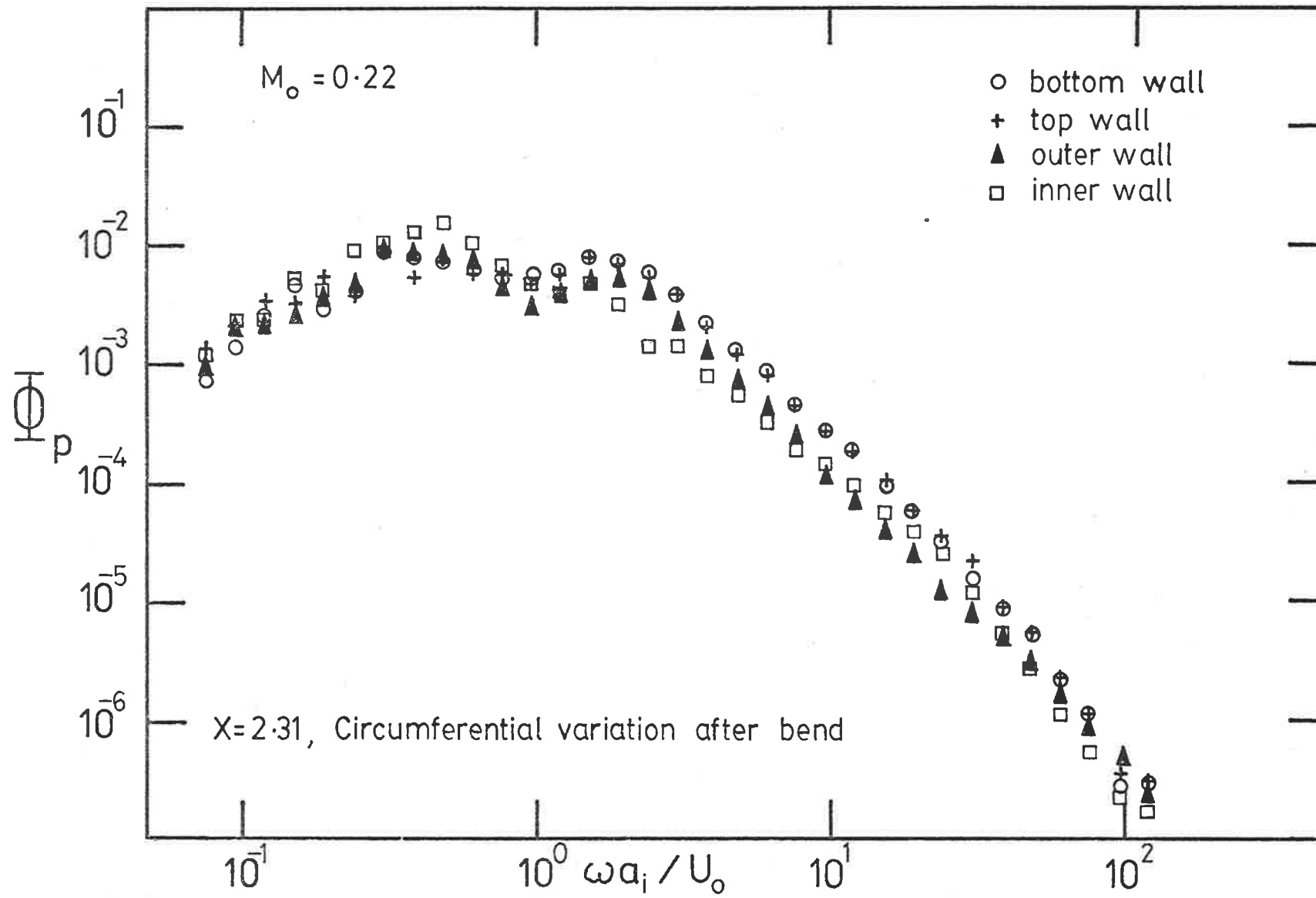


FIGURE 4.17 SPECTRAL DENSITY OF WALL PRESSURE FIELD

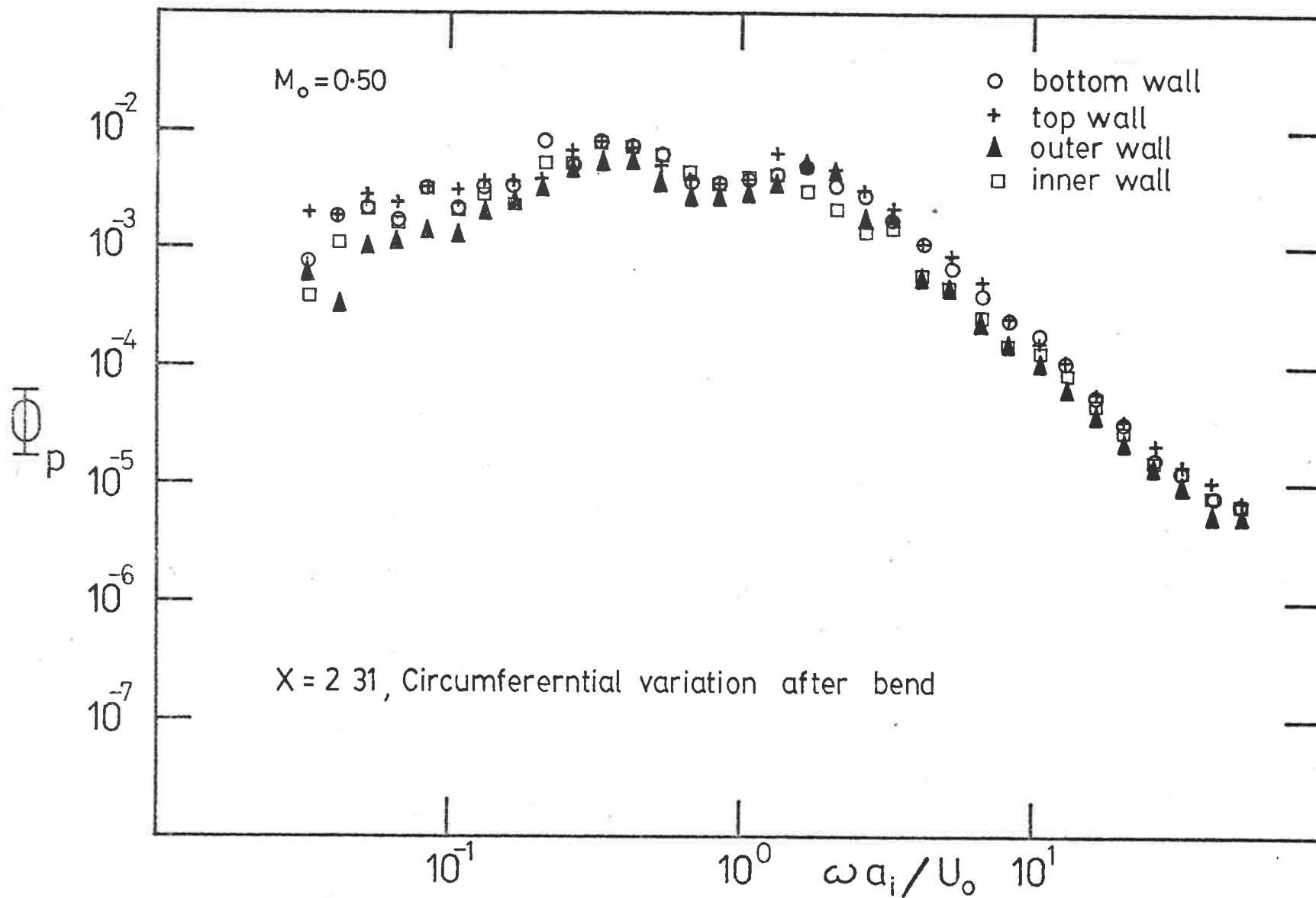


FIGURE 4.18 SPECTRAL DENSITY OF WALL PRESSURE FIELD

Figures 4.17 and 4.18 illustrate circumferential variation ($X = 2.3$) after the bend for $M_0 \sim 0.20$ and 0.50 , and show that they are negligible.

Extensive measurements of the overall root mean square wall pressure fluctuations $p' = \overline{(p^2)}^{1/2}$ were obtained for several flow speeds. Measurements of (p'/q_0) at four different axial positions are presented in Figure 4.19, for the 90° mitred bend. The r.m.s. pressure fluctuations, when non-dimensionalized by the centreline dynamic pressure at $X = 52.4$ (p'/q_0), were found to be essentially independent of flow speed at all axial positions. This is discussed in Section 4.4 where the flow dependence of the wall pressure fluctuations associated with the 90° mitred bend is discussed in considerable detail.

The overall r.m.s. pressure fluctuations show similar behaviour to that of the spectral density. In Figure 4.20, the variation of p'/q_0 with axial position at various circumferential positions is shown. Since p'/q_0 is essentially independent of flow speed the values shown are averages for the various flow speeds. At all circumferential positions, p'/q_0 has a maximum for X in the range of 1.1 to 1.3, that is near the position where the static pressure measurements indicate that reattachment occurs on the inner wall of the bend. Previous measurements of wall pressure fluctuations in separated flows, summarised by Mabey (1972), generally reveal the occurrence of a maximum value of p'/q some distance upstream of the re-attachment point (where q is the dynamic pressure based on a freestream velocity). On average the maximum value of p'/q occurs at a distance downstream of separation of about 0.84 times the streamwise length of the separation bubble. Looking specifically at the variation of p'/q_0 on the inner wall of the bend in the present experiments, the peak value occurs at $X = 1.15$. Applying the preceding result based on the data cited by Mabey, the corresponding reattachment

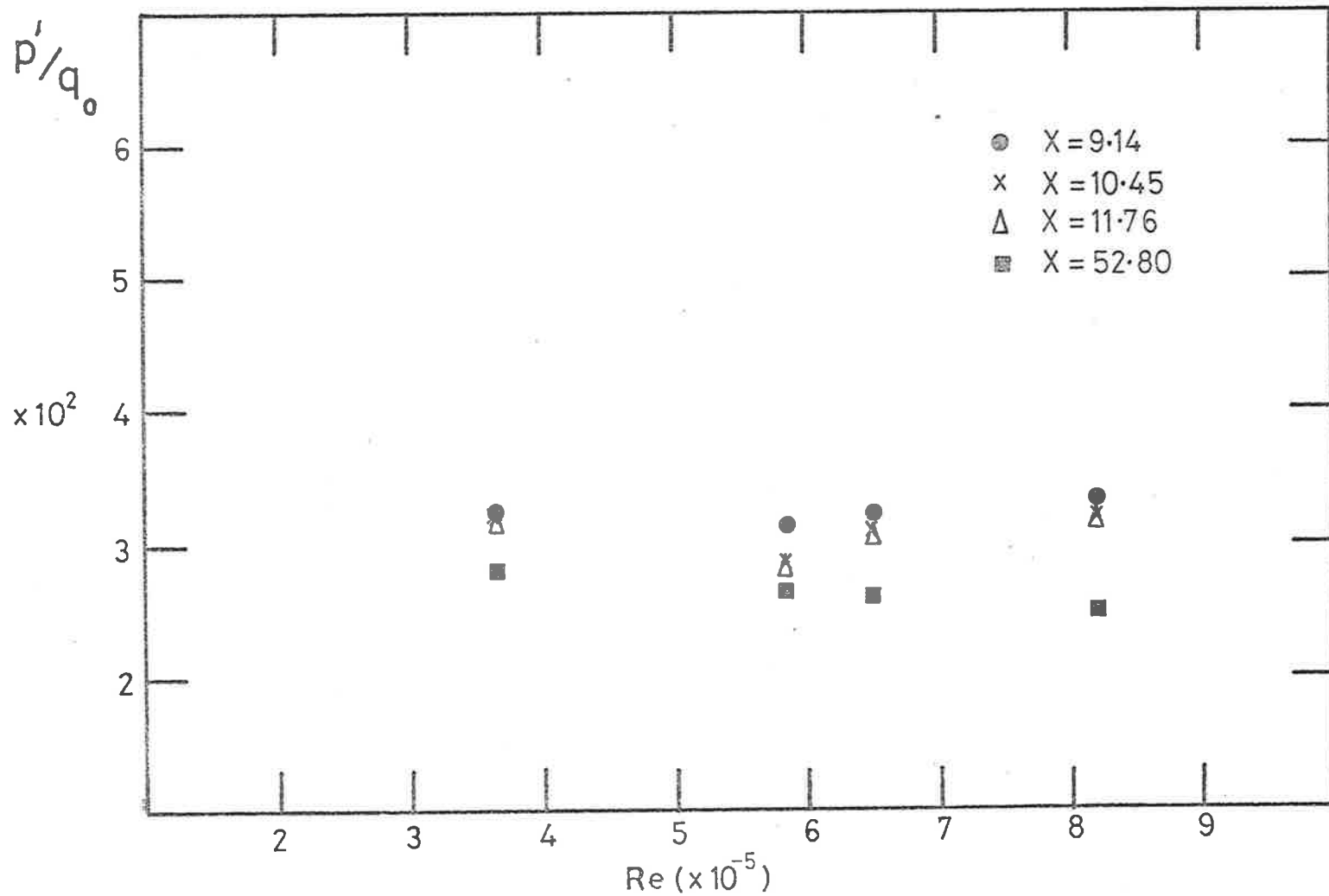


FIGURE 4.19 VARIATION OF p'/q_0 WITH REYNOLDS NUMBER

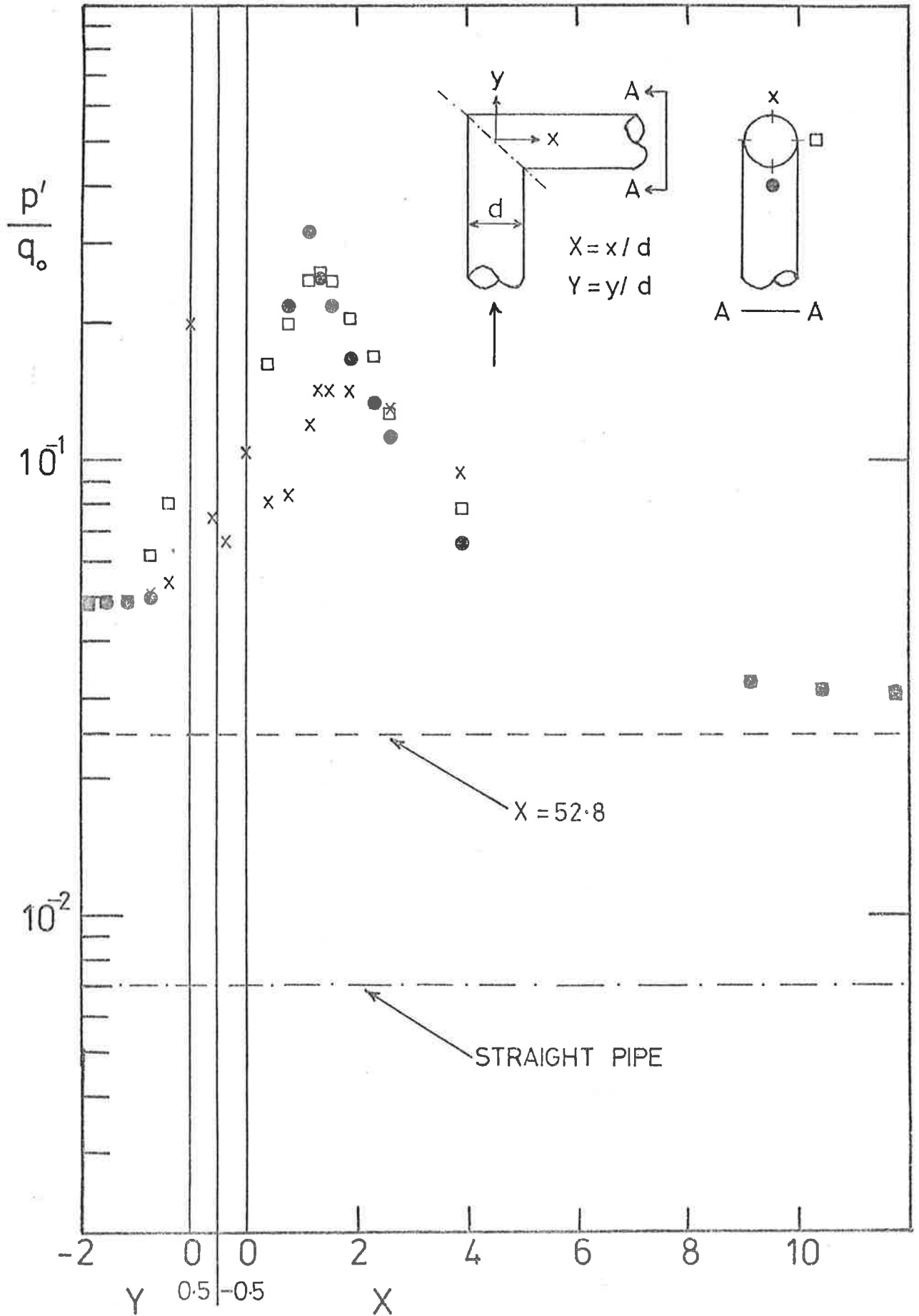


FIGURE 4.20 ROOT MEAN SQUARE WALL PRESSURE FLUCTUATIONS

position would be $X = 0.50 + (1.15 - 0.50)/0.84 = 1.27$, which is in good agreement with the deductions from the static pressure measurements.

Figure 4.20 also shows that p'/q_0 values for the outer wall have maxima at $X = 0$ and at $Y = 0$. The former, in the light of the foregoing, might be identified with the reattachment position. But there is no direct evidence (and certainly none from the data considered by Mabey, which are for the most part for flows in which a freestream can be identified) which would allow the latter to be identified with the position of separation, although it must be close to it.

It might also be noted that the maximum p'/q_0 value observed here is 0.33, considerably greater than the highest value (~ 0.1) in the data summarised by Mabey.

Figures 4.21 and 4.22 illustrate the circumferential variation in p'/q_0 for several axial positions upstream and downstream of the bend. From Figure 4.21 it can be seen that there is negligible circumferential variation before the mitre and at $Y = -0.76$ the effects of the bend start to appear. From Figure 4.22, it can be seen that p'/q_0 is a maximum along the inner wall ($\Theta = 180^\circ$) for $X < 1.28$ (regions inside the separation bubble), and that beyond $X = 1.28$ the circumferential variation progressively decreases.

The frequency ranges from which the dominant contributions to the mean square wall pressure come can be highlighted by plotting the spectral densities as $\Omega \Phi_p$ or $\Omega \Phi'_p = \omega \phi_p / \overline{p^2}$ (to linear scales) against Ω (to a logarithmic scale). The areas under the curves then directly represent contributions to the mean square pressure; in the former case the total area is $\overline{p^2}/q_0^2$ and in the latter unity. Such plots are shown in Figure 4.23 for the inner wall at various positions downstream of the mitred bend.

At $X = 52.8$, the wall pressure field can be identified as that of fully-developed turbulent pipe flow with a superimposed

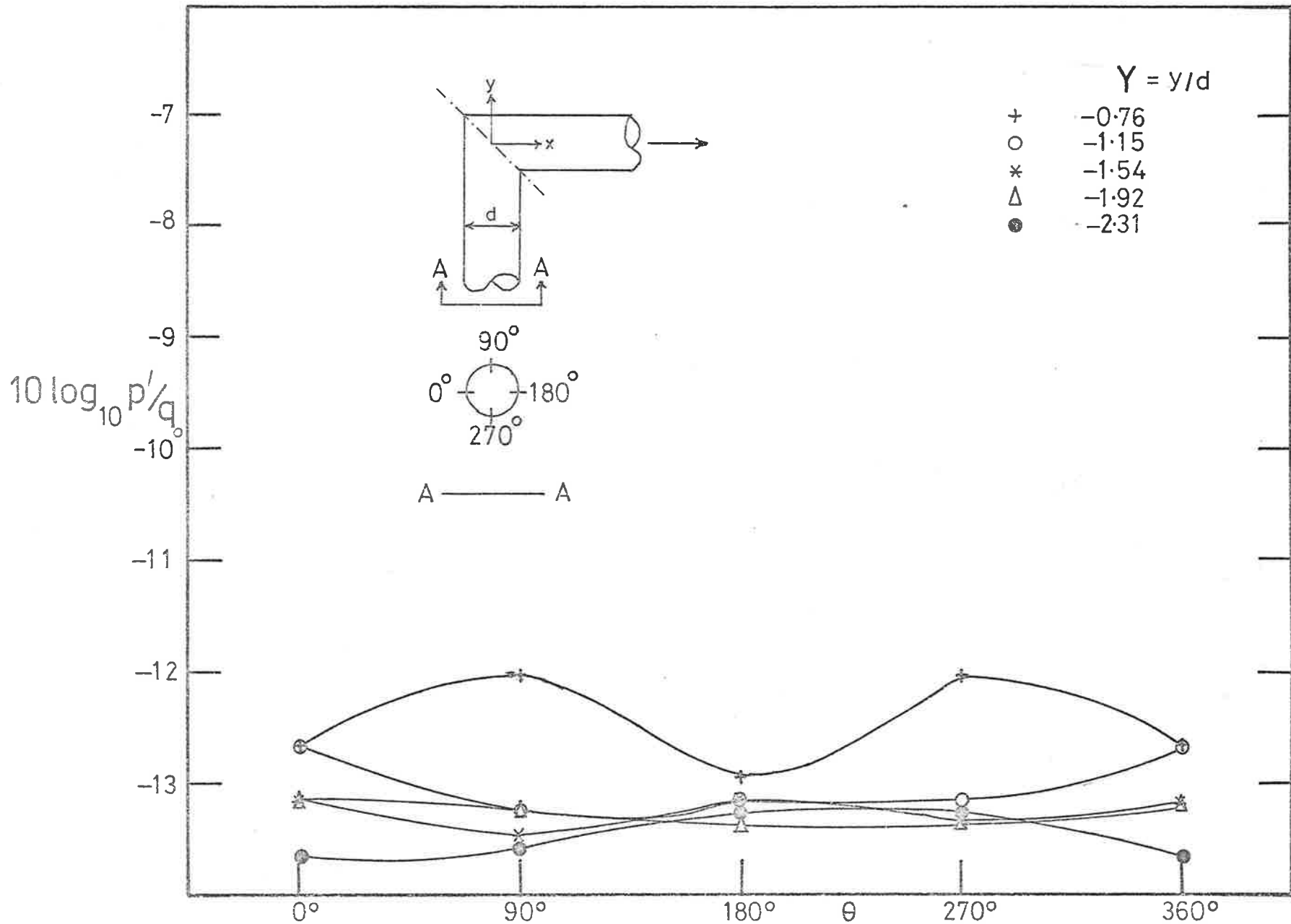
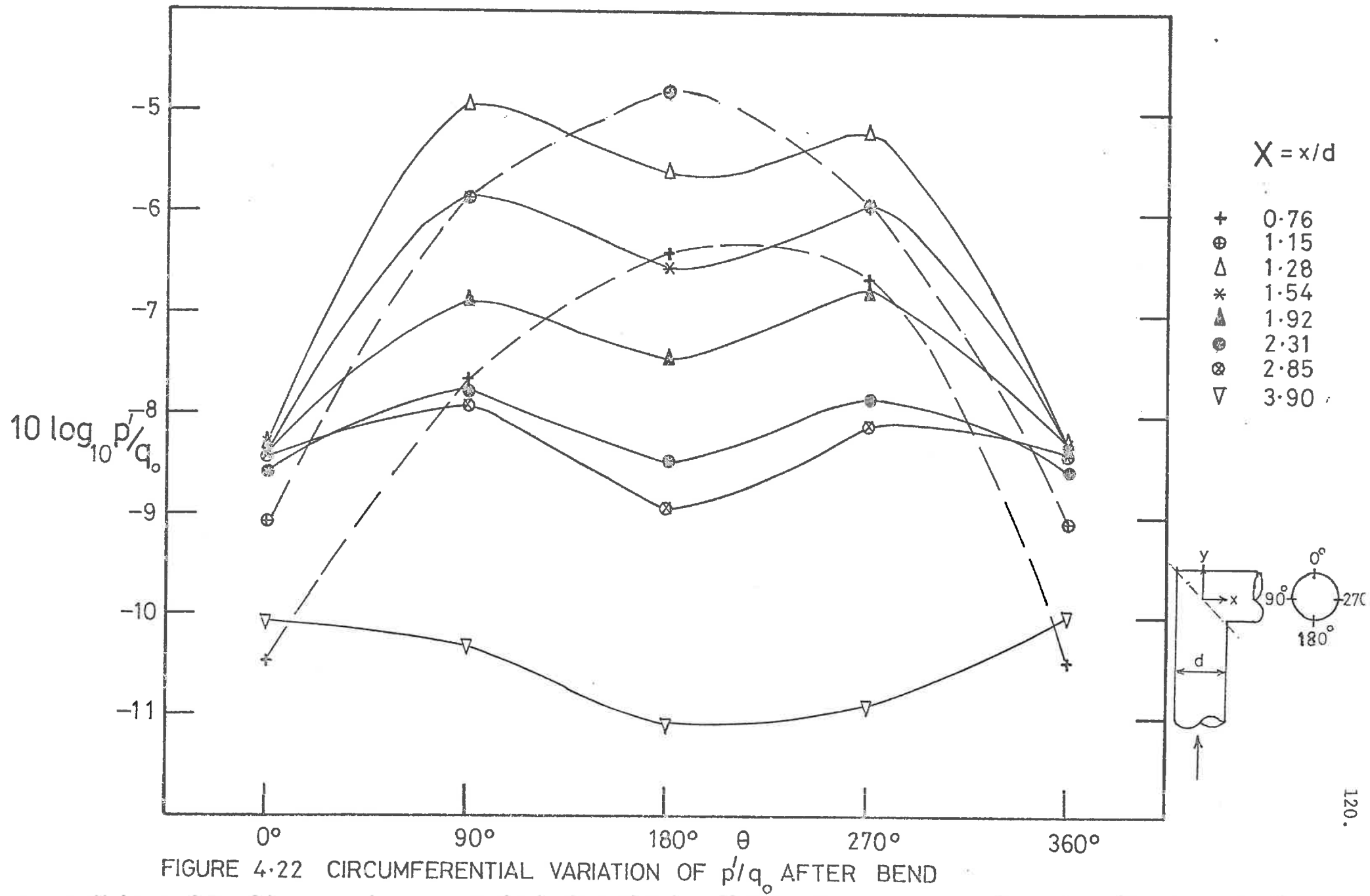


FIGURE 4-21 CIRCUMFERENTIAL VARIATION OF p'/q_0 BEFORE BEND



acoustic field generated by and radiated from the flow disturbance in the immediate vicinity of the bend. But it is clear from the wall pressure spectra and the r.m.s. pressure fluctuations that the acoustic contribution outweighs the basic pipe flow contribution.

For $M_0 = 0.40$, the cut-off frequencies for the (1,0) and (2,0) acoustic modes correspond to $\Omega = 4.6$ and 7.6. The presence of these two modes in the pressure field at $X = 52.8$ is indicated by peaks of the weighted spectral density close to these Ω values (and similar indications can be seen in the wall pressure spectra, Figure 4.7). The presence of still higher order modes may also be expected but considering that the modal density of the acoustic modes increases rapidly with frequency and that the data are derived from $1/3$ octave band measurements, one would not expect that higher frequency peaks would be observed. Since for $\Omega < 4.6$ only plane waves can propagate it is clear that the wall pressure field at $X = 52.8$ is dominated by plane acoustic waves. The energy associated with these propagating waves is concentrated mainly at frequencies $\Omega \sim 0.40$ with a minor concentration near $\Omega \sim 1.6$.

However, close to the bend ($X = 1.15$), where there are large additional non-propagating pressure fluctuations, the major energy concentration is at $\Omega \sim 1.6$ and the minor at $\Omega \sim 0.4$. As the measuring point on the inner wall is moved downstream, away from the bend, the relative contribution to $\overline{p^2}/q_0^2$ made by fluctuations with $\Omega < 1$ increases, while that made by fluctuations with frequencies in the range $1 < \Omega < 4.6$ decreases, the decrease being rather more marked at the lower than at the higher end of the range. This behaviour suggests the possibility that the energy concentration at $\Omega \sim 1.6$ close to the bend may be due to the generation in this region of non-propagating higher order modes at frequencies below their cut-off frequencies. These modes would then be attenuated with distance

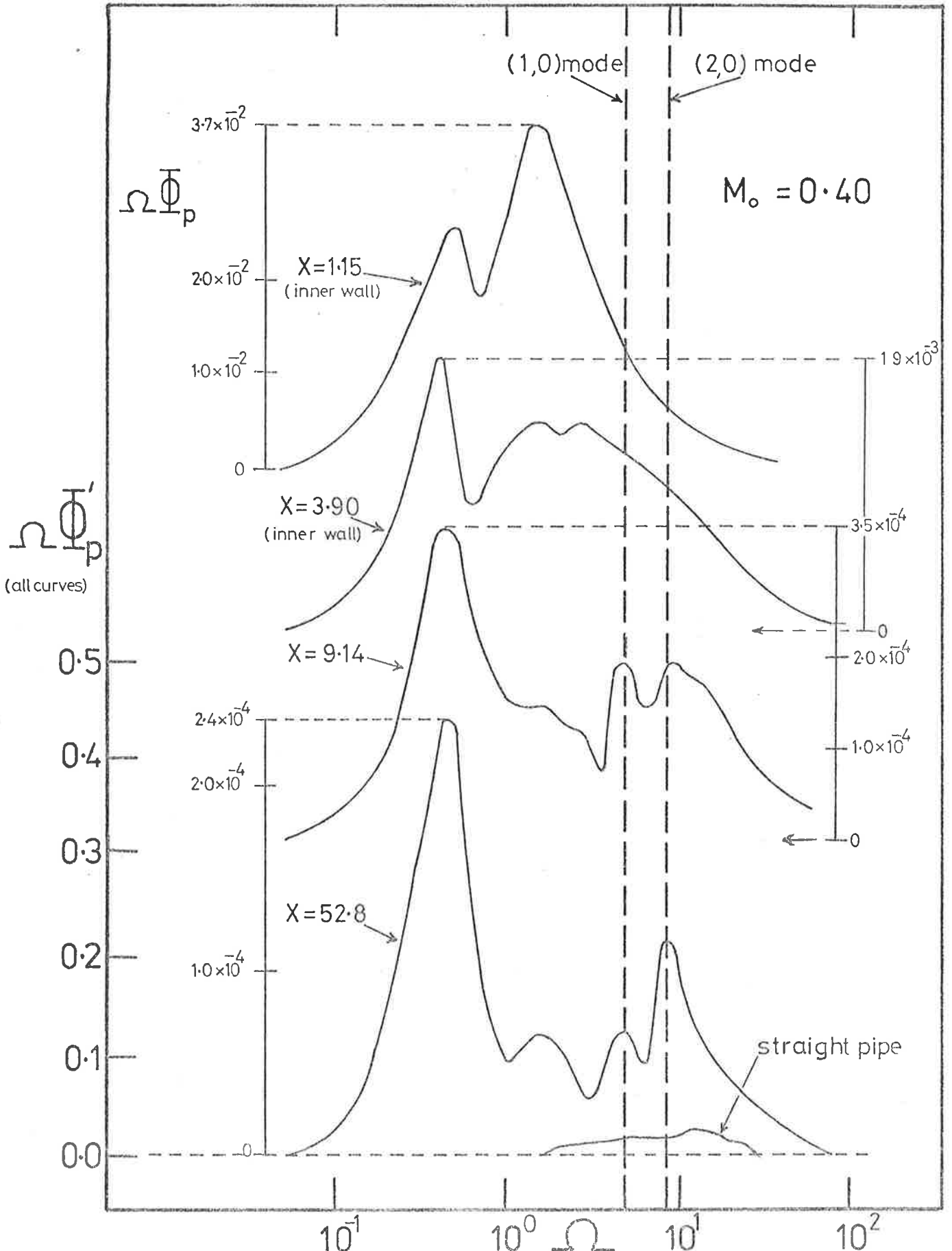


FIGURE 4.23 FREQUENCY WEIGHTED POWER SPECTRAL DENSITY OF Φ_p

downstream, the attenuation rate being greater the further a mode is removed in frequency from its cut-off frequency.

The spatial rate of attenuation of Φ_p in the vicinity of the separation bubble can be obtained from the wall pressure spectra or from Figure 4.23. It has about the same value, 4.7 dB for each pipe diameter increase in x , for all $\Omega < 4.6$. The attenuation rate for non-propagating higher order modes can be calculated on the basis of the solution of the wave equation represented by equations 2.1 and 2.2 or their equivalents for flowing fluid in a cylindrical pipe as given by Mason (1969). For the (1,0) mode the axial attenuation rate is found to be about 30 dB/diameter at $\Omega = 2$ and decreases only slowly as Ω increases towards the cut-off values. It falls significantly only at Ω very close to cut-off and would drop to the experimentally observed value only within a few percent of the cut-off frequency. In view of this disparity between observed and calculated values it is concluded that the major peak in the energy curves at $\Omega \sim 1.6$ in the vicinity of the bend is not due to non-propagating higher-order modes but to non-propagating fluctuations of the type associated with the generation of plane acoustic waves. It follows that for all frequencies $\Omega < 4.6$, the pressure fluctuations near the bend have this latter character.

The frequencies of the peaks at $\Omega \sim 0.4$ and 1.6 are far removed from the frequencies of switching and of oscillation of the separation bubbles from one side of the plane of the bend to the other ($\Omega \sim 0.02$). Tunstall and Harvey (1968), who also found pressure spectra close to the bend to have two peaks, associated the frequencies with those of peaks in the velocity fluctuation spectra corresponding to different directions of flow rotation at points off the plane of symmetry of the bend. But considering the rapid change in relative magnitude of the peaks with X observed here it seems that a more

detailed investigation of the flow and the separation at small X is required in order to identify what characteristics of the flow are associated with the frequencies at which the peaks occur.

The distance downstream of the bend at which the pressure disturbances due to the bend have become almost entirely acoustic (as at $X = 52.8$) can be seen from Figures 4.7, 4.20 and 4.23 to be given by $X \sim 12$. The same conclusion is reached for all values of Ω if the spectral densities of the pressure are similarly considered.

The experimental spectral results presented in this chapter so far, are all based on $1/3$ -octave measurements, but a finer resolution than is provided by $1/3$ -octave band analysis is desirable for a more positive interpretation of the spectral data and in particular for identification of regions close to the bend where propagating higher order modes are detectable. For this reason a narrow band spectral analysis has been carried out. It is based on constant (100 Hz) bandwidth measurements (using a Brüel and Kjaer heterodyne analyser) and covers the frequency range from 200 Hz to 20 kHz. Measurements of wall pressure spectra were obtained for several axial and circumferential positions (corresponding to Figure 4.1) both upstream and downstream of the mitred bend and are presented in Figures 4.24 to 4.29.

From Figures 4.24 and 4.25 it can be seen that several higher order modes are detectable immediately upstream of the mitred bend. This is consistent with the r.m.s. pressure fluctuations (Figure 4.20) and since there is negligible attenuation of Φ_p with variation in Y upstream, this indicates a propagating acoustic field. From Figure 4.26, it can be seen that the higher order modes are not observed for $Y = 0.0$ and 0.40 and that the overall level of Φ_p is greater by about an order of magnitude. These measurement ports lie

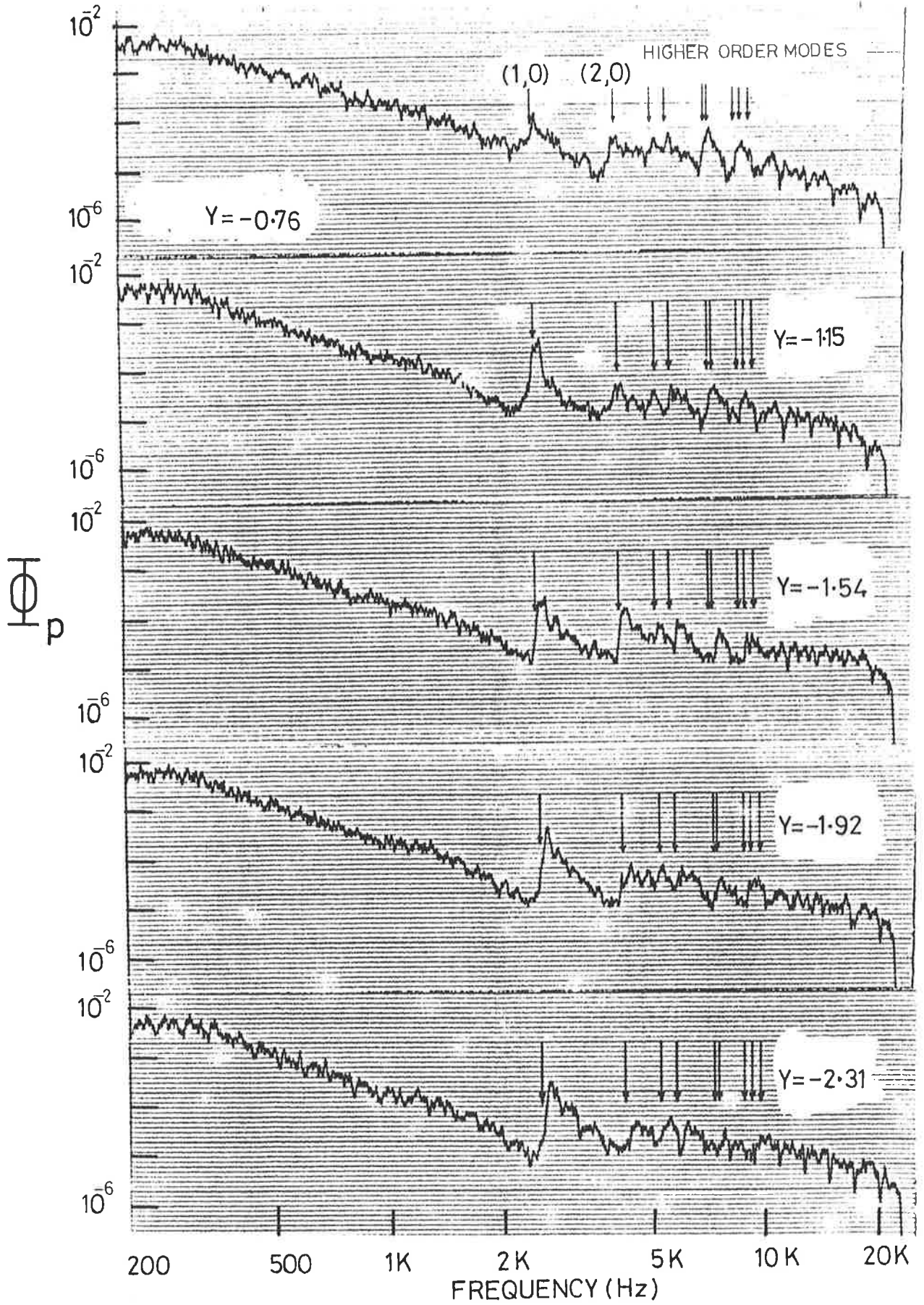


FIGURE 4.24 WALL PRESSURE FLUCTUATIONS ALONG INNER WALL BEFORE BEND
 $[M_0 = 0.40, 100 \text{ Hz Bandwidth}]$

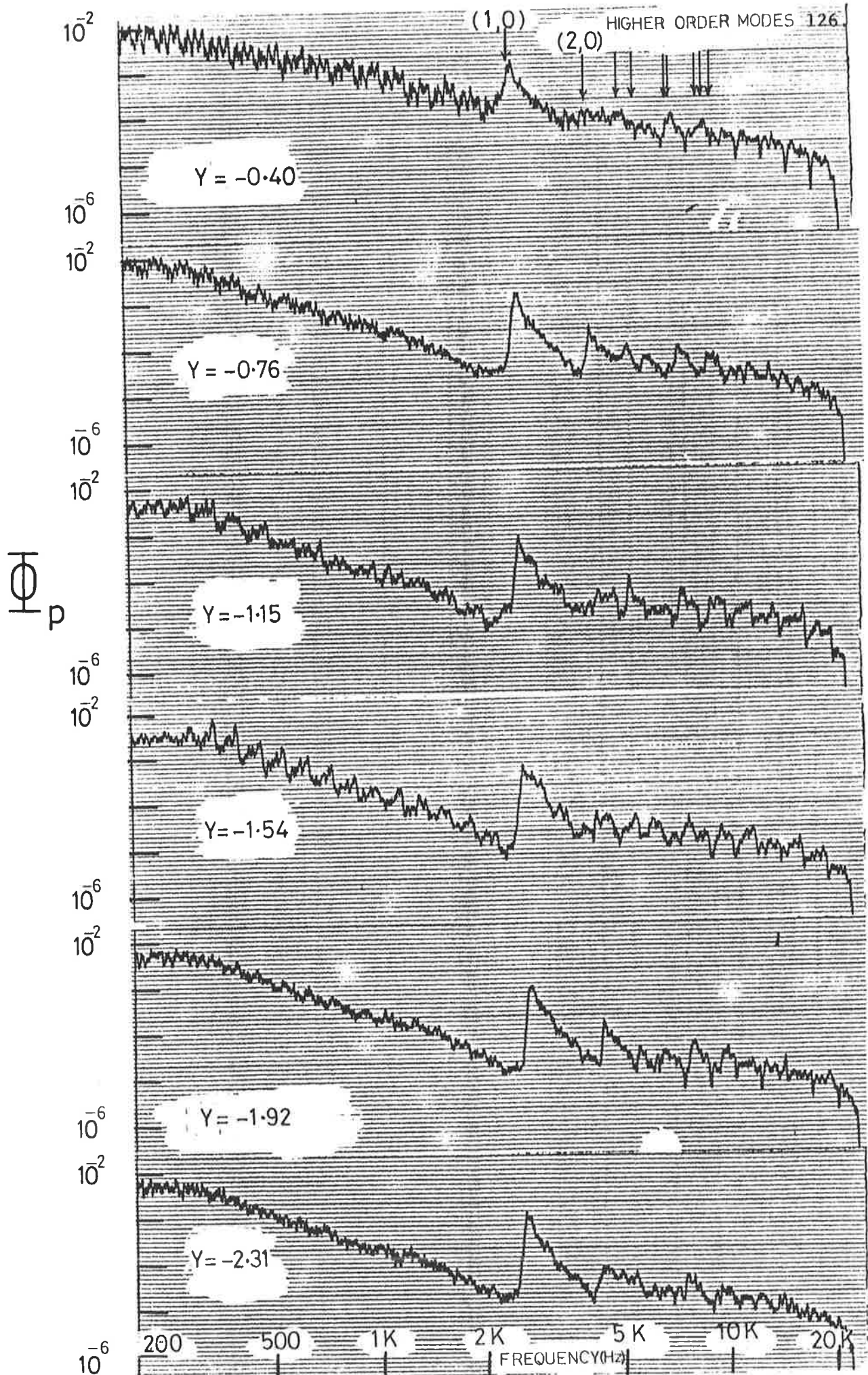


FIGURE 4.25 WALL PRESSURE FLUCTUATIONS ALONG SIDE WALL BEFORE BEND [$M_0 = 0.40$, 100 Hz Bandwidth]

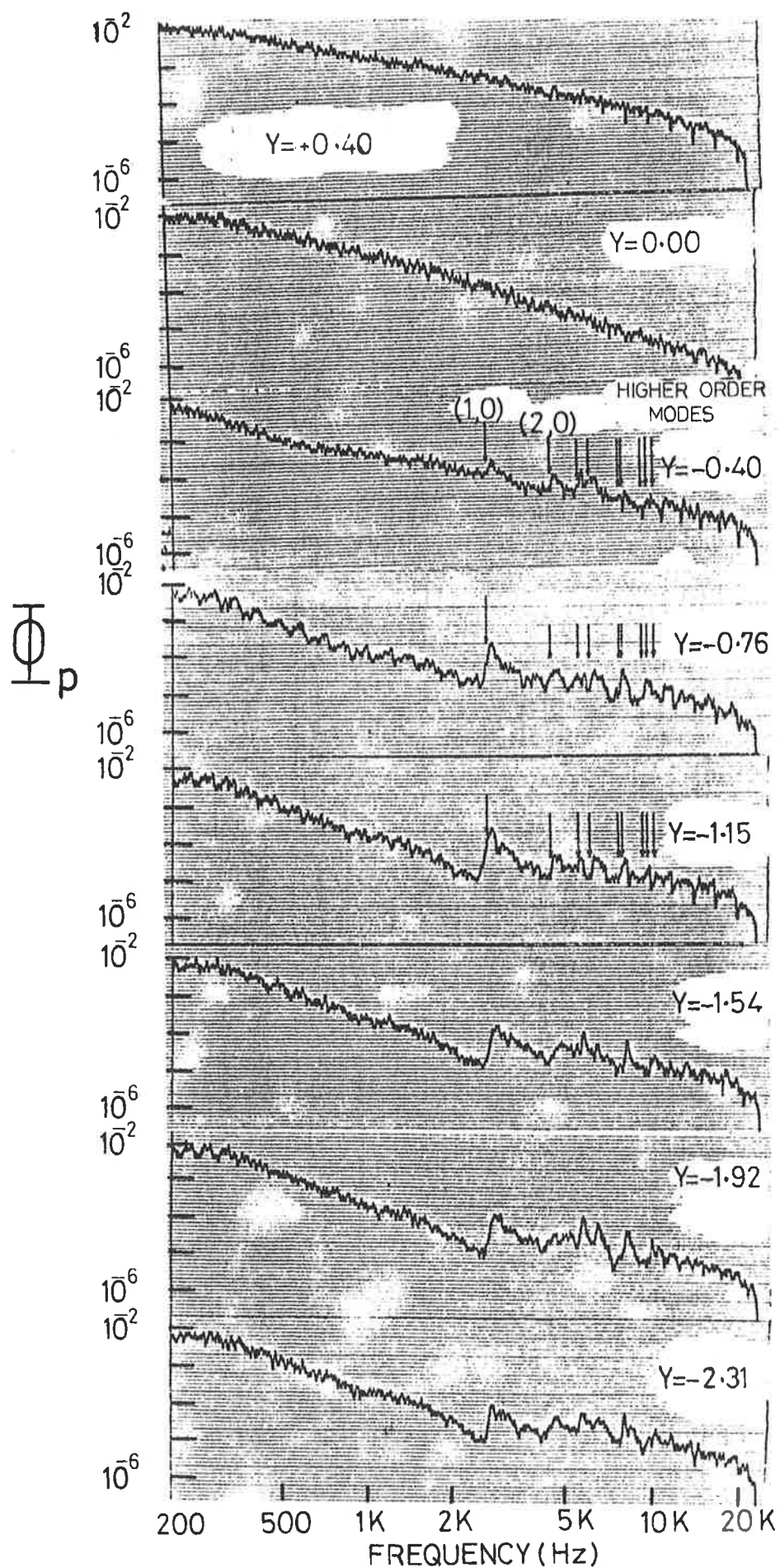


FIGURE 4.26 WALL PRESSURE FLUCTUATIONS
ALONG OUTER WALL BEFORE BEND
[$M_0 = 0.40$, 100 Hz Bandwidth]

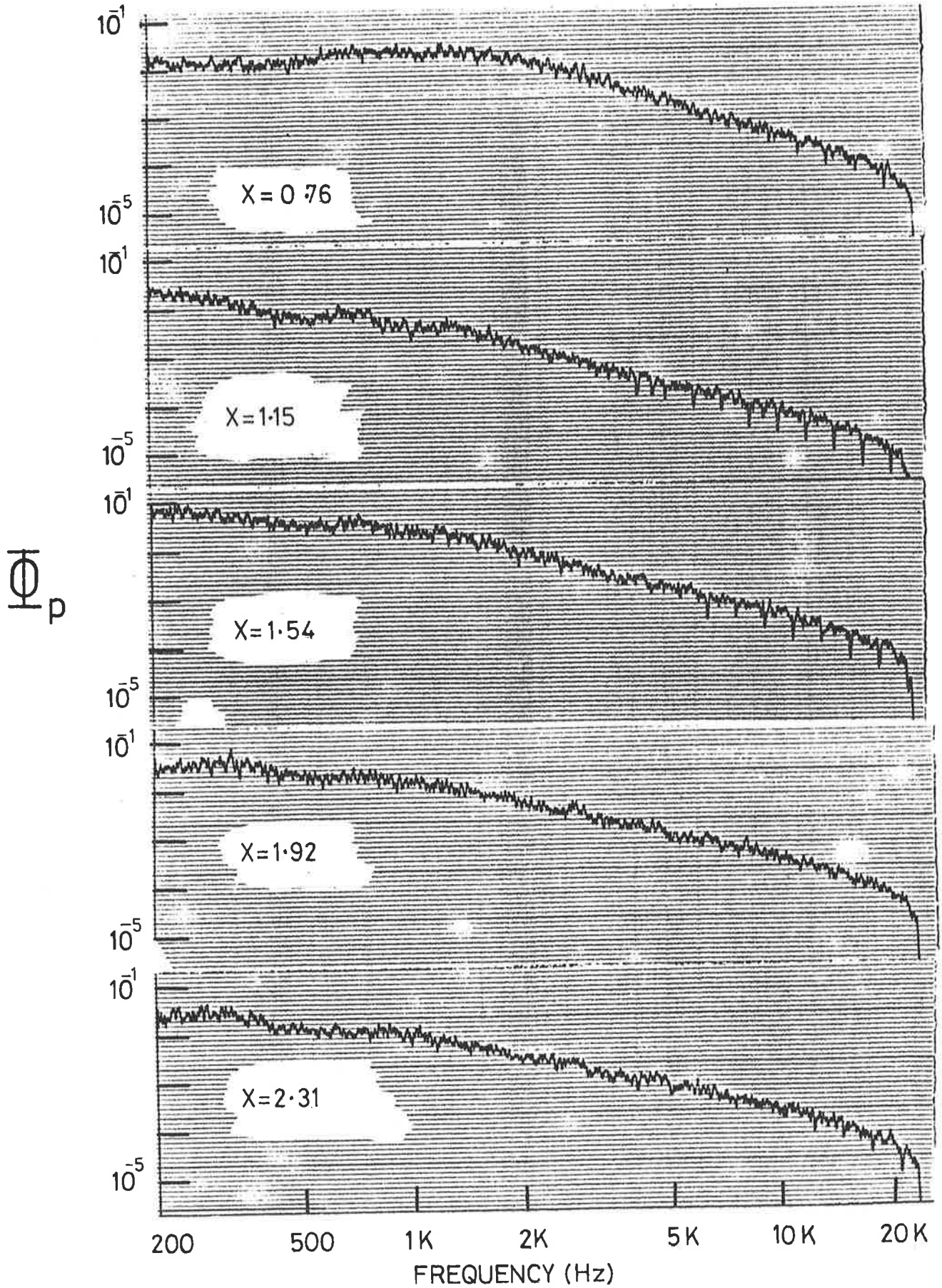


FIGURE 4.27 WALL PRESSURE FLUCTUATIONS ALONG
INNER WALL AFTER BEND

[$M_o = 0.40$, 100 Hz Bandwidth]

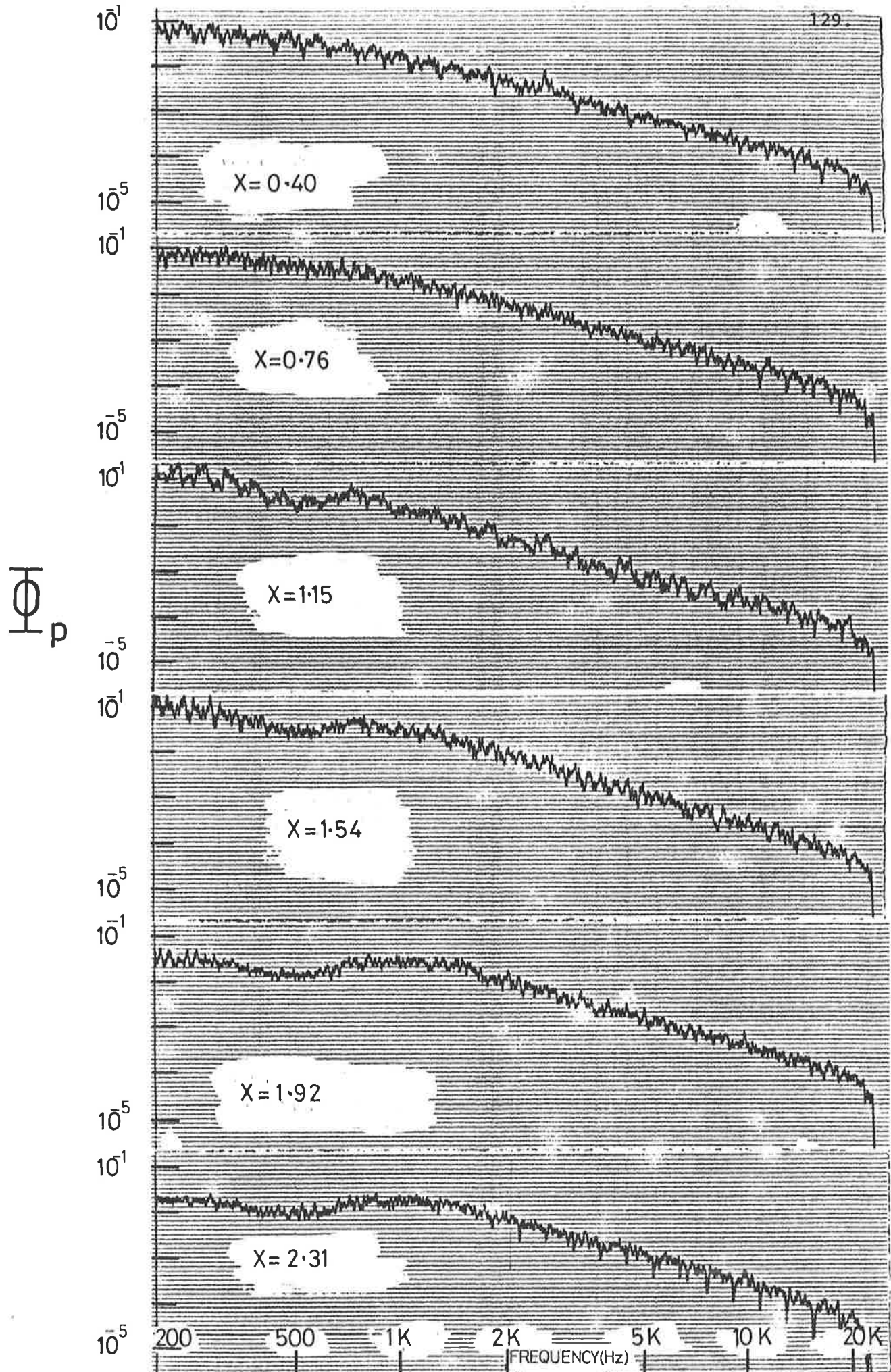


FIGURE 4.28 WALL PRESSURE FLUCTUATIONS ALONG SIDE WALL
AFTER BEND [$M_o=0.40$, 100 Hz Bandwidth]

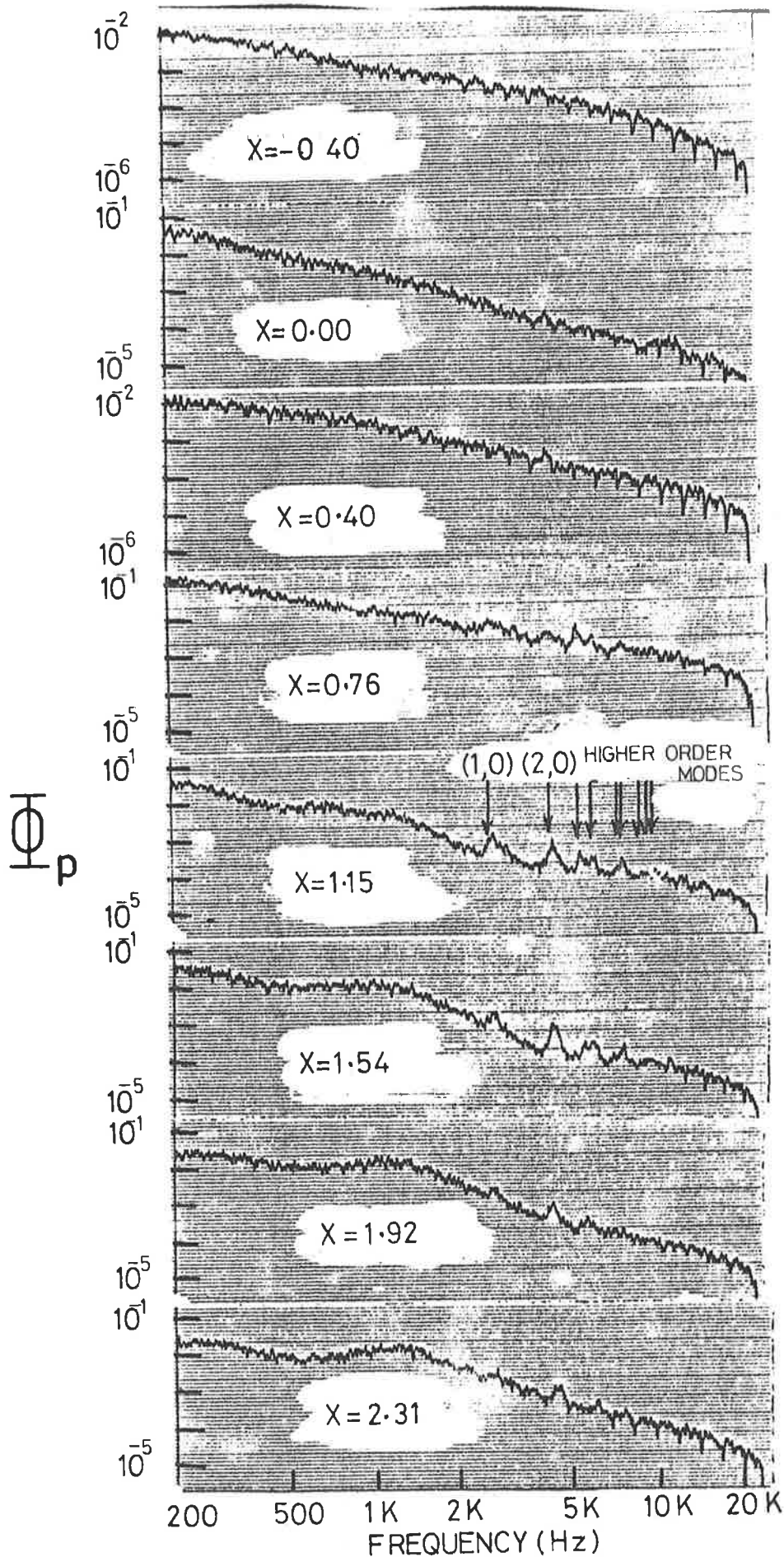


FIGURE 4.29 WALL PRESSURE FLUCTUATIONS
ALONG OUTER WALL AFTER BEND
[$M_0=0.40$, 100 Hz Bandwidth]

somewhere in the region of the outer separation bubble. Higher order modes are not detectable along the inner and side walls after the bend, as indicated in Figures 4.27 and 4.28 for $X \leq 2.3$. From Figure 4.29 it can be seen that the higher order modes start to be detectable at $X = 1.15$.

These narrow band spectra reinforce the results of the r.m.s. pressure fluctuations and the frequency weighted power spectral densities discussed earlier in this section and one can conclude that the character of the disturbance to the wall pressure field in the vicinity of the mitred bend is as follows:

- (1) Close to the bend (roughly $0 < X < 4$), over the region of flow separation and for some distance beyond it, the wall pressure field is not circumferentially uniform.
- (2) In this region it is dominated by intense non-propagating fluctuations at frequencies below that at which any higher order acoustic mode can propagate in the pipe.
- (3) The power spectral densities of these fluctuations are as much as 10^4 times as great as those of undisturbed turbulent pipe flow.
- (4) These non-propagating fluctuations are of the type associated with the production of plane acoustic waves.
- (5) They are attenuated rapidly with distance downstream, making negligible contributions to the mean square pressure at points further than about 1.2 diameters downstream of the bend, the remaining disturbance consisting entirely of propagating acoustic waves.
- (6) The major contribution to this acoustic field is made by plane waves at frequencies below the cut-off frequency of the first higher order mode. At higher frequencies higher-order modes, and almost certainly plane waves also are present.

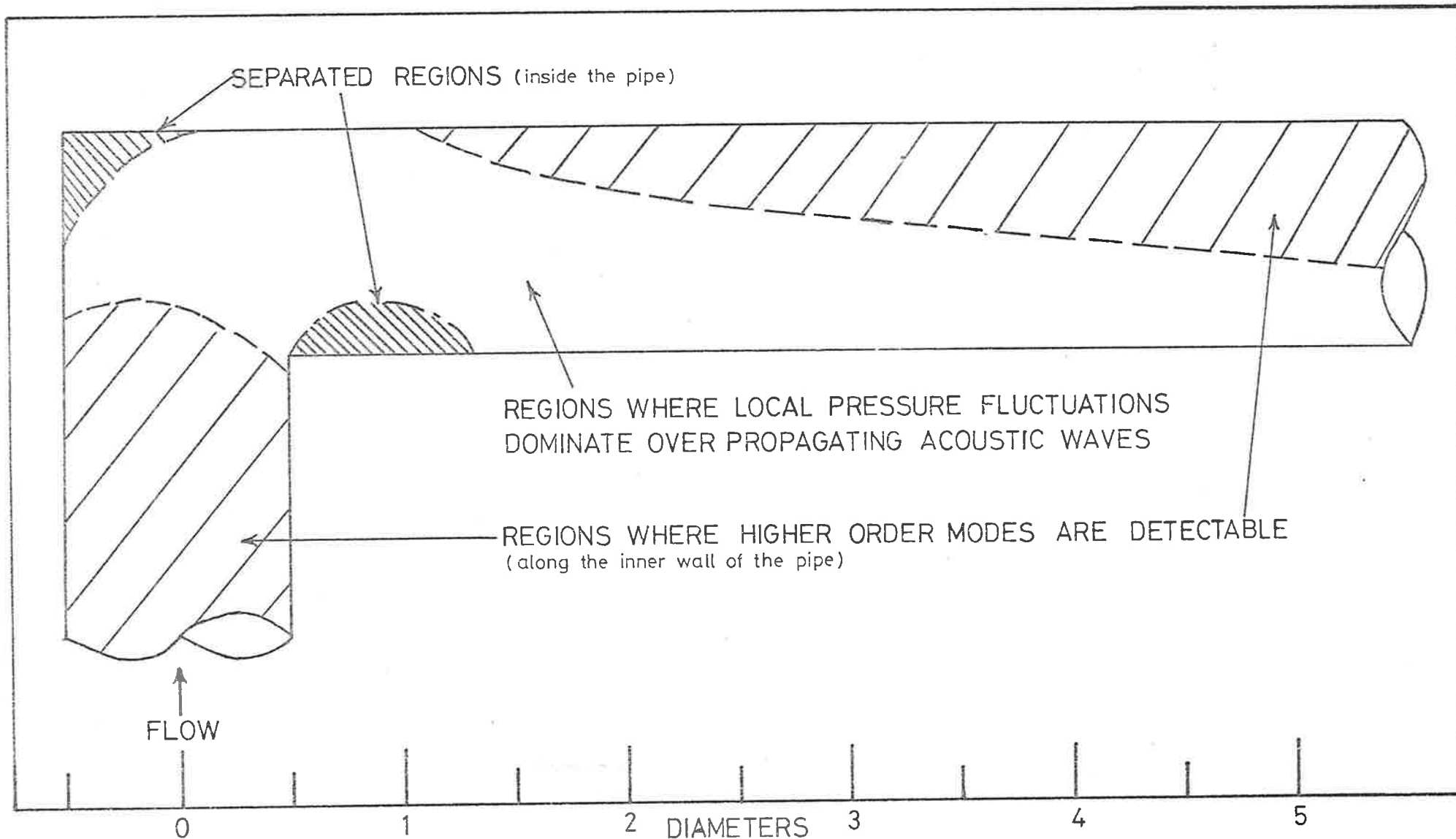


FIGURE 4.30 FLOW DISTURBANCES IN THE REGION OF THE BEND

Figure 4.30 illustrates the regions close to the bend where the higher order modes are detectable.

4.3 VIBRATIONAL AND ACOUSTIC EFFECTS DOWNSTREAM OF THE BEND

Spectral measurements of the wall pressure fluctuations, the acceleration response of and the acoustic power radiated from a cylindrical thin-walled test section with re-established fully-developed internal turbulent air flow at $X \geq 52$ (downstream of the mitred bend) are presented in this section. The data are for flow Mach numbers from 0.20 to 0.50. As seen in Chapter 3, there is fully-developed turbulent flow at entry to the bend, and at entry to the test section ($\approx X = 52.4$), an undisturbed fully-developed turbulent flow profile has been re-established.

4.3.1 Spectra of the Wall Pressure Fluctuations

The power spectrum of the wall pressure fluctuations has been measured at each speed just upstream of the test section ($X = 52.8$). The results of these measurements are shown in Figure 4.31; the data being presented in the form of the non-dimensional power spectral density, Φ_p , as a function of Strouhal number, Ω . Figure 4.31 shows two sets of experimental results - for straight pipe flow, and for the 90° mitred bend at $X = 52.8$. There is a fairly good collapse of the data for all flow speeds investigated, when they are scaled in this way. The scatter about the mean lines are generally less than ± 2 dB. The wall pressure fluctuations for both the 90° mitred bend and the straight pipe are flow dependent and this flow dependence is discussed in section 4.4. However, the spread (at any particular Strouhal number) over the range of flow speeds investigated is small enough to justify comparison between the 90° mitred bend and the straight pipe by comparing mean values. As will be shown in Chapter 5, this is also true of the other pipe fittings investigated and the

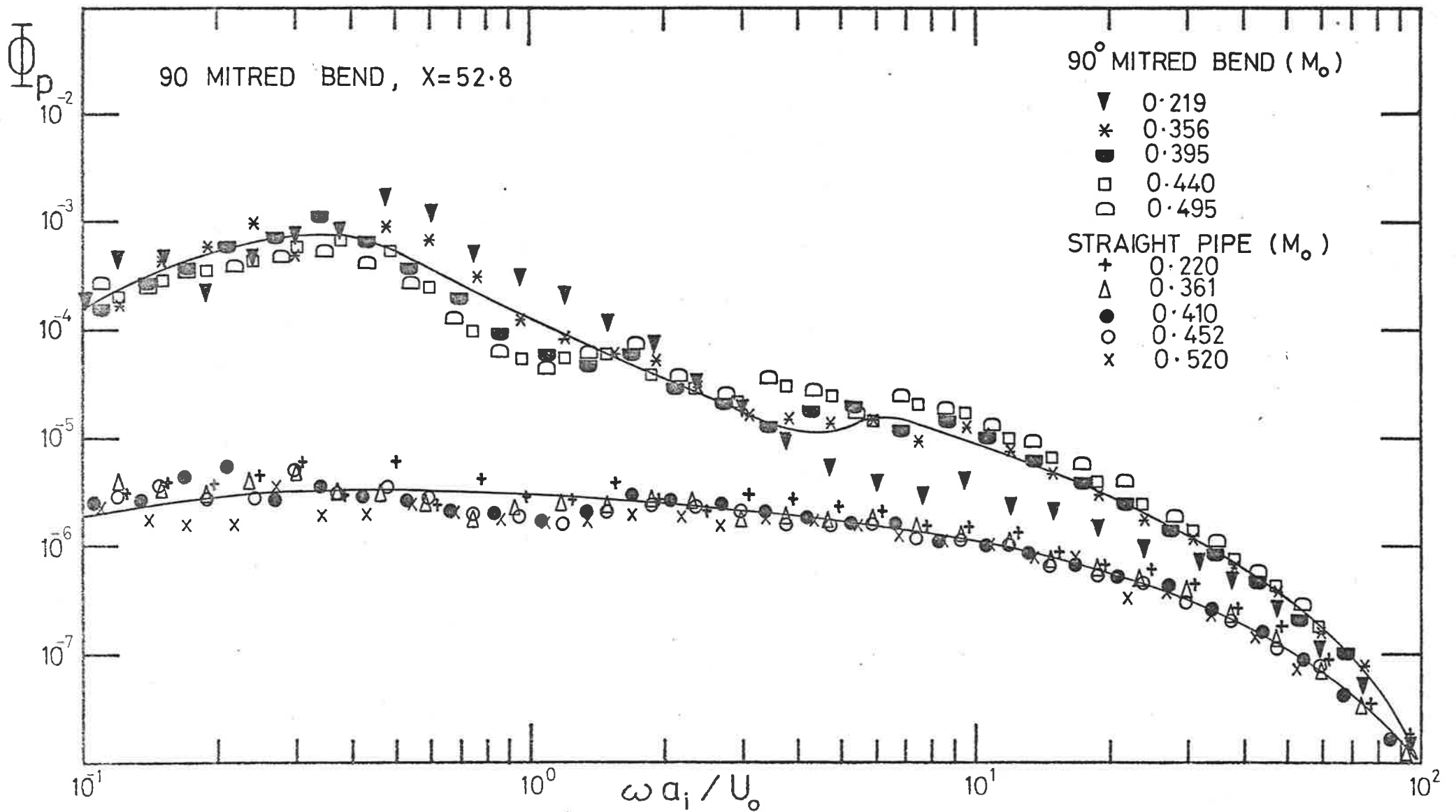


FIGURE 4.31 SPECTRAL DENSITY OF WALL PRESSURE FIELD

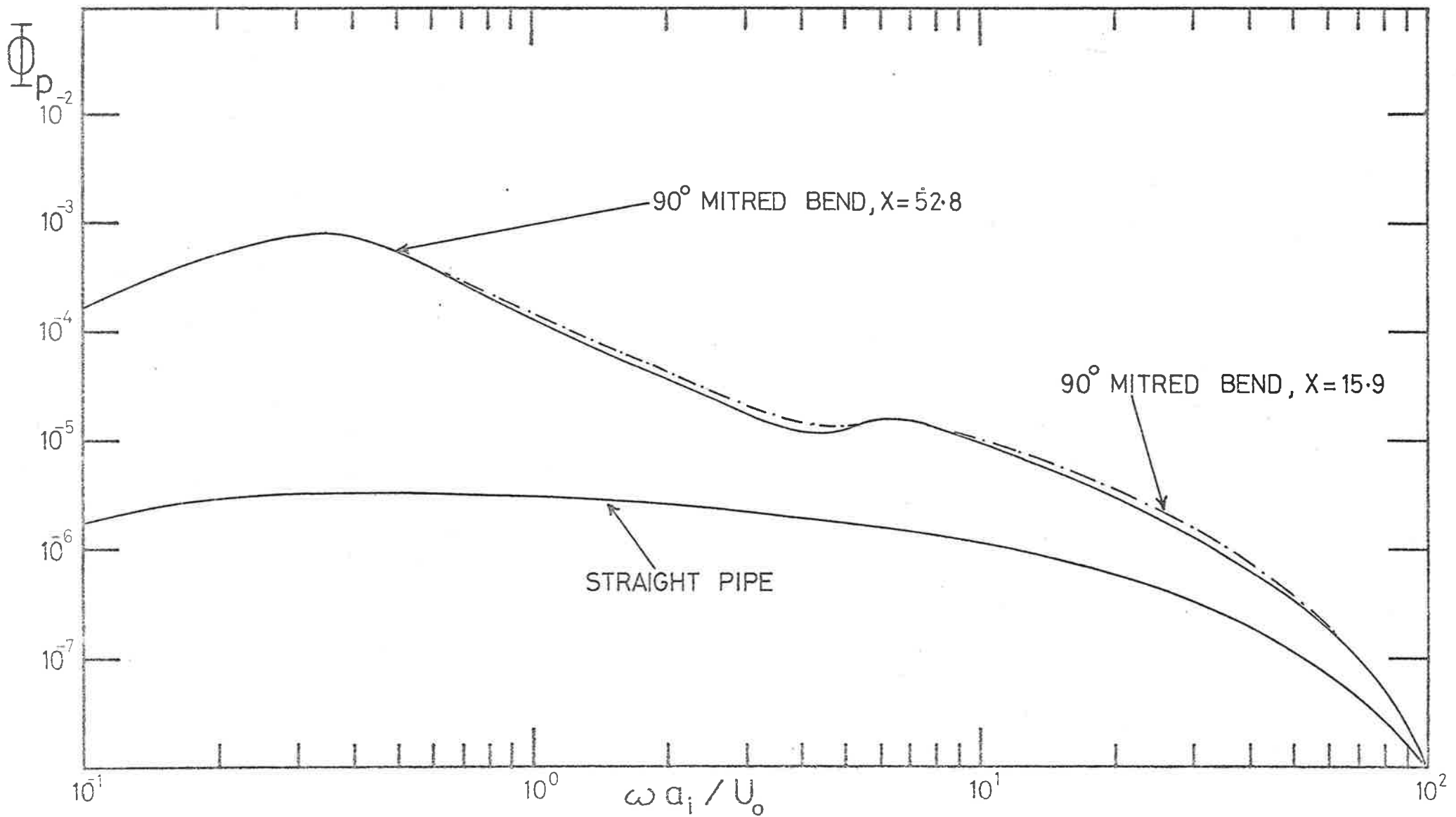


FIGURE 4.32 SPECTRAL DENSITY OF WALL PRESSURE FIELD (MEAN VALUES)

mean values are used for comparison between the various pipe fittings.

There is an increase in power spectral density of the wall pressure field over that for undisturbed fully-developed turbulent flow (at $X = 52.8$), large at low Strouhal numbers and progressively falling to almost nothing at the highest Strouhal numbers investigated. Spectra were also obtained at $X = 15.9$ and the spectral levels are almost the same as the corresponding ones measured close to the test-section ($X = 52.8$). This is illustrated in Figure 4.32.

In conjunction with the observed reversion of the mean velocity profiles to the undisturbed state at entry to the test section, together with an understanding of the experimental results presented in Section 4.2, this spectral behaviour indicates that the effect of the bend is to generate both near-field, non-propagating fluid dynamic pressure disturbances and acoustic pressure disturbances in its own vicinity, and that the disturbance observed at the test section is a combination of acoustic propagation from the bend and turbulent pressure fluctuations, the acoustic propagation being dominant at low Strouhal numbers. Hence, the wall pressure fluctuations are the sum of two pressure fields - a turbulent pressure field and an acoustic pressure field. These two pressure fields as will be seen in Chapter 6 can be separated using cross-correlation techniques.

Figures 4.33 to 4.35 shows the results for the non-dimensional power spectral density, Φ_p , based on constant (100 Hz) narrow bandwidth measurements; they cover the frequency range from 200 Hz to 20 kHz for $M_0 \sim 0.20, 0.40$ and 0.50 . The data for other flow speeds (not presented here) exhibit similar behaviour. For frequencies above cut-off, higher order modes are present and they are detectable from the narrow band spectral analysis of the wall pressure fluctuations. At higher frequencies, as the modes become closer together, the effects of individual modes become less obvious.

$X = 52.8, M_o = 0.22$

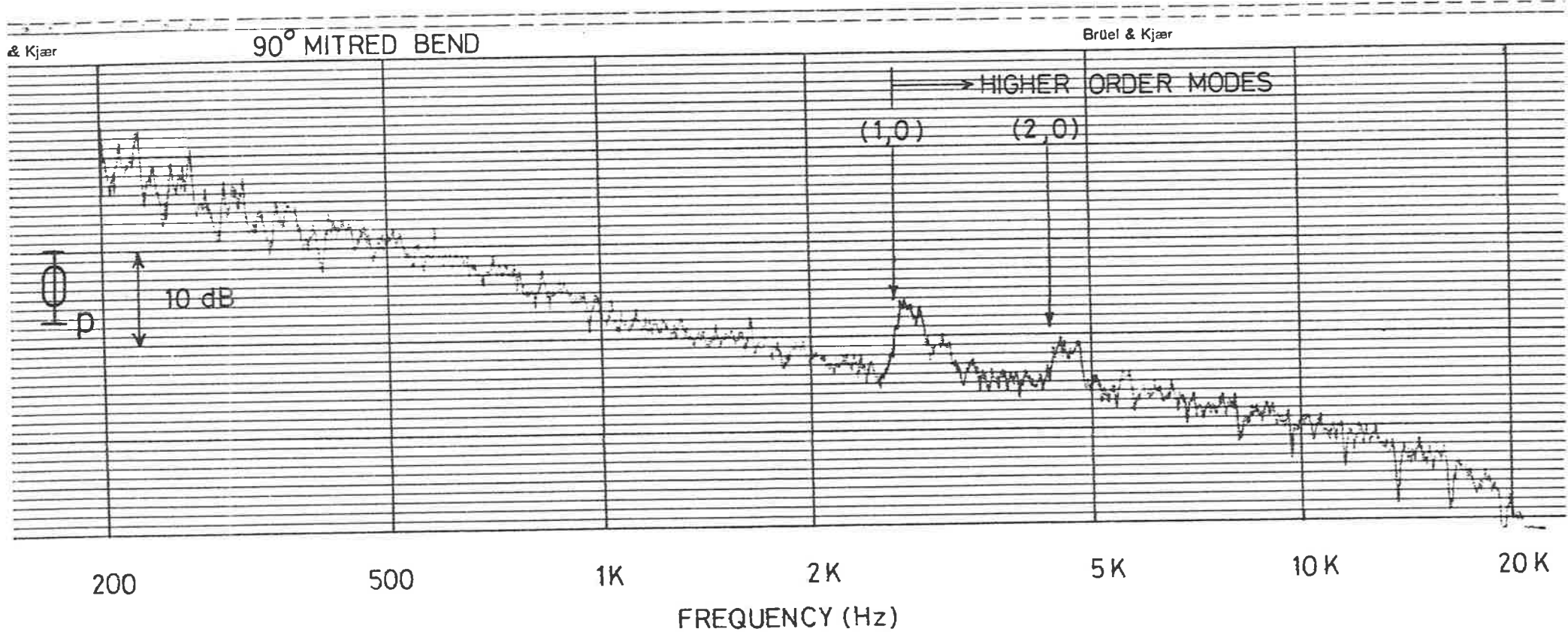


FIGURE 4.33 WALL PRESSURE FLUCTUATIONS [100 Hz Bandwidth]

$X = 52.8, M_0 = 0.40$

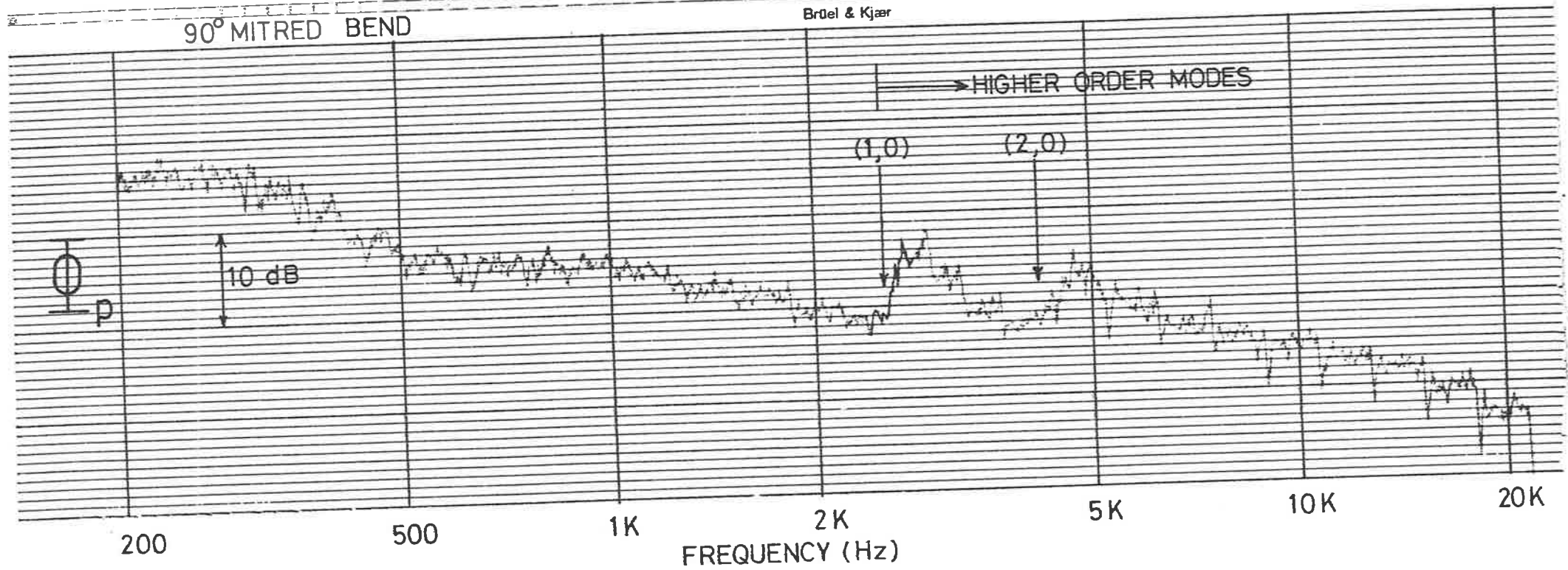


FIGURE 4.34 WALL PRESSURE FLUCTUATIONS [100 Hz Bandwidth]

$X=52.8, M_0=0.50$

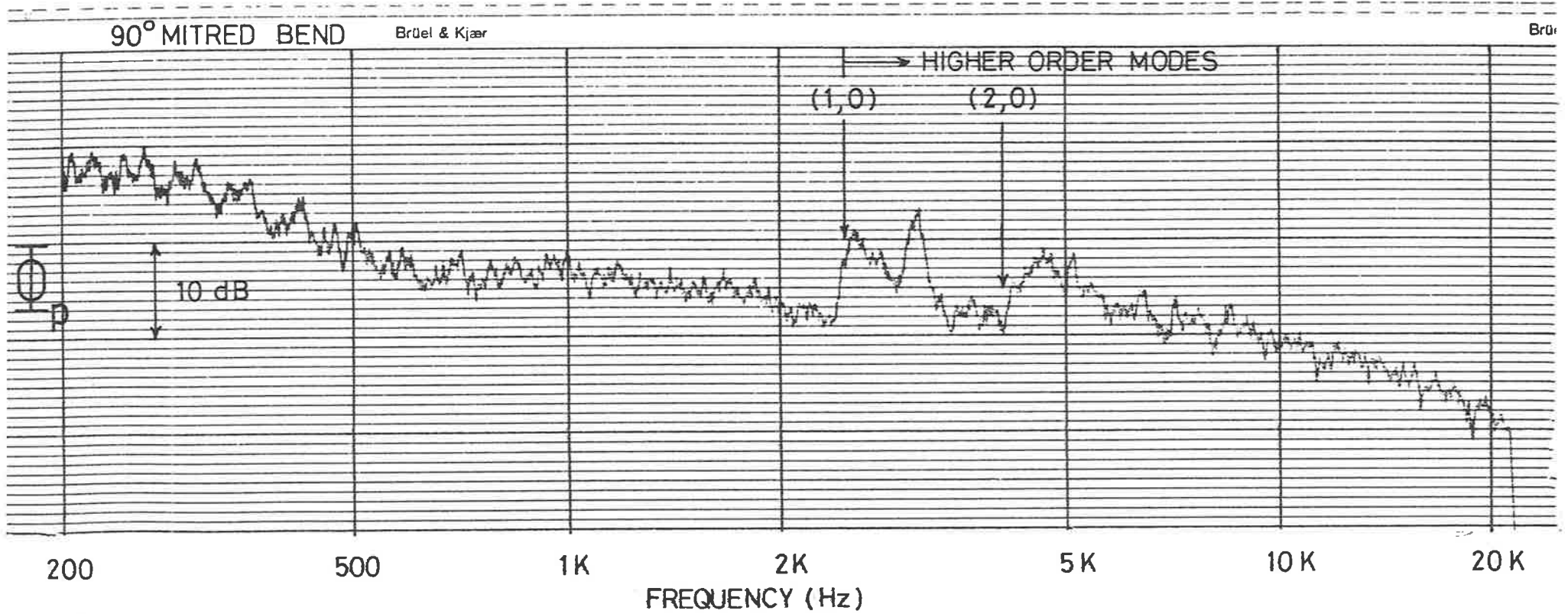


FIGURE 4.35 WALL PRESSURE FLUCTUATIONS [100 Hz Bandwidth]

4.3.2 Acceleration Response of and Acoustic Radiation from the Test Section

The power spectral density, ϕ_{ζ} , of the acceleration of the wall of the test section has been derived from $1/3$ -octave band measurements made with a 0.5 g Brüel and Kjaer accelerometer at each of the five flow speeds. The corresponding spectral density, ϕ_{π} , of the acoustic power radiated from the test section has been similarly derived from $1/3$ -octave band measurements of sound pressure levels under free field conditions. It is found experimentally that ϕ_{ζ} and ϕ_{π} are axially and circumferentially uniform over the test section within ± 1 dB. The results presented in Figures 4.36 and 4.37 are those obtained at the mid-point of the test section, $X = 74.4$. The results are shown in the form of the non-dimensional spectral density of wall acceleration Φ_{ζ} and acoustic radiation Φ_{π} against non-dimensional frequency ν ,

$$\text{where } \Phi_{\zeta} = \phi_{\zeta} / \omega_r^3 a_m^2 ; \quad \Phi_{\pi} = \phi_{\pi} / \rho_e c_e^2 S a_m ; \quad \nu = \omega / \omega_r ;$$

$\omega_r = c_{LP} / a_m$ is the ring frequency of the test section;

$c_{LP} = \sqrt{E / \rho_s \psi^2}$; $\psi^2 = 1 - \mu^2$; E , ρ_s , and μ are respectively Young's modulus, density and Poisson's ratio of the test section material; ρ_e and c_e are respectively the density of and the speed of sound in the fluid outside the pipe; and S is the surface area of the test section.

The spectral density of both the pipe wall acceleration and the acoustic power radiation increases dramatically as ν rises above 0.10. Furthermore, this behaviour occurs despite the fact that the greatest acoustic disturbance to the wall pressure spectrum occurs at Strouhal numbers corresponding to frequencies for which $\nu < 0.10$ (see Figure 4.31 and 4.32). Effects are greatest at frequencies close to the cut-off frequencies of the various higher order acoustic modes discussed in Chapter 2. This is even more apparent from a narrow

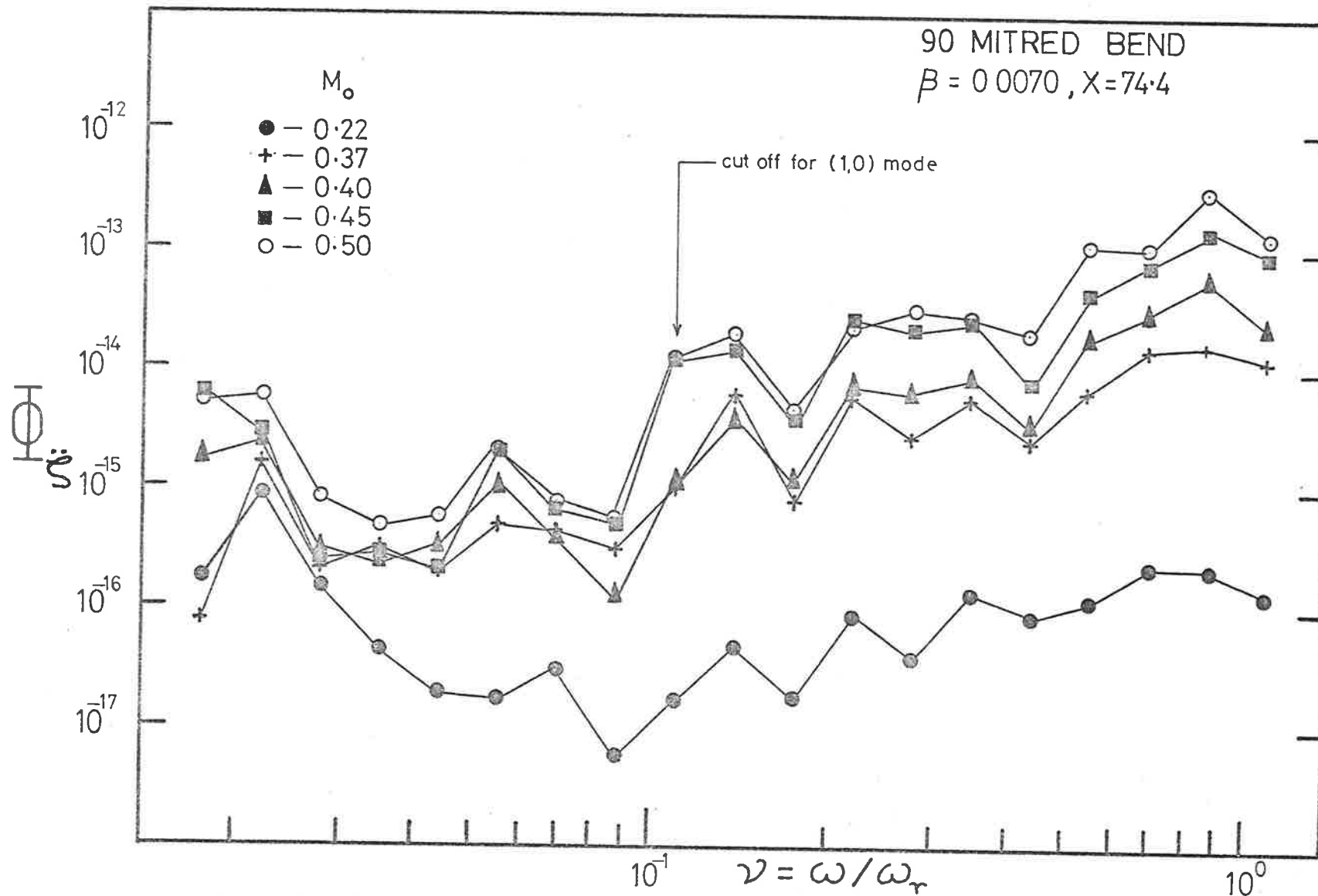


FIGURE 4.36 NON-DIMENSIONAL PIPE WALL ACCELERATION

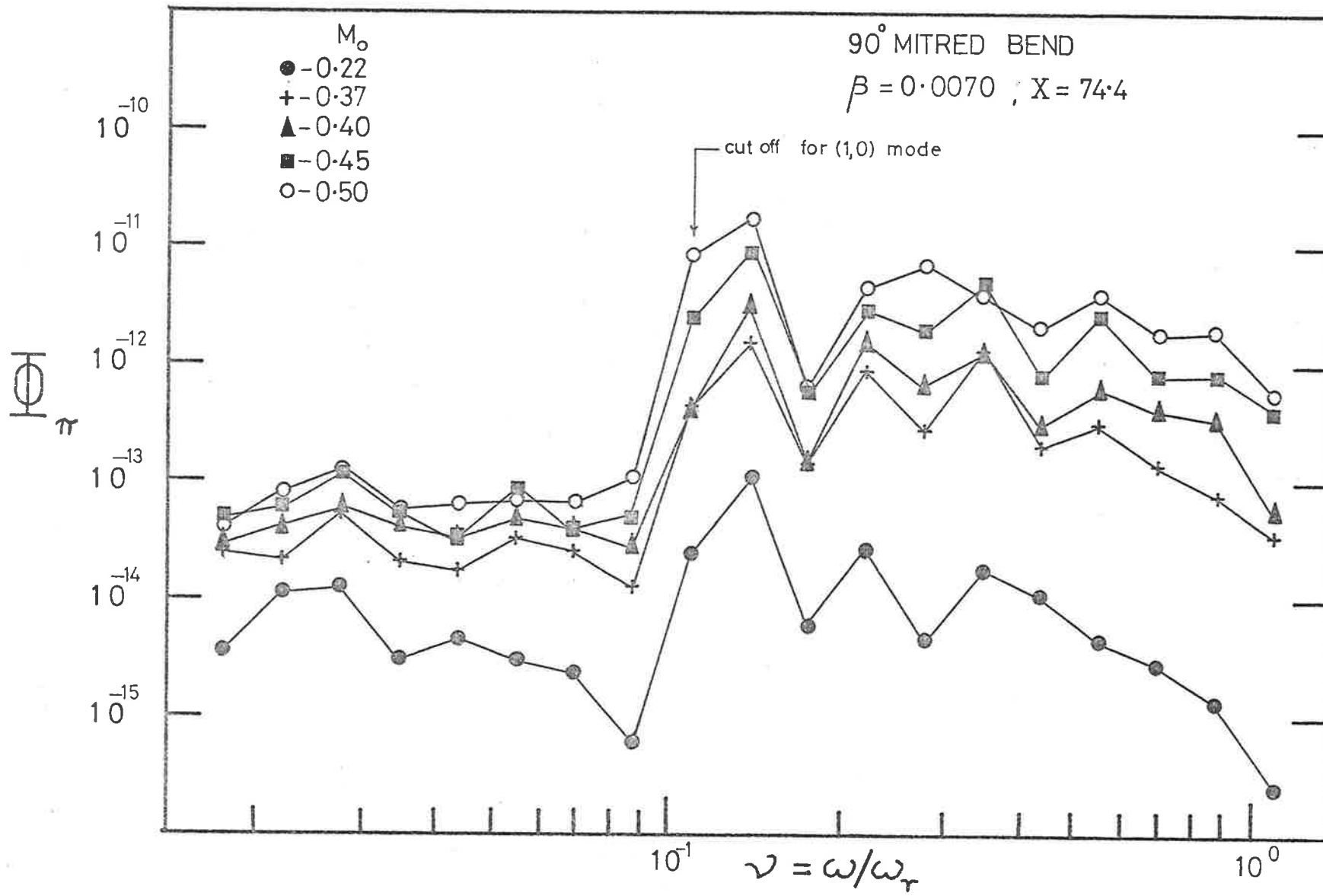


FIGURE 4.37 NON-DIMENSIONAL ACOUSTIC POWER RADIATION

band analysis giving finer resolution than provided by the $1/3$ -octave bands. Figures 4.38 to 4.40 are narrow band analyses for Φ_{ζ} for $M_o \sim 0.20, 0.40$ and 0.50 , and Figures 4.41 to 4.43 for Φ_{π} for the same flow Mach numbers. Sharp peaks in pipe wall response and acoustic power radiation can be seen at frequencies close to the cut-off frequencies of the various higher order modes. Absolute scales are not included on Figures 4.38 to 4.43, and in the narrow band analysis of the wall acceleration (Figures 4.38 to 4.40) accelerometer mass loading effects (as discussed in Chapter 3) are not accounted for, so that the relative acceleration contributions at and above 8 kHz are larger than indicated on Figures 4.38 to 4.40. Nevertheless, the narrow band analyses clearly illustrate the point that effects are greatest at frequencies close to the cut-off frequencies of the various higher order modes.

The same $1/3$ -octave results for Φ_{ζ} and Φ_{π} are shown in Figure 4.44 in the alternative form of the non-dimensional spectral density of wall acceleration Φ_{ζ} and acoustic radiation Φ_{π} relative to the corresponding values for the straight pipe $[(\Phi_{\zeta})_o]$ and $[(\Phi_{\pi})_o]$ against the non-dimensional frequency ν . Results for the straight pipe (fully-developed turbulent) flow itself are presented in the next chapter.

The efficiency of the pipe as an acoustic radiator can be expressed by the radiation ratio,

$$\sigma = \frac{\omega^2 \Phi_{\pi}}{\rho_e c_e S [[\Phi_{\zeta}]]} \quad , \quad [4.1]$$

so that,

$$\frac{\sigma}{\sigma_o} = \frac{\Phi_{\pi} / (\Phi_{\pi})_o}{[[\Phi_{\zeta}]] / [[\Phi_{\zeta}]]_o} \quad , \quad [4.2]$$

$X = 52.8, M_0 = 0.22$

HIGHER ORDER MODES

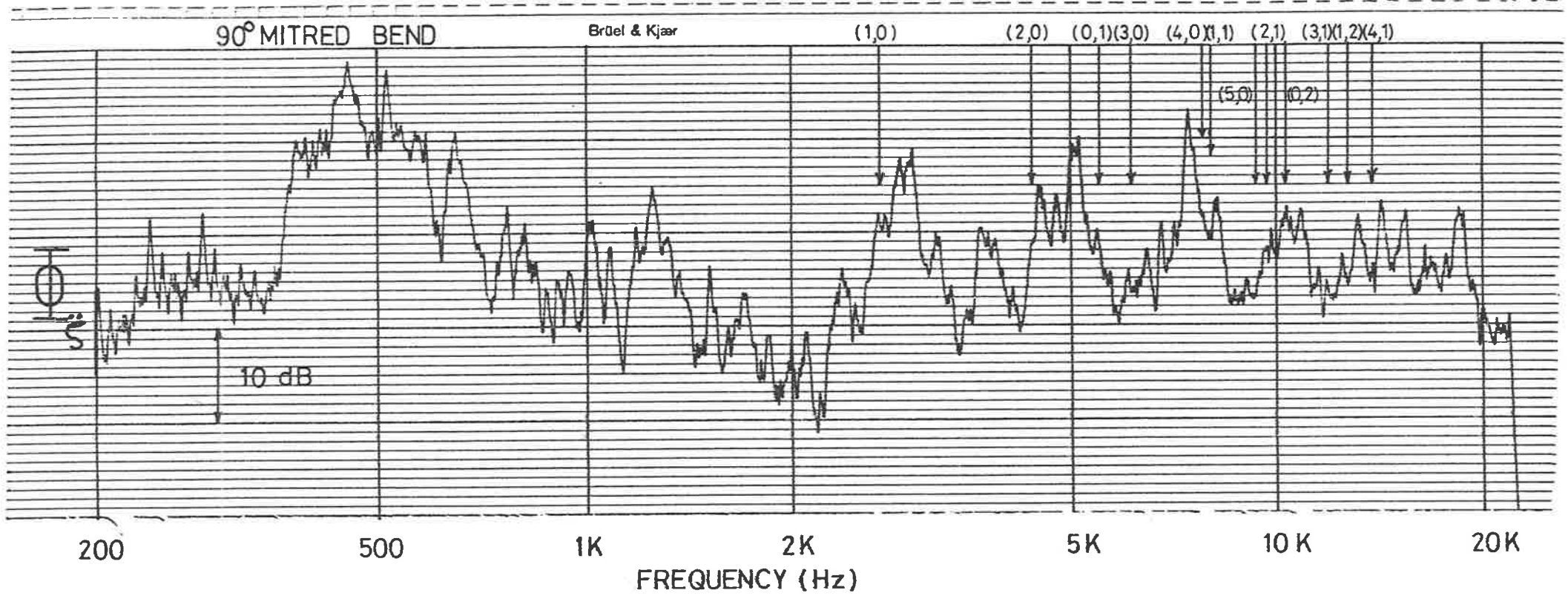


FIGURE 4.38 PIPE WALL ACCELERATION [100 Hz Bandwidth]

$X = 52.8, M_o = 0.40$

HIGHER ORDER MODES

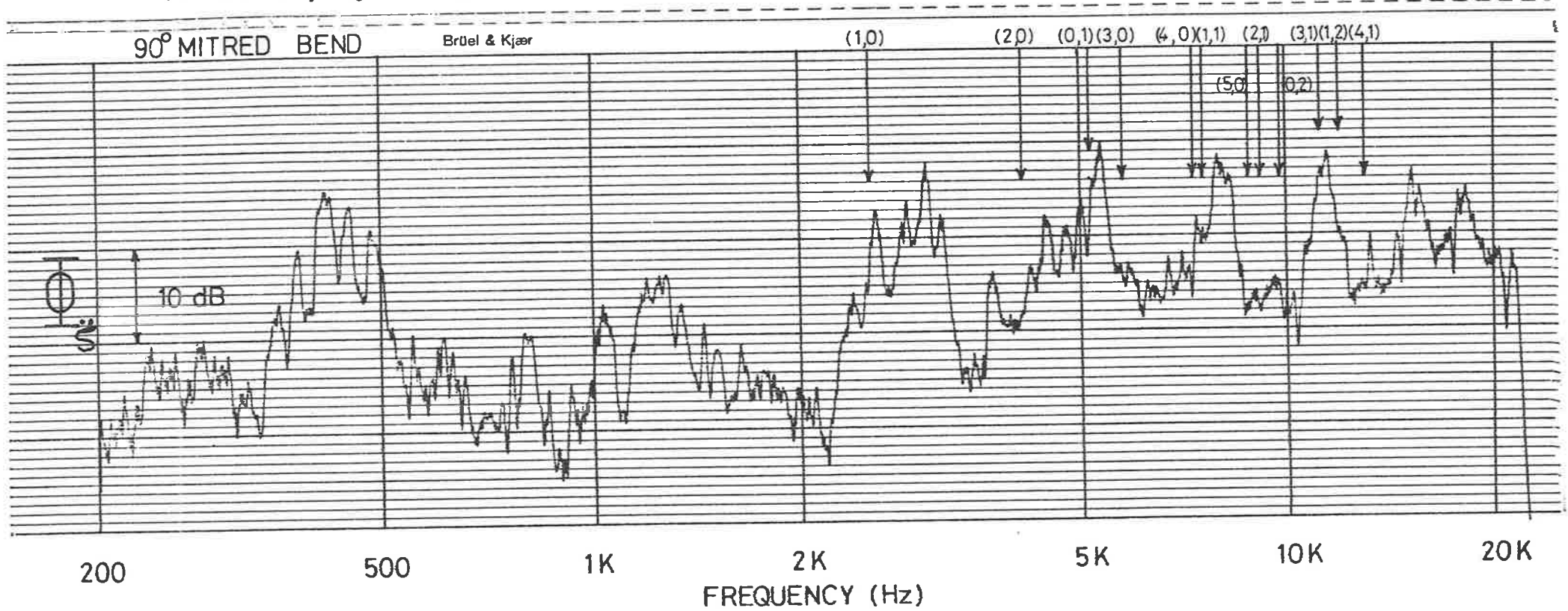


FIGURE 4.39 PIPE WALL ACCELERATION [100 Hz Bandwidth]

$X = 52.8, M_o = 0.50$

HIGHER ORDER MODES

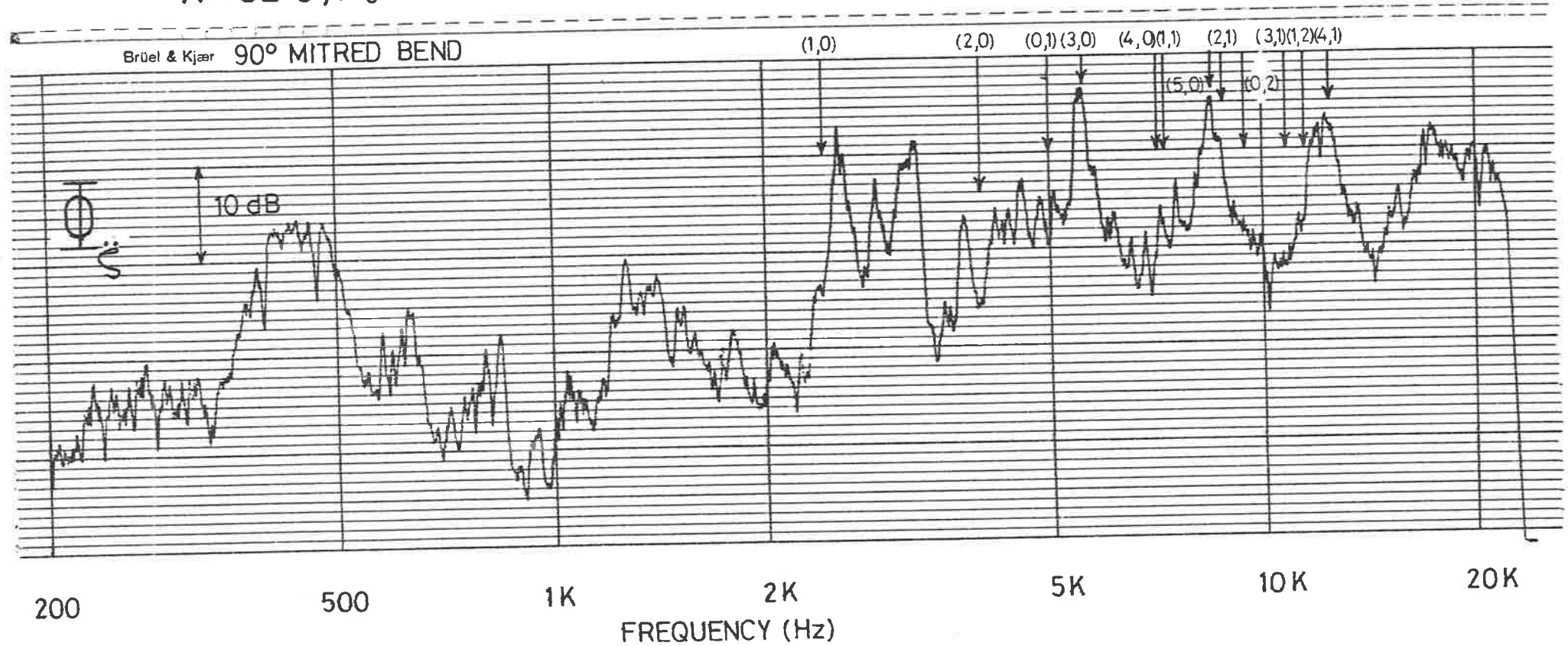


FIGURE 4.40 PIPE WALL ACCELERATION [100 Hz Bandwidth]

$X = 52.8, M_0 = 0.22$

HIGHER ORDER MODES

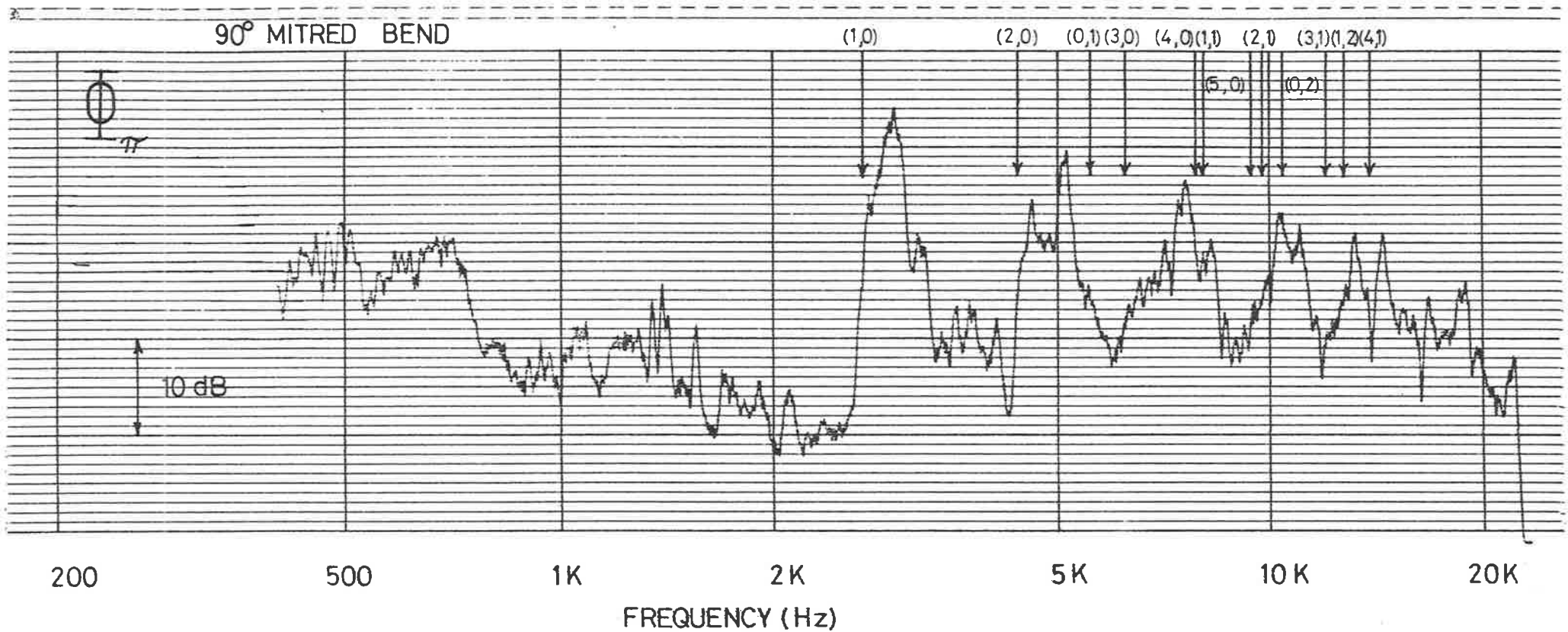


FIGURE 4-41 ACOUSTIC POWER RADIATION [100 Hz Bandwidth]

$X = 52.8, M_0 = 0.40$

HIGHER ORDER MODES

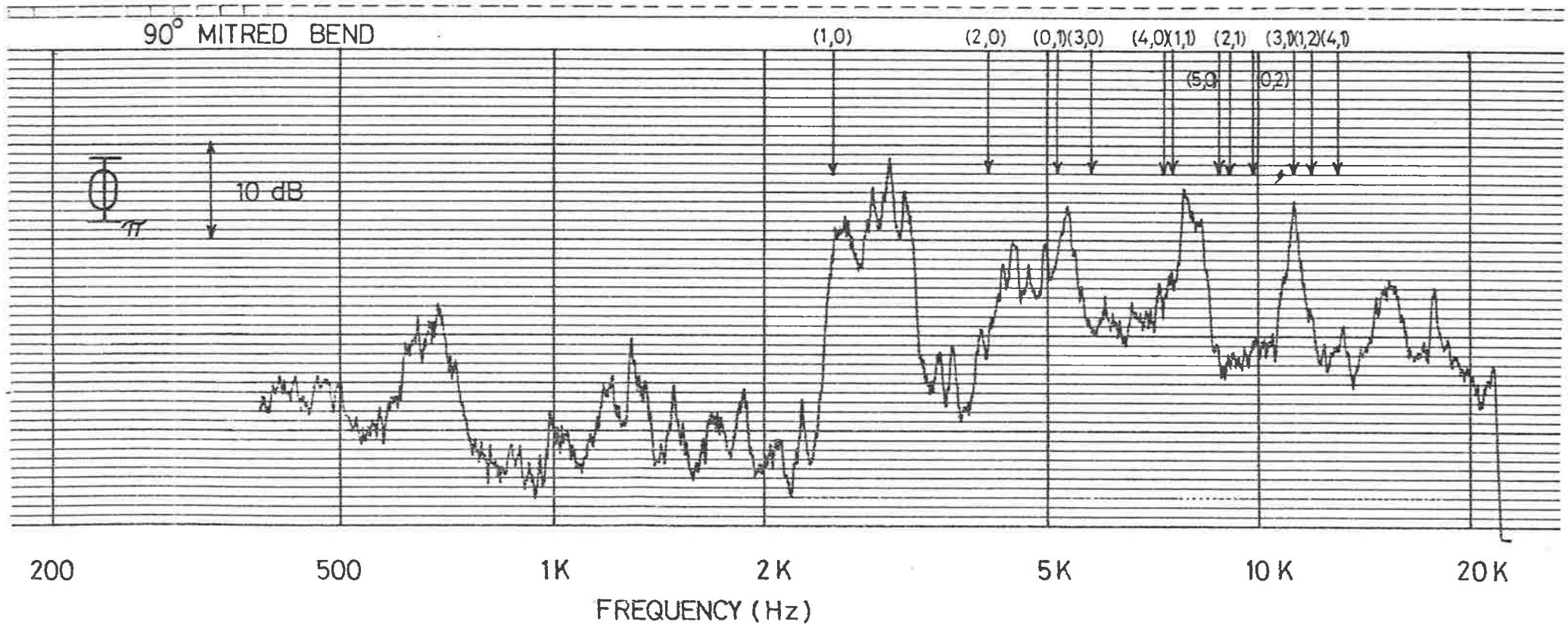


FIGURE 4.42 ACOUSTIC POWER RADIATION [100 Hz Bandwidth]

$X = 52.8, M_o = 0.50$

HIGHER ORDER MODES

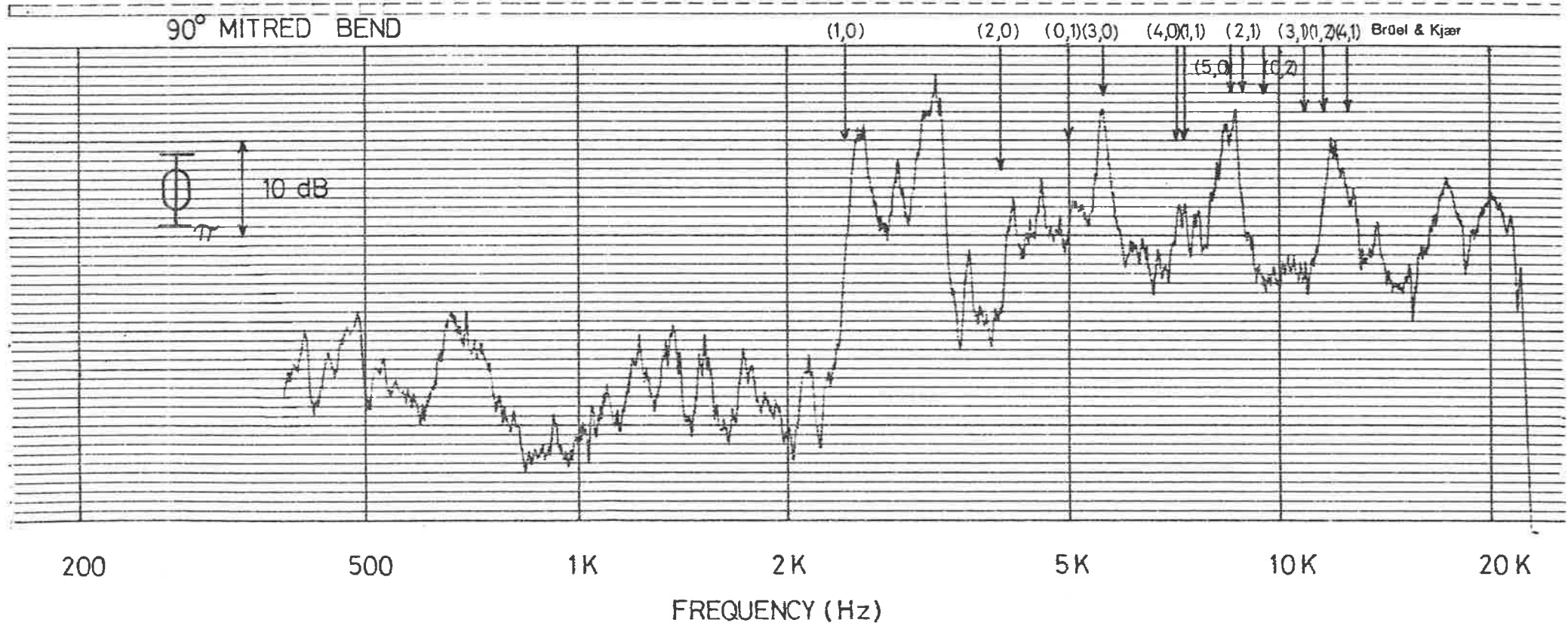


FIGURE 4.43 ACOUSTIC POWER RADIATION [100 Hz Bandwidth]

where $[[\]]$ indicates a spatial average over the vibrating surface.

As indicated above, experimental measurements show that Φ_{ζ} is uniform over the test section, and hence $[[\Phi_{\zeta}]]$ is essentially equal to the value of Φ_{ζ} at the mid-point of the test section.

From Figure 4.44 it can be seen that the 90° mitred bend produces increases in both acceleration and radiation levels (over that of straight pipe flow) over the whole frequency range in addition to the dramatic increases as ν rises above 0.10. Increases in acceleration and radiation levels in the frequency range $0.08 < \nu < 0.30$ are accompanied by increases in σ/σ_0 , but there is no significant change in σ/σ_0 for $\nu > 0.30$.

It can be seen from Figure 4.36 and from the narrow band analyses (Figures 4.38 to 4.40) that for the low frequency pipe wall response, the effects are greatest for $0.02 < \nu < 0.03$ and for $0.05 < \nu < 0.07$. These low frequency increases in pipe wall acceleration level are associated with plane waves coupling with various resonant structural modes. Rennison (1976) and Rennison and Bull (1977) investigated the modal density of various cylindrical pipes. Calculations of the experimental modal density at low frequencies were made in $1/3$ -octave bands, and compared with theoretical predictions. Rennison's experimental results and theoretical prediction for the thin walled pipe used in this investigation ($\beta = 0.0070$, $\Lambda = 79.4$, $\psi = 0.960$) are presented in Figure 4.45. Rennison (1976) associates the experimental peaks with the grouping together of low axial order resonant modes of fixed circumferential order, and as the total number of modes in a band increases the groupings have less influence on the experimental modal density. For the particular thin-walled test section used in this investigation, there is a significant grouping of $n=2$ circumferential order modes for $0.014 < \nu < 0.029$ and $n=3$ circumferential order modes for $0.048 < \nu < 0.058$ (Rennison, 1976). Hence the observed increases

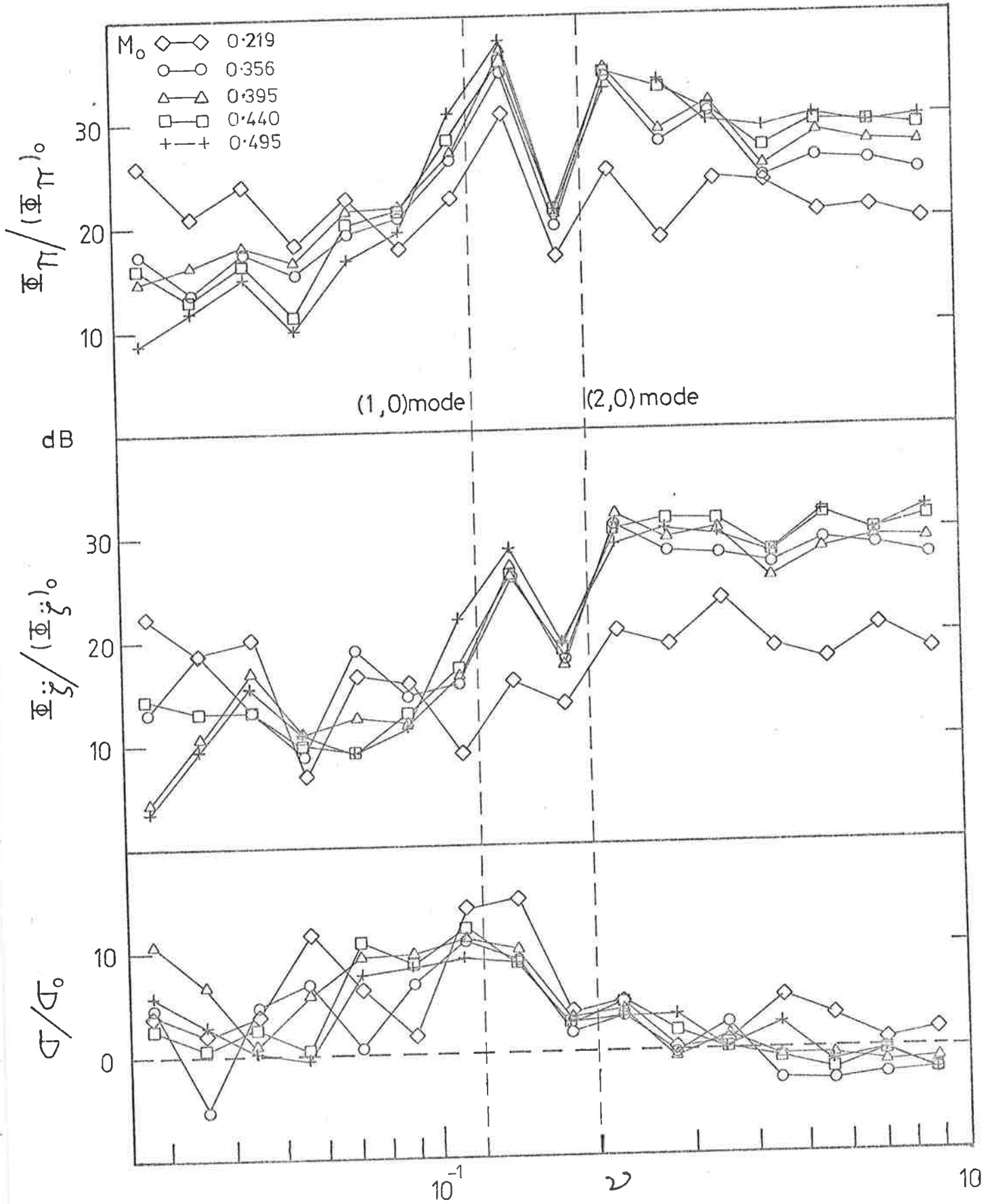


FIG 4.44 SPECTRAL DENSITIES OF Φ_{ξ} AND Φ_{π} RELATIVE TO STRAIGHT PIPE FLOW AND THE CORRESPONDING RADIATION RATIO σ / σ_0 FOR 90° MITRED BEND

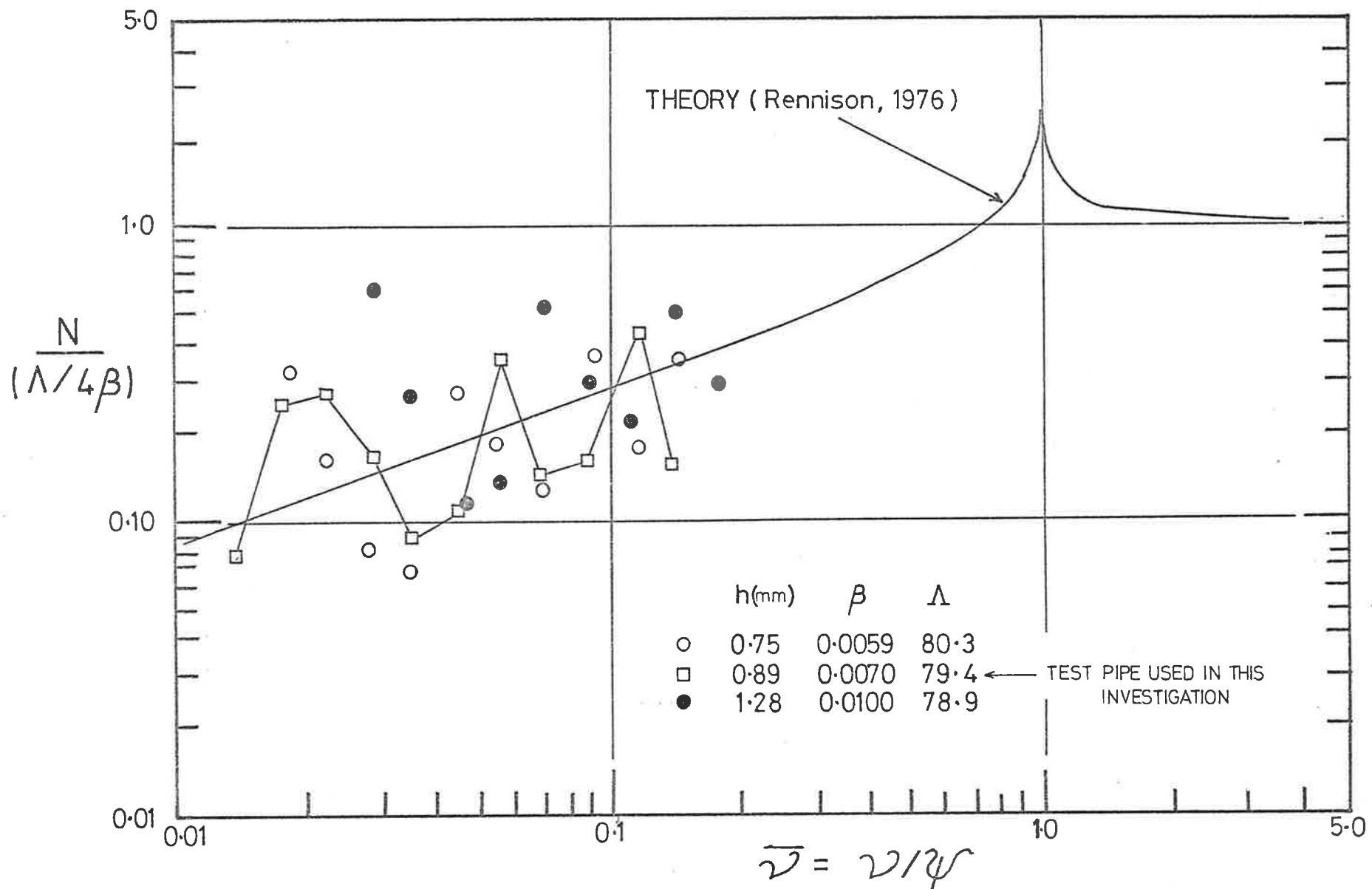


FIGURE 4.45 MODAL DENSITY OF EXPERIMENTAL TEST PIPE
(FROM RENNISON, 1976)

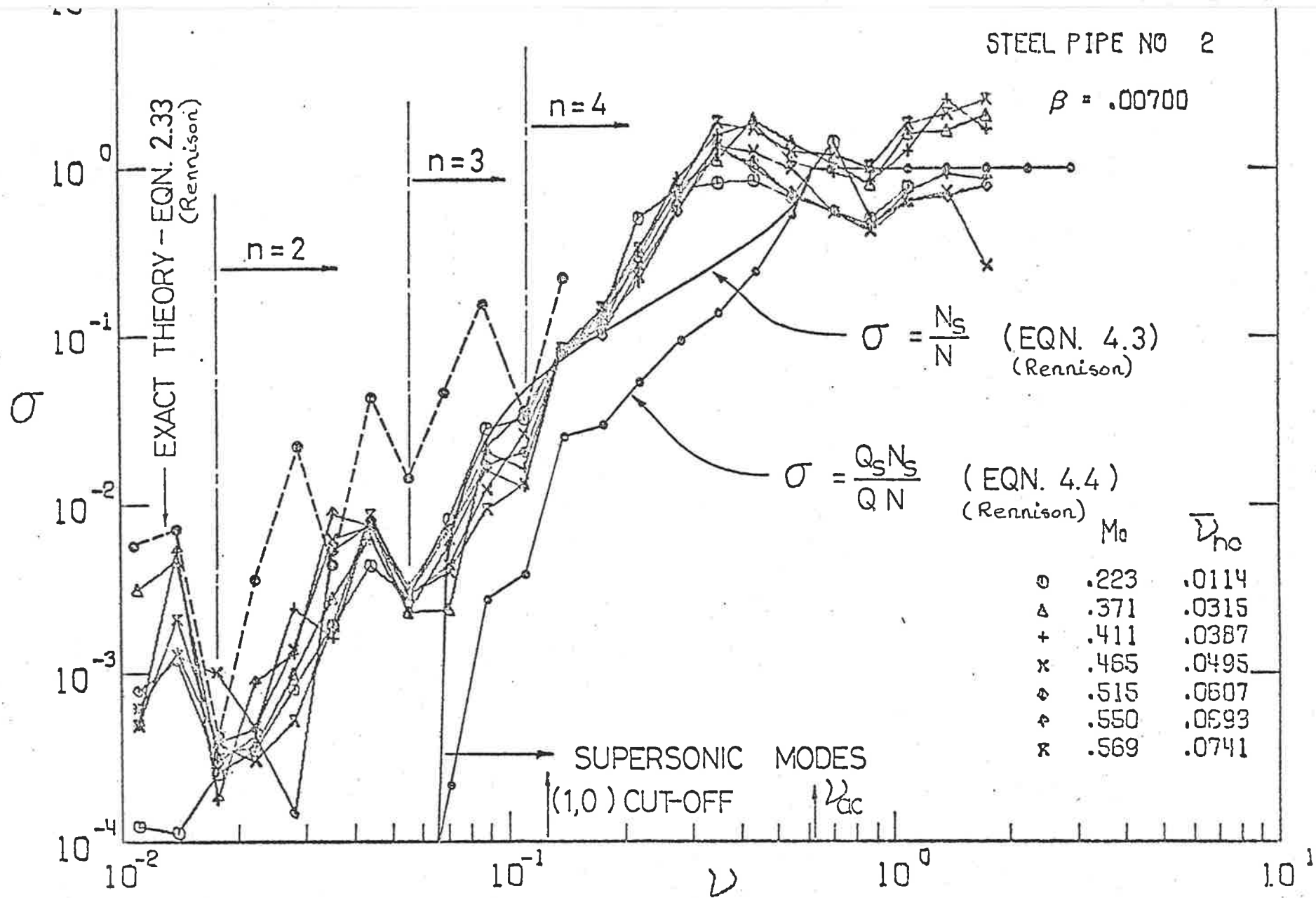


FIG. 4.45 (a) σ FOR VARIOUS M_0 . STEEL PIPE $\beta = .00700$
from Rennison (1976)

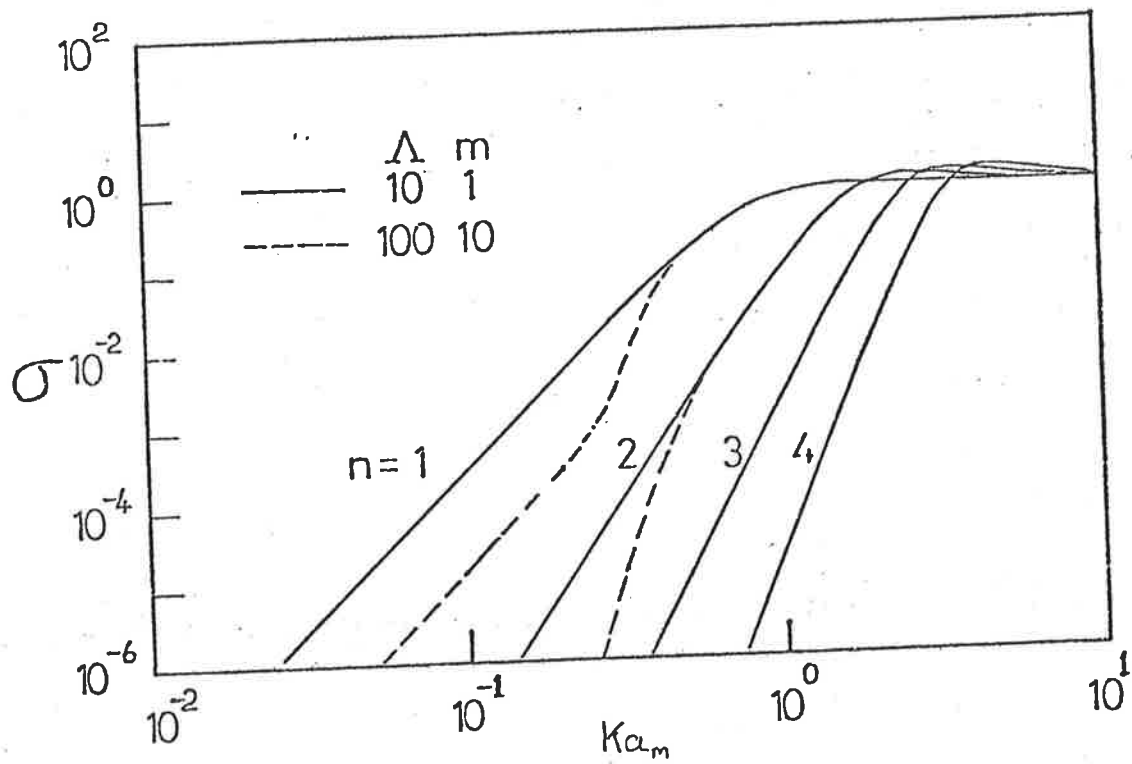


FIG. 4.45(b) EFFECT OF Ka_m ON σ FOR VARIOUS n
 from Rennison (1976)

in pipe wall response at these frequencies to plane wave excitation from the 90° mitred bend, as determined in the present investigation. Rennison (1976) showed that in pipes ($\Lambda \gg 1$), the radiation ratios of these low n subsonic modes are not negligible and they tend to have a strong influence on the external acoustic radiation. The observed increases in external acoustic radiation at these low frequencies to plane wave excitation from the 90° mitred bend confirm Rennison's observations. On average, these plane wave excitations cause the pipe to radiate more efficiently than the undisturbed fully-developed turbulent flow excitation (see σ/σ_0 in Figure 4.44) although it appears that most of the low frequency scatter in σ/σ_0 is experimental scatter. Comparisons are made in the next chapter with various internal flow disturbances.

4.4 THE FLOW DEPENDENCE OF THE INTERNAL WALL PRESSURE FIELD

The mean square value and the power spectral density of the wall pressure fluctuations associated with a turbulent boundary layer or fully-developed turbulent (straight) pipe flow are dependent on the flow speed. Many independent researchers (e.g. Bull, 1967) have found that the overall mean square pressure, $\overline{p^2}$, is fairly closely proportional to U_0^4 and that the power spectral density, ϕ_p , is fairly closely proportional to U_0^3 at any given Strouhal number, Ω . The non-dimensional power spectral density of the wall pressure fluctuations, Φ_p , which is non-dimensionalized on the basis of U_0^3 is therefore very nearly independent of flow speed.

An approximate U_0^3 dependence of ϕ_p (and hence a U_0^0 dependence of Φ_p) for straight pipe wall pressure fluctuations has been found in this investigation also (see Figure 4.31). The flow dependence for several Strouhal numbers is shown in Figure 4.46, where Φ_p is plotted against $\log_{10} M_0$. As can be seen, the non-dimensional spectral density,

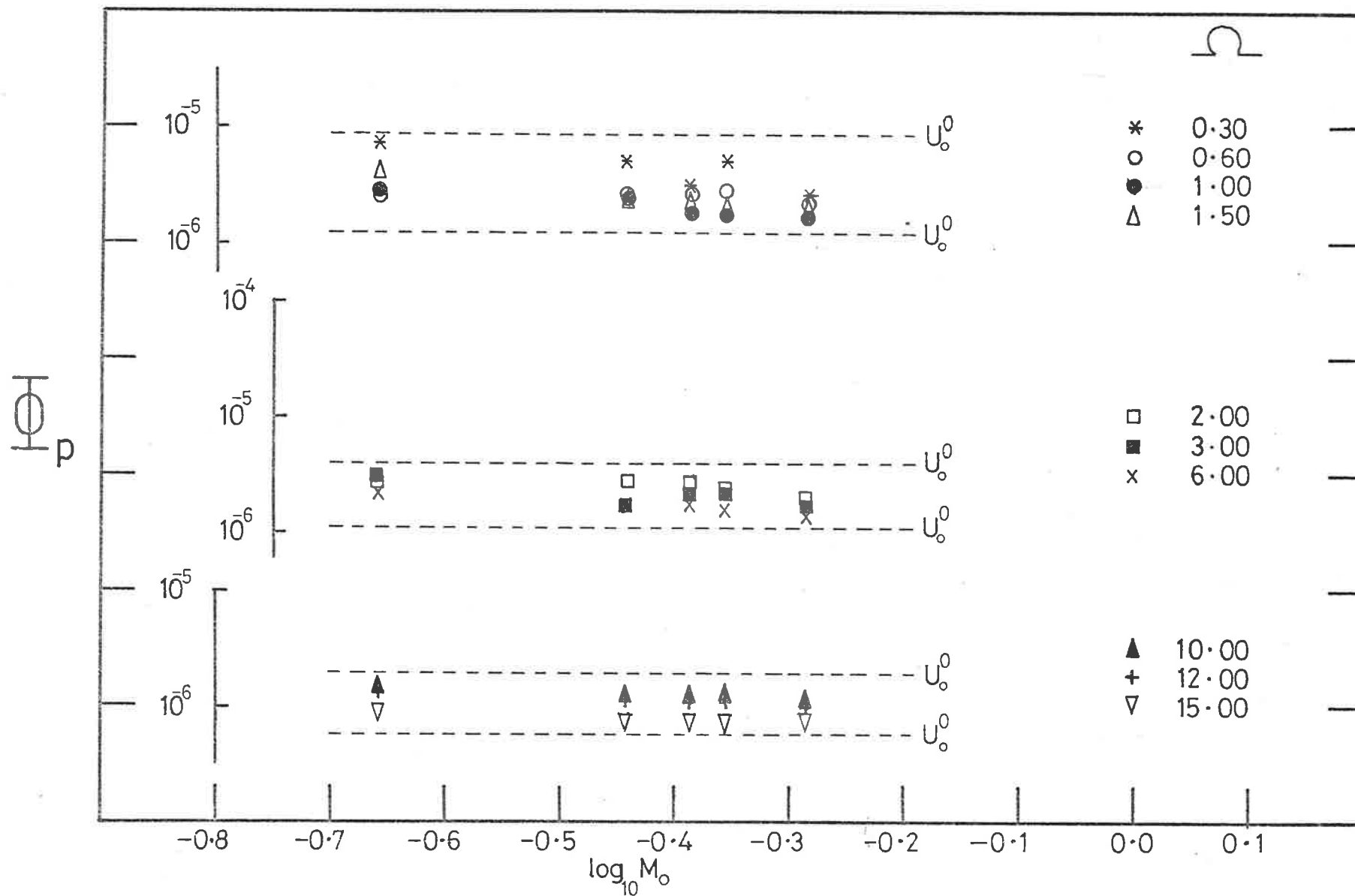


FIGURE 4.46 FLOW DEPENDENCE OF $\bar{\Phi}_p$ FOR STRAIGHT PIPE

Φ_p , is essentially independent of U_o , which implies that ϕ_p scales as U_o^3 and that $\overline{p^2}$ scales as U_o^4 . There is however experimental scatter in the spectra (Figure 4.31) and this is evident in Figure 4.45 at some Strouhal numbers. However for the majority of Strouhal numbers, Φ_p scales approximately as U_o^0 .

In the case of the 90° mitred bend, the overall picture is somewhat different. Values of $(\Phi_p - \Phi_{p_o})$ against $\log_{10} M_o$, where Φ_{p_o} is the non-dimensional power spectral density of the wall pressure fluctuations associated with undisturbed fully-developed turbulent pipe flow, are presented in Figure 4.47 for several Strouhal numbers. The data are presented for Strouhal numbers corresponding to frequencies below and above the cut-off frequency of the first higher order acoustic mode. There is experimental scatter in the spectra (see Figure 4.31) as in the case of the fully-developed turbulent pipe flow but it can be seen from Figure 4.47 that Φ_p scales approximately as U_o^0 for most Strouhal numbers below and as U_o^2 for most Strouhal numbers above the cut-off frequency of the first higher order mode. Thus, at a given Strouhal number, ϕ_p scales as U_o^3 and U_o^5 below and above cut-off of the first higher order mode respectively, and $\overline{p^2}$ scales correspondingly as U_o^4 and U_o^6 . However, despite this, the overall mean square pressure associated with a 90° mitred bend scales approximately as U_o^4 (see Figure 4.19 where over the range of flow conditions investigated, p'/q_o is roughly independent of Reynolds number). It can be seen from the frequency weighted power spectral densities in Figure 4.23 (at $X = 52.8$), that the largest contributions to the mean square pressure fluctuations come from frequencies below the cut-off frequency of the first higher order acoustic mode. These $\overline{p^2}$ contributions, scaling as U_o^4 , clearly outweigh the contributions from the higher order modes, which scale as U_o^6 , in the overall mean square pressure fluctuations, thus the U_o^4 overall dependence.

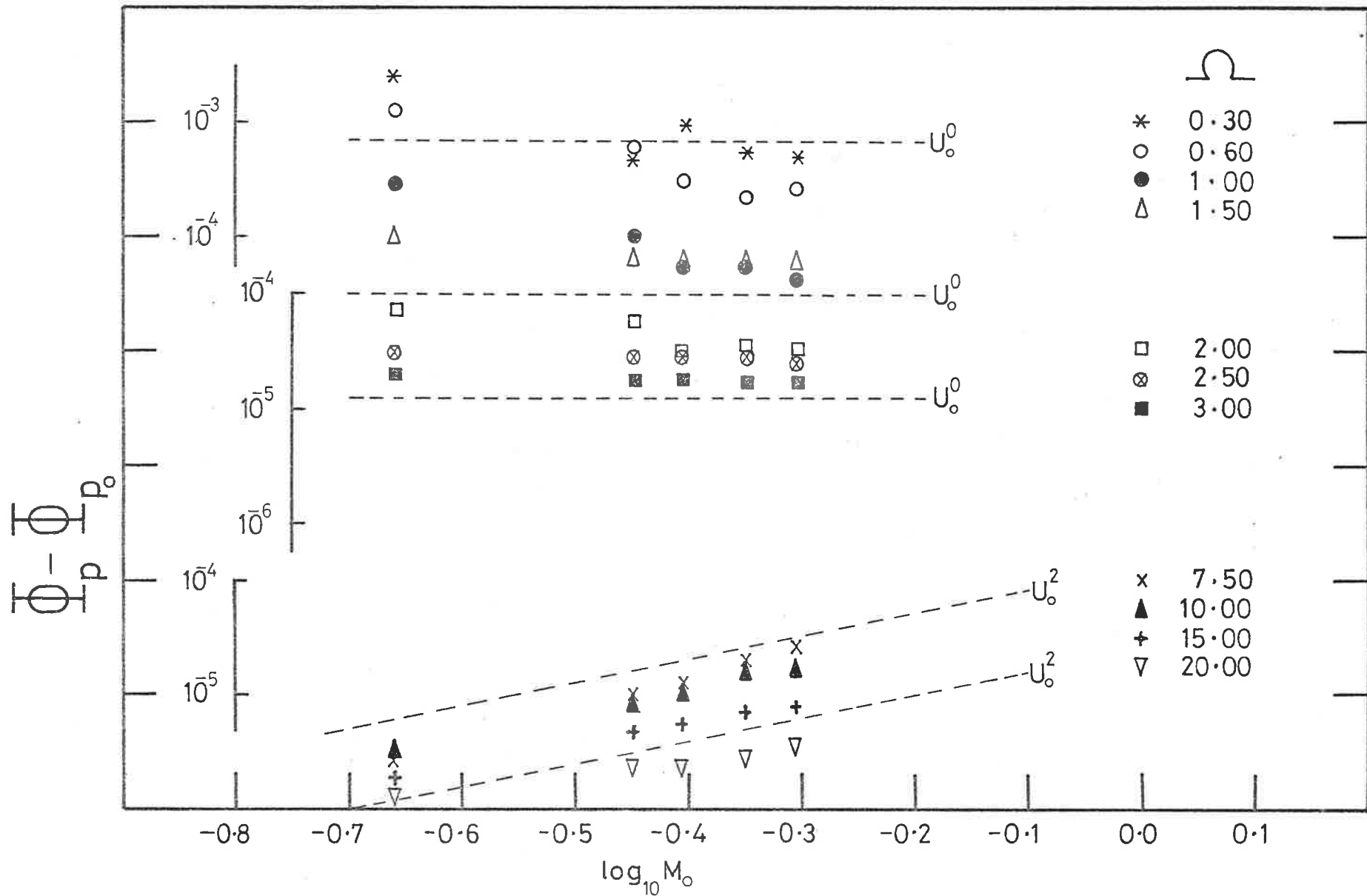


FIGURE 4.47 FLOW DEPENDENCE OF $\frac{K_p}{U_0^2}$ FOR 90° MITRED BEND

The flow dependence of the wall pressure fluctuations associated with the other internal flow disturbances that were investigated are discussed in the next chapter.

4.5 GENERAL DISCUSSION

It has been established that the flow disturbances produced by the 90° mitred bend generate an intense internal acoustic field. The non-propagating fluctuations are attenuated rapidly with distance downstream (and upstream) and, at points greater than 12 diameters downstream of the bend, the remaining disturbance consists entirely of propagating acoustic waves. The major contribution to this internal acoustic field is made by plane acoustic waves at frequencies below the cut-off frequency of the first higher order mode. This is consistent with the observations of Kuhn and Morfey (1976), on noise due to turbulent pipe flow exhausting from a pipe containing a 90° mitred bend. In their work, the bend was found to give rise to significantly increased noise levels. The radiated acoustic power was found to grow approximately as U^6 , where U is the flow velocity at the pipe exit. The wall pressure fluctuations associated with the internal acoustic field in this investigation scale as U_0^4 for frequencies below the cut-off frequency of the first higher order acoustic mode, and as U_0^6 for frequencies above the cut-off frequency of the first higher order acoustic mode.

At all flow Mach numbers investigated, there is an increase in the power spectral density of both the wall acceleration and the acoustic power radiation over those for undisturbed flow, over the whole frequency range. Low frequency increases are associated with plane acoustic waves but the increases abruptly become much larger as the higher order acoustic modes become propagational, for $v > 0.10$. Furthermore, this behaviour occurs despite the fact that the greatest acoustic disturbance to the wall pressure spectra occurs at frequencies

which correspond to $\nu < 0.10$.

The fact that the effects for a particular higher order mode appear to be confined to frequencies near its cut-off frequency is explained by the considerations of Chapter 2 (section 2.5 in particular), namely that it is a consequence of the occurrence of the sharp maximum in the joint acceptance at coincidence. By means of the phenomenon of coincidence, the higher order acoustic modes select and enhance the vibration of those resonant modes of the structure which radiate most efficiently into the fluid outside the pipe. In addition, these efficiently radiating structural modes now make a proportionately greater contribution to the radiated sound power. Radiation ratios (σ/σ_0) are a maximum in the region of the (1,0) and (2,0) higher order acoustic modes.

Acoustic plane waves generated by the bend, contribute to the vibrational response and the power radiation at frequencies below the cut-off frequency of the first higher order mode, resulting in an overall increased radiation ratio (σ/σ_0) in comparison to undisturbed fully-developed turbulent pipe flow. Acoustic plane waves may also contribute to the vibrational response and the power radiation at frequencies above the cut-off frequency of the first higher order mode. The component of the wall pressure fluctuations associated with the plane waves can be estimated from longitudinal space-time cross-correlations of the wall pressure fluctuations with appropriate time delays and spatial separations. This is discussed in considerable detail in Chapter 6.

For an ideal pipe with no asymmetry, propagating acoustic plane waves do not constitute a very efficient form of vibrational excitation, since they necessarily give rise to a forced response of the same wavenumber in the pipe wall. But if flow conditions in the pipe are such that the speed of sound inside the pipe is greater than

in the external fluid, then this forced peristaltic wave motion in the pipe wall will generate acoustic radiation very efficiently. For real pipes, inhomogeneities in pipe structure and end conditions will give rise to coupling between plane wave excitation and resonant modes of the pipe, so that the vibrational response will in general be greater than the forced response which would be expected in the ideal case (see Rennison and Brown, 1976).

The explanation of the observed overall behaviour of the pipe wall response and the external acoustic radiation therefore lies both in the ability of higher order acoustic modes, which occur only for $\nu > 0.10$, to excite resonant pipe wall modes and in the phenomenon of coincidence of the higher order acoustic modes with selected structural resonant modes. The spectral increases in pipe wall vibration response and external acoustic radiation at frequencies at and above the cut-off frequency of the first higher order mode dominate over those spectral increases at frequencies where only plane waves can propagate in the particular case of the 90° mitred bend although the internal acoustic field is dominated by low frequency plane waves.

CHAPTER 5

EXPERIMENTS WITH OTHER INTERNAL FLOW DISTURBANCES

5.1 INTRODUCTION

Measured values of the effects of several internal flow disturbances on the wall accelerations of and external acoustic radiation from a pipe carrying a fully-developed internal turbulent air flow (at a distance greater than 50 diameters downstream of the disturbance) are presented in this chapter together with spectral measurements of the wall pressure fluctuations. Some spectral measurements are also presented for the wall pressure fluctuations upstream of the disturbances. The internal flow disturbances investigated were those due to a 45° mitred bend, two 90° radiused bends with ratios of bend radius to mean pipe radius R/a_m of 3.0 and 6.4, a gate valve and a butterfly valve.

Some of the results already presented in Chapter 4 on the 90° mitred bend are also included in this chapter for comparison with these various internal flow disturbances. Also, spectral measurements of the wall pressure fluctuations, wall acceleration of and acoustic power radiated from a pipe carrying a fully-developed internal turbulent air flow, with no flow disturbance - i.e. "straight pipe flow", are presented. These data form a standard against which the measured effects of the various flow disturbances can be judged. We are not concerned in this chapter with "local" non-propagating disturbances in the region of the various flow disturbances but only with the propagating acoustic field superimposed on a wall pressure field associated with fully-developed turbulent pipe flow.

Mean velocity profiles have been obtained at all five flow speeds for the various flow disturbances at measuring points upstream of the disturbances ($X = -12.9$) and just upstream of the test section ($X = 52.4$). As seen in Chapter 3, in all cases there is fully-developed turbulent flow at entry to the disturbances ($X = -12.9$), and at entry to the test section ($X = 52.4$) an undisturbed fully-developed turbulent flow profile has been re-established.

All the experimental results for the vibration response and the acoustic radiation presented in this chapter apply to the thin-walled cylindrical test-section described in Chapter 4.

5.2 SPECTRA OF WALL PRESSURE FLUCTUATIONS

As in the case of the 90° mitred bend, the power spectra of the wall pressure fluctuations has been measured at each flow speed just upstream of the test section ($X = 52.8$) and, the data are presented in the form of the non-dimensional power spectral density, Φ_p , as a function of Strouhal number, Ω . The results are presented in Figure 5.1 to 5.4 for the 90° radiused bend ($R/a_m = 3.0$), the 45° mitred bend, the gate valve and the butterfly valve. The mean lines presented in Figure 5.5 have been obtained from the preceding curves, the scatter about these mean lines being generally less than ± 2 dB. As for the 90° mitred bend, the mean lines have been used to facilitate comparison between the various flow disturbances. The flow dependences of the various disturbances, above and below the cut-off frequency of the first higher order mode, are discussed in section 5.4. The mean lines for both the 90° radiused bends are almost identical and therefore only that for the $R/a_m = 6.4$ ratio is presented in Figure 5.5. Mean lines for the 90° mitred bend and the straight pipe "datum" are also included for comparison; they were obtained from the results in Chapter 4. The results presented in Figures 5.6 to 5.8 are for the 90° radiused bend

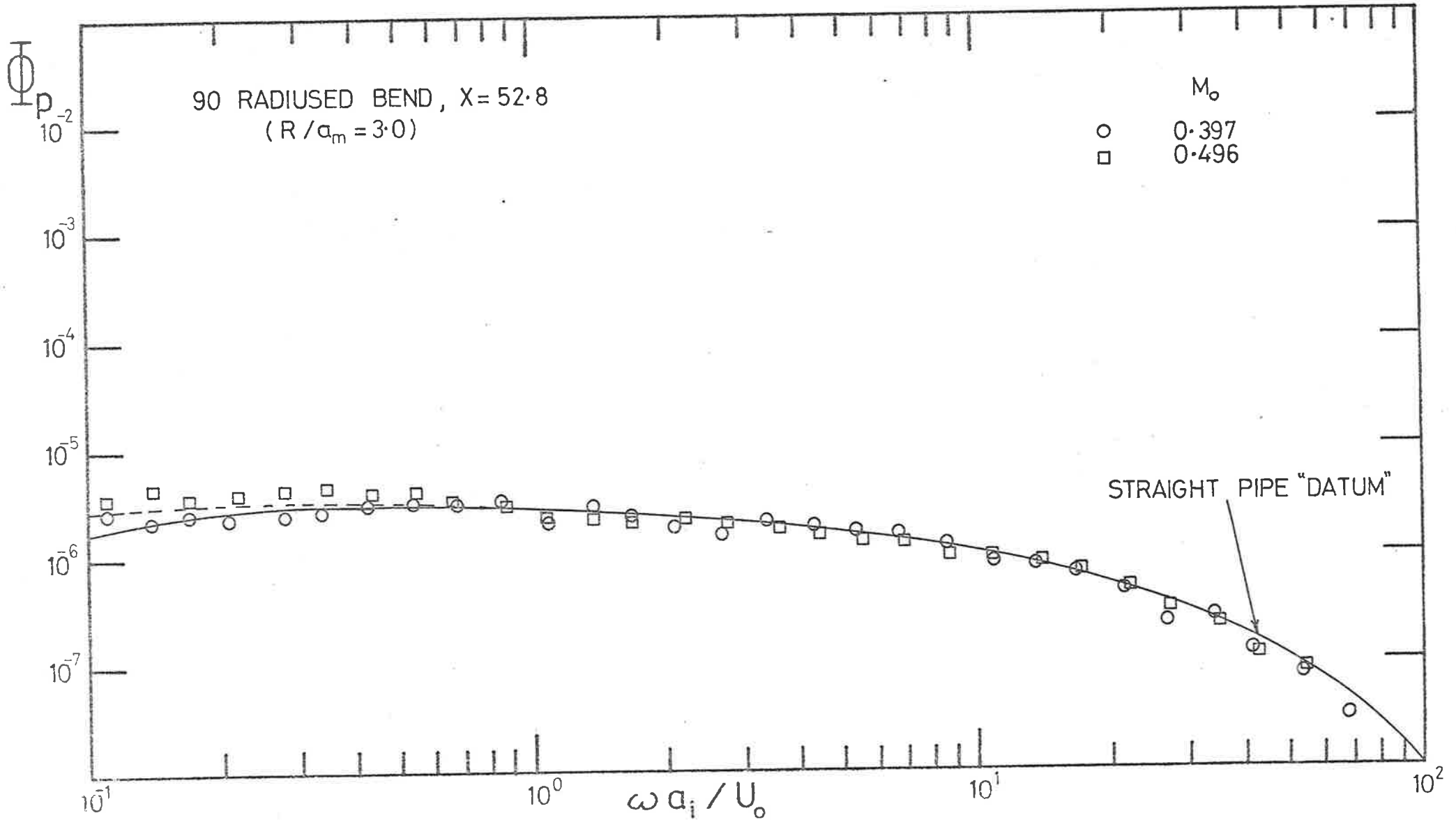


FIGURE 5.1 SPECTRAL DENSITY OF WALL PRESSURE FIELD

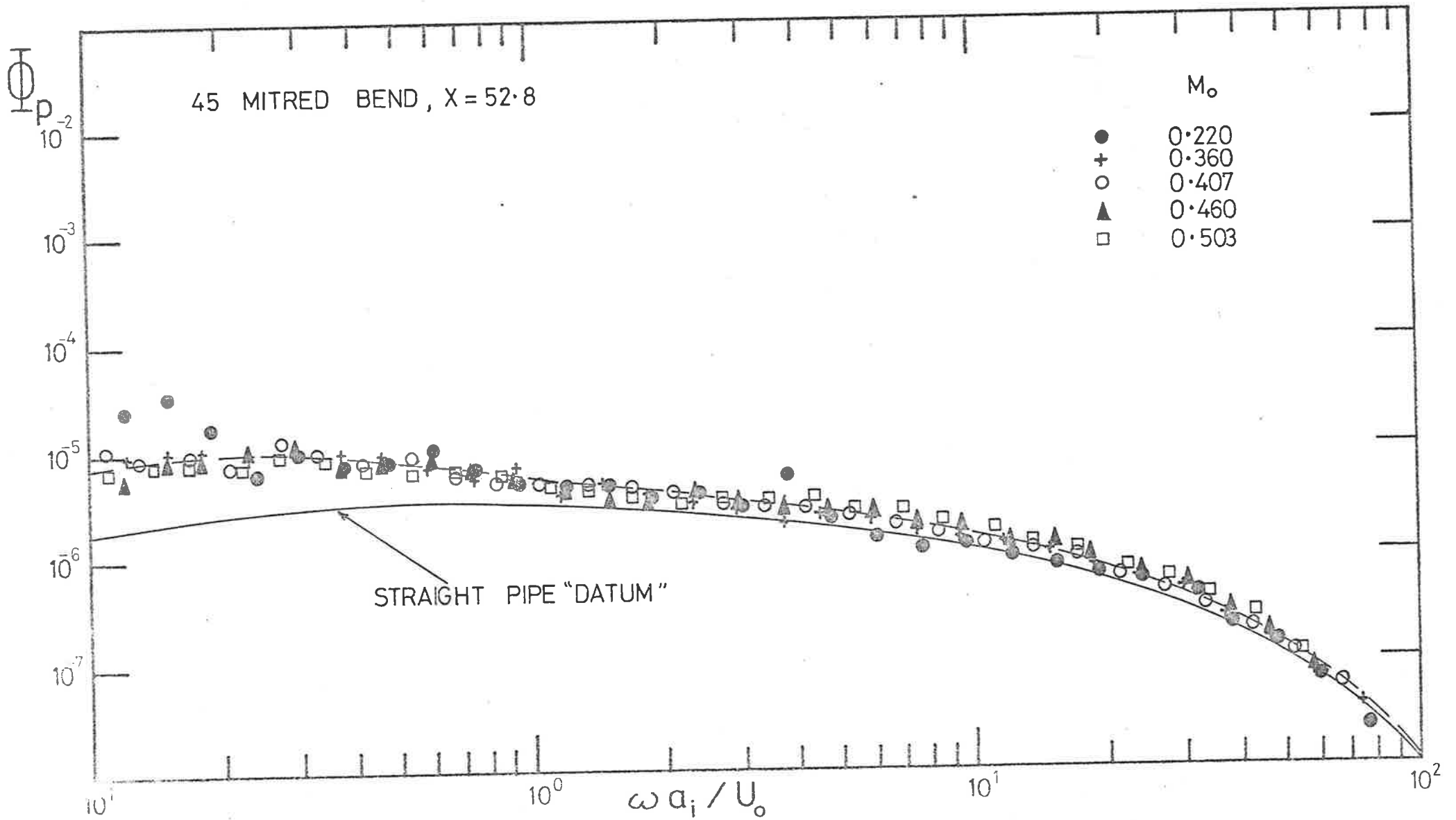


FIGURE 5.2 SPECTRAL DENSITY OF WALL PRESSURE FIELD

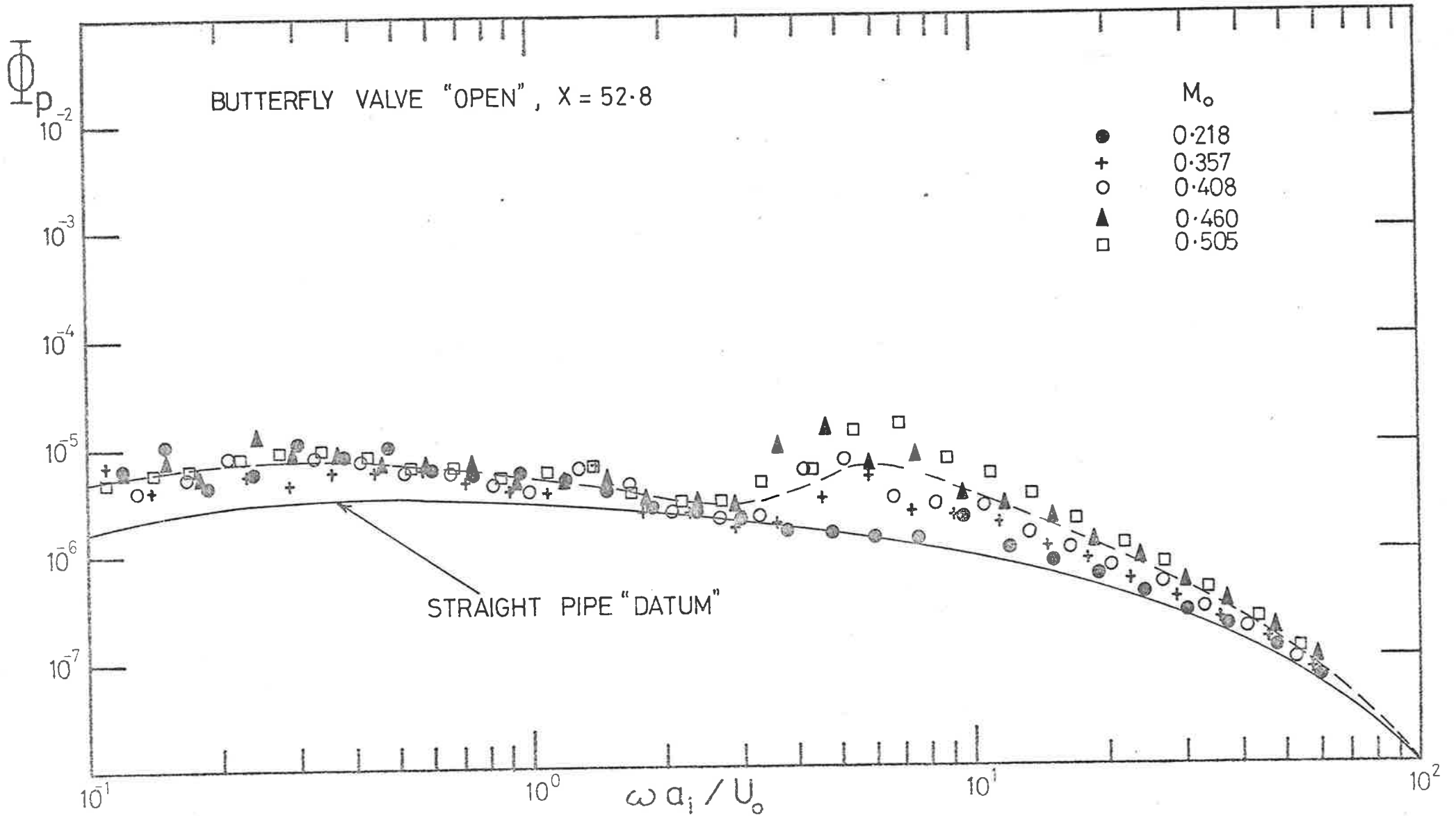


FIGURE 5.3 SPECTRAL DENSITY OF WALL PRESSURE FIELD

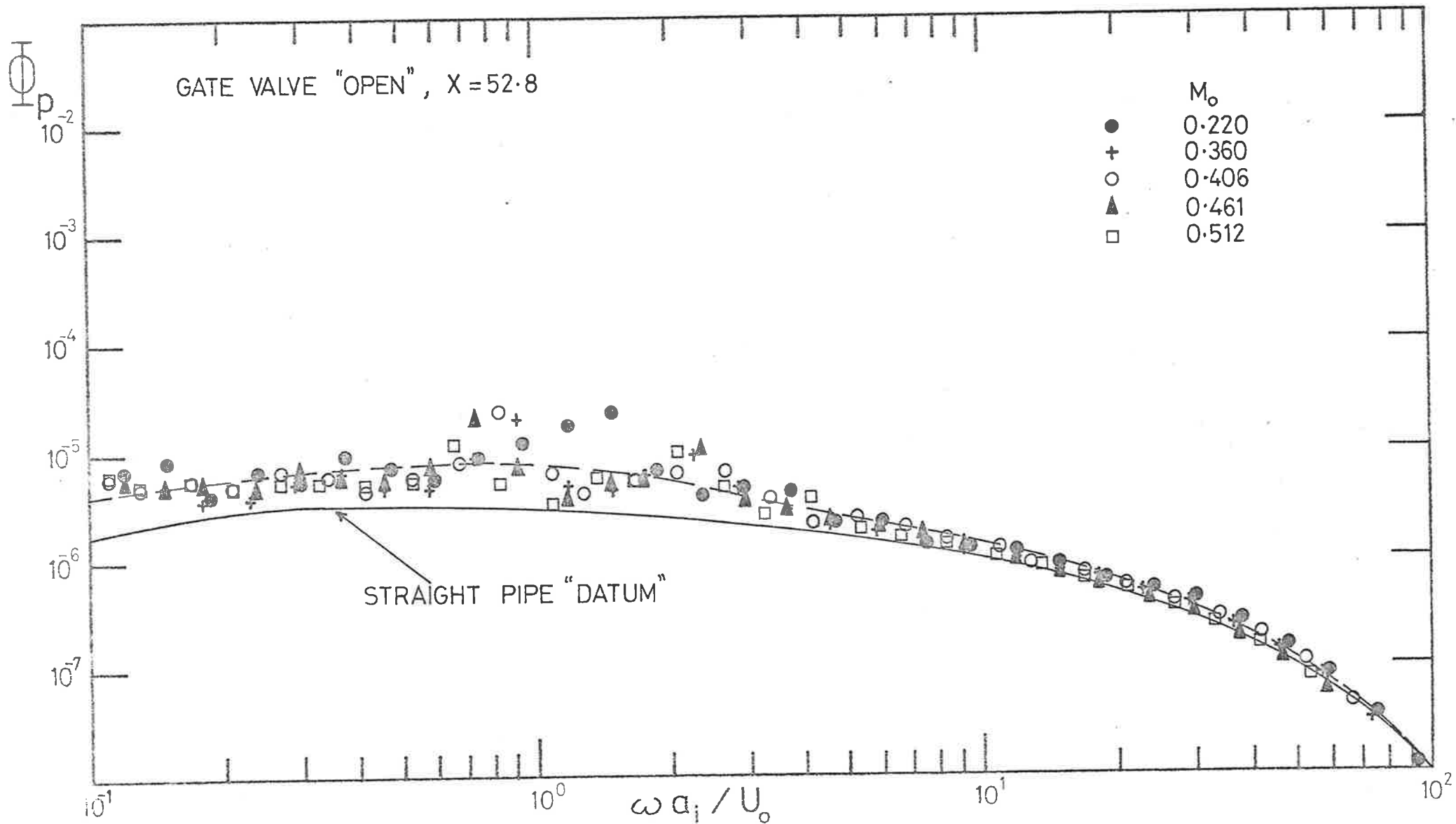


FIGURE 5.4 SPECTRAL DENSITY OF WALL PRESSURE FIELD

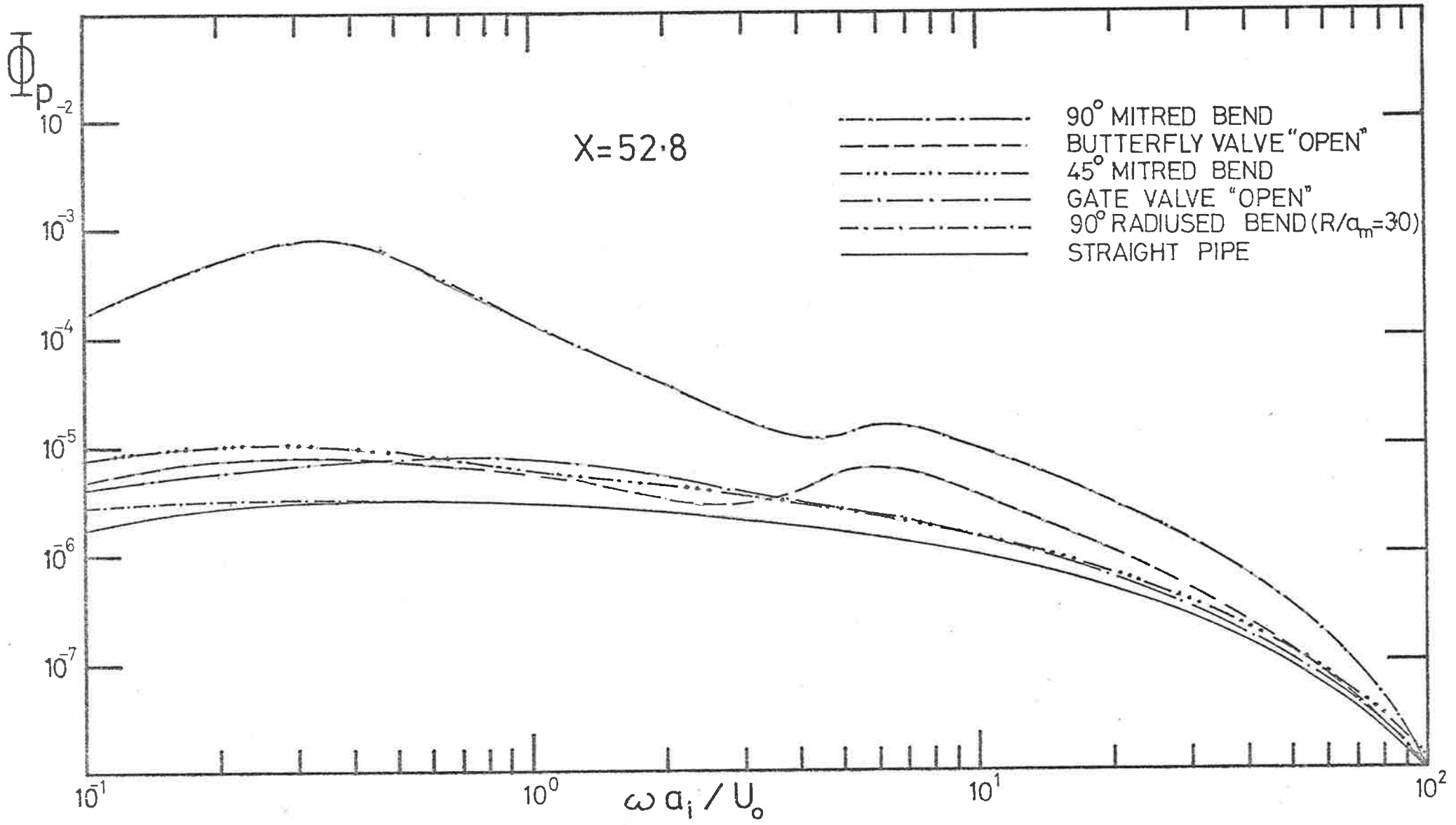


FIGURE 5.5 SPECTRAL DENSITY OF WALL PRESSURE FIELD (MEAN VALUES)

($R/a_m = 6.4$), the 45° mitred bend and the 90° mitred bend at a position, $X = -12.9$, upstream of the respective disturbances. Curves representing mean values of these data are presented in Figure 5.9; the scatter about the mean lines presented in Figure 5.9 is generally less than ± 2 dB. Again, the straight pipe "datum" is included for comparison. Once again, the flow dependence of the various disturbances is not totally accounted for, when the spectral data are presented in this manner but the spread of the data over the speed range investigated still allows gross differences between the various disturbances to be highlighted in this way.

From Figure 5.5, it can be seen that the wall pressure fluctuations associated with the 90° mitred bend are much more severe than those due to the other flow disturbances, in particular at low Strouhal numbers. The butterfly valve, also produces significant increases for Strouhal numbers in the region where higher order modes propagate but not at low Strouhal numbers where only plane waves can propagate. The two 90° radiused bends produce only mild increases in the wall pressure fluctuations at low Strouhal numbers and almost nothing at the highest Strouhal numbers investigated. At the measuring position upstream of the disturbance ($X = -12.9$) the Strouhal number dependence of the various disturbances investigated is similar to that at the entrance to the test section ($X = 52.8$). Measurements were not obtained at $X = 12.9$ for the two valves investigated.

That the flow disturbances due to the bends and valves do indeed give rise to acoustic disturbances in the pipe is readily confirmed qualitatively by listening to the sound radiation into the reverberation chamber from the inlet bell-mouth, and has been confirmed quantitatively by measurements of sound pressure levels by a microphone located on the pipe-axis in the inlet plane of the bell-mouth. The results of such measurements are shown in Figure 5.10. At the highest flow speed,

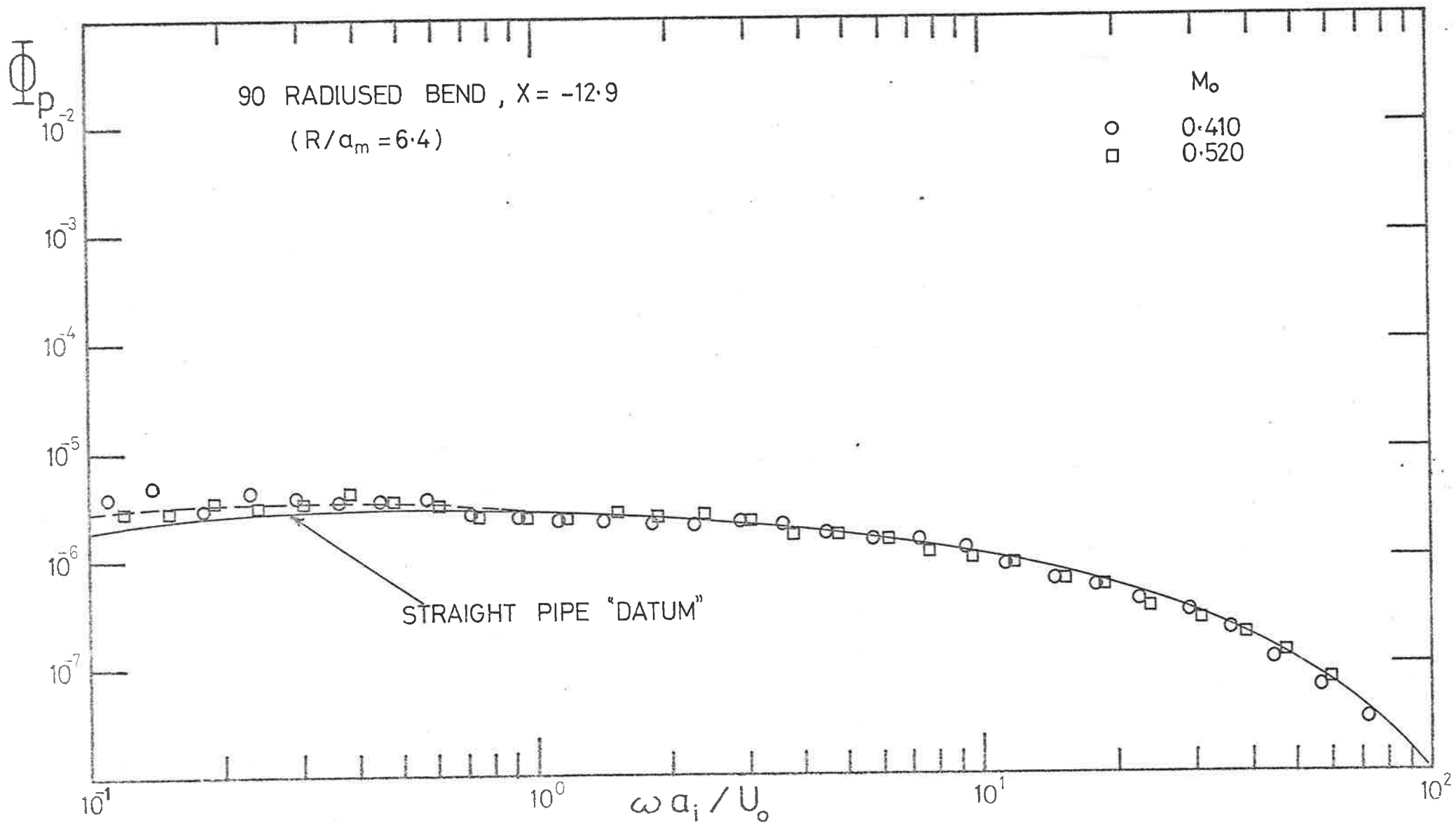


FIGURE 5.6 SPECTRAL DENSITY OF WALL PRESSURE FIELD

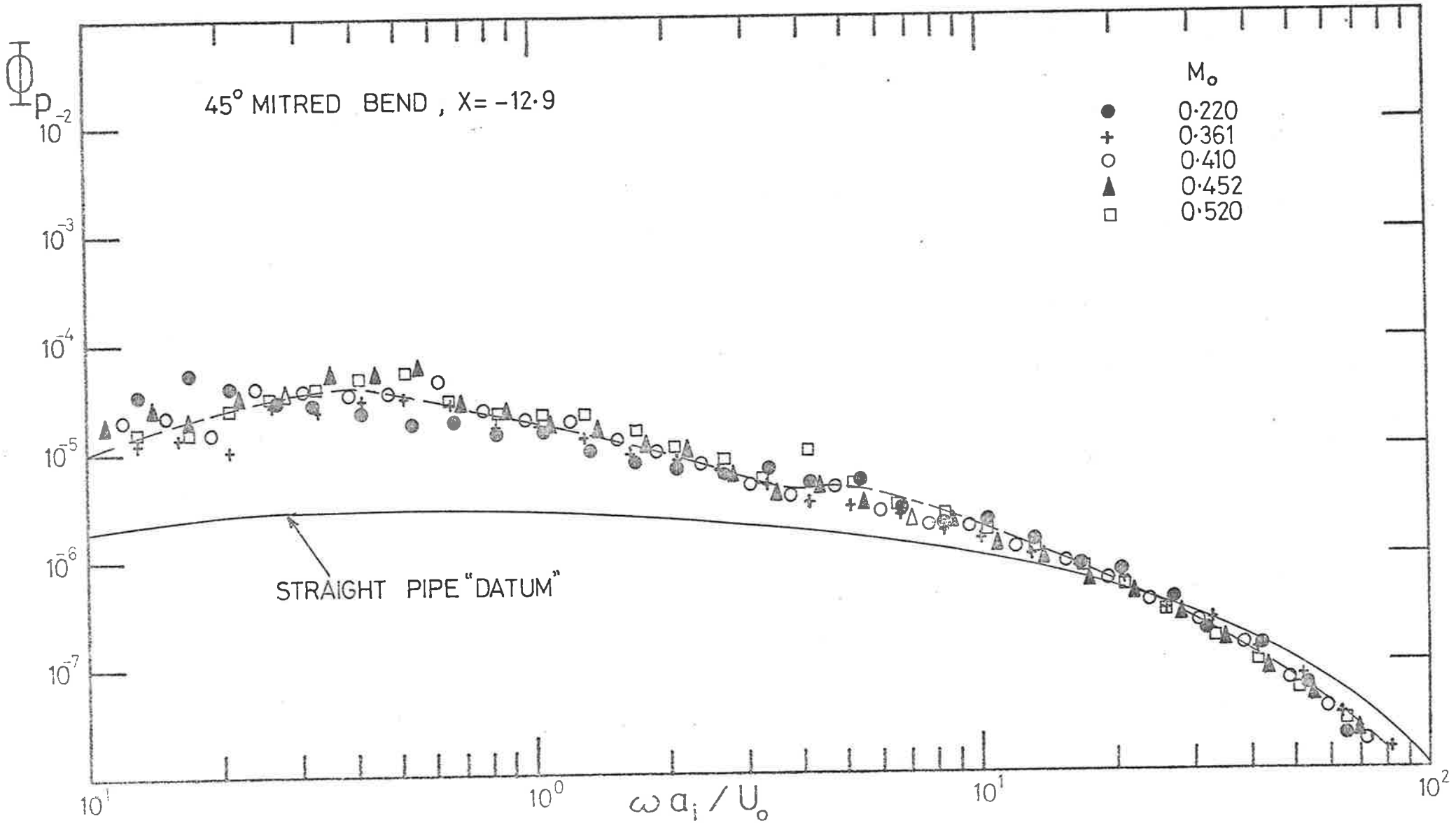


FIGURE 5.7 SPECTRAL DENSITY OF WALL PRESSURE FIELD

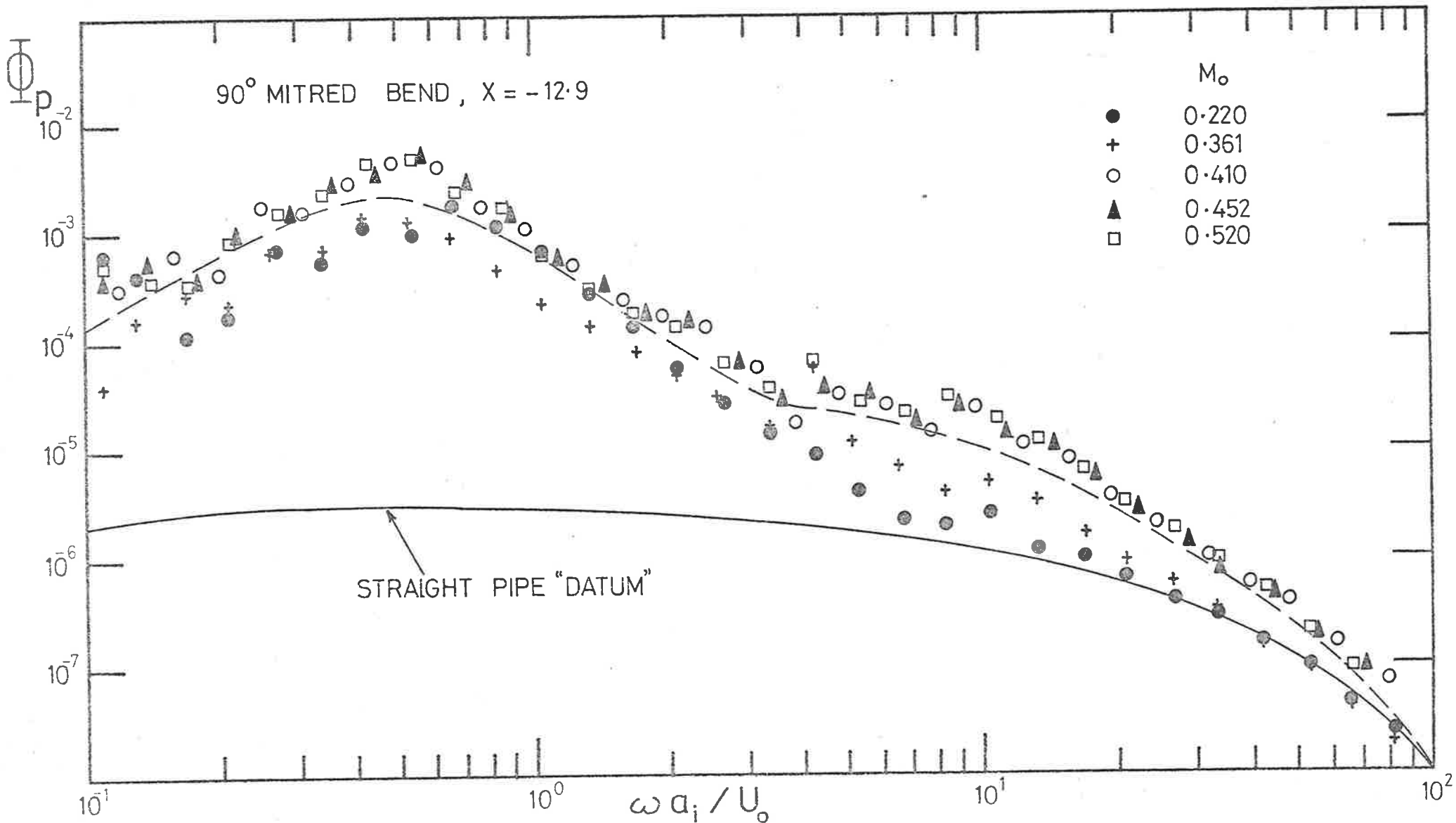


FIGURE 5.8 SPECTRAL DENSITY OF WALL PRESSURE FIELD

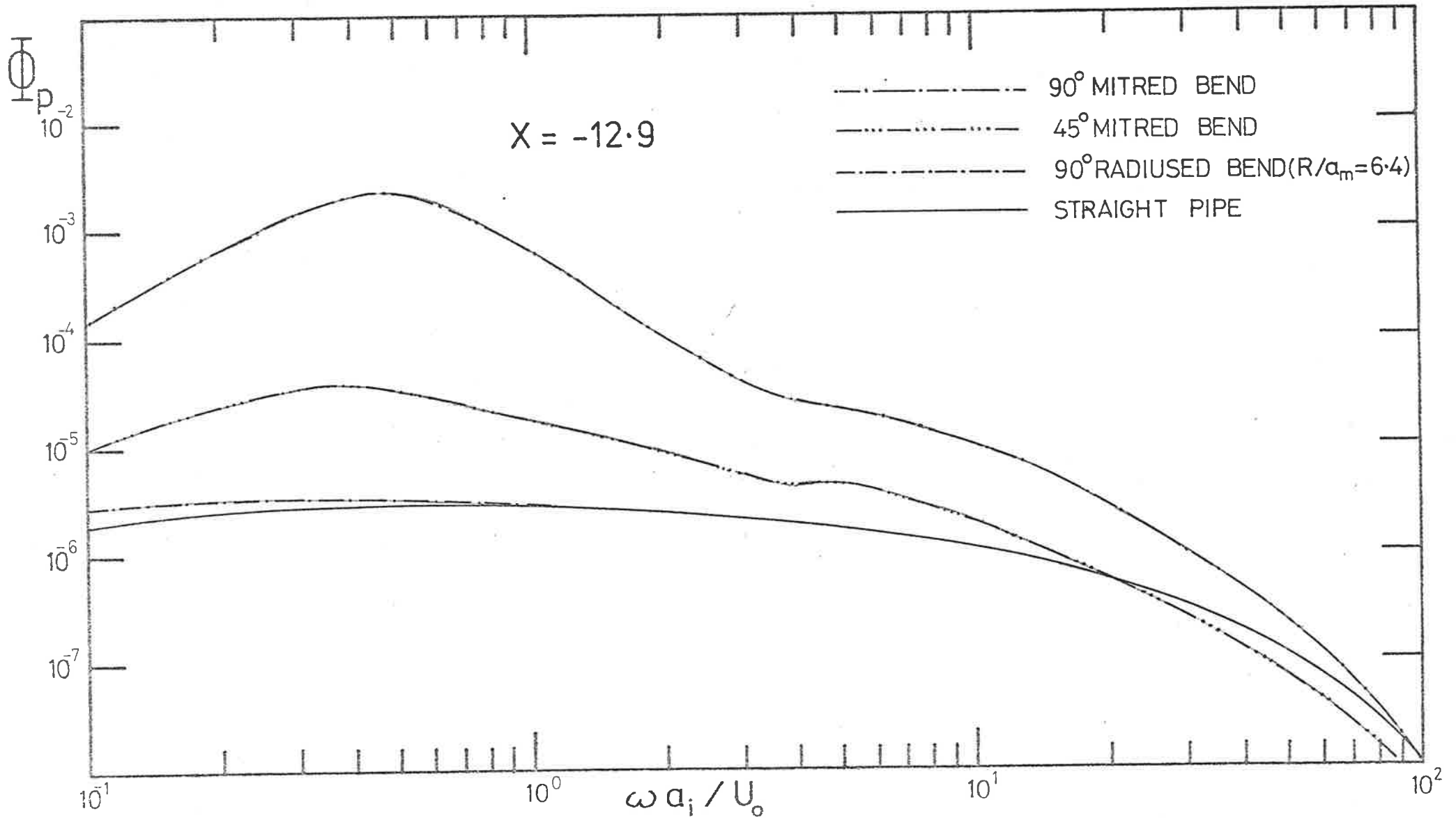


FIGURE 5.9 SPECTRAL DENSITY OF WALL PRESSURE FIELD (MEAN VALUES)

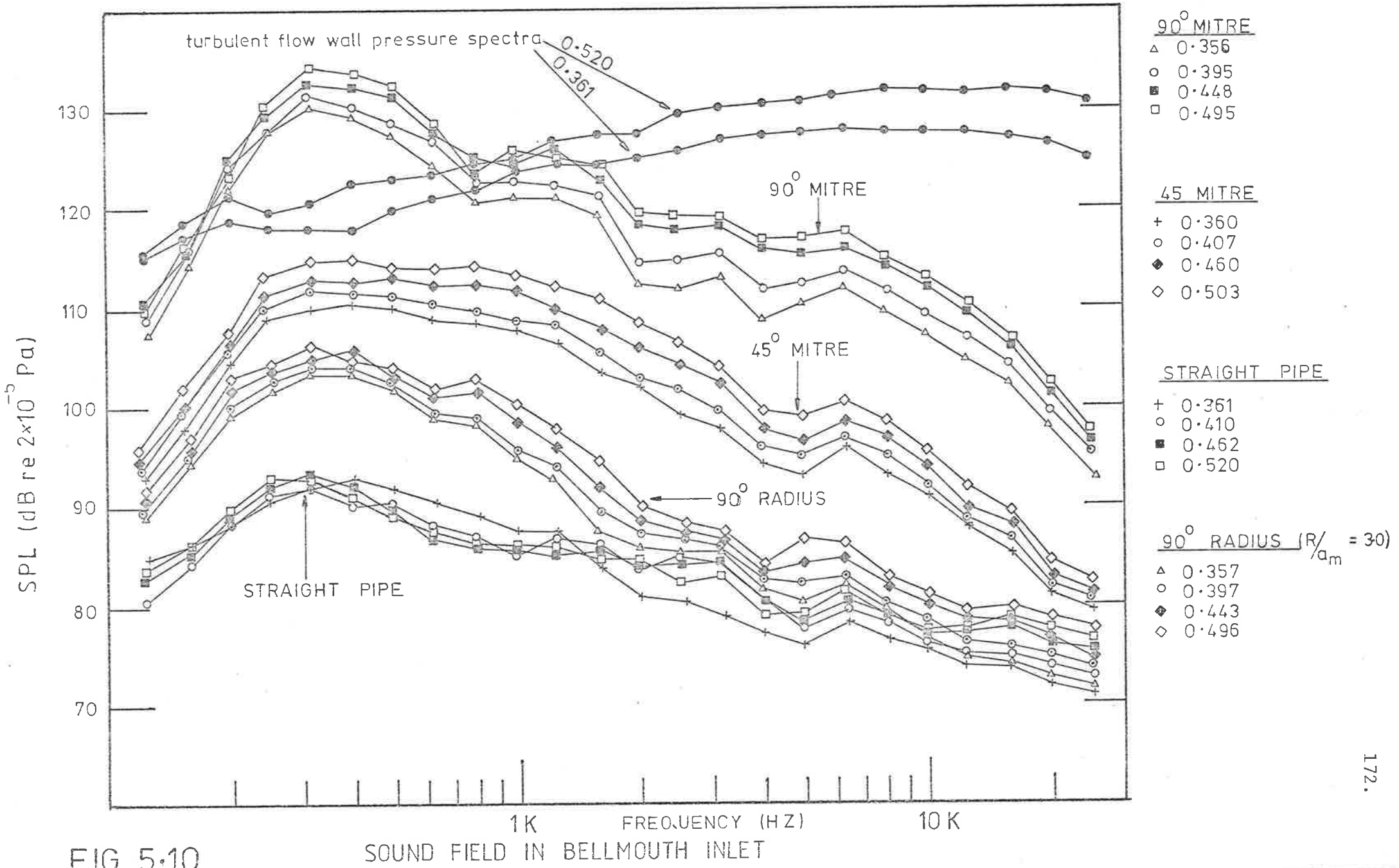


FIG 5.10

increases in sound pressure level at the bell-mouth, above that for a pipe of the same length but with no internal flow disturbance, are generally less than about 4 dB throughout the frequency range for the 90° radiused bend with $R/a_m = 6.4$ (data not shown); but they are as great as 15, 26, and 43 dB in some frequency bands for the 90° radiused bend with $R/a_m = 3.0$, the 45° mitred bend, and the 90° mitred bend respectively. For the gate valve and the butterfly valve (data presented in Section 5.5), the increases are as great as 25 and 35 dB respectively in some frequency bands.

5.3 ACCELERATION RESPONSE OF AND ACOUSTIC RADIATION FROM THE TEST SECTION

The acceleration response of and the acoustic radiation from the thin-walled test section were obtained in a similar manner to that described in Chapter 4 and the results are presented in the form of the non-dimensional spectral density of wall acceleration Φ_{ζ} and acoustic radiation Φ_{π} against non-dimensional frequency ν . As in Section 5.2, results for the 90° mitred bend and straight pipe flow are also presented for comparison.

The results presented in Figures 5.11 to 5.15 are for Φ_{ζ} against ν for the five flow speeds and are those obtained at the mid-point of the test section $X = 74.4$. It was found experimentally that Φ_{ζ} and Φ_{π} are axially and circumferentially uniform over the test section. Figures 5.16 to 5.20 are for Φ_{π} against ν . Because of the similarity in pipe wall acceleration and acoustic radiation levels for the two radiused bends, the results for both bends are not included simultaneously in all of Figures 5.11 to 5.20; instead each bend ($R/a_m = 3.0$ and $R/a_m = 6.4$) is included in alternate figures, to minimise confusion.

From Figures 5.11 to 5.20 it can be seen that the radiused bends do not cause significantly more acoustic power radiation than undisturbed fully-developed turbulent flow in a straight pipe, except

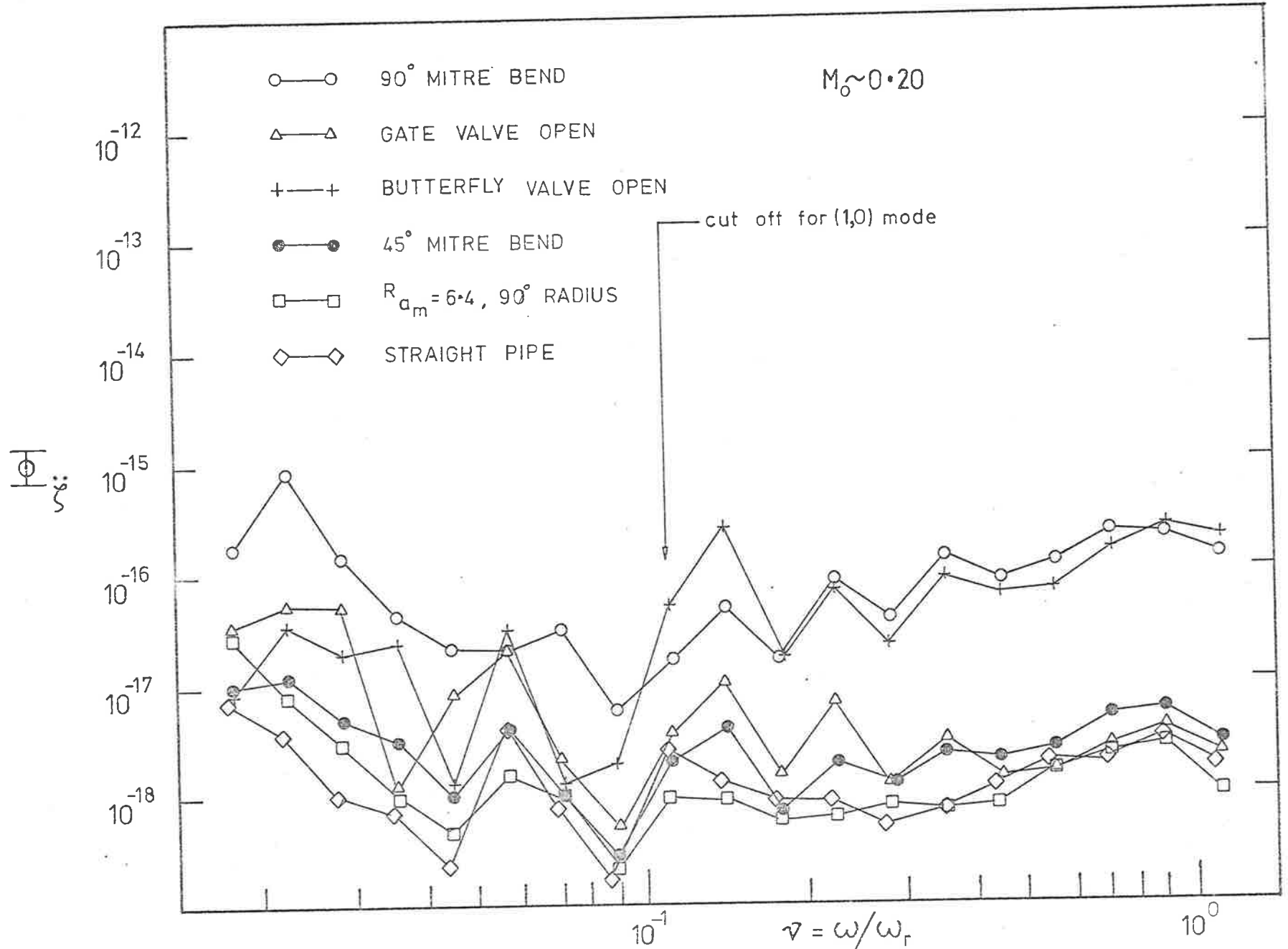


FIG 5.11

NON-DIMENSIONAL PIPE WALL ACCELERATION

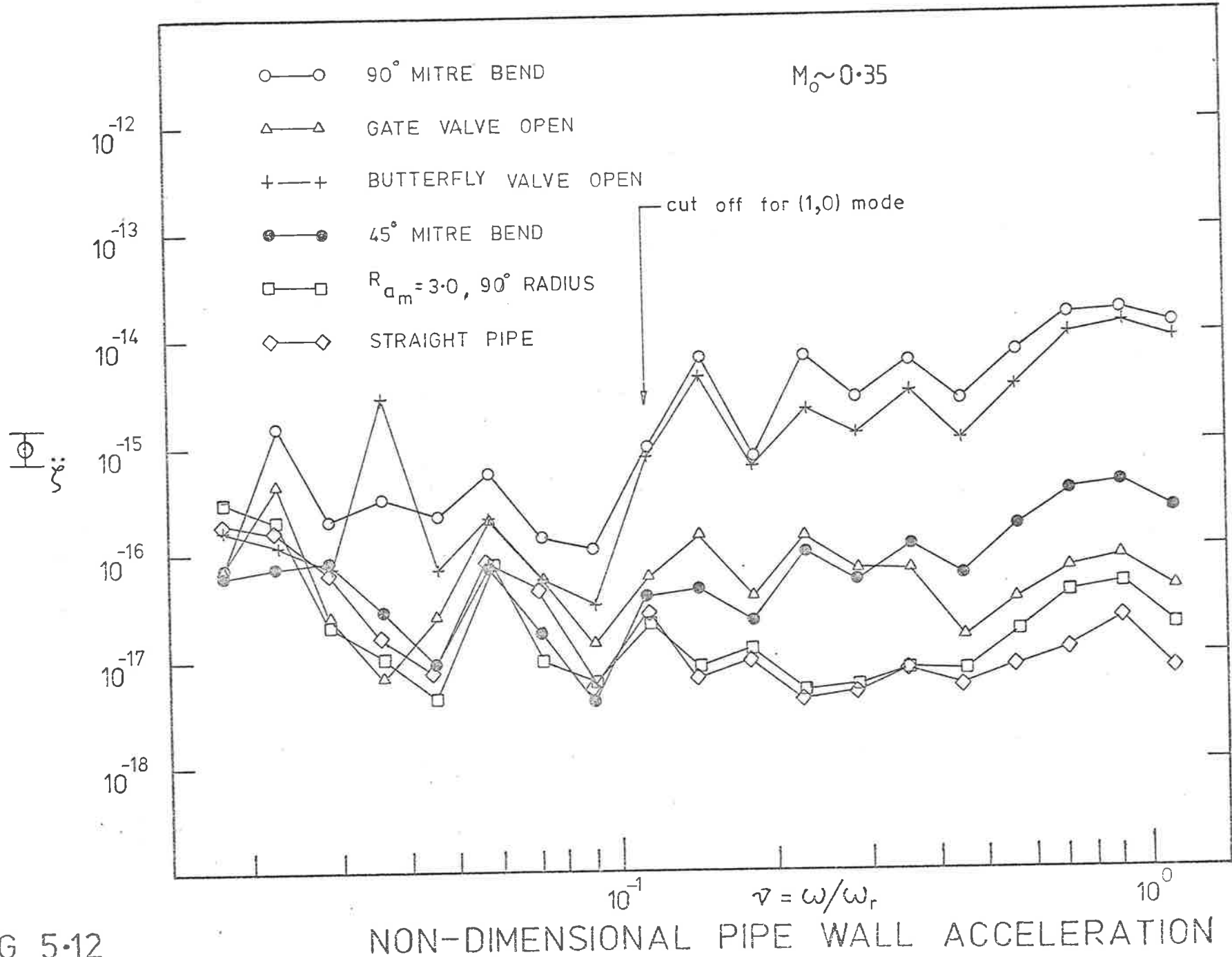


FIG 5-12

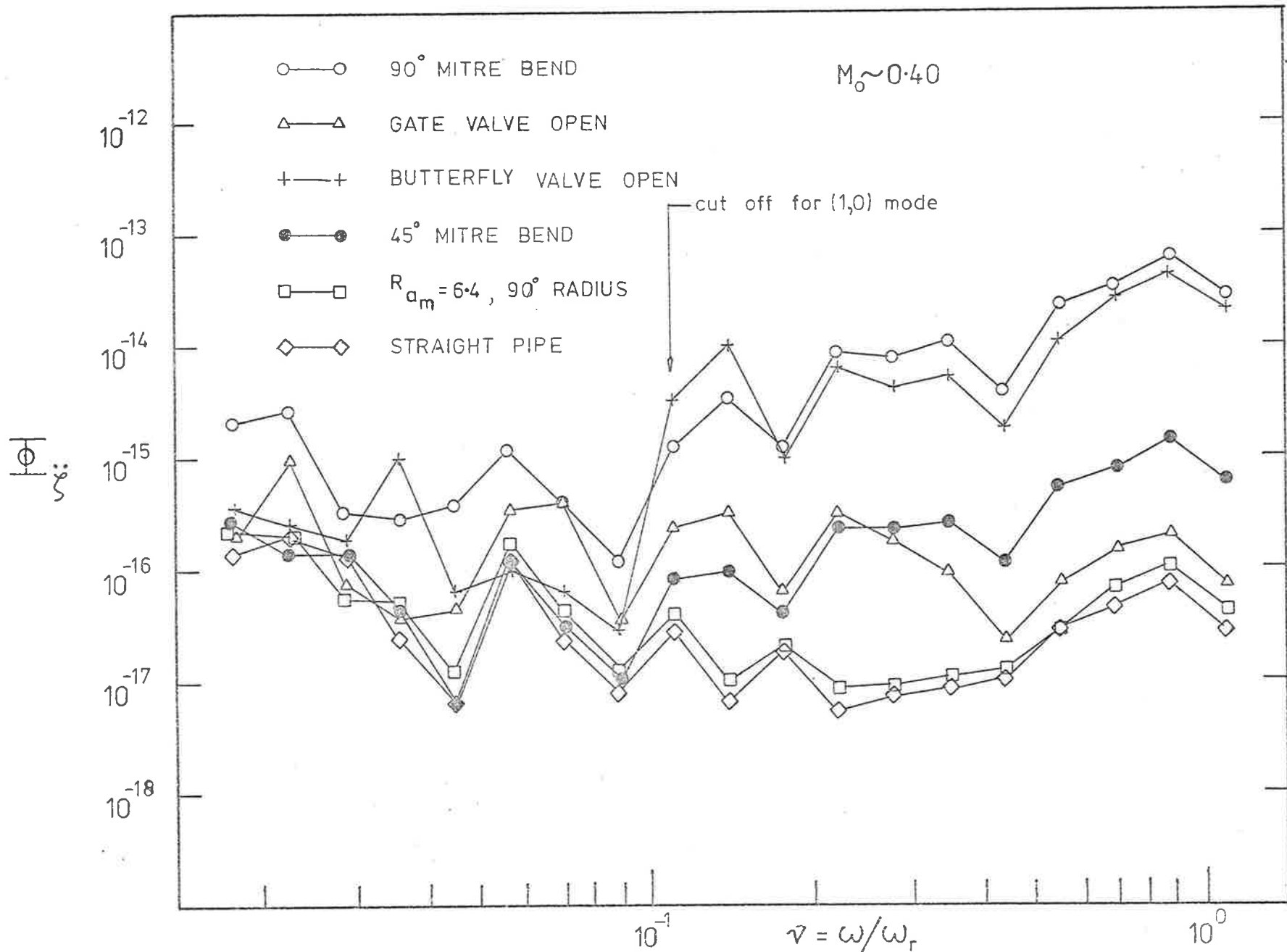


FIG 5.13

NON-DIMENSIONAL PIPE WALL ACCELERATION

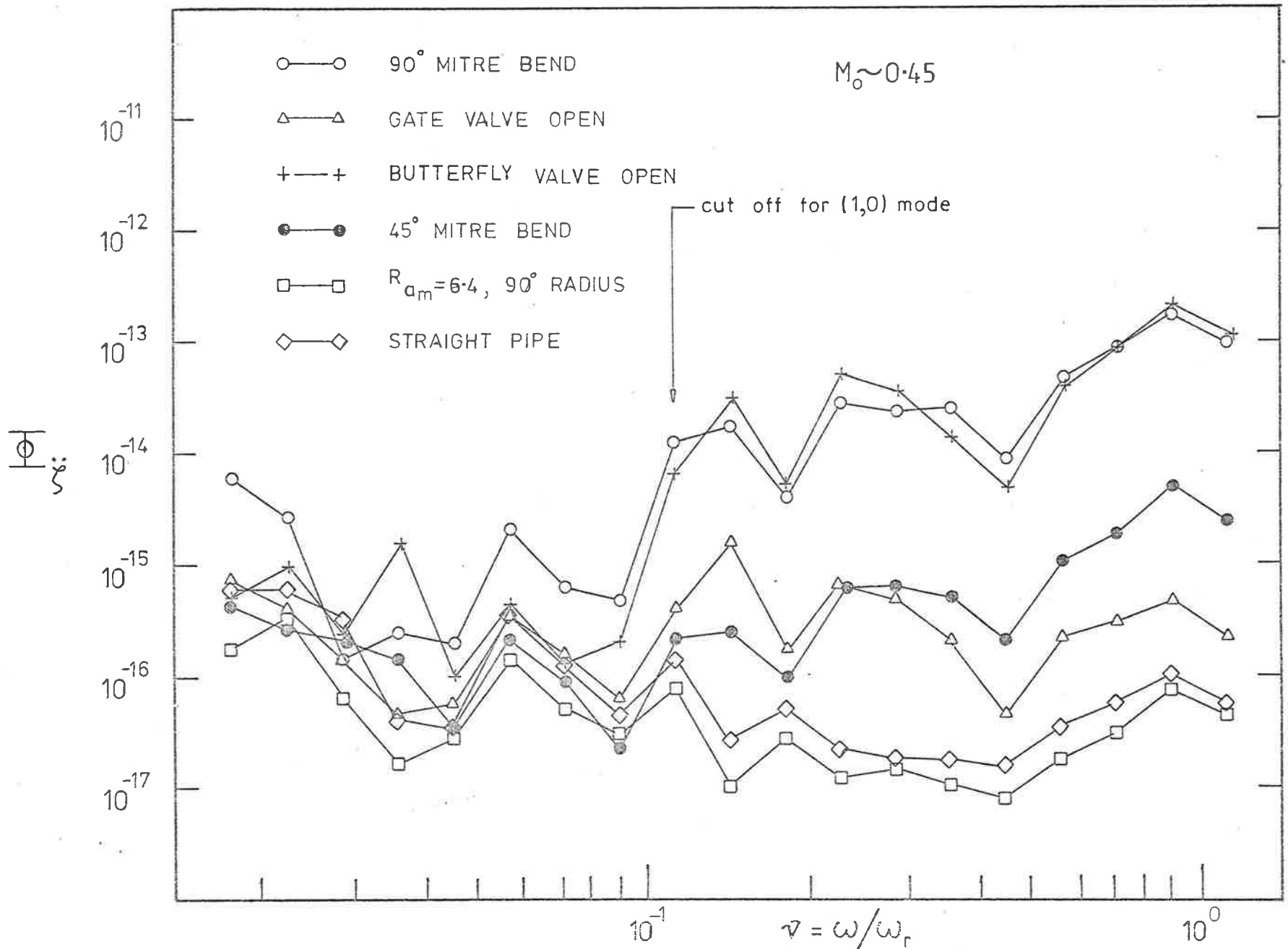


FIG 5.14

NON-DIMENSIONAL PIPE WALL ACCELERATION

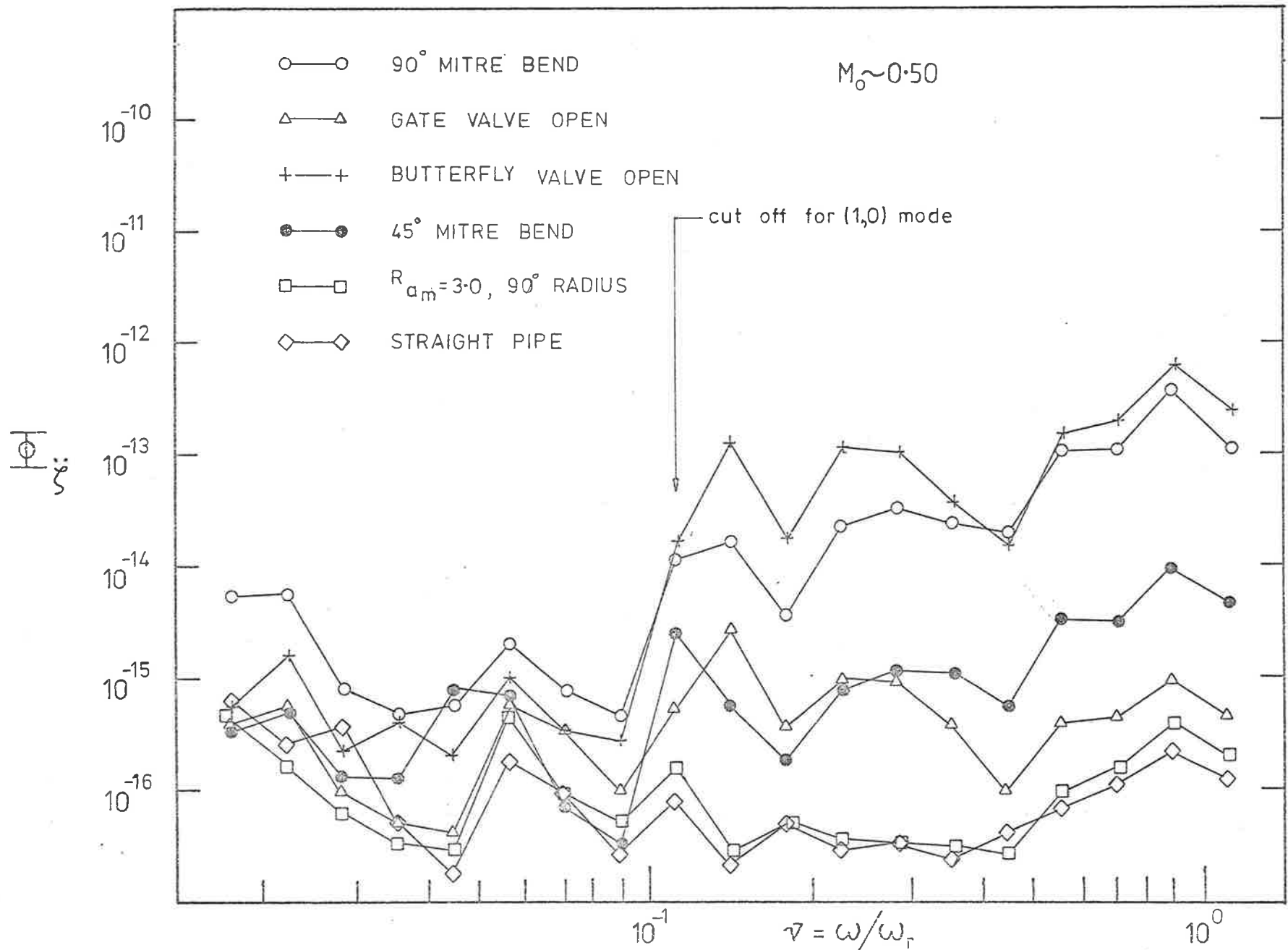


FIG 5.15

NON-DIMENSIONAL PIPE WALL ACCELERATION

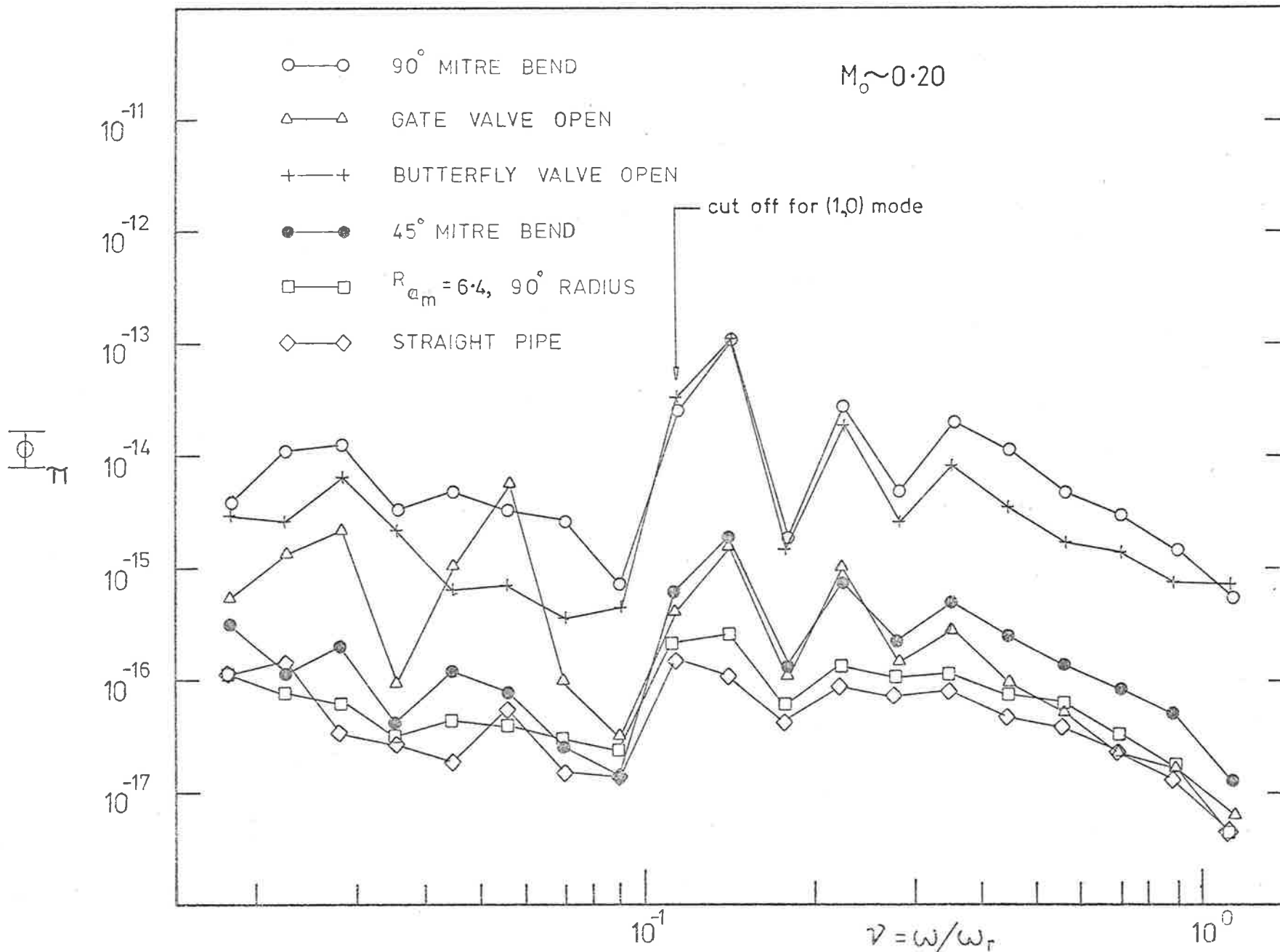


FIG 5-16

NON-DIMENSIONAL ACOUSTIC POWER RADIATION

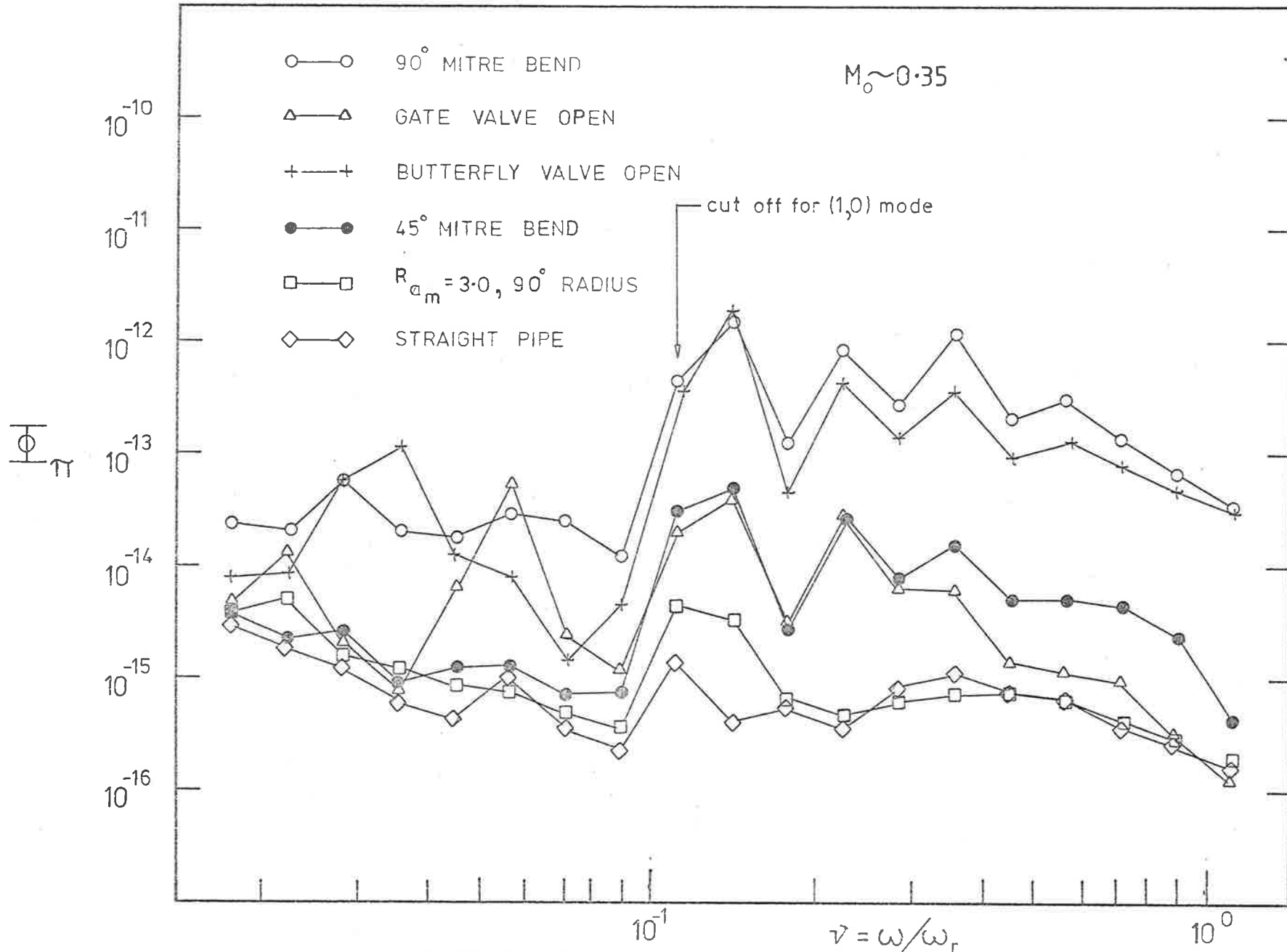


FIG 5.17

NON-DIMENSIONAL ACOUSTIC POWER RADIATION

$\frac{\overline{P}}{\pi}$

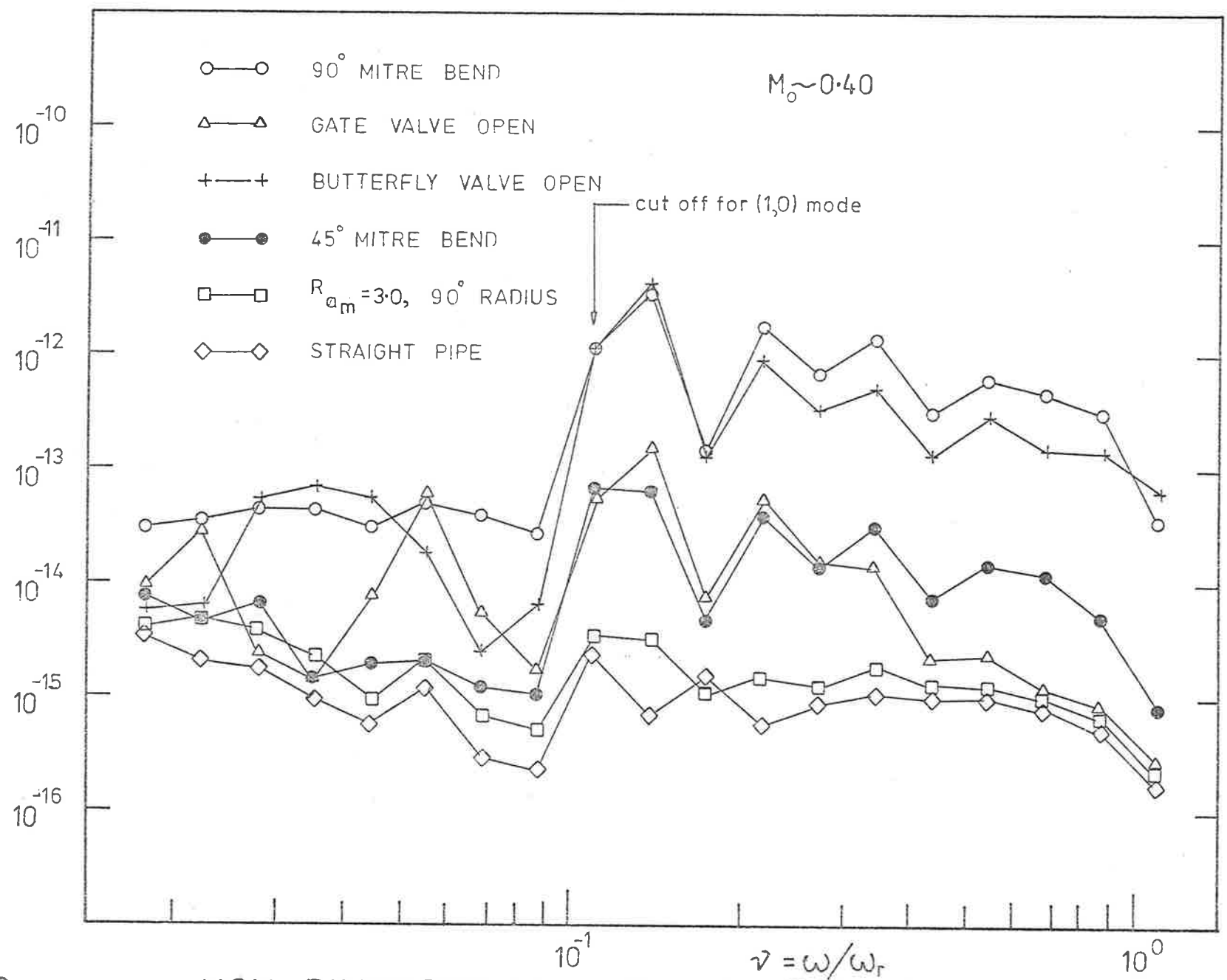


FIG 5-18

NON-DIMENSIONAL ACOUSTIC POWER RADIATION

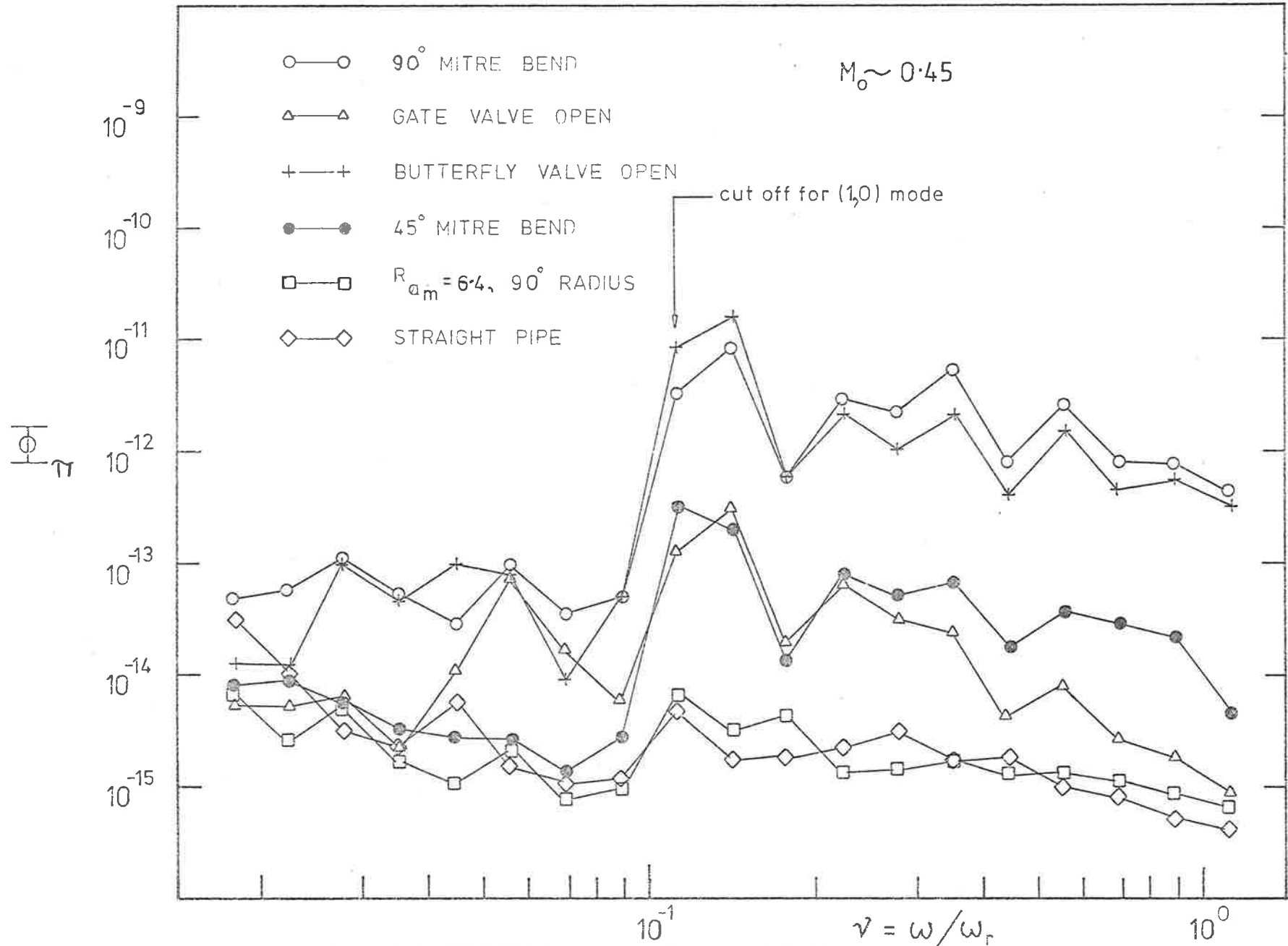


FIG 5.19

NON-DIMENSIONAL ACOUSTIC POWER RADIATION

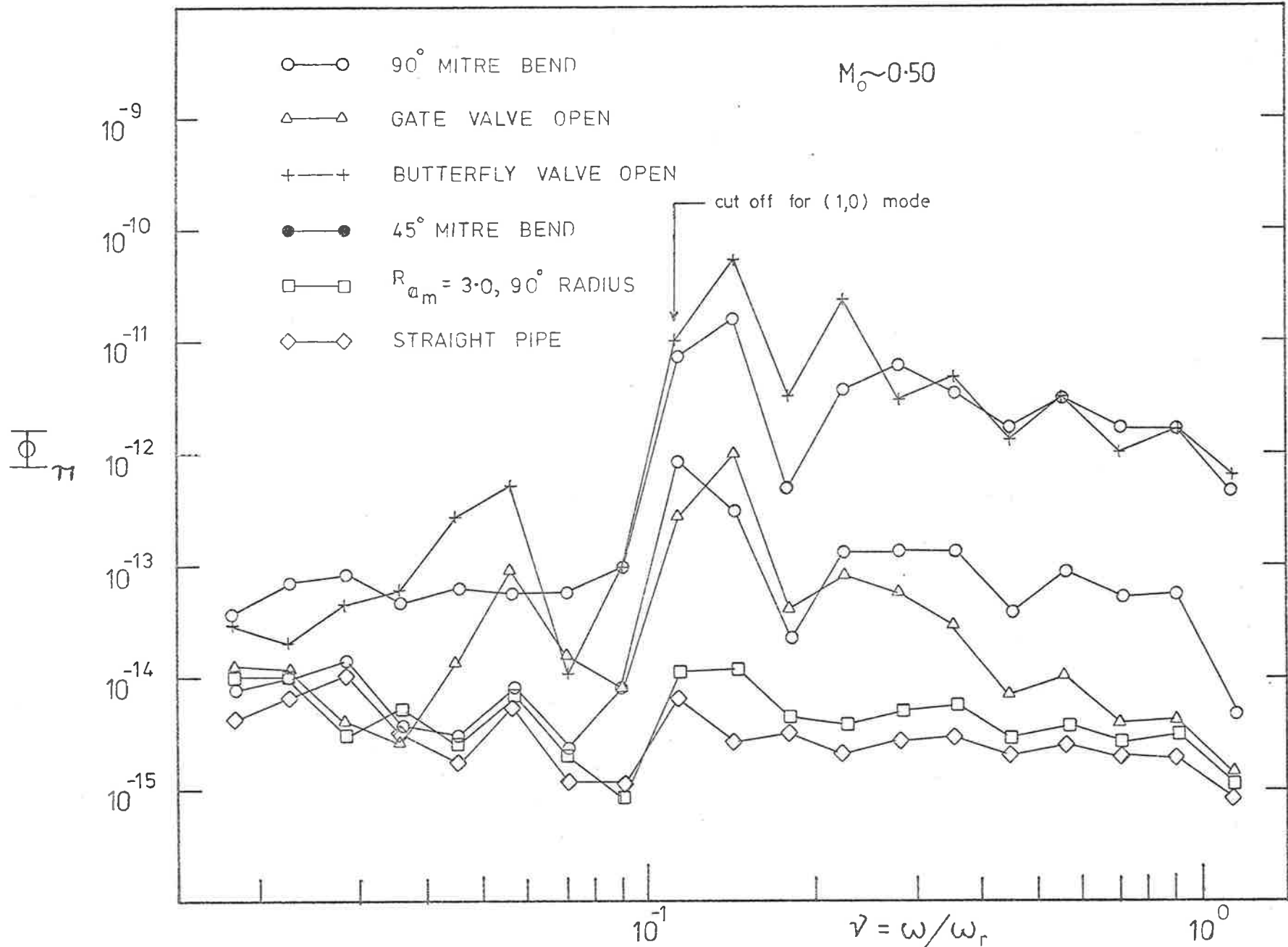


FIG 5.20

NON-DIMENSIONAL ACOUSTIC POWER RADIATION

perhaps in the region of the first higher order mode i.e. the (1,0) mode (at $\nu \approx 0.12$). The 45° mitred bend and the gate valve produce significant increases in pipe wall vibrational response and acoustic power radiation at frequencies above the cut-off frequency of the (1,0) mode and, the butterfly valve, like the 90° mitred bend, discussed in Chapter 4, produces increases (compared with results for the straight pipe datum) that are even more substantial. Low frequency increases for the gate and butterfly valves will be discussed later on in this section. As in the case of the 90° mitred bend, the most dramatic effects for the 45° mitred bend, the gate valve, and the butterfly valve are confined to frequencies close to the cut-off frequencies of the various higher order modes, and are associated with the coincidence between propagating higher order acoustic modes and selected resonant structural modes. This is illustrated in Figures 5.21 to 5.32 for the particular cases of the butterfly and gate valves. The narrow band analyses provides a finer resolution than the $\frac{1}{3}$ -octave analyses and the effects of coincidence are illustrated much more clearly. As for the 90° mitred bend absolute scales are not included on Figures 5.21 to 5.32, and accelerometer mass loading effects are not accounted for in the narrow band analysis of the pipe wall acceleration. Narrow band analyses were not made for the radiused bends or the 45° mitred bend.

The radiused bends produce insignificant increases in pipe wall vibration response and external acoustic radiation at frequencies below the cut-off frequency of the first higher order mode, in comparison with undisturbed fully-developed turbulent pipe flow. This is also generally true of the 45° mitred bend. The two radiused bends produce wall pressure fluctuations, at most Strouhal numbers investigated, that are comparable with undisturbed fully-developed turbulent pipe flow, although there is some evidence of a mild acoustic disturbance

$X = 52.8, M_0 = 0.22$

HIGHER ORDER MODES

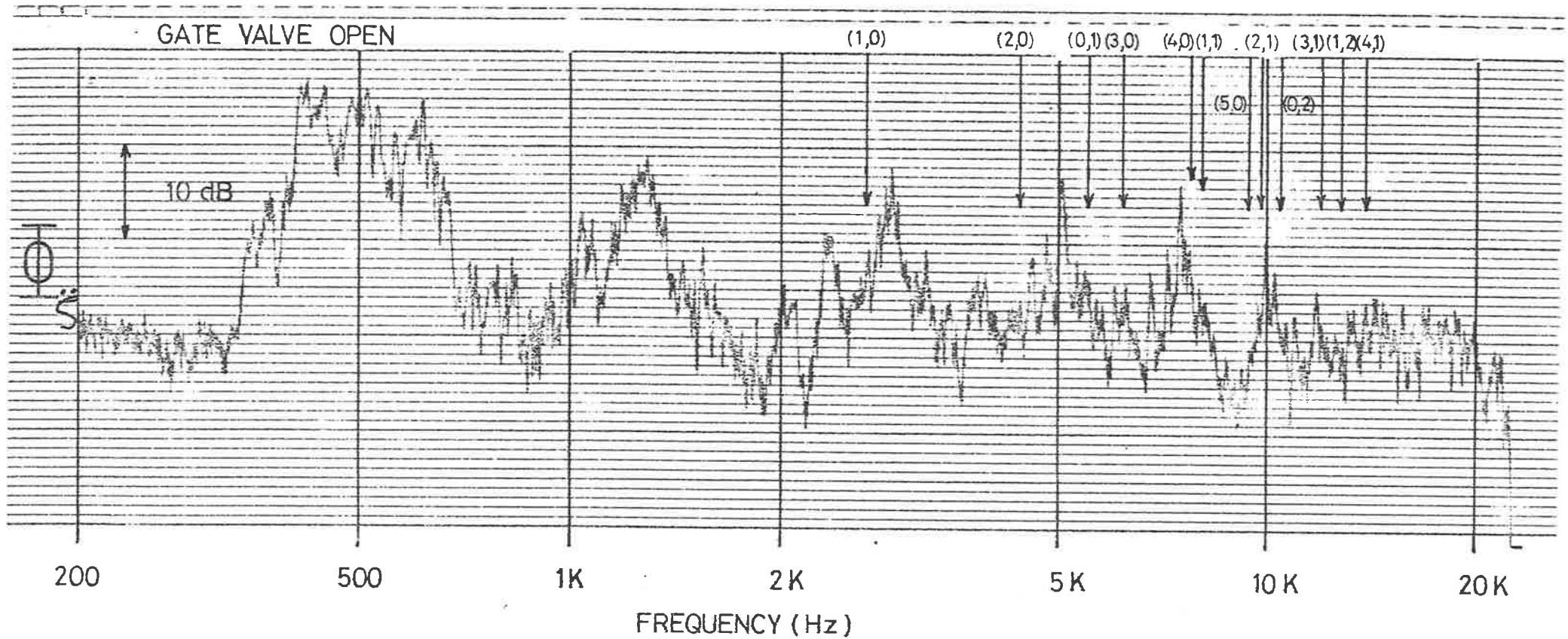


FIGURE 5.21 PIPE WALL ACCELERATION [100 Hz Bandwidth]

$X = 52.8, M_0 = 0.40$

HIGHER ORDER MODES

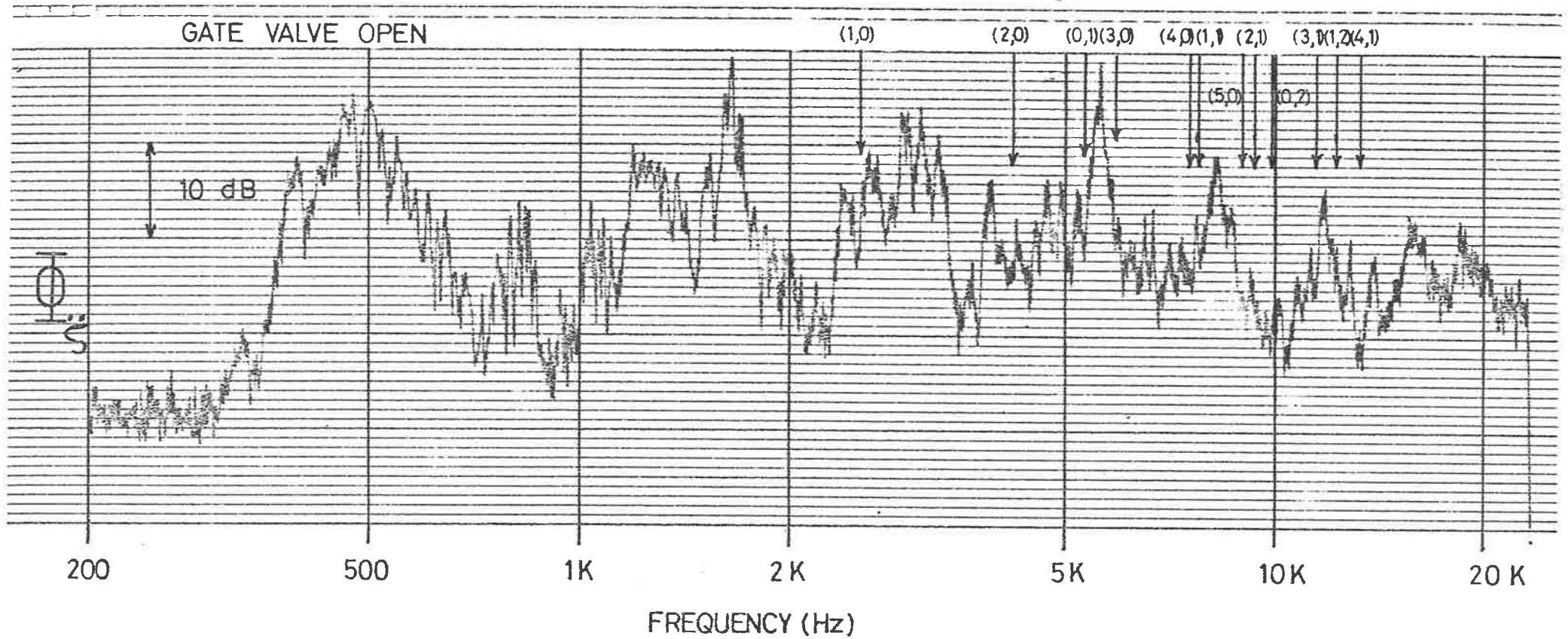


FIGURE 5.22 PIPE WALL ACCELERATION [100 Hz Bandwidth]

$X = 52.8, M_o = 0.50$

HIGHER ORDER MODES

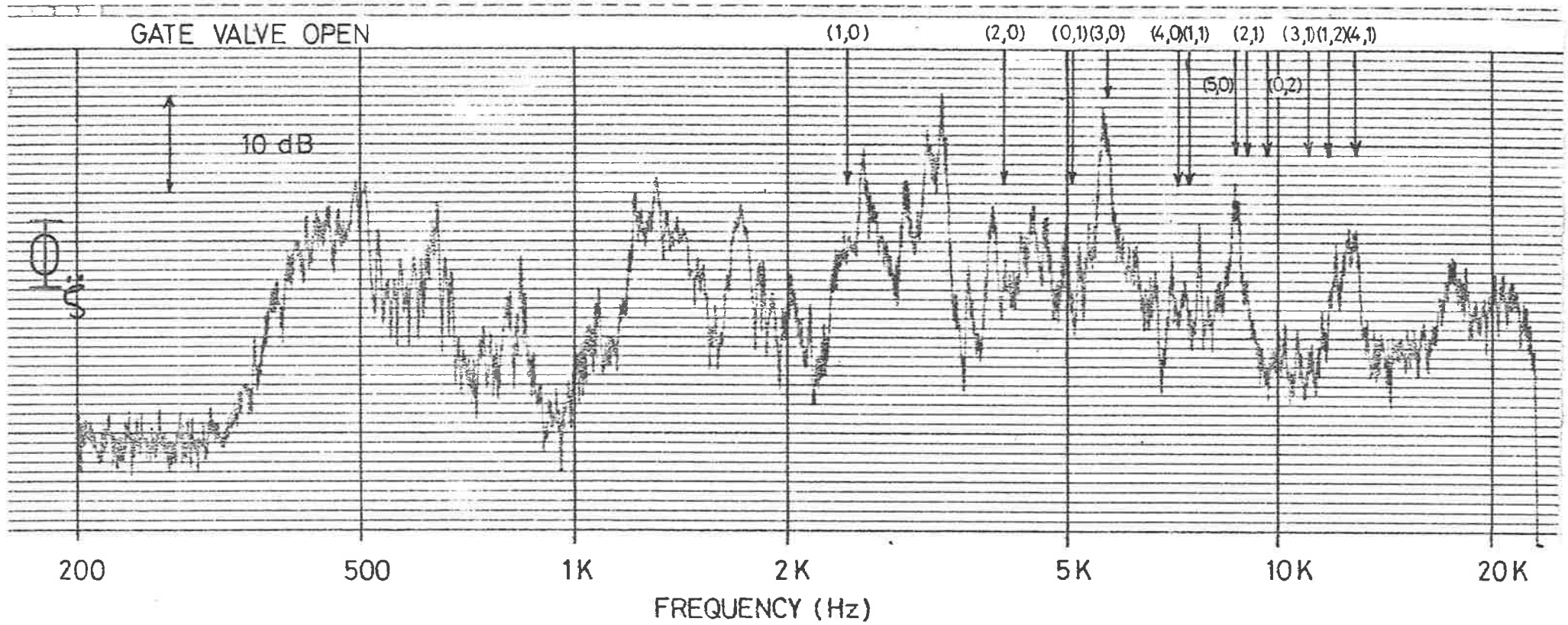


FIGURE 5-23 PIPE WALL ACCELERATION [100 Hz Bandwidth]

$$X = 52.8, M_o = 0.22$$

HIGHER ORDER MODES

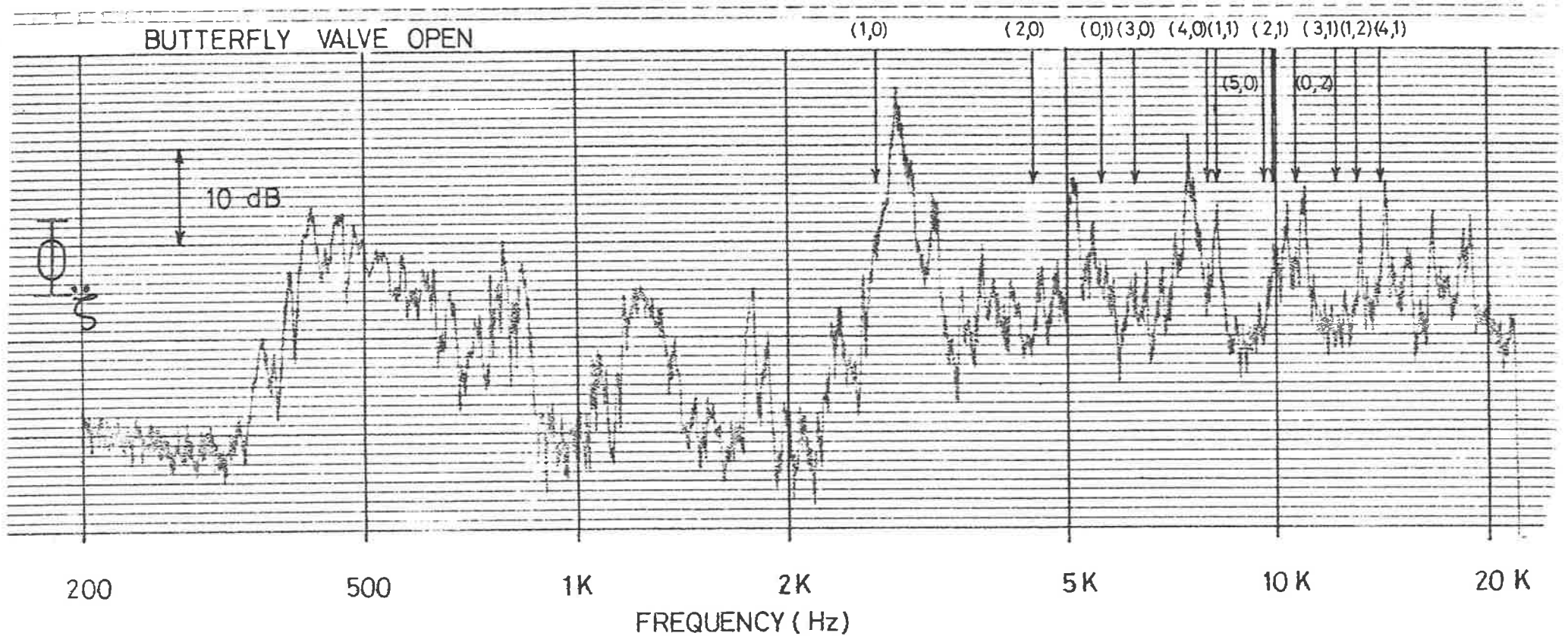


FIGURE 5.24 PIPE WALL ACCELERATION [100 Hz Bandwidth]

$X = 52.8$, $M_o = 0.40$

HIGHER ORDER MODES

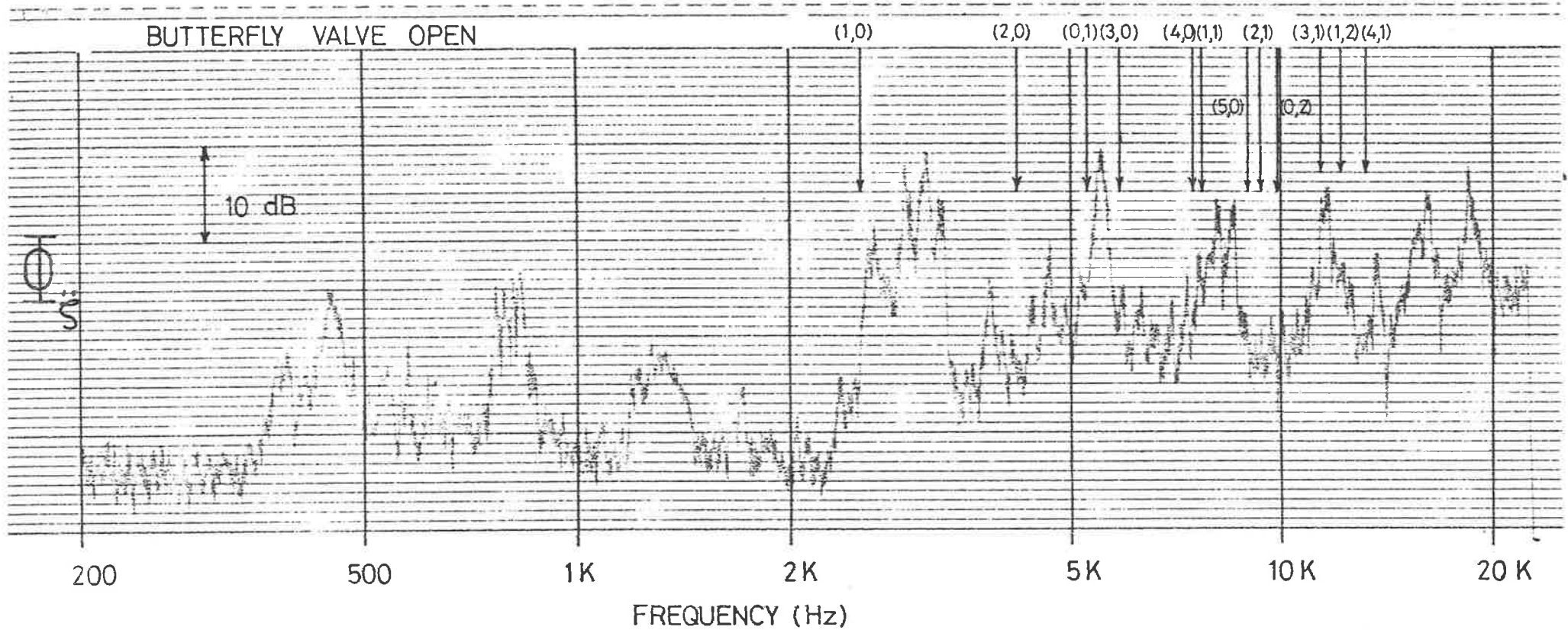


FIGURE 5.25 PIPE WALL ACCELERATION [100 Hz Bandwidth]

$$X = 52.8, M_0 = 0.50$$

HIGHER ORDER MODES

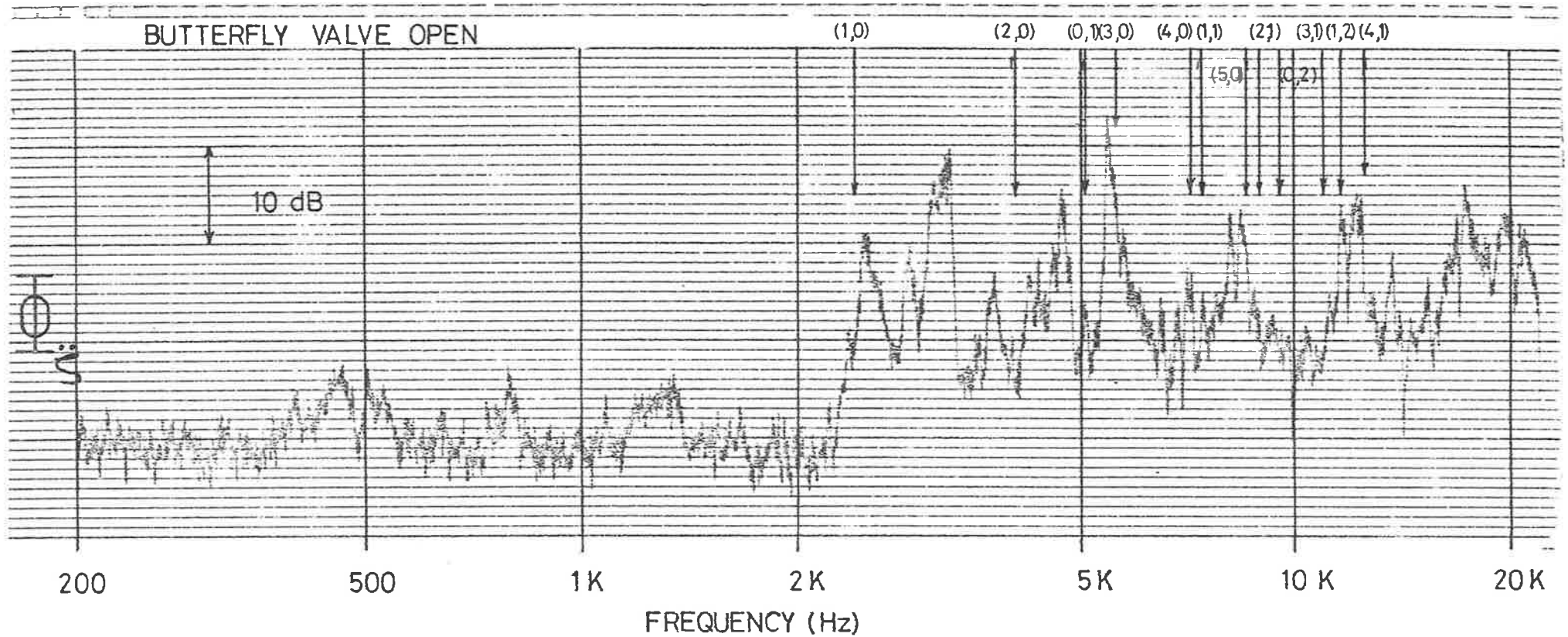


FIGURE 5.26 PIPE WALL ACCELERATION [100 Hz Bandwidth]

$$X = 52.8, M_o = 0.22$$

HIGHER ORDER MODES

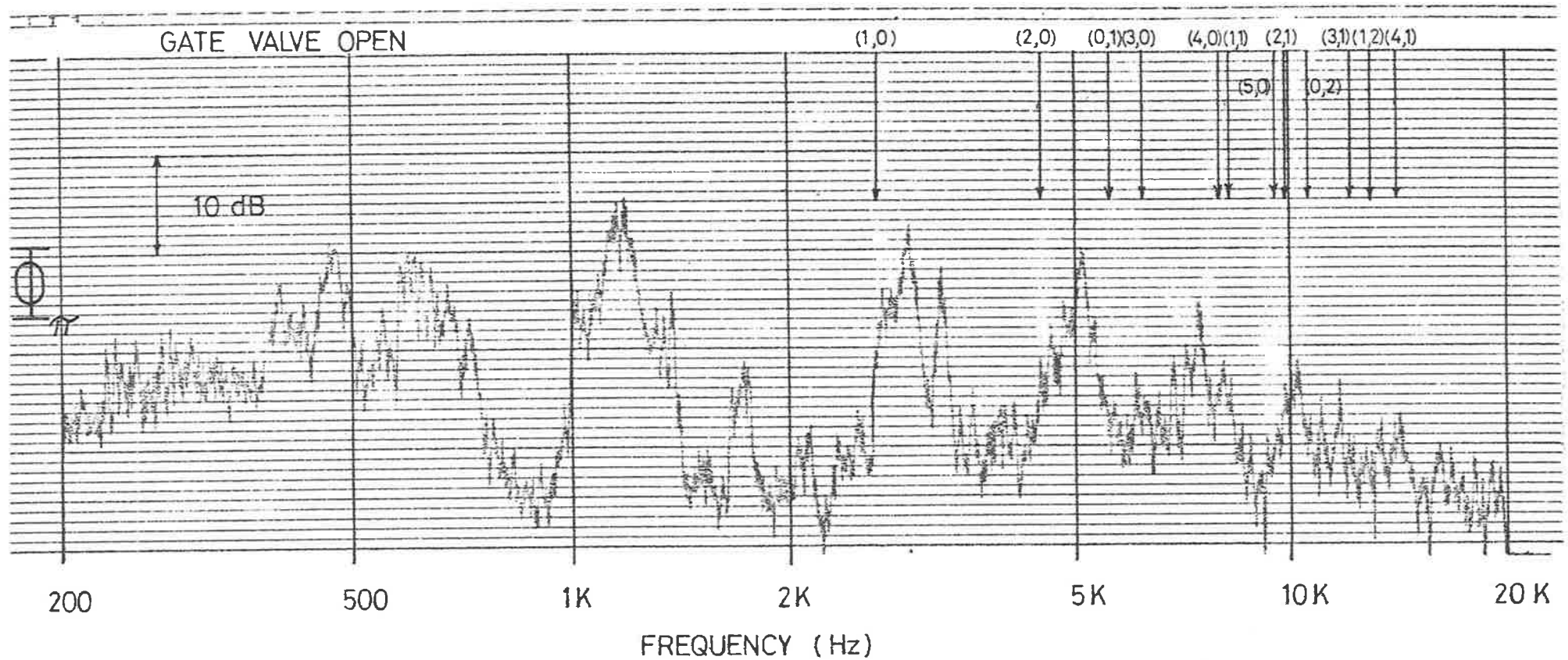


FIGURE 5.27 ACOUSTIC POWER RADIATION [100 Hz Bandwidth]

$$X = 52.8, M_0 = 0.40$$

HIGHER ORDER MODES

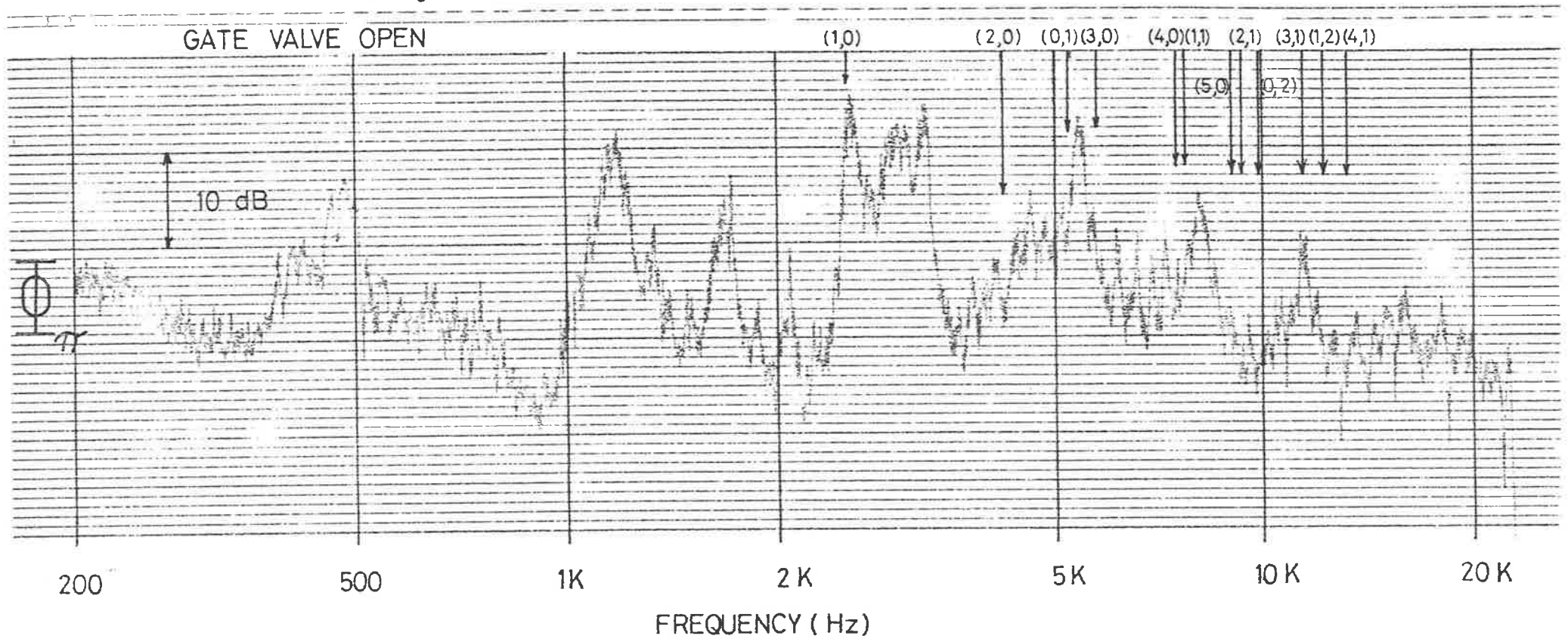


FIGURE 5-28 ACOUSTIC POWER RADIATION [100 Hz Bandwidth]

$X = 52.8$, $M_0 = 0.50$

HIGHER ORDER MODES

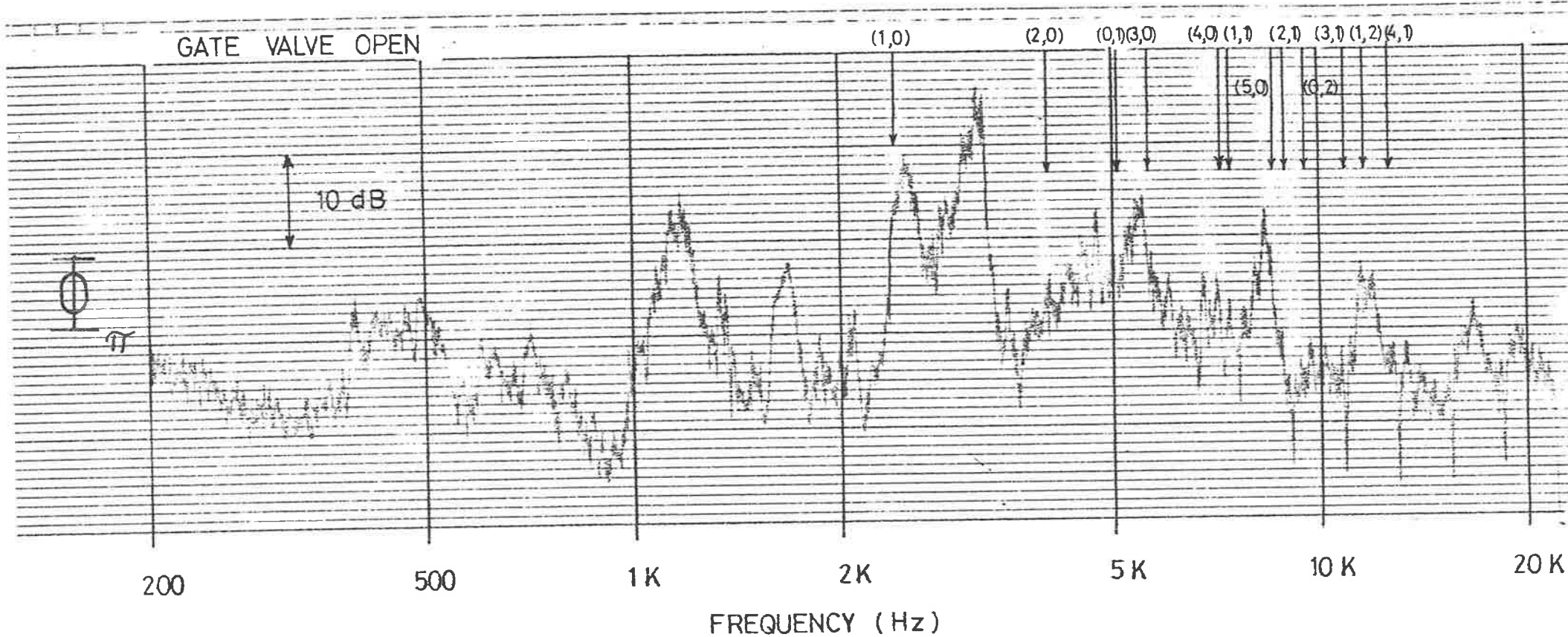


FIGURE 5.29 ACOUSTIC POWER RADIATION [100 Hz Bandwidth]

$X = 52.8, M_0 = 0.22$

HIGHER ORDER MODES

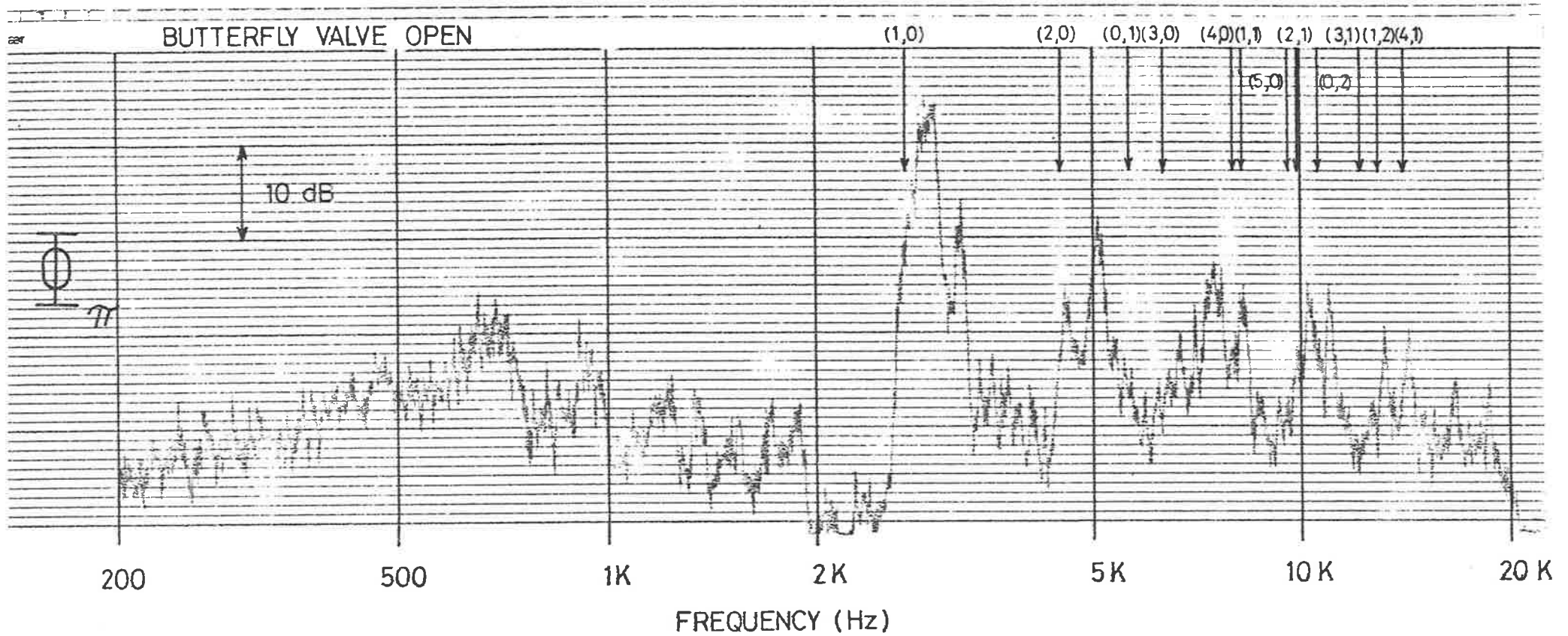


FIGURE 5-30 ACOUSTIC POWER RADIATION [100 Hz Bandwidth]

$X = 52.8, M_0 = 0.40$

HIGHER ORDER MODES

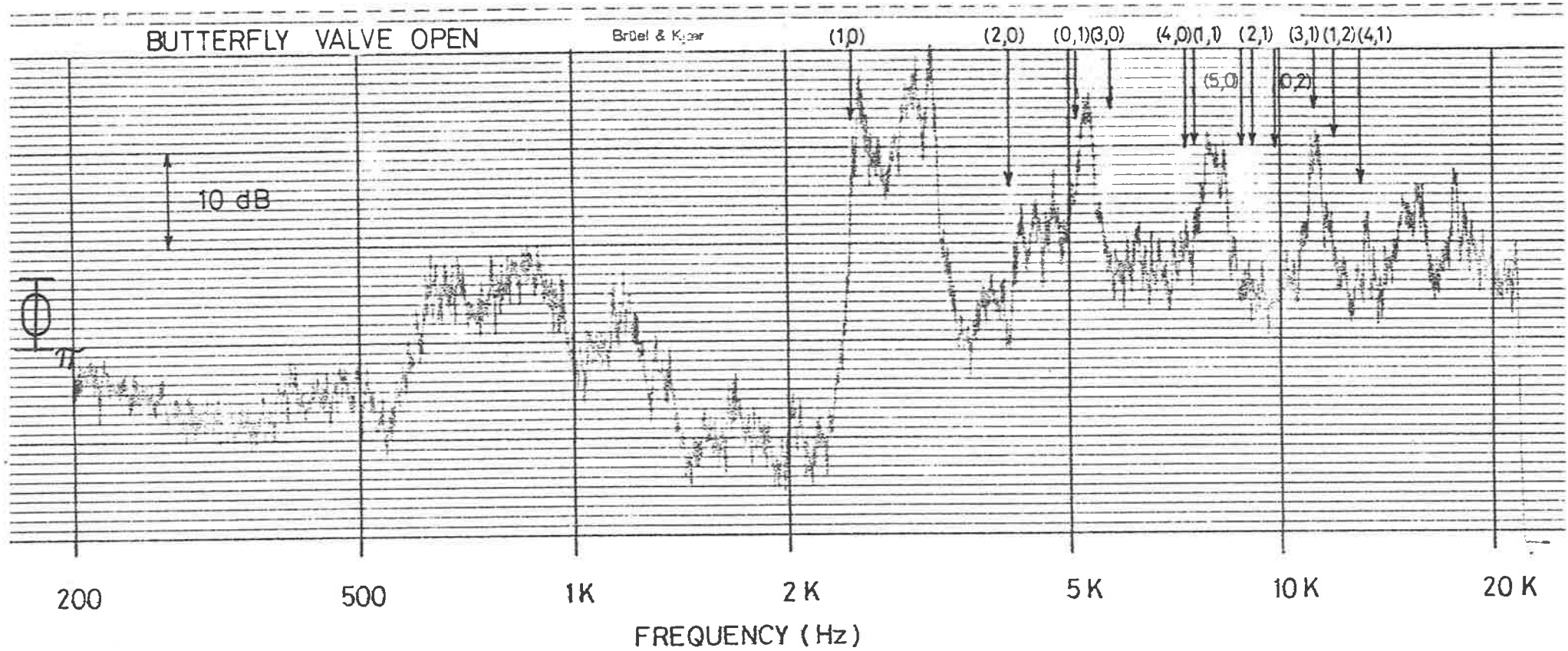


FIGURE 5-31 ACOUSTIC POWER RADIATION [100 Hz Bandwidth]

$X = 52.8, M_0 = 0.50$

HIGHER ORDER MODES

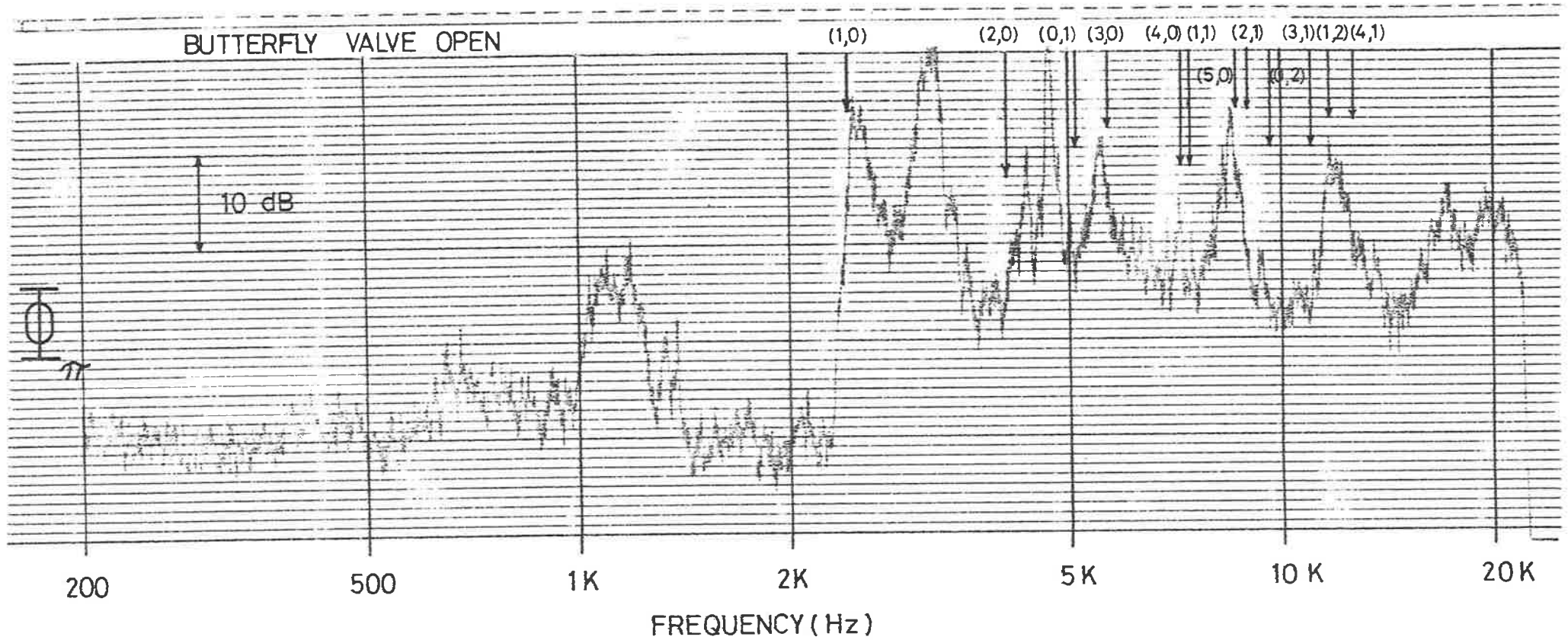


FIGURE 5.32 ACOUSTIC POWER RADIATION [100 Hz Bandwidth]

that dominates over the wall pressure fluctuations associated with straight pipe flow at very low Strouhal numbers (see Figure 5.5). This does not, however, cause any detectable increases in pipe wall response or external acoustic radiation (see Figures 5.11 to 5.20). The 45° mitred bend is also a generator of mild acoustic plane waves that dominate over the wall pressure fluctuations associated with straight pipe flow at low Strouhal numbers (see Figure 5.5) and once again there are no low frequency vibration or radiation increases over undisturbed turbulent flow excitation.

The gate valve produces low frequency increases in both the pipe wall acceleration and the external acoustic radiation at $\nu \approx 0.022$ (500 Hz) and $\nu \approx 0.055$ (1250 Hz) at all flow speeds investigated. This is evident from the $1/3$ -octave spectra (Figures 5.11 to 5.20) and the narrow band analyses (Figures 5.21 to 5.23, and 5.27 to 5.29). Increases in the wall pressure spectra at Strouhal numbers corresponding to these frequencies are also observed (see Figure 5.4). These observed increases in wall pressure fluctuations, pipe wall acceleration and external acoustic power radiated do not increase in frequency with increasing flow speed. Hence they are not associated with the periodic shedding of vortices (which give rise to force fluctuations which in turn radiate noise), which might be expected from a flow spoiler. The gate valve, in its fully open position, comprises of a circumferential slot in the pipe wall (as illustrated in Chapter 3) and does not represent a significant protrusion into the flow and as such does not generate periodic vortices. Thus, the low frequency increases in the wall pressure fluctuations associated with a gate valve are probably attributable to plane acoustic waves, although further experimental investigation would be required to substantiate this. Cross-correlation techniques (as discussed in Chapter 6) could establish whether or not the increases in the wall pressure fluctuations are associated

with plane acoustic waves. As illustrated in Chapter 4, there is a significant grouping of resonant structural modes in the 500 Hz and 1250 Hz $\frac{1}{3}$ octave bands. This grouping appears to be responsible for the observed increases in pipe wall acceleration and external acoustic power radiation at these frequencies, for the range of flow speeds in this investigation.

The vane - spindle assembly of the butterfly valve, on the other hand, splits the flow (see Figure 3.3) and periodic vortex shedding into the wake and force fluctuations are to be expected. These force fluctuations are produced at a discrete frequency given by

$$f = \frac{S_o U_o}{t_c} \quad , \quad [5.1]$$

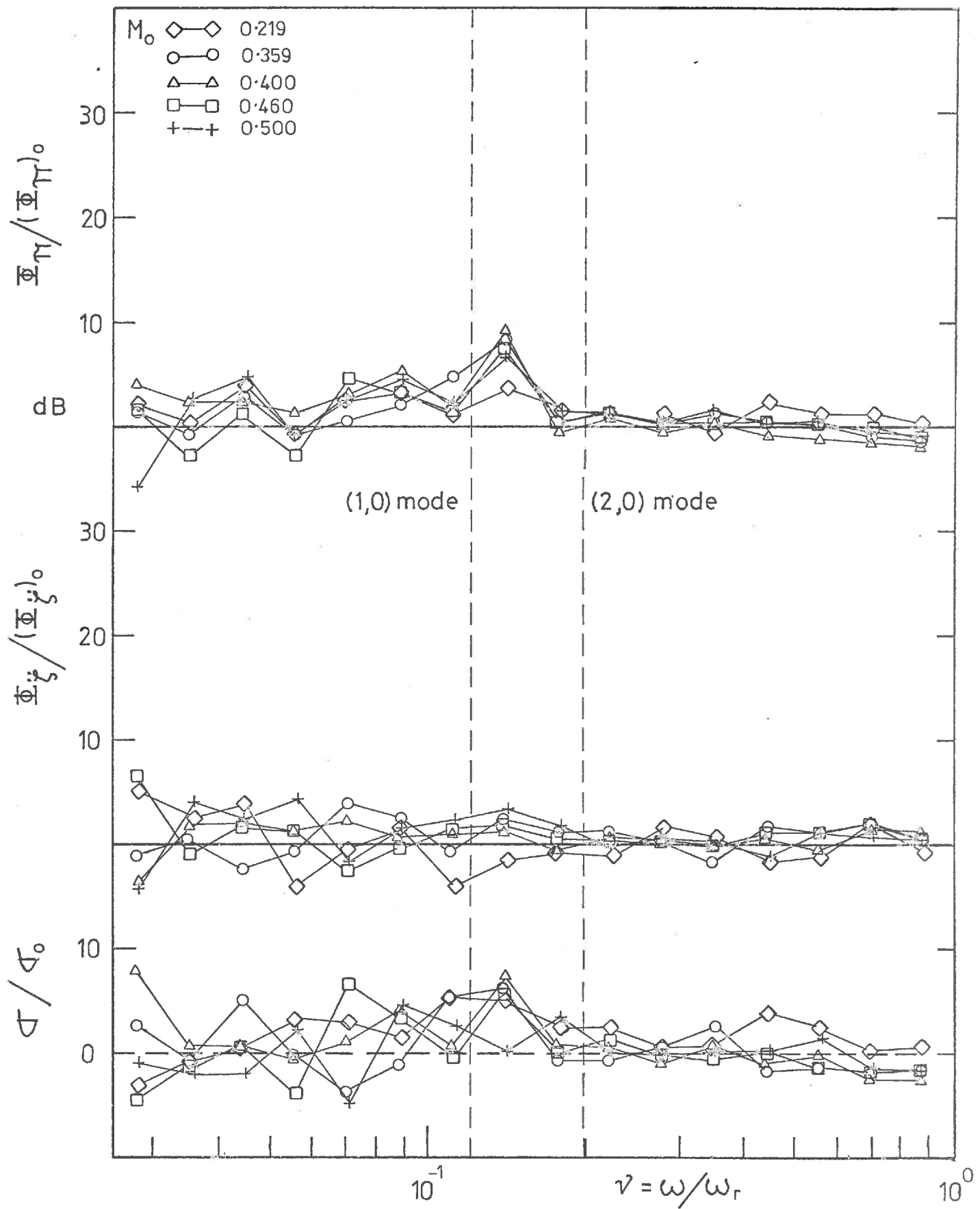
where U_o is the mean flow speed, S_o is the peak Strouhal number associated with turbulent mixing, typically 0.20 (Goldstein, p. 570, 1965 and Beranek, p. 512, 1971), and t_c is a characteristic length (which is in this case the thickness of the aerodynamic disturbance, the vane and spindle, and is 28.5 mm). If a disturbance is associated with this phenomenon its frequency will increase with flow speed.

For the butterfly valve used in this investigation, there is a broadband increase in the wall pressure fluctuations, at low Strouhal numbers, over that of undisturbed fully-developed turbulent pipe flow (see Figure 5.3). This could possibly be associated with plane acoustic waves, and wall pressure fluctuation cross-correlations (as discussed in Chapter 6) would have to be performed to confirm this. However, the corresponding low frequency increases in pipe wall acceleration and external acoustic radiation, for the butterfly valve, shift to higher frequencies as flow speed is increased. This is apparent in the $\frac{1}{3}$ -octave spectra (see Figures 5.11 to 5.20) and is clearly illustrated in the narrow band spectra (see Figures 5.24 to 5.26 and Figures 5.30

to 5.32). For this particular butterfly valve, where t_c (as defined in equation [5.1]) is approximately 28.5 mm, the vortex shedding frequency corresponds to 562 Hz, 984 Hz and 1218 Hz for $M_0 = 0.218$, 0.408 and 0.505 respectively.

As mentioned earlier in this section (and as illustrated in Chapter 4), there is a significant grouping of resonant structural modes in the 500 Hz and 1250 Hz $\frac{1}{3}$ -octave bands, and the radiation ratios of these structural modes are not negligible (Rennison, 1976). It appears that the force fluctuations associated with the vortex shedding and the plane acoustic waves at these low frequencies couple to these resonant structural modes and produce the observed increases in pipe wall vibration response and external acoustic radiation. The experimental evidence suggests that the vibration response and external acoustic radiation associated with the vortex shedding dominates over that associated with plane wave wall pressure fluctuations in the same frequency band. From the $\frac{1}{3}$ -octave spectral measurements of the wall pressure fluctuations (see Figure 5.3) there is no evidence of any discrete peaks at low Strouhal numbers corresponding to the vortex shedding frequencies; instead the spectra are broadband in character. However, no narrow band measurements, which might have shown something, were made. The conclusion drawn from this observation is that the fluctuations associated with the vortex shedding are "submerged" under the wall pressure fluctuations associated with plane acoustic waves, but despite this, they excite the pipe wall far more efficiently than the plane waves. Extensive wall pressure fluctuation cross-correlations are required to further substantiate the above conclusions.

The results for the various flow disturbances investigated are shown again in Figures 5.33 to 5.37 in the form of the non-dimensional spectral density of wall acceleration Φ_{ζ} and acoustic radiation Φ_{π}



SPECTRAL DENSITIES OF Φ_{ξ} AND Φ_{π} RELATIVE TO
 STRAIGHT PIPE FLOW AND THE CORRESPONDING
 RADIATION RATIO. σ/σ_0
 FOR 90° RADIUS BEND ($R/a_0 = 6.4$)

FIG 5.33

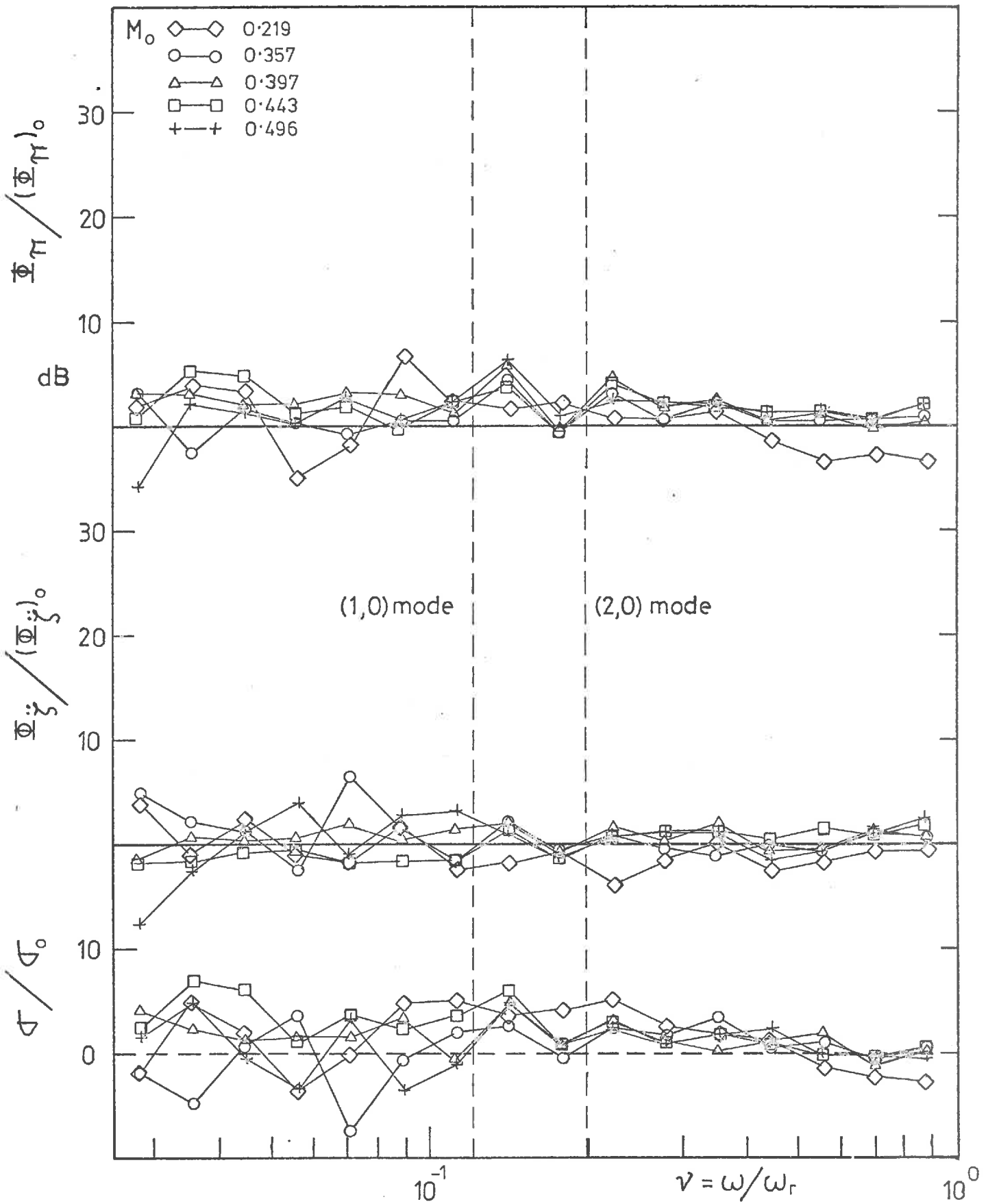


FIG 5.34

SPECTRAL DENSITIES OF $\Phi_{\dot{\xi}}$ AND Φ_π RELATIVE TO
 STRAIGHT PIPE FLOW AND THE CORRESPONDING
 RADIATION RATIO. σ / σ_0
 FOR 90° RADIUS BEND ($R/a_m = 3.0$)

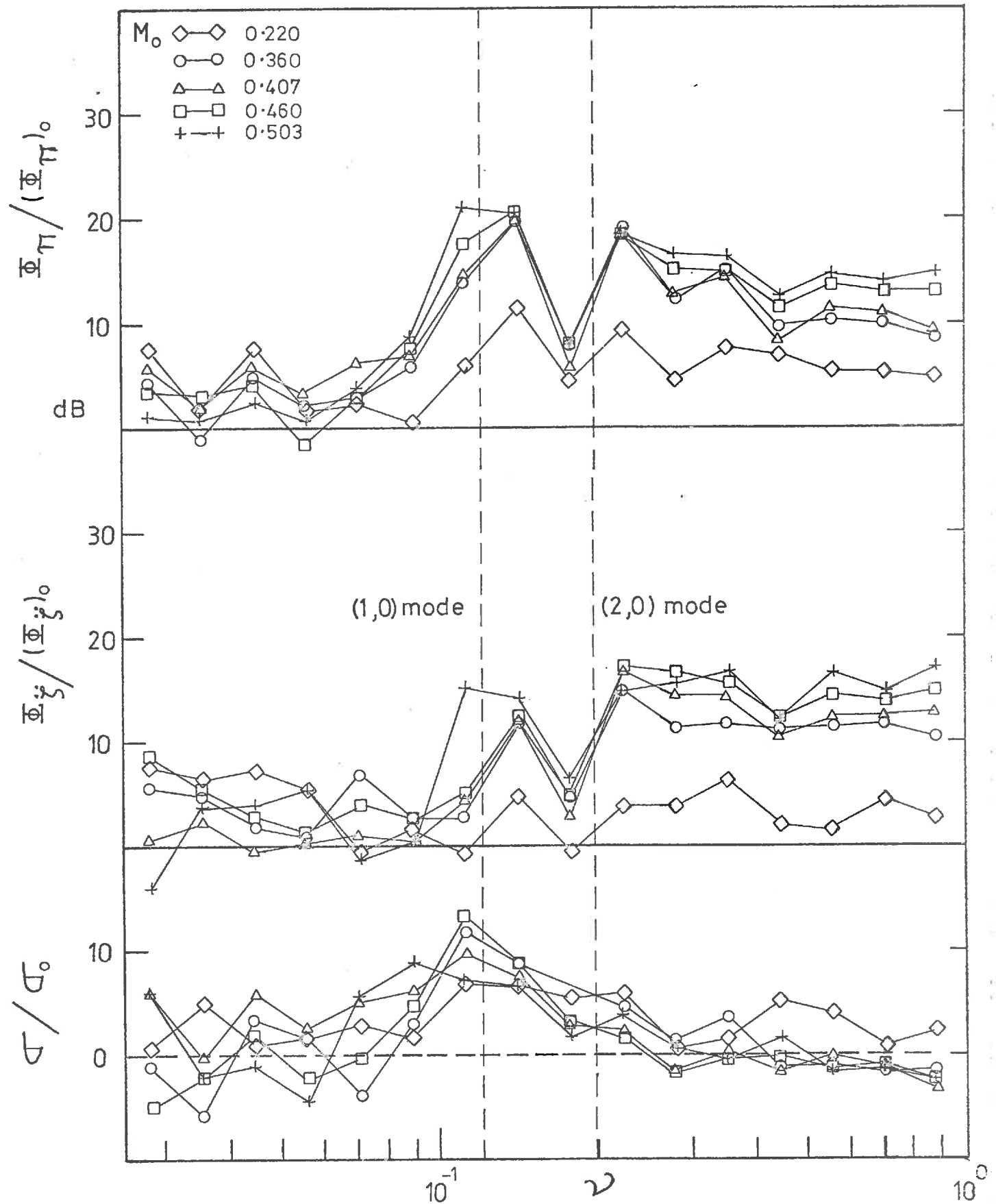
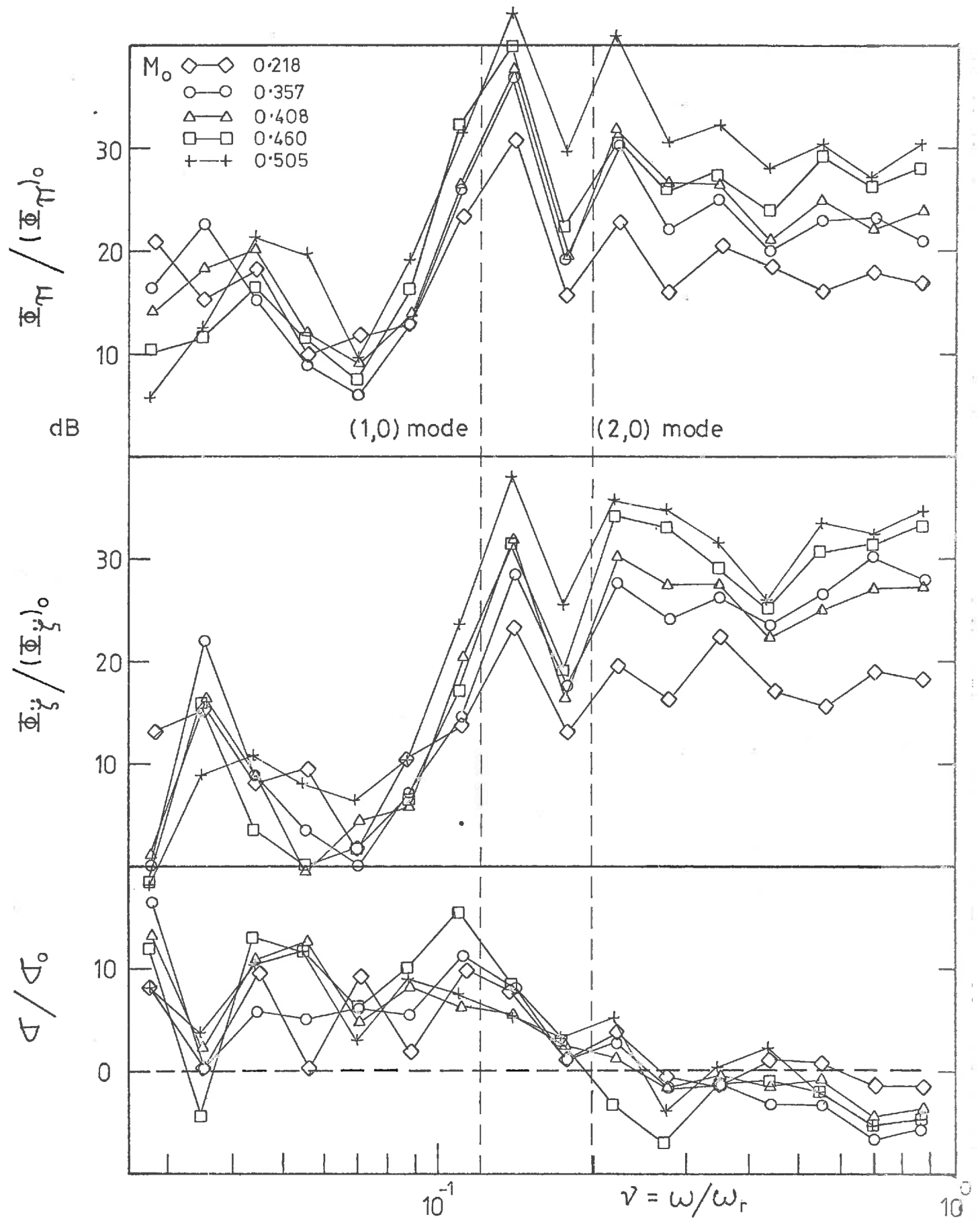


FIG 5.35

SPECTRAL DENSITIES OF Φ_{ξ} AND Φ_{π} RELATIVE TO
 STRAIGHT PIPE FLOW AND THE CORRESPONDING
 RADIATION RATIO. σ / σ_0
 FOR 45° MITRED BEND



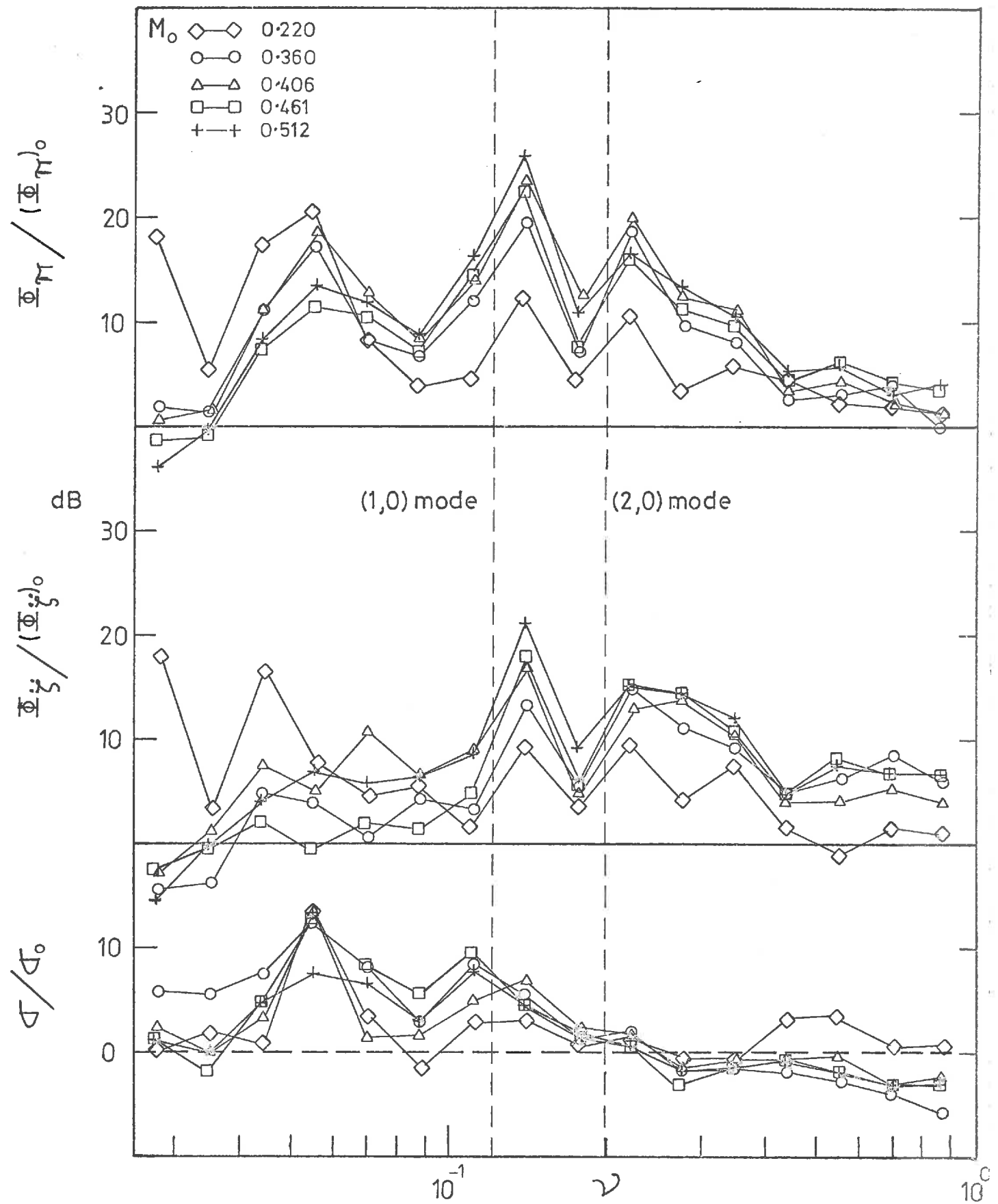
SPECTRAL DENSITIES OF $\Phi_{\dot{u}}$ AND $\Phi_{\dot{u}^2}$ RELATIVE TO

STRAIGHT PIPE FLOW AND THE CORRESPONDING

RADIATION RATIO. σ/σ_0

FOR BUTTERFLY VALVE (OPEN)

FIG 5.36



SPECTRAL DENSITIES OF Φ_{ξ} AND Φ_{η} RELATIVE TO
 STRAIGHT PIPE FLOW AND THE CORRESPONDING
 RADIATION RATIO, σ / σ_0
 FOR GATE VALVE (OPEN)

FIG 5.37

relative to the corresponding values for the straight pipe $[(\Phi_{\zeta})_0$ and $(\Phi_{\pi})_0]$ against the non-dimensional frequency ν ; the corresponding radiation ratios σ/σ_0 (see equation [4.2]) are also shown. These will be referred to again in the general discussion section.

5.4 THE FLOW DEPENDENCE OF THE INTERNAL WALL PRESSURE FIELD

As discussed in Chapter 4, the power spectral density, ϕ_p , of the wall pressure fluctuations associated with undisturbed fully-developed turbulent (straight) pipe flow scales as U_0^3 at any given Strouhal number. The power spectral density, ϕ_p , of the wall pressure fluctuations associated with flow through a pipe, downstream of a 90° mitred bend scales as U_0^3 below the cut-off frequency of the first higher order mode and as U_0^5 at any given Strouhal number above it. In this section, the flow dependence of the internal wall pressure field downstream of the other flow disturbances investigated is discussed, and comparisons made with the straight pipe and 90° mitred bend.

For the two radiused bends investigated, the wall pressure spectral levels (at $X = 52.8$) are similar to those of straight pipe flow. The bends generate a mild internal acoustic field as can be seen from the sound pressure levels in the bell mouth inlet (see Figure 5.10). But, the pressure fluctuations associated with fully-developed turbulent pipe flow dominate the wall pressure field at all, except perhaps at very low, Strouhal numbers, and the contribution from the acoustic field is generally negligible. Hence, the spectral density of the wall pressure fluctuations downstream of the radiused bends investigated would be expected to scale as U_0^3 at any given Strouhal number.

Similar arguments can be presented for the 45° mitred bend and the gate valve. The internal acoustic fields generated are again

comparatively mild and the wall pressure fluctuation levels are comparable with those of straight pipe flow, particularly at frequencies above the cut-off frequency of the first higher order mode. Both the 45° mitred bend and the gate valve do however generate plane acoustic waves at low Strouhal numbers (below cut-off of the first higher order mode) whose wall pressure fluctuations are larger than those associated with straight pipe flow at the same Strouhal numbers. Results for $(\Phi_p - \Phi_{p_0})$ against $\log_{10} M_0$ (where Φ_{p_0} is the non-dimensional spectral density of the wall pressure fluctuations associated with fully-developed turbulent pipe flow at the same flow speed), are presented in Figures 5.38 and 5.39 for the 45° mitred bend and the gate valve respectively. The data presented are for several $\frac{1}{3}$ -octave bands at frequencies below and above the cut-off frequency of the first higher order mode. At Strouhal numbers above the cut-off frequency, the wall pressure fluctuations associated with both devices are similar to those associated with straight pipe flow. Bearing in mind that coincidence of these modes and pipe wall modes can occur, the implication is that the acoustic components are very much less intense than the turbulent pressure fluctuations. At these Strouhal numbers, results are presented for Φ_p (instead of $\Phi_p - \Phi_{p_0}$) against $\log_{10} M_0$, in Figures 5.38 and 5.39. The non-dimensional spectral density of the wall pressure fluctuations scales approximately as U_0^0 at all Strouhal numbers (above and below cut-off of the first higher order mode). There is however some experimental scatter, and this is evident in Figures 5.38 and 5.39. Since Φ_p is essentially independent of U_0 at most Strouhal numbers, this implies that ϕ_p scales approximately as U_0^3 at all Strouhal numbers for both the 45° mitred bend and the gate valve. Hence, the overall mean square pressure $\overline{p^2}$ scales as U_0^4 .

The butterfly valve generates both acoustic plane waves and higher order modes, which dominate over the wall pressure fluctuations

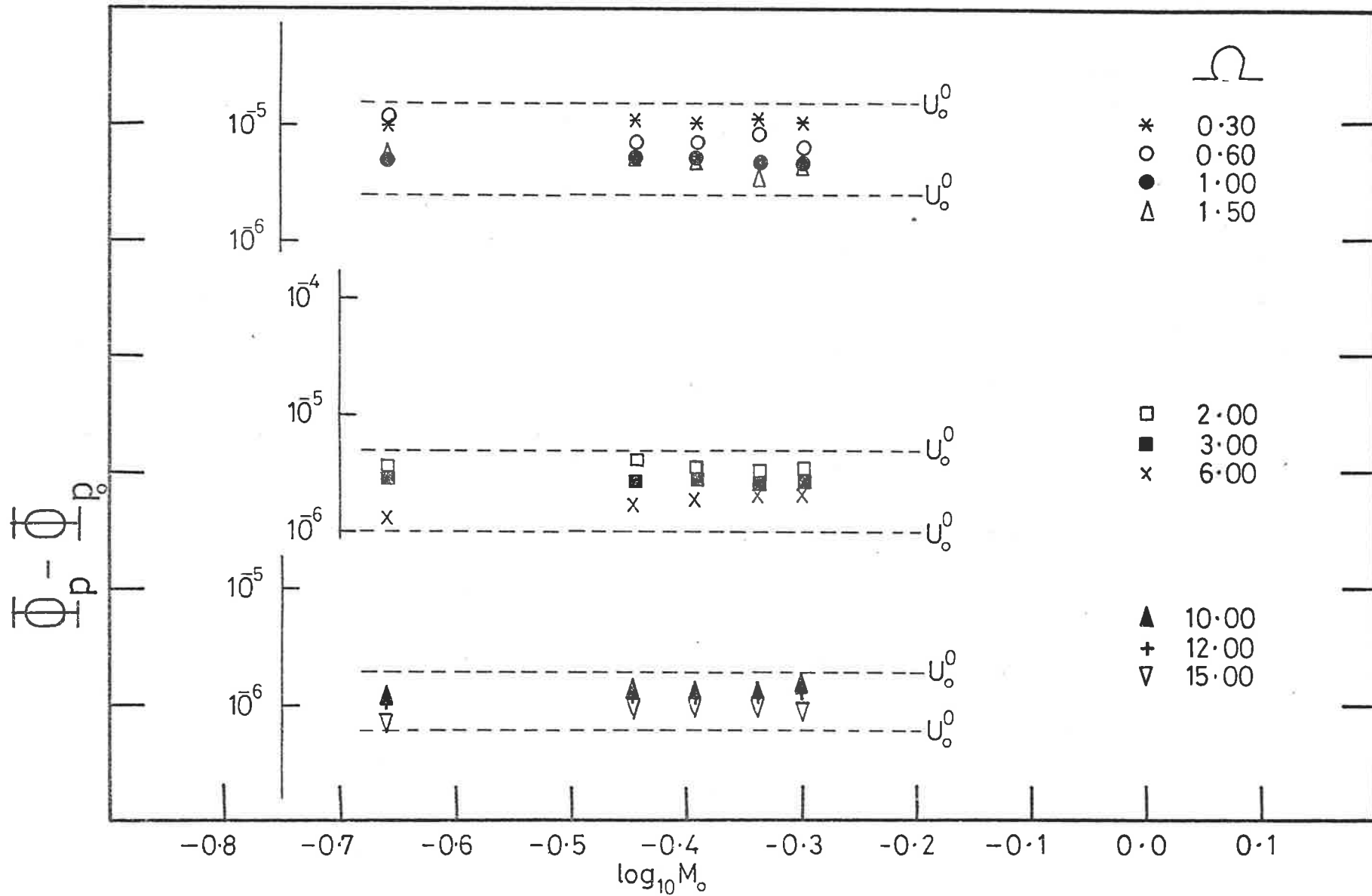


FIGURE 5.38 FLOW DEPENDENCE OF K_p FOR 45° MITRED BEND

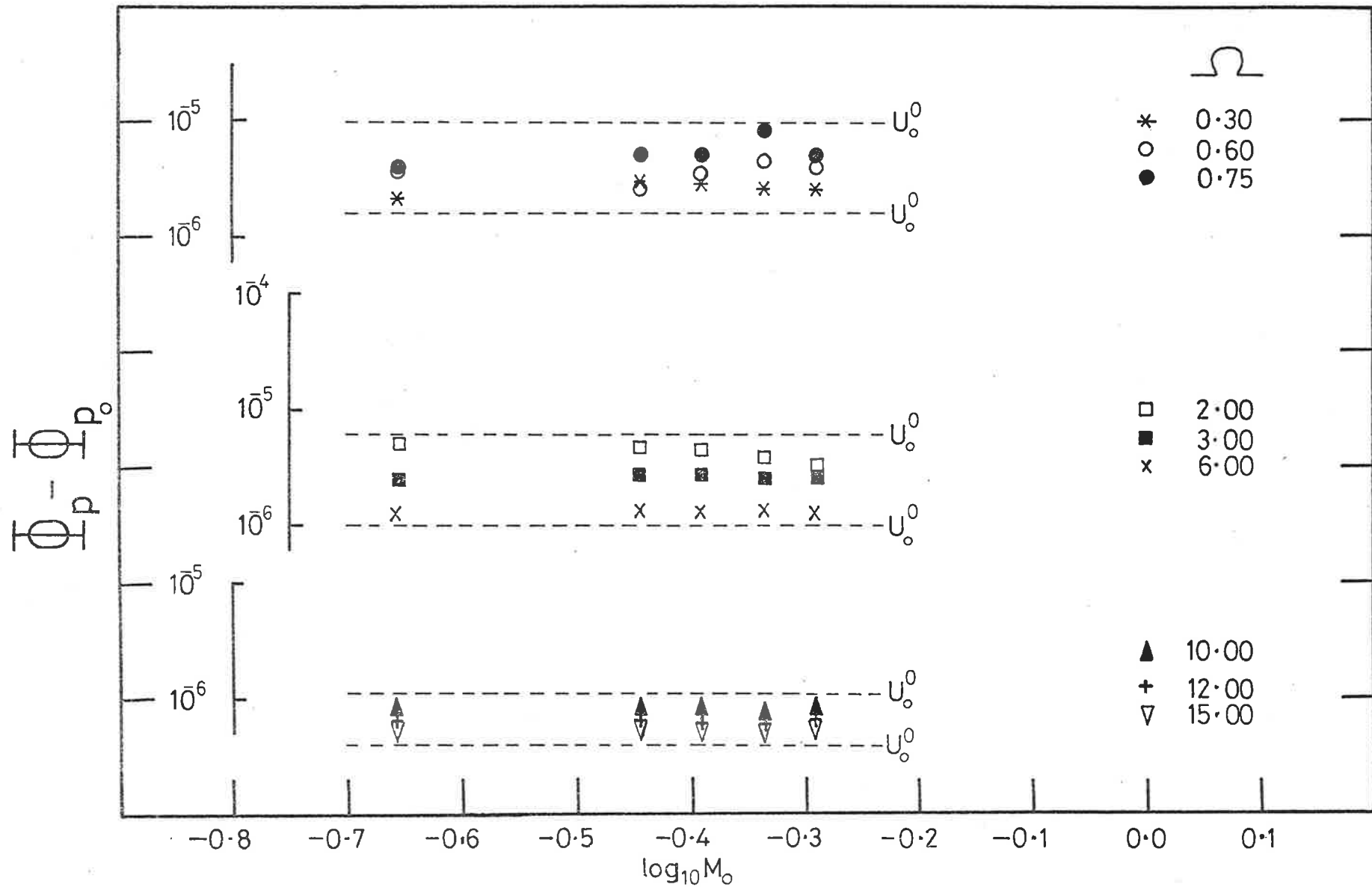


FIGURE 5.39 FLOW DEPENDENCE OF Φ_p FOR GATE VALVE

associated with undisturbed fully-developed turbulent pipe flow. The plane waves generated are not as intense as those generated by the 90° mitred bend. Results of $(\Phi_p - \Phi_{p_0})$ against $\log_{10} M_0$ are presented in Figure 5.40 for Strouhal numbers below and above the cut-off frequency of the first higher order mode. The non-dimensional power spectral densities of the wall pressure fluctuations scales essentially as U_0^0 below cut-off (of the first higher order mode) and as U_0^2 above it for any given Strouhal number. This implies that ϕ_p scales as U_0^3 below cut-off for the first higher order mode and as U_0^5 above it, and that $\overline{p^2}$ scales as U_0^4 below cut-off for the first higher order mode and as U_0^6 above it. This flow dependence is similar to that of the 90° mitred bend.

The wall pressure spectra for the 55 mm orifice plate are presented in Figure C-3 in Appendix C. It can be seen that there is a considerable spread in the wall pressure fluctuations, Φ_p , at Strouhal numbers above the cut-off frequency of the first higher order mode. The 55 mm orifice plate is a strong generator of higher order acoustic modes and the wall pressure fluctuations are strongest at these Strouhal numbers. This is apparent from the frequency weighted power spectral density in Figure C-5. The higher order acoustic modes dominate the internal acoustic field which is in direct contrast to the 90° mitred bend. As in the case of the 90° mitred bend and the butterfly valve the spectral density of the wall pressure fluctuations, ϕ_p , scales as U_0^3 at Strouhal numbers below the cut-off frequency of the first higher order mode and as U_0^5 above it. Because the higher order modes dominate the spectra, it would be expected that the overall mean square pressure fluctuations $\overline{p^2}$ scale as U_0^6 (as opposed to U_0^4 for the 90° mitred bend). Hence p'/q_0 will not be independent of Reynolds number. This is indeed the case as can be seen from Figure C-2.

In comparison, the 65 mm orifice plate is not a strong generator

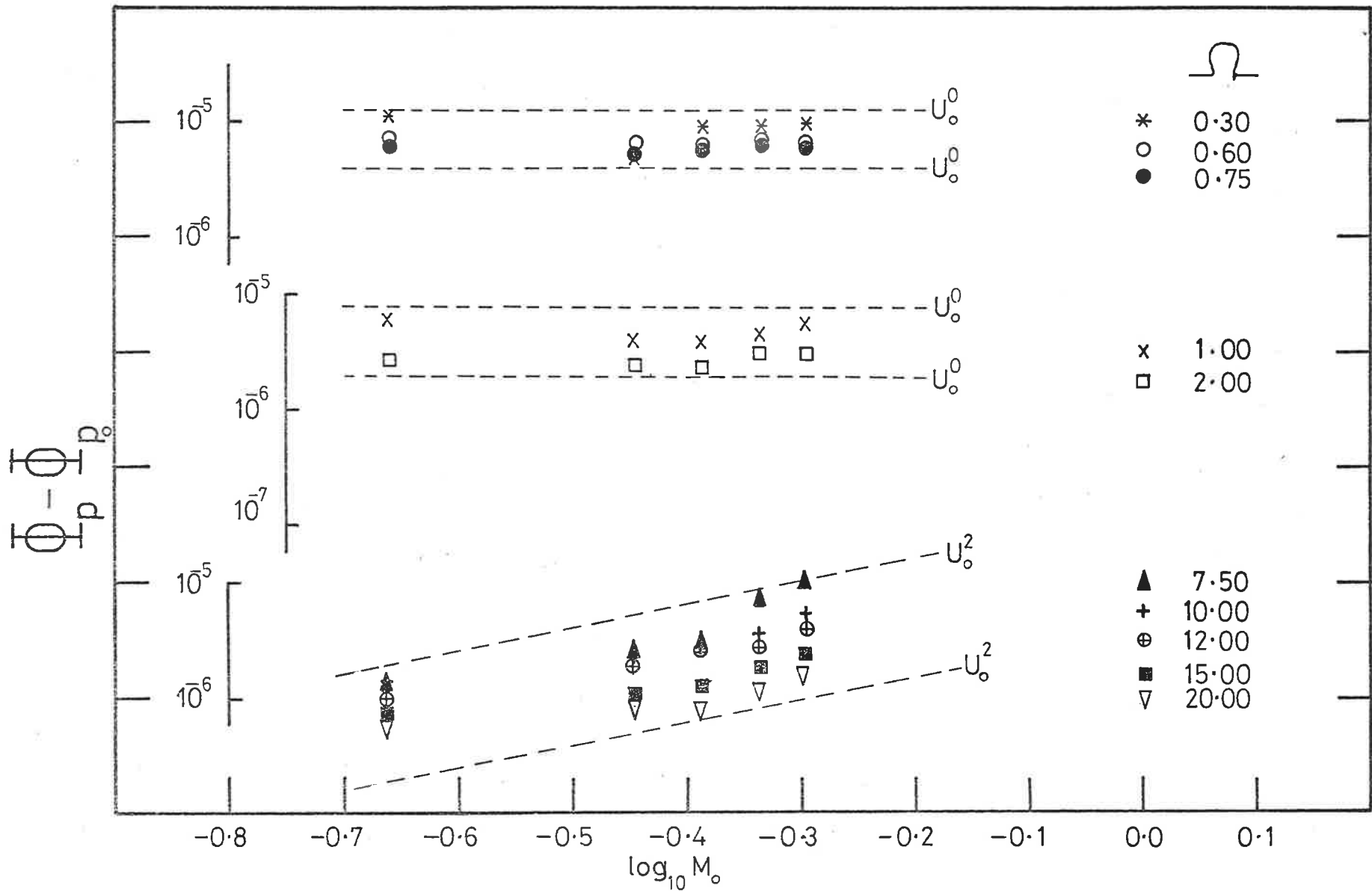


FIGURE 5.40 FLOW DEPENDENCE OF \bar{Q}_p FOR BUTTERFLY VALVE

of either plane waves or higher order modes. This is evident from Figure C-4. Hence, as in the case of the 45° mitred bend and the gate valve, one could expect the wall pressure spectral density, ϕ_p , to scale as U_o^3 at all Strouhal numbers, and the overall mean square pressure fluctuations to scale as U_o^4 .

A summary of the flow dependence associated with the various internal flow disturbances investigated is presented in Table 5.1.

There appears to be no published work available on the flow dependence of the wall pressure fluctuations associated with various internal flow disturbances. Gordon and Maidanik (1967), and Gordon (1968, 1969) were concerned with spoiler generated flow noise and in particular with the acoustic power radiated by the turbulent flow exhausting from the pipe. The acoustic power radiated was found to scale as U_ℓ^6 where U_ℓ is the local flow velocity in the vicinity of the spoiler. Hayden (1972) extended Gordon and Maidanik's work and concluded that the acoustic power radiated by the turbulent flow exhausting from the pipe scales as U_ℓ^6 below the cut-off frequency of the first higher order acoustic mode in the pipe and as U_ℓ^8 above it. Kuhn and Morfey (1976) determined that the exhaust from a pipe run containing a 90° mitred bend produces radiated acoustic power which scales as U^6 , where U is the flow velocity at the pipe exit. They were only concerned with Strouhal numbers below the cut-off frequency of the first higher order acoustic mode (i.e. regions where only plane waves can propagate) and they concluded that the plane wave acoustic field inside the pipe dominated the acoustic radiation exhausting from the pipe. As observed, there are differences in flow dependence between the wall pressure fluctuations, as determined in this investigation, and the radiated acoustic power exhausting from the pipe as determined by Gordon and Maidanik, Hayden, and Kuhn and Morfey. Morfey (p. 233, 1968) and Fuchs (1969) have shown that the

TABLE 5-1

The flow dependence of the spectral density of the internal wall pressure field, and the overall mean square wall pressure fluctuations, associated with the various flow disturbances investigated.

	ϕ_p		$\overline{P^2}$
	Below Cut Off	Above Cut Off	
90° Radiused Bends	U_o^3	U_o^3	U_o^4
45° Mitred Bend	U_o^3	U_o^3	U_o^4
90° Mitred Bend	U_o^3	U_o^5	U_o^4
Gate Valve	U_o^3	U_o^3	U_o^4
Butterfly Valve	U_o^3	U_o^5	U_o^4
55 m.m. Orifice Plate	U_o^3	U_o^5	U_o^6
65 m.m. Orifice Plate	U_o^3	U_o^3	U_o^4
Straight Pipe	U_o^3	U_o^3	U_o^4

sound power travelling along a duct is increased by a factor of $(1+M_0)^2$ for the acoustic waves propagating in the direction of flow, and that it is reduced by a factor of $(1-M_0)^2$ for the acoustic waves propagating against the direction of flow. Alfredson and Davies (1970) investigated the radiation of sound from an engine exhaust. They reported that the nett acoustic energy flux out of the tailpipe depended on the mean flow and the reflection coefficient. They developed an expression for this nett acoustic energy flux, which is,

$$I = \frac{P_{\text{r.m.s.}}^2}{\rho_e c_e} [(1+M_0)^2 - R^2(1-M_0)^2] \quad , \quad [5.2]$$

where $P_{\text{r.m.s.}}$ is the root mean square amplitude of the incident pressure wave at the exhaust outlet and R is the reflection coefficient. If the end of the pipe is open (as in the case of Gordon, and Kuhn and Morfey), for the no flow case, it can be assumed that the terminal impedance is the same as that acting upon a piston mounted in an infinite baffle (Kinsler and Frey, p.199, 1962) and little if any acoustic energy flux is reflected, and consequently almost all of the incident acoustic power is radiated out through the end of the pipe. Alfredson and Davies (1970) showed that the magnitude of the reflection coefficient at an engine exhaust outlet is greater than is predicted for the zero flow case, and that the reflection coefficient increases with flow speed. In the presence of a steady mean flow at ambient conditions, the reflection coefficient increases with flow, from that at no flow, by a factor of $1 + 2M_0$. For the case of air flowing out of an open pipe (Gordon, Kuhn and Morfey), since the reflection coefficient is negligible, for the no flow case, the effects of flow on the reflection coefficient would appear to be of second order for $M_0 < 1$. Hence, equation [5.2] reduces to

$$I = \frac{p^2}{\rho_e c_e} (1 + M_o)^2 \quad [5.3]$$

Hence the nett acoustic energy flux out of an open piping system with flow, scales as $(1 + M_o)^2$. For the range of flow speeds in this investigation ($M_o \sim 0.20$ to 0.50) this approximates as a $M_o^{0.5}$ dependence. This additional flow dependence does not totally account for the difference between the flow dependence for the mean square wall pressure fluctuations (U_o^4 and U_o^6 below and above cut-off respectively) and the acoustic power radiated (U_o^6 and U_o^8 below and above cut-off respectively).

5.5 GENERAL DISCUSSION

5.5.1 90° Radiused Bends

It has been shown that for the 90° radiused bend with $R/a_m = 6.4$, both the acceleration response of the test section and the acoustic power radiated from it are essentially the same as for undisturbed fully-developed turbulent pipe flow, over the whole of the speed range of the present tests. This is consistent with the wall pressure spectra for this bend, and the observation that additional acoustic radiation into the reverberation chamber due to the bend is very small. It is clear that the flow disturbance produced by bends of this radius ratio is a mild one, which results in generation of neither a significant wall pressure field nor a significant acoustic field as compared with fully-developed turbulent pipe flow.

The most consistent and obvious difference between the results for this bend and those for undisturbed flow, is a slight increase in acoustic radiation for ν values of 0.10 to 0.15. Sound will propagate in the pipe as plane waves if $ka_1 < 1.84$ and as higher order modes (and plane waves) if $ka_1 \geq 1.84$. For the steel test section used, the propagation of the lowest of the higher order modes -

the (1,0) mode - occurs for $\nu_{co} \sim 0.12$. The increase in Φ_{π} referred to is associated with this (1,0) mode becoming propagational and with the phenomenon of coincidence (discussed in Chapter 2), a conclusion which is supported by the experimental results presented in Chapter 4 and by the discussion of the other flow disturbances in following subsections.

As in the case of the radiused bend with $R/a_m = 6.4$, there is no significant difference in either acceleration response of the test section or acoustic radiation from it between the $R/a_m = 3.0$ bend and the straight pipe, again with the exception of increased radiation at frequencies in the range $0.10 < \nu < 0.15$.

The flow disturbance due to the $R/a_m = 3.0$ radiused bend gives rise to sound pressures in the inlet bell-mouth and, it may be inferred, also to an internal acoustic field, both of which have considerably higher levels than those in the straight pipe; but even so the wall pressure fluctuations associated with these acoustic levels (see Figure 5.10) do not dominate over the wall pressure fluctuations associated with straight pipe flow. This is shown by the fact that the wall pressure spectral levels associated with the radiused bend are similar to those associated with undisturbed fully-developed turbulent pipe flow (see Figure 5.5), except for slight increases at very low Strouhal numbers.

From Figures 5.33 and 5.34 it can be seen that the efficiency of the pipe as an acoustic radiator (with the radiused bends) is only greater than that of fully-developed turbulent pipe flow in the proximity of $\nu = 0.10$, where there is a consistent increase in radiation ratio. The low frequency scatter is fairly inconsistent and on the average produces $\sigma/\sigma_0 \approx 0$ as in the case for $\nu \geq 0.20$. The implication here is that low frequency plane waves and higher order modes above the first ((1,0)) mode, generated by the two radiused bends are of very

low intensity and do not radiate any more efficiently than the turbulent pressure fluctuations or are non-existent, the (1,0) higher order mode being the exception.

5.5.2 45° Mitred Bend

The 45° mitred bend produces no significant effect on the power spectral density of the acceleration of the pipe wall or the acoustic power radiation for $\nu < 0.10$ (as compared with straight pipe flow). However, as the frequency increases above this value, there are increases in spectral density, coinciding with the higher order acoustic modes in the pipe becoming propagational. As for the case of the 90° mitred bend (Chapter 4), this behaviour occurs despite the fact that the greatest acoustic disturbance to the wall pressure spectrum occurs at frequencies which correspond to $\nu < 0.10$.

It can be deduced from Figure 5.35 that the low intensity plane waves generated by the 45° mitred bend do not radiate efficiently (for $\nu < 0.10$). It is clear that the consequent experimentally observed increases in radiation ratio in the region of $\nu = 0.10$, coincide with the (1,0) mode becoming propagational. There is a suggestion of a further peak in the experimental curves at the frequency of the (2,0), (4,0) and (1,1) modes (bearing in mind that the experimental results are for $\frac{1}{3}$ -octave bands), but at these and higher frequencies, as the modes become closer together, the effects of individual modes become less obvious.

As has been seen in Chapter 4, the 90° mitred bend is a strong generator of low frequency plane acoustic waves in comparison with the 45° mitred bend. These intense plane waves generated by the 90° mitred bend couple to the pipe wall and radiate more efficiently than the turbulent pressure fluctuations (see σ/σ_0 in Figure 4.44). This is in contrast to the 45° mitred bend which does not radiate more

efficiently than turbulent pressure fluctuations associated with straight pipe flow (see σ/σ_0 in Figure 5.35), except at frequencies associated with the (1,0) and (2,0) higher order modes. This is because the low frequency plane waves generated by the 45° mitred bend are very much less intense than those generated by the 90° mitred bend (see Figure 5.5) and the excitations produced by the turbulent pressure fluctuations dominate at these low frequencies.

5.5.3 Butterfly Valve

The butterfly valve, like the 90° mitred bend, is also responsible for the generation of a strong acoustic field in the pipe, as evidenced by sound pressure level measurements in the inlet bell mouth presented in Figure 5.41. At the highest flow speed investigated, some band levels are 40 dB or more greater than those in an undisturbed flow (see Figure 5.10).

In this case, at all flow speeds, there is an increase in the power spectral density of both the wall acceleration and the acoustic power radiation over those for undisturbed flow, over the whole frequency range, although, as in the case of the 90° mitred bend, the increase abruptly becomes much larger as the higher order acoustic modes become propagational. This is illustrated in Figure 5.36. There are also significant increases in both the wall acceleration and the acoustic power radiated at frequencies below the cut-off frequency of the first higher order mode, and as discussed earlier in this chapter these are attributed to vortex shedding and plane acoustic waves, the vortex shedding dominating. As can be seen from the radiation ratios (σ/σ_0) in Figure 5.36, these low frequency excitations radiate much more efficiently than undisturbed fully-developed turbulent flow excitation. As for the other pipe fittings, the (1,0) and (2,0) higher order modes also radiate more efficiently.

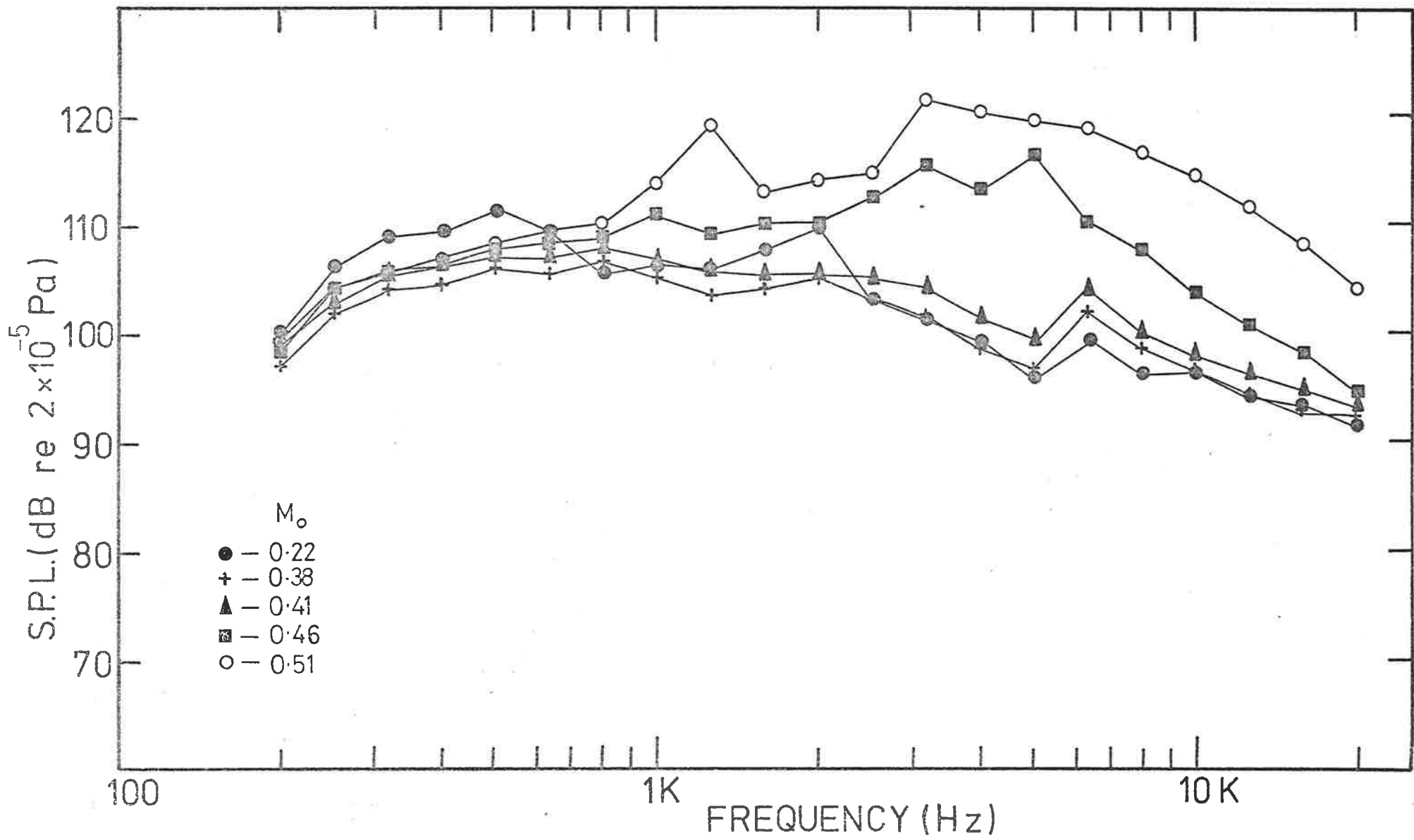


FIGURE 5.41 BUTTERFLY VALVE "FULLY OPEN" →
SOUND FIELD IN BELLMOUTH INLET

5.5.4 Gate Valve

The gate valve is a milder flow disturbance than either the butterfly valve or the 90° mitred bend; it is responsible for the generation of an internal acoustic field with approximately the same magnitude as the 45° mitred bend. The results of sound pressure level measurements on the pipe axis in the bell mouth inlet are presented in Figure 5.42.

It can be seen, however, from Figure 5.37 that the character of the pipe wall vibration and the external acoustic radiation produced by the gate valve is different from that produced by the butterfly valve, the 90° mitred bend or the 45° mitred bend, in that the low frequency increases of pipe wall acceleration and acoustic radiation are of the same order of magnitude as the increases for the (1,0) and (2,0) higher order modes. In fact, the low frequency increases are greater than those at frequencies above the cut-off frequency of the (2,0) higher order mode. From the radiation ratio (σ/σ_0) it can be seen that the pipe is a particularly efficient acoustic radiator at $v = 0.055$. The implications of these observations are that the gate valve when fully open, while exciting the (1,0) and (2,0) higher order modes efficiently, is not a strong generator of many higher order modes. Perhaps this is not surprising in that one would perhaps expect the internal configuration of the valve to have some influence on the degree of flow excitation induced. Whereas the mitred bends cause flow separation and the butterfly valve is subject to vortex shedding from the vane, the flow through the gate valve is not subjected to any intense disturbance when the valve is fully open, as it does not represent a significant protrusion into the flow in this state.

In view of this, several experiments were performed with the gate valve " $\frac{2}{3}$ open", so that the flow through the valve contracted

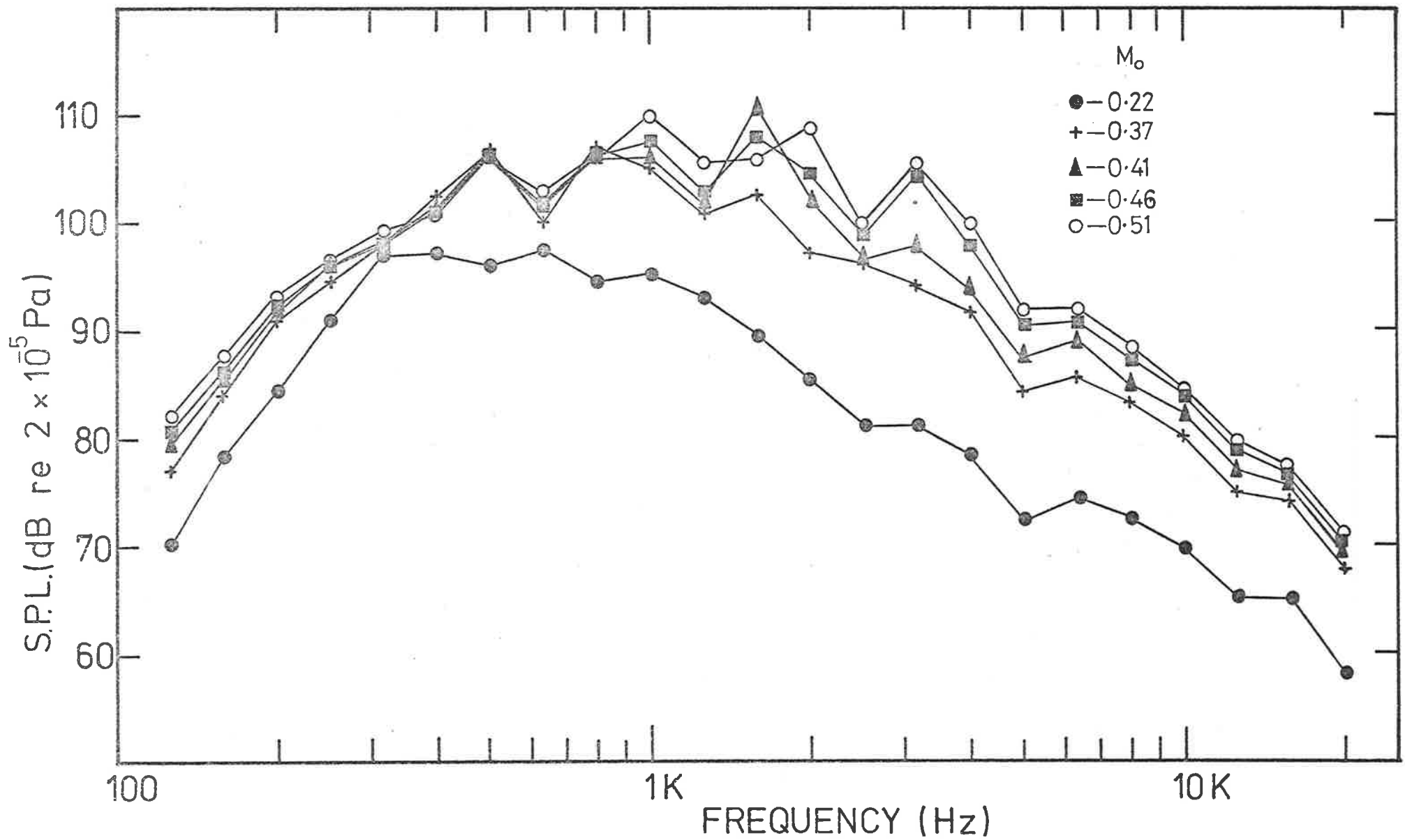


FIGURE 5.42 GATE VALVE "FULLY OPEN"—SOUND FIELD IN BELLMOUTH INLET

and separated. In this position the gate represented a partial blockage to the flow through the valve, whereas in the "fully open" position, the gate is completely removed from the path of the fluid flow. Figures 5.43 and 5.44 are narrow band analyses of the pipe wall acceleration and the acoustic power radiated from the test section with the valve " $\frac{2}{3}$ open". Comparing the pipe wall vibration response in Figures 5.23 and 5.43 it can be seen that the relative contribution to the spectra of the higher order modes in comparison with the low frequency plane waves is much greater in the latter. The same conclusion is reached by comparison of the external acoustic power radiated in Figures 5.28 and 5.44. The $\frac{1}{3}$ -octave band spectral measurements of Φ_{ζ} and Φ_{π} relative to the corresponding value for the straight pipe, and the corresponding radiation ratios, for the gate valve $\frac{2}{3}$ open are presented in Figure 5.45. It can be seen that the higher order modes dominate the pipe wall response and the external acoustic radiation in this case.

It will also be observed from Figure 4.44, 5.36 and 5.37 (for the 90° mitred bend, butterfly valve and gate valve respectively), that there is a general tendency for the amount by which the low frequency ($\nu < 0.10$) radiation from the test section exceeds that for the straight pipe at the same flow speed to decrease as the flow speed increases. It would therefore appear, even though the spectra of the wall pressure fluctuations all appear to scale in roughly the same way with flow speed (for a particular pipe fitting), the effectiveness of the fluid dynamic pressure field in forcing pipe modes which radiate efficiently increases more rapidly with flow speed than does that of the plane wave component of the acoustic pressure field; the result is a reduced relative contribution from the low frequency acoustic disturbance as the flow speed is increased.

$X = 52.8, M_o = 0.50$

HIGHER ORDER MODES

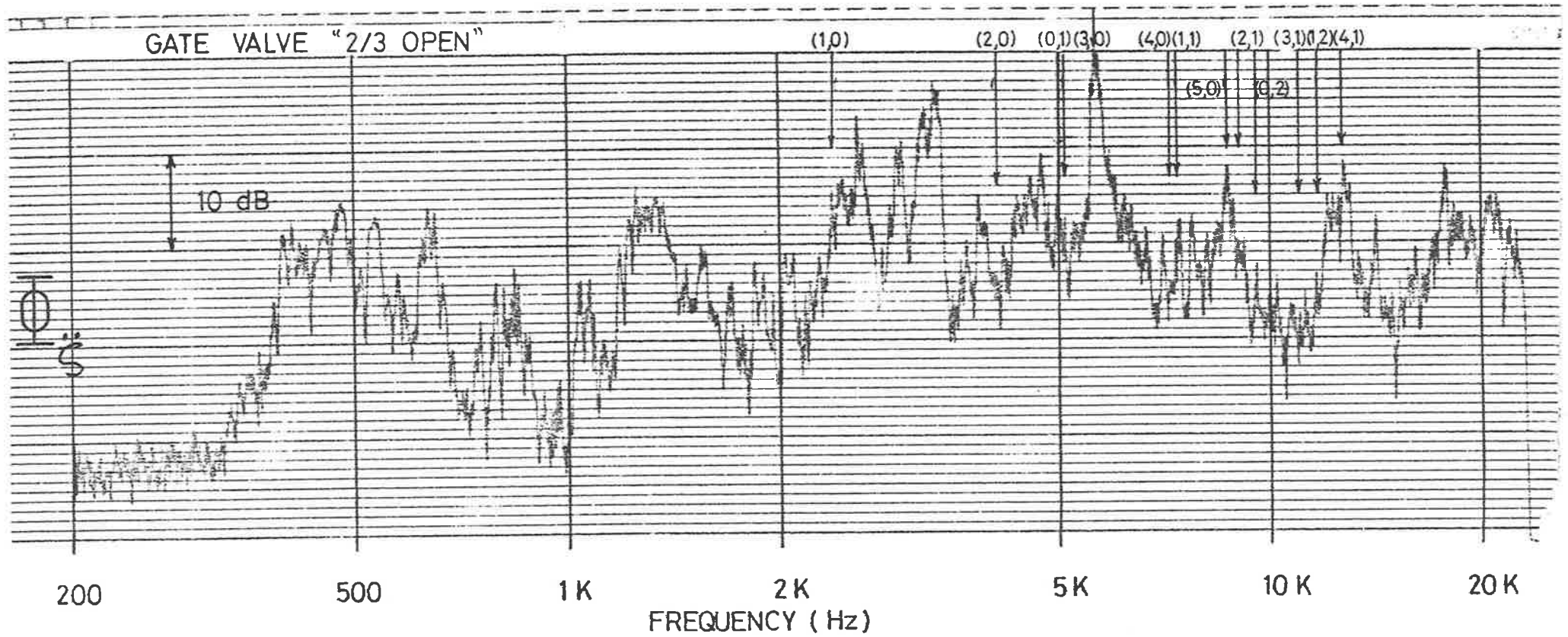


FIGURE 5-43 PIPE WALL ACCELERATION [100 Hz Bandwidth]

$X = 52.8, M_0 = 0.40$

HIGHER ORDER MODES

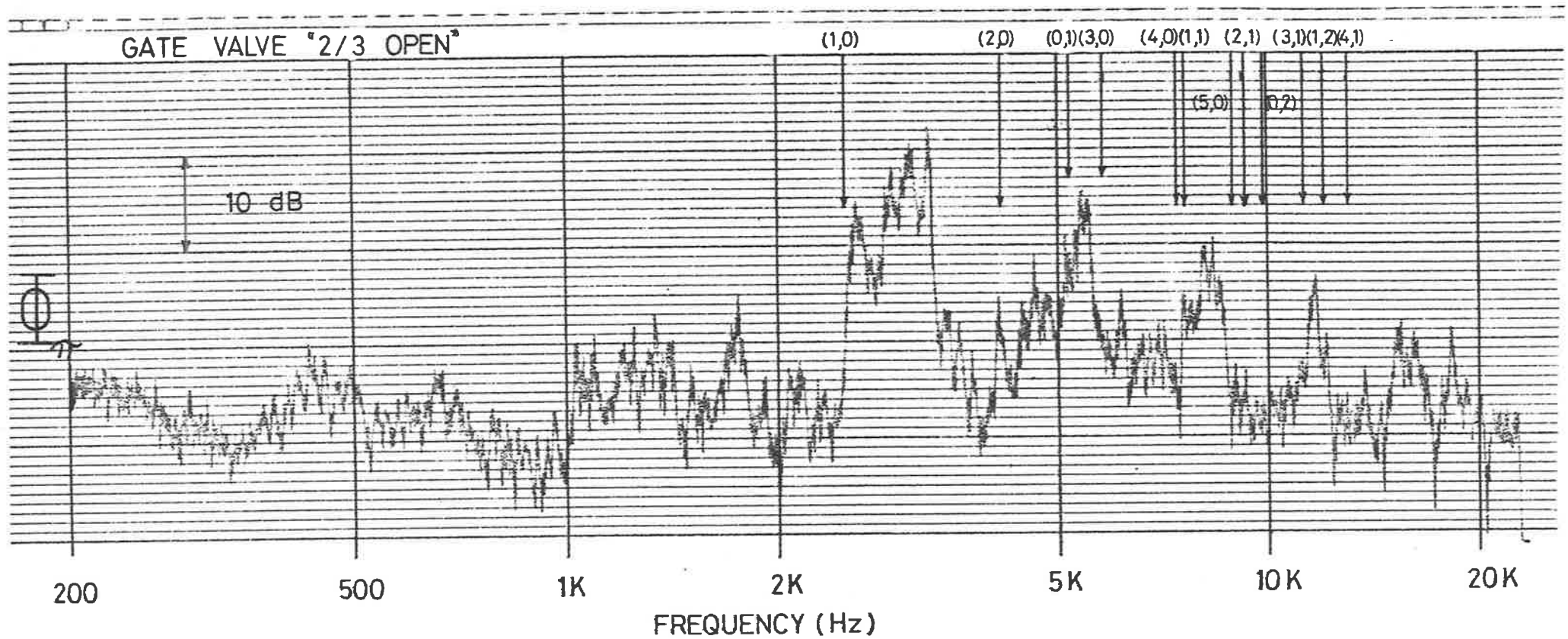


FIGURE 5-44 ACOUSTIC POWER RADIATION [100 Hz Bandwidth]

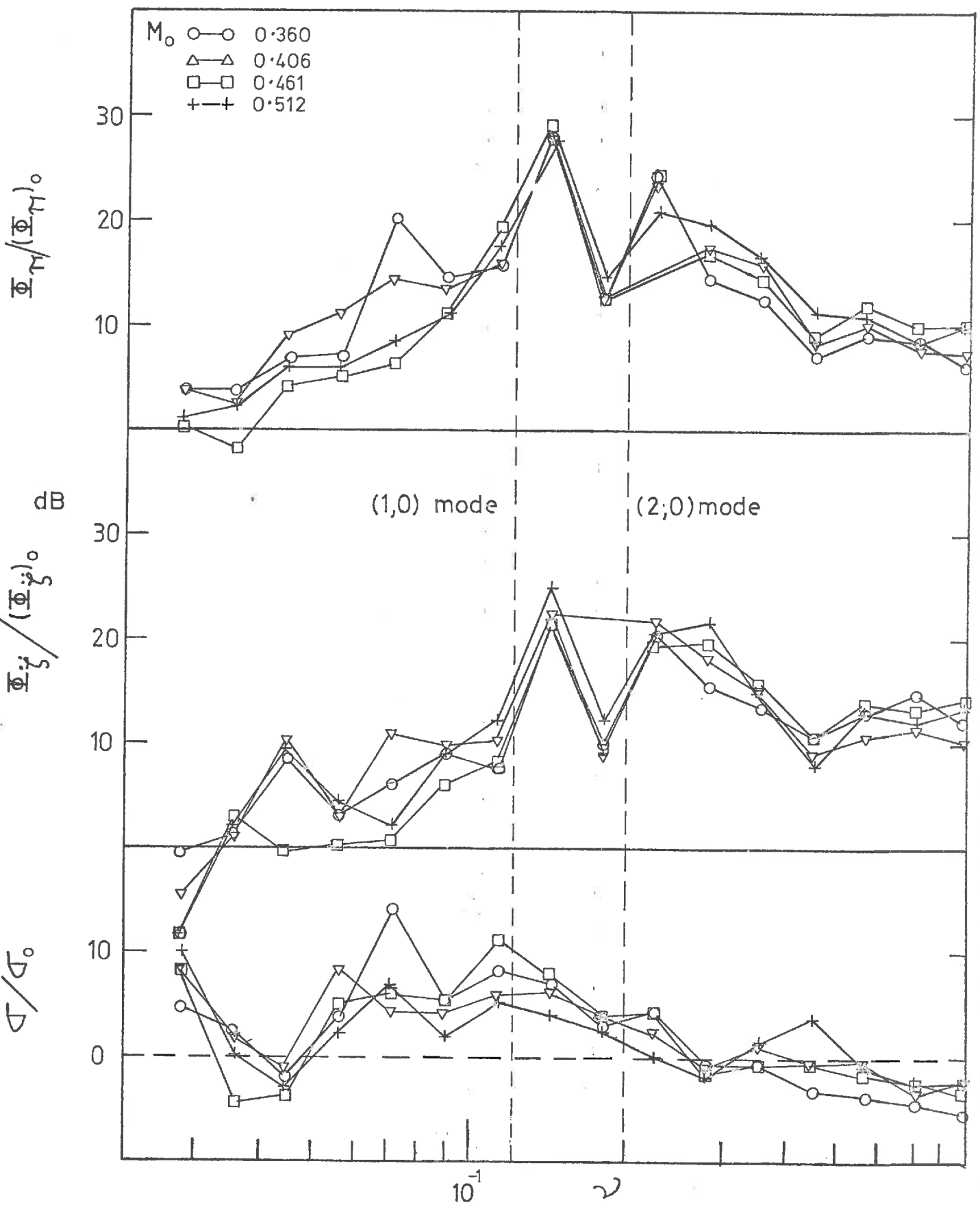


FIG 5.45 SPECTRAL DENSITIES OF Φ_{ξ} AND Φ_{η} RELATIVE TO STRAIGHT PIPE FLOW AND THE CORRESPONDING RADIATION RATIO, σ/σ_0 FOR GATE VALVE (2/3 OPEN)

5.5.5 Summary

Measured values of the effects of several internal flow disturbances on the wall acceleration of and the external acoustic radiation from a pipe carrying a turbulent air flow have been presented in this chapter. The disturbances produce acoustic wall pressure fluctuations, most of which are larger than those associated with undisturbed fully-developed turbulent pipe flow. In all cases, however, enhanced vibrational response and external acoustic radiation are observed when compared with straight pipe flow. Effects are greatest at frequencies close to the cut-off frequencies of the higher order internal acoustic modes.

Of the several internal flow disturbances investigated, the 90° mitred bend, the butterfly valve and the 55 mm orifice plate (Appendix C) give rise to intense internal sound fields. The spectral densities of the wall pressure fluctuations associated with these devices scale as U_0^3 at Strouhal numbers below which the higher order modes can propagate and as U_0^5 at Strouhal numbers at which the higher order modes are propagational. There are large increases in external sound radiation due to the vibrations of the pipe wall. Both plane acoustic waves (at low frequencies) and higher order modes are responsible for these increases. In the particular case of the butterfly valve, force fluctuations due to vortex shedding off the vane generate additional low frequency pipe wall vibrations which dominate over the plane waves at these frequencies.

There is negligible plane wave excitation of the pipe wall in the case of the 45° mitred bend although the higher order modes are responsible for vibration and radiation increases at frequencies above the cut-off frequency of the (1,0) mode. Here, the spectral density of the wall pressure fluctuations scale as U_0^3 at all Strouhal numbers.

The gate valve in its fully open state excites propagating plane waves at low frequencies. The (1,0) and (2,0) higher order modes are excited, but the experimental evidence suggests that the other higher order modes do not contribute significantly to the pipe wall response. The spectral density of the wall pressure fluctuations scale as U_0^3 at all Strouhal numbers.

The radiused bends do not produce any appreciable increases in pipe wall response at any frequency, perhaps with the exception of a small increase in the filter band containing the (1,0) mode. Here too, the spectral density of the wall pressure fluctuations, ϕ_p , scales as U_0^3 at all Strouhal numbers.

CHAPTER 6

WALL PRESSURE FLUCTUATION CROSS CORRELATIONS

6.1 INTRODUCTION

As has been shown in Chapters 4 and 5, a flow disturbance such as a mitred bend, a valve or an orifice plate in a piping system containing a fully-developed turbulent flow generates intense internal wall pressure fluctuations. This in turn gives rise to a correspondingly increased pipe wall acceleration and acoustic power radiation to the surroundings. Sufficiently far downstream (or upstream) of the flow disturbance (away from any regions of separated flow in the vicinity of the disturbance), the wall pressure fluctuations are the sum of two pressure fields: a turbulent pressure field and an acoustic pressure field. The acoustic pressure field comprises contributions from propagating plane waves and propagating higher order modes. Longitudinal space-time cross-correlations of the wall pressure fluctuations with appropriate time delays and spatial separations, allow the acoustic pressure field to be separated from the turbulent pressure field. Furthermore, cross-correlations in a frequency band can also show whether the acoustic energy is being propagated in a plane wave mode or in a higher order mode in that band. This approach was originally used by Goff (1955), Bolleter and Chanaud (1971), and more recently by Karvelis (1975); it is based on the assumption that the turbulent pressure fluctuations and the acoustic pressure fluctuations are uncorrelated.

In the present investigation, various techniques developed by Goff (1954) and Karvelis (1975) are extended and applied to the particular case of the 90° mitred bend with the intention of

identifying the contribution of plane waves and higher order modes to the wall pressure fluctuations in various frequency bands. At low frequencies ($k a_i < 1.84$), only plane waves can propagate; these fundamental waves propagate in the axial direction with their wave-fronts normal to the pipe axis and the acoustic pressure uniform over the pipe cross-section. The mean-square acoustic pressure, associated with plane waves (at frequencies below the cut off frequency of the first higher order mode) propagating inside the pipe can be extracted from the wall pressure fluctuation cross-correlations (Karvelis, 1975). For $k a_i \geq 1.84$, the higher order modes become propagational and these waves reflect back and forth from the pipe wall as they propagate down it and here the wave fronts (pressure distribution) are not uniform over the pipe cross-section. Further, since the phase velocity of these higher order modes is frequency dependent they are dispersive in character. For these reasons the mean-square acoustic pressure propagating inside the pipe cannot be obtained directly at these frequencies by cross-correlation techniques.

To predict the acoustic radiation from, and the acceleration response of, pipes downstream (or upstream) of an internal flow disturbance, it must be possible to calculate the dynamic response of the pipe, with the wall pressure fluctuations as the forcing function. Karvelis (1975) was mainly concerned with the mean square acoustic pressure inside the pipe and stated that the calculation of the pipe response was outside the scope of his investigation. Hence his work did not contain any analysis of the components of the wall pressure fluctuations in frequency bands containing higher order modes. While observing that all the flow disturbances that he

investigated showed dispersion in the frequency bands where higher order modes propagate he did not attempt to extract the individual components of the wall pressure fluctuations associated with the various higher order modes. The wall pressure fluctuations due to fully-developed turbulent pipe flow constitute a "lower limit" for the pipe wall excitation. They have been experimentally investigated by Rennison (1976) and by Bull and Norton (1977), and are readily available in a non-dimensional form. The plane wave component of the wall pressure fluctuations in filter bands containing higher order modes can be obtained from the cross-correlations (By the techniques applied by Karvelis (1975) to filter bands where only plane wave propagation is possible). Karvelis's statement that it is not possible, due to the dispersion, to associate a peak value corresponding to the plane wave motion in these filter bands that contain higher order modes is not correct because the group velocity c_g of the higher order modes is less than the internal speed of sound c_i , at which the plane waves propagate. Correlations to be presented in this Chapter contain a clearly defined peak at a time delay corresponding to plane wave propagation in all filter bands. Thus, an estimate of the component of the wall pressure fluctuations associated with the higher order modes in various filter bands can be obtained by subtracting the turbulent and plane wave components from the total wall pressure fluctuations in those bands. The extraction of this information is useful in predicting the pipe wall response, as will be discussed in Chapter 7. The theoretical background for the extraction of the various components of the wall pressure fluctuations will now be discussed in this chapter and experimental results presented for the 90° mitred bend.

6.2 THEORETICAL BACKGROUND

The wall pressure fluctuations in a piping system containing various internal flow disturbances (away from any region of separated flow in the vicinity of a disturbance) are the sum of an acoustic and a turbulent pressure field. Both the acoustic pressure fluctuations, \tilde{p} , and the turbulent pressure fluctuations, p' , are stochastic processes, being random functions of space and time. Furthermore, the two variables are stationary in the wide sense (their expected values are constant and their autocorrelations depend only on the time delay τ). That is;

$$E\{\underline{p}'(t)\} = \int_{-\infty}^{\infty} p' f(p'; t) dp' = \eta' = \text{constant}$$

$$E\{\underline{\tilde{p}}(t)\} = \int_{-\infty}^{\infty} \tilde{p} f(\tilde{p}; t) d\tilde{p} = \tilde{\eta} = \text{constant}$$

and

$$E\{\underline{p}'(t_1) \underline{p}'^*(t_2)\} = \int_{-\infty}^{\infty} p'_1 p'_2 f(p'_1, p'_2; t_1, t_2) dp'_1 dp'_2$$

$$= R_{p'_1 p'_2}(\tau)$$

$$E\{\underline{\tilde{p}}(t_1) \underline{\tilde{p}}^*(t_2)\} = \int_{-\infty}^{\infty} \tilde{p}_1 \tilde{p}_2 f(\tilde{p}_1, \tilde{p}_2; t_1, t_2) d\tilde{p}_1 d\tilde{p}_2$$

$$= R_{\tilde{p}_1 \tilde{p}_2}(\tau), \quad [6.1]$$

where f is the probability density function, $\tau = t_1 - t_2$, and $p(t) = p(\underline{x}; t)$ where \underline{x} is a position vector and the asterisk (*) denotes the complex conjugate.

The instantaneous wall pressure fluctuation at a point \underline{x} at time t , is given by

$$p(\underline{x};t) = p'(\underline{x};t) + \tilde{p}(\underline{x};t) . \quad [6.2]$$

The variable $p(\underline{x};t)$ is also a random stochastic process which is stationary in the wide sense.

The cross-correlation of two arbitrary processes, real or complex, is defined in the space and time domain by;

$$E\{\underline{x}(t_1)\underline{y}^*(t_2)\} = R_{xy}(\xi, t_1, t_2) . \quad [6.3]$$

If it is assumed that $\underline{x}(t)$ and $\underline{y}(t)$ are ergodic with respect to the mean (time averages equal expected values or ensemble averages (Papoulis, 1965)), then

$$R_{xy}(\xi, t_1, t_2) = R_{xy}(\xi, \tau), \quad \text{and}$$

$$R_{xy}(\xi, \tau) = \lim_{T \rightarrow \infty} \frac{1}{2T} \int_{-T}^T \underline{x}(t)\underline{y}^*(t+\tau)dt . \quad [6.4]$$

For the purposes of this investigation, it is assumed that all the various wall pressure fluctuation components are random, stationary, ergodic stochastic processes.

The longitudinal space-time cross-correlation of the wall pressure fluctuations can be expressed as

$$R_{pp}(\xi, \tau) = \lim_{T \rightarrow \infty} \frac{1}{2T} \int_{-T}^T \underline{p}(t)\underline{p}^*(t+\tau)dt , \quad [6.5]$$

where $\underline{p}(t) = p(\underline{x}_1; t) = p'(\underline{x}_1; t) + \tilde{p}(\underline{x}_1; t)$ and $\underline{p}^*(t+\tau) = p^*(\underline{x}_2; t+\tau) = p'^*(\underline{x}_2; t+\tau) + \tilde{p}^*(\underline{x}_2; t+\tau)$. Furthermore for $ka_i \geq 1.84$, the acoustic component of the wall pressure fluctuations, \tilde{p} can be broken up into a plane wave and a higher order mode component. Hence:

$$\tilde{p}(\underline{x};t) = \tilde{p}_{P.W.}(\underline{x};t) + \tilde{p}_{H.O.}(\underline{x};t) \quad \text{for } ka_i \geq 1.84$$

$$\tilde{p}_{P.W.}(x;t) \quad \text{for } k a_1 < 1.84. \quad [6.6]$$

Thus,

$$\begin{aligned} R_{PP}(\xi, \tau) = & R_{p'p'}(\xi, \tau) + R_{\tilde{p}_{P.W.}\tilde{p}_{P.W.}}(\xi, \tau) + R_{\tilde{p}_{H.O.}\tilde{p}_{H.O.}}(\xi, \tau) + 2R_{p'\tilde{p}_{P.W.}}(\xi, \tau) \\ & + 2R_{p'\tilde{p}_{H.O.}}(\xi, \tau) + 2R_{\tilde{p}_{P.W.}\tilde{p}_{H.O.}}(\xi, \tau). \end{aligned} \quad [6.7]$$

For $\tau = 0$ and $x_1 = x_2$,

$$\begin{aligned} R_{p'p'}(0,0) &= \lim_{T \rightarrow \infty} \frac{1}{2T} \int_{-T}^T p'(x_1;t)p'(x_1;t)dt \\ &= \langle p'^2 \rangle, \end{aligned} \quad [6.8]$$

and similarly:

$$\begin{aligned} R_{\tilde{p}_{P.W.}\tilde{p}_{P.W.}}(0,0) &= \langle \tilde{p}_{P.W.}^2 \rangle, \\ R_{\tilde{p}_{H.O.}\tilde{p}_{H.O.}}(0,0) &= \langle \tilde{p}_{H.O.}^2 \rangle, \\ R_{p'\tilde{p}_{P.W.}}(0,0) &= \langle p'\tilde{p}_{P.W.} \rangle, \\ R_{p'\tilde{p}_{H.O.}}(0,0) &= \langle p'\tilde{p}_{H.O.} \rangle, \\ R_{\tilde{p}_{P.W.}\tilde{p}_{H.O.}}(0,0) &= \langle \tilde{p}_{P.W.}\tilde{p}_{H.O.} \rangle. \end{aligned} \quad [6.9]$$

If we define the correlation coefficient of two arbitrary random processes as:

$$\rho_{xy}(\xi, \tau) = \frac{R_{xy}(\xi, \tau)}{\sqrt{R_{xx}(0,0)}\sqrt{R_{yy}(0,0)}} = \frac{R_{xy}(\xi, \tau)}{\sqrt{\langle x^2 \rangle}\sqrt{\langle y^2 \rangle}}, \quad [6.10]$$

then, Equation [6.7] can be re-written as

$$\begin{aligned} \rho_{pp}(\xi, \tau) \langle p^2 \rangle &= \rho_{p'p'}(\xi, \tau) \langle p'^2 \rangle + \rho_{\tilde{p}_{P.W.}\tilde{p}_{P.W.}}(\xi, \tau) \langle \tilde{p}_{P.W.}^2 \rangle \\ &+ \rho_{\tilde{p}_{H.O.}\tilde{p}_{H.O.}}(\xi, \tau) \langle \tilde{p}_{H.O.}^2 \rangle + 2\rho_{p'\tilde{p}_{P.W.}}(\xi, \tau) \langle p'^2 \rangle^{\frac{1}{2}} \langle \tilde{p}_{P.W.}^2 \rangle^{\frac{1}{2}} \\ &+ 2\rho_{p'\tilde{p}_{H.O.}}(\xi, \tau) \langle p'^2 \rangle^{\frac{1}{2}} \langle \tilde{p}_{H.O.}^2 \rangle^{\frac{1}{2}} + 2\rho_{\tilde{p}_{P.W.}\tilde{p}_{H.O.}}(\xi, \tau) \langle \tilde{p}_{P.W.}^2 \rangle^{\frac{1}{2}} \langle \tilde{p}_{H.O.}^2 \rangle^{\frac{1}{2}}. \end{aligned} \quad [6.11]$$

The correlation coefficient is a normalized quantity, and as such its values will lie between -1 and $+1$. Random variables whose correlation coefficient is zero are uncorrelated.

Goff (1954), Bolleter and Chanaud (1971) and Karvelis (1975) in utilizing wall pressure fluctuation cross-correlations to separate the acoustic component and the turbulent component of the wall pressure fluctuations, made the assumption that the turbulent and acoustic pressures are uncorrelated. Karvelis (1975) puts forward two arguments for the above statement: (i) Turbulent pressure fluctuations are an exponentially decaying random field convected at a large fraction of the mean velocity, whereas acoustic pressure fluctuations propagate at the local speed of sound. (ii) Interaction between turbulent and acoustic wall pressure fluctuations is of the second order since their length and time scales are not of the same order of magnitude.

Thus p' and $\tilde{p}_{P.W.}$ or p' and $\tilde{p}_{H.O.}$ are uncorrelated and the $\rho_{p'\tilde{p}_{P.W.}}$ and $\rho_{p'\tilde{p}_{H.O.}}$ terms in equation [6.11] are zero. The group velocity of the higher order modes (the velocity at which the energy associated with the higher order modes propagates) is always less than the speed of sound c_i , hence interaction between plane wave wall

pressure fluctuations and higher order mode wall pressure fluctuations is also of the second order (i.e. their length and time scales are not of the same order of magnitude). Hence, $\tilde{p}_{P.W.}$ and $\tilde{p}_{H.O.}$ are uncorrelated and the $\rho_{\tilde{p}_{P.W.}\tilde{p}_{H.O.}}$ term in equation [6.11] can be assumed to be zero also and equation [6.11] reduces to

$$\begin{aligned} \rho_{pp}(\tau)\langle p^2 \rangle &= \rho_{p'p'}(\tau)\langle p'^2 \rangle + \rho_{\tilde{p}_{P.W.}\tilde{p}_{P.W.}}(\tau)\langle \tilde{p}_{P.W.}^2 \rangle \\ &+ \rho_{\tilde{p}_{H.O.}\tilde{p}_{H.O.}}(\tau)\langle \tilde{p}_{H.O.}^2 \rangle \end{aligned} \quad [6.12]$$

Several studies have been made of the statistical properties of the fluctuating wall pressure field associated with a turbulent boundary layer and fully-developed turbulent pipe flow, for example Willmarth and Woolridge (1962), Bull (1967), Corcos (1963) and Cockburn and Robertson (1974). In general, these indicate that the cross spectral density of the wall pressure field, for both types of flow can be fairly well represented by:

$$\phi_p(\xi, \eta, \omega) = \phi_p(\omega) \exp\left(-c_x \frac{\omega|\xi|}{U_c} - c_y \frac{\omega|\eta|}{U_c} + i \frac{\omega\xi}{U_c}\right), \quad [6.13]$$

where ξ and η are spatial separations in the x -direction (longitudinal) and y -direction respectively and U_c is the convection velocity of the pressure field at frequency ω . The corresponding narrow band normalized space-time correlation coefficient is

$$\begin{aligned} \rho_{p'p'}(\xi, \eta, \tau; \omega) &= \exp\left(-c_x \frac{\omega|\xi|}{U_c} - c_y \frac{\omega|\eta|}{U_c}\right) \\ &\cdot \frac{\sin \Delta\omega/2(\tau-\tau_{p'})}{\Delta\omega/2(\tau-\tau_{p'})} \cos\omega(\tau-\tau_{p'}) \end{aligned} \quad [6.14]$$

This can also be written as

$$\rho_{p',p'}(\xi, \eta, \tau; \omega) = \rho_{x_{p',p'}}(\xi, \tau; \omega) \cdot \rho_{y_{p',p'}}(\eta, \tau; \omega) \quad , \quad [6.15]$$

where the normalized longitudinal space time correlation coefficient is

$$\rho_{x_{p',p'}}(\xi, \tau; \omega) = \exp\left(-c_x \frac{\omega |\xi|}{U_c}\right) \frac{\sin \Delta\omega/2(\tau - \tau_{p'})}{\Delta\omega/2(\tau - \tau_{p'})} \cdot \cos \omega (\tau - \tau_{p'}) \quad [6.16]$$

where $\Delta\omega$ is the bandwidth, $c_x \approx 0.10$ is an experimentally determined constant and $\tau_{p'} = \xi/U_c$.

Karvelis (1975) has derived an expression for the space-time longitudinal cross-correlation coefficient of acoustic waves of random phase and amplitude, where there is a uniform mean flow, in a filter band $\Delta\omega$. If we assume anechoic termination (i.e. there is no reflection of the propagating acoustic waves, as is approximately the case with choked nozzle flow because the acoustic waves cannot propagate back upstream past the nozzle throat, where the flow is sonic), then Karvelis's expression can be simplified to

$$\rho_{x_{pp}}(\xi, \tau; \omega) = \frac{\sin \Delta\omega/2(\tau - \tau_{\tilde{p}})}{\Delta\omega/2(\tau - \tau_{\tilde{p}})} \cos \Delta\omega(\tau - \tau_{\tilde{p}}) \quad , \quad [6.17]$$

where for plane waves

$$\tau_{\tilde{p}} = \tau_{\tilde{p}P.W.} = \frac{\xi}{c_i + U_0} = \frac{\xi}{c_i(1+M_0)} \quad , \quad [6.18]$$

and for higher order modes,

$$\tau_{\tilde{p}} = \tau_{\tilde{p}_{H.O.}} = \frac{\xi}{c_g + U_0} = \frac{\xi}{c_i (c_g / c_i + M_0)} \quad [6.19]$$

The peaks of the various longitudinal cross-correlation coefficients occur when $\tau = \tau_{p'}$, $\tau_{\tilde{p}}$, etc., hence;

$$\rho_{x_{p'p'}}(\xi, \tau; \omega)_{\text{peak}} = \exp\left(-0.1 \frac{\omega|\xi|}{U_c}\right) \delta(\tau - \tau_{p'}) ,$$

$$\rho_{x_{\tilde{p}_{P.W.}\tilde{p}_{P.W.}}}(\xi, \tau; \omega)_{\text{peak}} = \delta(\tau - \tau_{\tilde{p}_{P.W.}}) ,$$

and $\rho_{x_{\tilde{p}_{H.O.}\tilde{p}_{H.O.}}}(\xi, \tau; \omega)_{\text{peak}} = \delta(\tau - \tau_{\tilde{p}_{H.O.}}) . \quad [6.20]$

It should be noted that if $\Delta\omega$ is chosen appropriately then the respective peaks are distinct and sharp; the δ 's are not genuine delta functions but the maxima of well behaved and damped $\cos(\tau - \tau_p)$ correlation functions (See Bull, 1967).

Thus, equation 6.12 reduces to:

$$\begin{aligned} \rho_{pp}(\tau) \langle p^2 \rangle &= \exp\left(-0.1 \frac{\omega|\xi|}{U_c}\right) \delta(\tau - \tau_{p'}) \langle p'^2 \rangle \\ &+ \delta(\tau - \tau_{\tilde{p}_{P.W.}}) \langle \tilde{p}_{P.W.}^2 \rangle + \delta(\tau - \tau_{\tilde{p}_{H.O.}}) \langle \tilde{p}_{H.O.}^2 \rangle . \end{aligned} \quad [6.21]$$

It should be noted that Equation [6.21] is based on the following assumptions:

- (1) The turbulent flow and the plane wave contributions to the wall pressure fluctuations are uncorrelated.
- (2) The turbulent flow and the higher order mode contributions to the wall pressure fluctuations are uncorrelated.
- (3) The plane wave and the higher order mode wall pressure fluctuations are uncorrelated.

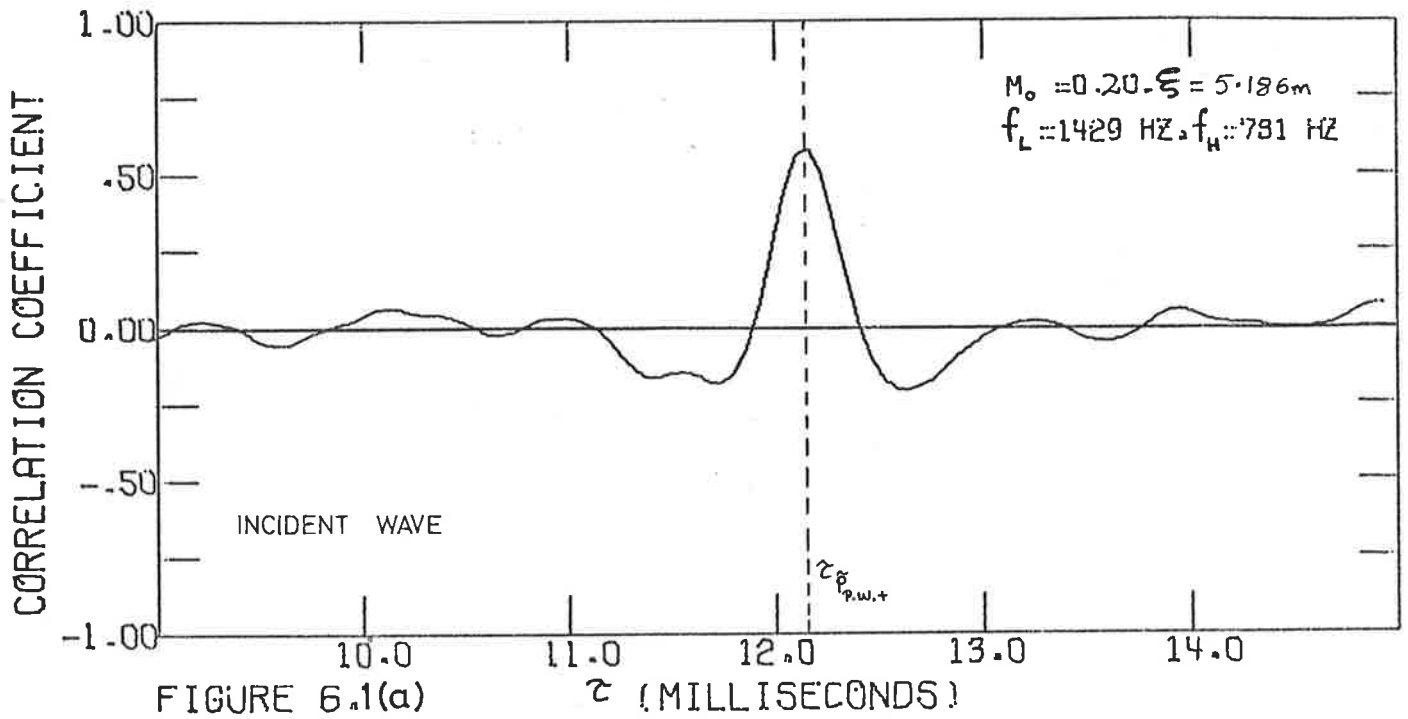
- (4) The choked nozzle in the system behaves as an anechoic termination; hence there are no reflections of the propagating acoustic waves.
- (5) Only the peak cross-correlation coefficients (which are associated with the various time delays corresponding to the various modes of energy propagation) are relevant to the evaluation of the components of the wall pressure fluctuations associated with the various modes of energy propagation (turbulent, plane wave and higher order mode wall pressure fluctuations).

Figure 6.1 is a typical correlogram, for $M_0 \sim 0.20$, $\xi = 5.186\text{m}$ and a filter band of 709-1412 Hz (1000 Hz octave). Here, since $k a_i < 1.84$, only plane wave propagation is possible and because of the large separation distance, the turbulence is essentially uncorrelated. The peak at $\tau \approx 12.2$ msec. corresponds to plane wave propagation ($\tau_{P.W.} = \xi/c_i(1+M_0)$) in the positive longitudinal (x) direction and the peak at $\tau \approx 33.7$ msec. corresponds to the positive time delay associated with the reflected wave propagating past the two transducers. This latter time delay can be represented as

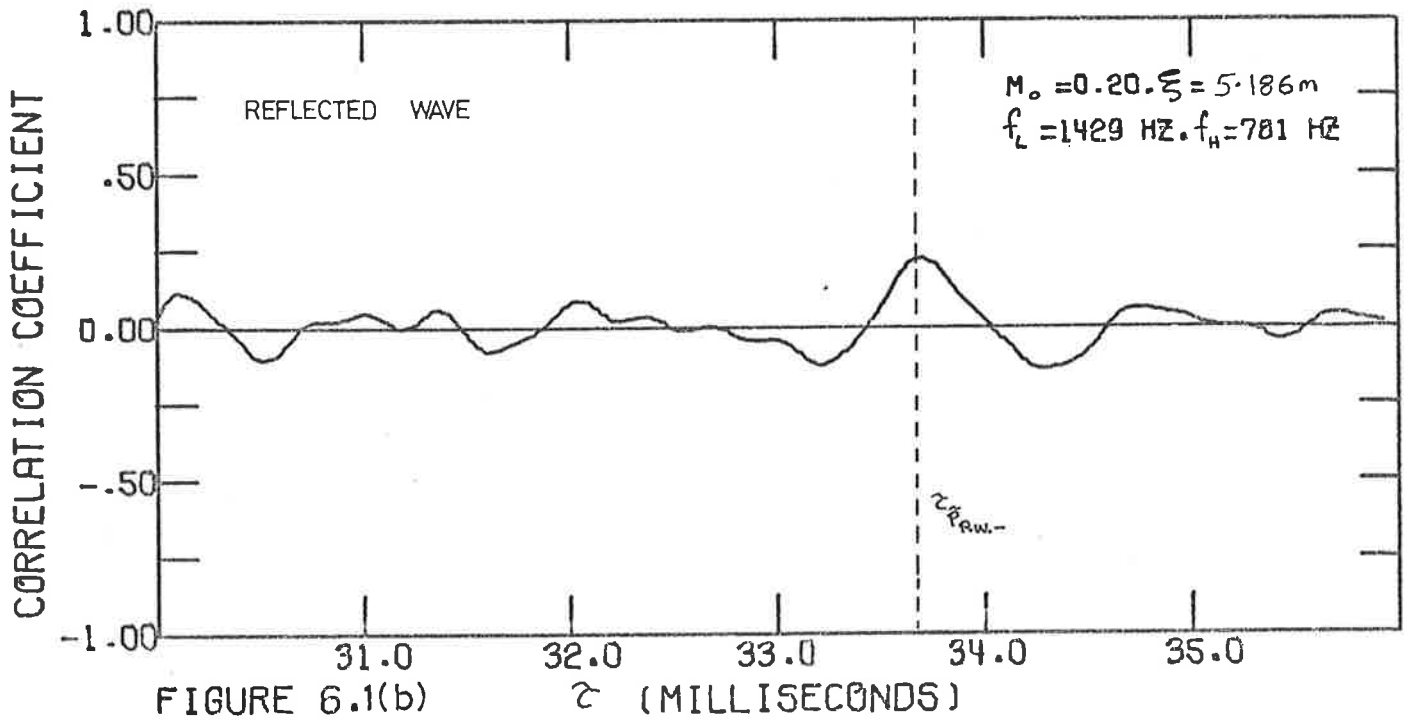
$$\tau_{P.W.-} = \frac{\xi + 2\xi_T - \xi M_0}{c_i(1 - M_0^2)}, \quad [6.22]$$

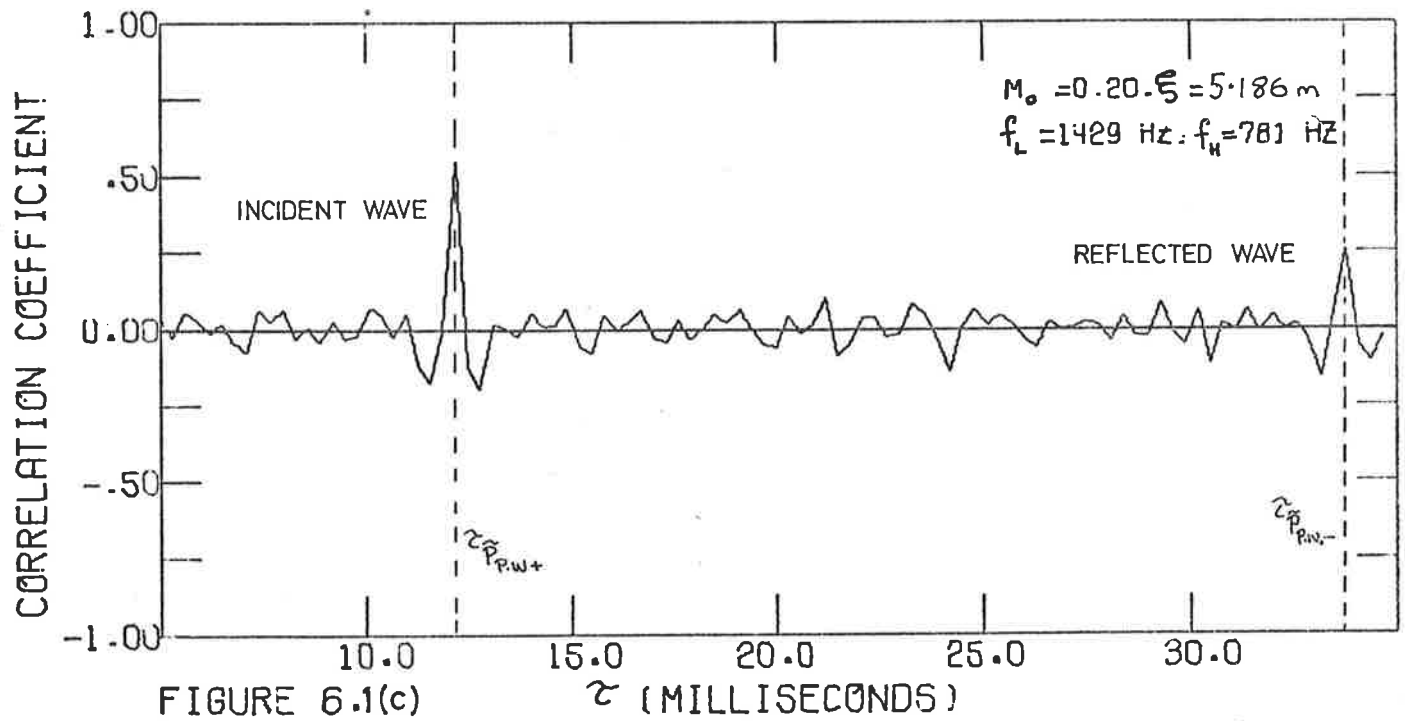
where ξ_T is the distance from the downstream transducer to the anechoic termination ($\xi_T \approx 3.5$ m for this experimental set up). The absorption coefficient of the termination, α , is the ratio of the absorbed energy to the incident energy and can be related to the incident and reflected pressure waves. We have

$$\alpha = 1 - \frac{\langle \tilde{p}_-^2 \rangle}{\langle \tilde{p}_+^2 \rangle} = 1 - r^2, \quad [6.23]$$



CORRELATION COEFFICIENTS OF INCIDENT AND REFLECTED WAVES





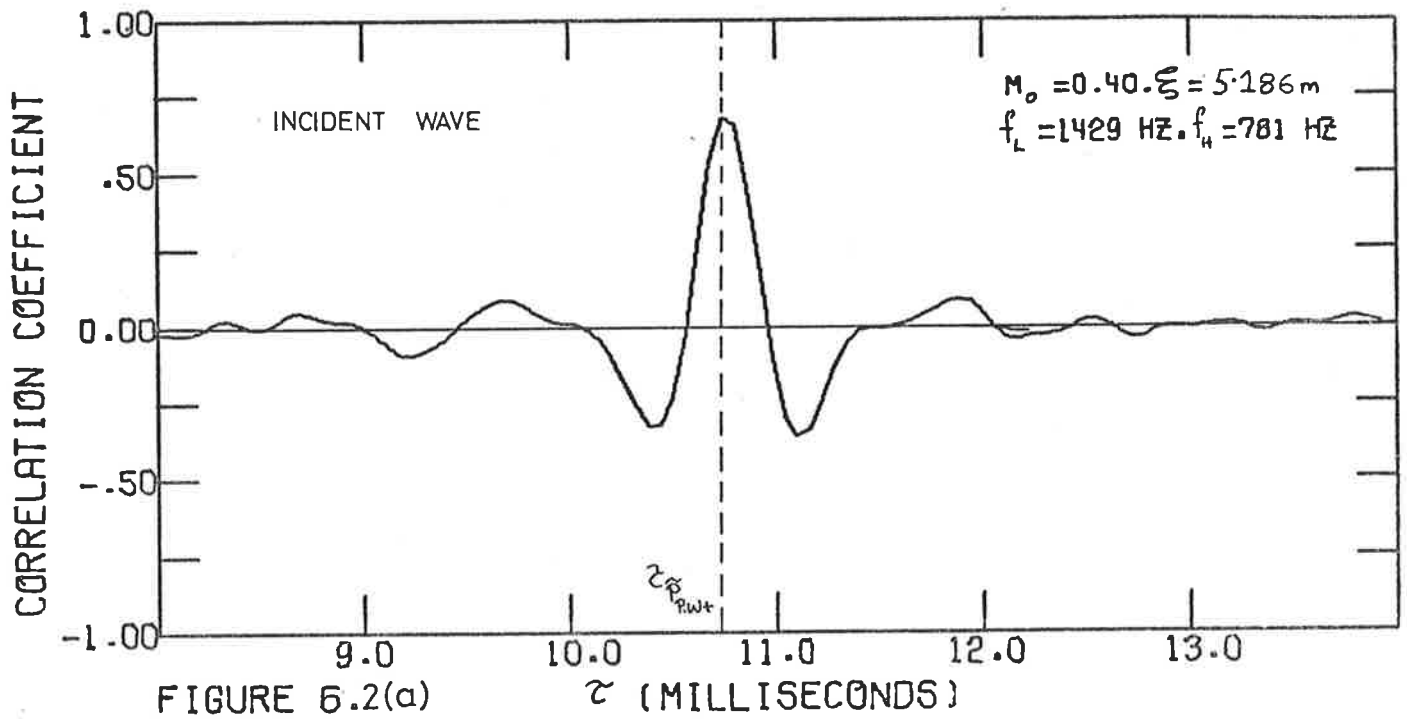
where r is the magnitude of the reflection coefficient.

Karvelis (1975) has shown that the real part of the reflection coefficient, $r \cos \phi$ (where ϕ is the complex phase angle of the termination impedance), is the ratio of the correlation peak associated with the reflected wave to that associated with the incident wave; that is

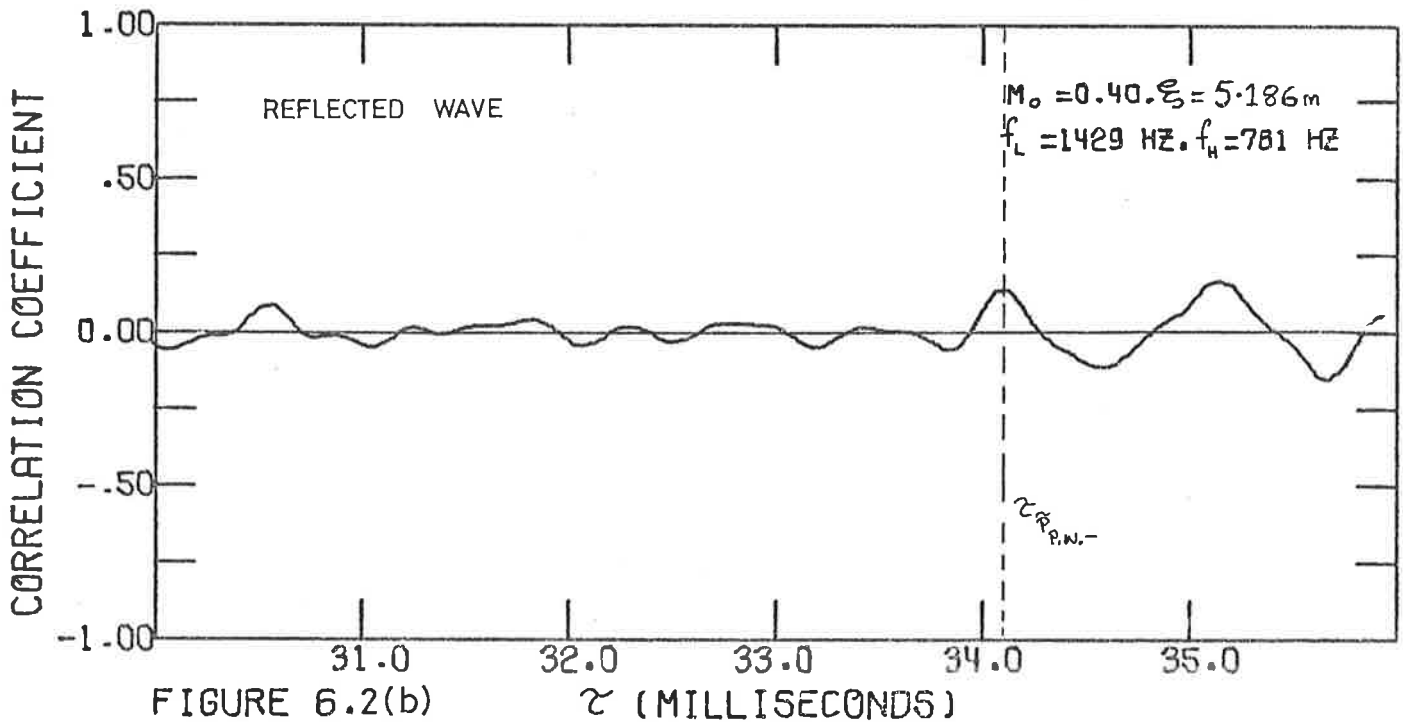
$$r \cos \phi = \rho(\tau_{P.W.-}^{\sim}) / \rho(\tau_{P.W.}^{\sim}) . \quad [6.24]$$

From Figure 6.1, $\rho(\tau_{P.W.-}^{\sim}) = 0.553$ and $\rho(\tau_{P.W.}^{\sim}) = 0.246$.

If we assume that $\cos \phi = 1.0$ (or -1.0), corresponding to a maximum real part of the correlation coefficient, then $\alpha = 0.802$. The intensity of the reflected wave is thus ≈ 7.0 dB less than that of the incident wave for $M_0 \sim 0.20$. Figure 6.2 is a correlogram for $M_0 \sim 0.40$, all other variables being the same as in figure 6.1. Here $\rho(\tau_{P.W.-}^{\sim}) = 0.686$ and $\rho(\tau_{P.W.}^{\sim}) = 0.138$, giving $\alpha = 0.956$. Here, the intensity of the reflected wave is 14.3 dB less than that of the incident wave. The absorption and reflection coefficients are approximately the same in all frequency bands of interest so that the values just given are typical of all filter bands. Thus it can be assumed in general that any correlation peak associated with a reflected wave due to the tapered entry to the nozzle throat is of a second order and the assumption that the choked nozzle represents an anechoic termination, and that there are no reflections, is justified. Table 6.1 lists the absorption coefficients (α) and the reflection coefficients (r) for four flow speeds for the 500 Hz and 1000 Hz octave bands.



CORRELATION COEFFICIENTS OF INCIDENT AND REFLECTED WAVES



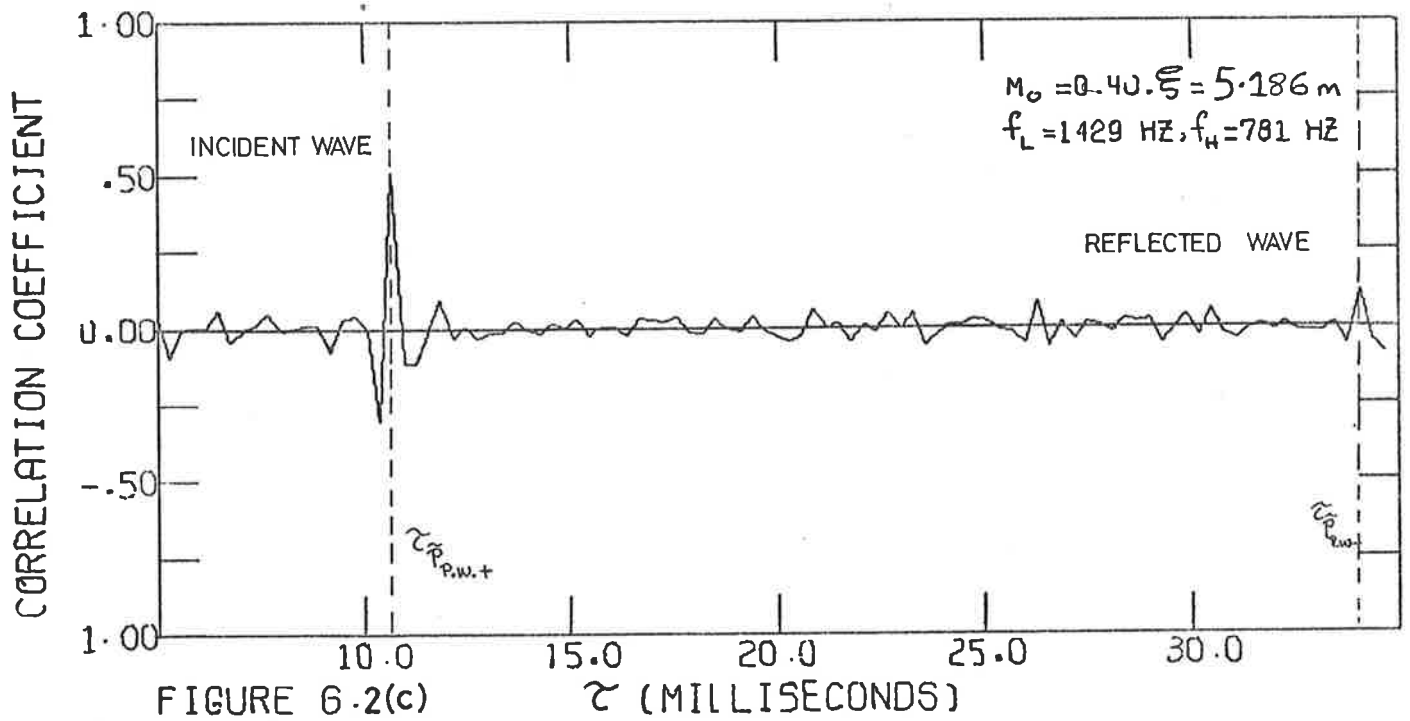


TABLE 6.1

Estimated absorption and reflection coefficients
for several flow speeds

M_0	Octave filter (Hz)	r	α	$10 \log_{10} (1-\alpha)$ dB
0.20	500	0.557	0.690	5.1
0.20	1000	0.445	0.802	7.0
0.35	500	0.424	0.820	7.5
0.35	1000	0.247	0.939	12.1
0.40	500	0.385	0.852	8.3
0.40	1000	0.201	0.956	13.6
0.50	500	0.246	0.939	12.1
0.50	1000	0.192	0.963	14.3

The wall pressure fluctuations due to a fully-developed turbulent pipe flow as discussed in Chapter 4 constitute a lower limit, which is readily available in a non-dimensional form that is independent of flow speed and pipe diameter. Hence, the turbulent wall pressure fluctuations $\langle p'^2 \rangle$ can be readily estimated in any frequency band. Plane wave contributions to the total wall pressure fluctuations can also be estimated using equation [6.21] at $\tau = \tau_{\tilde{p}_{P.W.}} = \xi/c_i(1+M_0)$. Here, equation [6.21] becomes,

$$\rho(\tau_{\tilde{p}_{P.W.}}) \langle p^2 \rangle = \langle \tilde{p}_{P.W.}^2 \rangle . \quad [6.25]$$

Because of the dispersive nature of the higher order modes, no particular time delay can account for all of the wall pressure fluctuations associated with them in a particular filter band.

For $ka_i < 1.84$, no higher order modes exist and for $ka_i \geq 1.84$, the number of higher order modes in a particular filter band will depend on the band width and its centre frequency. The wall pressure fluctuations associated with higher order modes in a particular filter band can be estimated by subtracting the turbulent and plane wave components from the total wall pressure fluctuations.

$$\begin{aligned} \tilde{p}_{H.O.}(\underline{x};t) &= p(\underline{x};t) - (p'(\underline{x};t) + \tilde{p}_{P.W.}(\underline{x};t)) && \text{for } ka_i \geq 1.84 \\ &= 0 && \text{for } ka_i < 1.84 \end{aligned}$$

or

$$[6.26(a)]$$

$$\begin{aligned} \langle \tilde{p}_{H.O.}^2 \rangle &= \langle p^2 \rangle - (\langle p'^2 \rangle + \langle \tilde{p}_{P.W.}^2 \rangle) && \text{for } ka_i \geq 1.84 \\ &= 0 && \text{for } ka_i < 1.84 \end{aligned}$$

$$[6.26(b)]$$

The wall pressure fluctuations associated with the first order mode, the (1,0) mode, can be estimated fairly readily, using the method described, in a filter band containing no other higher order modes. In subsequent bands containing other higher order modes (e.g. a filter band containing the (2,0) mode and some contribution from the (1,0) mode), the contributions to the wall pressure fluctuations from preceding higher order modes cannot be separated from the particular higher order mode of interest. Thus, only the intensity of the wall pressure fluctuations associated with all the higher order modes in these filter bands can be obtained. While this is a limitation, the information extracted is useful in predicting the pipe wall response and hence the acoustic radiation in various filter bands containing one or more higher order modes. This is discussed in detail in Chapter 7.

6.3 DIGITAL TECHNIQUES

The wall pressure fluctuation cross-correlation discussed in this chapter were performed on the Control Data Corporation CYBER 173 computer of the University of Adelaide utilizing digital cross-correlation techniques. This involved the digitalization of the analog wall pressure fluctuation signals (obtained from the piezo-electric crystal transducers using the general data acquisition system described in Chapter 3), digitally filtering the data to the required filter bandwidth and cross-correlating the two filtered digital signals. The digitalized sample records consist of discrete time series values representing sample records from a stationary, ergodic, random stochastic process. Figure 6.3 is a schematic diagram illustrating the key steps in the data acquisition and in the processing of the wall pressure fluctuation cross-correlations.

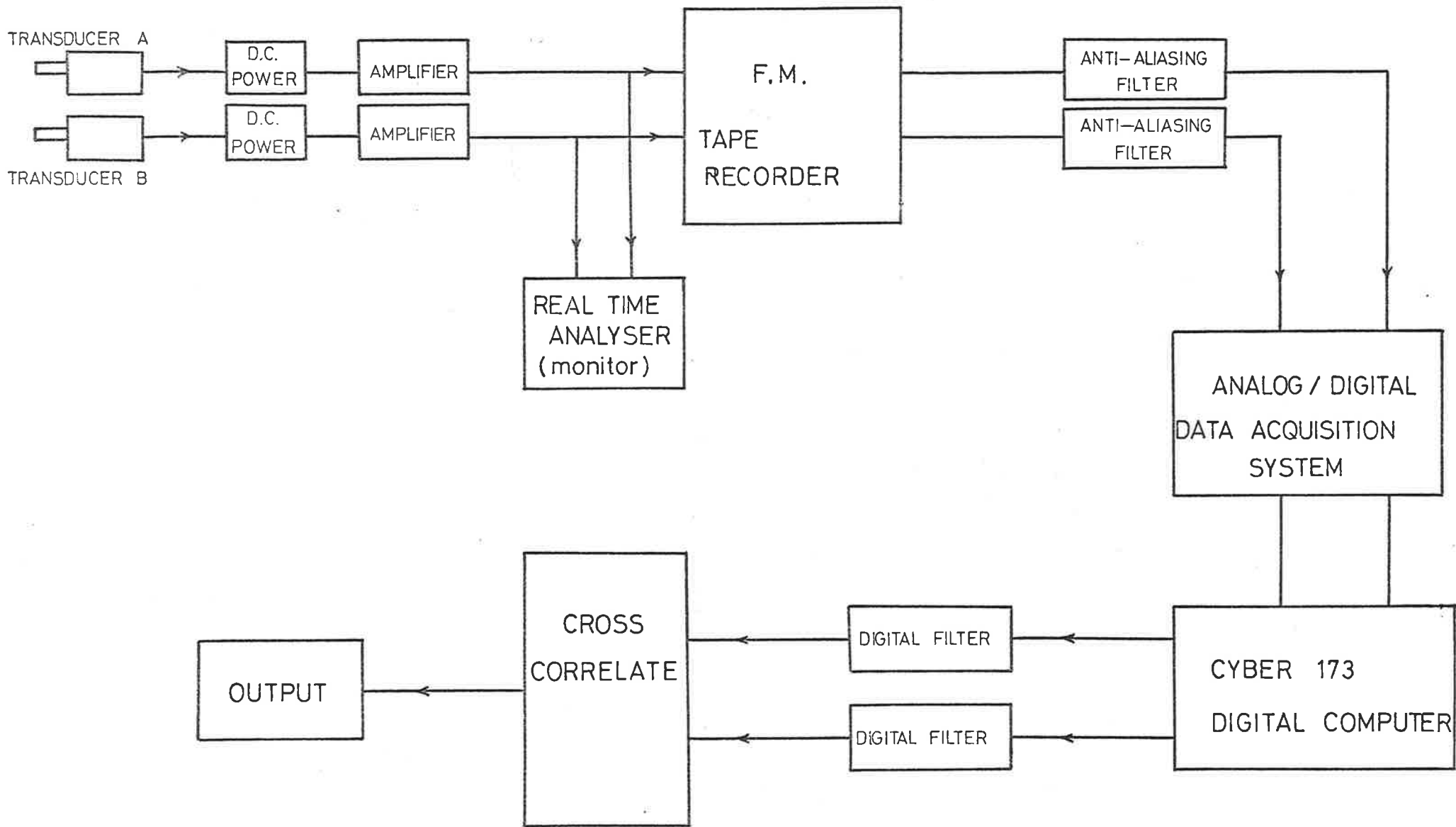


FIGURE 6.3 KEY STEPS IN THE WALL PRESSURE CROSS CORRELATIONS

6.3.1 Statistical Considerations

The analog signals from the wall pressure transducers were stored on magnetic tape using a Hewlett Packard 3955A frequency modulated recording system. The tape recorder provided a 0-20KHz frequency response bandwidth at 60 inches per second with an F.M. centre carrier frequency of 108 kHz and a signal to noise ratio of 48dB. The taped signals were then passed through an analog dual 4-pole Butterworth filter at 20kHz and digitalized (sampled) on a general purpose data acquisition system at 50kHz (20×10^{-6} sec) corresponding to a Nyquist or folding frequency (f_N) of 25kHz where

$$f_N = \frac{1}{2h} , \quad [6.27]$$

and h is the sampling or digitalizing interval. This was done to overcome the well known "aliasing" phenomenon. This is well described by Bendat and Pierson (1966) and if not taken into account will give rise to inaccurate digital reproduction of the analog signal. The analog to digital converters used within the data acquisition system were the ADC-HY12BC models with 8 bit converters and a conversion time of 4 μ sec. Negligible energy exists within the wall pressure fluctuations at frequencies corresponding to the conversion time. For 8 bit resolution, quantization errors are negligible and quantization and conversion time (aperture time) errors are essentially uncorrelated with the signals and with themselves. (Windrow, 1956 and Watts, 1962). If we consider the quantized signal x' (or y') to be the original signal x (or y) plus an additive ϵ_x (or ϵ_y) due to quantization and aperture time errors such that,

$$x' = x + \epsilon_x$$

and
$$y' = y + \epsilon_y, \quad [6.28]$$

then the normalized correlation coefficient between the two quantized variables is

$$\begin{aligned} \rho_{x'y'}(\tau) &= \rho_{xy}(\tau) + \rho_{x\epsilon_y}(\tau) + \rho_{y\epsilon_x}(\tau) + \rho_{\epsilon_x\epsilon_y}(\tau) \\ &= \rho_{xy}(\tau), \end{aligned} \quad [6.29]$$

since $\rho_{x\epsilon_y}(\tau) \approx \rho_{y\epsilon_x}(\tau) \approx \rho_{\epsilon_x\epsilon_y}(\tau) \approx 0$.

As an illustration that the system used functions correctly and gives satisfactory results, Figure 6.4 is the spectra of the pressure transducer voltage output as a function of frequency, for $M_0 \sim 0.40$. It compares the spectra obtained from direct analysis of the analog signal (F.M. Tape Recorder) by a Brüel and Kjaer Real Time $\frac{1}{3}$ -Octave Analyser with the spectra obtained by the digitized version of the same analog signal being fed through the digital to analog converter on the data acquisition system and then on to the real time analyser. There is excellent agreement between the two spectra (± 0.5 dB) up to 16kHz.

Another important factor that has to be considered is the selection of the filter bandwidth and the separation distance between the two transducers. A problem arises in the detection of the appropriate time delays if the separation distances are not adequate, thus preventing identification of the peaks. White (1969) has developed a criterion whereby an envelope is completely unambiguous if it decays to a value less than one-tenth of its peak value by the time it gets to the adjacent path delay time. For plane acoustic waves and turbulent wall pressure fluctuations, this criterion yields

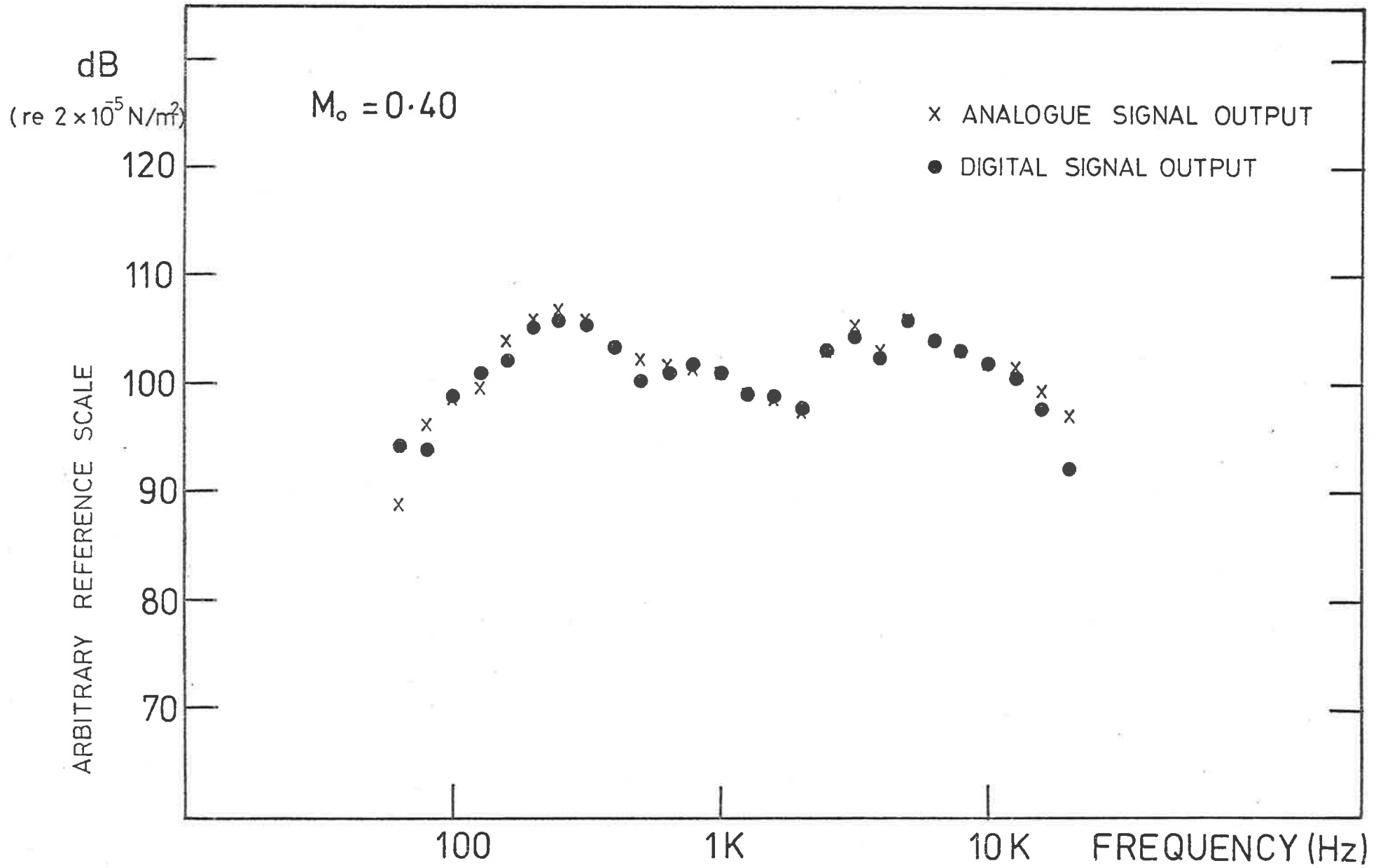


FIGURE 6.4 PRESSURE TRANSDUCER VOLTAGE OUTPUT

$$\Delta\omega \xi \left(\frac{1}{M_0(M_0+1)} \right) \geq 6c_i . \quad [6.30]$$

Because of the dispersive nature of the higher order modes (the phase velocity is frequency dependent) it is also desirable to have the transducers sufficiently separated so that in frequency ranges where the group velocity is approximately constant (sufficiently away from cut-off such that c_g approaches c_i) the time delay associated with plane wave propagation can be readily detected. It should be remembered that the group velocity of the higher order modes cannot be greater than or equal to c_i . Hence, for higher order modes and plane acoustic waves, White's (1969) criterion yields

$$\Delta\omega \xi \left(\frac{1-G}{(M_0+G)(M_0+1)} \right) \geq 6c_i , \quad [6.31]$$

where $G = c_g/c_i$.

Finally, there is a statistical uncertainty related to the correlation estimates themselves, and one is interested in the equivalent resolution bandwidth B_e and the sample length T_r required to keep within a particular level of normalised standard error ϵ_r where,

$$\epsilon_r = \sqrt{1/B_e T_r} , \quad [6.32]$$

and $B_e = 1/mh$, $T_r = Nh$, m is the maximum number of correlation lag values ($m = \tau_{\max}/h$) and h is the sampling or digitizing interval. This is well discussed in the literature and in particular by Bendat and Pierson (1966) and Kinns (1973). A normalised standard error of $\epsilon_r = 0.10$ was deemed sufficient for our purposes (see Bendat and

Piersol, Chapter 6).

6.3.2 Linear Phase Digital Filters

The wall pressure fluctuation cross-correlations in the various filter bandwidths discussed in this chapter have to be obtained by digitally filtering the data to the required filter bandwidth and cross-correlating the two filtered digital signals. Recursive digital filters with linear phase characteristics as described by Lynn (1972, 1970) and Thomas (1977) have been used. A linear phase response means that all the frequency components that constitute the input signal are time shifted by the same amount when passed through the filter. The filter is thus free from phase distortion and can be made physically realisable by accounting for this time shift (phase shift). Hence the filter can be made to have precisely zero time shift.

Linear phase digital filters can be described in the z -plane where $z = e^{j\omega T}$, ω is the circular frequency, T is the sample period, $j^2 = -1$ and, the z -transform theory used is the digital equivalent of Laplace transform theory. The filters make use of z -plane zeros equally distributed around a unit circle, which are cancelled in one position ($\omega = 0$) by a coincident pole (or poles) giving rise to a recursive linear phase digital filter of the low pass realization with a passband centred upon $\omega = 0$. The particular low pass realization filter transfer function that was used is the same as that used by Thomas (1977) and can be expressed as

$$H(z) = \left[\frac{1 - z^k}{1 - z} \right]^n \quad [6.33]$$

where k is the order of the filter and n is the number of applications of the filter. Raising the transfer function $H(z)$ to

the integer power n sharpens the cutoff and reduces the filter sidelobe levels. The time domain operation (difference equation) corresponding to equation [6.33] can be derived by inspection (Lynn, 1970) as

$$y_{i+1} = y_i + x_{i+k} - x_i, \quad [6.34]$$

where x and y are the input and output respectively. The time shift through the filter is $n(k-1)/2$ and by appropriate choice of n and k , this can be made an integer. Thus phase correction and physical realization may be made by time shifting each sample by the correct amount (Thomas, 1977).

If f_L is defined as the low pass breakpoint, and f_H as the highpass breakpoint (where the breakpoint is the point in the frequency response at which there is a 3dB drop), then a required filter bandwidth Δf for cross-correlating, where $\Delta f = f_L - f_H$ and $f_L > f_H$, can be obtained by the following process.

- (a) Applying the low pass filter to the original data array (array 1) at f_L .
- (b) Applying the low pass filter to the f_L filtered array (array 2) at f_H to produce array 3.
- (c) Subtracting array 3 from array 2 to yield the band pass filtered array, where $\Delta f = f_L - f_H$.

Figure 6.5, illustrates the above steps schematically and Table 6.2 lists the 3dB cut-off for several values of n and k . The response of the transfer function (Equation [6.33]) to a step input for $n = 4$ and $k = 4$ is shown in Figure 6.6.

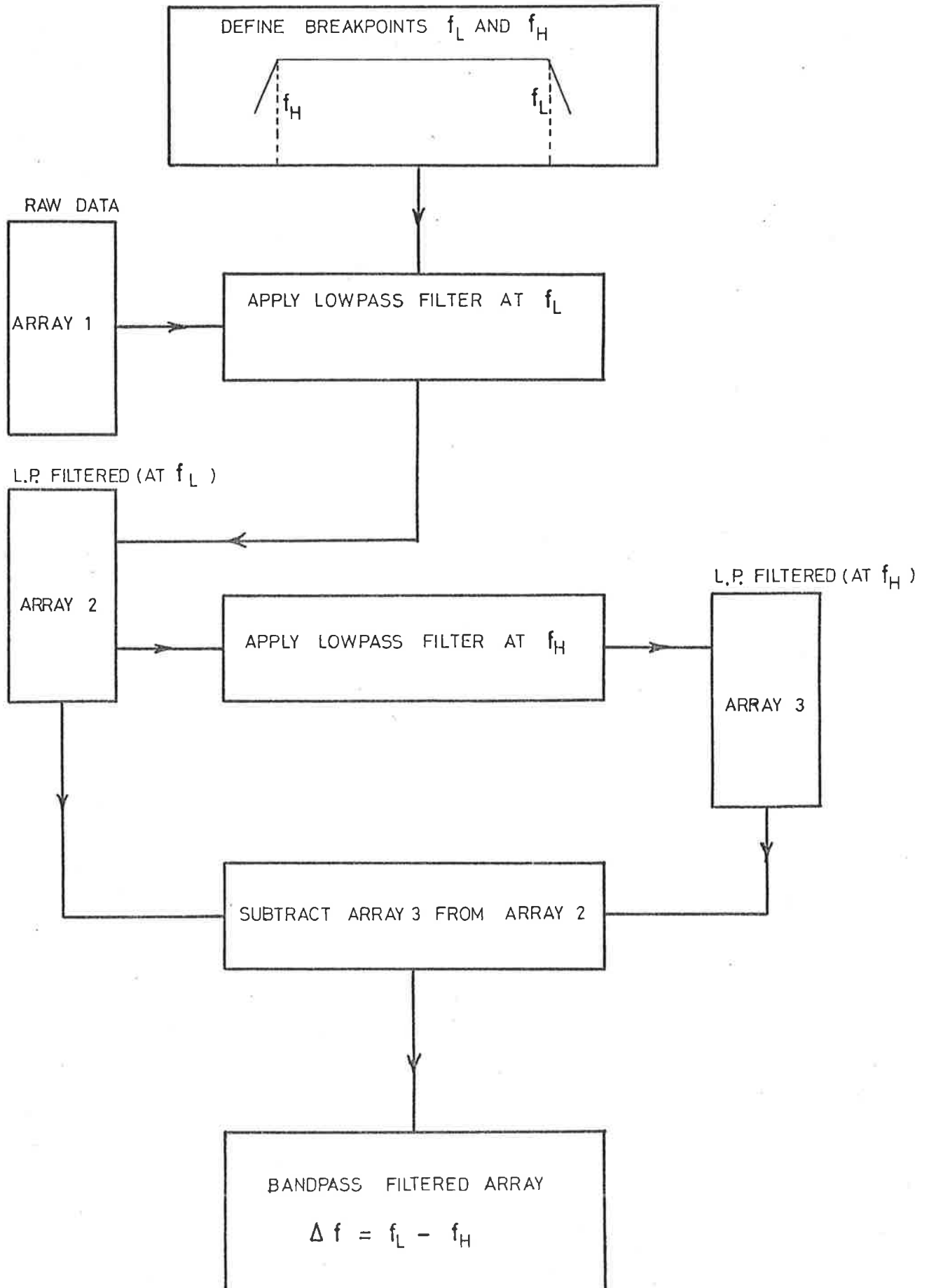


FIGURE 6.5 DIGITAL FILTER FLOWCHART

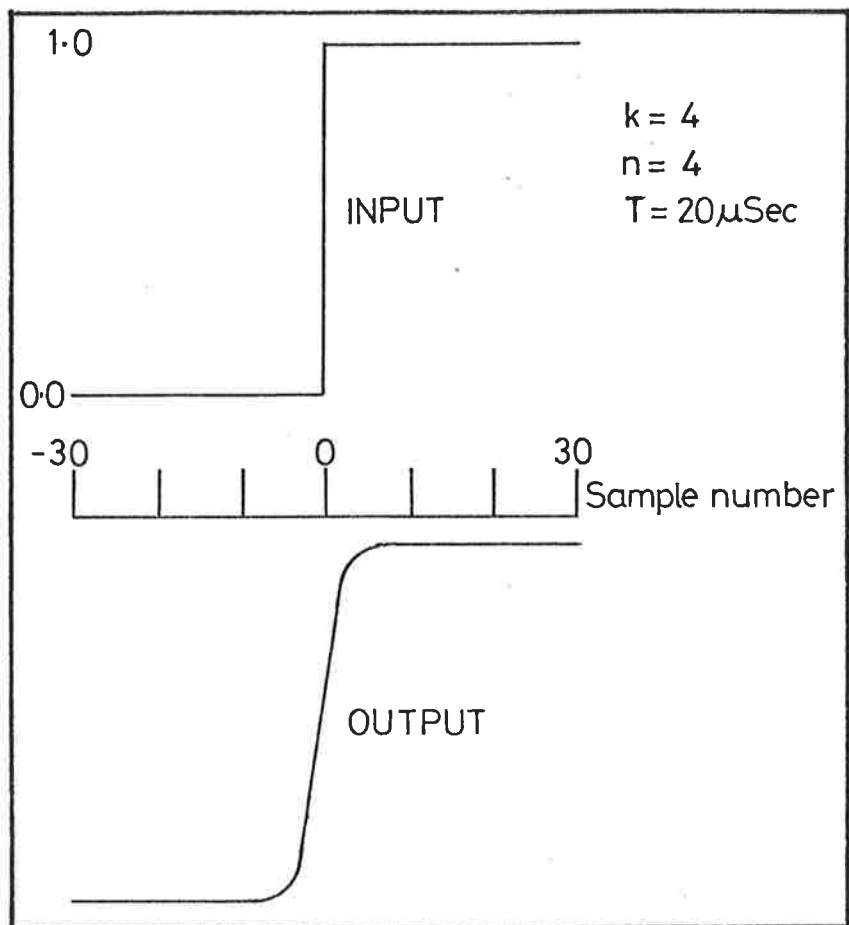


FIGURE 6.6 RESPONSE OF A DIGITAL FILTER TO A STEP INPUT

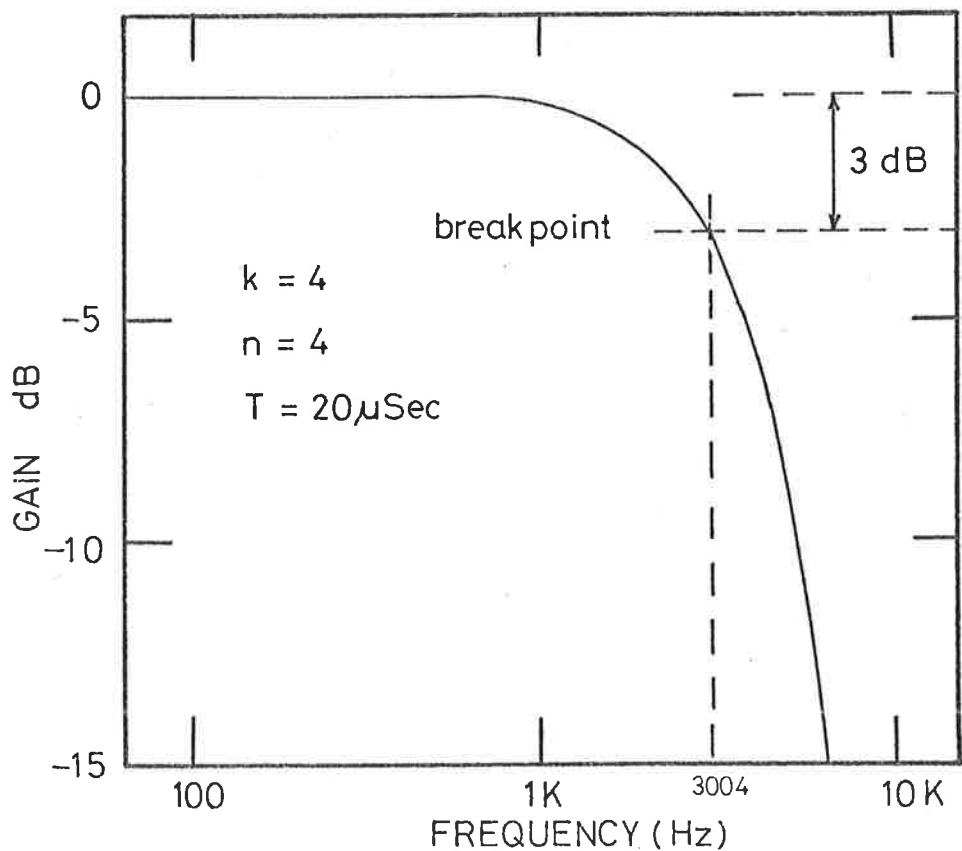


FIGURE 6.7 FREQUENCY RESPONSE OF A TYPICAL DIGITAL FILTER USED

TABLE 6.2

3dB Cut-off Frequency for several Digital
Filters Used.

Required Frequency (Hz)	n	k	3dB cut-off (Hz)
355	4	35	312
709	4	18	614
781	4	16	684
890	4	14	780
1122	4	11	960
1412	5	7	1422
2280	4	5	2194
2820	4	4	2800
3550	4	3	3004
4460	2	4	4510
5680	2	3	5817

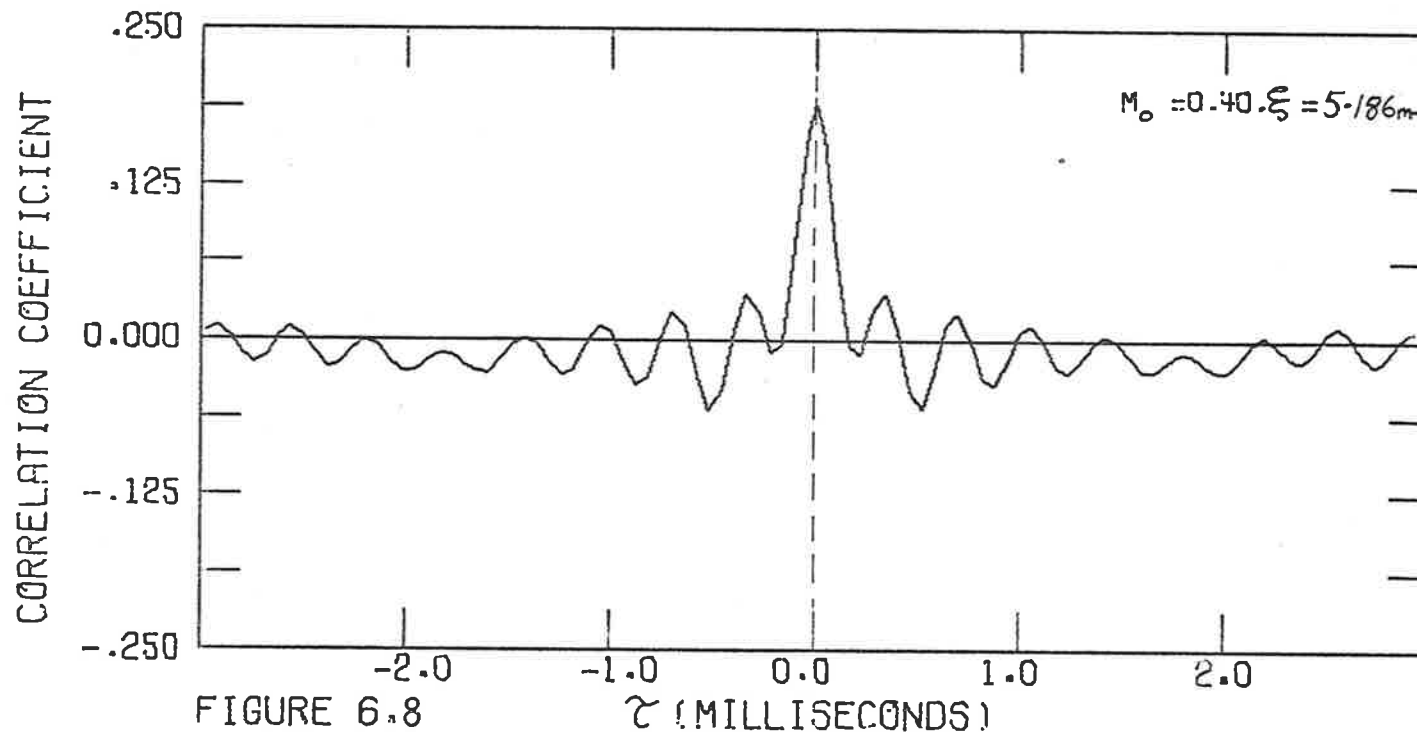
It should be noted that the output has been phase shifted by $n(k-1)/2$. A typical frequency response for this transfer function (Equation [6.33]) is shown in Figure 6.7 where $n = 4$, $k = 4$ and the 3dB point corresponds to 3004 Hz.

A bandpass filtered signal was correlated with the unfiltered signal and the correlogram, Figure 6.8, peaked at zero time delay and was symmetrical about that value. This indicated that the programming of the digital filter was correct and that there was zero phase shift. To further ensure that the programming of the correlation was correct, a square wave input signal was correlated with itself. The correlogram, Figure 6.9, consisted of a triangular wave form of constant amplitude, which is the correct autocorrelation function for a square wave (Newland, 1975).

6.4 CROSS CORRELATIONS ASSOCIATED WITH A 90° MITRED BEND

As mentioned in the introduction to this Chapter, cross correlation techniques for analysing the propagation of energy in the pipe flow system were confined to the particular case of the 90° mitred bend. The theory described in section 6.2 could be applied to any internal flow disturbance, and the 90° mitred bend was chosen because it represented a severe flow disturbance. The constraint of time was the only reason that the other flow disturbances were not considered but the results presented in this chapter form a useful base from which a detailed investigation of various internal flow disturbances could be undertaken.

The wall pressure fluctuation cross-correlations were obtained for several flow speeds ($M_q \sim 0.20 - 0.50$) and for four transducer spatial separations ($\xi = 5.186\text{m}, 3.182\text{m}, 0.187\text{m}$ and 0.036m). For the



CORRELATION OF A BANDPASS FILTERED SIGNAL WITH AN
 UNFILTERED SIGNAL

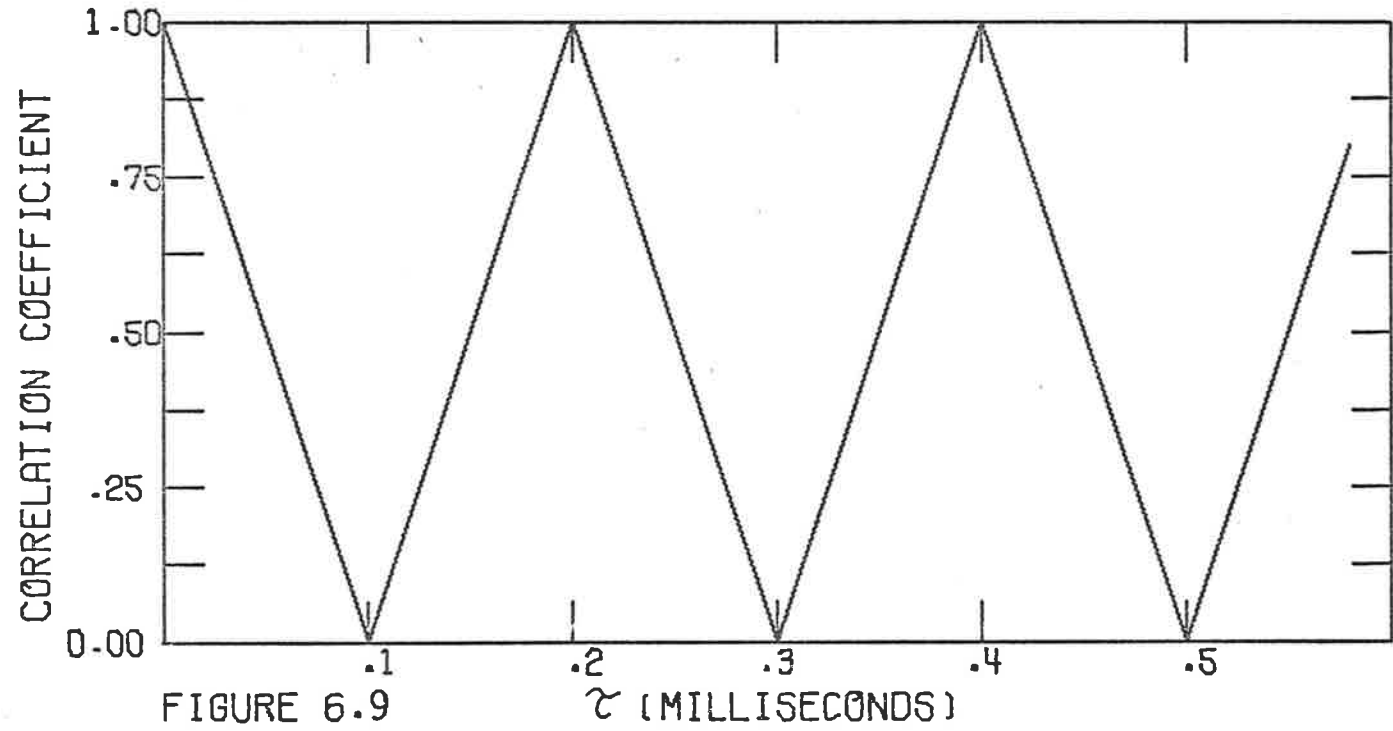
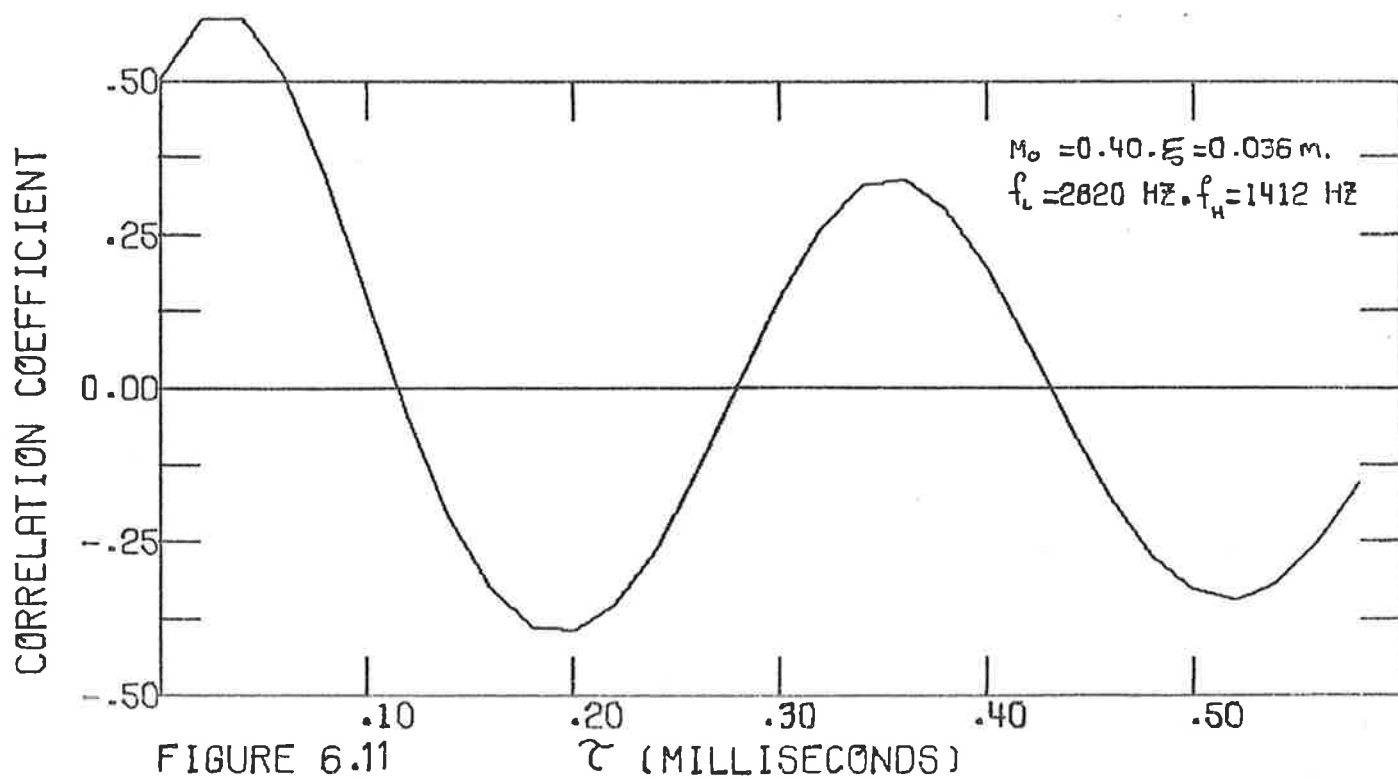
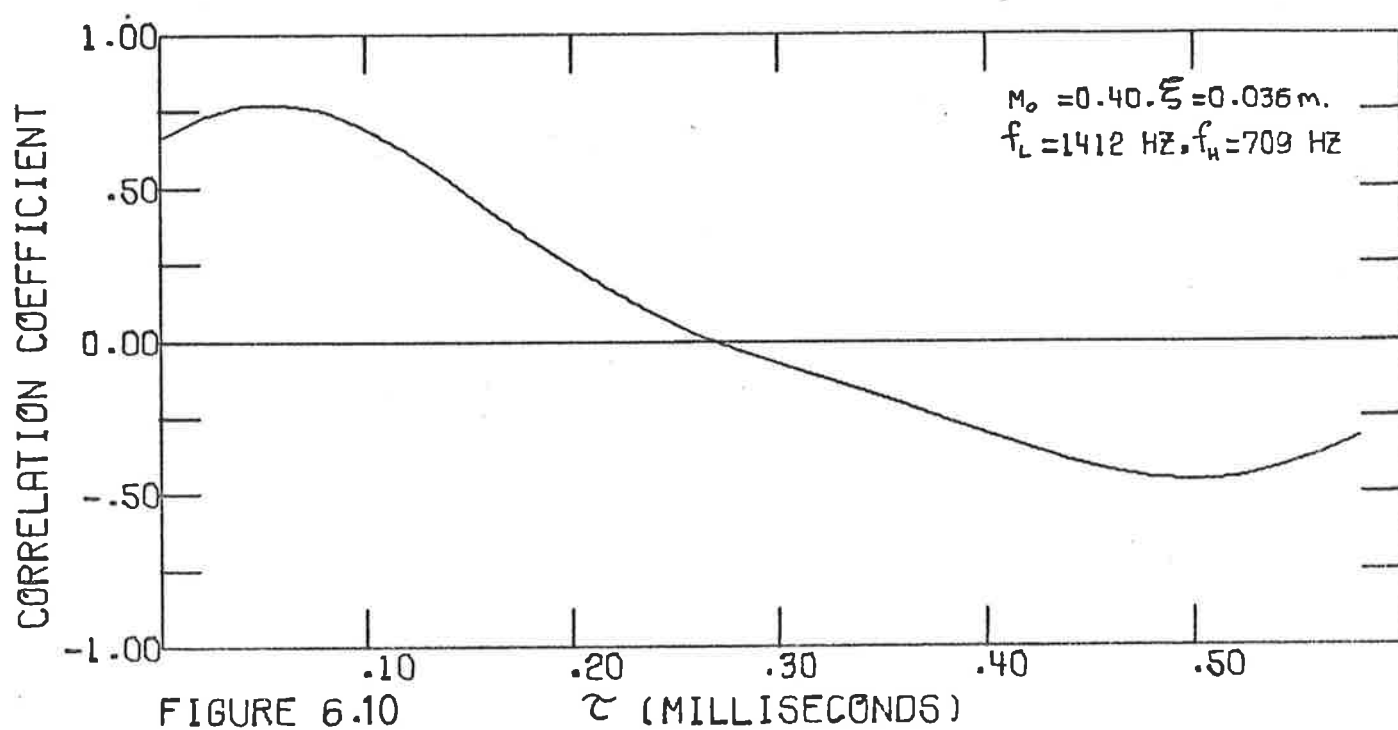
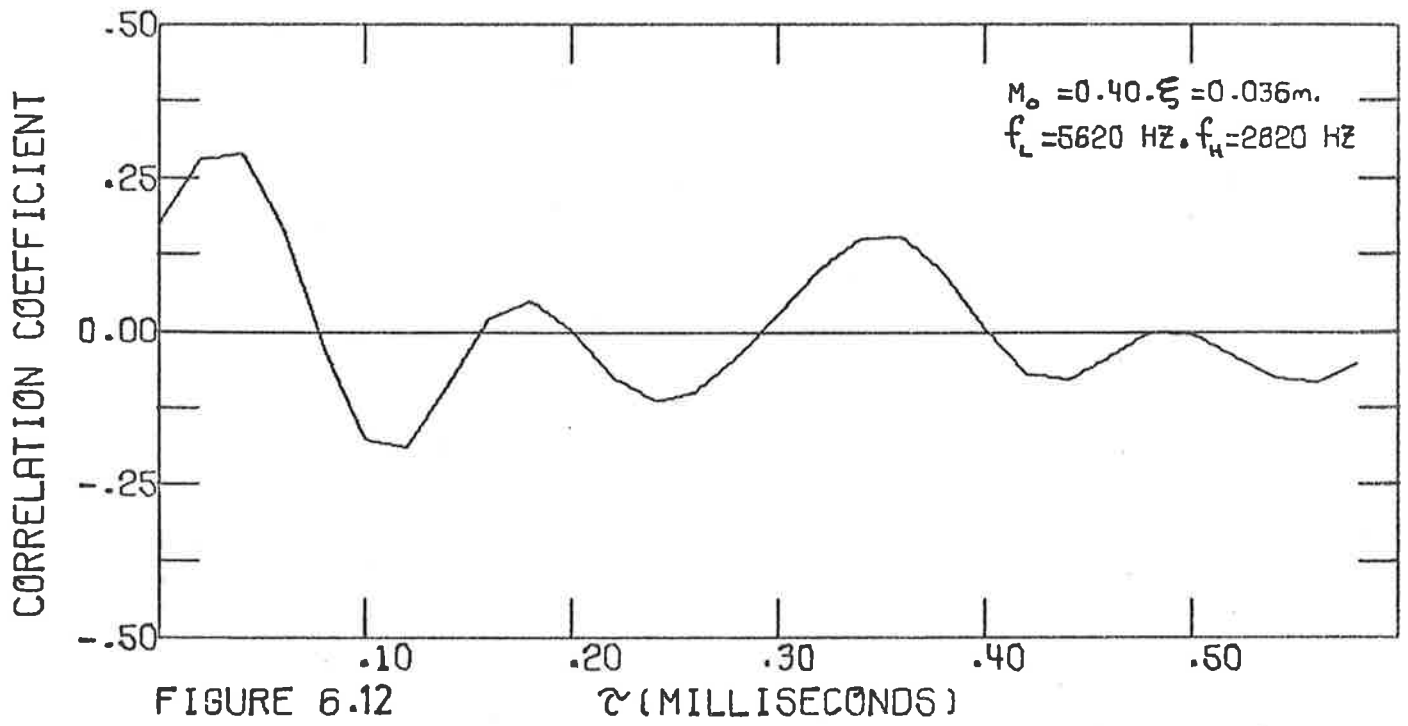


FIGURE 6.9
AUTOCORRELATION OF A SQUARE WAVE

$\xi = 0.036$ m case, equation [6.30] was not satisfied for various octave and $\frac{1}{3}$ -octave bands of interest. In these bands, the transducer separation was insufficient, thus preventing identification of true peak values. However, the turbulent pressure fluctuations are still correlated to a significant extent at this spatial separation (Bull, 1967) and one would expect to be able to detect a peak at the appropriate time delay even though the actual numerical value of the correlation coefficient would be "contaminated" due to the insufficient transducer separation mentioned above. Figures 6.10, 6.11 and 6.12 are correlograms for $M_0 \sim 0.40$, $\xi = 0.036$ m for the 1000 Hz, 2000 Hz and 4000 Hz octave filter bands respectively. The primary peak at $\tau_{P.W.} \approx 0.04$ msec can be associated with plane waves and the secondary peak at $\tau_p \approx 0.36$ msec can be associated with turbulent pressure fluctuations, bearing in mind that both peaks are contaminated. It is interesting to note that a peak associated with turbulent pressure fluctuations cannot be detected in the 1000 Hz octave filter band. At these low frequencies the acoustic pressure fluctuations are of the order of 12-16 dB above the turbulent pressure fluctuations (Chapter 4) and no higher order modes exist. There is strong plane wave correlation, and the turbulence is undetectable as it is submerged in the oscillations of the low frequency plane wave envelope. In the other two octave bands, the wall pressure fluctuations contain contributions from all three components and the plane waves are not dominant. Hence a peak associated with turbulent pressure fluctuations is detectable.

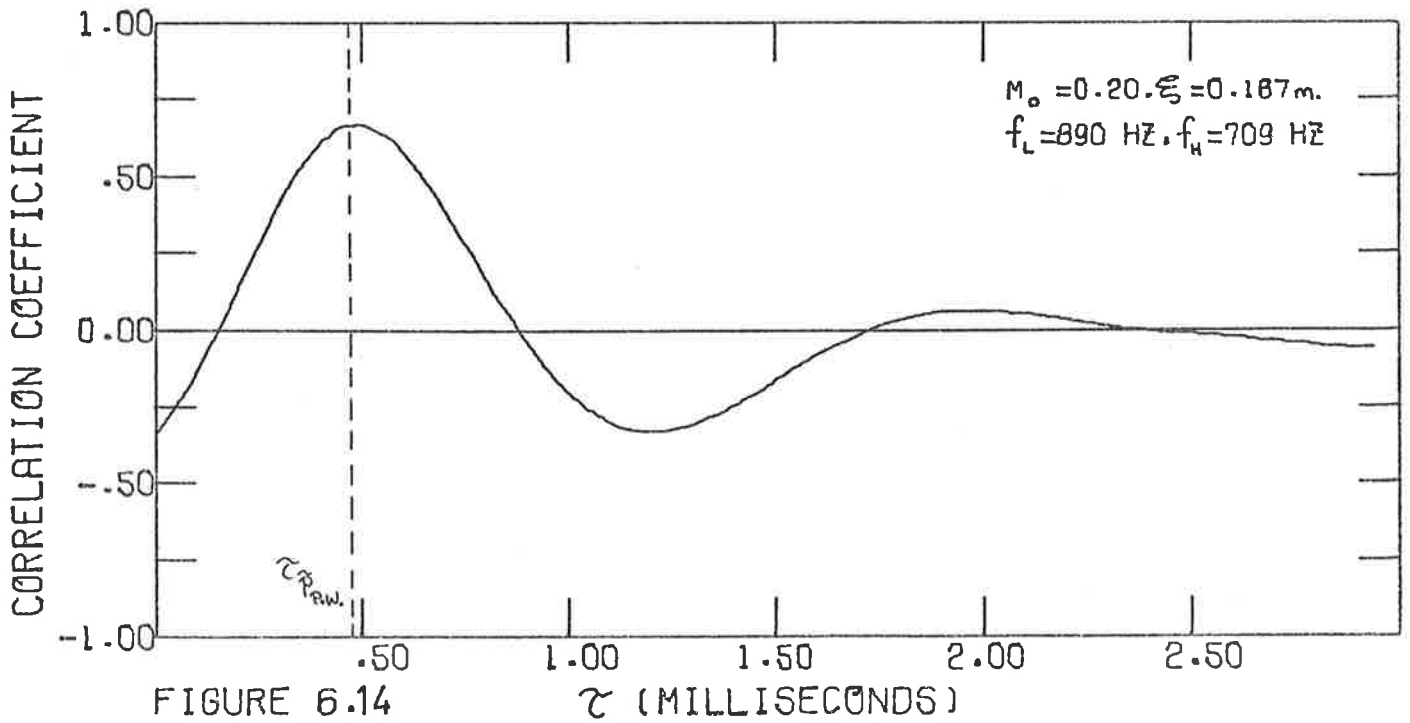
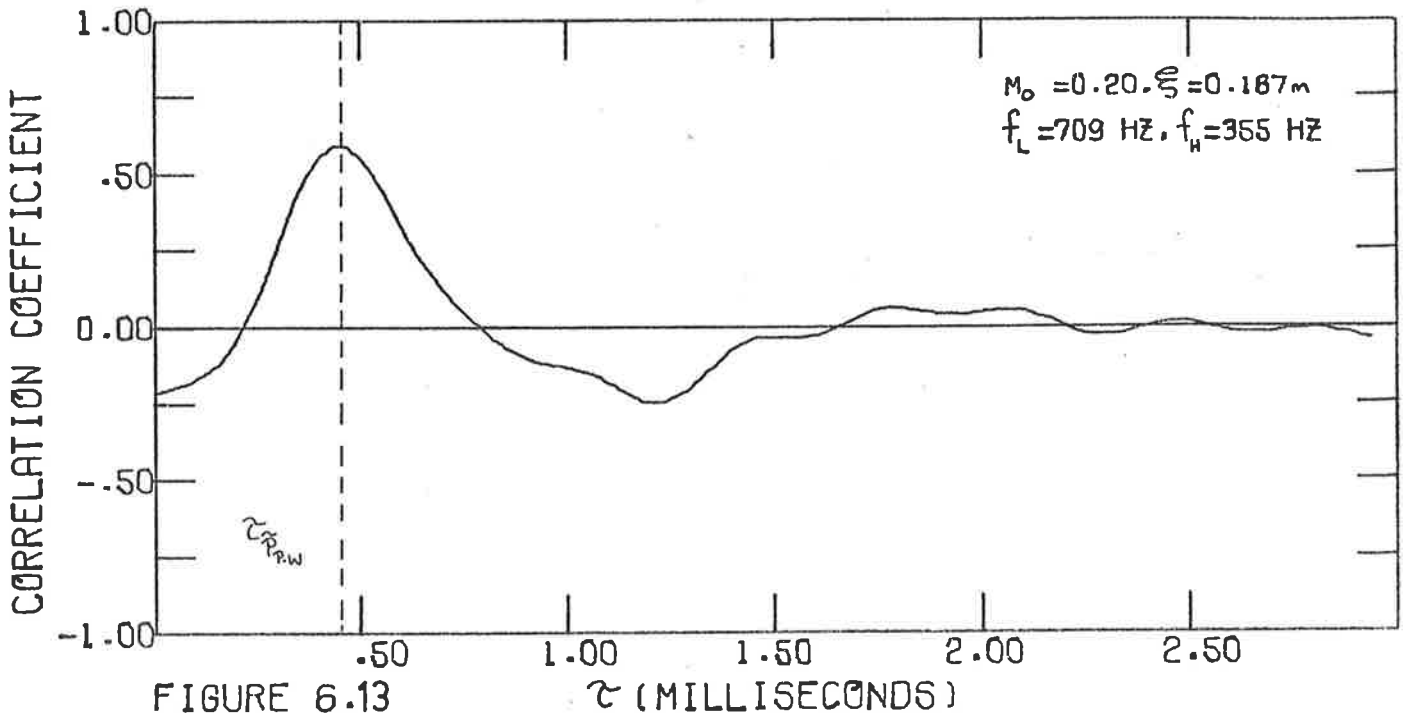
For a transducer spatial separations, ξ , of 0.187 m, equation [6.30] is just satisfied in some octave bands and generally not satisfied in most $\frac{1}{3}$ -octave bands. Furthermore, equation [6.31] is

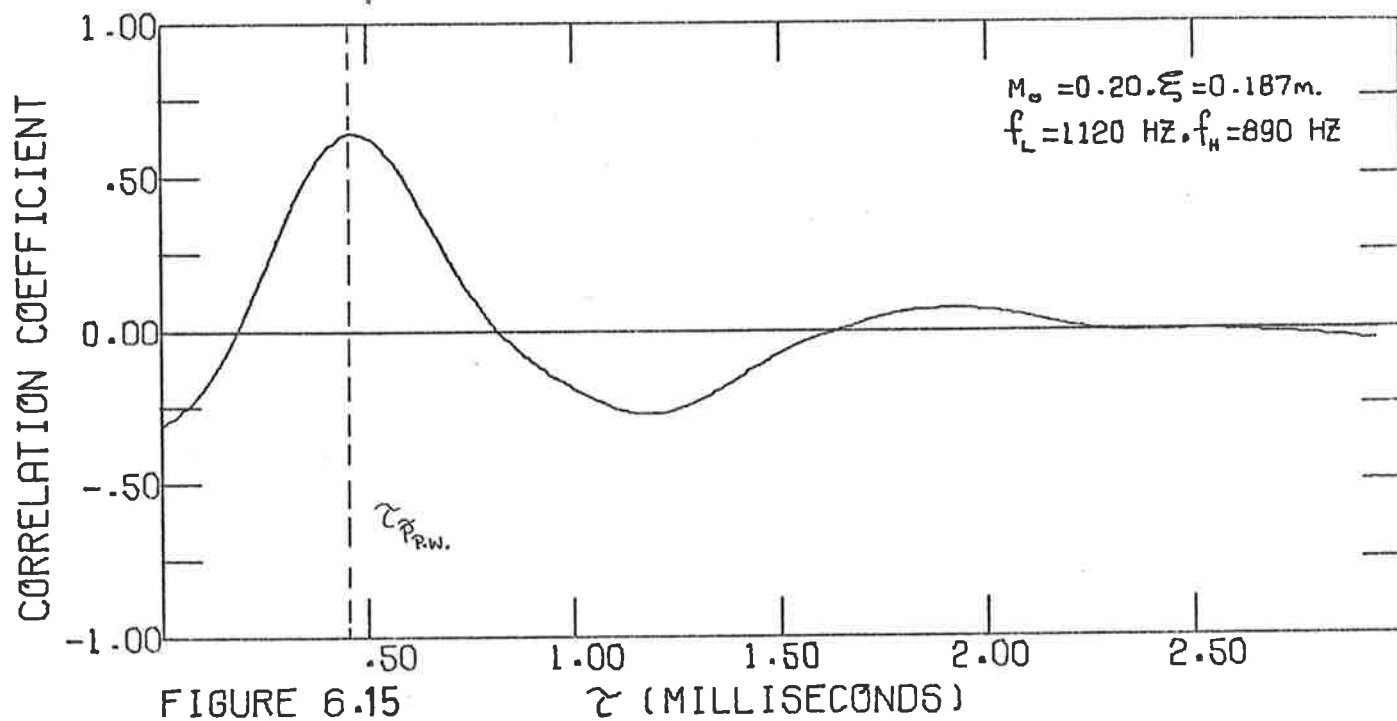




not satisfied and hence the time delay associated with plane wave propagation cannot be readily detected in filter bands containing higher order modes. However, at this separation there is a very small turbulence correlation and a distinct peak at a time delay associated with plane wave propagation can be observed in filter bands where $ka_i < 1.84$. Figures 6.13, 6.14 and 6.15 are correlograms for $M_0 \sim 0.20$, $\xi = 0.187$ m for the 500 Hz octave, the 800 Hz $\frac{1}{3}$ -octave and the 1000 Hz $\frac{1}{3}$ -octave filter bands respectively. The peak at $\tau = 0.46$ msec corresponds to plane wave propagation ($\tau_{P.W.} = \xi/c_i + U_0$) and it is very well defined. There is also quite high correlation, confirming the presence and dominance of plane waves at these low frequencies. Figures 6.16, 6.17 and 6.18 are correlograms for $M_0 \sim 0.40$, $\xi = 0.187$ m for similar filter bands as in the previous three figures and the peaks at $\tau = 0.39$ msec correspond to plane wave propagation. Figures 6.19, 6.20 and 6.21 are correlograms for $M_0 \sim 0.20$, $\xi = 0.187$ m for the 2500 Hz $\frac{1}{3}$ -octave, 2000 Hz octave and the 4000 Hz octave filterbands respectively. Propagating higher order modes are present in these filter bands; hence the dispersion of the correlation curves. The time delay associated with plane wave propagation ($\tau_{P.W.} = 0.46$ msec) cannot be readily detected because of the insufficient transducer separation. Figures 6.22, 6.23 and 6.24 are correlograms for $M_0 \sim 0.40$, $\xi = 0.187$ m for the same filter bands as in the previous three figures ($\tau_{P.W.} = 0.39$ msec).

The important point to be made regarding the series of correlograms presented for $\xi = 0.187$ m, is that while the separation distance is sufficient to isolate the plane waves from the turbulent pressure fluctuations, it is insufficient to isolate the plane waves from the dispersive higher order modes. In particular for the $M_0 \sim 0.40$





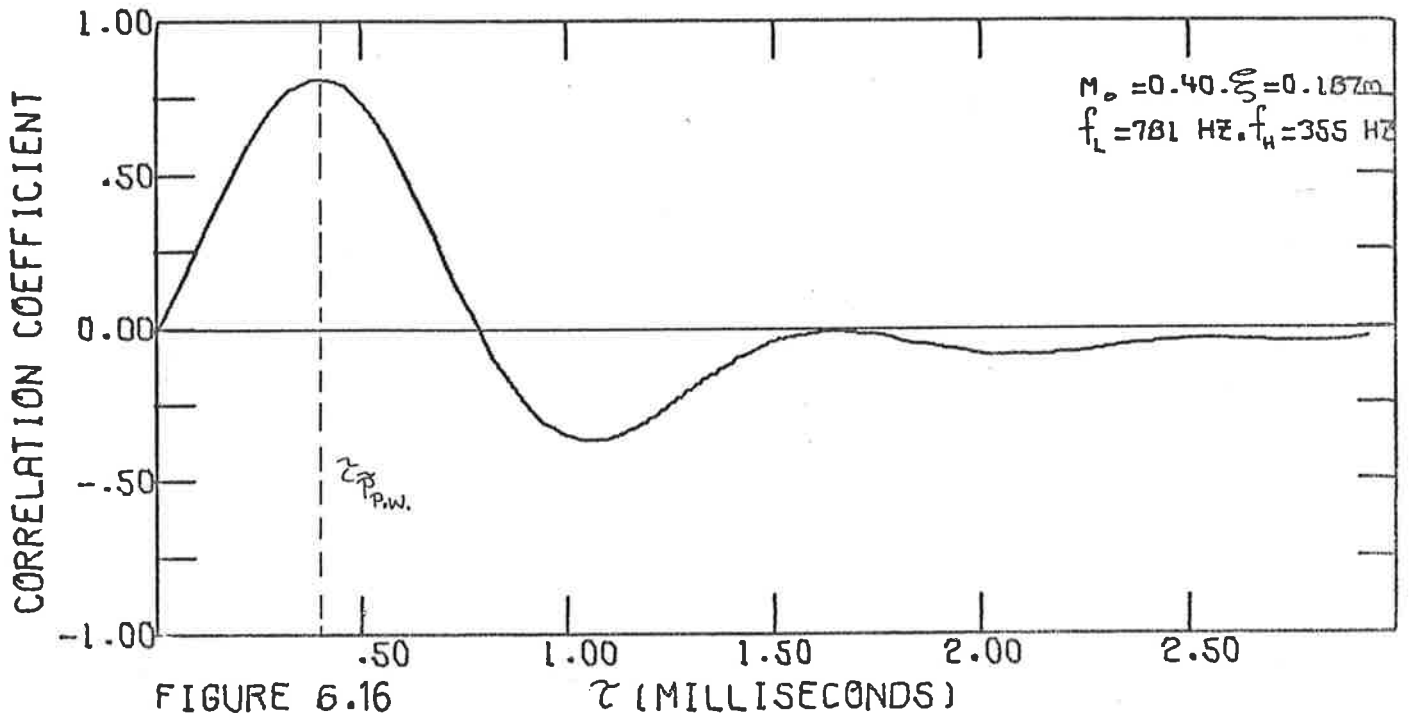


FIGURE 6.16

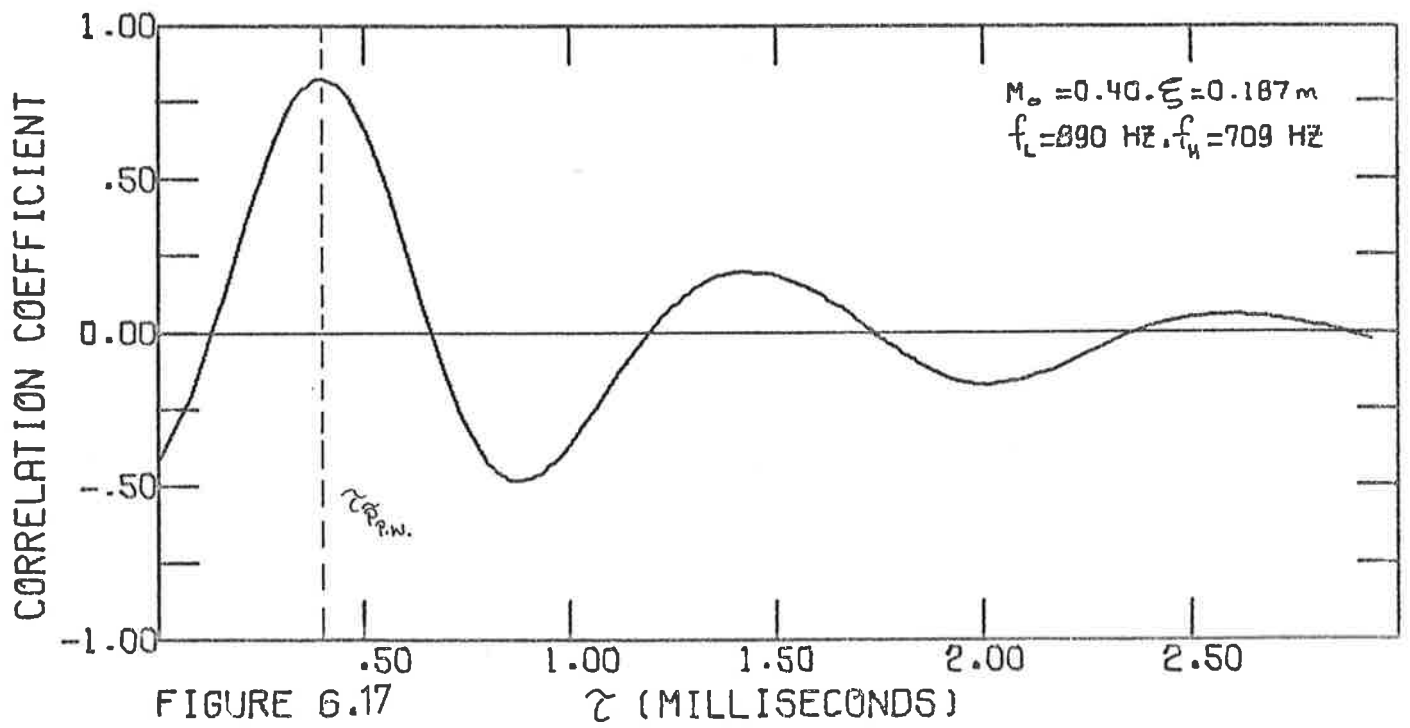
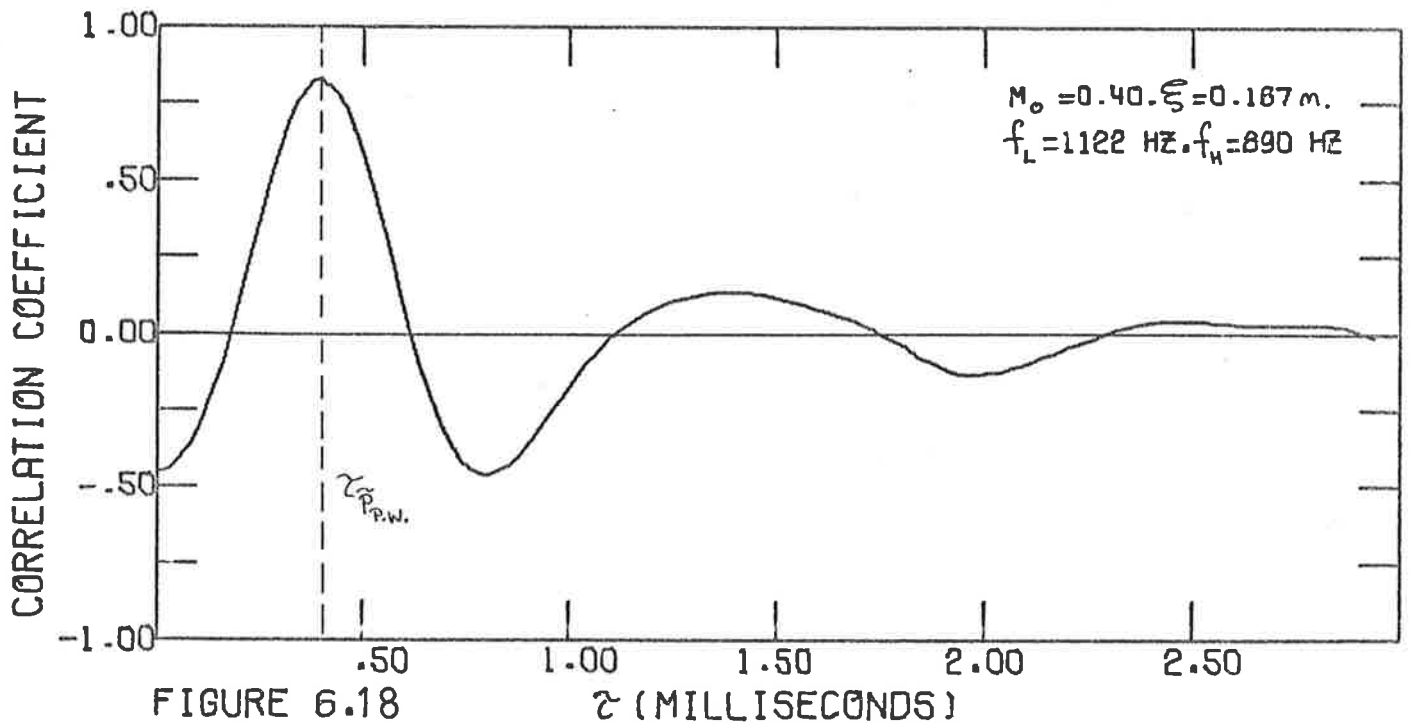
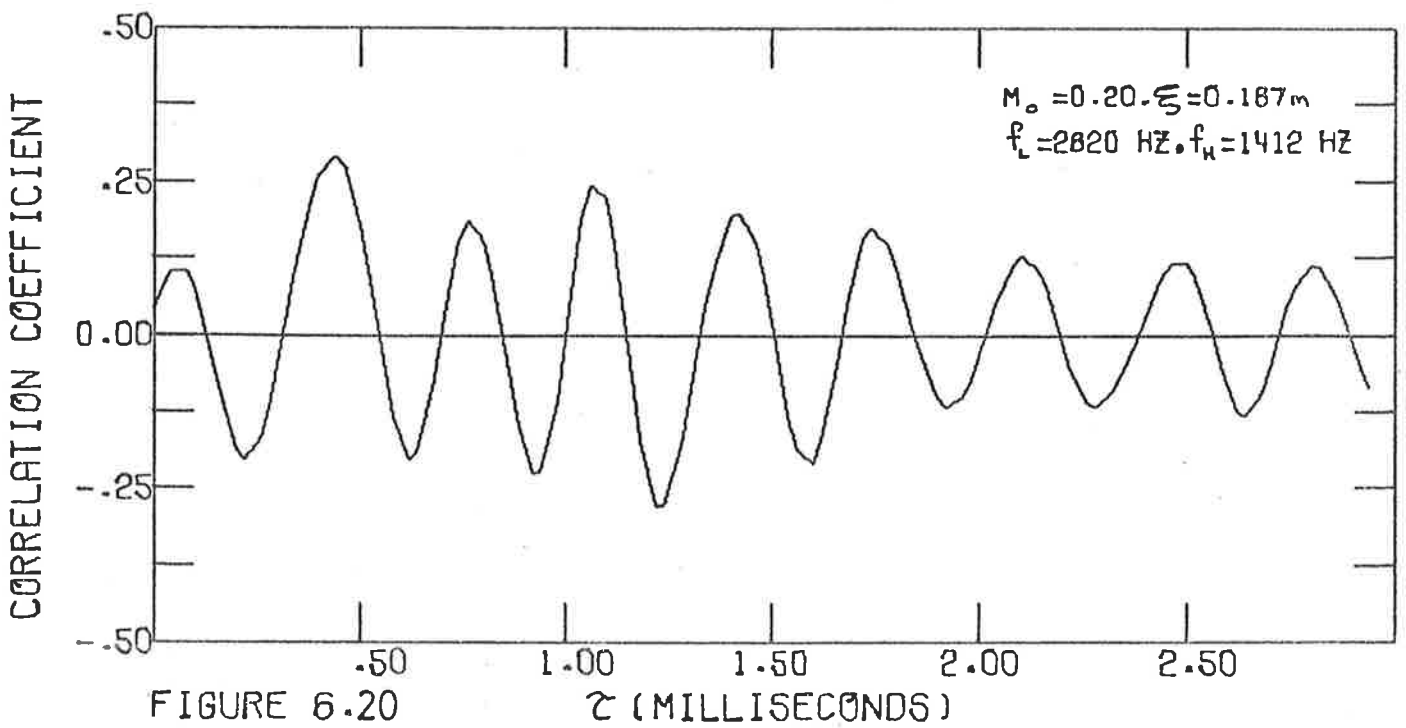
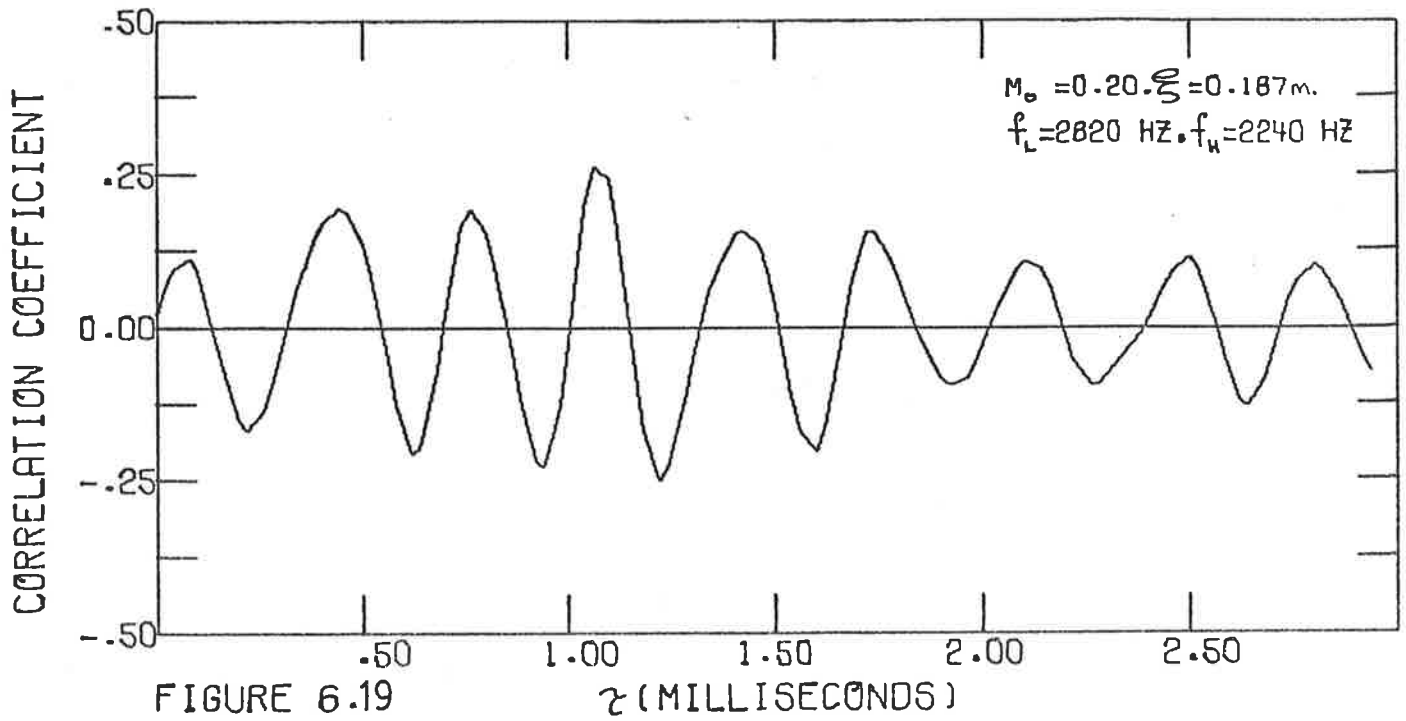
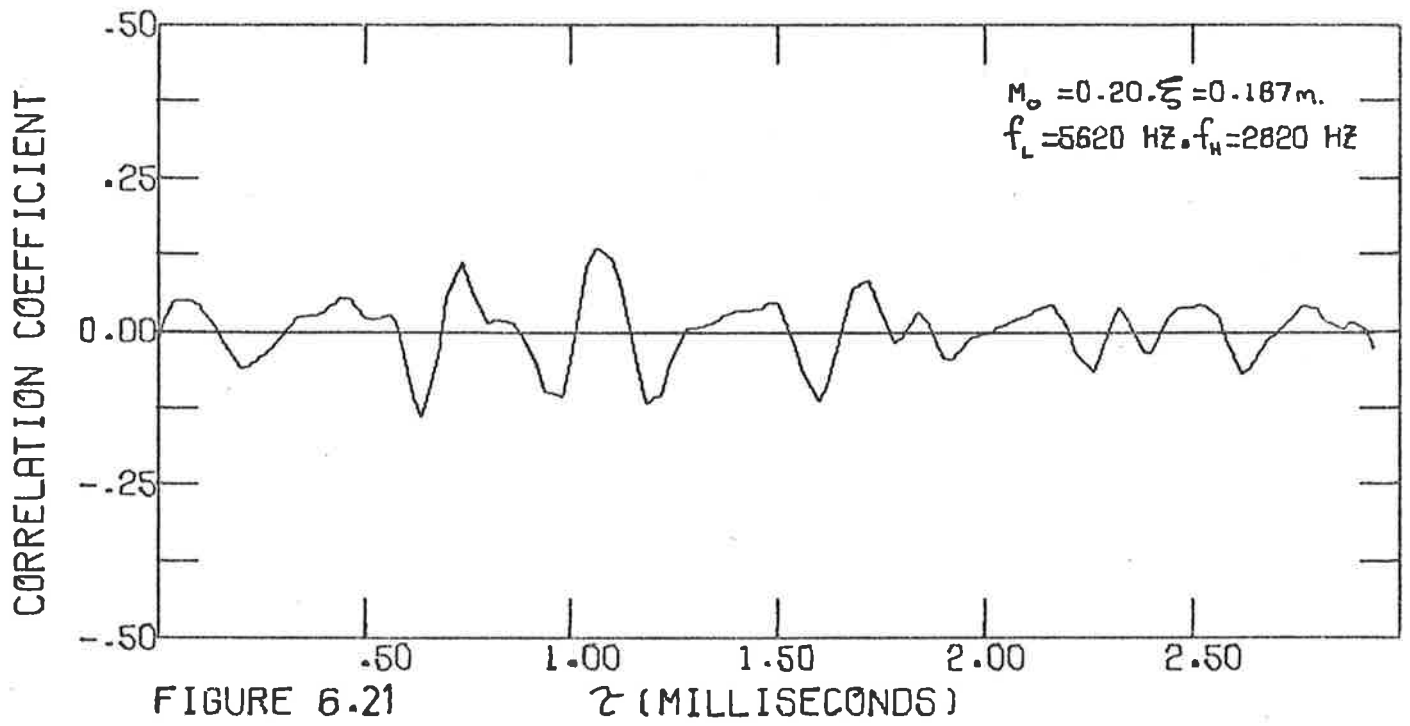


FIGURE 6.17







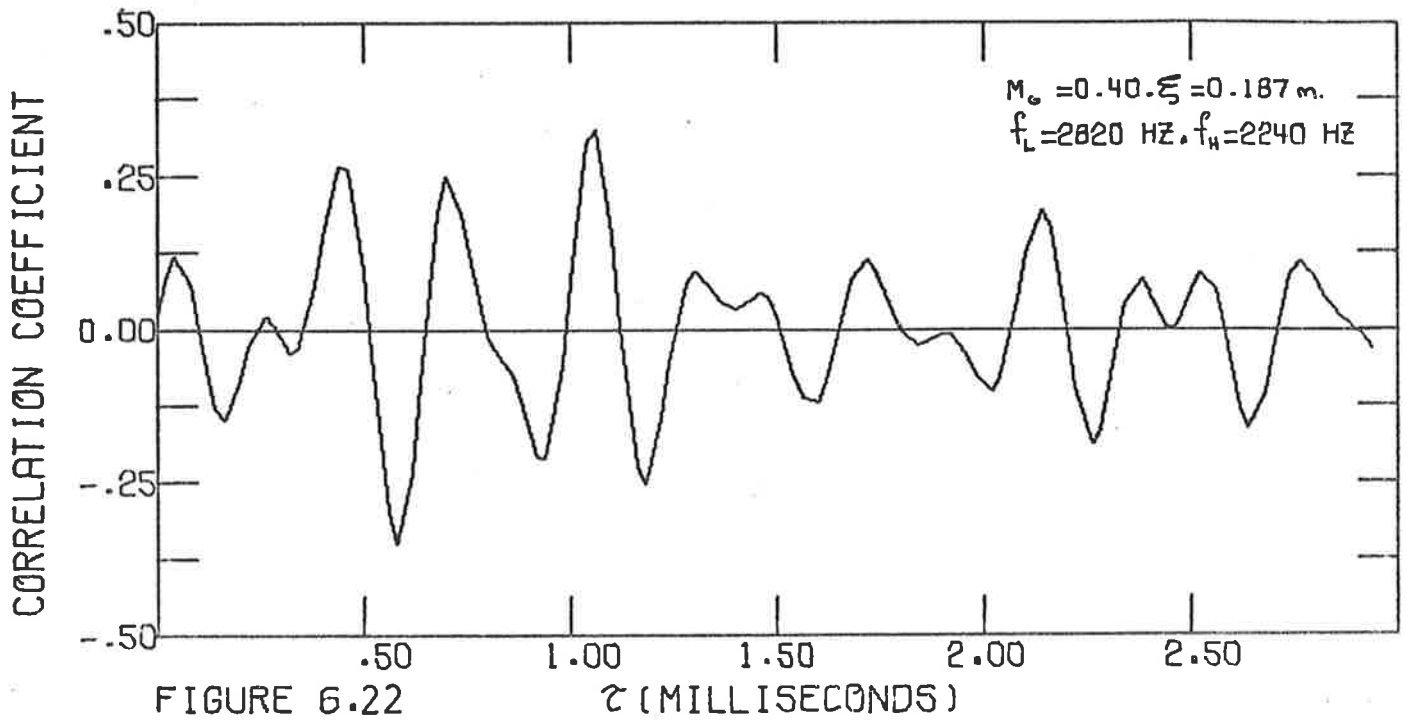


FIGURE 6.22

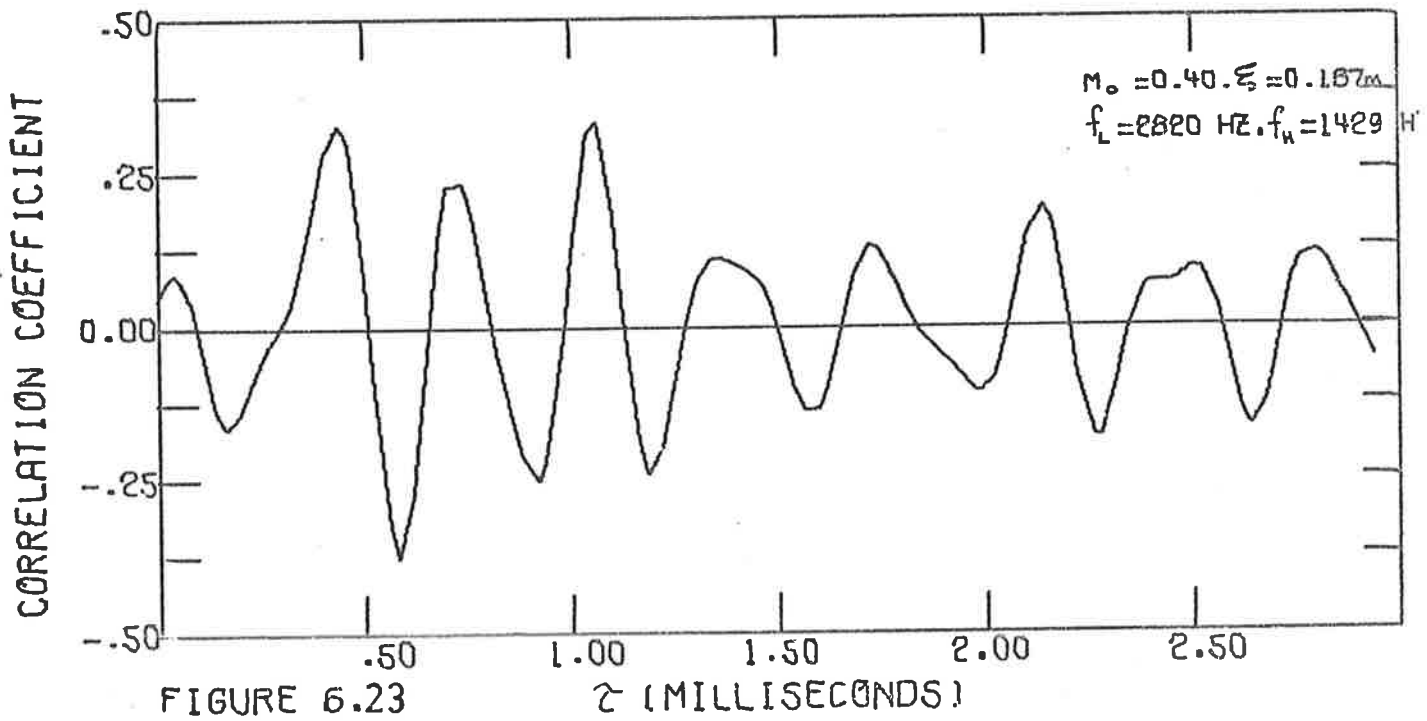
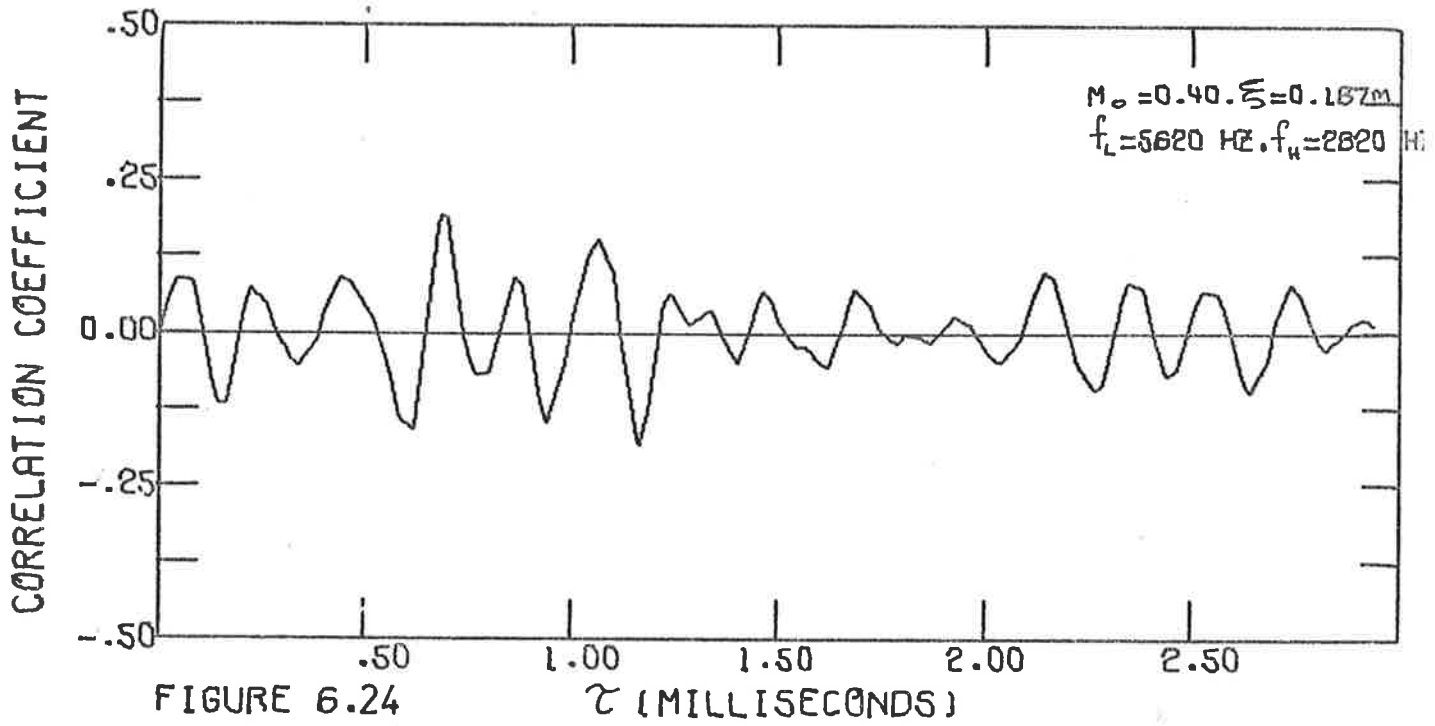
 τ (MILLISECONDS)

FIGURE 6.23

 τ (MILLISECONDS)

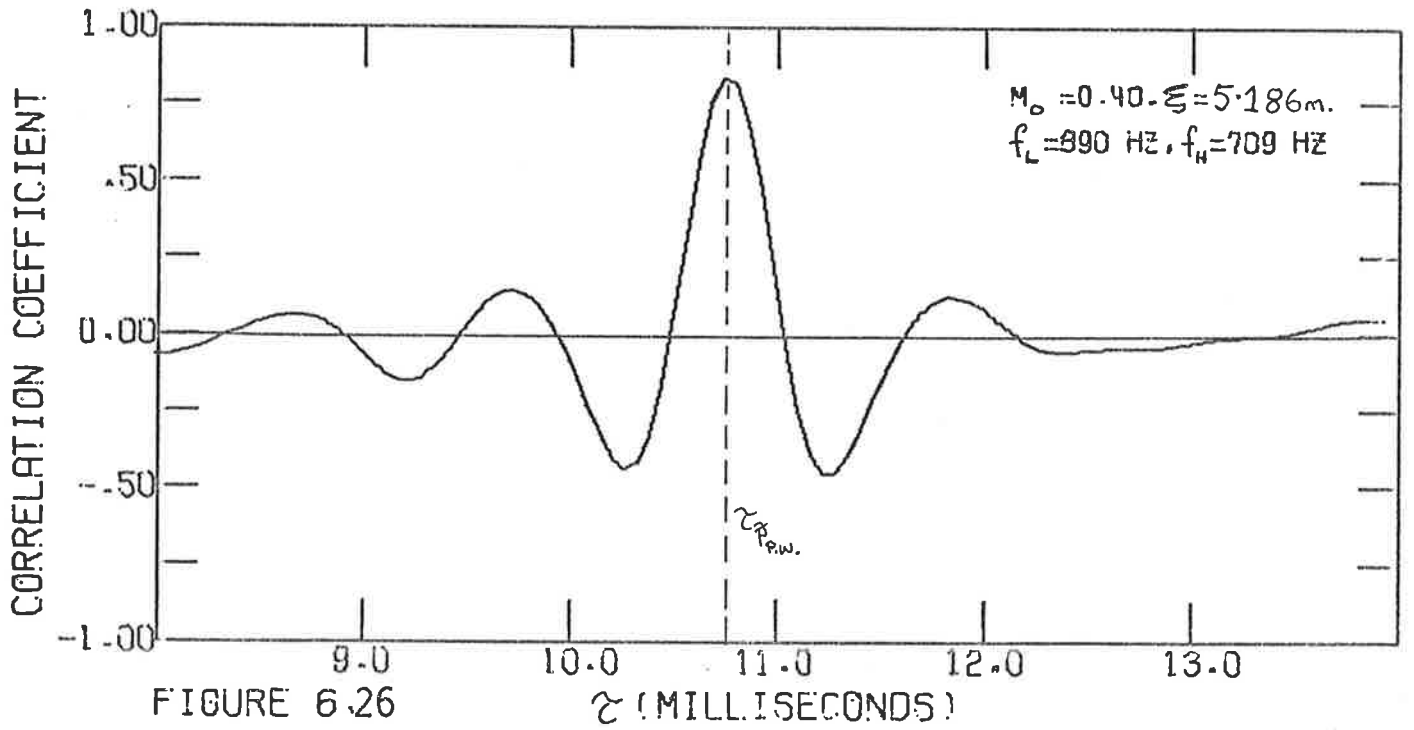
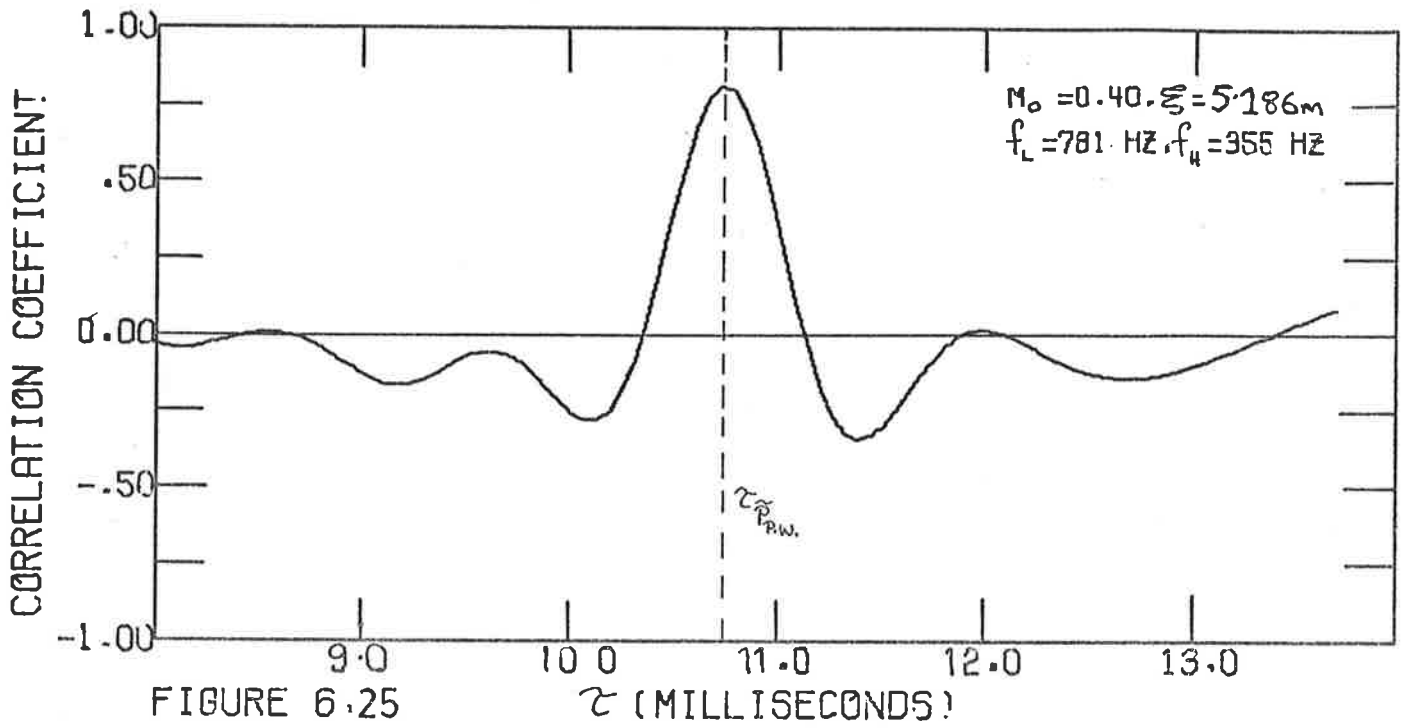


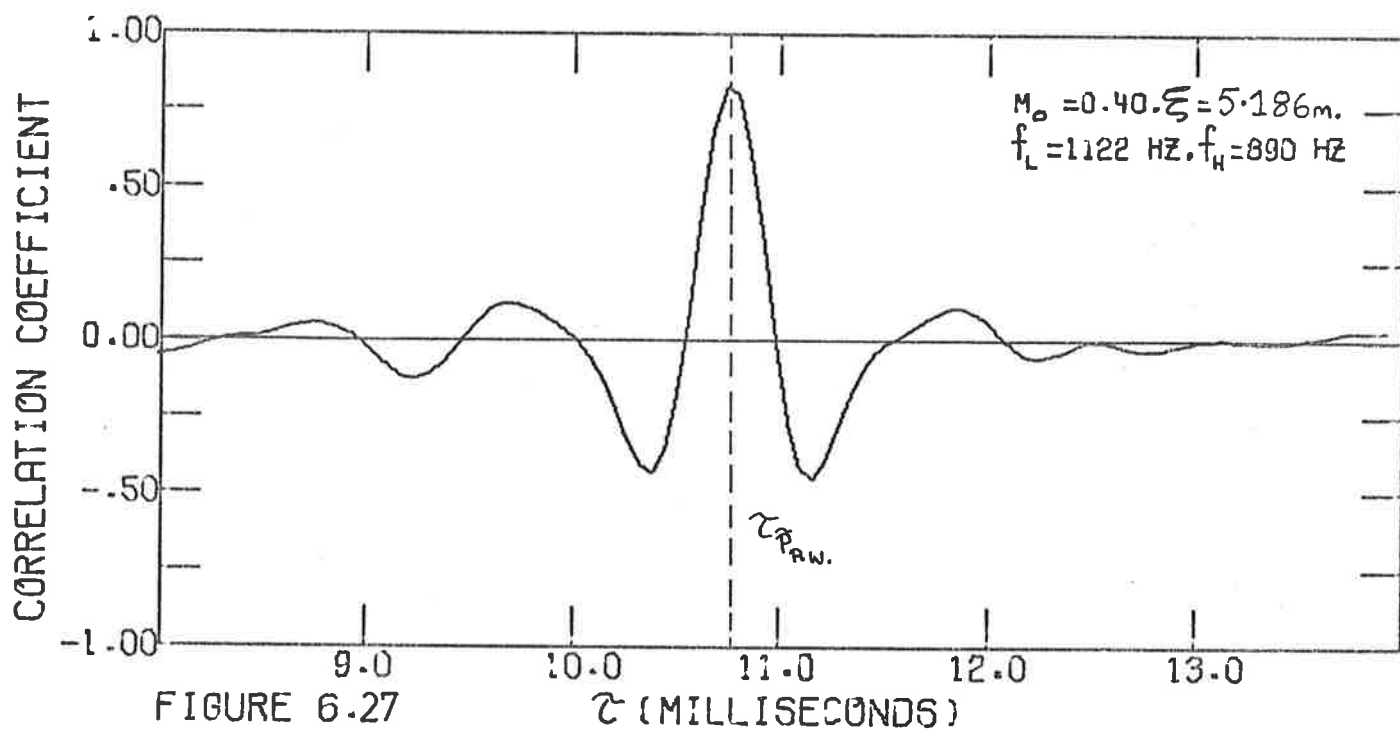
case (Figures 6.22 to 6.24) there is no peak at $\tau = 0.39$ msec corresponding to plane wave propagation implying that oscillations in the correlation curves due to the dispersive higher order modes prevent identification of the plane wave peak. Hence, to extract the plane wave component of the wall pressure fluctuations in filter bands containing higher order modes it is imperative that equation [6.31] is satisfied.

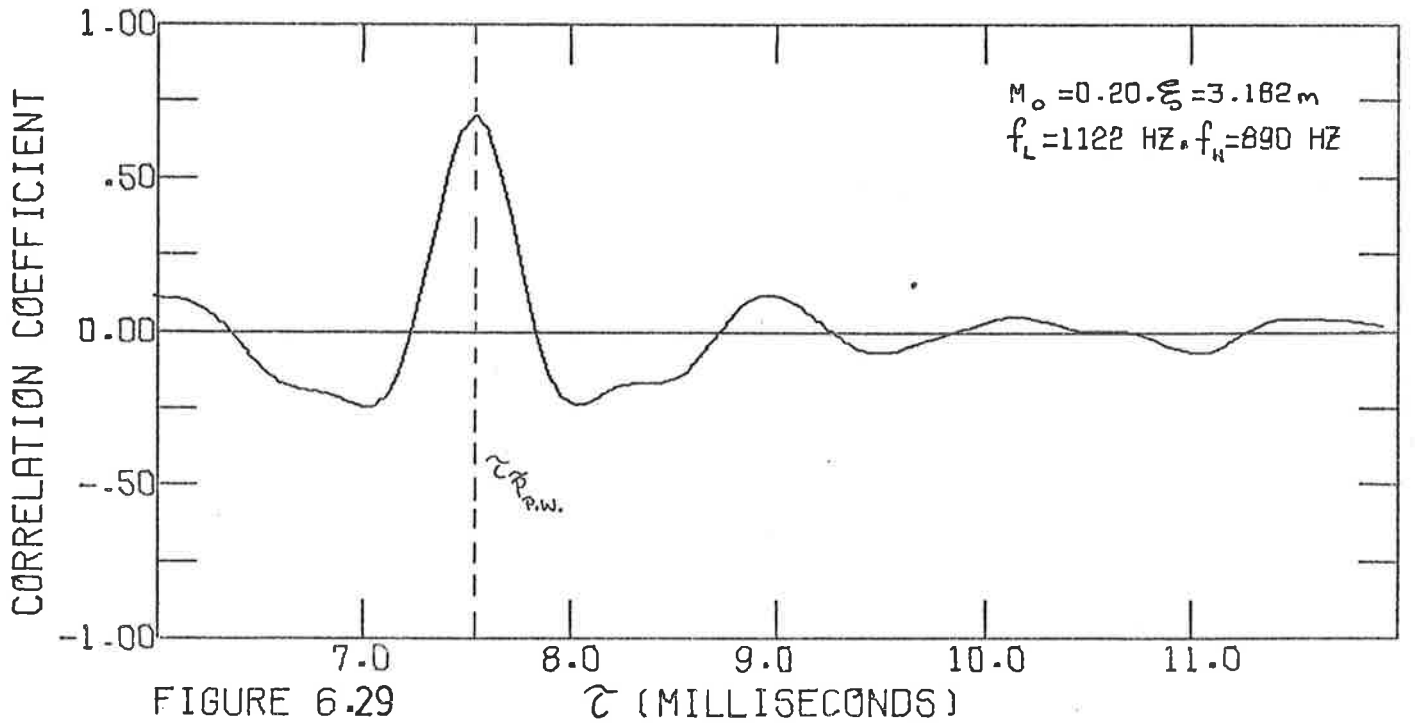
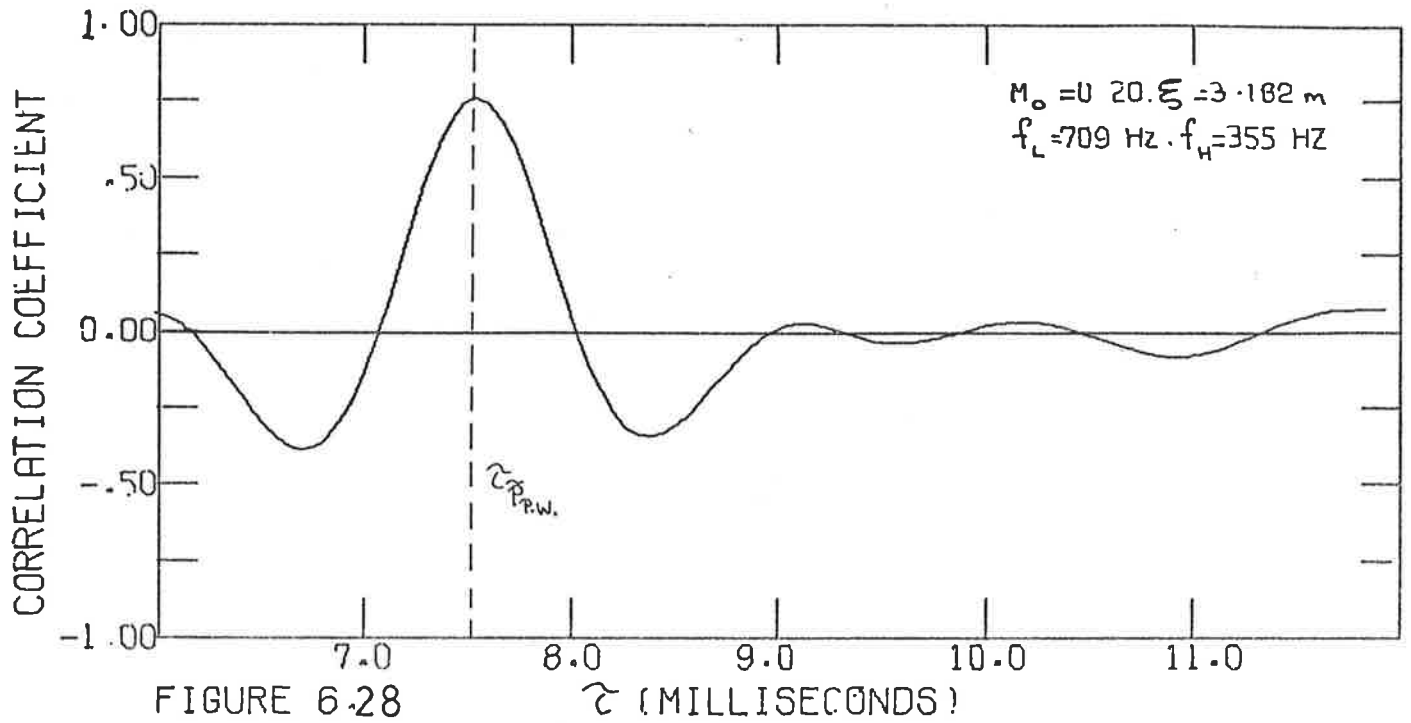
Thus, it was decided that a fairly large transducer separation was essential, and two particular separation distances were chosen:

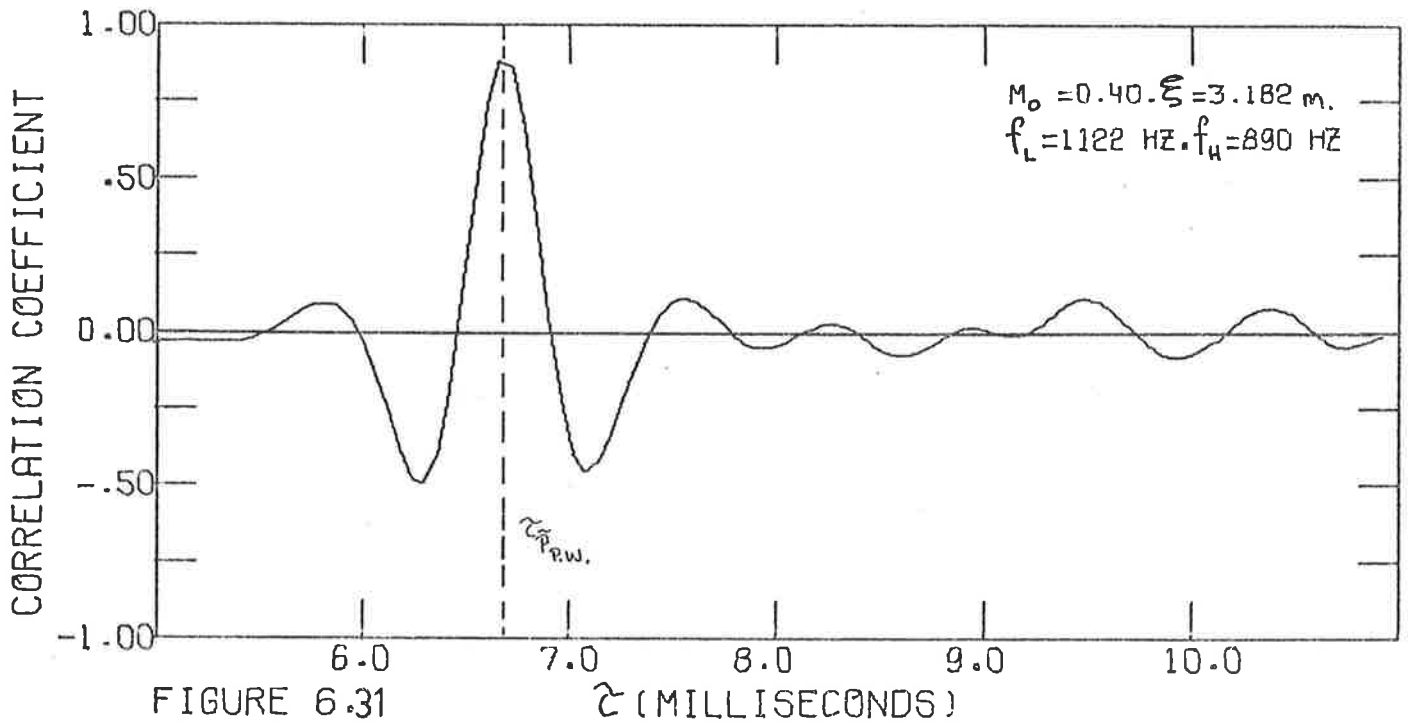
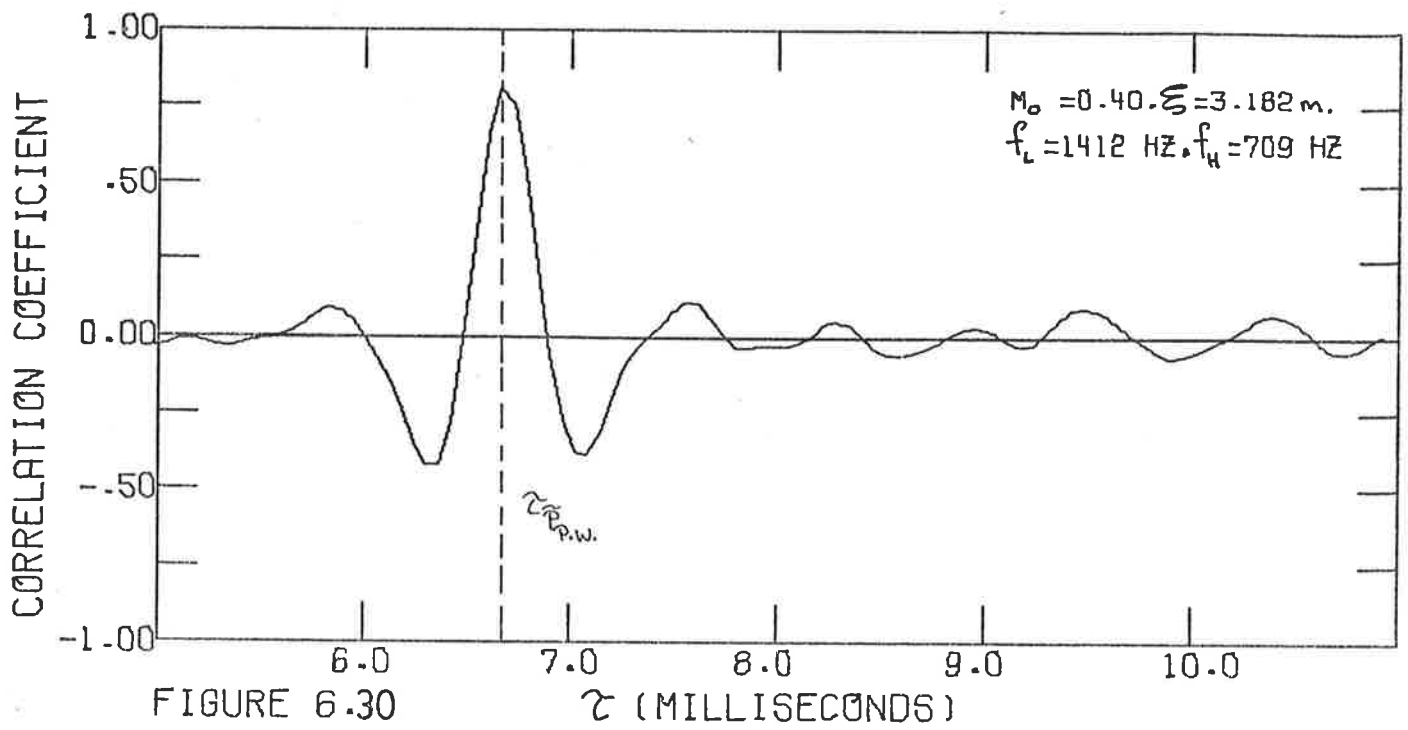
(i) $\xi = 3.182$ m. and (ii) $\xi = 5.186$ m. The first separation distance corresponds to the span of the thin-walled test section (including the two instrumentation sections on which the transducers were mounted) and the second corresponds to the span of the thin-walled test section and a section of piping upstream of it, 2.004 m long. For both separations, cross-correlations were performed in several octave and $\frac{1}{3}$ -octave bands. Figures 6.25, 6.26 and 6.27 are correlograms for $M_0 \sim 0.40$, $\xi = 5.186$ m for the 500 Hz octave, 800 Hz $\frac{1}{3}$ -octave and 1000 Hz $\frac{1}{3}$ -octave filter bands respectively. The well defined peaks at $\tau = 10.8$ msec corresponds to plane wave propagation, which once again confirms earlier conclusions that the plane waves dominate the wall pressure field at these low frequencies ($ka_i < 1.84$). Similar results are obtained for a spatial separation of $\xi = 3.182$ m. Results are presented for $M_0 \sim 0.20, 0.40$ and 0.50 for several octave and $\frac{1}{3}$ -octave filter bands in Figures 6.28 to 6.33 where $\tau_{P.W.} = 7.6$ msec, 6.63 msec and 6.14 msec for the three flow mach numbers respectively.

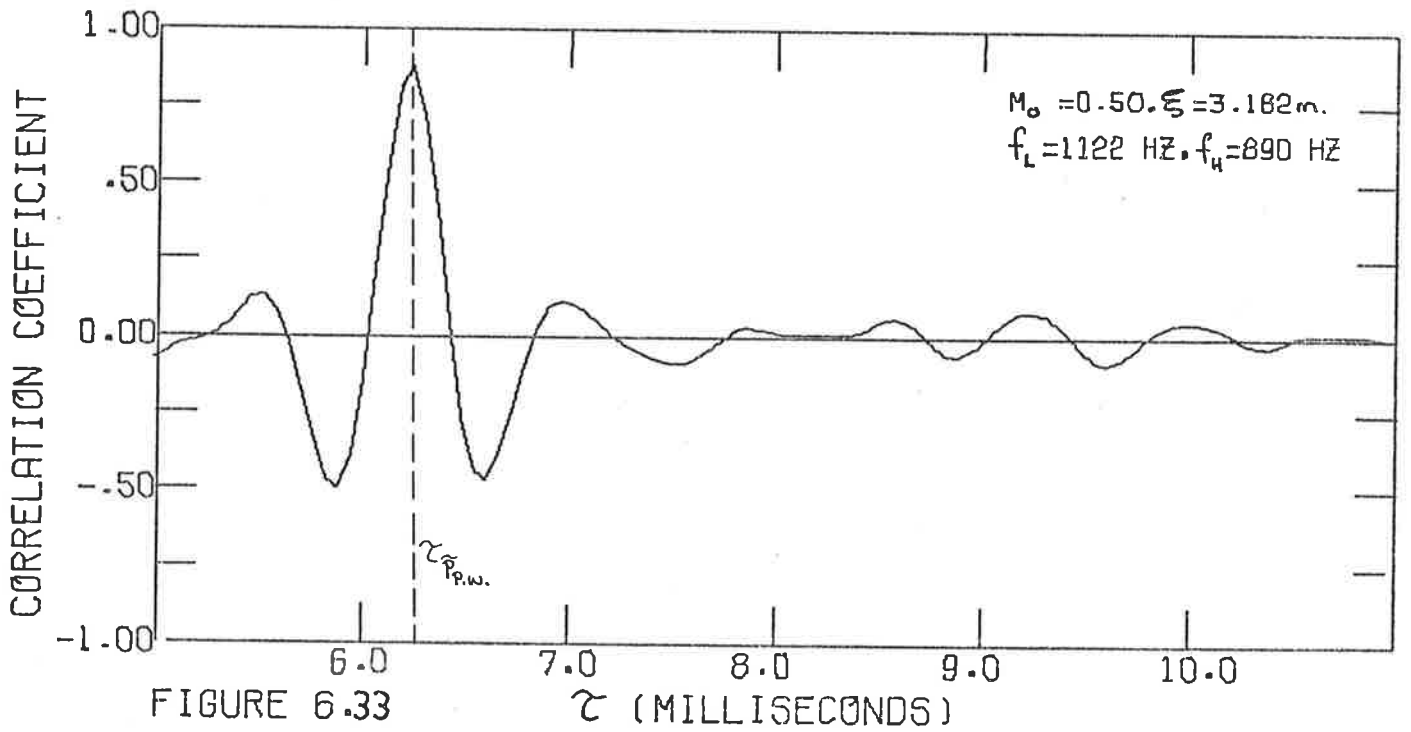
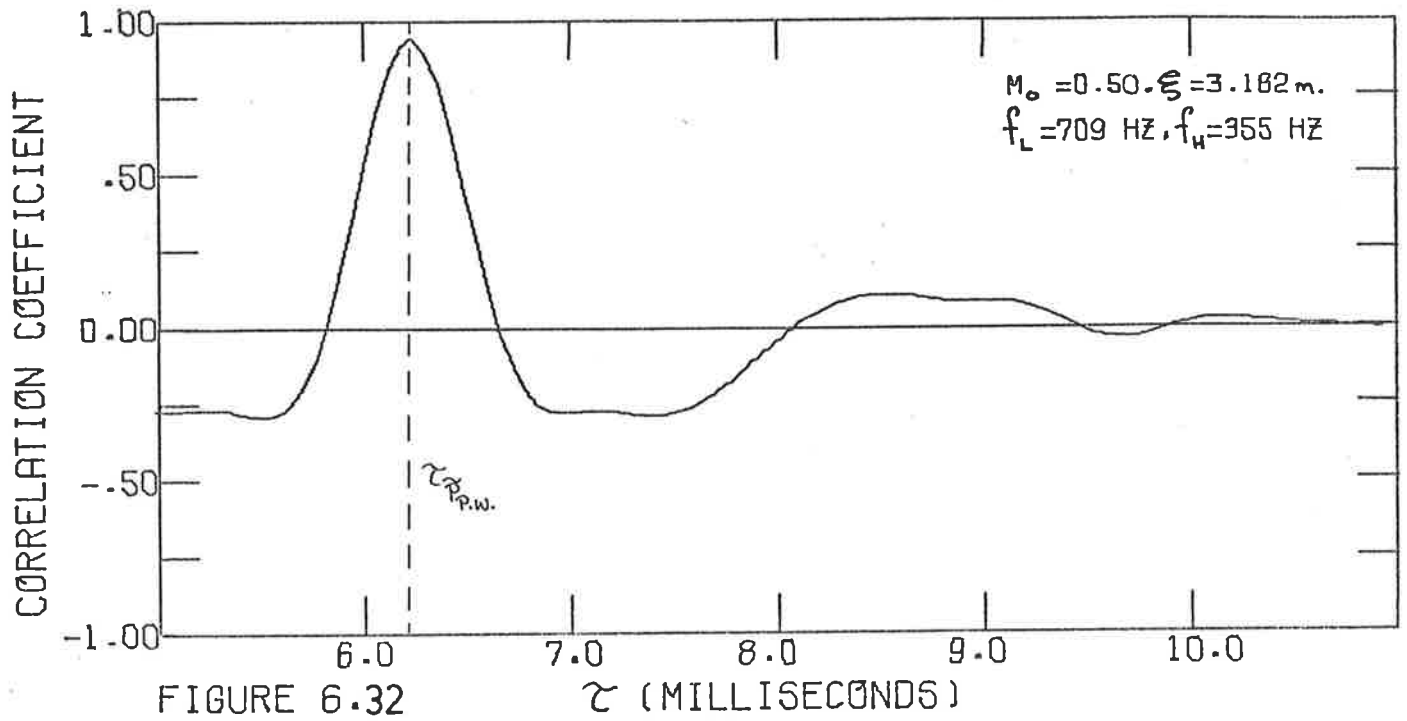
The main objective in doing the wall pressure fluctuations cross-correlations was to extract the plane wave component in filter bands where $ka_i \geq 1.84$. The results presented so far (for $ka_i < 1.84$)



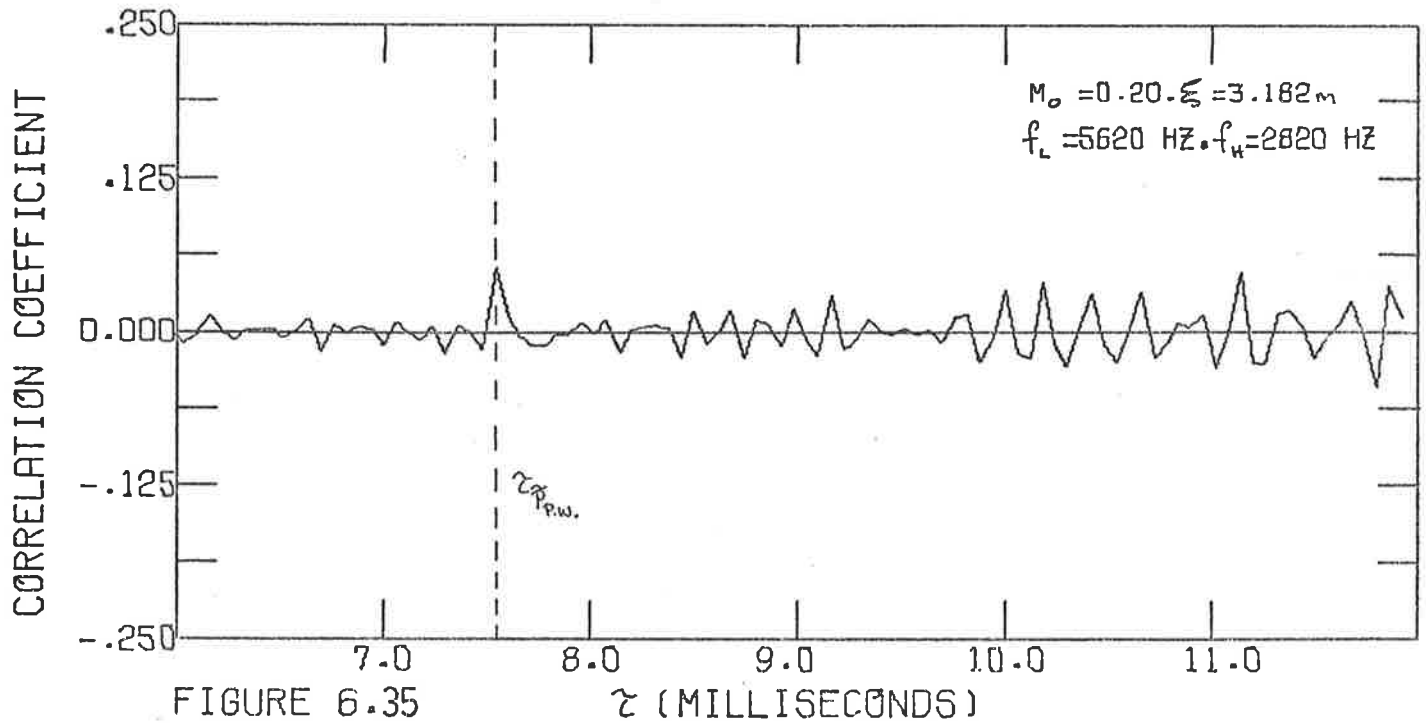
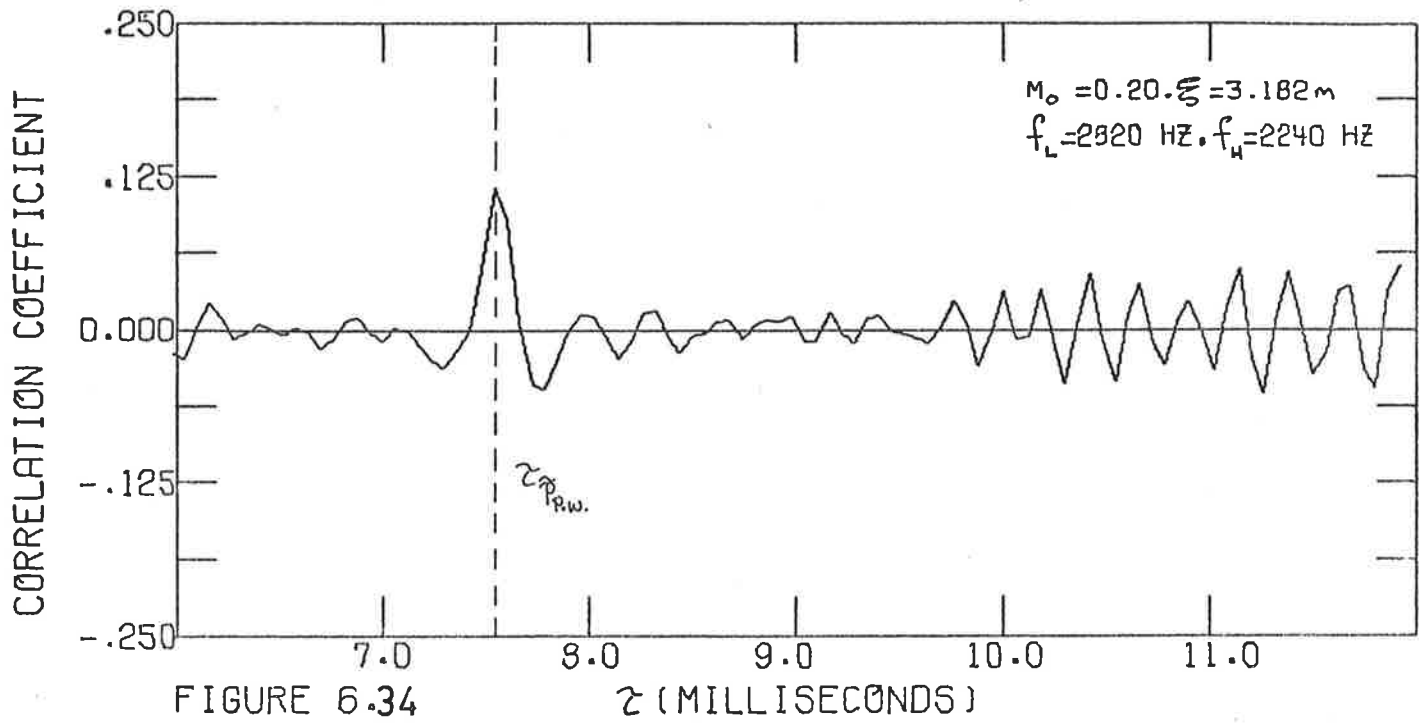


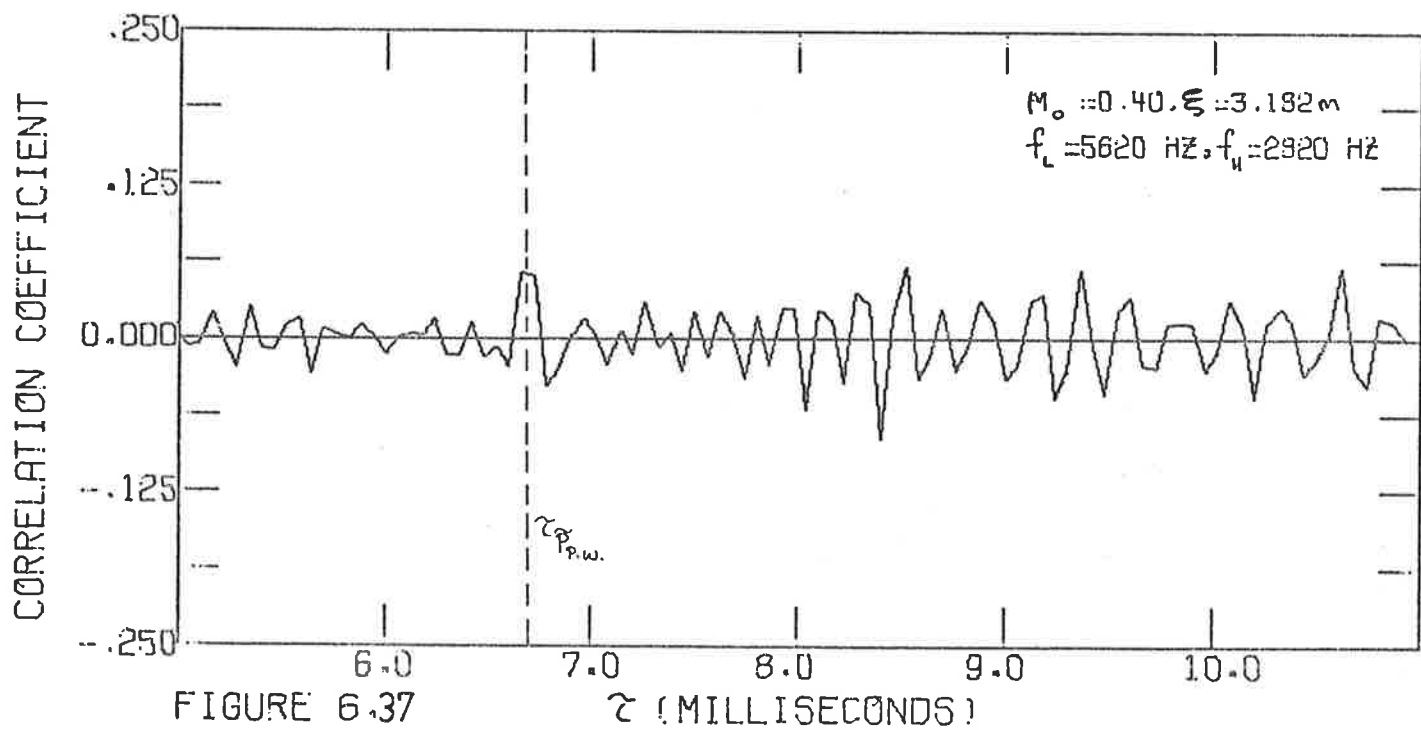
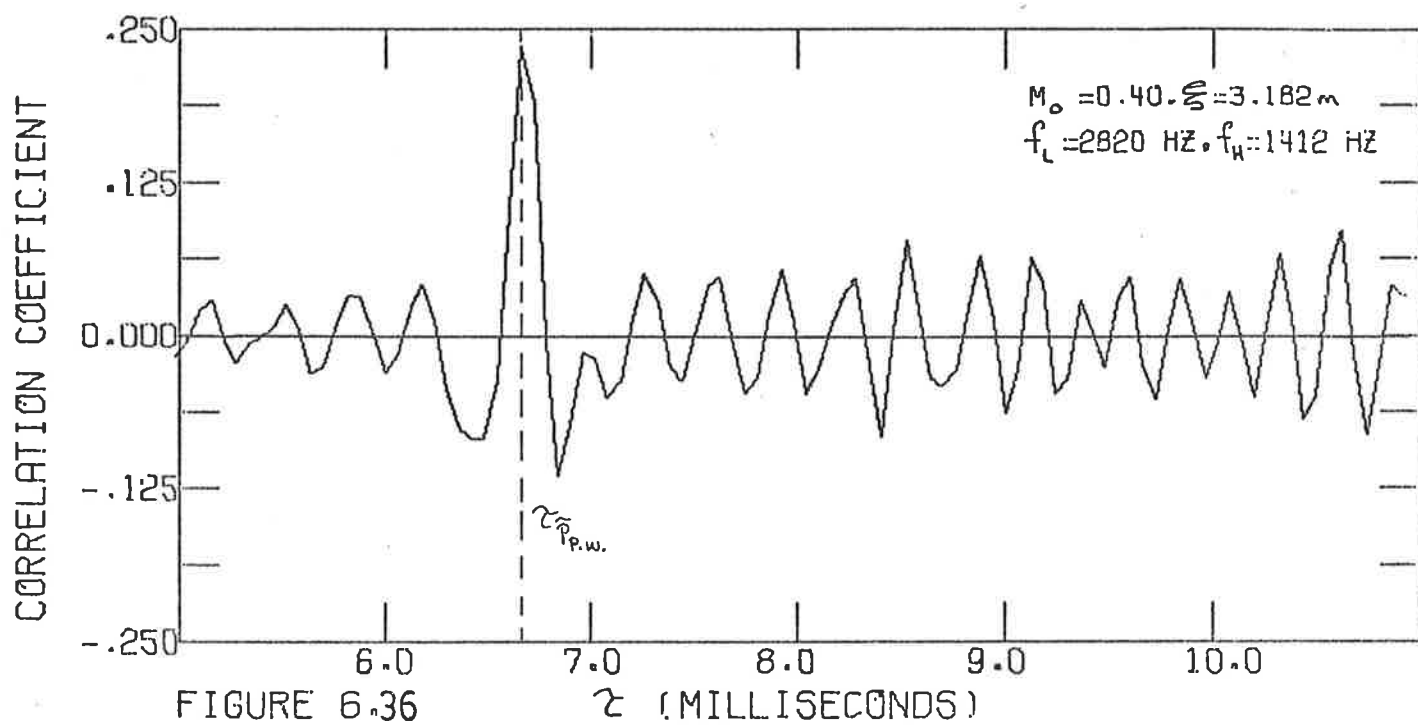


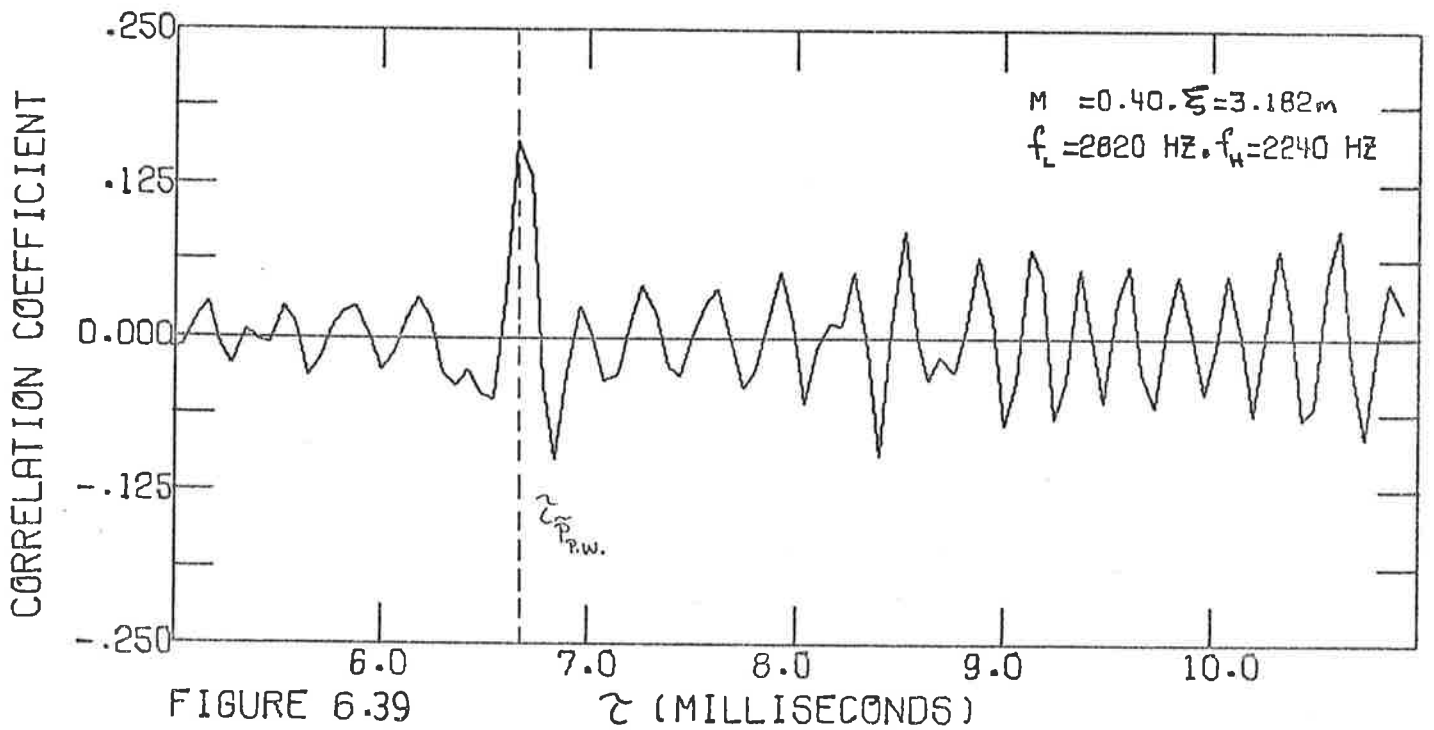
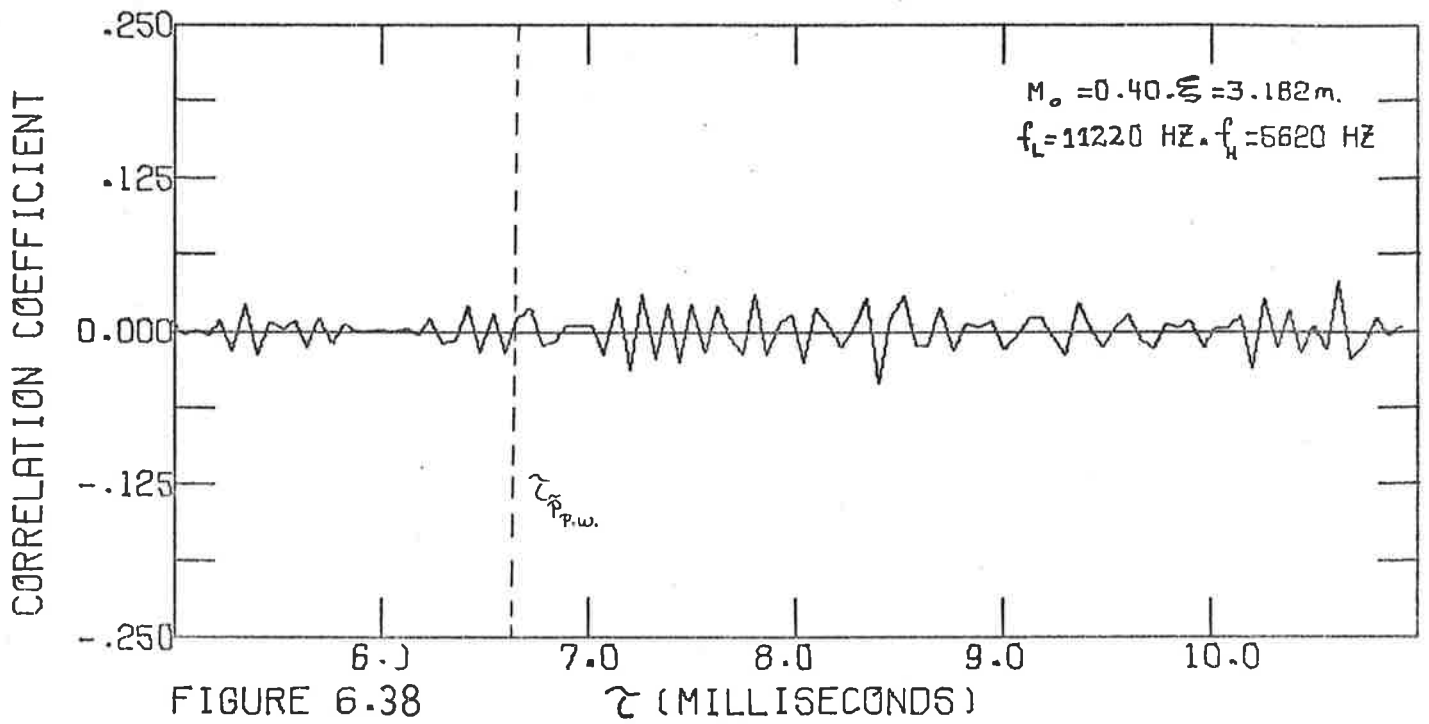


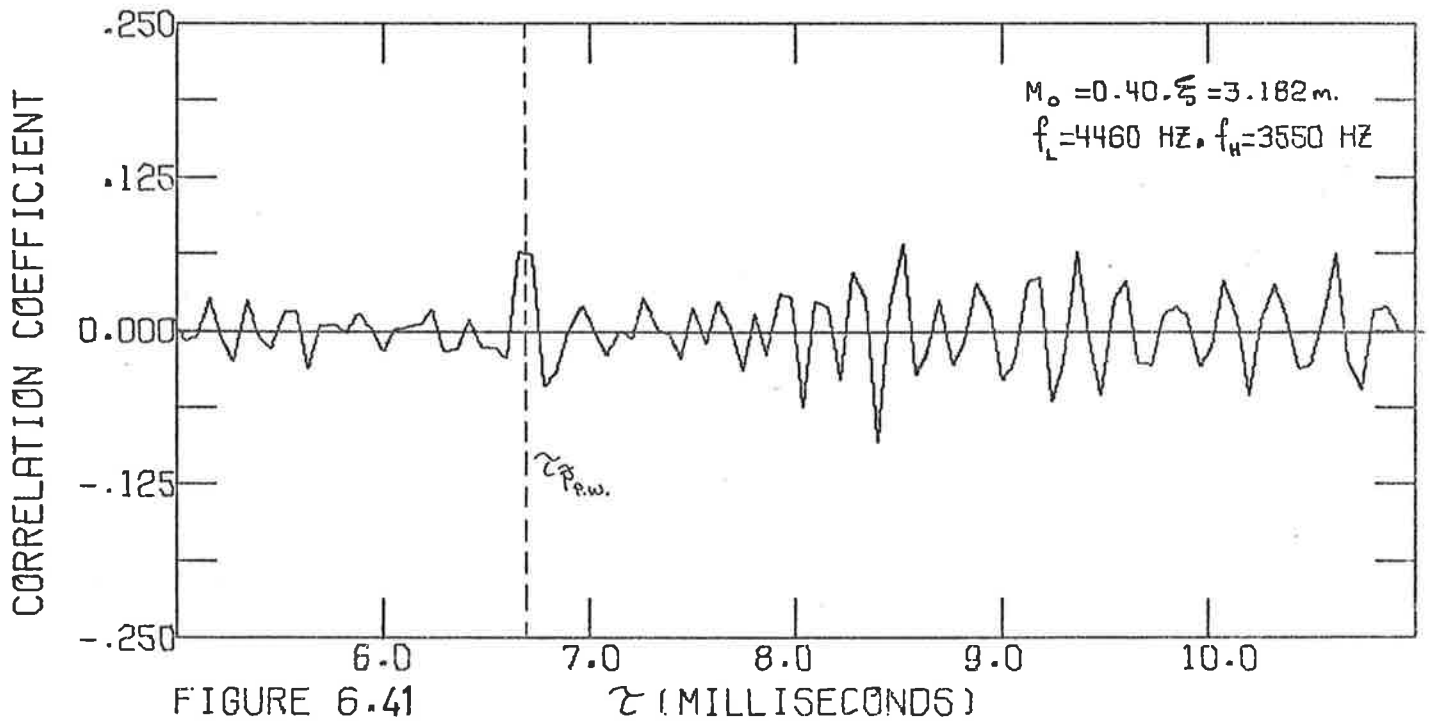
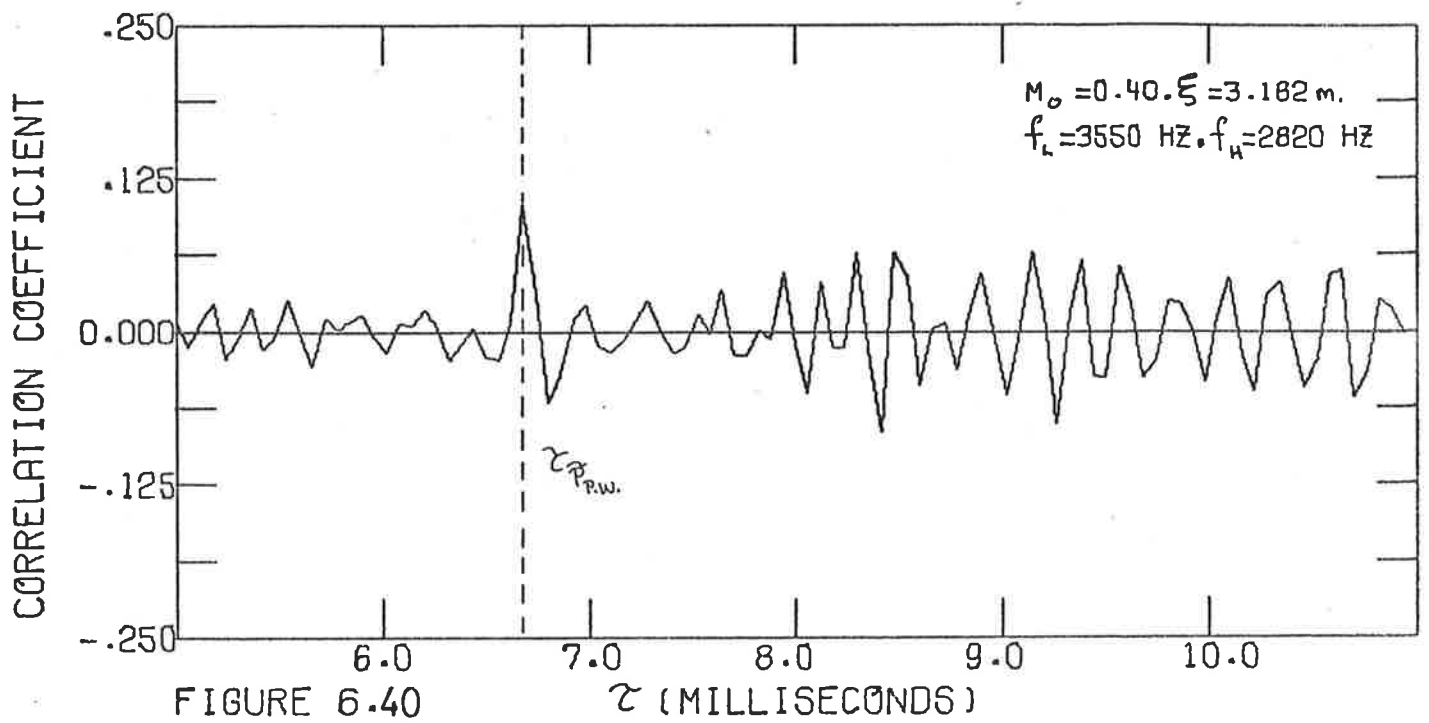


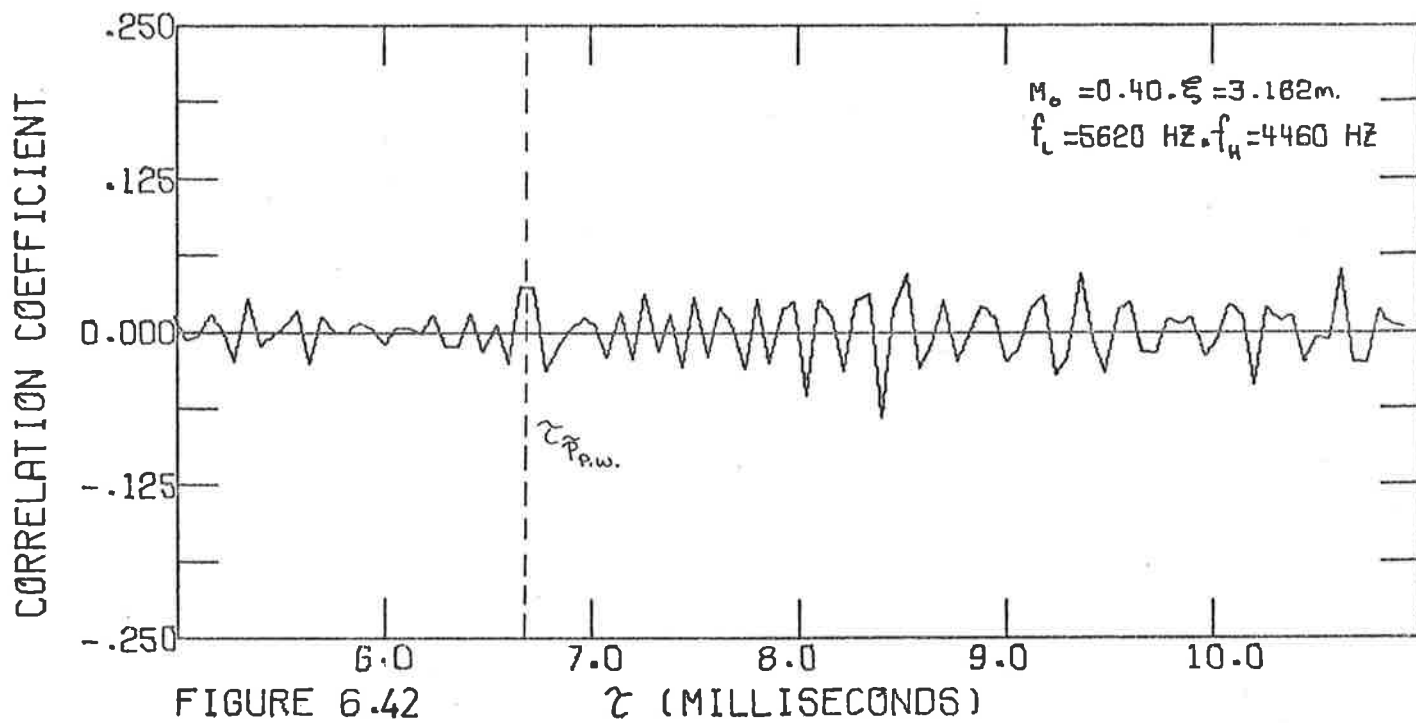
are in close agreement with previously published work (Karvelis, 1975), and this provided ample proof that the data acquisition, digital filtering and cross correlation computer programs were free of any faults. Detailed cross correlations were then performed in several octave and $\frac{1}{3}$ -octave filter bands. A typical selection of results is presented for $M_0 \sim 0.20, 0.40$ and 0.50 for $\xi = 3.182$ m and for $M_0 \sim 0.40, \xi = 5.186$ m for several octave and $\frac{1}{3}$ -octave bands in Figures 6.34 to 6.50. Three immediate observations are that (1) there are distinct peaks at the appropriate time delays corresponding to plane wave propagation (2) the correlation curve is dispersive at time delays $> \tau_{P.W.}$, and (3) the magnitude of the correlation coefficient corresponding to plane wave propagation is independent of spatial separation (provided equations [6.30] and [6.31] are satisfied). The third observation confirms that the plane waves propagate essentially unattenuated down the pipe (the correlation coefficient associated with plane wave propagation is directly proportional to the component of the wall pressure fluctuations associated with the plane waves and hence the corresponding sound power in the duct (see Section 6.2)). Furthermore as the center frequency of the filter bands increase the component of the wall pressure fluctuations associated with plane waves decreases. Typical examples are Figure 6.38 for the 8000 Hz octave, Figure 6.50 for the 5000 Hz $\frac{1}{3}$ -octave and Figures 6.35 and 6.44 for the 4000 Hz octave filter bands. The implications of this are that at these frequencies, the wall pressure field comprises contributions from turbulent pressure fluctuations and higher order modes with a small plane wave contribution. For the 90° mitred bend, the component of the wall pressure fluctuations associated with plane acoustic waves starts to become insignificant at center frequencies greater than 8000 Hz. This is illustrated in

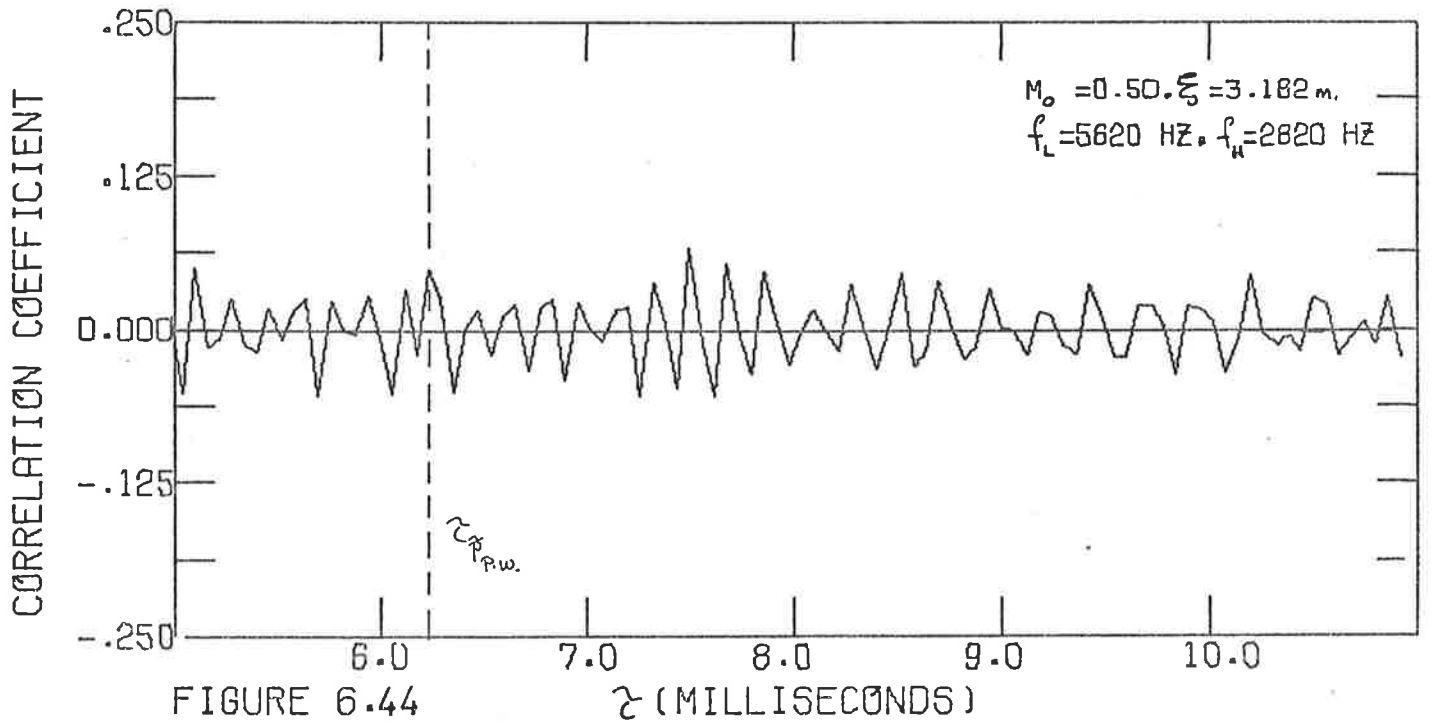
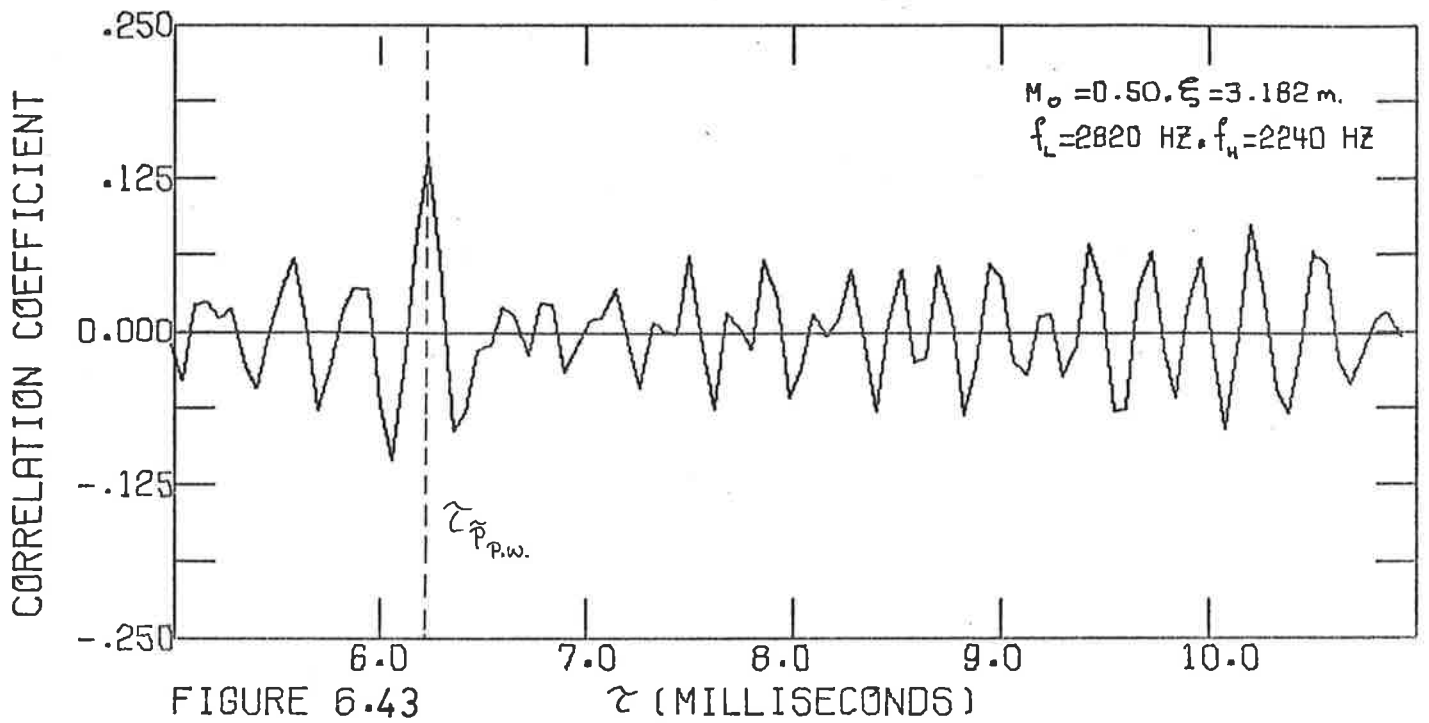


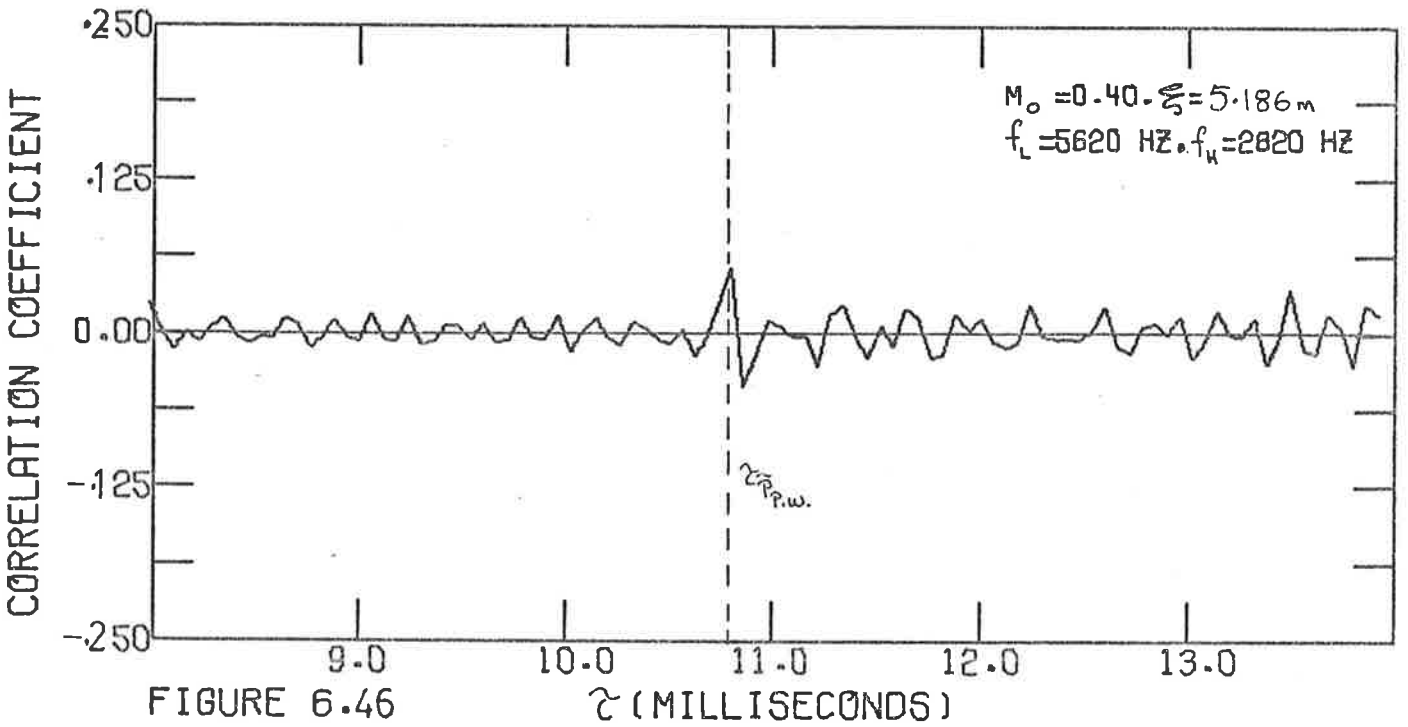
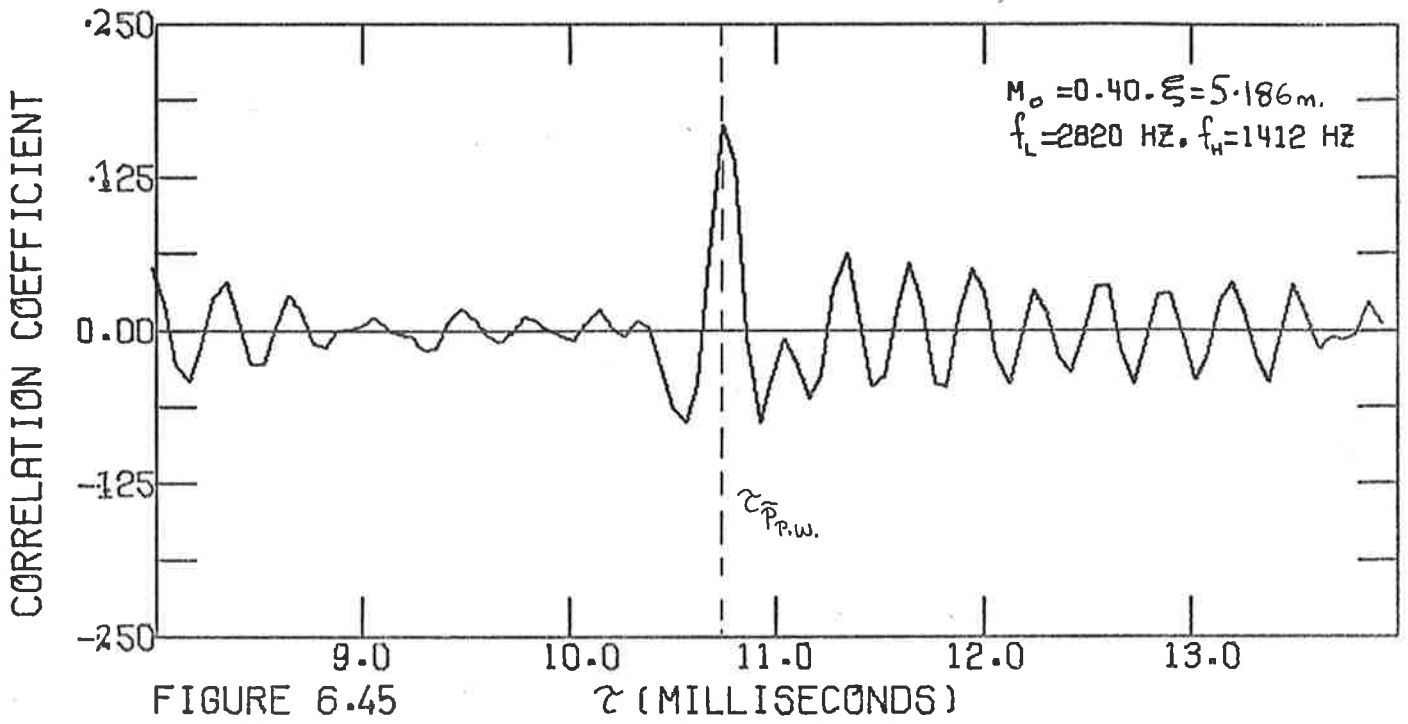


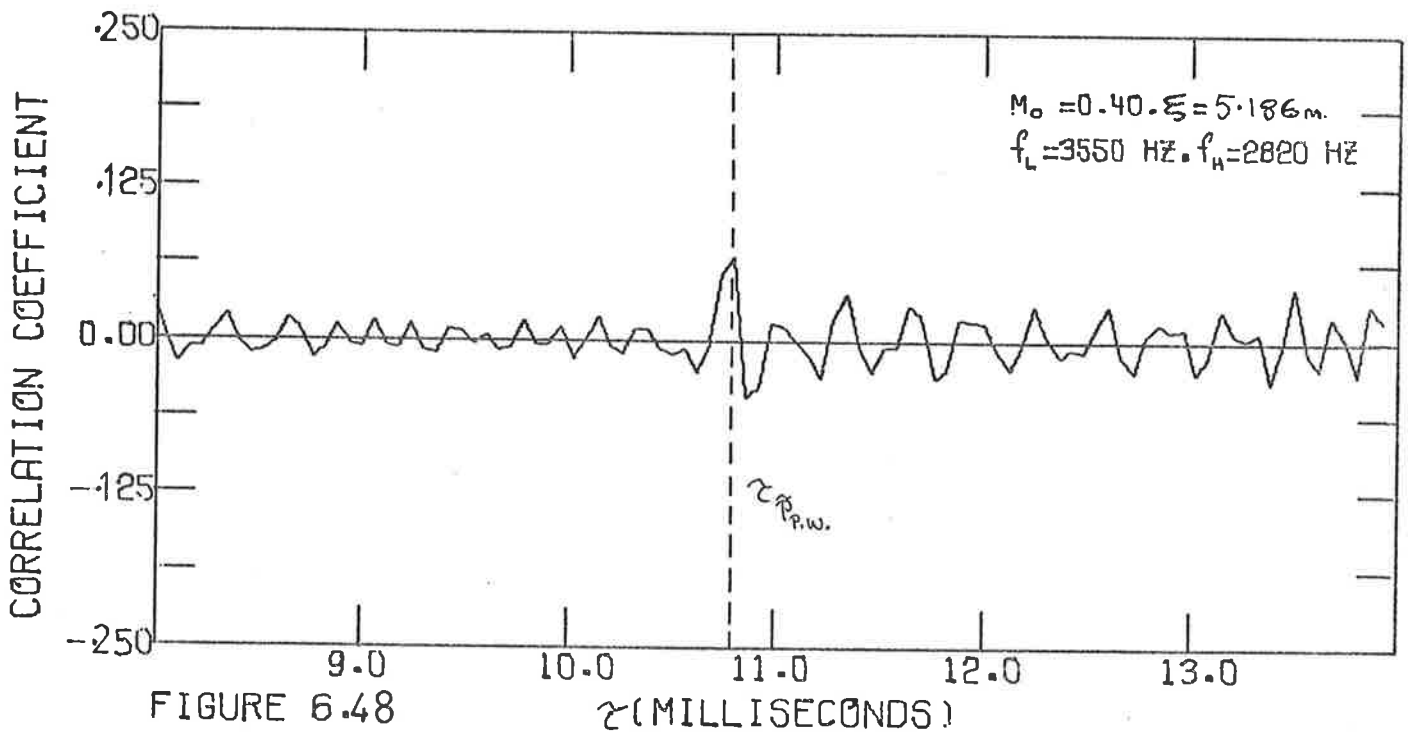
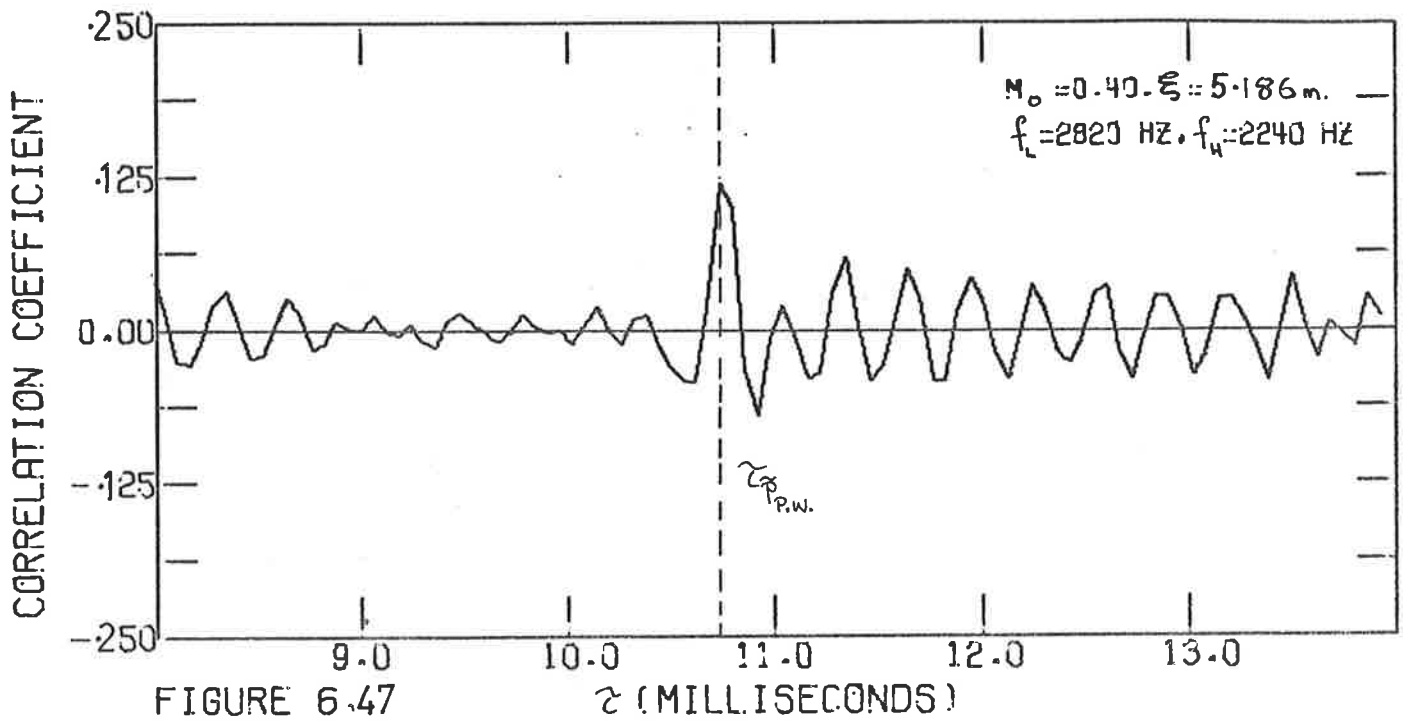


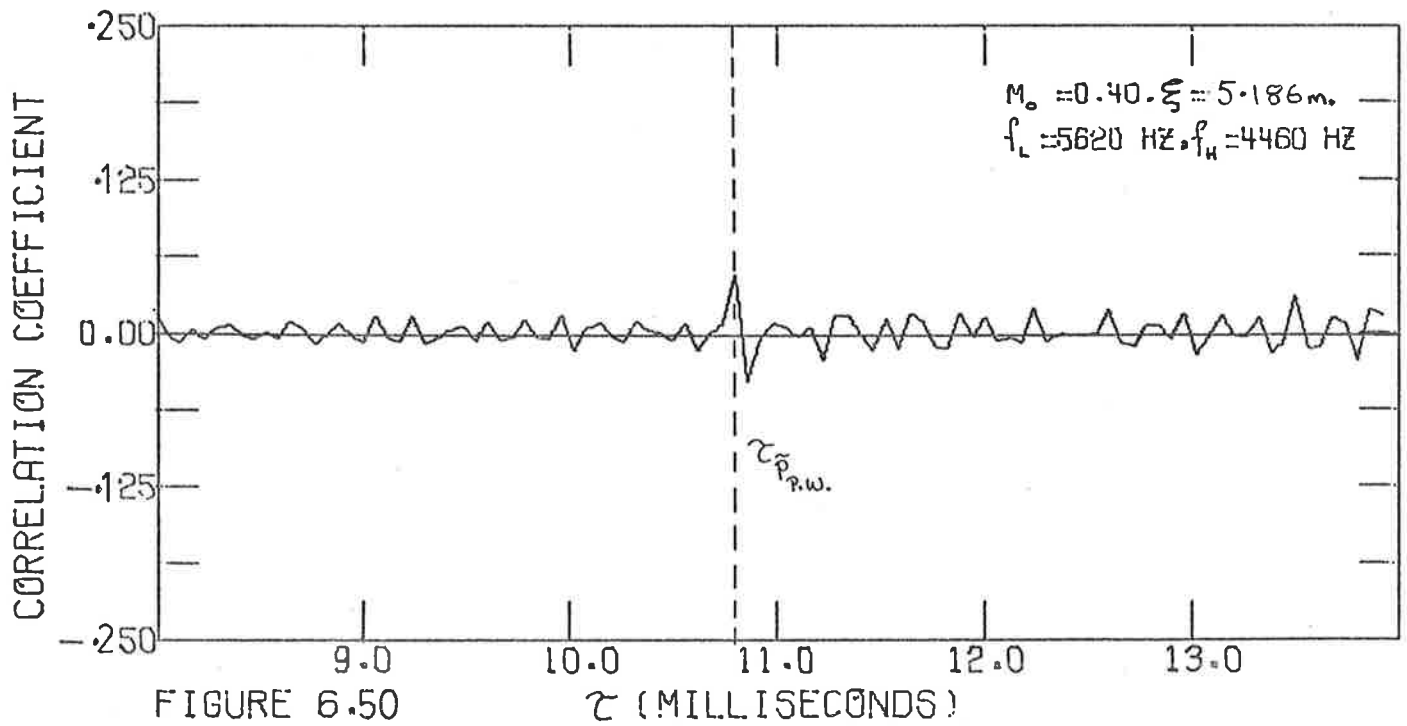
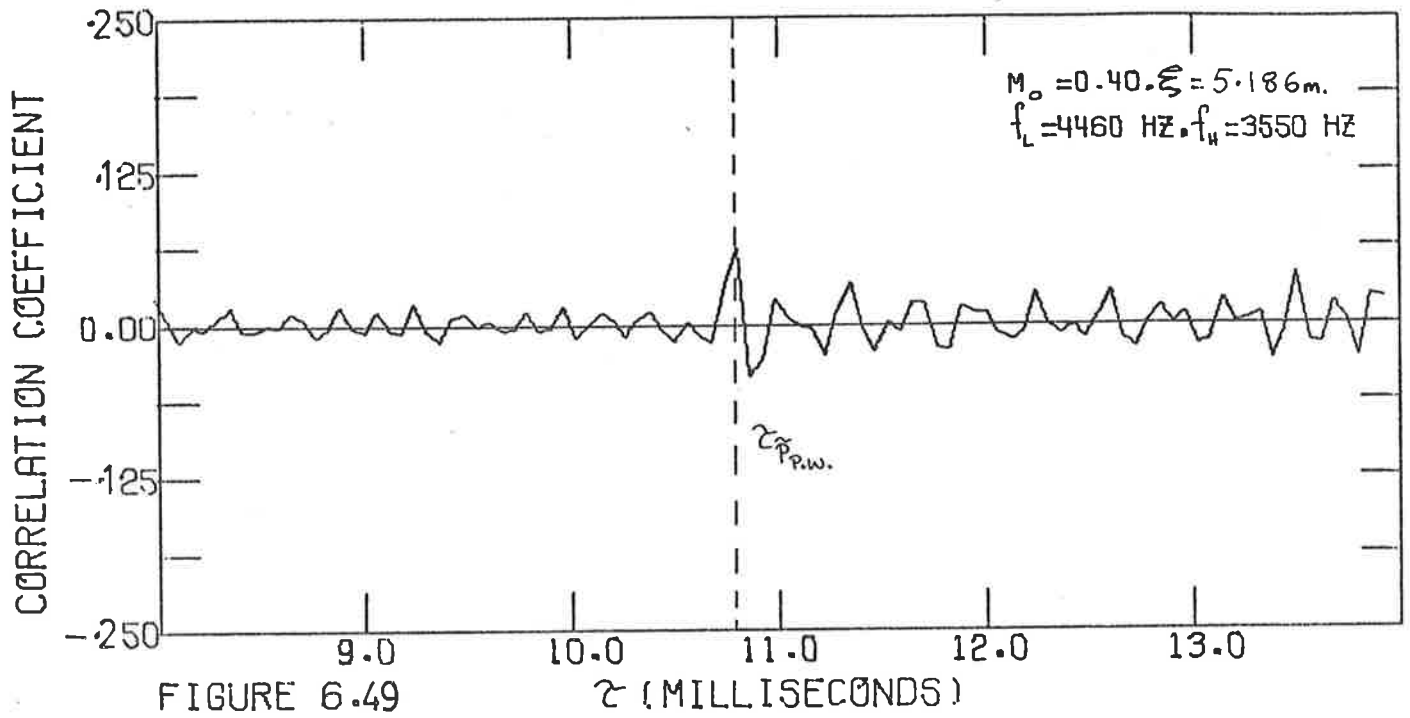












Figures 6.51 and 6.52 where the correlation coefficient associated with plane wave propagation is plotted against band centre frequency for several octave and $\frac{1}{3}$ -octave filter bands for various flow speeds and spatial separations. For regions where $k a_i \geq 1.84$ (~ 2500 Hz) the plane wave contribution rapidly decreases for all flow speeds and spatial separations. Hence it was concluded that it was unnecessary to correlate in filter bands above the 8000 Hz octave filter band as no useful information could be extracted at these frequencies.

This information can now be used in conjunction with equations [6.25] and [6.26] to estimate the wall pressure fluctuations associated with plane waves and higher order modes in various filter bands. Table 6.3 shows the results for the $M_0 \sim 0.40$ case. At high frequencies ($k a_i \geq 1.84$) this is representative of all flow speeds since $\rho(\tau_{P.W.})$ is approximately constant in these filter bands. It can be seen that for $k a_i < 1.84$ plane waves dominate the wall pressure fluctuations and the turbulent pressure fluctuations are about 13 dB less than the acoustic pressure fluctuations. The higher order modes dominate the wall pressure field for $k a_i \geq 1.84$. The percentage of $\langle p^2 \rangle$ associated with the higher order modes remains approximately constant with an increase in filter band center frequency, but in the 12.5 kHz and 16 kHz filter bands in particular, the turbulent pressure fluctuations are starting to make a noticeable contribution towards the overall pressure fluctuations. This has to be taken into account in the estimation of the pipe wall response to higher order mode excitation, and this is discussed in Chapter 7. It is of particular importance when studying some of the milder internal flow disturbances where the higher order modes do not dominate the wall pressure field although they do dominate the pipe wall response (Chapters 4 and 5).

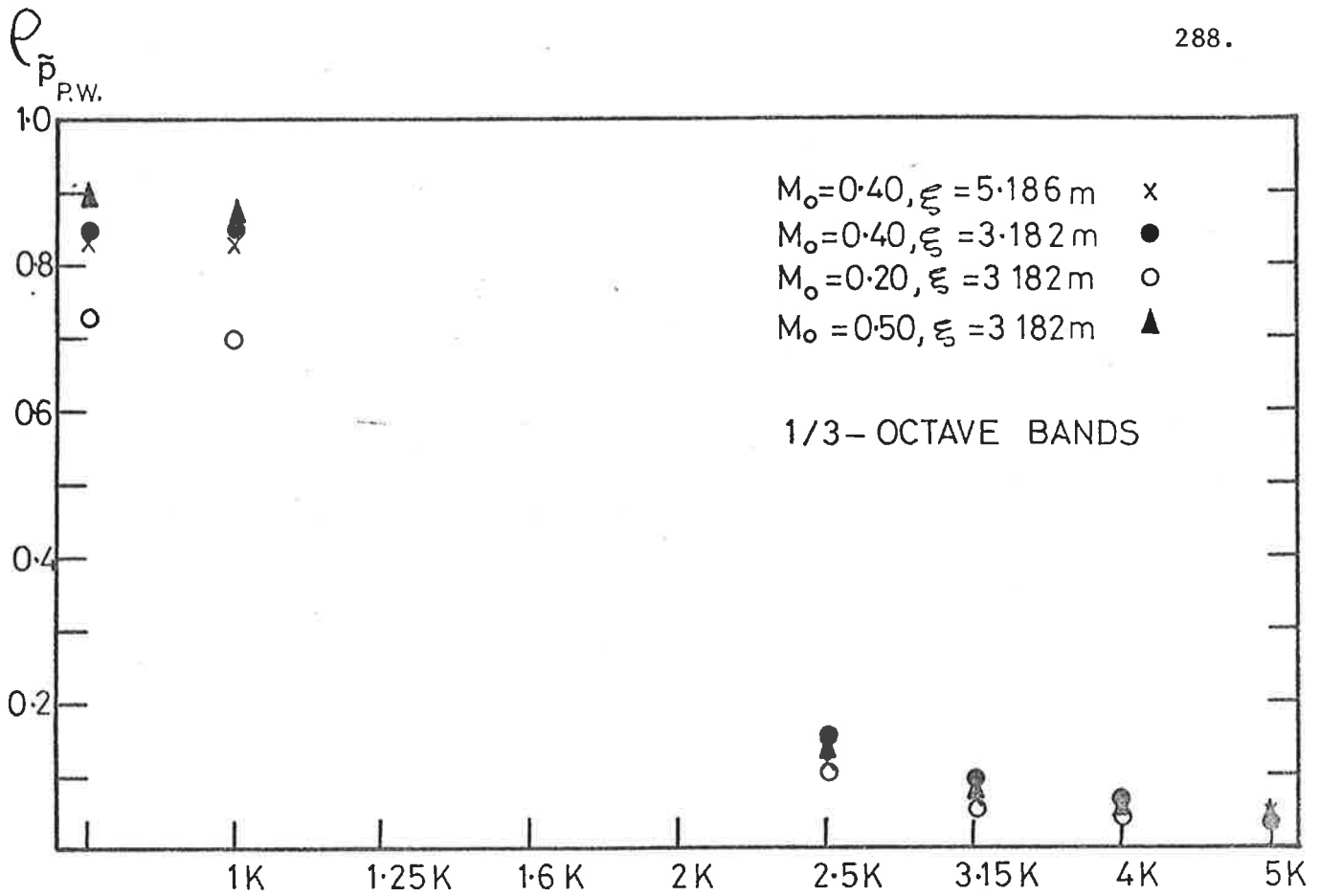


FIGURE 6.51 CORRELATION COEFFICIENT ASSOCIATED WITH $\tau_{\bar{p}_{P.W.}}$

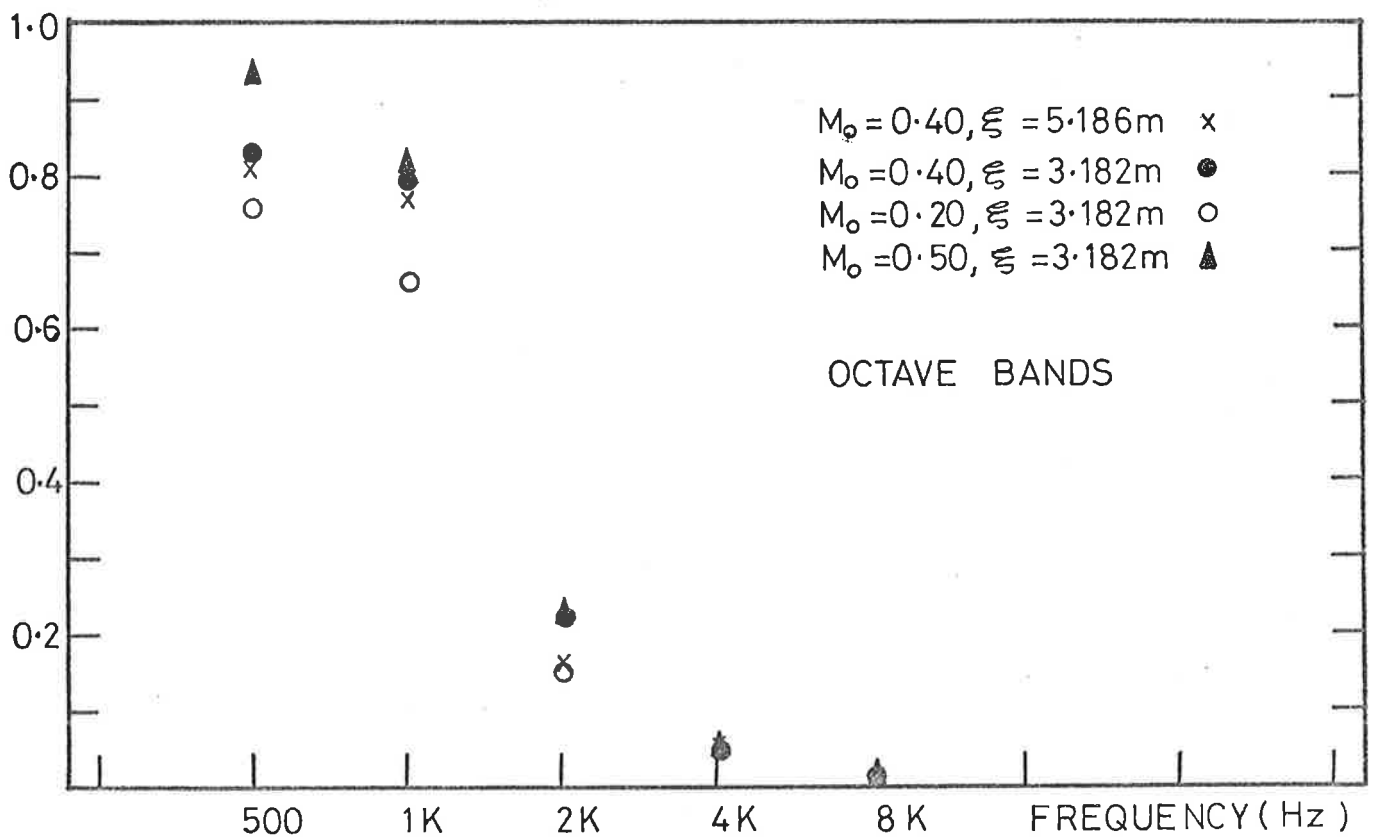


FIGURE 6.52 CORRELATION COEFFICIENT ASSOCIATED WITH $\tau_{\bar{p}_{P.W.}}$

TABLE 6.3

The components of the wall pressure fluctuations associated with plane waves and higher order modes in several filter bands. (90° mitred bend, $M_0 \sim 0.40$)

FILTER BAND (HZ)	$\rho(\tau_{P.P.W.})$	$10 \log_{10} \Phi_p$	$10 \log_{10} \Phi_p'$	$10 \log_{10} \Phi_{P.P.W.}$	$10 \log_{10} \Phi_{H.O.}$
800	.840	-43.1	-56.8 (4.3%)	-43.4 (93.1%)	No higher order modes
1000	.830	-41.9	-55.2 (4.7%)	-42.2 (93.0%)	No higher order modes
2500	.140	-47.3	-57.2 (10.2%)	-55.8 (14.0%)	-48.5 (75.7%)
3150	.080	-46.9	-57.8 (8.1%)	-57.9 (7.9%)	-47.7 (83.2%)
4000	.0625	-49.3	-57.6 (14.8%)	-61.3 (6.3%)	-50.3 (79.4%)
5000	.0460	-48.1	-59.4 (7.4%)	-61.5 (4.6%)	-48.7 (87.1%)
6300	<0.03	-49.7	-59.6 (10.2%)	-66.7 (2.0%)	-50.3 (87.1%)
8000	<0.03	-51.9	-60.4 (14.1%)	-	-52.6 (85.1%)
10000	<0.03	-53.7	-61.4 (17.0%)	-	-54.5 (83.0%)
12500	-	-55.9	-62.7 (20.9%)	-	-56.9 (79.4%)
16000	-	-58.0	-63.6 (27.5%)	-	-59.4 (72.4%)

Note: (i) Higher order modes can propagate in filter bands ≥ 2500 Hz for this particular case ($k a_1 \geq 1.84$).

(ii) Corresponding percentages of mean square pressure fluctuations $\langle p^2 \rangle$ are included in parentheses.

6.5 GENERAL DISCUSSION

The main aim of the work discussed in this chapter was to extract the component of the wall pressure fluctuations associated with the higher order modes in several filter bands. The component of the wall pressure fluctuations associated with plane waves can be obtained from the correlations, and thus the component associated with the higher order modes can be estimated by subtracting the turbulent and plane wave components from the total wall pressure fluctuations. In this way, the wall pressure fluctuations associated with the (1,0) higher order acoustic mode can be estimated fairly readily in the 2.5 kHz and 3.15 kHz filter bands. However in the frequency bands containing other higher order modes, the contribution to the wall pressure fluctuations from modes already propagating at lower frequencies cannot be separated from that due to the particular mode of interest, since the higher order modes are dispersive in character. Thus, as mentioned previously, only the intensity of the wall pressure fluctuations associated with ALL the higher order modes in these filter bands (including the higher order modes that have their cut off frequencies in the preceding filter bands) can be made. This is a limitation in that the component of the wall pressure fluctuations associated with individual higher order modes cannot be obtained and furthermore the component associated with several higher order modes in a filter band contains higher order modes from previous bands. These higher order modes from previous bands do not contribute significantly to the pipe wall response in the filter band of interest (because their coincidence frequencies are in the previous bands), and hence the wall pressure fluctuations due to the higher order modes in the filter band of interest are over estimated (this is discussed in Chapter 7).

In summary, the conclusions to be drawn from this chapter are:

- (1) The 90° mitred bend is a strong generator of plane acoustic waves for $k a_i < 1.84$.
- (2) Higher order acoustic modes dominate the wall pressure field for $k a_i \geq 1.84$.
- (3) With a sufficient spatial separation of the transducers, a distinct peak at a time delay corresponding to plane wave propagation can be obtained in filter bands containing higher order modes.
- (4) The plane wave component of the wall pressure field can thus be extracted from the correlogram and hence the higher order mode component can be estimated.
- (5) This technique will be useful when attempting to estimate the pipe wall response due to a mild flow disturbance, where an estimate of the higher order mode component of the wall pressure fluctuations is essential since in these cases, the higher order modes make major contributions to the pipe wall response but do not dominate the wall pressure field.

CHAPTER 7THEORETICAL ESTIMATION OF THE ACOUSTICRADIATION DUE TO VARIOUS INTERNAL FLOW DISTURBANCES7.1 INTRODUCTION

This chapter is concerned with theoretically estimating the increased vibration response of the pipe wall and the external acoustic radiation due to the various internal flow disturbances; to do this the nature of the internal acoustic field has to be known and in particular the component of the wall pressure fluctuations associated with the higher order modes.

The wall pressure fluctuations (Chapters 4 and 5) and the cross-correlations (Chapter 6) indicate that for the 90° mitred bend, which is a severe flow disturbance, at frequencies below the cut-off frequency of the first higher order mode plane waves dominate the wall pressure field, and for frequencies above cut-off, the higher order modes dominate. The pipe wall response and acoustic radiation effects show maxima at frequencies just after cut-off for the various higher order modes, because coincidence (between higher order acoustic and structural resonant modes) occurs there, for steel pipes in particular. Thus, theoretical estimates can be obtained from the general solution for the dynamic response of a thin-walled cylindrical shell to an acoustic pressure field, with approximations based on a detailed understanding of the higher order acoustic modes that are excited and the degree to which they dominate the internal wall pressure field. These theoretical estimates together with the various spectral data of the wall pressure fluctuations presented, make it possible to estimate the acceleration response of and the acoustic radiation from a pipe, downstream of an internal flow

disturbance, where a fully-developed turbulent profile has been re-established.

7.2 ESTIMATION OF THE ACCELERATION RESPONSE AND ACOUSTIC RADIATION

For the purposes of estimating the acceleration response of and the acoustic radiation from pipes, it is convenient to perform the analysis in $\frac{1}{3}$ -octave bands. Over a $\frac{1}{3}$ -octave band ranging from a non-dimensional frequency ν_1 to ν_2 , equation [2.17] can be rewritten as;

$$\frac{I_{\ddot{\zeta}}}{I_p} = \frac{\rho_{fs}^2 M_0^3 a_i}{12 \beta^2 M_{LP}^3 a_m} \frac{\int_{\nu_1}^{\nu_2} \Phi_p(\nu) \sum_{\alpha} \frac{j_{\alpha\alpha}^2(\nu)}{(1 - (\frac{\nu\alpha}{\nu})^2)^2 + (\frac{\nu\alpha}{\nu Q_{\alpha}})^2} d\nu}{I_p}, \quad [7.1]$$

where

$$I_{\ddot{\zeta}} = \int_{\nu_1}^{\nu_2} \Phi_{\ddot{\zeta}}(\nu) d\nu,$$

and,

$$I_p = \int_{\nu_1}^{\nu_2} \Phi_p(\nu) d\nu. \quad [7.2]$$

$I_{\ddot{\zeta}}$ is the non-dimensional mean square acceleration response and I_p is the non-dimensional mean square fluctuating wall pressure in the frequency band being considered. To evaluate equation [7.1], several approximations have to be made: to the overall modal quality factor Q_{α} , to the wall pressure fluctuations $\Phi_p(\nu)$ and I_p , to the joint acceptance function $j_{\alpha\alpha}^2(\nu)$, and to the receptance function.

Coincidence, as defined in Chapter 2, is the condition in which the circumferential distance along the pipe surface between diametral nodes of the (p,q) th acoustic mode is equal to half the

wavelength of the (m,n) th structural mode in the same direction ($n=p$), and also in which the structural and acoustic wavenumbers in the axial direction are equal ($K_x = K_m$). Besides this "wavenumber coincidence", for exact coincidence there must also be a "frequency coincidence" (i.e. $v_\alpha = v_c$). At coincidence, the joint acceptance function is a maximum (the j_{mm}^2 component of the joint acceptance has a very sharp peak) and the (p,q) th acoustic mode couples most effectively with the closest (m,p) th structural mode for which $K_x = K_m$. Because of the nature of the joint acceptance function and the receptance functions of the various resonant structural modes, coupling with other (more distant) structural modes produces secondary effects that can be neglected. If the two structural modes on either side of the acoustic mode are approximately equidistant in frequency from it, then the acoustic mode couples equally effectively with both structural modes. If there were an "exact coincidence" between a particular acoustic and structural mode, then we should have $v_\alpha = v_c$ and the "receptance function" term in equation [7.1] would be inversely proportional to $(Q_\alpha)^2$. Hence the pipe wall response at the "exact coincidence" frequency is dependent only on modal damping. For the "wavenumber coincidence" situation however, $v_\alpha \neq v_c$ and the "receptance function" term in Equation [7.1] now depends on v_α , v_c and Q_α . Hence the ratio of (v_α/v_c) needs to be known to estimate the receptance function and the pipe wall response at this "wavenumber coincidence" frequency. For steel pipes (low modal damping), small differences between v_α and v_c make the $(1-(v_\alpha/v_c)^2)^2$ term dominate over the $(v_\alpha/v_c Q_\alpha)^2$ term whereas the latter term dominates if v_α is exactly equal to v_c . Thus the ratio of (v_α/v_c) is important in the estimation of the receptance function for the coincidences

associated with the various higher order modes of interest. This ratio can be estimated from the wavenumber plots (as presented in Chapter 2), v_α being obtained either approximately by using equation [2.8] or more accurately by using a computer program based on Arnold and Warburton's (1953) frequency equation which is derived by the energy method based on strain relations. Figures 7.1, 7.2 and 7.3 are wavenumber plots for coincidence of acoustic and structural modes for the (m,1), (m,2) and (m,3) structural modes respectively as obtained from Equation [2.8] (Heckl, 1962) and from Arnold and Warburton's (1953) analysis, all diagrams corresponding to $\beta = 0.0070$, $\Lambda = 79.4$, $\Psi = 0.960$ and $M_{LP} = 15.37$. As mentioned in Chapter 2 and as observed in Figure 7.1 to 7.3, equation [2.8] underestimates the resonant structural modes for low K_m values for the $n=1$ and $n=2$ modes in particular (i.e. at any given frequency, the axial mode order m is underestimated by equation [2.8]). However, since the difference in frequency between consecutive resonant structural modes is predicted fairly well there is justification for using the simpler and more readily evaluated equation [2.8] for the purposes of estimating the pipe wall response and hence the acoustic radiation. As the circumferential structural mode order n increases, the density of the structural modes in any particular frequency band increases and the axial structural wavenumber (K_m) increases with increasing n for a given frequency. Thus, the difference in frequency between consecutive structural modes decreases and the ratio of v_α/v_c becomes smaller. However, as will be shown later on in this chapter with numerical examples, it is important to take account of any difference between v_α and v_c in any theoretical estimate, for this can completely alter the predicted pipe wall response owing to the sensitivity of the receptance function to the value of v_α/v_c , as

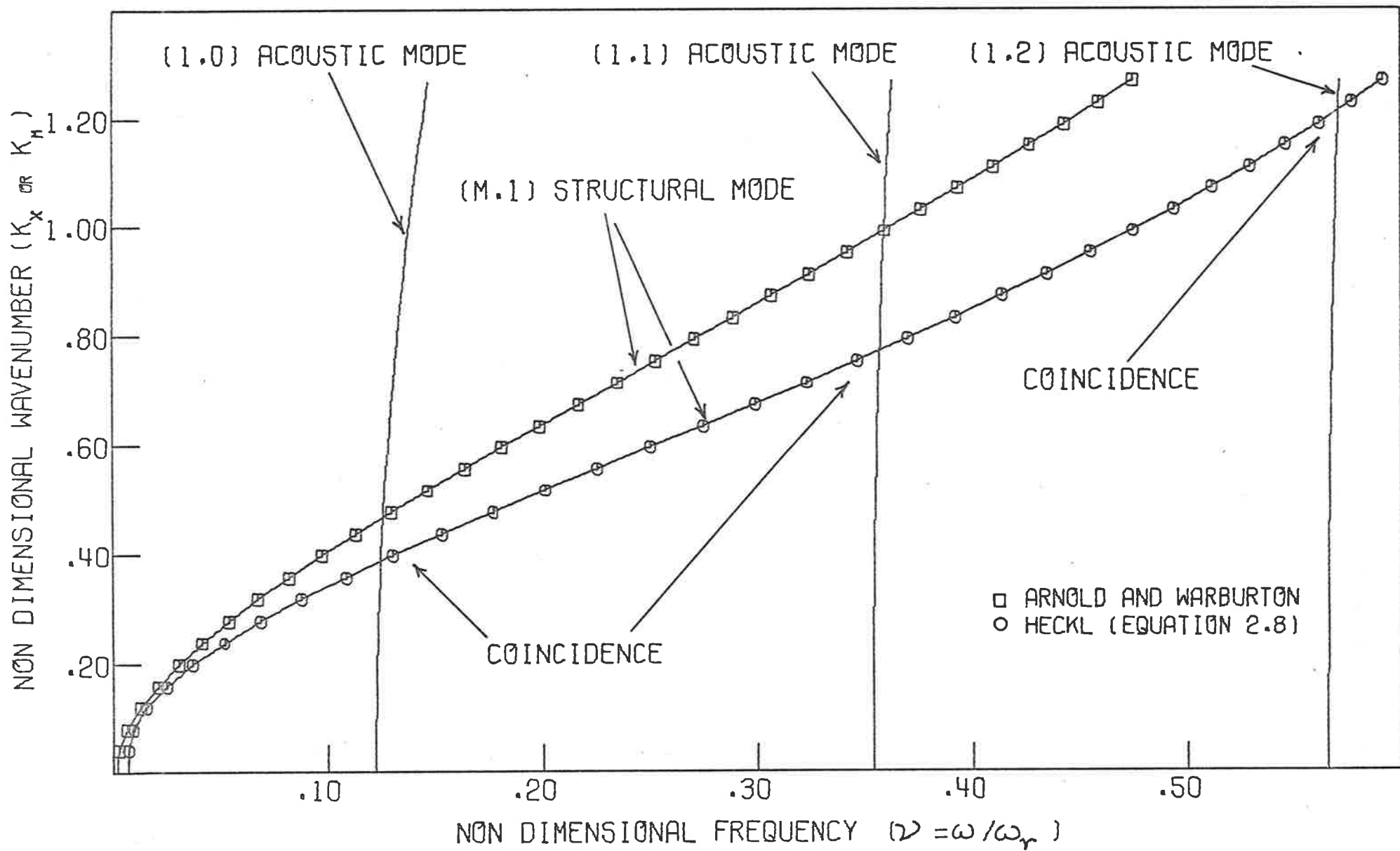


FIGURE 7.1 COINCIDENCE OF ACOUSTIC AND STRUCTURAL MODES.

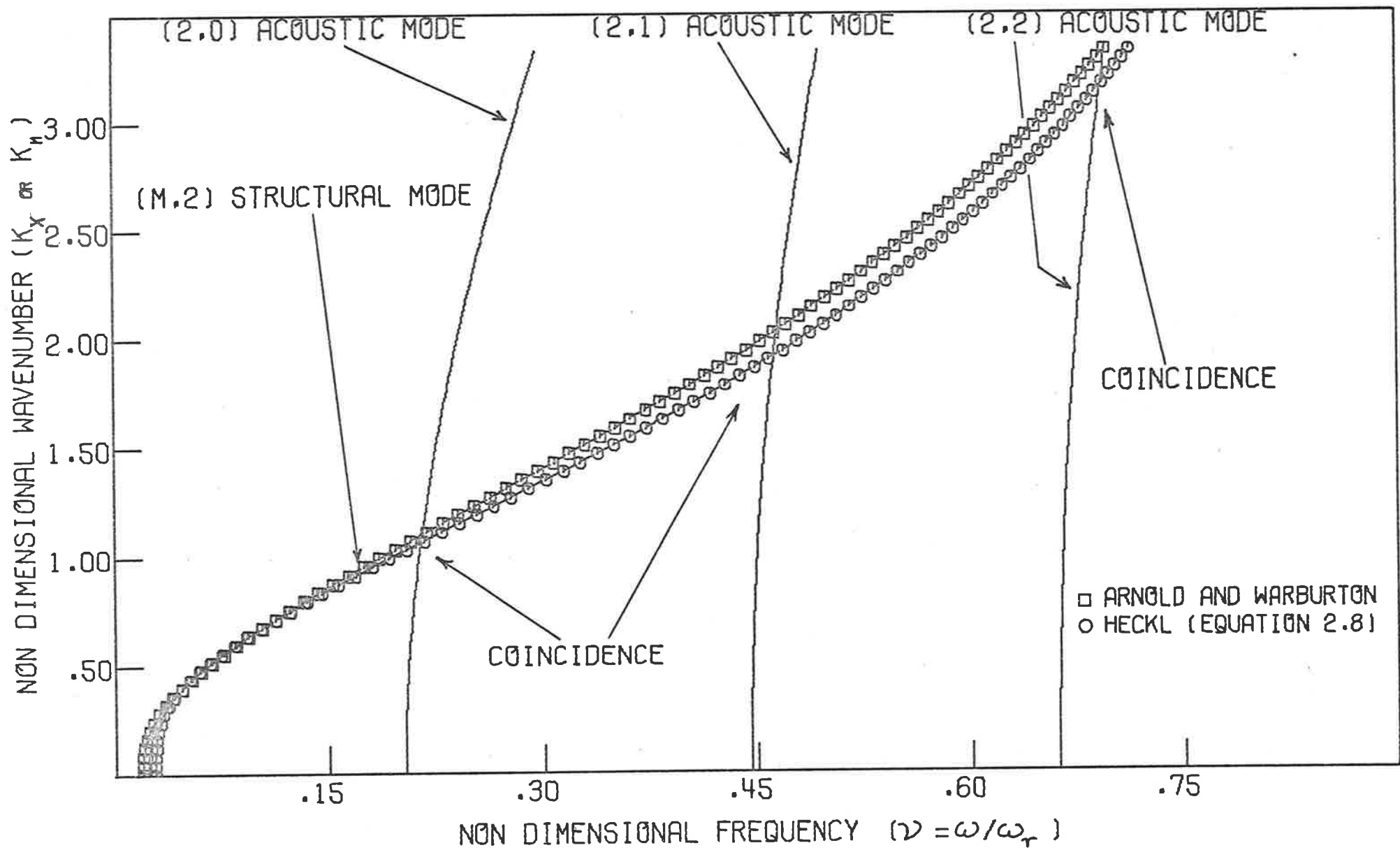


FIGURE 7.2 COINCIDENCE OF ACOUSTIC AND STRUCTURAL MODES.

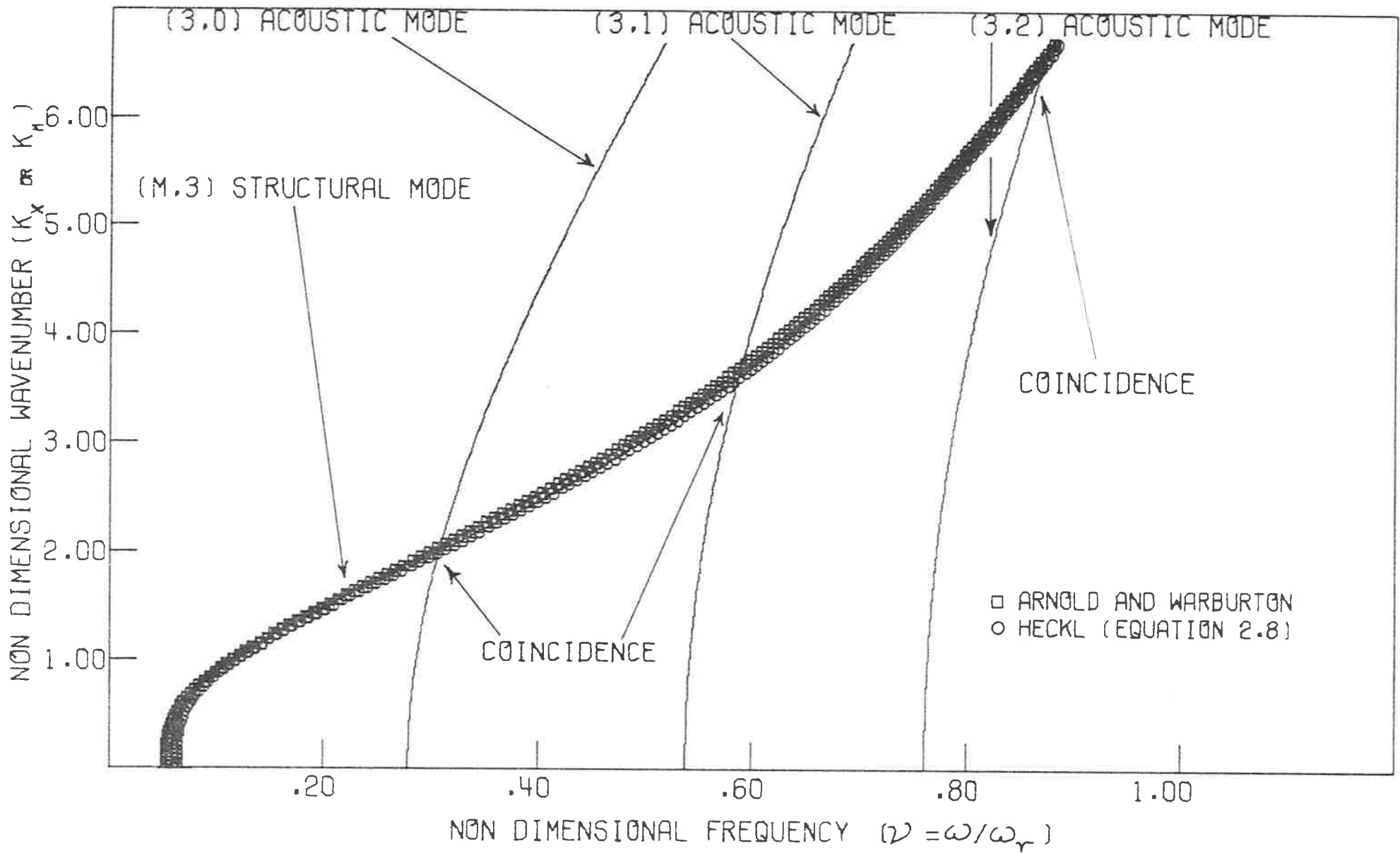


FIGURE 7.3 COINCIDENCE OF ACQUSTIC AND STRUCTURAL MODES.

mentioned earlier. Comparisons are made later in this chapter, between various theoretical predictions based on

(1) an "exact coincidence" approach where there is both wavenumber and frequency coincidence and where $K_m = K_x$ and $v_\alpha = v_c$, for the various higher order acoustic modes concerned. This approach assumed that K_m is continuous and that coincidence can occur at a non-integer values of m , thus there is no need for an estimation of individual resonance frequencies.

(2) a "wavenumber coincidence" approach where the various resonant frequencies are estimated using Heckl's equation (equation [2.8]). Here when $K_m = K_x$, v_α is not necessarily equal to v_c , but coincidence can only occur at integer m values.

(3) a "wavenumber coincidence" approach where the various resonant frequencies are estimated using Arnold and Warburton's (1953) method. Here, as in (2) above, when $K_m = K_x$, v_α is not necessarily equal to v_c , but coincidence can only occur at integer m values.

(4) a "mean wavenumber coincidence" approach based on the assumption that the acoustic mode wavenumber function intersects the resonant structural mode wavenumber function at a frequency that is equidistant from the structural modes on either side of it (i.e. for v_c lying between $v_{m,n}$ and $v_{m+1,n}$ then $v_c = (v_{m+1,n} + v_{m,n})/2$).

The "mean wavenumber coincidence" approach recognises the inability to accurately predict the various resonant structural modes for a practical piping system (since pipe wall thickness, end conditions,

effective length, etc are not precisely known). Since the ratio $(1-(v_\alpha/v_c)^2)^2$ is essentially the same for both structural modes in this case, the acoustic mode couples equally effectively with both structural modes and it is important that this is recognised when using this method. A discussion on the relative advantages and disadvantages of the four methods will be presented in the next section, following comparisons with several sets of experimental results.

The axial joint acceptance function, $j_{mm}^2(\omega)$, as given by equation [2.13] peaks sharply over a narrow frequency range for a particular structural mode order m . Hence coupling between the higher order acoustic mode and a particular structural mode is significant only within this narrow frequency range, which for purposes of estimation is taken to be the half-power bandwidth of the primary peak in $j_{mm}^2(\omega)$ (See Figure 2.3, section 2.4).

Theoretical estimates of the vibration response of and the acoustic radiation from the pipe depend on estimates of the total vibrational damping. The resonant response of a particular structural mode is dependent on its overall modal quality factor Q_α , as well as the degree of coupling between the excitation and the mode. The overall modal quality factor Q_α may be expressed by the relation

$$1/Q_\alpha = 1/Q_i + 1/Q_j + 1/Q_{rad} , \quad [7.3]$$

where Q_i is the internal quality factor corresponding to material damping, Q_j is the quality factor associated with the dissipation at structural joints and Q_{rad} is the modal quality factor associated with acoustic radiation damping. Rennison and Bull (1977) have investigated and reported on the modal density and damping of cylindrical pipes in considerable detail. The modal quality factor resulting from acoustic

radiation damping, Q_{rad} , is given by;

$$Q_{\text{rad}} = \omega M_{\alpha} / R_{\text{rad}} = \omega \rho_s h / \rho_f c_e \sigma_{\alpha}, \quad [7.4]$$

where ω is the radian frequency, M_{α} is the generalized mass of the mode, R_{rad} is the radiation resistance and σ_{α} is the radiation ratio. For steel structures, Q_i and Q_j are essentially independent of frequency and furthermore, for lightly damped structures, $Q_i \geq 1000$ and for rigid joints allowing no relative motion between the component parts, $Q_j > Q_i$ (Rennison and Bull, 1977).

The wavenumbers and phase velocities of the resonant sonic or supersonic vibrational modes of the pipe wall (i.e. modes having sonic or supersonic structural wavespeeds with respect to the external acoustic medium) are more closely matched by the higher order propagating acoustic modes than the subsonic modes, hence $\sigma_{\alpha} \approx 1$ for these structural modes. Cylindrical pipes have supersonic structural modes at frequencies well below the acoustic coincidence frequency, v_{ac} , of a flat plate with the same thickness as the pipe wall. For the test section used in the present work ($\beta = 0.0070$), it has been found experimentally by Rennison (1976), and in the present work that supersonic vibrational modes occur for $v \geq 0.078$, while higher order acoustic modes can occur for $v \geq 0.121$. Under these conditions, Q_{rad} is very much less than both Q_i and Q_j , and dominates the modal quality factor Q_{α} . In the subsequent theoretical estimates, a value of $Q_i = 2000$ is assumed and Q_j is neglected (Rennison and Bull, 1977); hence

$$Q_{\alpha} \approx 2000 \omega \rho_s h / (\omega \rho_s h + 2000 \rho_f c_e) . \quad [7.5]$$

A narrow-band analysis of the wall pressure fluctuations (Chapter 4) shows that there is a sharp rise in power spectral density

(of the order of 4 to 10dB) at the cut-off frequencies of the first few higher order modes and in particular the (1,0) and (2,0) higher order modes. The asymmetric flow disturbances do not appear to excite the symmetric (0,1) higher order mode. Above the (3,0) mode, the density of the higher order modes becomes increasingly greater and the individual higher order modes become harder to detect. To theoretically estimate the pipe wall response, the wall pressure fluctuations have to be estimated (a) over the frequency band of interest (ν_1 to ν_2) in order to estimate I_p , and (b) over the narrow bandwidth over which the joint acceptance function peaks and coincidence occurs to estimate the numerator in equation [7.1].

For any particular severe flow disturbance and the piping geometry used in this investigation, the first few higher order acoustic modes are well separated in frequency, and the wall pressure fluctuations display a sharp rise at cut-off. Then in a $\frac{1}{3}$ -octave band ranging from ν_1 to ν_2 containing one of these higher order modes

$$I_p = \int_{\nu_1}^{\nu_2} \Phi_p(\nu) d\nu \approx \int_{\nu_{co}}^{\nu_2} \Phi_p(\nu) d\nu \approx \Phi_p \Delta\nu_B, \quad [7.6]$$

where $\Delta\nu_B = \nu_2 - \nu_{co}$. This is illustrated in Figure 7.4. At higher frequencies, where the density of the higher order modes is greater and there is no obvious sharp rise in the wall pressure fluctuations at the cut-off frequencies of the various higher order modes in the $\frac{1}{3}$ -octave band of interest,

$$I_p = \int_{\nu_1}^{\nu_2} \Phi_p(\nu) d\nu \approx \Phi_p(\nu_2 - \nu_1). \quad [7.7]$$

In general if there are several higher order modes in a $\frac{1}{3}$ -octave band, there is no obvious sharp rise in the wall pressure fluctuations at the

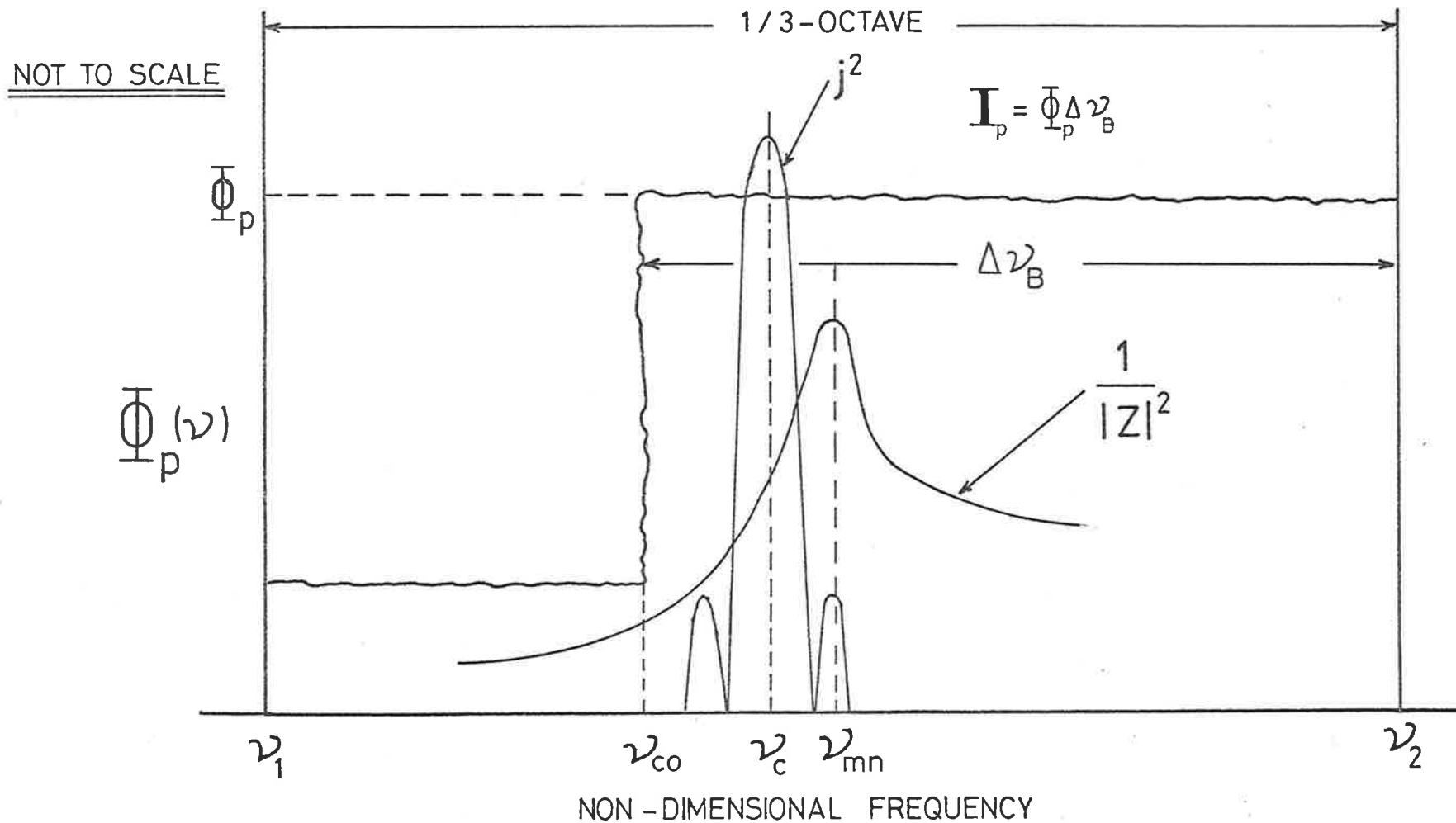


FIGURE 7.4 SCHEMATIC ILLUSTRATION OF THE ESTIMATION OF \mathbf{I}_p IN A 1/3-OCTAVE BAND

cut-off frequencies of the various higher order modes, as can be seen from the present experiments, at frequencies well above the cut-off frequency of the (2,0) higher order acoustic mode. However, the occasion could arise for a particular piping geometry when the first two or three higher order modes are sufficiently close in frequency that they occur in a single $\frac{1}{3}$ -octave band. In that case, equation [7.7] would overestimate the wall pressure fluctuations. Equation [7.6] with v_{co} as the cut off frequency of the first higher order mode would give a more accurate estimation.

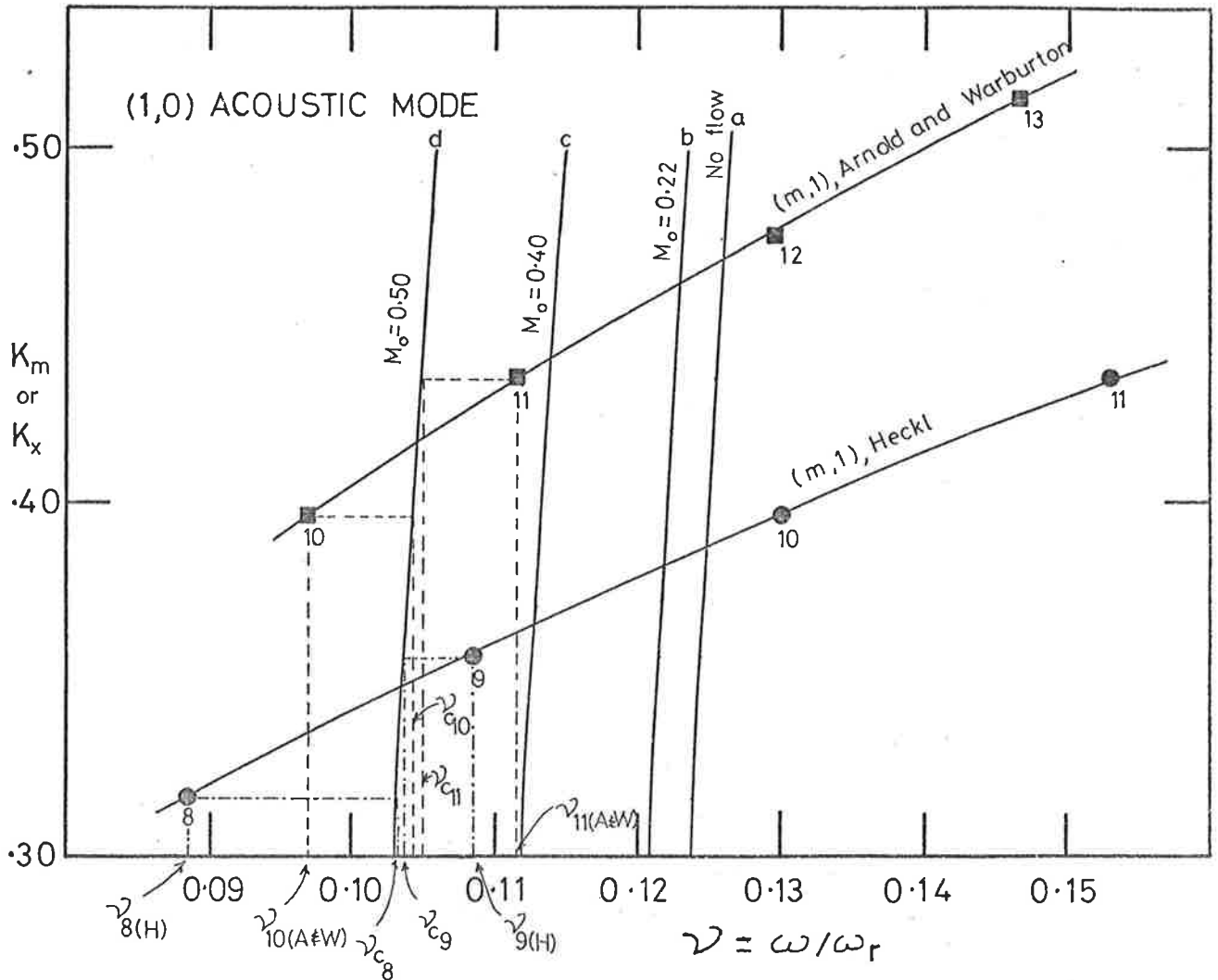
Over the narrow frequency bandwidth over which the joint acceptance function peaks and coincidence occurs, $\Phi_p(v)$ is essentially constant and equal to Φ_p (see Figure 7.4).

Hence, with this understanding of the behaviour of the receptance function, the modal quality factor Q_{α} , the joint acceptance function $j_{\alpha\alpha}^2$ and the wall pressure fluctuations, a theoretical estimation of the pipe wall vibration response and hence the acoustic radiation due to the higher order acoustic modes in various $\frac{1}{3}$ -octave bands can be made. It should be remembered that this "theoretical estimate" is based on the experimental observation that pipe wall response and acoustic radiation effects are greatest at frequencies close to the cut-off frequencies of the various higher order internal acoustic modes due to the coincidence effects that have been discussed in Chapter 2 and in this section. Of the four methods mentioned for making the theoretical estimates, it should be mentioned that the fourth method (for the case where $v_c = (v_{m+1,n} + v_{m,n})/2$) is the most realistic one for a practical piping system; this will become evident from a reading of the next section.

7.3 COMPARISON WITH VARIOUS EXPERIMENTAL MEASUREMENTS

The results and discussion presented in this section relate to a comparison between theoretical estimates for "exact coincidence", the three separate "wavenumber coincidences" and experimental measurements for the various internal flow disturbances. They all relate to the vibrational response of and the acoustic radiation from the thin-walled cylindrical test-section, for which $\beta=0.0070$, $\Psi=0.960$, $\Lambda=79.4$ and $M_{LP}=15.37$, which spans the anechoic chamber.

The frequencies of the $(m,1), \dots, (m,5)$ resonant structural modes were computed using both equation [2.8] (Heckl, 1962) and Arnold and Warburton's (1953) thin shell theory. The first fifteen higher order acoustic modes that would couple to these structural modes were considered (excluding the $(0,1)$, $(0,2)$ and $(0,3)$ modes which do not couple to structural modes) and these are listed in Table A-1 (Appendix A). These fifteen "coincidences" were found to be distributed in frequency in various ways (depending on M_0 , since flow affects the cut-off frequency and hence the frequency for coincidence) in $\frac{1}{3}$ -octave bands ranging from 2.5kHz to 16 kHz. The two structural modes (one on each side) closest to the acoustic mode, for each of the fifteen acoustic modes can then be determined for the two respective theories used. The frequencies at which $K_x = K_m$ correspond to the coincidences between the two structural modes and the acoustic mode, hence v_α/v_c can be found for both structural modes for both theories used. This is illustrated in Figure 7.5 for coincidence between the $(1,0)$ higher order acoustic mode and the $(m,1)$ structural modes. The half-power bandwidth of the primary peak in the axial joint acceptance function, $j_{mm}^2(\omega)$, can be estimated for a particular coincidence to be



n	m	K_x or K_m	$\nu_{A\&W}$	ν_{Heckl}	$\nu_{(1,0)_a}$	$\nu_{(1,0)_b}$	$\nu_{(1,0)_c}$	$\nu_{(1,0)_d}$
1	8	.3166	—	.0878	.1238	.1209	.1119	.1031
1	9	.3562	—	.1084	.1243	.1214	.1126	.1036
1	10	.3957	.0969	.1302	.1248	.1219	.1131	.1042
1	11	.4353	.1129	.1532	.1253	.1225	.1137	.1048
1	12	.4749	.1294	—	.1259	.1231	.1144	.1054
1	13	.5145	.1464	—				

NOTE COINCIDENCES ILLUSTRATED (ie. $\nu_{c8}, \nu_{c9}, \nu_{c10}, \nu_{c11}$) ARE FOR (1,0) ACOUSTIC MODE, $M_0 = 0.50$.

FIGURE 7.5 ILLUSTRATION OF ESTIMATION OF ν_{mn} / ν_c USING (a) HECKL'S, and (b) ARNOLD & WARBURTON'S EQUATIONS

$$\Delta v_{j_m} \approx 0.45(v_b - v_a) \quad [7.8]$$

where $v_i^2 = v_{co}^2 + \left(\frac{K_{x_i}}{M_{LP}}\right)^2$ for $i=a,b$, and where $K_{x_a} = \left(\frac{m-2}{m}\right)K_m$ and $K_{x_b} = \left(\frac{m+2}{m}\right)K_m$ represent the minima associated with the primary peak in the axial joint acceptance function for a particular K_m . This is illustrated in Figure 7.6. The modal quality factor Q_α and the wall pressure fluctuations, I_p and ϕ_p , can be estimated fairly readily as described in section 7.2, and ρ_{fs} , M_0 , β and M_{LP} can be obtained for a particular flow speed and cylinder geometry. Hence, if it is assumed that because of the sharp maximum associated with the joint acceptance and the narrow frequency bandwidth associated with it, the effects of coincidence for a particular structural and acoustic mode are confined to frequencies within the range Δv_{j_m} , then equation [7.1] reduces to

$$\frac{I_\zeta}{I_p} = \frac{(0.250)^2 \rho_{fs}^2 M_0^3 a_i}{12\beta^2 M_{LP}^3 a_m \Delta v_B} \sum_{\alpha} \frac{\Delta v_{j_m}}{\left(1 - \left(\frac{v}{v_c}\right)^2\right)^2 + \left(\frac{v}{v_c} \frac{1}{Q_\alpha}\right)^2} \quad [7.9]$$

where $j_{mm(max)}^2(v) \cdot j_{nn}^2(v) = (0.250)^2$, v_c is the coincidence frequency and $\Delta v_B = (v_2 - v_{co})$ or $(v_2 - v_1)$ depending on the $\frac{1}{3}$ -octave band under consideration (see Equation [7.6] and [7.7]). Hence the problem reduces to one of estimating Δv_b , Δv_j , v_α , v_c and Q_α for various coincidences between resonant structural and higher order acoustic modes in several $\frac{1}{3}$ -octave bands, and hence computing corresponding values of I_ζ/I_p . The non-dimensional mean square acoustic radiation, I_π , can be expressed as (see Appendix B)

$$\frac{I_\pi}{I_p} = \frac{I_\zeta}{I_p} \cdot \frac{M_{LP}}{v_c^2} \quad [7.10]$$

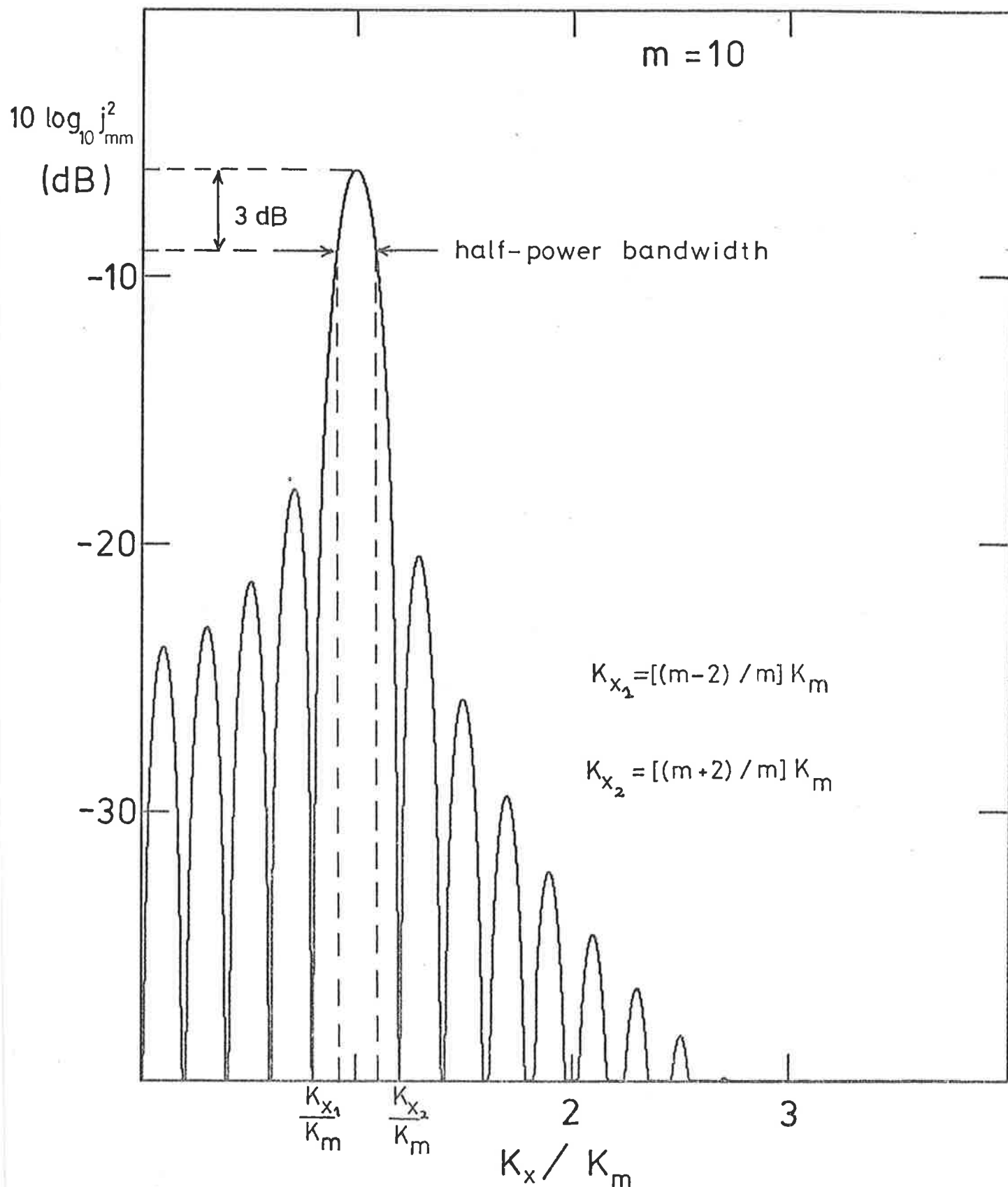


FIGURE 7.6 AXIAL JOINT ACCEPTANCE
(estimation of half-power bandwidth)

As mentioned in the previous section, equations [7.9] and [7.10] were evaluated in $\frac{1}{3}$ -octave bands ranging from 2.5 kHz to 16 kHz, using the four methods mentioned. It should be noted that the various higher order acoustic modes were allocated to the $\frac{1}{3}$ -octave bands in which the corresponding coincidence occurred: if cut-off for the (1,0) mode occurred in the 2.5 kHz frequency band and for a particular flow speed, $v_{c(1,0)}$ occurred in the 3.15 kHz frequency band, then the sum was computed for the 3.15 kHz band with $\Delta v_B = (v_2 - v_1) 3.15 \text{ kHz}$ instead of $\Delta v_B = (v_2 - v_{co}) 2.5 \text{ kHz}$.

A comparison of the four theoretical estimates and experimental results for various internal flow disturbances for $M_0 \sim 0.20, 0.40, 0.50$ for (a) I_ζ/I_p and (b) I_π/I_p is presented in Figures 7.7 to 7.12. All the theoretical estimate points were computed following the procedures described earlier in this section and in section 7.2. The experimental results as presented in Chapters 4 and 5 were derived from $\frac{1}{3}$ -octave band measurements.

The most striking observation from all six figures is that the "exact coincidence" approach overestimates both the pipe wall response and the acoustic radiation by 30-45 dB. Exact coincidence implies that $v_\alpha = v_c$ and that the receptance function is only dependent on the modal quality factor Q_α . The "wavenumber coincidence" approaches based on (1) Equation [2.8] and (2) Arnold and Warburton's "exact" equation yield better estimates. Here $v_\alpha \neq v_c$, and the $(1 - (v_\alpha/v_c)^2)^2$ term dominates the receptance function. Because neither v_α nor v_c cannot be predicted sufficiently accurately to give an accurate prediction of v_α/v_c , these two approaches could possibly yield gross overestimates in certain $\frac{1}{3}$ -octave bands in comparison with the actual experimental results; this is evident in several $\frac{1}{3}$ -octave bands in Figures 7.7 to

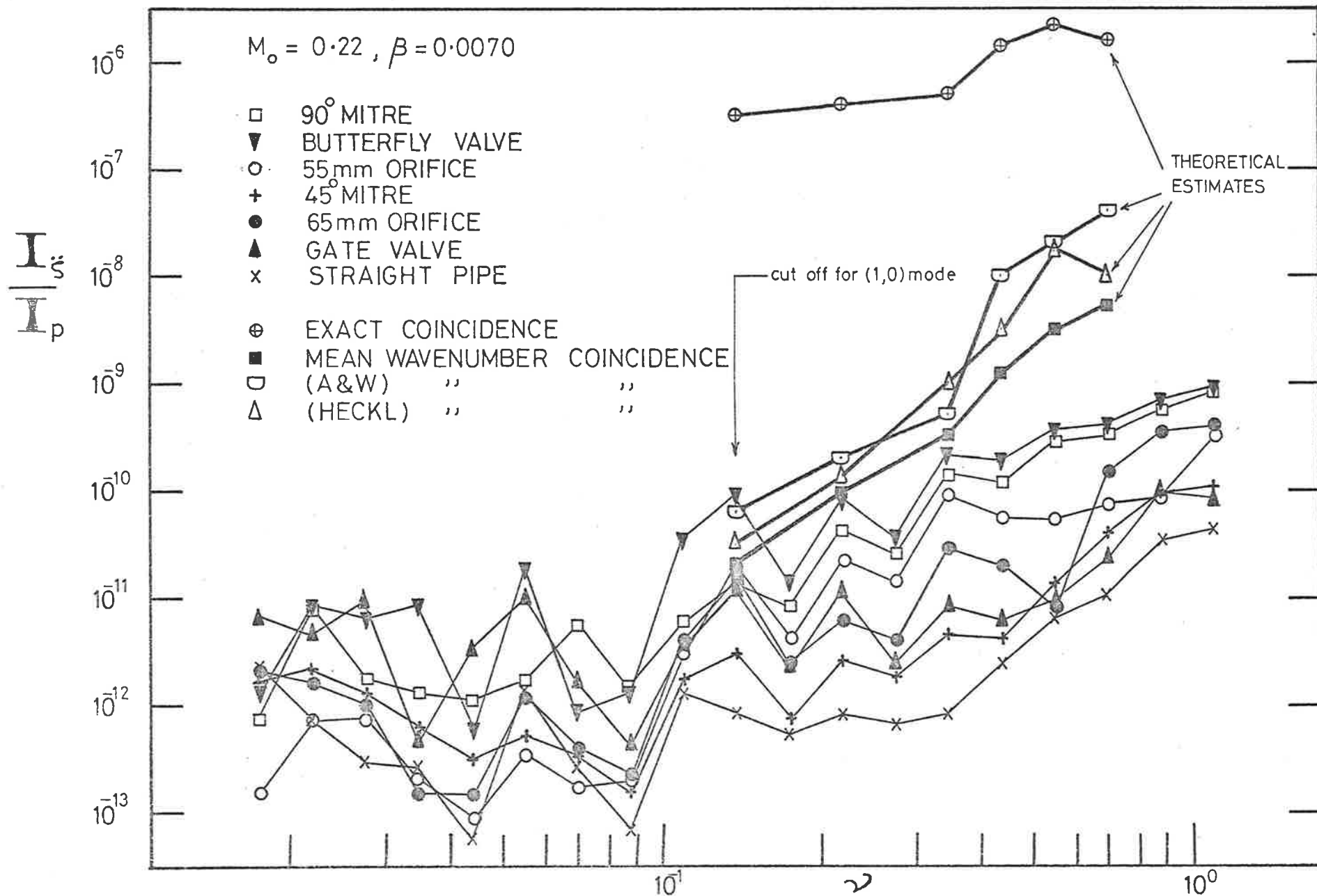


FIGURE 7.7 I_s/I_p - COMPARISON OF THEORETICAL ESTIMATES AND EXPERIMENTAL RESULTS

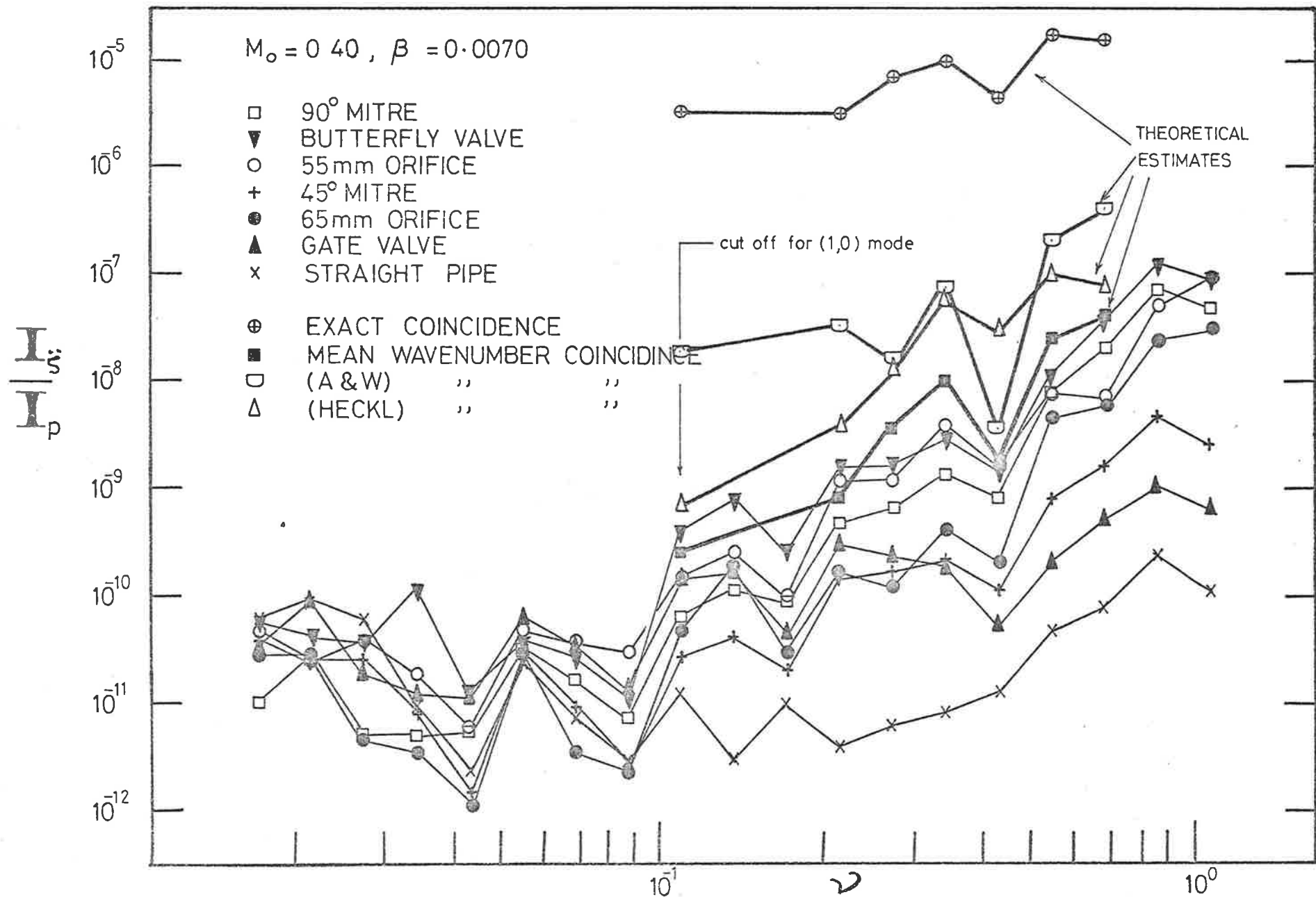


FIGURE 7.8 I_s / I_p - COMPARISON OF THEORETICAL ESTIMATES AND EXPERIMENTAL RESULTS

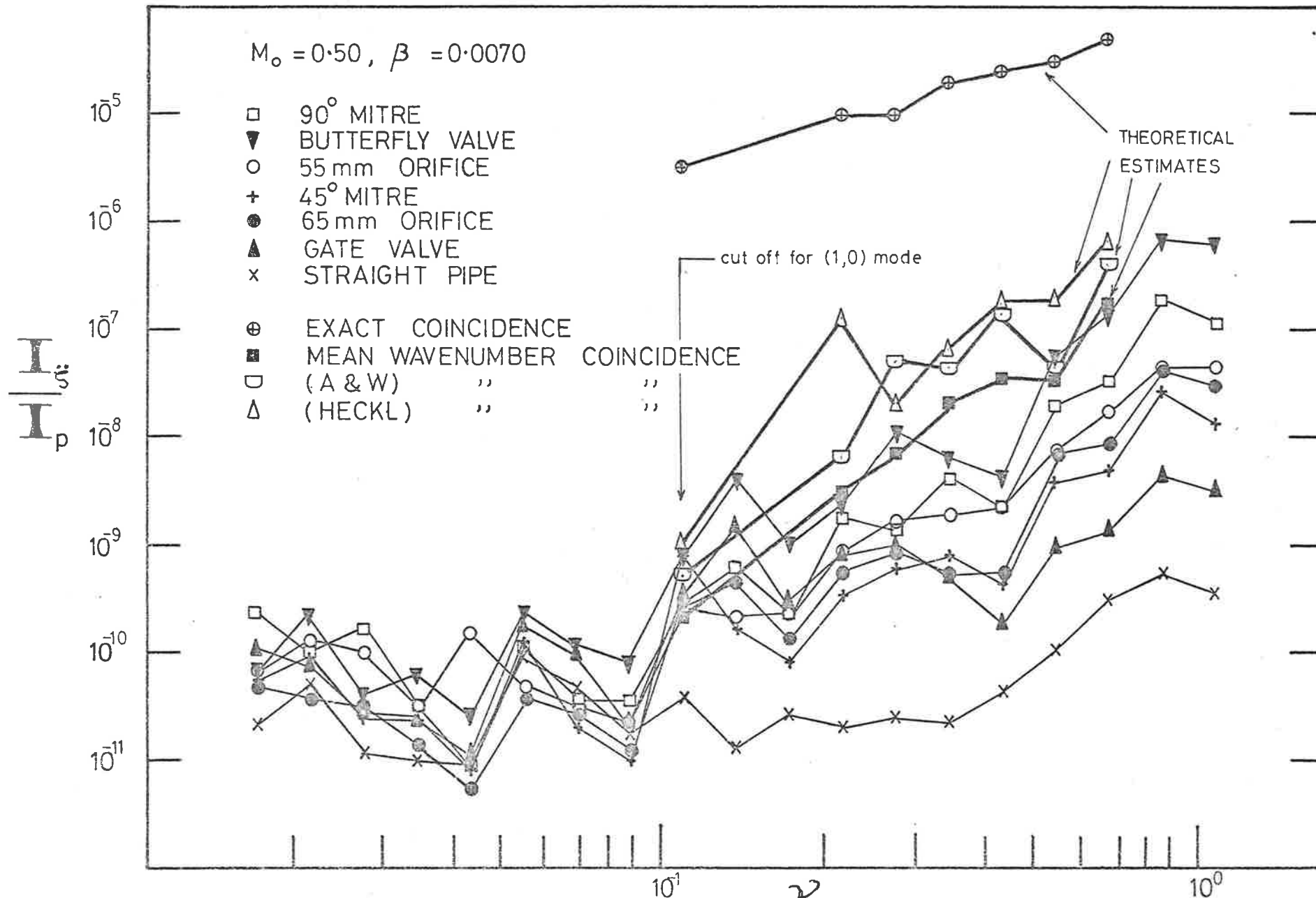


FIGURE 7-9 I_s/I_p - COMPARISON OF THEORETICAL ESTIMATES AND EXPERIMENTAL RESULTS

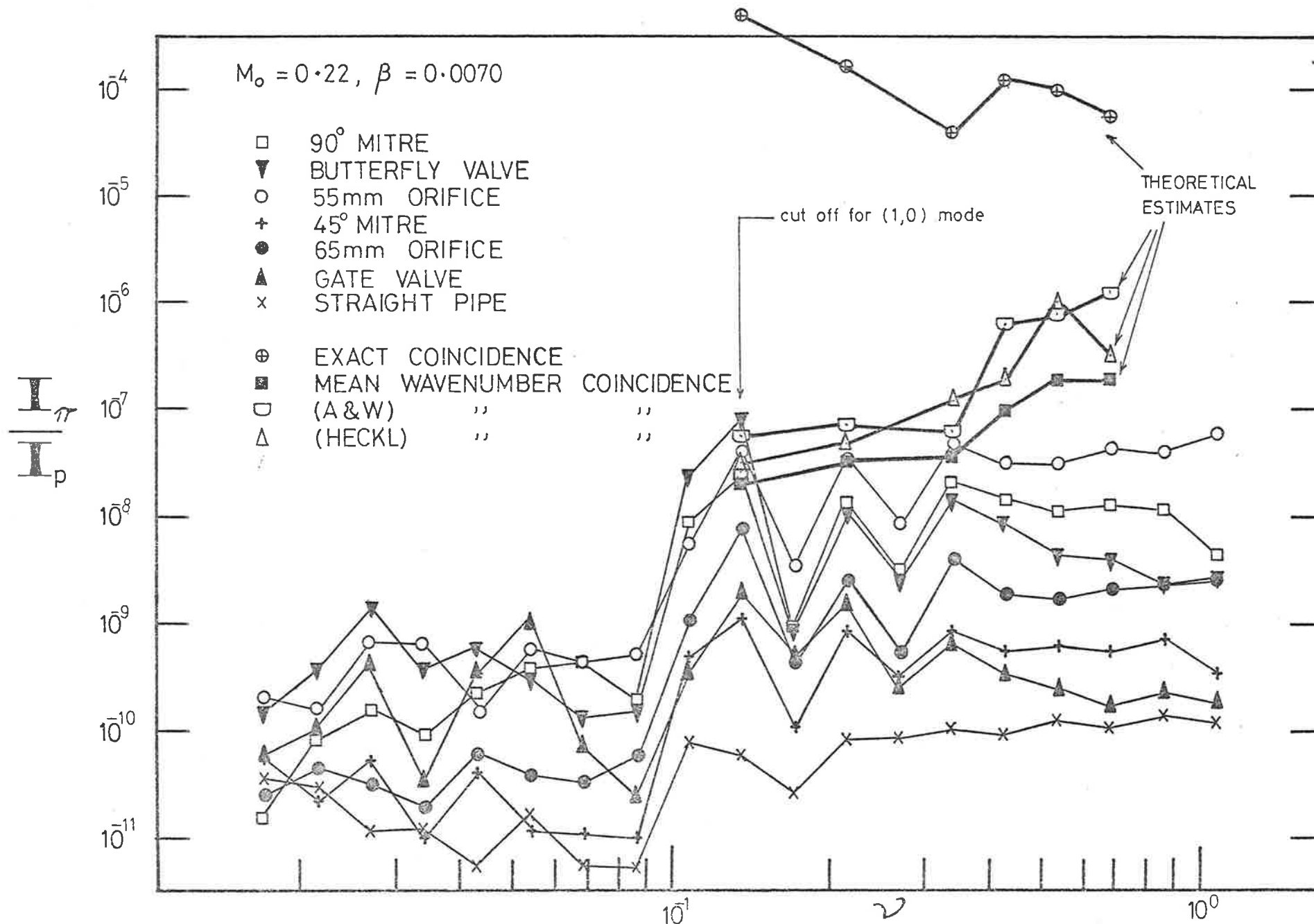


FIGURE 7.10 I_{π} / I_p - COMPARISON OF THEORETICAL ESTIMATES AND EXPERIMENTAL RESULTS

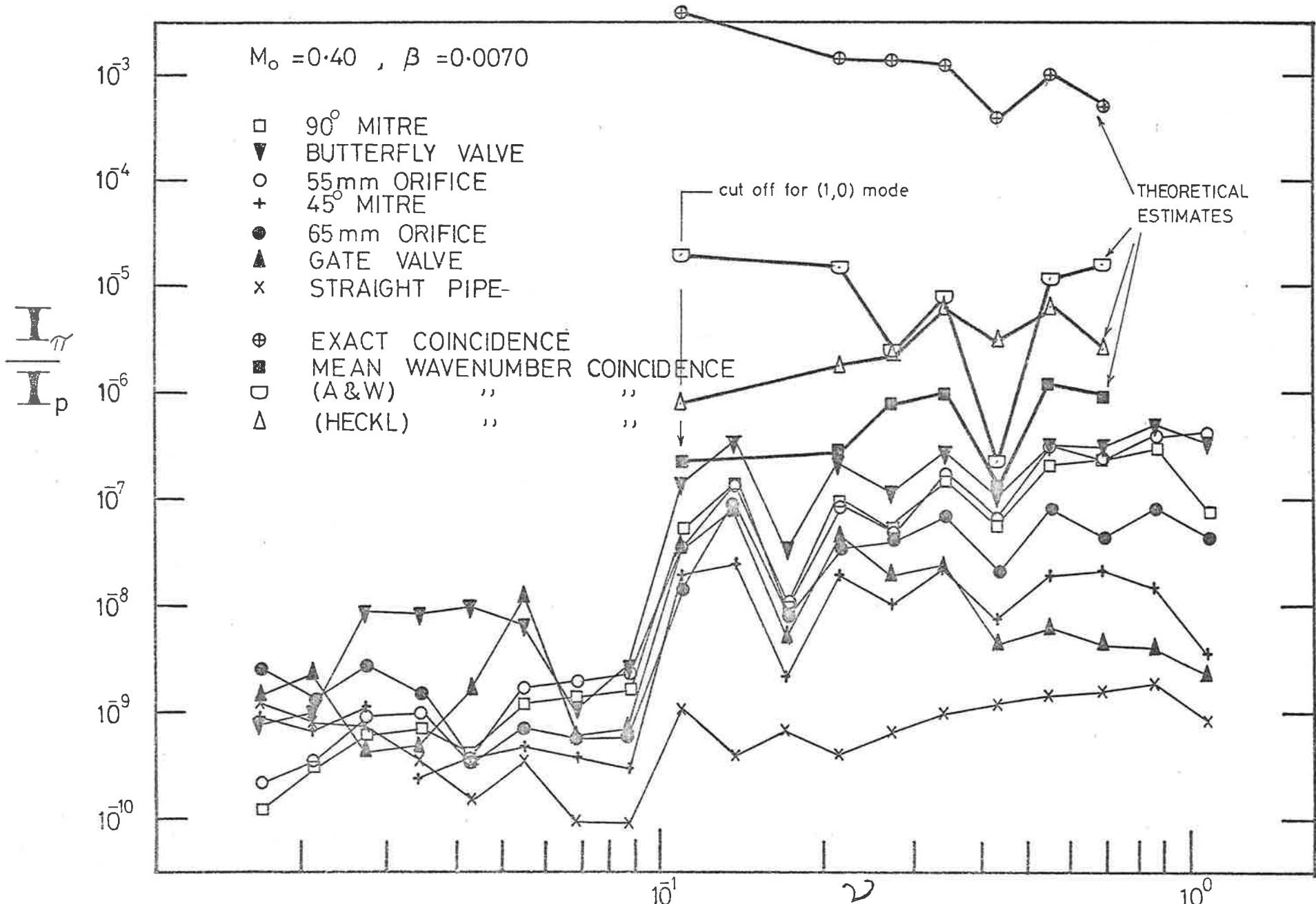


FIGURE 7.11 I_{η} / I_p - COMPARISON OF THEORETICAL ESTIMATES AND EXPERIMENTAL RESULTS

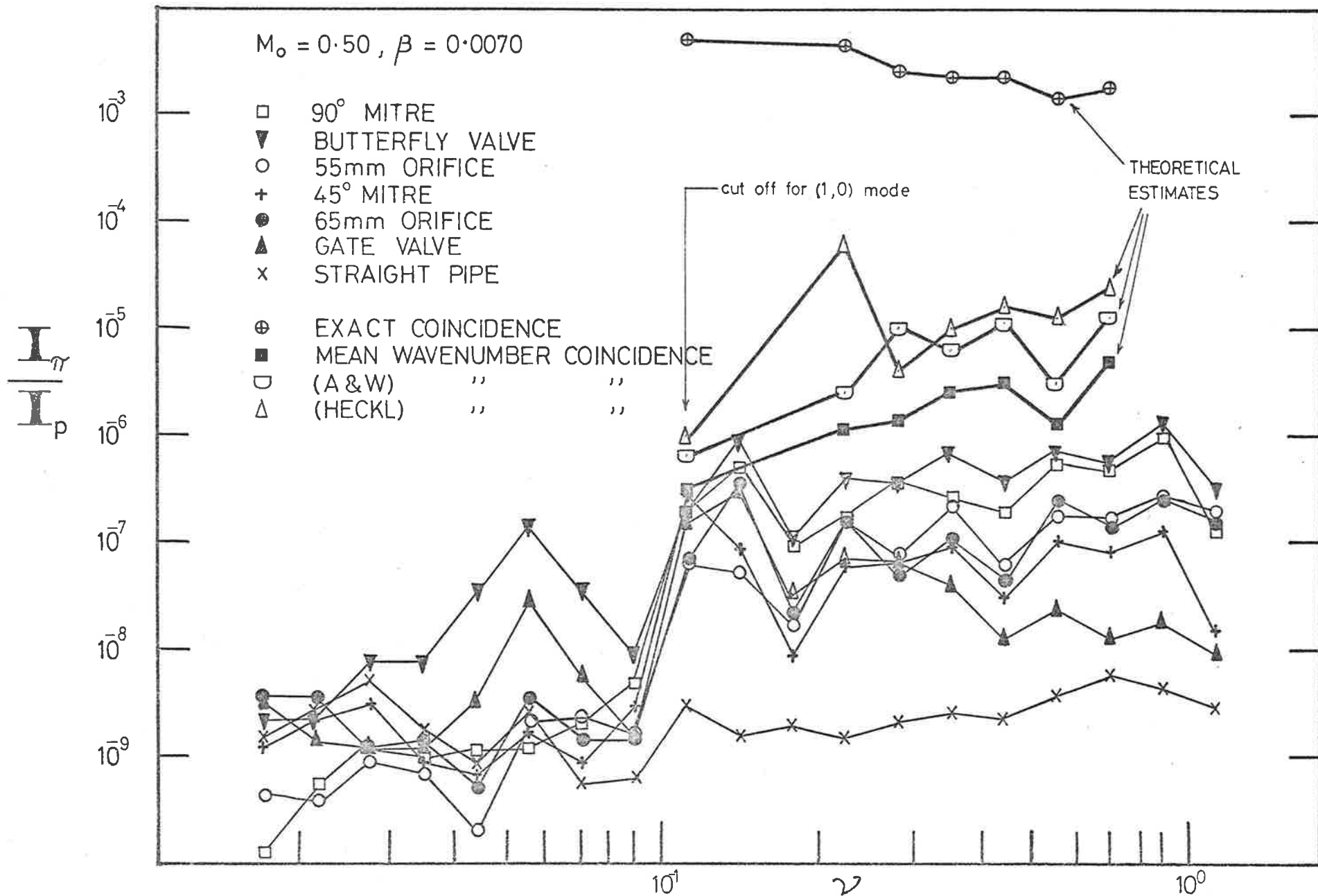


FIGURE 7.12 I_π / I_p - COMPARISON OF THEORETICAL ESTIMATES AND EXPERIMENTAL RESULTS

7.12. These gross overestimates occur because the structural mode is predicted to be closer to the acoustic modes than it is. A gross underestimate cannot occur because the acoustic mode couples to structural modes on either side, and as it moves away from one structural mode it moves closer to the other. The problem of gross overestimation can be overcome by adopting the "mean wavenumber coincidence" approach based on the assumption that the acoustic mode wavenumber function intersects the resonant structural mode wavenumber function at a frequency that is equidistant from the structural modes on either side of it. This approach might yield a slight underestimate in the pipe wall response, but the gross overestimates that could occur in the other two wavenumber coincidence approaches are avoided. This is observed in Figures 7.7 to 7.12 and this approach yields the best agreement between experiment and theory.

It should be pointed out here, that equations [7.9] and [7.10] which were used to obtain the results, assume that all the wall pressure fluctuations in the $\frac{1}{3}$ -octave bands considered are directly attributable to the higher order acoustic modes, and that contributions from turbulent pressure fluctuations and plane waves are negligible. The results of Chapter 6 indicate that this is indeed the case for the (1,0) and the (2,0) higher order modes for the 90° mitred bend in particular. This is confirmed by the wall pressure spectra themselves which shows a sharp rise in $\Phi_p(\omega)$ at cut-off for the first two higher order modes. This trend is also observed in the results for the butterfly valve and the 55 mm orifice plate. For these three flow disturbances, at higher frequencies, $\Phi_p(\omega)$ approaches straight pipe pressure fluctuation levels and any higher order modes present are not detectable in the spectra.

This is also the case at all frequencies for the milder flow disturbances. Nevertheless, for the milder flow disturbances investigated (with the exception of the radiused bends), the higher order modes couple more efficiently to the structural modes than either the plane waves or the turbulent pressure fluctuations. This is apparent from their dominance of the spectral data presented in Chapters 4 and 5 - i.e. the higher order modes dominate the pipe wall response and the acoustic radiation at frequencies above cut off for the (1,0) mode for the 90° mitred bend, the butterfly valve, the 45° mitred bend, the gate valve and both orifice plates. Equations [7.9] and [7.10] assume that all the wall pressure fluctuations are due to the higher order modes. When the higher order modes are not dominant and make up a proportion, α_p , of the total power spectral density of the wall pressure fluctuations, then equation [7.9] has to be multiplied by this factor, α_p . Hence, the procedures used would be expected to overestimate the pipe wall response at higher frequencies (above the (2,0) mode) for the severe flow disturbances and at all frequencies for the mild flow disturbances. This can be overcome by using the techniques described in Chapter 6 (which were applied to the 90° mitred bend only) to estimate the contribution of the higher order modes to the wall pressure fluctuations for the various disturbances. There is extensive experimental work involved, but it is beyond the scope of this investigation. However it is felt that the use of such information could greatly reduce the discrepancy between the "mean wavenumber coincidence" theoretical estimate and the experimental results for the mild flow disturbances.

7.4 THICK WALLED CYLINDERS

All of the analysis so far presented relates to thin-walled pipes and all experimental results presented relate to thin-walled pipes

with $\beta=0.0070$. Additional experimental data are introduced here, for a pipe with much greater wall thickness, $\beta=0.04648$ (i.e. approximately 7 times the wall thickness of the thin-walled pipe), in order to give some indication of the effect of wall thickness as such, and to establish whether or not the estimation procedures discussed in the previous sections of this Chapter can be applied to much thicker cylindrical shells which are more representative of industrial piping systems.

The thick-walled cylinder, for which $\Psi=0.960$, $\Lambda=75.7$, $h=6.35$ mm, and $M_{LP}=15.37$, was situated in the same position as the thin-walled cylindrical test section i.e. spanning the anechoic chamber. Measured values of the effects of the various internal flow disturbances on the pipe wall acceleration and the acoustic radiation are presented and comparisons are made with the thin-walled cylinder.

7.4.1 Acceleration Response of and Acoustic Radiation from the Test Section

The power spectral density, $\phi_{\zeta}^{\ddot{}}$, of the acceleration of the test section wall, and, ϕ_{π} , of the acoustic power radiated have been measured in the same way as for the thin-walled pipe. Here too, it was found experimentally that $\phi_{\zeta}^{\ddot{}}$ and ϕ_{π} are axially and circumferentially uniform over the test section within ± 1 dB. The results presented in Figures 7.13 to 7.16 are those obtained at the mid point of the test section for $M_0 \sim 0.40$ and 0.50 .

As for the thin-walled cylinder, there are substantial increases in spectral density as ν rises above 0.10; effects are greatest at frequencies close to the cut-off frequencies of various higher order internal acoustic modes, due to coincidence between the various acoustic modes and particular resonant structural modes. The results presented are

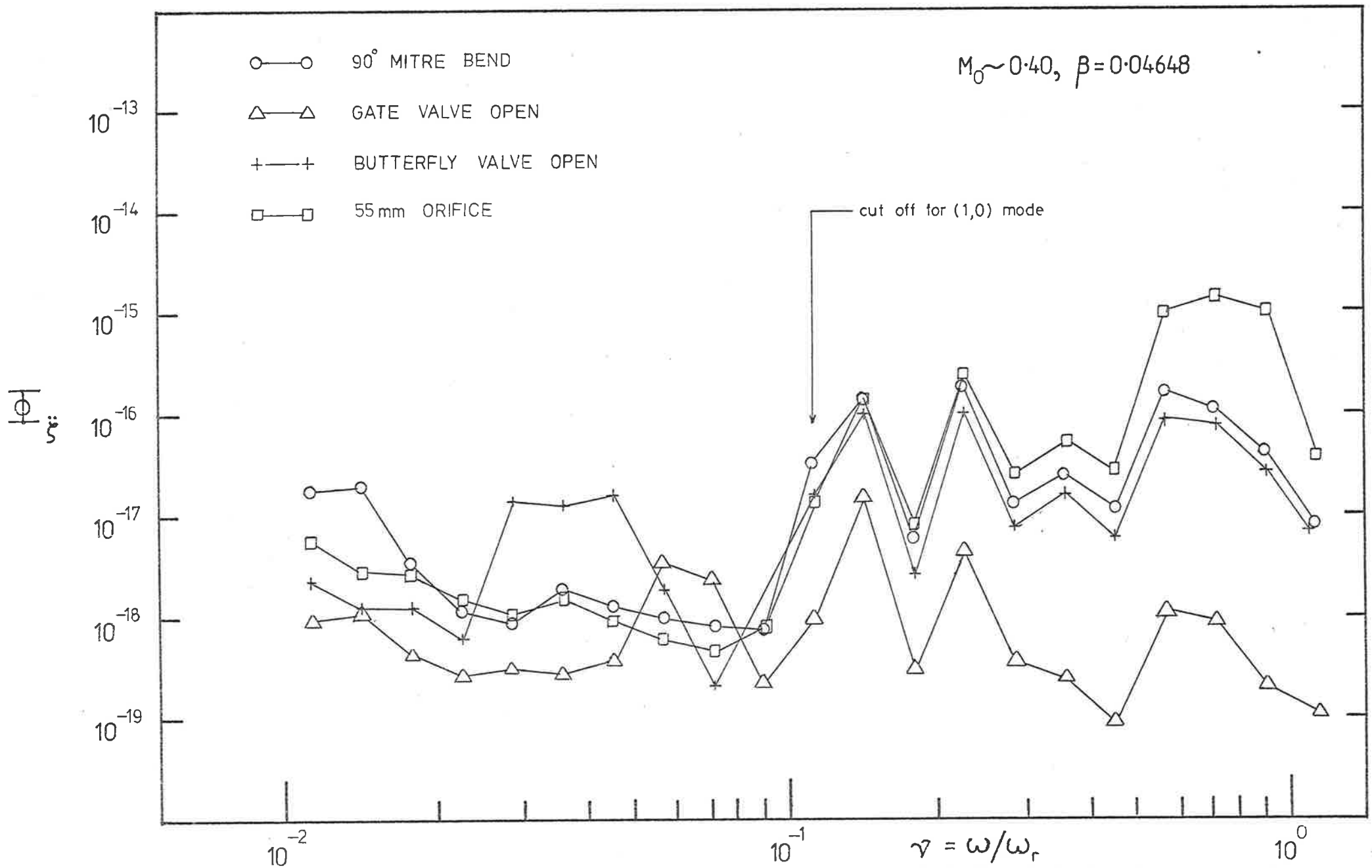


FIG 7.13 THICK WALL PIPE NON-DIMENSIONAL ACCELERATION SPECTRA

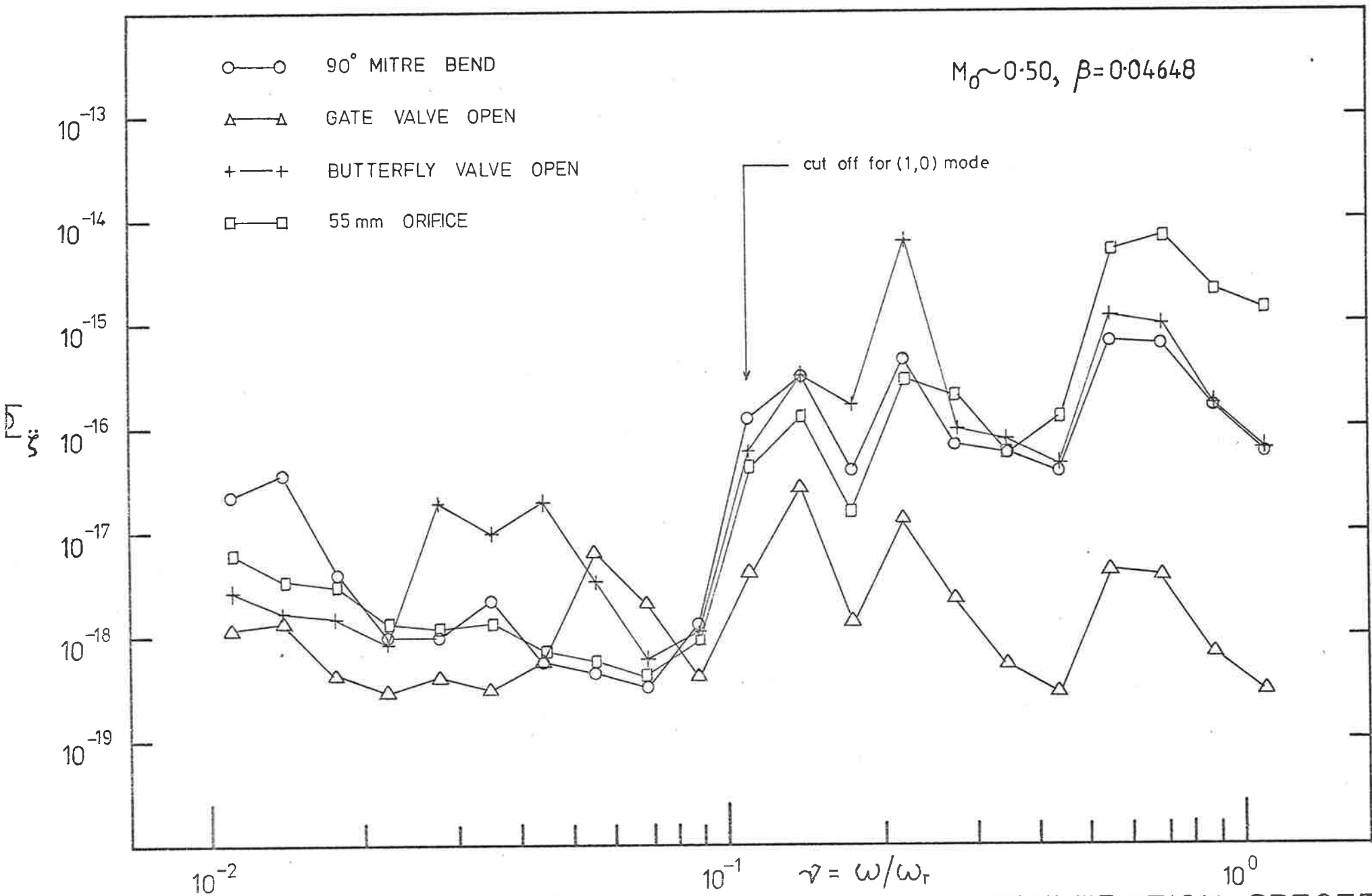


FIG 7.14 THICK WALL PIPE NON-DIMENSIONAL ACCELERATION SPECTRA

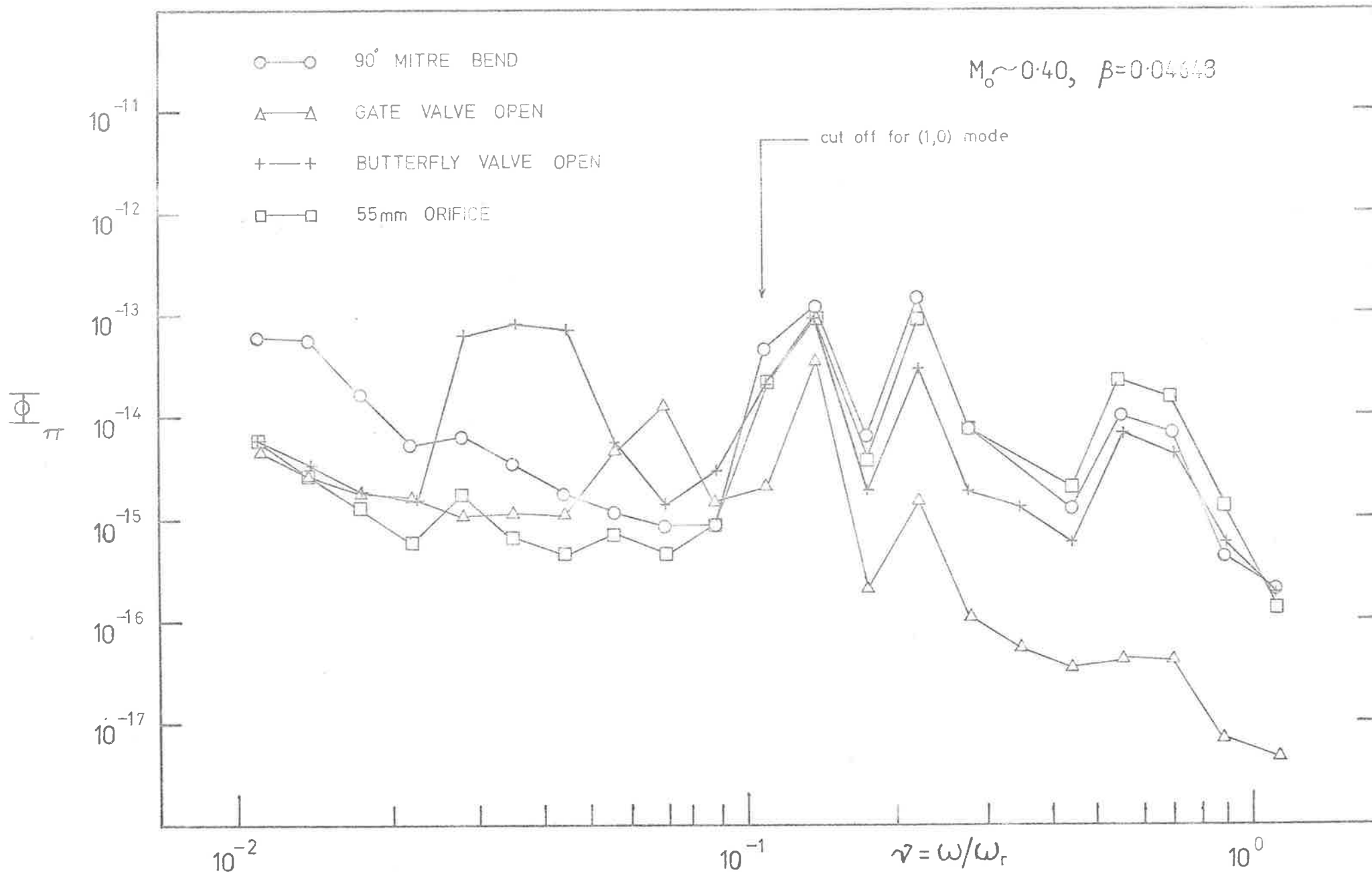


FIG 7.15 THICK WALL PIPE NON-DIMENSIONAL ACOUSTIC POWER RADIATION

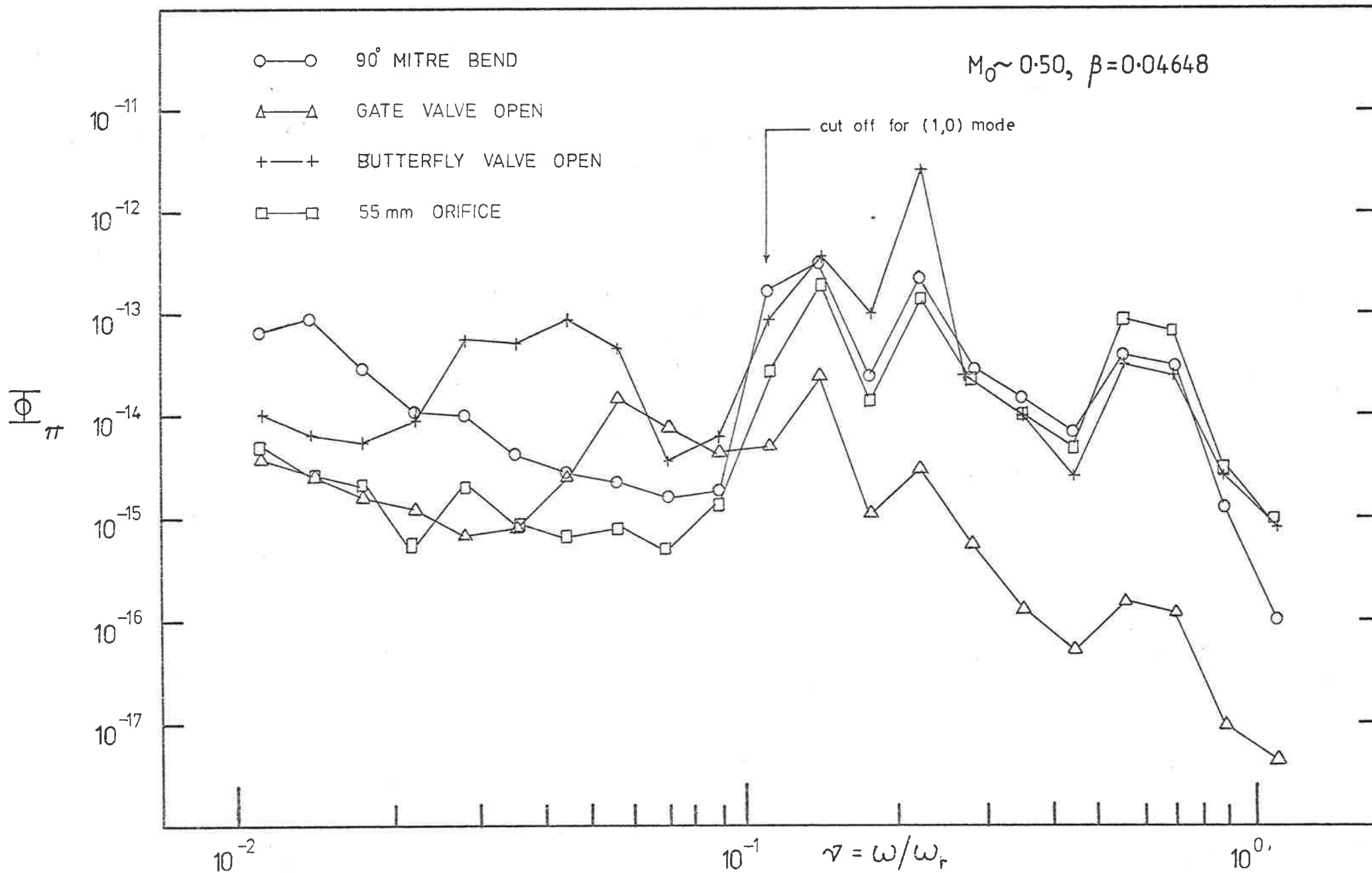


FIG 7.16 THICK WALL PIPE NON-DIMENSIONAL ACOUSTIC POWER RADIATION

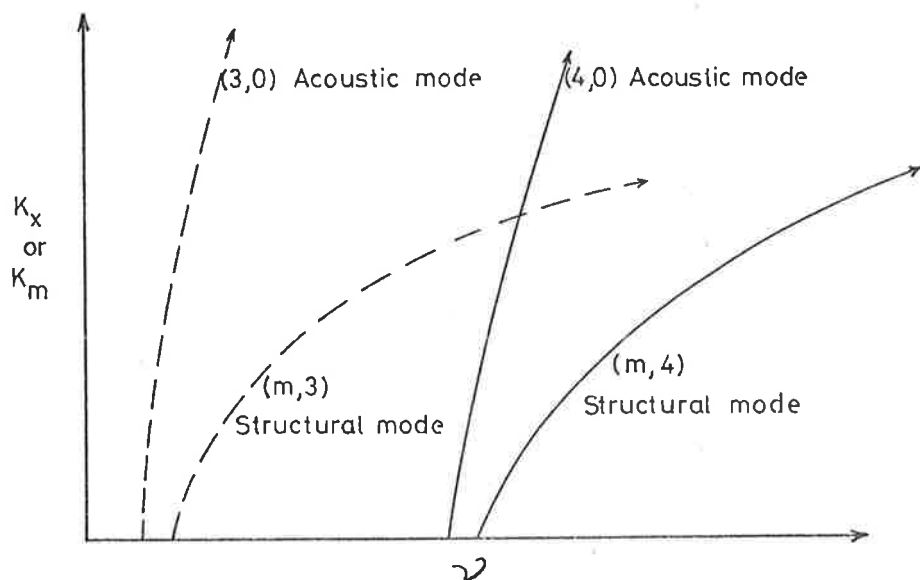
typical of all flow speeds investigated. The interesting point to be noted here is that there is a drop in pipe wall response and acoustic power radiation in the frequency range $0.30 \leq \nu \leq 0.47$ when compared with other frequencies above the cut off frequency of the (1,0) higher order acoustic mode. The reason for this is as follows. For the $\beta=0.04648$ pipe, calculation of the resonance frequencies of the pipe structural modes, using Arnold and Warburton's (1953) theory, shows that in the frequency range $0.30 \leq \nu \leq 0.47$, the only coincidence possible is that between the (m,1) resonant structural modes and the (1,1) higher order acoustic mode. This is because the cut-off frequencies of the other higher order acoustic modes in this frequency range occur at frequencies well below the lowest possible frequency of the resonant structural modes with matching circumferential wavenumbers ($n=p$); because of the nature of the dispersion (wavenumber - frequency) characteristics of the higher order acoustic modes (see Figures 7.1 to 7.3) this implies that in these particular cases, coincidence can never occur. This is illustrated in Table 7.1, where the (m,3) resonant structural modes "cut off" at a higher frequency than the (3,0) higher order acoustic mode, the (m,4) resonant structural modes "cut off" above the (4,0) higher order acoustic mode, and the (m,5) resonant structural modes "cut off" above the (5,0) higher order acoustic mode. Hence in the frequency range $0.30 \leq \nu \leq 0.47$, coincidence can only occur between the (m,1) resonant structural modes and the (1,1) higher order acoustic mode, whereas for the thin-walled pipe, all coincidences are possible - thus the drop in pipe wall response and acoustic power radiation in the $\frac{1}{3}$ -octave bands corresponding to those frequencies.

TABLE 7.1

Structural Mode	Acoustic Mode	ν
(1,1)	-	0.0028
	(1,0)	0.1314
(1,2)	-	0.1339
	(2,0)	0.2179
	(3,0)	0.2996
(1,3)	-	0.3783
	(4,0)	0.3794
	(1,1)	0.3803
	(5,0)	0.4577
	(2,1)	0.4783
	(3,1)	0.5785
(1,4)	-	0.7249
(1,5)	-	1.1720

NOTE

$\nu = f/f_r$, and $f_r = 21.1$ kHz for $\beta=0.04648$.



7.4.2 Comparison between prediction for thick and thin walled cylinders

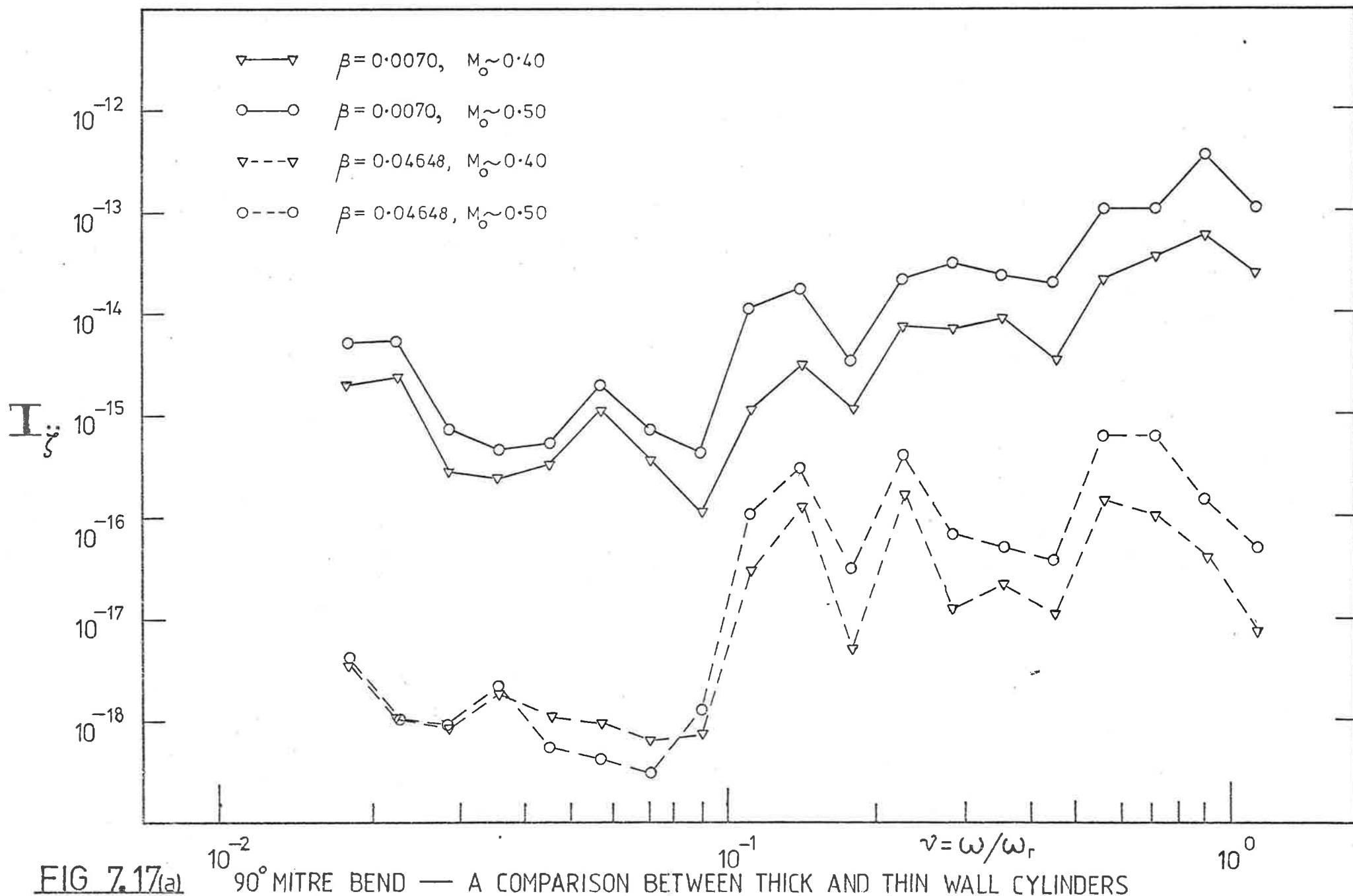
Comparison of prediction for the thick and thin-walled pipes is made on the basis of the "mean wavenumber coincidence" approach.

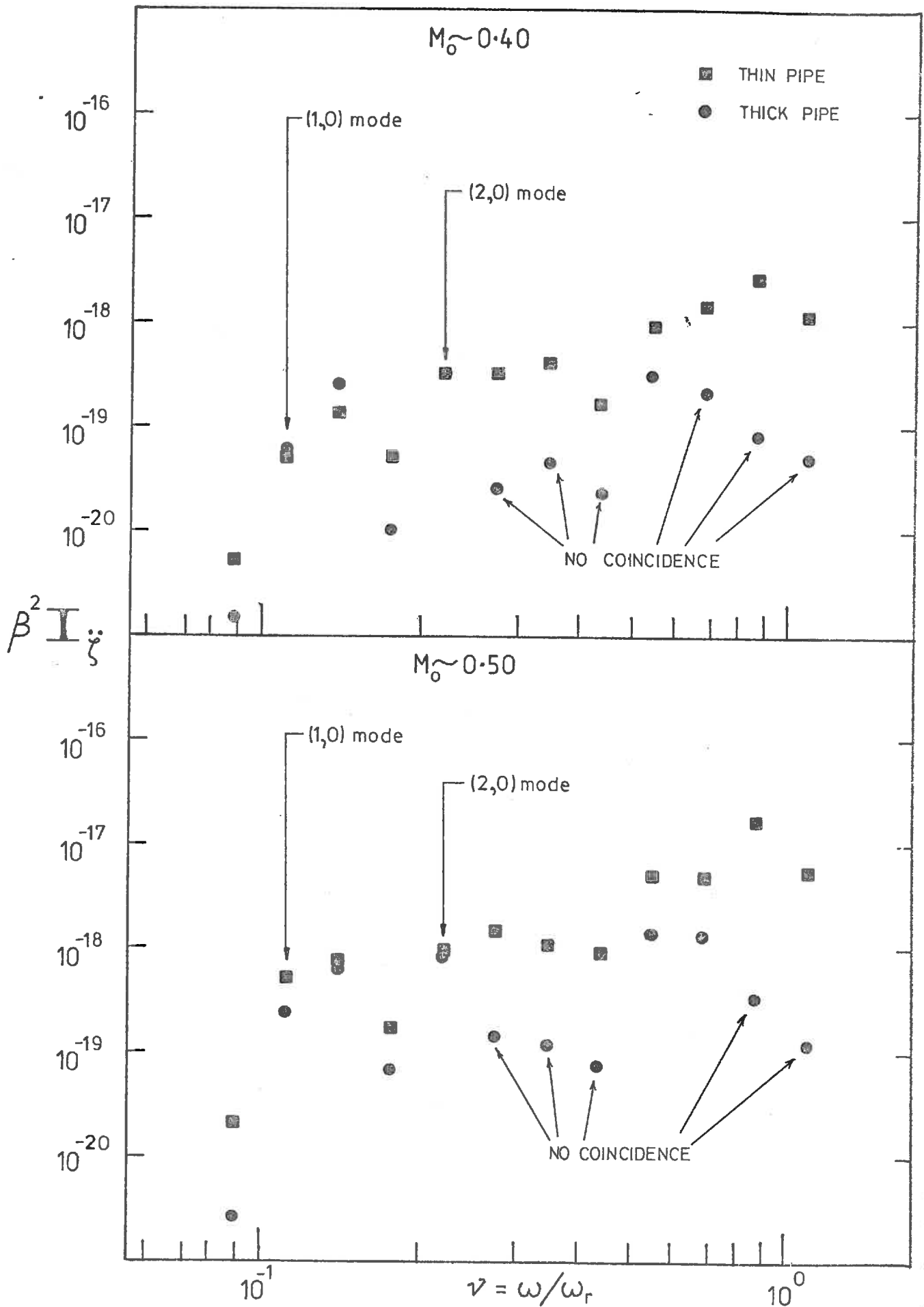
The modal density, $N(\nu)$, (i.e. number of structural modes per unit non-dimensional frequency band, $dN/d\nu$) of the resonant structural modes of all orders, is proportional to $1/\beta$ (Rennison and Bull, 1977) - in any particular frequency band, $\Delta\nu$, this includes resonant structural modes of various axial and circumferential mode orders ($m=1,2,3,\dots$, etc. and $n=1,2,3,\dots$, etc.). However, while the overall modal density is proportional to $1/\beta$, the modal density for modes of fixed circumferential order is roughly independent of β - hence the difference in frequency between consecutive axial structural mode orders for a particular circumferential structural mode order is almost the same for the thick and thin-walled pipes being considered. Thus the value of ν_{α}/ν_c is essentially the same for the thick and thin-walled pipes, for any particular higher order acoustic mode. Thus, the summation term, (\sum_{α}) , in equation [7.9] is approximately constant and independent of β . In this case, for a particular flow speed, pipe radius, pipe length, and internal flow disturbance, I_{ζ}/I_p should according to equation [7.9], be proportional to $1/\beta^2$ (in the regions where higher order modes dominate the pipe wall response). The two particular pipe wall thicknesses, ($\beta=0.0070$ and 0.04648), yields a β^2 ratio of 16.5 dB. Then, in the regions where higher order coincident acoustic modes dominate the pipe wall response, according to the "mean wavenumber coincidence" approach, the thin-walled pipe should produce a pipe wall vibrational response that is 16.5 dB

greater than the thick-walled pipe response. This is indeed essentially the case for the various devices investigated in the frequency bands in which coincidences occur (and this excludes the $0.30 \leq \nu \leq 0.47$ region). This is illustrated in Figures 7.17 to 7.19 for the 90° mitred bend, butterfly valve and gate valve respectively.

The pipe wall acceleration spectra, I_{ζ} , for the thin and thick-walled pipes, are compared in Figures 7.17(a), 7.18(a) and 7.19(a) for $M_0 \sim 0.40, 0.50$ for the three respective disturbances. The same data are presented in Figures 7.17(b), 7.18(b) and 7.19(b) as $\beta^2 I_{\zeta}$, which according to the preceding discussion should lead to a collapse of the data for regions where coincidence occurs. The differences between thick and thin-walled pipe wall response in the particular $\frac{1}{3}$ -octave bands of interest vary from 14 to 24 dB with an average of 18 dB. The approximate collapse at these frequencies ($\nu=0.118, 0.149, 0.237, 0.569, 0.758$) can be observed in Figures 7.17(b) to 7.19(b). As can be seen from Table 7.1, coincidence can only occur between: the $(m,1)$ structural modes and all the $(1,q)$ acoustic modes; the $(m,2)$ structural modes and all the $(2,q)$ acoustic modes; and, for other higher order modes whose cut-off frequency is greater than the "cut off" frequency of the resonant structural modes with matching circumferential wavenumbers.

The implications of this are that theoretical estimation procedures, as discussed in previous sections, can only be expected to yield good results in $\frac{1}{3}$ -octave bands where coincidences occur. For thin-walled pipes, coincidence generally occurs in all $\frac{1}{3}$ -octave bands above the cut off frequency of the $(1,0)$ mode, but, as has been illustrated, this is not necessarily the case with thicker pipes.





A COMPARISON BETWEEN THICK AND THIN WALLED
CYLINDERS

FIG 7.17(b)

FOR 90° MITRED BEND

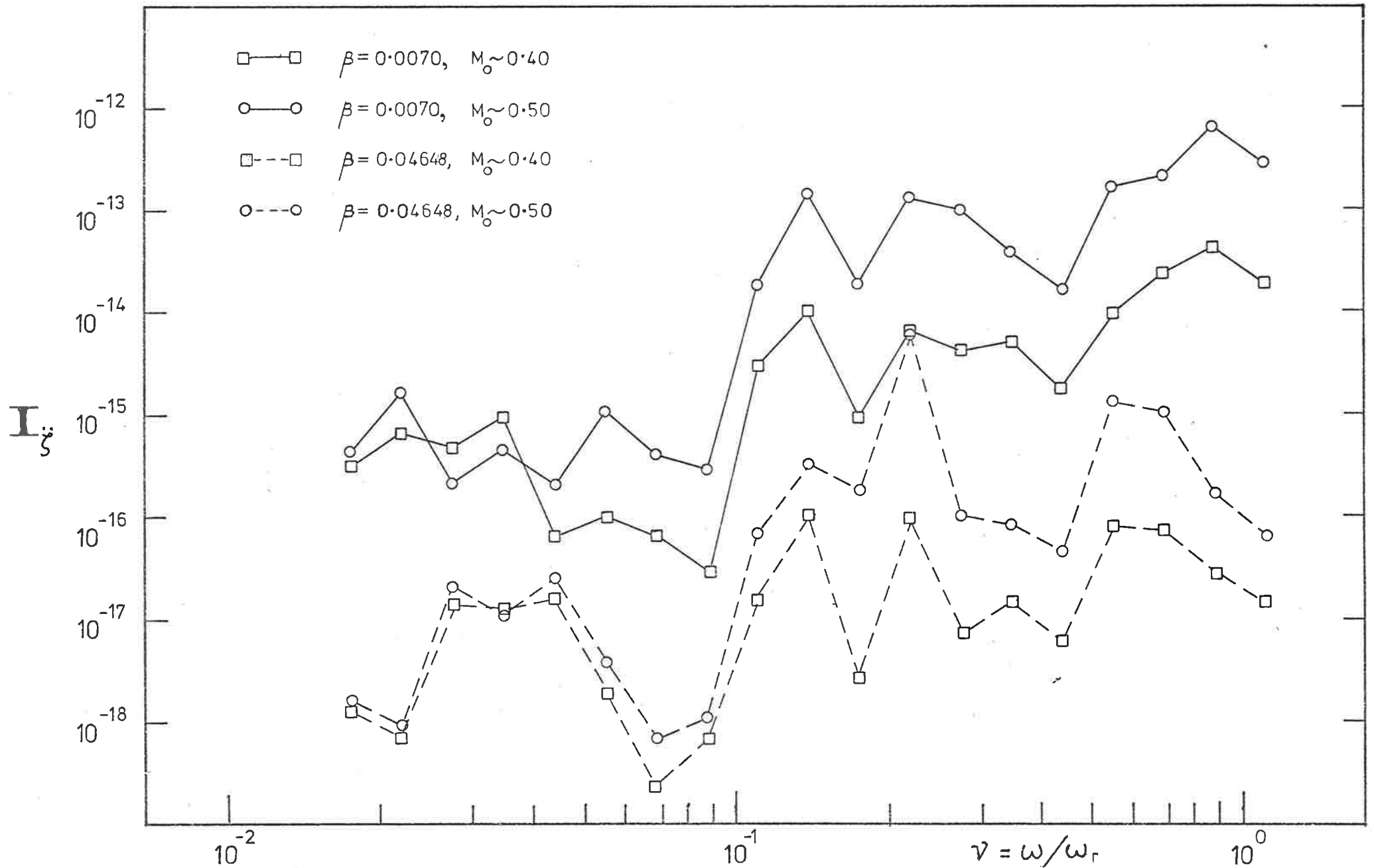
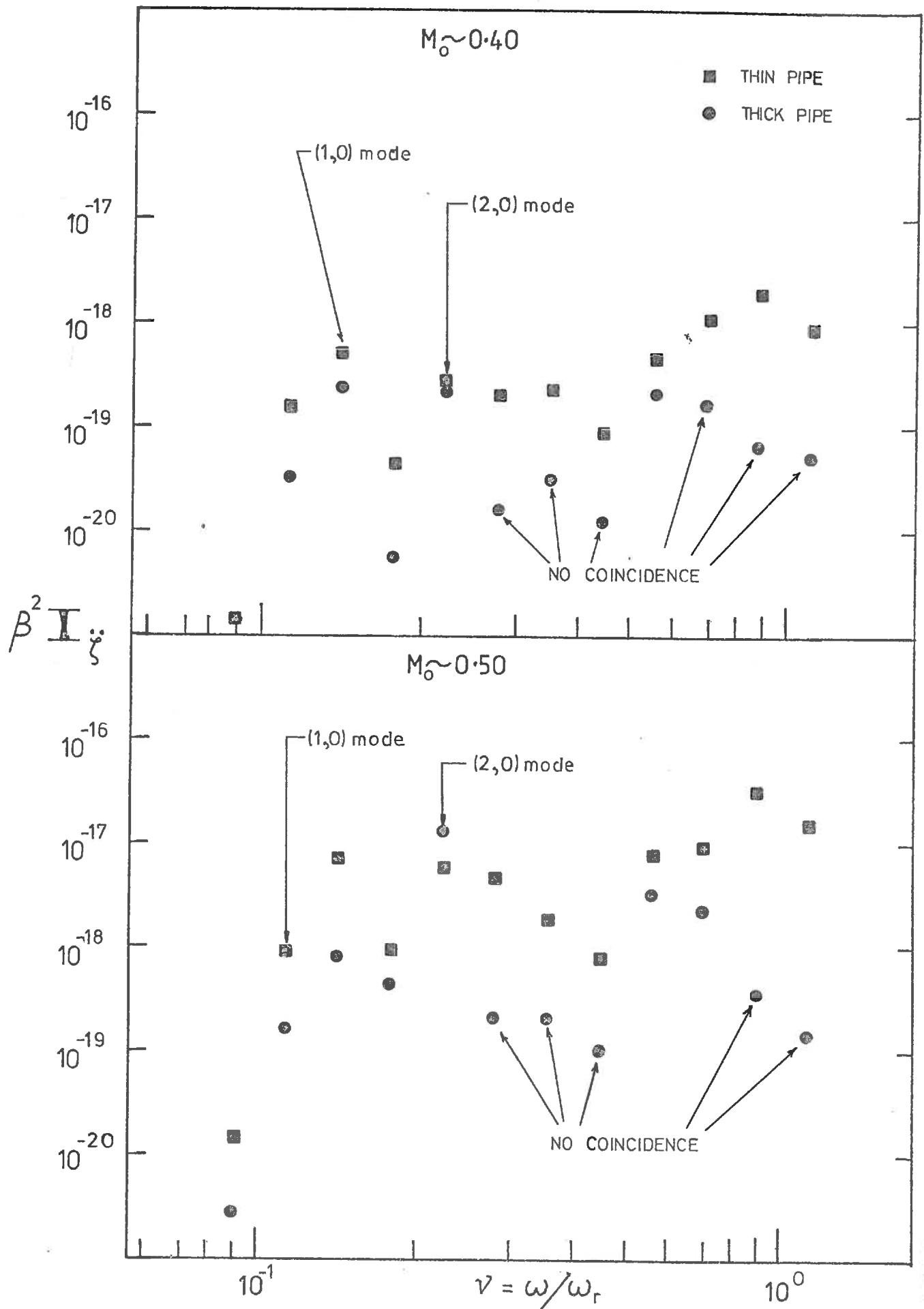


FIG 7.18(a)

BUTTERFLY VALVE OPEN — A COMPARISON BETWEEN THICK AND THIN WALLED CYLINDERS



A COMPARISON BETWEEN THICK AND THIN WALLED
CYLINDERS
FOR BUTTERFLY VALVE (OPEN)

FIG 7.18(b)

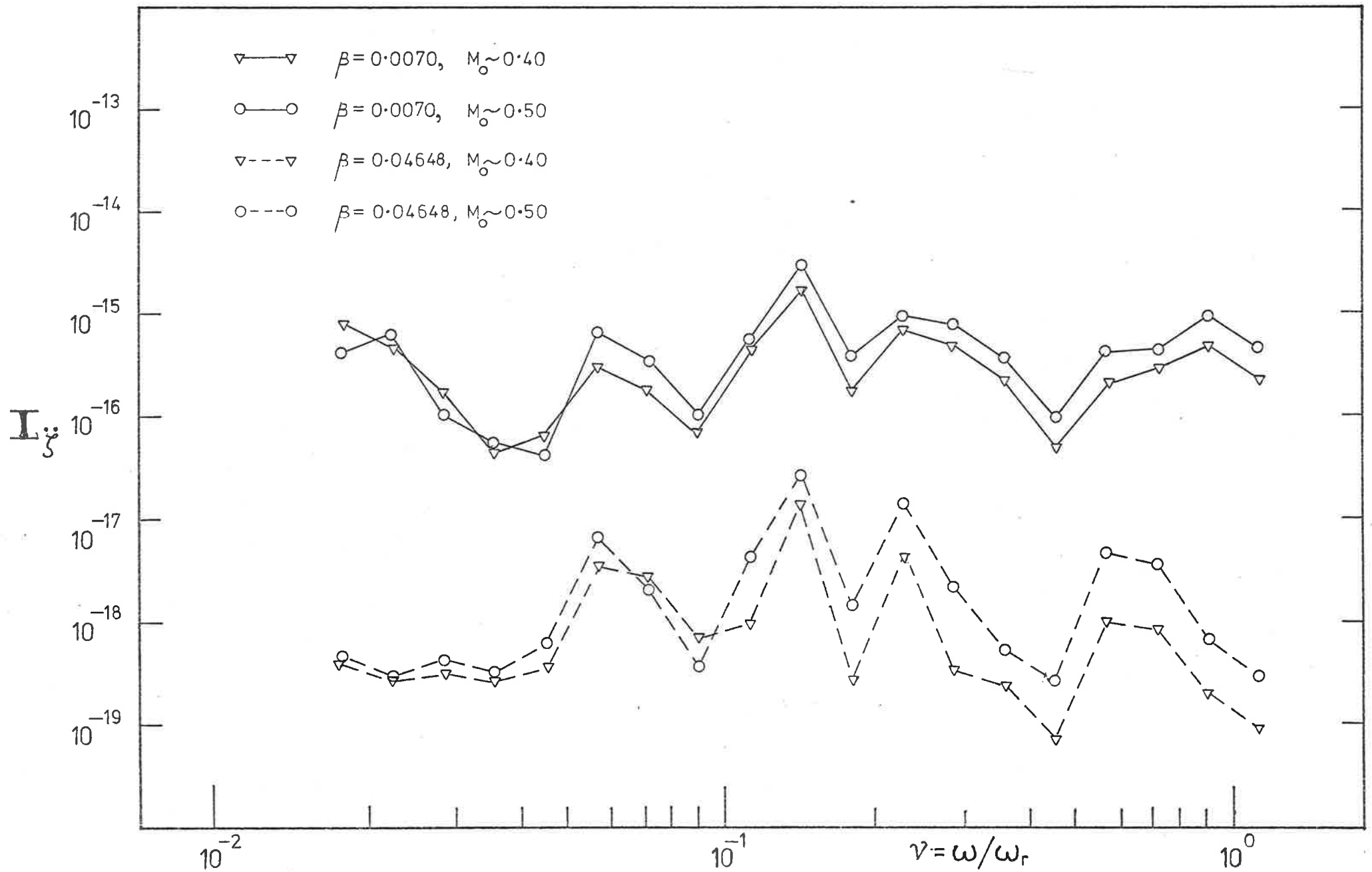
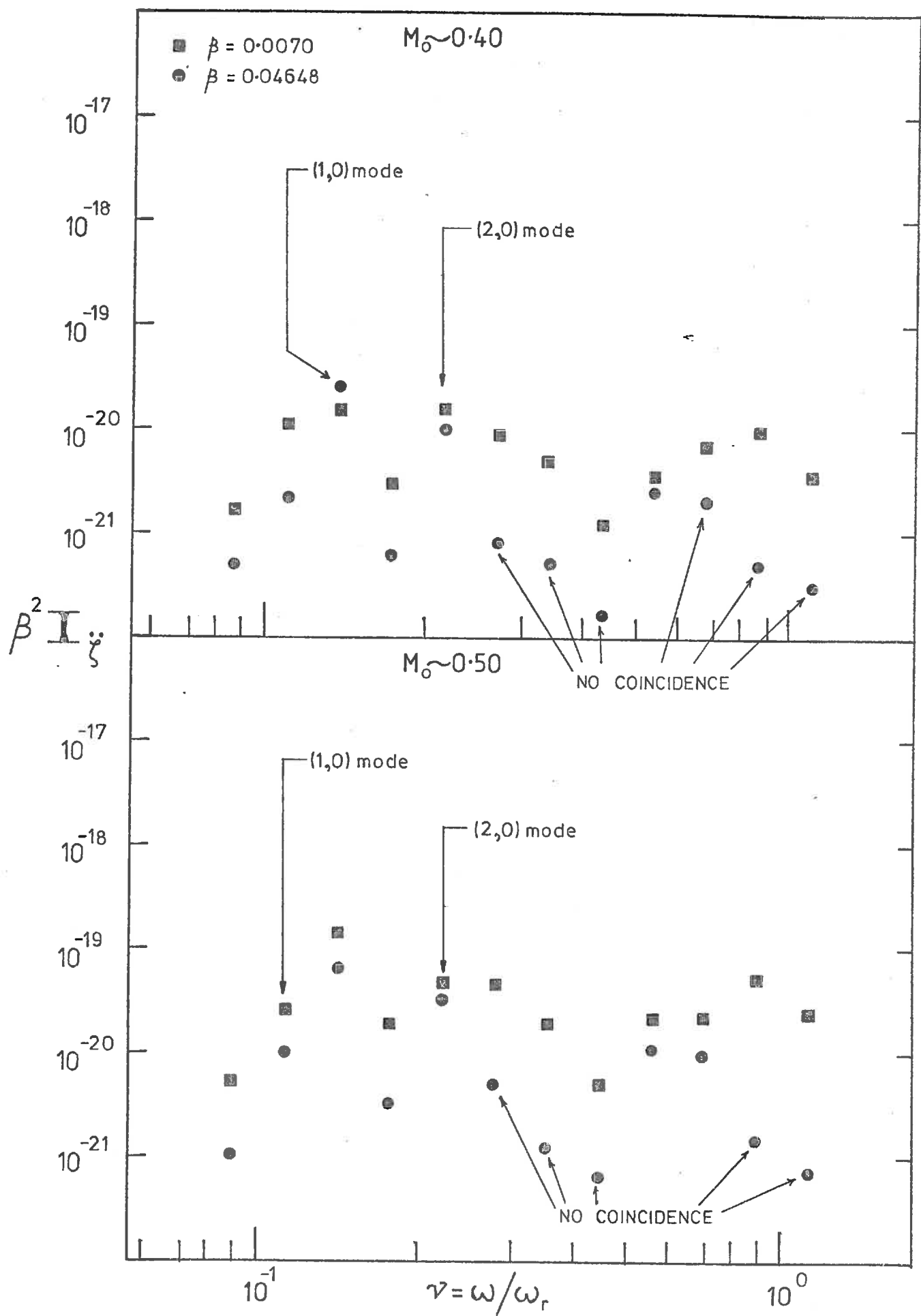


FIG 7. 19(a) GATE VALVE OPEN — A COMPARISON BETWEEN THICK AND THIN WALLED CYLINDERS



A COMPARISON BETWEEN THICK AND THIN WALLED CYLINDERS

FIG 7.19(b)

FOR GATE VALVE (OPEN)

However, since these coincident higher order acoustic modes do indeed dominate the pipe wall response and the acoustic power radiation, these procedures can be used to provide an upper bound estimation. Figures 7.20 to 7.23 present a comparison between experiment and theory for the thick-walled pipe for (a) I_{ζ}/I_p and (b) I_{π}/I_p for $M_0 \sim 0.40$ and 0.50 . The theoretical estimates were obtained by scaling the thin-walled pipe theoretical estimates to account for the change in β . There is very good agreement for the (1,0) and (2,0) higher order modes for which coincidence occurs and also for the higher order modes in the frequency range $0.474 \leq \nu \leq 0.758$ where there are some coincident acoustic modes.

On the whole, the theoretical estimates give reasonable agreement with experiment for the severe flow disturbances, especially when compared with "exact coincidence" predictions. The approximations at frequencies where there are coincident acoustic modes could perhaps be improved by obtaining the frequencies of resonant structural modes from a thick shell theory and then applying the same procedure as discussed in the earlier part of this chapter in relation to thin walled pipes.

7.5 GENERAL DISCUSSION

The arguments presented in this Chapter relate to developing appropriate techniques for the prediction of acoustic radiation from and the acceleration response of pipes with various internal flow disturbances, in view of the fact that assuming exact coincidence (i.e. $\nu_{\alpha} = \nu_c$) gives gross overestimates. There are obvious practical applications and limitations both of which will be discussed in this section.

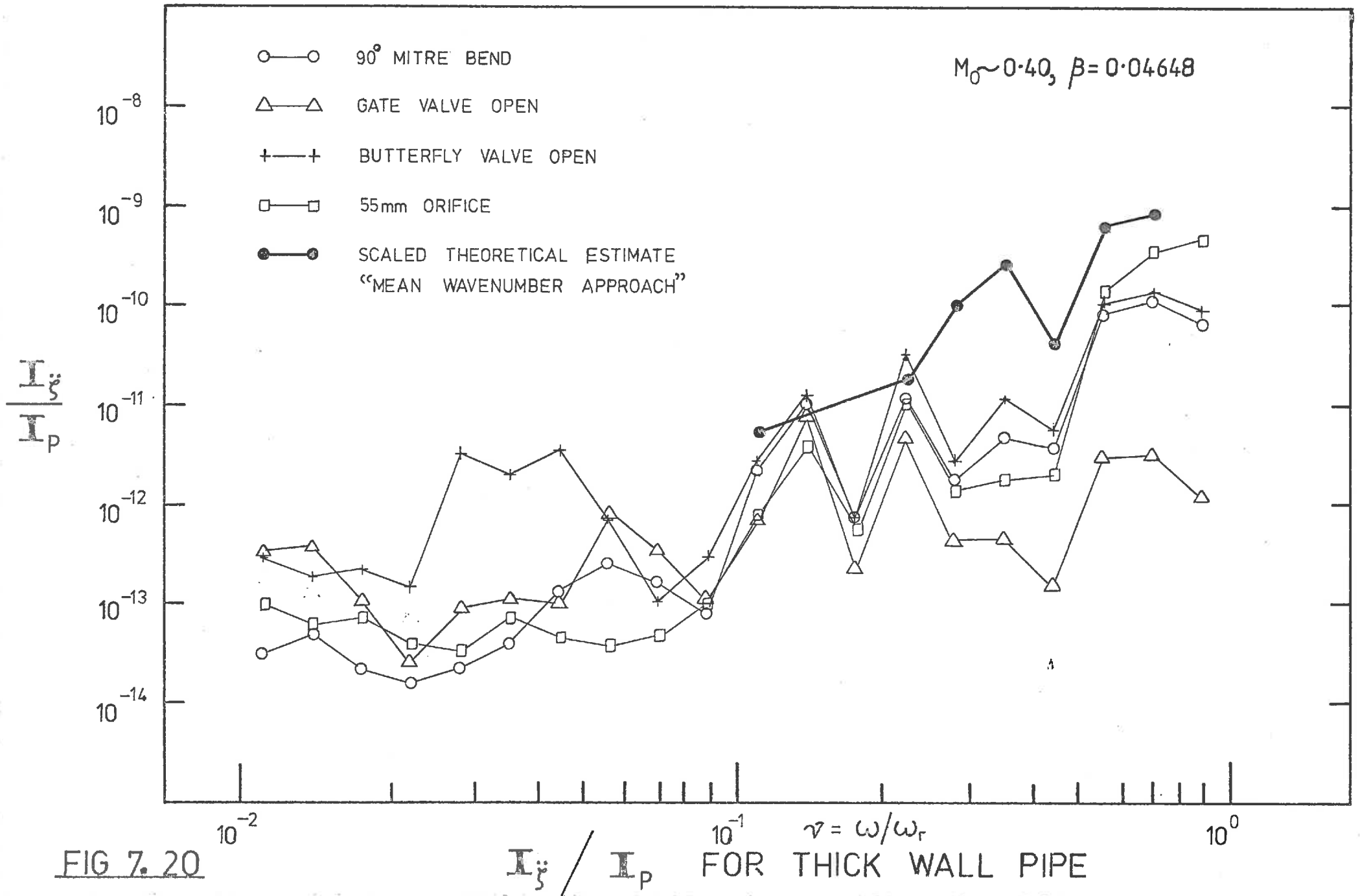


FIG 7.20

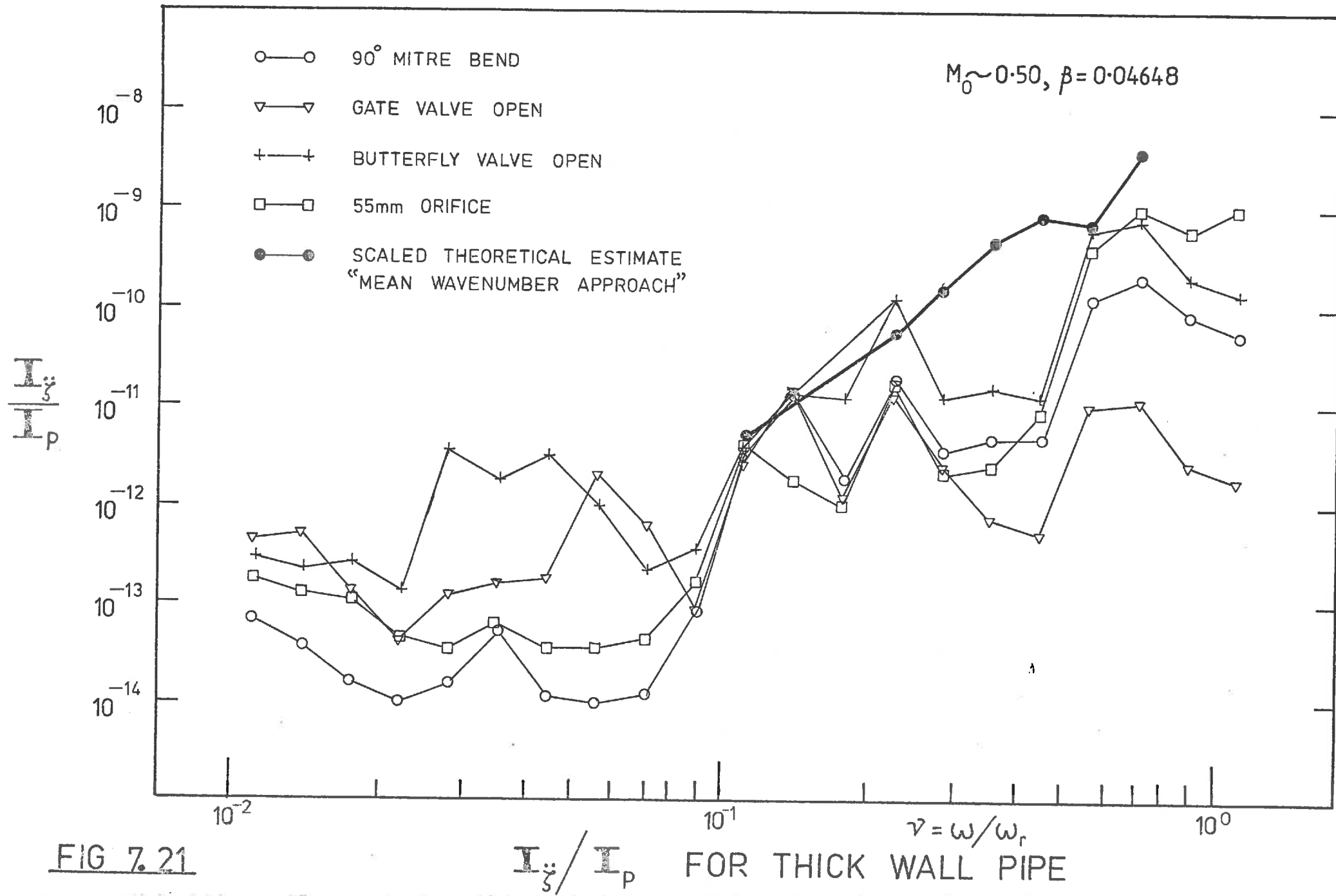


FIG 7.21

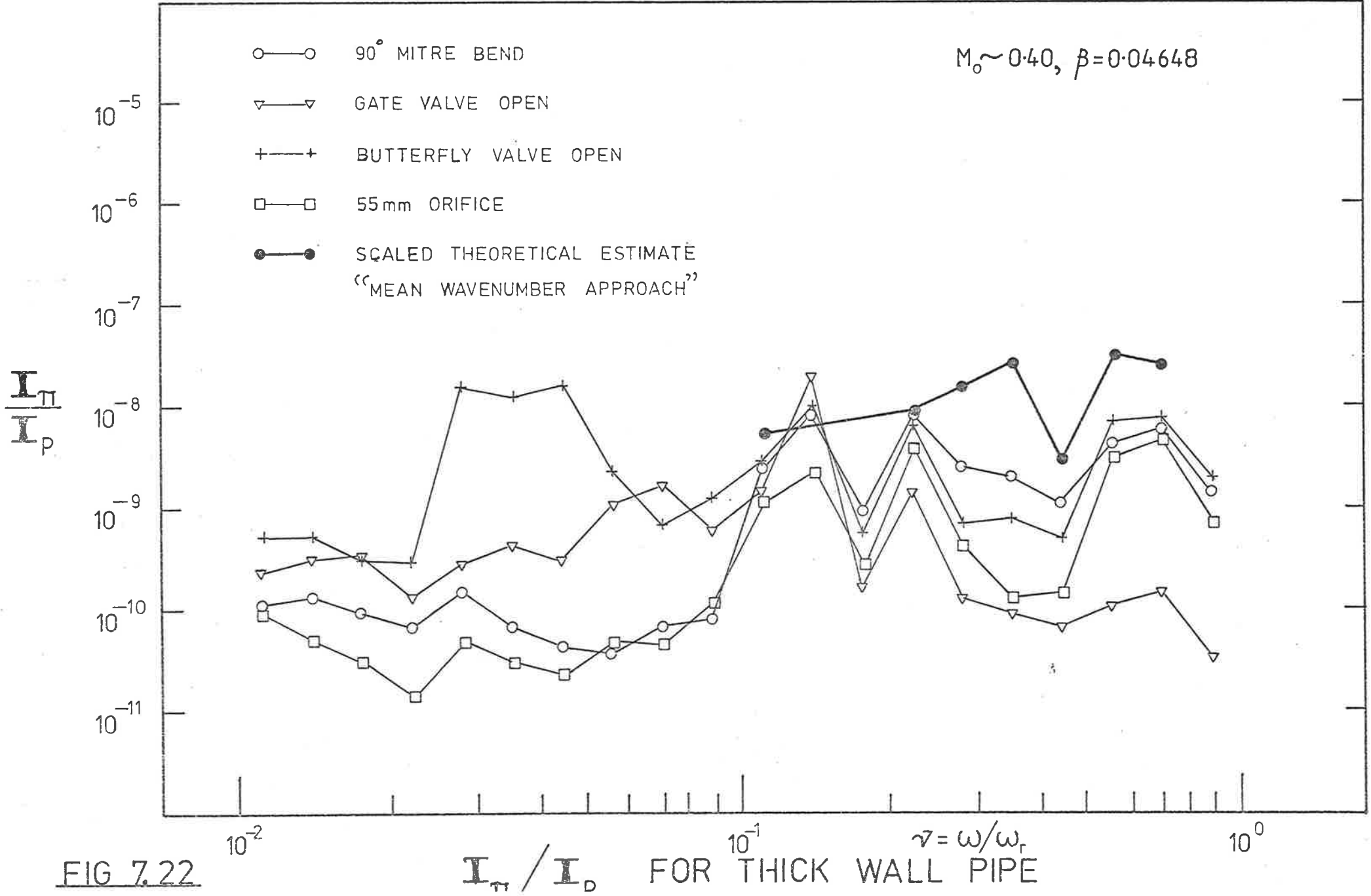


FIG 7.22

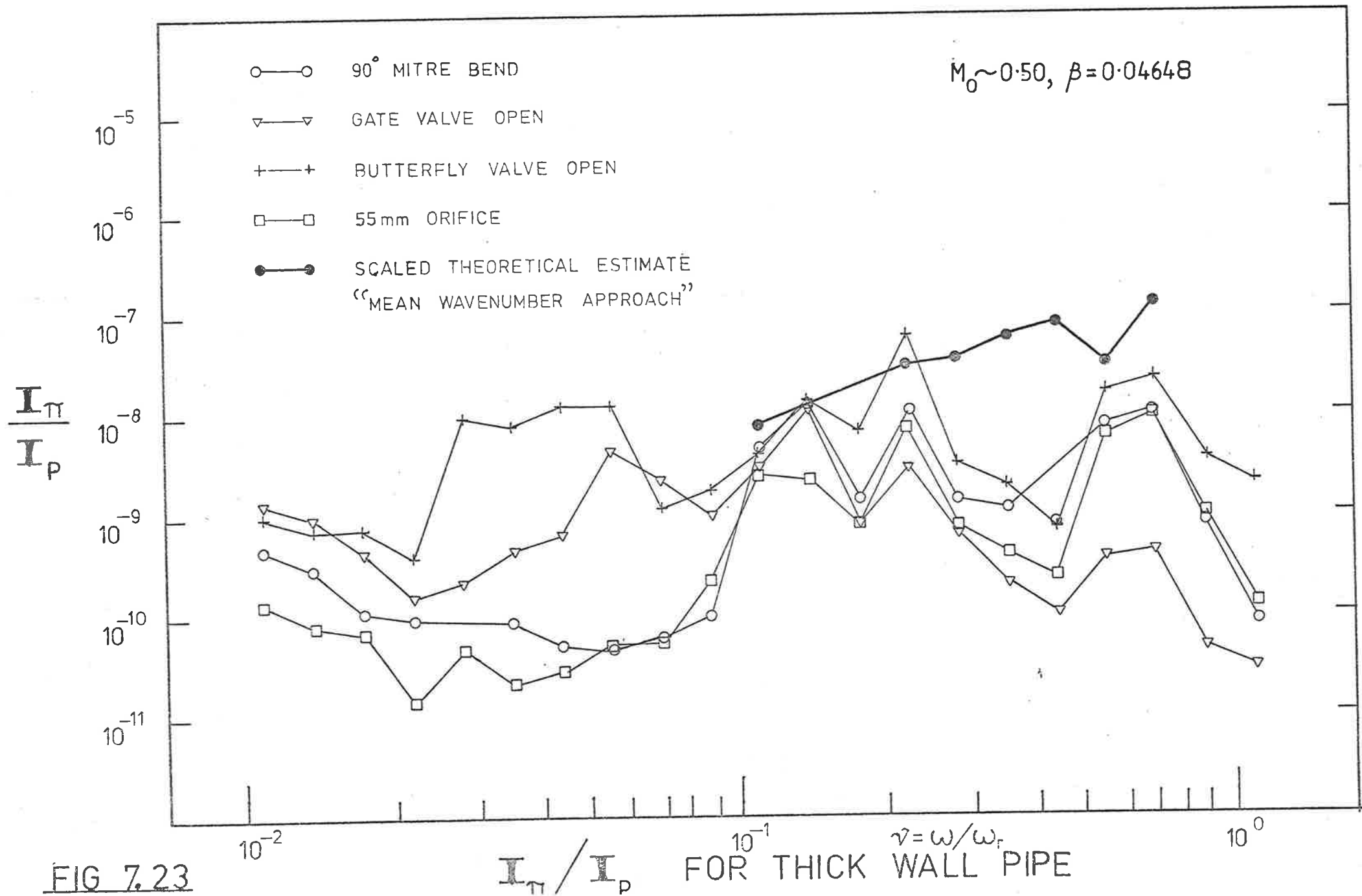


FIG 7.23

7.5.1 Practical Applications and Limitations

The theoretical estimates as presented in this chapter, allow for an estimation of both I_{ζ}/I_p and I_{π}/I_p . To estimate the mean square acceleration response, I_{ζ} , and the mean square acoustic radiation, I_{π} , for a particular internal flow disturbance, the mean square wall pressure fluctuations associated with that particular disturbance have to be known. The wall pressure spectral data at $X = 52.8$ (just upstream of the test section) represent the wall pressure fluctuations associated with a propagating acoustic field superimposed on fully-developed turbulent pipe flow. Estimates of Φ_p can be obtained from the spectral data presented in Chapters 4 and 5, for various flow speeds and pipe sizes. The "mean wavenumber coincidence" approach discussed in this chapter appears to be the best of those considered as a basis for pipe work design. It should provide a designer with a reliable indication of the acoustic radiation to be expected from various pipe fittings; it avoids the gross overestimation given by the other three approaches.

All the theoretical estimates presented in this chapter are based on the assumption that the higher order modes dominate the wall pressure field in the $\frac{1}{3}$ -octave bands of interest ($ka_1 \geq 1.84$). Extensive wall pressure fluctuation cross correlations are necessary to obtain the actual components of the spectra that are associated with the higher order modes, for the various internal flow disturbances. This has been discussed in Chapter 6, for the particular case of the 90° mitred bend, in which the higher order modes dominate the wall pressure field in the region of the (1,0) and (2,0) acoustic modes. The wall pressure fluctuation levels associated with the mild flow disturbances (the radiused bends, the gate valve and the 45° mitred bend) are not very different

from those associated with straight pipe flow. Hence the assumption that the higher order modes dominate the wall pressure field is not valid for these mild flow disturbances. The theoretical procedures given will therefore lead to an overestimate of the pipe wall response in these cases. A more comprehensive study of the wall pressure spectra associated with various internal flow disturbances (utilizing cross correlation techniques) is required to allow estimation of the contribution of the higher order modes to the wall pressure fluctuations in various filter bands in all cases. Nevertheless, the techniques described in this chapter provide an "order of magnitude" estimate for the mild flow disturbances and in these cases they provide an "upper bound" prediction of acoustic radiation from and the acceleration response of pipes downstream (or upstream) of an internal flow disturbance. The I_{ζ}/I_p and I_{π}/I_p data for the straight pipe flow constitute a lower limit for all practical flow disturbances. Both the I_{ζ}/I_p and I_{π}/I_p theoretical estimates are essentially proportional to M_0^3 , and inversely proportional to β^2 , and can be scaled accordingly.

The theoretical estimation procedure is limited in that it can only be expected to yield good results in $\frac{1}{3}$ -octave bands where coincidences occur, and those are at frequencies at which the higher order modes can propagate ($ka_i \geq 1.84$). For the thin pipe ($\beta=0.0070$) coincidences occur with all the higher order modes (with the exception of those acoustic modes with radial mode order $p = 0$, e.g. (0,1), (0,2)). As has been seen in the preceding section, for thicker pipes ($\beta=0.04648$), not all the higher order acoustic modes are coincident. For propagating plane acoustic waves, neither wavenumber nor frequency coincidence with the resonant structural modes of the pipe can occur. Rennison (1976)

has discussed the concept of a lower bound to the acoustic radiation from pipes excited by propagating acoustic plane waves, based on the radiation from a forced vibrational response. He obtained good agreement between theory and prediction for a highly-damped (P.V.C.) pipe. However, in the case of a lightly-damped steel pipe, the "forced vibrational lower bound" underestimated the pipe wall response by 30 to 60 dB and the acoustic power radiated by 20 to 30 dB. The maximum increases in both acceleration response and acoustic power radiated were found to occur in those frequency bands in which the density of resonant structural modes is highest. Rennison (1976) showed both experimentally and theoretically that the pipe wall response is resonant and not forced and that the resonant response and the associated acoustic radiation resulted from inhomogeneities in the pipe and in particular from variations in pipe wall thickness. Hence, the joint acceptance between plane acoustic waves and the pipes resonant structural modes is never zero in practice although it is still small in comparison to the higher order acoustic mode coincidences. In order to present theoretical predictions for $k a_1 < 1.84$, a procedure for estimating this joint acceptance has to be developed.

7.5.2 Summary of the Theoretical Estimation Procedure

To estimate pipe wall acceleration levels and hence acoustic radiation levels for $k a_1 \geq 1.84$, in a piping system downstream of an internal flow disturbance the following procedures should be adopted,

- (1) Compute the various resonant structural modes and the corresponding axial structural wavenumbers in the regions of interest using the modified form of Heckl's (1962) result as presented in equation [2.8]

- (2) Estimate the overall modal quality factors (Q_{α}) using equations [7.4] and [7.5]. Estimates have to be made of the internal quality factor of the material damping (Q_i) and the quality factor associated with the dissipation at structural joints (Q_j). Rennison and Bull (1977) discuss this in considerable detail.
- (3) Evaluate the receptance function for the various coincidences using the "mean wavenumber coincidence" approach.
- (4) Estimate the bandwidth of the joint acceptance function ($j_{\alpha\alpha}^2(\omega)$) for the various coupled modes of interest, assuming that the half-power bandwidth of the primary peak is sufficient for the purposes of estimation. Equation [7.8] can be used to estimate this bandwidth ($\Delta\nu_{j_m}$).
- (5) Estimate the bandwidth ($\Delta\nu_B$) over which the wall pressure fluctuations are significant in the $\frac{1}{3}$ -octave bands of interest. Equations [7.6] and [7.7] can be used for these estimations.
- (6) Hence, evaluate I_{ζ}/I_p and I_{π}/I_p .
- (7) For different flow Mach numbers (M_0) or pipe wall thicknesses (β), I_{ζ}/I_p and I_{π}/I_p can be scaled accordingly as M_0^3 or β^2 respectively.
- (8) An estimation of the pipe wall acceleration (I_{ζ}) and the acoustic power radiated (I_{π}) can be obtained using the data presented in Chapters 4 and 5 on the wall pressure fluctuations. Using these data, I_p can be estimated in the $\frac{1}{3}$ -octave bands of interest and I_{ζ} and I_{π} can hence be evaluated.

CHAPTER 8CONCLUSIONS AND RECOMMENDATIONS8.1 CONCLUSIONS

This investigation has been concerned with the effects of various internal flow disturbances on the vibration response of and the acoustic radiation from cylindrical pipes with a fully-developed turbulent flow. Detailed experimental results have been presented for several internal flow disturbances, and certain experimentally observed phenomena have been explained. Procedures have been developed for theoretically estimating the vibration response of and the acoustic radiation from cylindrical pipes downstream of these flow disturbances, at positions where a fully-developed turbulent pipe flow has been re-established. Specific conclusions relating to the various sections of this thesis have been presented in the relevant earlier chapters. This section reiterates the more important of these conclusions, summarises them and makes more general conclusions about the overall problem.

As illustrated in the literature survey, very little work has been published to date on the internal acoustic fields generated at and propagating from pipe fittings. In particular, there has been very little attempt to study the associated internal fluctuating pressure fields (comprising turbulent and acoustic pressure fluctuations) and their excitation of the pipe wall. This investigation represents an extensive experimental and theoretical study of pipe flow noise associated with internal flow disturbances and is the first such comprehensive study to be attempted. The main conclusions are as follows.

[1] Internal flow disturbances generate internal sound fields which may range from mild internal sound fields (associated with the radiused bends, the 45° mitred bend and the gate valve) to intense internal sound fields (associated with the 90° mitred bend, the butterfly valve and the 55 mm orifice plate).

[2] The power spectral density of the wall pressure fluctuations associated with the 90° mitred bend, the butterfly valve and the 55 mm orifice plate is many times larger than that associated with fully-developed turbulent pipe flow. On the other hand the radiused bends, the 45° mitred bend and the gate valve generate milder wall pressure fluctuations that are not generally significantly greater than those associated with fully-developed turbulent pipe flow.

[3] For the particular case of the 90° mitred bend, in the region of the flow separation at the bend itself, the disturbance to the wall pressure field of fully-developed turbulent pipe flow consists of intense non-propagating fluctuations. These have a maximum value near reattachment. They are readily attenuated with downstream distance, and beyond 12 diameters downstream, the only remaining disturbance is an acoustic field containing propagating higher order modes but dominated by plane waves.

[4] For all fittings, the wall pressure field well downstream of the fitting ($X \approx 53$) can be identified as that of fully-developed turbulent pipe flow with a superimposed acoustic field generated by and radiated from the flow disturbance in the immediate vicinity of the fitting.

[5] At positions sufficiently far away from the flow disturbance, such that a fully-developed turbulent pipe flow has been re-established, the power spectral density ϕ_p at a given Strouhal

number and the mean square pressure $\overline{p^2}$ of the wall pressure fluctuations associated with the radiused bends, the 45° mitred bend, the gate valve and the 65 mm orifice plate scale essentially as U_0^3 and U_0^4 respectively. For the 90° mitred bend, the butterfly valve and the 55 mm orifice plate, the scaling is as U_0^3 and U_0^4 below the cut-off frequency of the first higher order acoustic mode, and U_0^5 and U_0^6 above it. The overall mean square pressure scales as U_0^4 for the radiused bends, the 45° mitred bend, the 90° mitred bend, the gate valve, the butterfly valve and the 65 mm orifice plate, and as U_0^6 for the 55 mm orifice plate (Table 5.1). The 55 mm orifice plate differs from the other pipe fittings because the higher order acoustic modes dominate the wall pressure field in this case - hence the U_0^6 flow dependence for the overall mean square pressure fluctuations.

[6] The experimentally observed increases in pipe wall acceleration and acoustic power radiation (over those for straight pipe flow), in a region where a fully-developed turbulent flow has been re-established, are associated with the internal sound fields generated by the flow disturbances. In particular, as v increases above 0.10, the increases in pipe wall acceleration and acoustic power radiation correspond to first the (1,0) and then other higher order modes becoming propagational. From both the $\frac{1}{3}$ -octave band measurements and the narrow band analyses, it appears that the increases in pipe wall acceleration and acoustic radiation due to any particular higher order acoustic mode are greatest at and essentially confined to frequencies close to the cut off frequency of that acoustic mode. From the $\frac{1}{3}$ -octave data presented, this is most obvious where the modes are well separated in frequency; it can be seen most clearly in the case of the (1,0) and (2,0) modes, and to a lesser extent in the case of the (4,0) and (1,1) modes

which are fairly well separated from the next higher mode (the (3,0) mode). In other parts of the frequency range examined, a $\frac{1}{3}$ -octave band is not sufficiently narrow to allow the effects of individual modes to be seen in isolation, but the observation has been very clearly confirmed by the narrow (100 Hz constant bandwidth) band analysis.

[7] Associated increase in pipe wall response and external acoustic radiation at frequencies below the cut-off frequency of the first higher order mode are due to plane acoustic waves generated by the various internal flow disturbances. These plane waves propagate away from the source essentially unattenuated and excite the pipe wall. According to Rennison (1976), the wall of a lightly damped steel pipe response in its resonant natural modes of vibration as opposed to a "breathing" forced response which would be the case if the pipe were heavily damped. Rennison found that this resonant pipe wall response and the corresponding acoustic power radiation are associated with the inherent inhomogeneties in the pipe and in particular the non-uniformity of the pipe wall thickness. For all the internal flow disturbances investigated here, even though the response to plane waves may be resonant, with the exception of the two radiused bends (which do not generate any significant additional pipe wall vibration and acoustic radiation over that of fully-developed turbulent pipe flow), the pipe wall vibration and acoustic power radiated by the higher order modes dominate over the vibration and radiation associated with the low frequency plane waves. This is despite the fact that in some cases, the low frequency plane waves dominate the internal wall pressure field.

[8] The reasons why the effects of the internal acoustic field, generated by flow disturbances, on the pipe wall vibration and acoustic radiation are greatest at and confined to frequencies close to the cut-off frequencies of the higher order acoustic modes are (i) the joint acceptance of structural and acoustic modes peak very sharply at wavenumber coincidence; (ii) wavenumber coincidence occurs at the resonance frequency of a structural mode (exact coincidence) or very close to it, so that the modal receptance is also at or close to its maximum value at coincidence; and (iii) by the nature of the dispersion (wavenumber-frequency) relations of the acoustic and structural modes, coincidence occurs at a frequency very close to the cut-off frequency of the acoustic mode. Thus, as a result of coincidence, the higher order acoustic modes select and enhance the vibration of those resonant pipe modes which radiate most efficiently into the external fluid.

[9] While in general, at distances sufficiently downstream of the fitting such that non-propagating disturbances have been attenuated, the excitation comprises of turbulent pressure fluctuations and an internal propagating acoustic field, there are cases where this is augmented by convected fluid dynamic disturbances, originating at the fitting. Such a case is the vane-spindle assembly of the butterfly valve which splits the flow, resulting in periodic vortex shedding into the wake. The force fluctuations associated with this phenomenon are produced in a frequency band centred on a characteristic frequency which is flow dependent. The pipe wall response and external acoustic radiation resulting from these force fluctuations dominate over the plane waves at frequencies where this phenomenon occurs.

[10] The understanding of the rôle played by coincidence of structural and higher order acoustic modes is essential to the formulation of procedures for predicting pipe wall response and acoustic radiation associated with a given flow disturbance; for it appears that, particularly in the frequency range of the lowest order acoustic modes, which are fairly well separated in frequency attention must be paid to the details of the structural response. Since wall pressure fluctuations due to fully-developed turbulent pipe flow (which in practical applications represent a lower limit of pipe wall excitation) and acoustic plane waves generated by flow disturbances, as well as the higher order acoustic modes associated with flow disturbances, contribute to the vibrational response and acoustic power radiation, any successful prediction scheme will depend on knowledge of the relative proportions of these components in the total wall pressure fluctuations in any given frequency band.

[11] Longitudinal space-time correlations of the wall pressure fluctuations downstream of an internal flow disturbance, allow the internal acoustic field to be separated from the turbulent pressure field in various filter bands. The component of the wall pressure fluctuations associated with plane waves can be obtained directly from the cross-correlations, but that associated with the higher order modes cannot because of their dispersive nature. However, the component of the wall pressure fluctuations associated with the higher order modes can be estimated by subtracting the turbulent and plane wave components from the total wall pressure fluctuations. In this way, the wall pressure fluctuations associated with the (1,0) higher order acoustic mode, in a frequency band embracing the cut-off frequency, can be estimated fairly readily. However in the filter bands containing other higher order modes, the contribution to the wall pressure fluctuations from modes with lower frequency

cut-off frequencies cannot be separated from that due to the particular mode of interest, since the higher order modes are dispersive in character. Thus it is possible to estimate only the wall pressure fluctuations associated with all the higher order modes in these filter bands. While it would be an additional advantage to be able to make a modal decomposition, even this information is useful in predicting the pipe wall response. These techniques are particularly necessary for the milder flow disturbances where the higher order modes do not dominate the internal wall pressure field but do dominate the wall response and acoustic radiation. However, they are less powerful in cases where the turbulent wall pressure field dominates over the internal acoustic field, such as that of the radiused bends investigated. Here, the correlation techniques give only plane waves and a combination of turbulent pressure fluctuations and higher order modes, hence the higher order modes cannot be extracted from the total wall pressure fluctuations.

[12] For the 90° mitred bend, which is a severe flow disturbance, the correlations indicate that the turbulent wall pressure fluctuations and the plane wave components of the wall pressure fluctuations are of secondary importance compared to the components associated with the higher order modes ($k a_i \geq 1.84$). At low frequencies ($k a_i < 1.84$) plane acoustic waves dominate the internal wall pressure field.

[13] A theoretical prediction scheme which takes account of the dominant role of the coincidence phenomenon and the relative proportions of various components in the total wall pressure fluctuations in any given frequency band where higher order modes are propagational has been put forward. Four theoretical estimation

procedures, all based on a general solution for the dynamic response of a thin-walled cylindrical shell to an acoustic pressure field, with approximations based on a detailed knowledge of the higher order acoustic modes that are excited and the degree to which they dominate the internal wall pressure field are discussed. The mean wavenumber coincidence approach yields the best estimates. The approach is based on the assumption that the acoustic mode wavenumber function intersects the resonant structural mode wavenumber function at a frequency that is equidistant from the structural modes on either side of it. This approach avoids the gross overestimation given by the other three approaches, and in particular the "exact coincidence" approach which yields discrepancies between theory and experiment of up to 45 dB. This theoretical procedure together with the various spectral data of the wall pressure field make it possible to estimate the acceleration response of and the acoustic radiation from a pipe, downstream of an internal flow disturbance, where a fully-developed turbulent profile has been re-established.

[14] Agreement between theory and experiment is good in $\frac{1}{3}$ -octave bands in which coincidence occurs. For the thin-walled pipe investigated, these coincident higher order acoustic modes are present in all $\frac{1}{3}$ -octave bands at frequencies above the cut-off frequency of the first higher order mode. This is not the case for the thicker walled pipe investigated; in this case coincidence cannot occur for certain higher order acoustic modes because their cut-off frequencies occur at frequencies well below the lowest possible frequency of the resonant structural modes with matching circumferential wavenumbers. There is very good agreement for the (1,0) and (2,0) higher order modes, for which coincidence occurs for both pipes, and

on the whole, the theoretical estimates give a reasonable upper bound prediction, especially when compared with exact coincidence predicted values.

[15] As a consequence of the modal density for fixed circumferential structural mode order n being essentially independent of β , both the pipe wall vibration response and the acoustic power radiated are inversely proportional to β^2 in frequency bands in which there are coincident higher order acoustic modes.

The effects of radiused bends, orifice plates, a gate valve, a butterfly valve, a 45° mitred bend and a 90° mitred bend on the vibration response of and the acoustic radiation from a cylindrical pipe with a fully-developed turbulent flow have been comprehensively investigated together with the characteristics of the wall pressure fields associated with the internal flow disturbances. A theoretical prediction scheme has been put forward and agrees well with the experimental results.

8.2 RECOMMENDATIONS

The research reported herein is the second phase of a comprehensive, fundamental investigation of pipe flow noise. The first phase was directed towards a better understanding of the pipe wall vibration and acoustic radiation due only to undisturbed fully-developed internal turbulent pipe flow (Rennison, 1976). Even on completion of this second phase many significant questions still need to be answered before comprehensive design guidelines can be formulated concerning pipe flow noise.

Part of the work reported in this investigation has concentrated on establishing the pipe wall response and acoustic radiation from the pipe remote from the cause of the flow disturbance. It is now

possible to predict upper and lower bounds for the response and radiation in this region and, if the pipe wall pressure fluctuation spectrum is known to predict the response and radiation for that particular case. However, it is not yet possible to predict except on the basis of experience what form the wall pressure spectrum will take for any given type of flow disturbance. An extension of the correlation measurements, in regions remote from the disturbance, to the disturbances produced by orifice plates, valves, tee-junctions, and other bends, in addition to the 90° mitred bend is also required (these measurements allow the contributions from plane waves, higher order modes and fully-developed turbulence to be distinguished). In the absence of any procedure for predicting the form of the wall pressure spectrum there may be merit in valve and pipe fitting manufacturers providing this information with their products to assist pipe work designers.

Certain other aspects of the pipe flow noise problem which require further research and development are:

[1] The effects of various internal flow disturbances on pipes of different material and damping properties from steel e.g. brass, P.V.C., and in particular the role played by the propagating higher order modes;

[2] An extension of the flow speed range ($M_0 \sim 0.20-0.50$) covered in the present work to both lower and higher flow speeds;

[3] The effects of flanges, end conditions and effective length on the pipe wall vibration and acoustic radiation;

[4] The effects of flanges on the propagation of energy along the pipe walls from the immediate vicinity of the disturbance to regions remote from it;

[5] The vibration response of and acoustic radiation from the pipe wall in the immediate vicinity of the disturbance and their correlation with the local wall pressure field (in the immediate vicinity of the pipe fitting);

[6] The details of the flow in the region of the various disturbances themselves, and their correlation with the pipe wall fluctuating pressure spectra both in the region of the disturbance and remote from it;

[7] The effect of pipe wall thickness on the acoustic radiation from the pipe in regions near to the disturbance;

[8] The effects of several simultaneous flow disturbances (e.g. a valve and a bend in series) on the internal wall pressure field.

The present investigation has answered a number of important questions regarding the mechanism of noise generation due to turbulent flow in an elastic pipe. However, as can be seen from the preceding list, significant questions still remain unanswered, and this investigation has laid the foundations for further investigation.

REFERENCES

- ALFREDSON, R.J. and DAVIES, P.O.A.L. (1970) The radiation of sound from an engine exhaust. *J. Sound and Vib.* 13 (4), 389-408.
- ALLEN, E.E. (1971) Prediction and abatement of control valve noise. *Flow: Its measurement and control in science and industry. Symp. Proc. Pittsburg, Pa.*, 1 (3), 1167-1173.
- ARNOLD, R.N. and WARBURTON, G.B. (1953) The flexural vibrations of thin cylinders. *Proc. Inst. Mech. Engrs. (London)* 167 (1), 62-74.
- BAKEWELL, H.P. (1964) Narrow-band investigations of the longitudinal space-time correlation function in turbulent flow. *J. Acoust. Soc. Amer.* 36 (1), 146-148.
- BENDAT, J.S. and PIERSOL, A.G. (1971) *Random data: Analysis and measurement procedures* (Wiley Interscience, New York).
- BERANEK, L.L. (1971) *Noise and vibration control* (McGraw-Hill Book Company, New York).
- BOGER, H.W. (1971) Valve and downstream accessories as a low noise package. *Flow: Its measurement and control in science and industry. Symp. Proc. Pittsburg, Pa.*, 1 (3), 1161-1166.
- BOLLETER, U. and CHANAUD, R.C. (1970) Propagation of fan noise in cylindrical ducts. *J. Acoust. Soc. Amer.* 49 (3), 627-638.
- BULL, M.K. (1963) Wall pressure fluctuations associated with subsonic turbulent boundary layer flow. Ph.D. Thesis, University of Southampton.
- BULL, M.K. (1967) Wall pressure fluctuations associated with subsonic turbulent boundary layer flow. *J. Fluid Mech.* 28, 719-754.
- BULL, M.K. (1978) Personal Communication.

- BULL, M.K. and NORTON, M.P. (1976) Effects of internal flow disturbances on acoustic radiation from pipes. Proc. I.E. Aust. Vibration and Noise Control Engineering Conference, Sydney, 61-65.
- BULL, M.K. and NORTON, M.P. (1977,a) Higher order acoustic modes due to internal flow disturbances in relation to acoustic radiation from pipes. Proc. 9th International Congress on Acoustics, Madrid, Contributed Papers Vol. II, 726.
- BULL, M.K. and NORTON, M.P. (1977,b) Pressure fluctuations in turbulent pipe flow due to a mitred bend. Proc. I.E. Aust. 6th Australasian Hydraulics and Fluid Mechanics Conference, Adelaide, 273-277.
- BULL, M.K., PICKLES, J.M. and RENNISON, D.C. (1976) Sound generation by fully developed turbulent pipe flow. University of Adelaide Tech. Note No. 7.
- BULL, M.K. and RENNISON, D.C. (1974,a) Acoustic radiation from pipes with internal gas flows. Proc. Noise, Shock and Vibration conference, Monash Univ., Australia, 393-405.
- BULL, M.K. and RENNISON, D.C. (1974,b) Turbulent pipe flow as an acoustic noise source. Proc. 5th Australasian Hydraulics and Fluid Mechanics Conference, Christchurch, New Zealand, 583-590.
- BULL, M.K. and RENNISON, D.C. (1974,c) Noise generation by pipe flow: theory and experiment. Proc. I.E. Aust. Thermafluids Conference, Melbourne, 76-80.
- CLAUSER, F.H. (1954) Turbulent boundary layers in adverse pressure gradients. J. Aero. Sciences. 21, 91-108.
- CLINCH, J.M. (1970) Prediction and measurement of the vibrations induced in thin-walled pipes by the passage of internal turbulent waterflow. J. Sound and Vib. 12, 429-451.

- COCKBURN, J.A. and ROBERTSON, J.E. (1974) Vibration response of spacecraft shrouds to in flight fluctuating pressures. *J. Sound and Vib.* 33 (4), 399-425.
- CORCOS, G.M. (1962) Pressure fluctuations in shear flows. Univ. of California, Inst. of Eng. Res. Rept., Series 183, No. 2.
- CORCOS, G.M. (1963) The structure of the turbulent pressure field in boundary layer flows. *J. Fluid Mech.* 18, 353-378.
- CREMER, L. (1955) Theory of the transmission loss of cylindrical shells (in German). *Acustica* 5, 245-256.
- DYER, I. (1959) Response of plates to a decaying and convecting random pressure field. *J. Acoust. Soc. Amer.* 31 (7), 922-928.
- FRICKE, F.R. and STEVENSON, D.C. (1968) Pressure fluctuations in a separated flow region. *J. Acoust. Soc. Amer.* 44 (5), 1189-1200.
- FRICKE, F.R. and STEVENSON, D.C. (1971) Estimation of wall pressure fluctuations in a separated flow. *J. Acoust. Soc. Amer.* 50 (3), 985-991.
- FRICKE, F.R. (1971) Pressure fluctuations in separated flows. *J. Sound and Vib.* 17 (1), 113-123.
- FUCHS, H.V. (1969) Energy balance for small fluctuations in a moving medium. University of Southampton, J.S.V.R. Tech. Rept. 18.
- GOFF, K.W. (1955) The application of correlation techniques to some acoustical measurements. *J. Acoust. Soc. Amer.* 50 (1), 236-242.
- GOLDSTEIN, S. (1955) *Modern developments in Fluid Dynamics* (Dover Publications, New York).

- GORDON, C.G. and MAIDANIK, G. (1967) Influence of upstream flow discontinuities on the acoustic power radiated by a model air jet. N.A.S.A. Contractor Report, CR-679.
- GORDON, C.G. (1968) Spoiler generated flow noise. I - the experiment. J. Acoust. Soc. Amer. 43 (5) 1041-1048.
- GORDON, C.G. (1969) Spoiler generated flow noise. II - Results. J. Acoust. Soc. Amer. 45 (1) 214-223.
- HAYDEN, R.E. (1972) Noise from interaction of flow with rigid surfaces: A review of current status of prediction techniques. N.A.S.A. Contractor Report, CR-2126.
- HECKL, M. (1958) Experimental investigation of the transmission loss of cylinders (in German). Acustica 8, 259-265.
- HECKL, M. (1962) Vibrations of point driver cylindrical shells. J. Acoust. Soc. Amer. 34 (10), 1553-1557.
- HESKESTAD, G. (1971) Two dimensional mitre bend flow. Trans. A.S.M.E., J. Basic Engineering, Sept., 433-455.
- HYLAND, C.E. (1979) Noise generation due to orifices in pipework with flow. Master of Eng. Sc. Thesis, Adelaide University (thesis submitted, January 1979).
- KARVELIS, A.V. (1975) An experimental investigation of the wall pressure fluctuations in piping containing simple control devices. Ph.D. Thesis. The Pennsylvania State University.
- KINNIS, R. (1973) A guide to digital spectral analysis. University of Cambridge C.U.E.D./A - Aerodynamics/TR 3.
- KINSLER, L.F. and FREY, A.R. (1962) Fundamentals of Acoustics. (John Wiley and Sons, New York).
- KUHN, G.F. (1974) Sound transmission through ducts with and without flow. University of Southampton, I.S.V.R. Tech. Rept. 65.

- KUHN, G.F. and MORFEY, C.L. (1976,a) Transmission of low frequency internal sound through pipe walls. J. Sound and Vib. 47 (2), 147-161.
- KUHN, G.F. and MORFEY, C.L. (1976,b) Noise due to fully developed turbulent flow exhausting from straight and bent pipes. J. Sound and Vib. 44 (1), 27-35.
- LIM, K.B. (1971) A study of pressure fluctuations in turbulent shear flows under the effects of mean pressure gradients. Ph.D. Thesis. The University of Adelaide.
- LYNN, P.A. (1970) Economic linear phase recursive digital filters. Electron. Lett., 6, 143-145.
- LYNN, P.A. (1972) Recursive digital filters with linear phase characteristics. Computer Journal, 15, 337-342.
- LYON, R.H. (1956) Response of strings to random noise fields. J. Acoust. Soc. Amer. 28 (3), 391-398.
- MABEY, D.G. (1972) Analysis and correlation of data on pressure fluctuations in separated flow. J. Aircraft. 9 (1), 642-645.
- MAESTRELLO, L. (1965,a) Measurement of noise radiated by boundary layer excited panels. J. Sound and Vib. 2 (2), 100-115.
- MAESTRELLO, L. (1965,b) Measurement and analysis of the response field of turbulent boundary layer excited panels. J. Sound and Vib. 2 (3), 270-292.
- MAESTRELLO, L. (1967) Use of a turbulent model to calculate the vibration and radiation responses of a panel, with practical suggestions for reducing sound level. J. Sound and Vib. 5 (3), 407-448.
- MASON, V. (1969) Some experiments on the propagation of sound along a cylindrical duct containing flowing air. J. Sound and Vib. 10 (2), 208-226.

- MILLER, D.K. and HART, F.D. (1967) Modal density of thin circular cylinders. N.A.S.A. Contractor report. CR-897.
- MORFEY, C.L. (1964) Rotating pressure patterns in ducts: Their generation and transmission. J. Sound and Vib. 1, 60-87.
- MORFEY, C.L. (1968) A review of the sound generating mechanisms in aircraft engine fans and compressors. A.F.O.S.R. - U.T.I.A.S. Symposium on Aerodynamic Noise, Toronto.
- MORFEY, C.L. (1968) Noise and Acoustic Fatigue in Aeronautics (Richards, E.J. and Mead, D.J., Editors), Chapter 10, p. 233, John Wiley and Sons, London.
- MORFEY, C.L. (1971) Transmission through duct walls of internally propagated sound. Proc. 7th International Congress on Acoustics. Paper 24, A9, Budapest.
- MORSE, R.M. and INGARD, U. (1968) Theoretical Acoustics (McGraw Hill, New York).
- NEWLAND, D.E. (1975) Random Vibrations and Spectral Analysis (Longman, London).
- NORTON, M.P., HYLAND, C.E., and BULL, M.K. (1978) The prediction of acoustic radiation from and the acceleration response of pipes with various internal flow disturbances. Proc. I.E. Aust. Applied Mechanics Conf. and Workshop, Adelaide, 34-36.
- PAPOULIS, A. (1965) Probability, Random Variables, and Stochastic Processes (McGraw Hill, Tokyo).
- POWELL, A. (1958,a) On the fatigue failure of structures to the vibrations excited by random pressure fields. J. Acoust. Soc. Amer. 30 (12), 1130-1135.
- POWELL, A. (1958,b) On the approximation to the infinite solution by the method of normal modes from random vibrations. J. Acoust. Soc. Amer. 30 (12), 1136-1139.

- RATTAYYA, J.V. and JUNGER, M.C. (1964) Flow excitation of cylindrical shells and associated coincidence effects. *J. Acoust. Soc. Amer.* 36, (5), 878-884.
- RENNISON, D.C. (1976) The vibrational response of and the acoustic radiation from thin walled pipes, excited by random fluctuating pressure fields. Ph.D. Thesis. University of Adelaide.
- RENNISON, D.C. and BROWN, G.L. (1974) Sound radiation from pipes excited by plane acoustic waves. *Proc. Noise, Shock and Vib. Conf.*, Monash Univ., Melb., 416-425.
- RENNISON, D.C. and BULL, M.K. (1976) On the modal density and damping of cylindrical pipes. *J. Sound and Vib.* 54 (1), 39-53.
- SCHLICHTING, H. (1968) *Boundary layer theory* (McGraw Hill, New York).
- SEEBOLD, J.G. (1971) Valve noise and piping system design. *Flow: Its measurement and control in science and industry. Symp. Proc. Pittsburg, Pa.*, 1 (3), 1151-1159.
- STRAWDERMAN, W.A. and CHRISTMAN, R.A. (1972) Turbulence induced plate vibrations: Some effects of fluid loading on finite and infinite plates. *J. Acoust. Soc. Amer.* 52 (5) 1537-1552.
- SZECHENYI, E. (1971) Modal densities and radiation efficiencies of unstiffened cylinders using statistical methods. *J. Sound and Vib.* 19 (1), 65-81.
- THOMAS, A.S.W. (1977) Organised structures in the turbulent boundary layer. Ph.D. Thesis. University of Adelaide.
- TUNSTALL, M.J. and HARVEY, J.K. (1968) On the effect of a sharp bend in a fully developed turbulent pipe flow. *J. Fluid Mech.* 34 (3), 595-608.

- WALTER, J.L., McDANIEL, O.H. and REETHOF, G. (1977) The coincidence of higher order acoustic modes in pipes with the pipe vibrational modes. J. Acoust. Soc. Amer. 62, S84, JJ10.
- WALTER, J.L., McDANIEL, O.H. and REETHOF, G. (1978) The coincidence of higher order acoustic modes in pipes with the pipe vibrational modes. Proc. Internoise 78, San Francisco, 1049-1050.
- WATTS, D.G. (1962) A general theory of amplitude quantization with applications to correlation determination. Inst. Elec. Eng. Proc. 109 (C), 209-214.
- WHITE, P.H. (1969) Cross correlation in structural systems: Dispersion and non-dispersion waves. J. Acoust. Soc. Amer. 45, (5), 1118-1128.
- WHITE, P.H. and SAWLEY, R.J. (1972) Energy transmission in piping systems and its relation to noise control. A.S.M.E. Transactions, J. Eng. Industry, May, 746-751.
- WIDROW, B. (1956) A study of rough amplitude quantization by means of Nyquist sampling theory. I.R.E., Trans. Circuit Theory, CT-3 (2), 266-270.
- WILBY, J.F. (1967) The response of panels to turbulent boundary layer excitation. Ph. D. Thesis, University of Southampton.
- WILLMARTH, W.W. and WOOLDRIDGE, C.E. (1962) Measurements of the fluctuating pressure at the wall beneath a thick turbulent boundary layer. J. Fluid. Mech. 14, 187-210.

APPENDIX A

ESTIMATION OF ACOUSTIC COINCIDENCE FOR HIGHER ORDER MODES

From the solution to the wave equation for the pressure associated with acoustic propagation in a stationary internal fluid, the relationship between the cut-off frequency, $(v_{co})_{pq}$, of the (p,q)th acoustic mode and its axial wavenumber, K_x , as given by equation [2.4] is

$$v_{pq}^2 = (v_{co})_{pq}^2 + \left(\frac{K_x c_i}{M_{LP} c_e} \right)^2, \quad [A.1]$$

and, the resonance frequency of the (m,n)th structural mode of a thin cylindrical pipe, as given by equation [2.8], is

$$v_{mn}^2 = \beta^2 K^4 + \frac{\psi^2 K_m^4}{K^4}. \quad [A.2]$$

At coincidence,

- (i) the circumferential distance along the pipe surface between diametral nodes of the (p,q)th acoustic mode is equal to half the wavelength of the (m,n)th structural mode in the same direction, thus $n = p$.
- (ii) The structural and acoustic wavenumbers in the axial direction are equal - thus $K_x = K_m$.
- (iii) The coincidence frequency is the resonance frequency of the (m,n)th structural mode - $v_{m,n} = v_{n,q} = v_c$.

It should be noted here that the following derivation applies to the theoretical case of continuous K_m and does not take account of K_m having only discrete values. Thus at coincidence,

$$v_c^2 = (v_{co})_{pq}^2 + \left(\frac{K_m c_i}{M_{LP} c_e} \right)^2 = \beta^2 (K_m^2 + K_n^2)^2 + \frac{\psi^2 K_m^4}{(K_m^2 + K_n^2)^2} \quad [A.3]$$

K_m is always small in comparison to K_n for low order acoustic modes at frequencies in the region of coincidence ($K_m = m\pi a_m / \ell$ and $K_n = n$). Furthermore for steel pipes, $M_{LP} \gg 1$ and thus,

$$(v_{co})_{pq}^2 \approx \beta^2 K_n^4 + \frac{\psi^2 K_m^4}{K_n^4},$$

and hence,

$$K_m^4 \approx \frac{K_n^4}{\psi^2} [(v_{co})_{pq}^2 - \beta^2 K_n^4] \quad [A.4]$$

Substituting for K_m in equation [A.1] at coincidence and rearranging,

$$v_c^2 \approx (v_{co})_{pq}^2 + \frac{1}{\psi} \left(\frac{n c_i}{M_{LP} c_e} \right)^2 (v_{co})_{pq} \left[1 - \frac{\beta^2 n^4}{(v_{co})_{pq}^2} \right]^{\frac{1}{2}} \quad [A.5]$$

For thin cylindrical pipes, $\beta^2 n^4 \ll (v_{co})_{pq}^2$ and thus,

$$v_c^2 \approx (v_{co})_{pq}^2 + \frac{(v_{co})_{pq}}{\psi} \left(\frac{n c_i}{M_{LP} c_e} \right)^2 \quad [A.6]$$

Equation [A.6] can be rewritten as,

$$v_c \approx (v_{co})_{pq} \left[1 + \frac{1}{\psi (v_{co})_{pq}} \left(\frac{n c_i}{M_{LP} c_e} \right)^2 \right]^{\frac{1}{2}}$$

For steel pipes $M_{LP} \gg 1$ and if we assume that $c_i \approx c_e$, then

$$v_c \approx (v_{co})_{pq} + \frac{n^2}{2\psi M_{LP}^2} \quad [A.7]$$

From equation [A.3], at coincidence,

$$K_m^2 = M_{LP}^2 [v_c^2 - (v_{co})_{pq}^2] \quad , \quad [A.8]$$

and thus from equation [A.6],

$$K_m^2 \approx n^2 (v_{co})_{pq} / \psi \quad ,$$

and hence,

$$K_x = K_m \approx n \sqrt{(v_{co})_{pq} / \psi} \quad [A.9]$$

TABLE A-1

A comparison of the coincidence frequency with the corresponding cut-off frequency for several higher order acoustic modes for $M_{LP} = 15.37$, $\psi = 0.960$ and $a_i = 0.03627m$, as obtained from equations [A.7] and [A.9].

n or p	q	α_{nq}	$(v_{co})_{nq}$	v_c	K_m	v_c/v_{co}
0	0	0.0000	-	-	-	-
1	0	0.5861	0.1221	0.1243	0.3566	1.0181
2	0	0.9722	0.2025	0.2113	0.9186	1.0435
0	1	1.2197	0.2541	NOT APPLICABLE		
3	0	1.3369	0.2785	0.2983	1.6158	1.0711
4	0	1.6931	0.3527	0.3880	2.4245	1.1001
1	1	1.6970	0.3535	0.3557	0.6068	1.0062
5	0	2.0420	0.4254	0.4807	3.3284	1.1300
2	1	2.1346	0.4446	0.4534	1.3611	1.0198
0	2	2.2331	0.4652	NOT APPLICABLE		
3	1	2.5812	0.5377	0.5575	2.2452	1.0368
1	2	2.7140	0.5653	0.5675	0.7674	1.0039
4	1	2.9891	0.6226	0.6579	3.2213	1.0567
2	2	3.1734	0.6610	0.6698	1.6596	1.0133
0	3	3.2744	0.6821	NOT APPLICABLE		
5	1	3.3880	0.7057	0.7608	4.2869	1.0781
3	2	3.6533	0.7610	0.7808	2.6710	1.0260
1	3	3.7692	0.7851	0.7873	0.9043	1.0028
4	2	4.0835	0.8506	0.8859	3.7652	1.0415

TABLE A-2

A comparison between v_c/v_{co} as obtained from (a) Equation [A.7]; (b) a numerical solution of Heckl's equation and equation [2.4] and (c) a graphical solution of Arnold and Warburton's equation and equation [2.4].

p	q	Calculated	Heckl	A & W
		v_c/v_{co}	v_c/v_{co}	v_c/v_{co}
1	0	1.0181	1.0206	1.0302
1	1	1.0062	1.0104	1.0165
1	2	1.0039	1.0094	1.0152
2	0	1.0435	1.0582	1.0671
2	1	1.0198	1.0391	1.0457
2	2	1.0133	1.0456	1.0529
3	0	1.0771	1.1043	1.1126
3	1	1.0368	1.0902	1.0962
3	2	1.0260	1.1376	1.1443

TABLE A-3

A comparison of the coincidence frequency with the corresponding cut-off frequency for several higher order acoustic modes for $M_{LP}=15.37$, $\psi = 0.960$, $a_i = 0.03627\text{m}$ and $\beta = 0.0070$, as obtained from the improved approximation (Equation[2.17]). Values of v_c/v_{co} obtained from equation A-7 are presented in the last column for comparison.

n or p	q	$(v_{co})_{nq}$	v_c	Equation[2.17] v_c/v_{co}	Equation[A-7] v_c/v_{co}
0	0	NOT APPLICABLE			
1	0	0.1221	0.1247	1.0213	1.0181
2	0	0.2025	0.2144	1.0588	1.0435
0	1	0.2541	NOT APPLICABLE		
3	0	0.2785	0.3091	1.1099	1.0711
4	0	0.3527	0.4127	1.1701	1.1001
1	1	0.3535	0.3571	1.0102	1.0062
5	0	0.4254	0.5212	1.2252	1.1300
2	1	0.4446	0.4617	1.0385	1.0198
0	2	0.4652	NOT APPLICABLE		
3	1	0.5377	0.5842	1.0865	1.0368
1	2	0.5653	0.5702	1.0087	1.0039
4	1	0.6226	0.7208	1.1577	1.0567
2	2	0.6610	0.6849	1.0362	1.0133
0	3	0.6821	NOT APPLICABLE		
5	1	0.7057	0.8812	1.2487	1.0781
3	2	0.7610	0.8277	1.0876	1.0260
1	3	0.7851	0.7920	1.0088	1.0028
4	2	0.8506	0.9951	1.1699	1.0415

APPENDIX BGENERAL FORMALISM OF THE PIPE RESPONSE AND ACOUSTIC RADIATION

To estimate the vibration response of the pipe wall and the external acoustic radiation, the nature of the internal acoustic field has to be known and in particular the various components of the wall pressure fluctuations.

Equations derived from a general solution to the dynamic response of a thin-walled cylindrical shell to an acoustic pressure field dominated by higher order acoustic modes leads to an estimation of the acoustic radiation from and the acceleration response of pipes with various internal flow disturbances as discussed in Chapter 7. Bull and Rennison (1974) have developed a procedure for calculating the dynamic response of a thin-walled cylindrical shell to the random pressure field generated by a fully-developed turbulent pipe flow, and this procedure is summarized here for an arbitrary random wall pressure field $\phi_p(\omega)$. For the purposes of analysis, the pipe is modelled as a thin cylindrical shell with simply supported ends, and the calculation of the statistical properties of the vibration response is based on the normal mode method of generalised harmonic analysis (Powell, 1958). The pipe structure is considered to be homogeneous over its surface area and the resonant structural modes which make up the total response of the pipe structure are assumed to be independent and lightly damped i.e. no modal coupling due to damping occurs.

The spectral density of the displacement response, ϕ_ζ , averaged over the pipe surface, to a random, stationary and homogeneous pressure field as derived by Bull and Rennison (1974), following Powell (1958) is

$$[[\phi_{\zeta}]] = \phi_p(\omega) S^2 \sum_{\alpha} \frac{[[\psi_{\alpha}^2(\underline{r})]] j_{\alpha\alpha}^2(\omega)}{|Z_{\alpha}(\omega)|^2}, \quad [\text{B.1}]$$

where $[[\]]$ indicates a spatial average over the vibrating surface, $\phi_p(\omega)$ is the power spectral density of the random wall pressure field, S is the surface area of the pipe and \underline{r} defines the co-ordinates of the pipe surface. $\psi_{\alpha}(\underline{r})$ defines the shape of the $\alpha = 1, \dots, N$ independent normal modes which are assumed to be uncoupled and orthogonal. The joint acceptance, $j_{\alpha\alpha}^2(\omega)$ of the α th mode, expresses the degree of spatial coupling that exists between the pressure excitation and the structural mode, and $Z_{\alpha}(\omega)$ is the generalised obstructance, where

$$Z_{\alpha}(\omega) = M_{\alpha} \left[\omega_{\alpha}^2 - \omega^2 + i \left(\frac{\omega_{\alpha} \omega}{Q_{\alpha}} \right) \right], \quad [\text{B.2}]$$

and M_{α} , ω_{α} and Q_{α} are respectively the generalised mass, resonance frequency and quality factor of the α th mode.

The spectral density of the pipe acceleration response, $\phi_{\zeta}^{\ddot{}}$, averaged over the pipe surface is

$$[[\phi_{\zeta}^{\ddot{}}(\omega)]] = [[\phi_{\zeta}(\omega)]] \omega^4. \quad [\text{B.3}]$$

Hence from equation [B.1]

$$\frac{[[\phi_{\zeta}^{\ddot{}}(\omega)]]}{\phi_p(\omega)} = S^2 \sum_{\alpha} \frac{[[\psi_{\alpha}^2(\underline{r})]] j_{\alpha\alpha}^2(\omega)}{M_{\alpha}^2 \left[\left(1 - \left(\frac{\omega_{\alpha}}{\omega} \right)^2 \right)^2 + \left(\frac{\omega_{\alpha}}{\omega Q_{\alpha}} \right)^2 \right]}. \quad [\text{B.4}]$$

For homogeneous structures, and mode shapes corresponding to simply supported ends, $\psi_{\alpha}^2(\mathbf{r})$ and M_{α} are independent of α ; also $[\psi^2] = \frac{1}{4}$ and $M = \rho_s h S / 4$ for all modes (Both sets of modes as given by the separable functions, equation [2.11], must be considered for the calculation of a homogeneous vibration response to a circumferentially homogeneous excitation, Powell (1964)). Hence

$$\frac{[\phi_{\zeta}(\omega)]}{\phi_p(\omega)} = \frac{4}{\rho_s^2 h^2} \sum_{\alpha} \frac{j_{\alpha\alpha}^2(\omega)}{[1 - (\frac{\omega_{\alpha}}{\omega})^2]^2 + [\frac{\omega_{\alpha}}{\omega Q_{\alpha}}]^2} \quad [\text{B.5}]$$

The non-dimensional spectral density of the pipe wall acceleration, averaged over the pipe surface is $\Phi_{\zeta}(\omega)$, where $\Phi_{\zeta}(\omega) = [\phi_{\zeta}(\omega)] / a_m^2 \omega^3$. Experimental data of the power spectral density of the wall pressure fluctuations are presented in the form of the mean non-dimensional power spectral density $\Phi_p(\omega) = \phi_p(\omega) U_o / q_o^2 a_i$. Hence, equation B.5 can be non-dimensionalised

$$\frac{\Phi_{\zeta}(\omega)}{\Phi_p(\omega)} = \frac{\rho_{fs}^2 M_{oi}^3 a_i}{12 \beta^2 M_{LP}^3 a_m} \sum_{\alpha} \frac{j_{\alpha\alpha}^2(\omega)}{[1 - (\frac{\omega_{\alpha}}{\omega})^2]^2 + [\frac{\omega_{\alpha}}{\omega Q_{\alpha}}]^2} \quad [\text{B.6}]$$

The spectral density of the acoustic power radiation from the pipe can be defined as

$$\phi_{\pi}(\omega) = R_{\text{rad}} [\phi_{\zeta}] \omega^2, \quad [\text{B.7}]$$

where $R_{\text{rad}} = \rho_e c_e S \sigma_{\alpha}$ is the pipe radiation resistance, σ_{α} is the radiation ratio, ρ_e and c_e are respectively the density of and the speed of sound in the fluid outside the pipe and S is the surface area of the pipe. The non-dimensional spectral density of the acoustic

power radiation, Φ_{π} , is defined as $\Phi_{\pi}(\omega) = \phi_{\pi}(\omega) / \rho_e c_e^2 S a_m$, hence

$$\Phi_{\pi}(\omega) = \frac{\Phi_{\zeta}(\omega) \sigma_{\alpha} M_{LP}}{v^2}, \quad [\text{B.8}]$$

and

$$\frac{\Phi_{\pi}(\omega)}{\Phi_p(\omega)} = \frac{\rho_{fs}^2 M_o^3 a_i}{12\beta^2 v^2 M_{LP}^2 a_m} \sum_{\alpha} \frac{j_{\alpha\alpha}^2(\omega) \sigma_{\alpha}}{\left[1 - \left(\frac{\omega}{\omega_{\alpha}}\right)^2\right]^2 + \left[\frac{\omega}{\omega Q_{\alpha}}\right]^2}. \quad [\text{B.9}]$$

Equations [B.6] and [B.9] can be used to predict the acoustic radiation from and the acceleration response of pipes with various internal flow disturbances by averaging over $1/3$ octave bands (by integrating and dividing by the bandwidth), as discussed in detail in Chapter 7.

APPENDIX CVARIOUS EXPERIMENTAL RESULTS FOR ORIFICE PLATES

As mentioned in chapter 3, most of the results presented for the orifice plates (chapter 7) were obtained in conjunction with Hyland (1979). A more extensive selection of Hyland's (1979) results are presented here for comparison with the other internal flow disturbances reported on in this thesis.

The data presented comprise (i) Non dimensional spectra of wall pressure fluctuations; (ii) Non dimensional spectra of acoustic power radiated; (iii) Narrow band analysis of acoustic power radiated; (iv) Non dimensional pipe wall acceleration spectra; (v) Narrow band analysis of pipe wall acceleration; and (vi) Spectral densities of pipe wall acceleration, acoustic power radiation and radiation ratios relative to straight pipe flow.

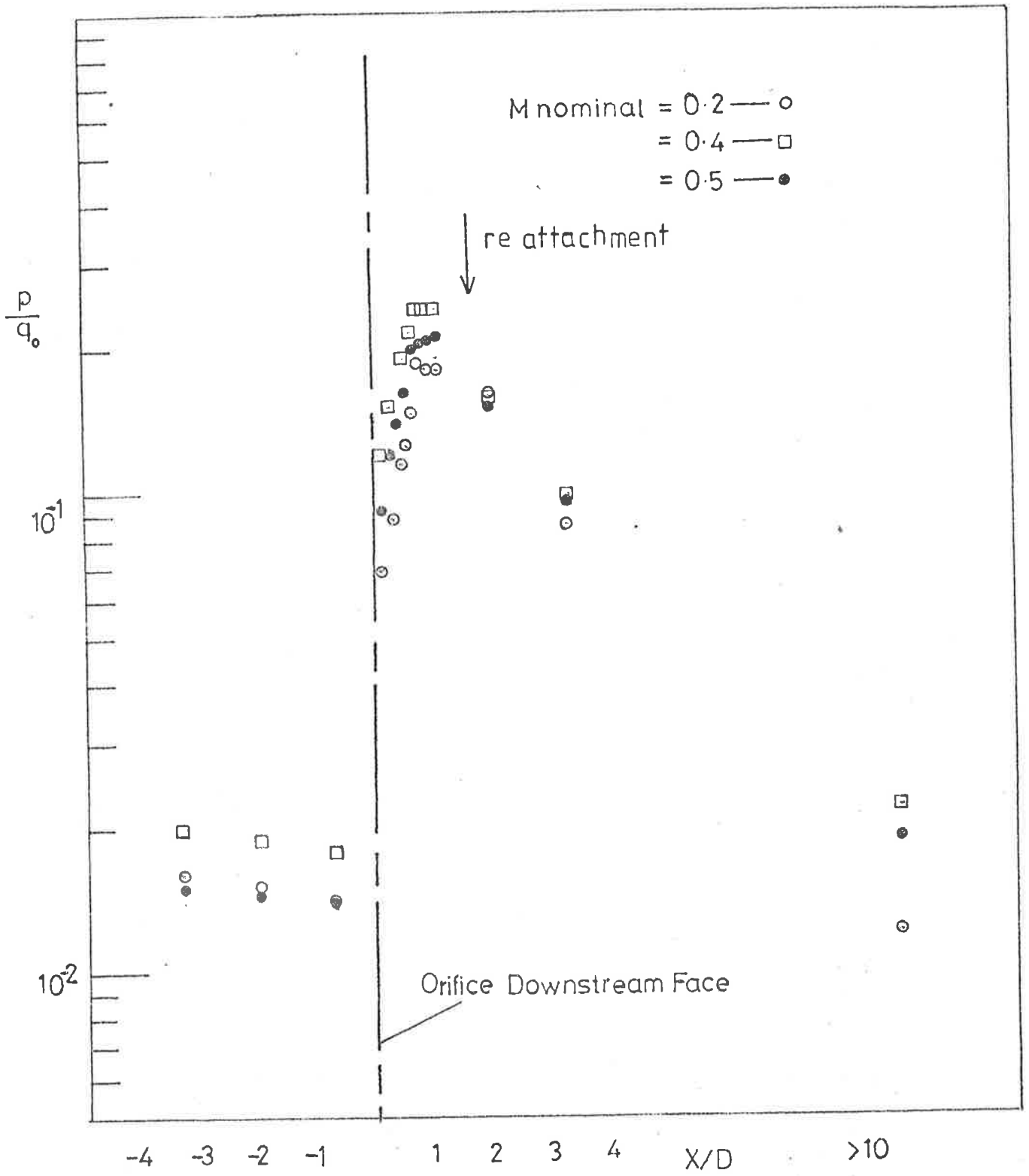


FIG C-2 R.M.S. PRESSURE FLUCTUATIONS

55mm Orifice

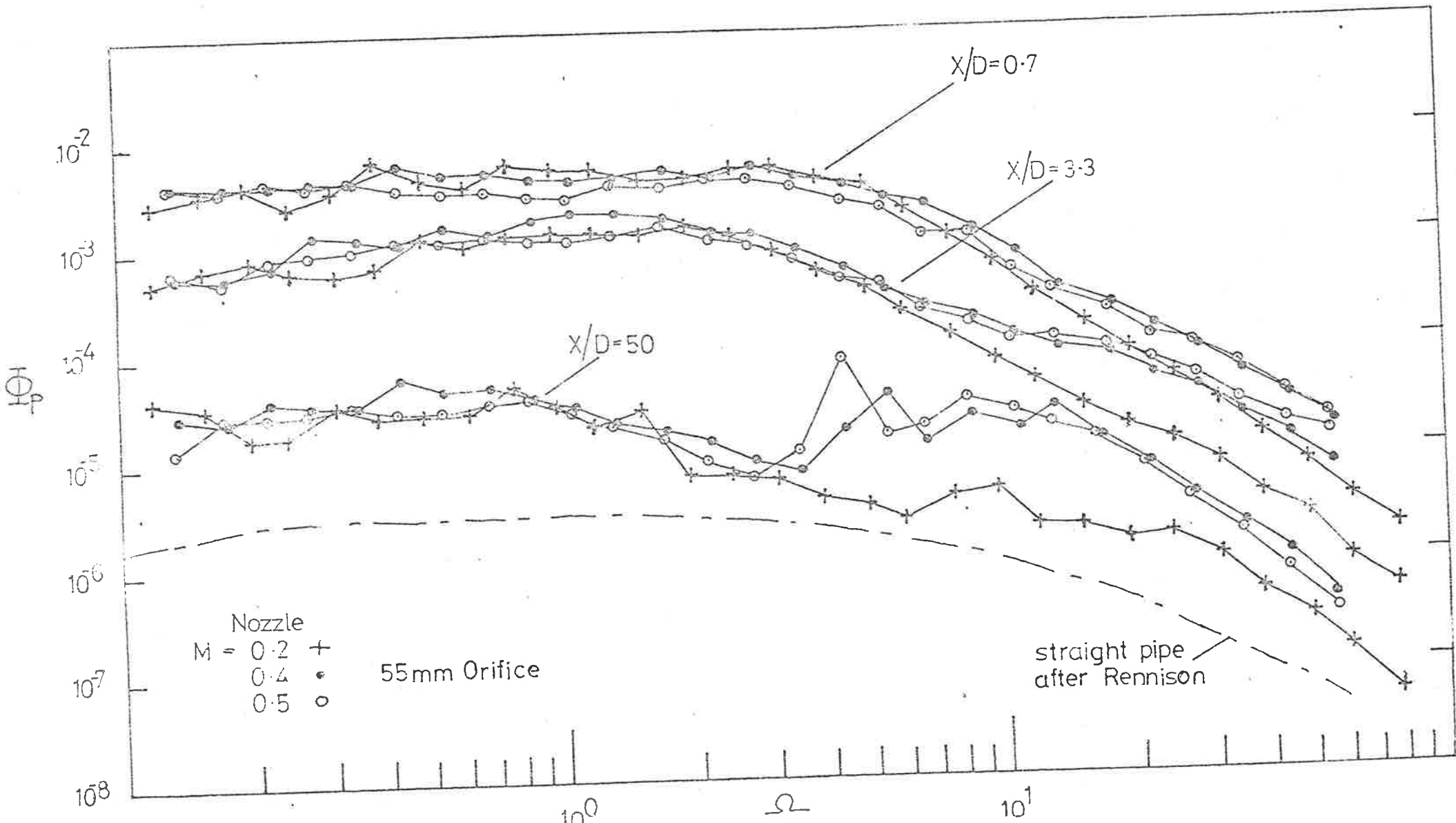


FIG C-3

NON DIMENSIONAL SPECTRA of WALL-PRESSURE FLUCTUATIONS

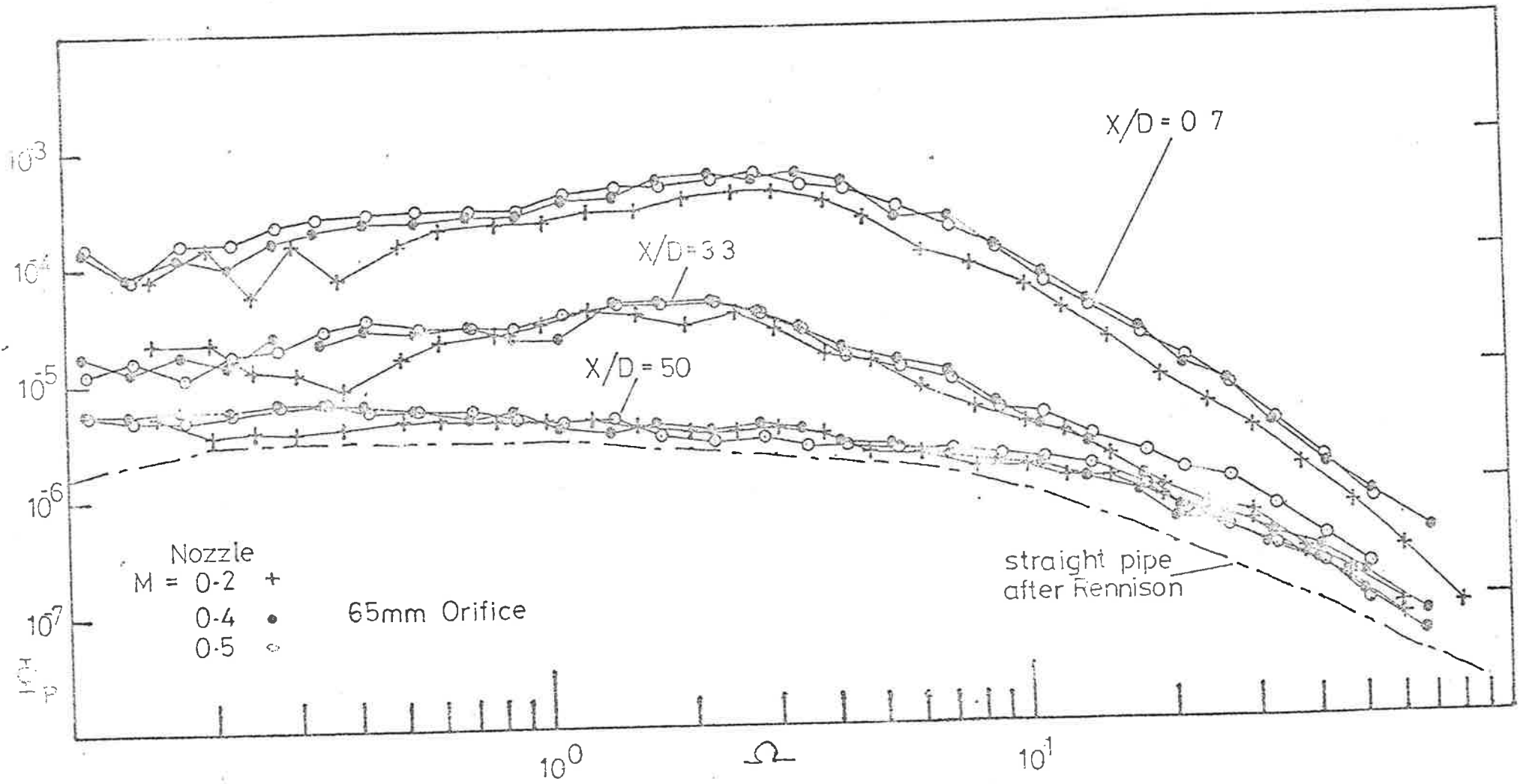
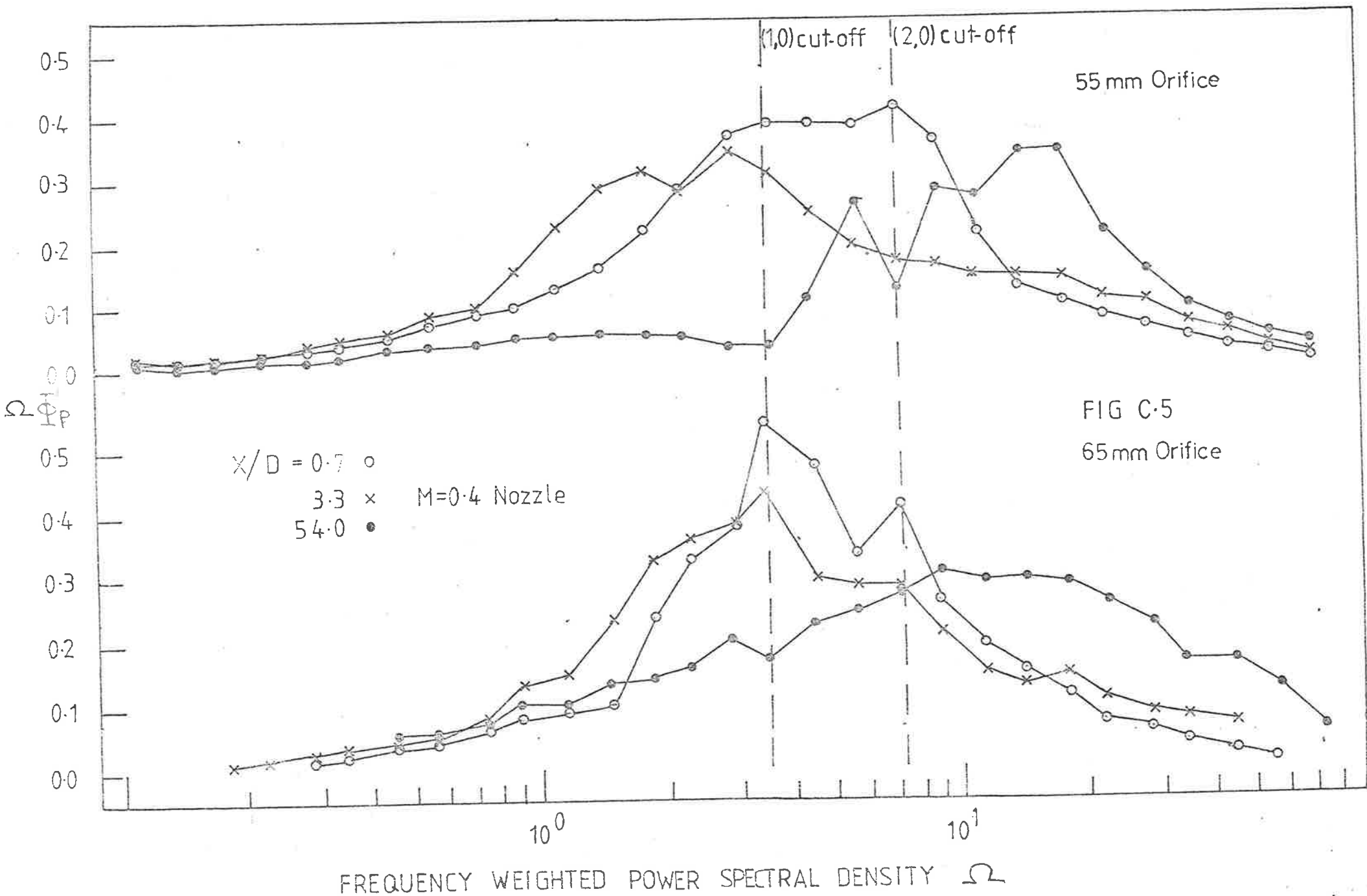


FIG C-4

NON DIMENSIONAL SPECTRA of WALL-PRESSURE FLUCTUATIONS



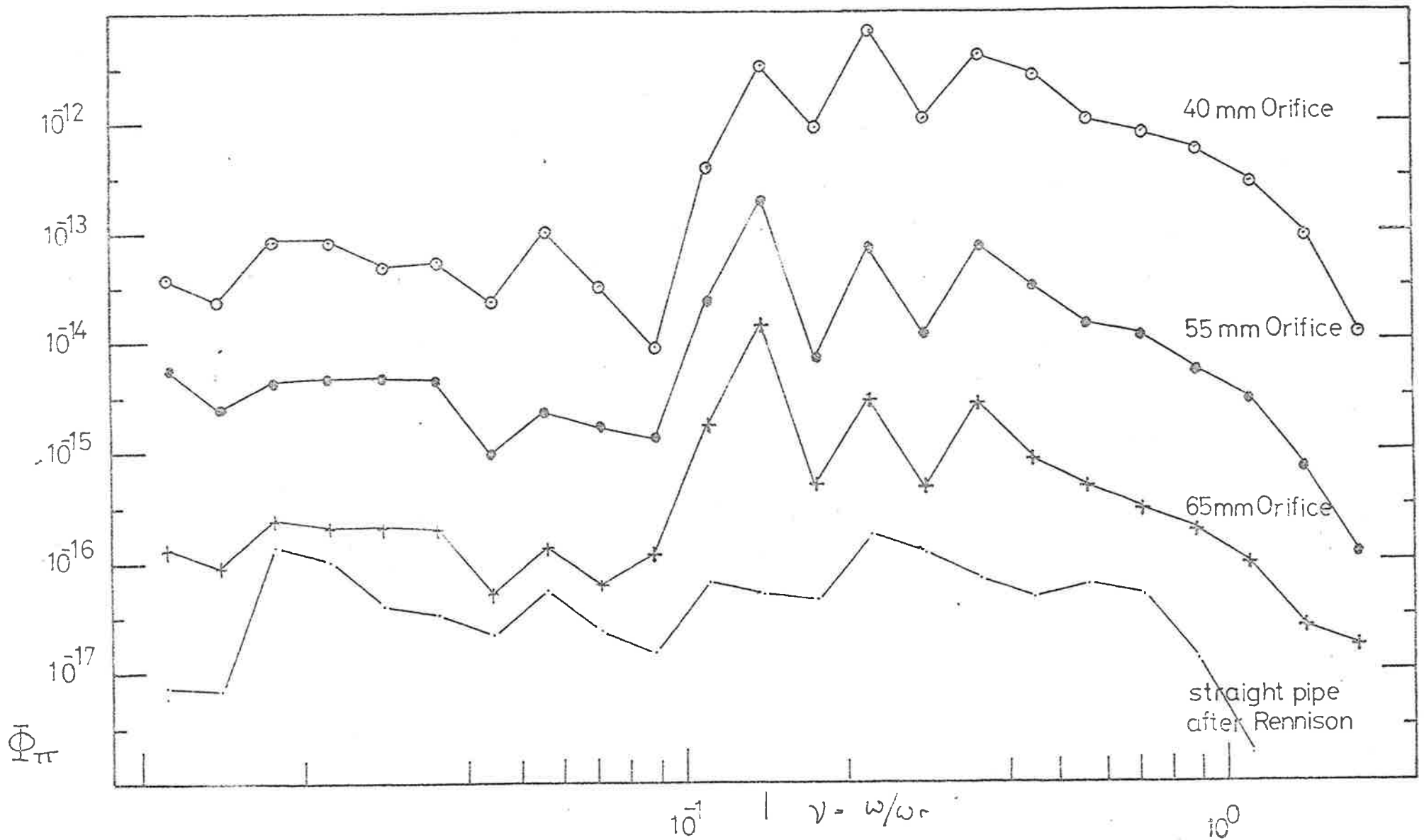


FIG.C.6 NON-DIMENSIONAL SPECTRA OF ACOUSTIC POWER RADIATED

M nominal = 0.2 for various orifices.

thin walled pipe. $X/D = 50$

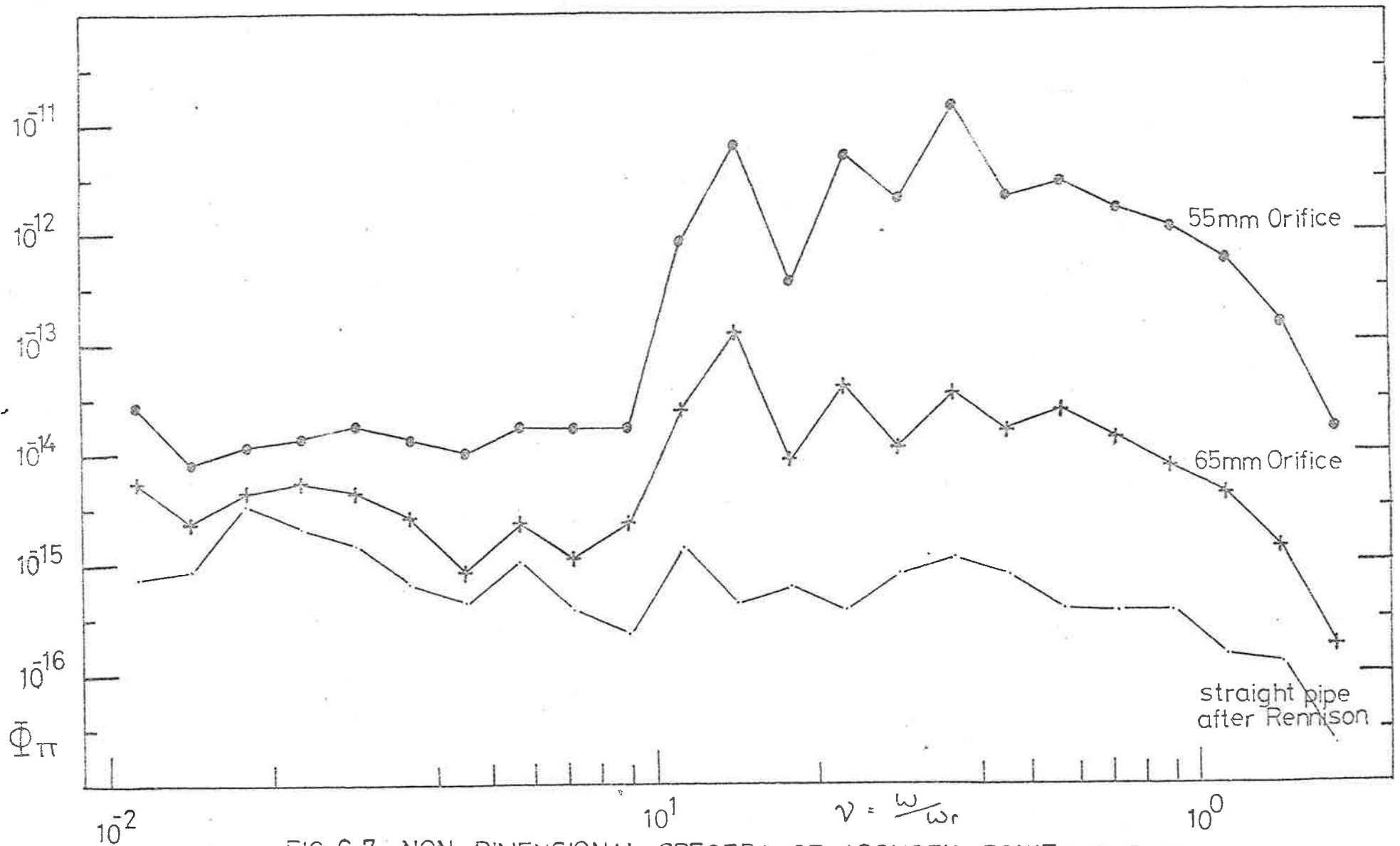


FIG. C.7 NON-DIMENSIONAL SPECTRA OF ACOUSTIC POWER RADIATED

M nominal = 0.35 for various orifices.

from thin walled pipe $X/D = 50$

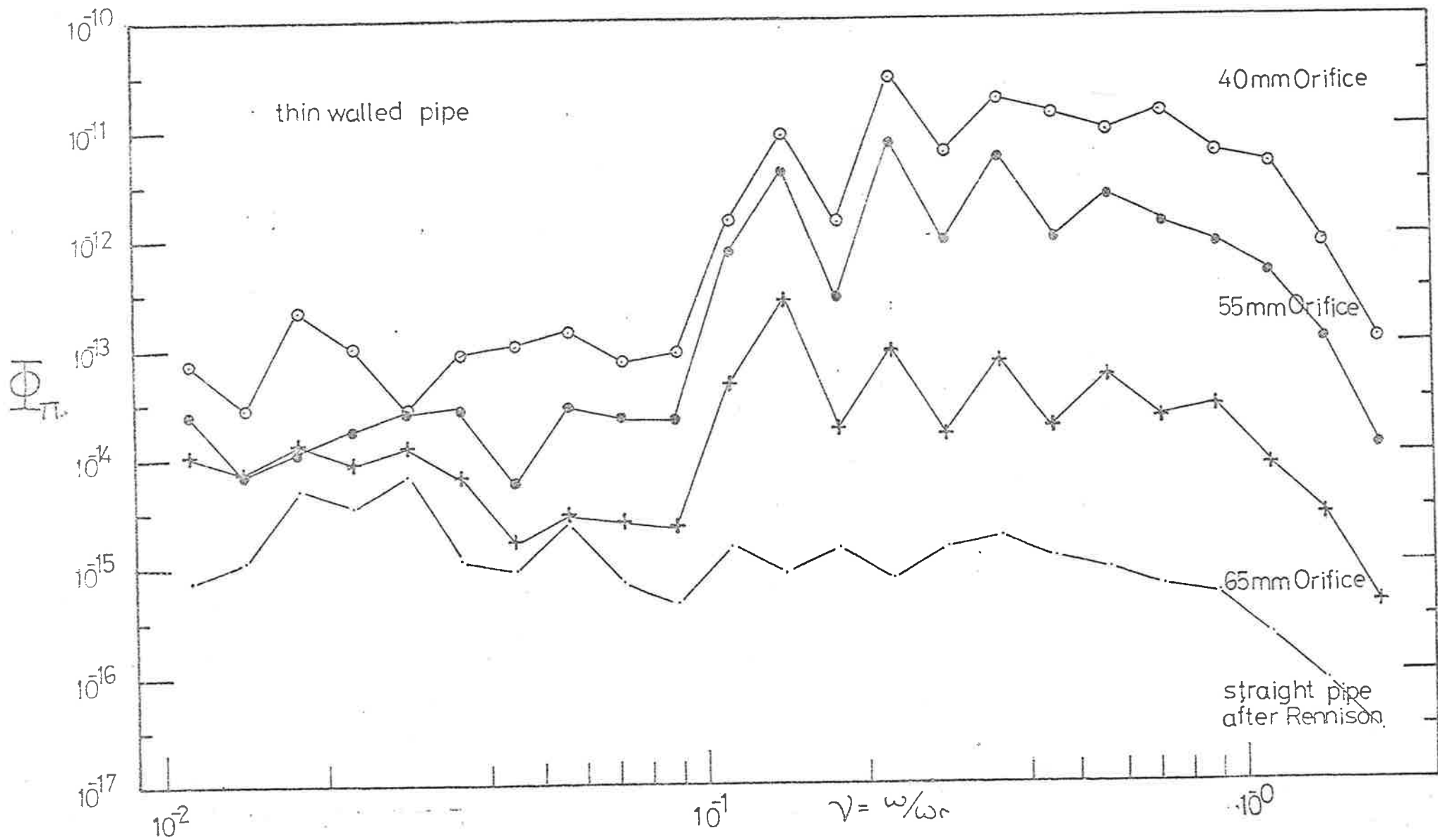


FIG. C-8 NON-DIMENSIONAL SPECTRA OF ACOUSTIC POWER RADIATED

M nominal = 0.4 for various orifices. at $X/D = 50$

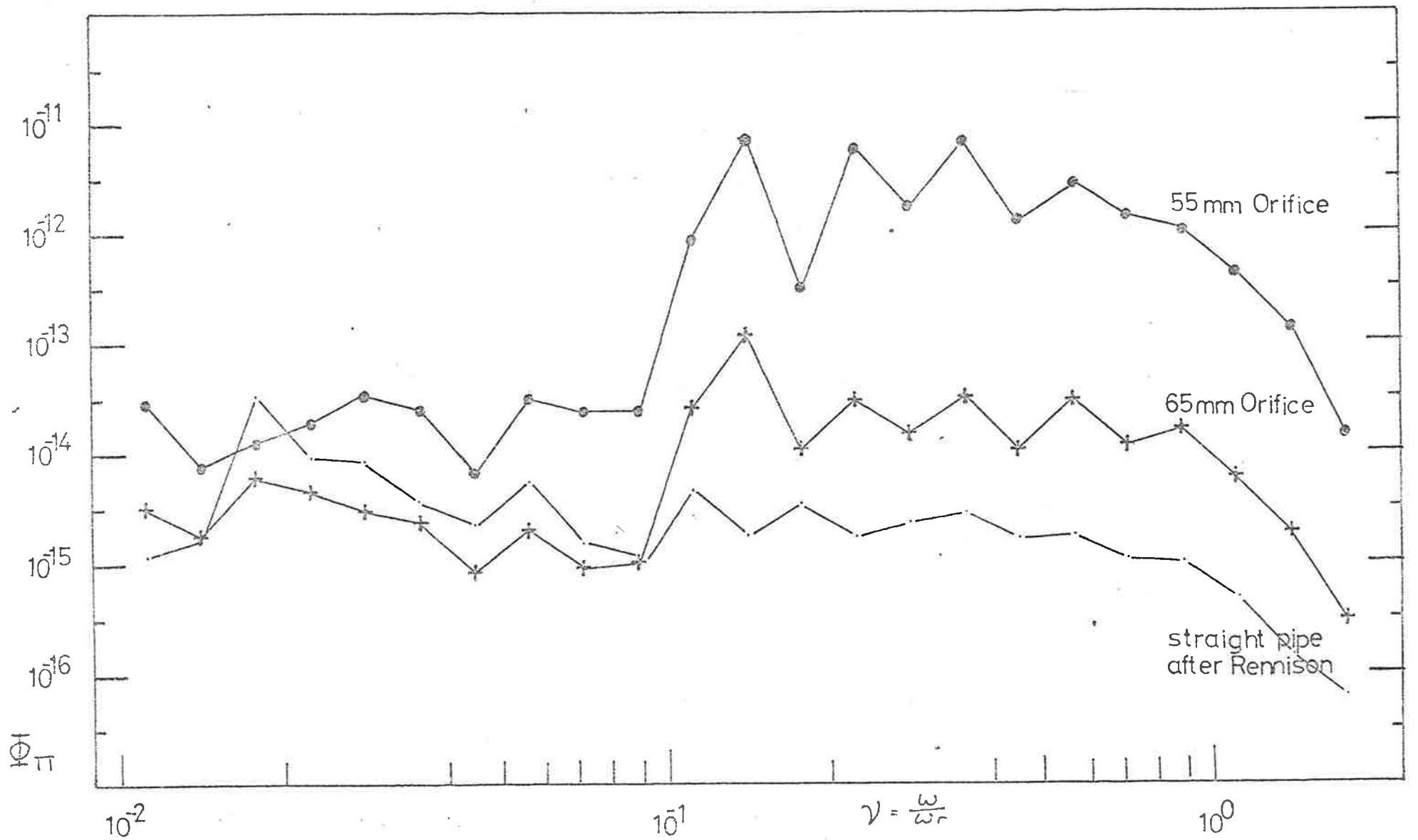


FIG. C.9 NON-DIMENSIONAL SPECTRA OF ACOUSTIC POWER RADIATED

M nominal = 0.45 for various orifices.

thin walled pipe $X/D = 50$

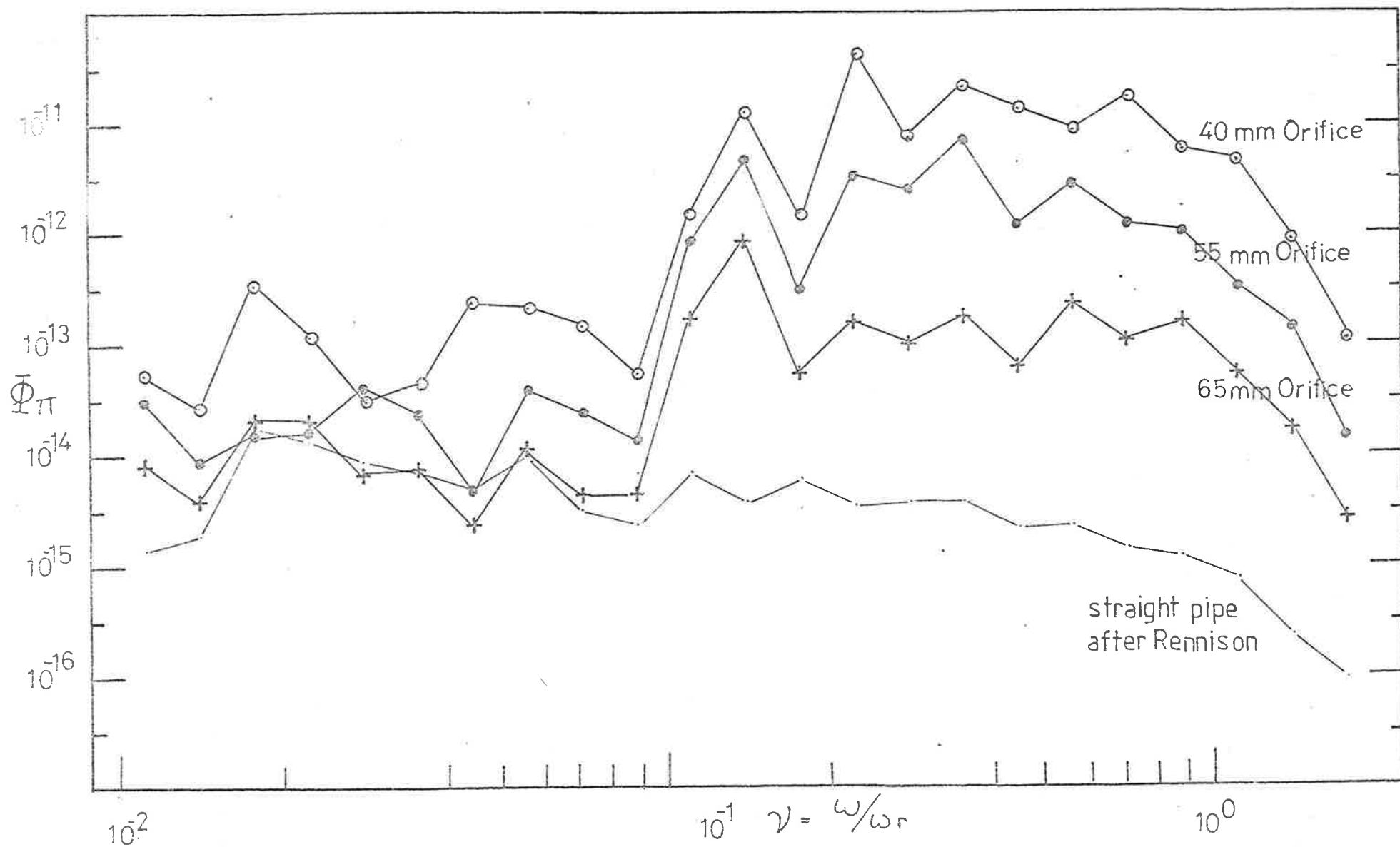


FIG. C.10 NON-DIMENSIONAL SPECTRA OF ACOUSTIC POWER RADIATED

M nominal = 0.5 for various orifices.

thin walled pipe $x/D = 50$

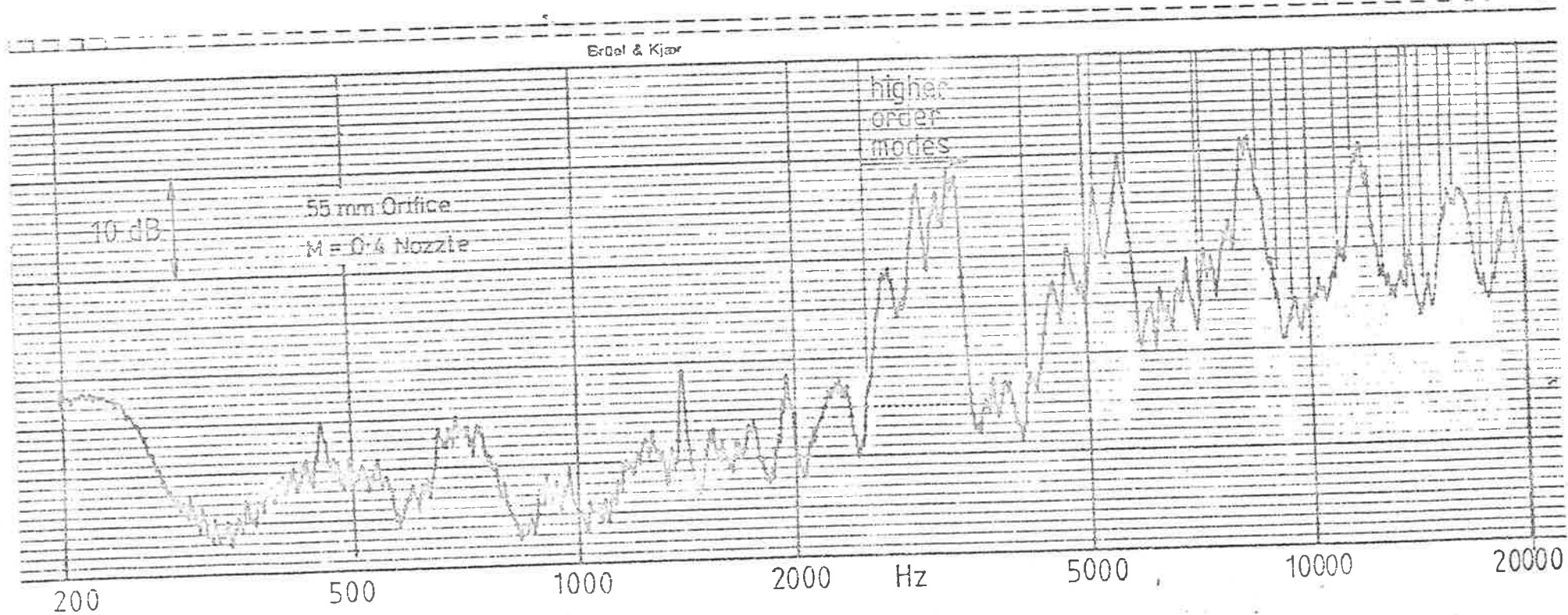


FIG C-11 NARROW BAND ANALYSIS of ACOUSTIC POWER RADIATED
 $X/D=50$

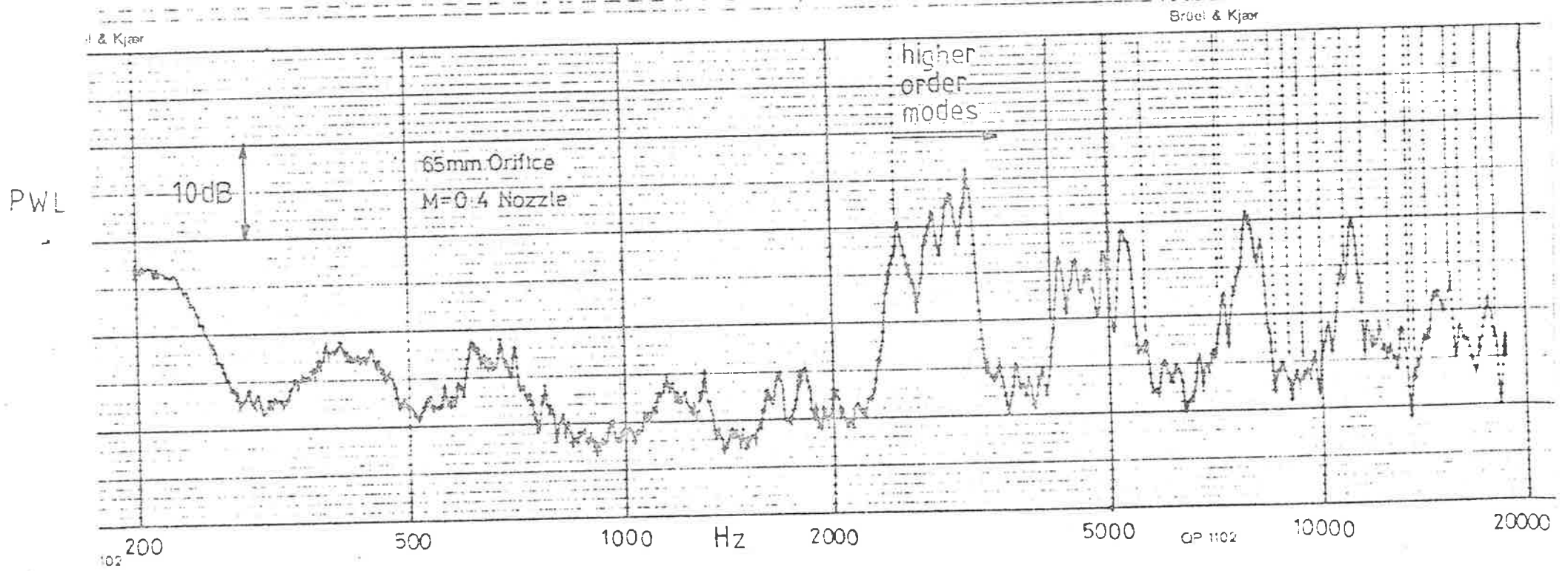


FIG C-12 NARROW BAND ANALYSIS of ACOUSTIC POWER RADIATED

$$X/D = 50$$

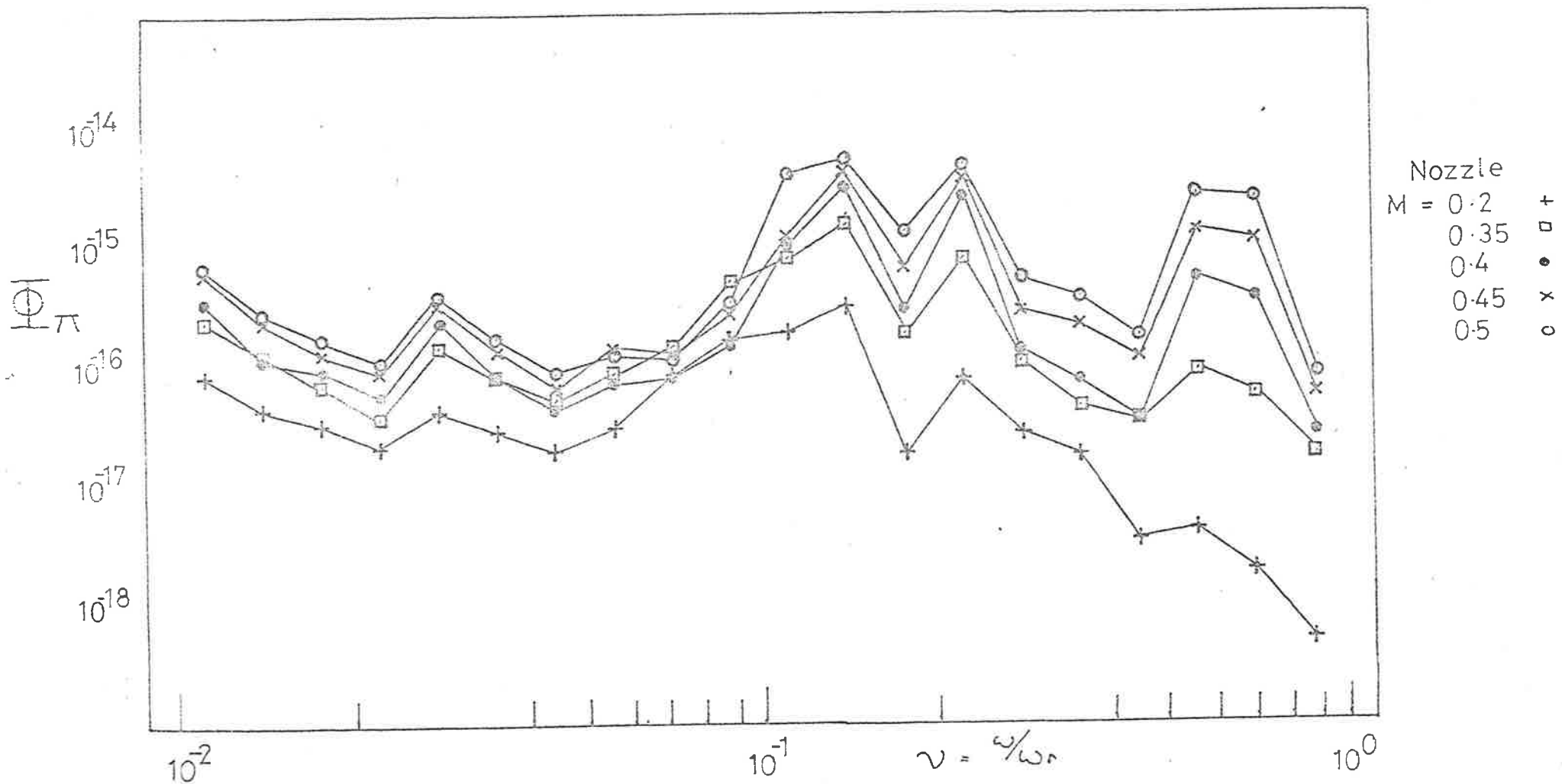


FIG C-13 NON-DIMENSIONAL SPECTRA OF ACOUSTIC POWER RADIATED

thick walled pipe 65mm Orifice $x/D = 50$

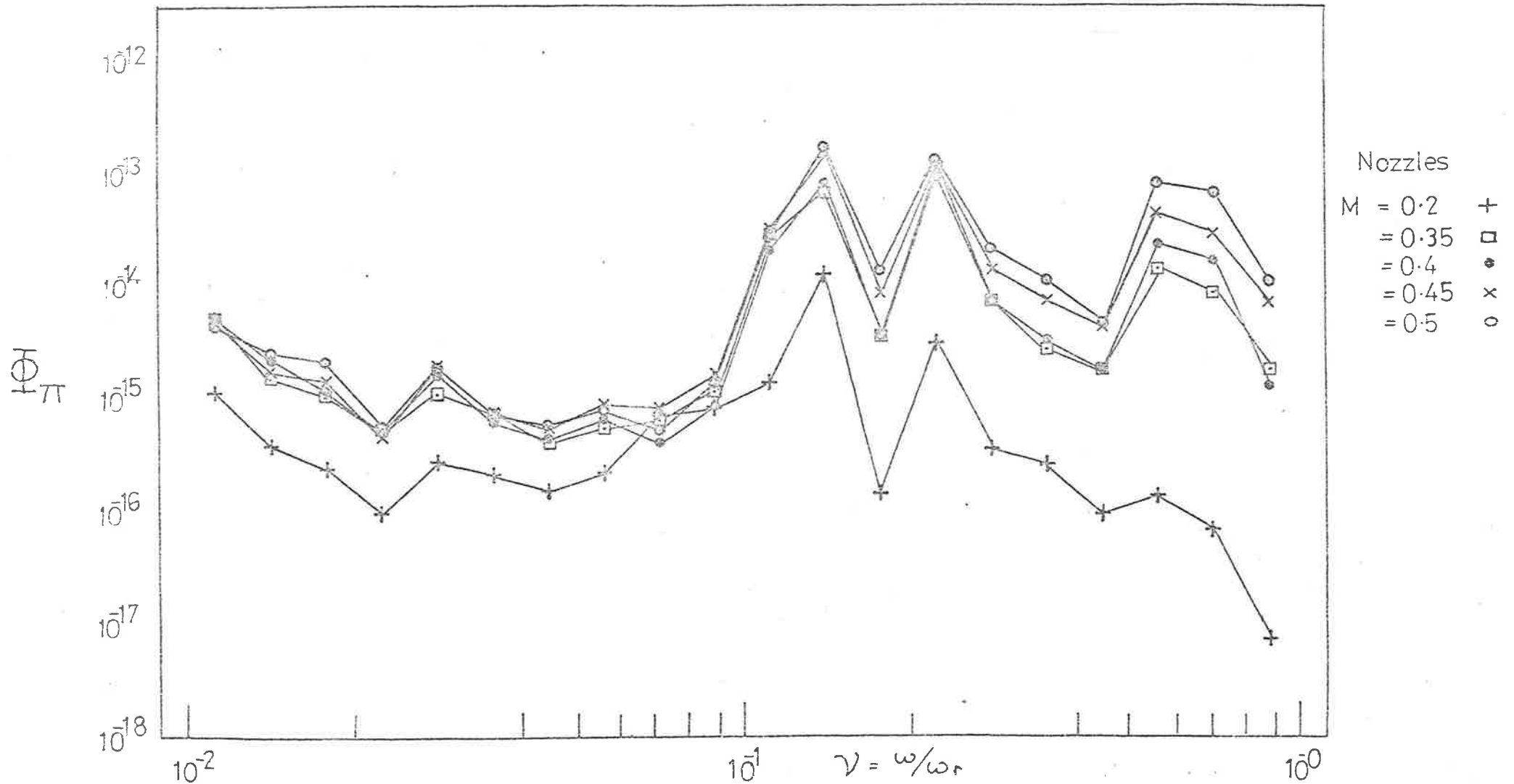


FIG C-14

NON DIMENSIONAL SPECTRA OF ACOUSTIC POWER RADIATED

thick walled pipe

55 mm Orifice

$x/D = 50$

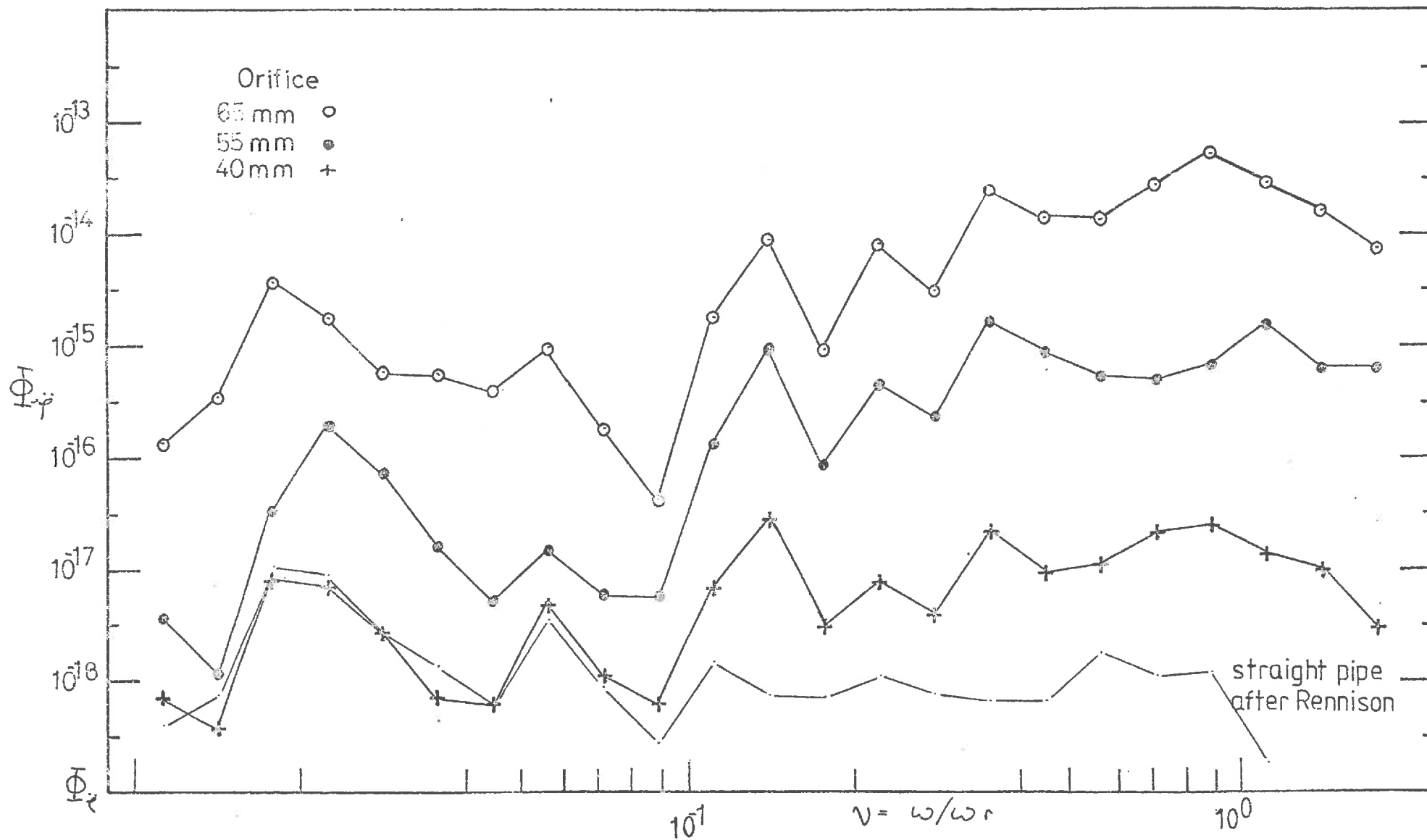


FIG C.15 NON-DIMENSIONAL ACCELERATION SPECTRA

at mid point of test section

thin walled pipe 0.89mm.

M nominal = 0.2

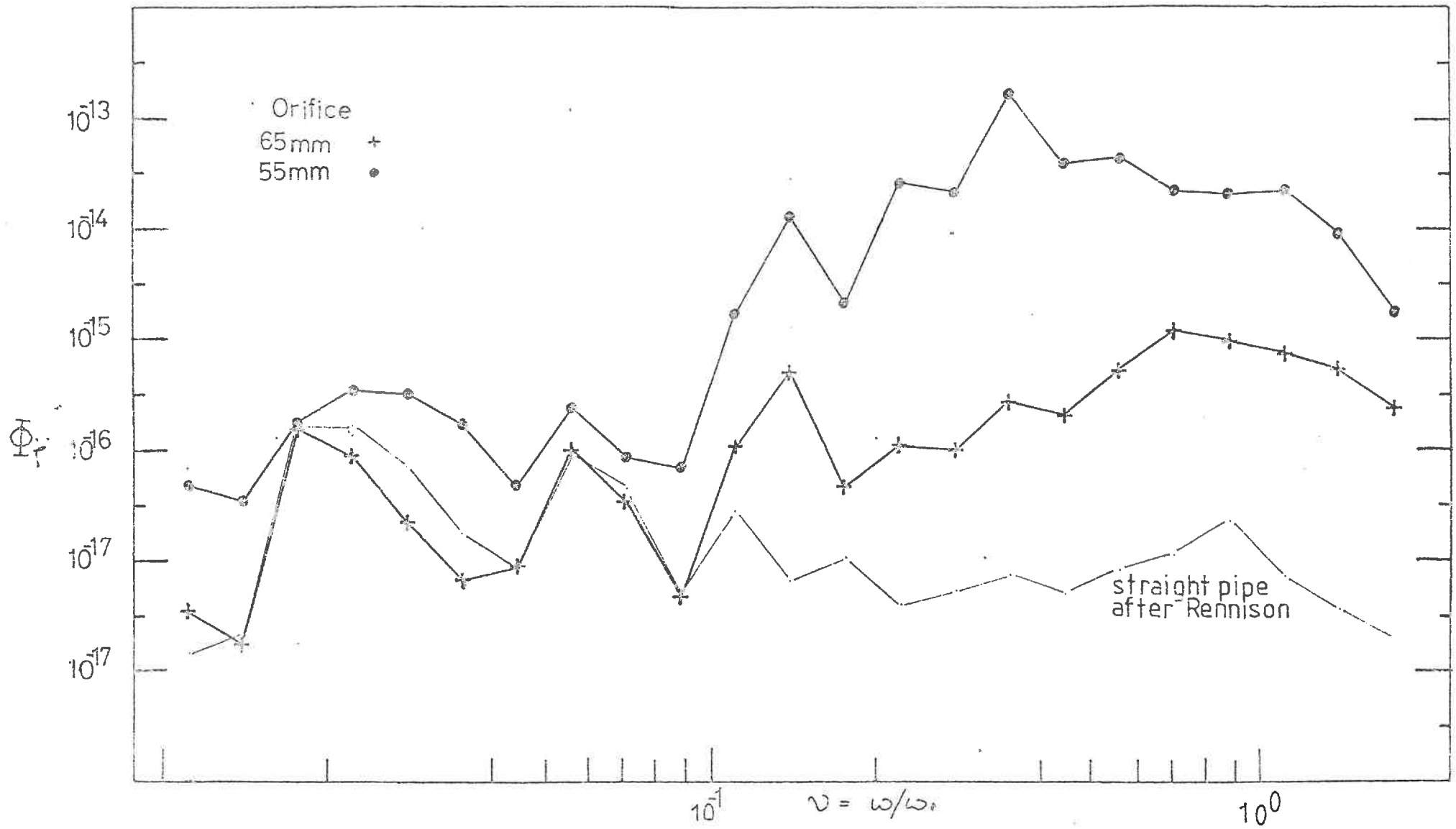


FIG C-16 NON-DIMENSIONAL ACCELERATION SPECTRA

at mid point of test section

thin walled pipe 0.89mm.

M nominal = 0.35

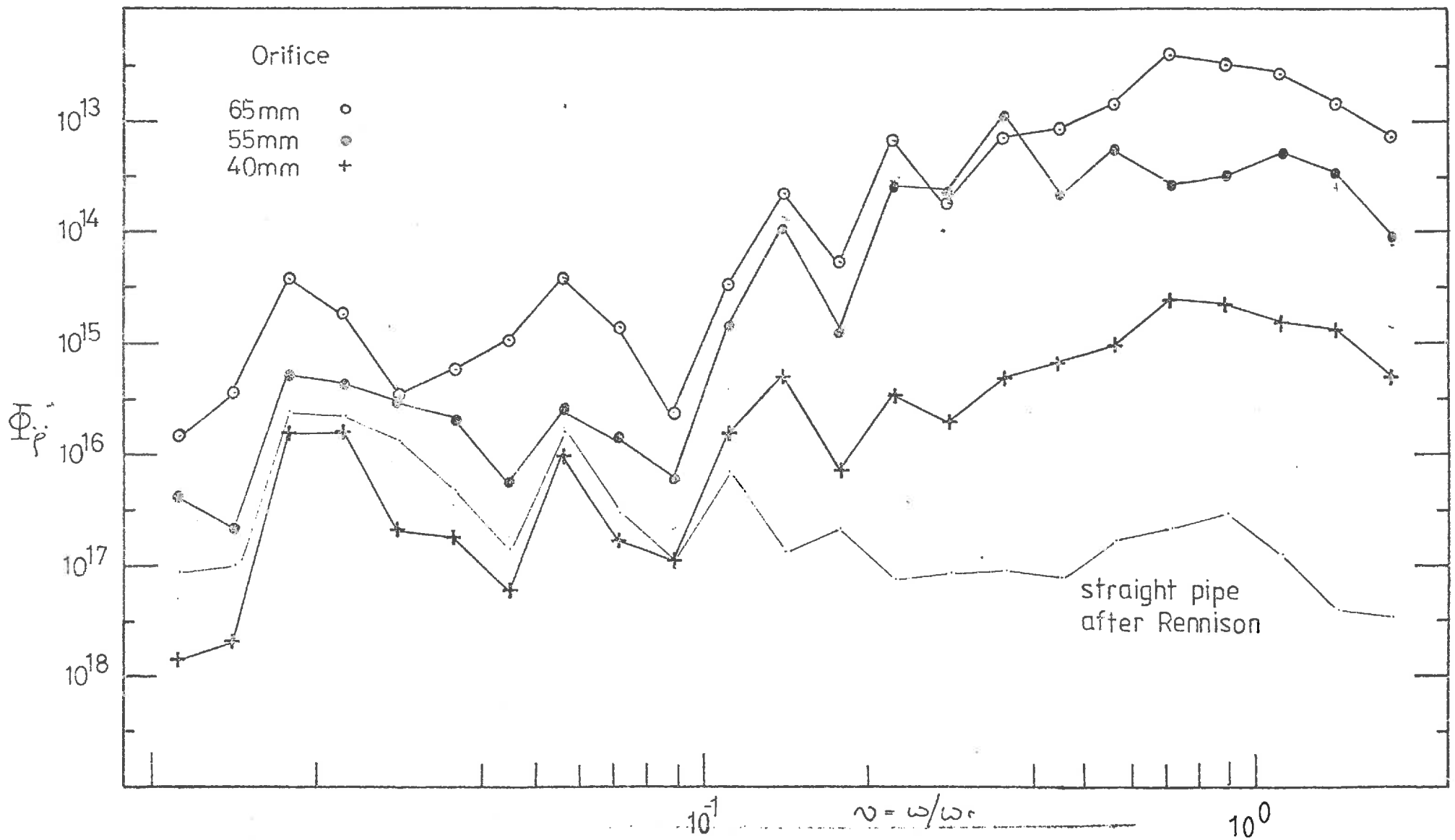


FIG C-17 NON-DIMENSIONAL ACCELERATION SPECTRA
 at mid point of test section thin walled pipe 0.89mm.
 M nominal = 0.4

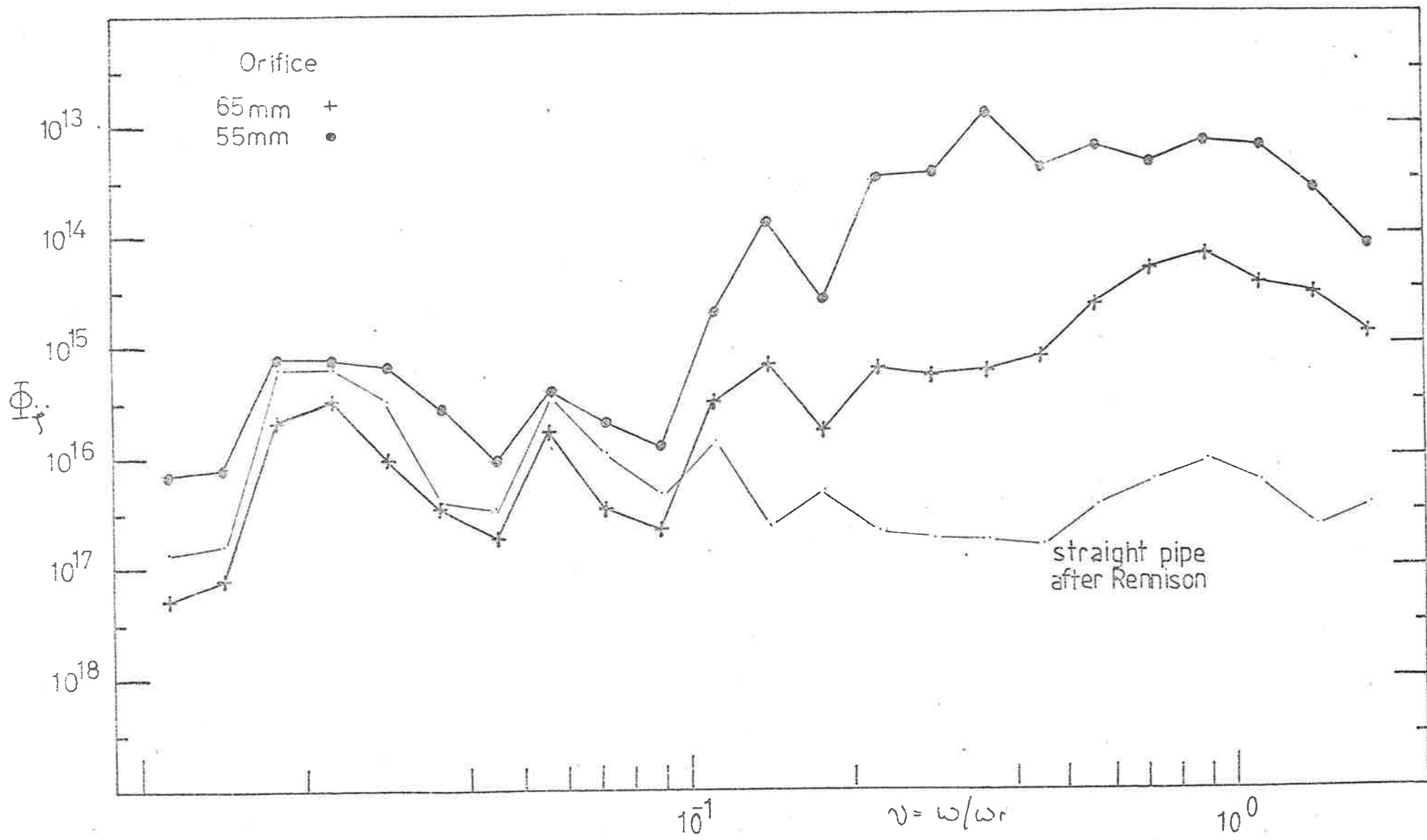


FIG C.18 NON-DIMENSIONAL ACCELERATION SPECTRA
 at mid point of test section thin walled pipe 0.89mm.
 $M_{nominal} = 0.45$

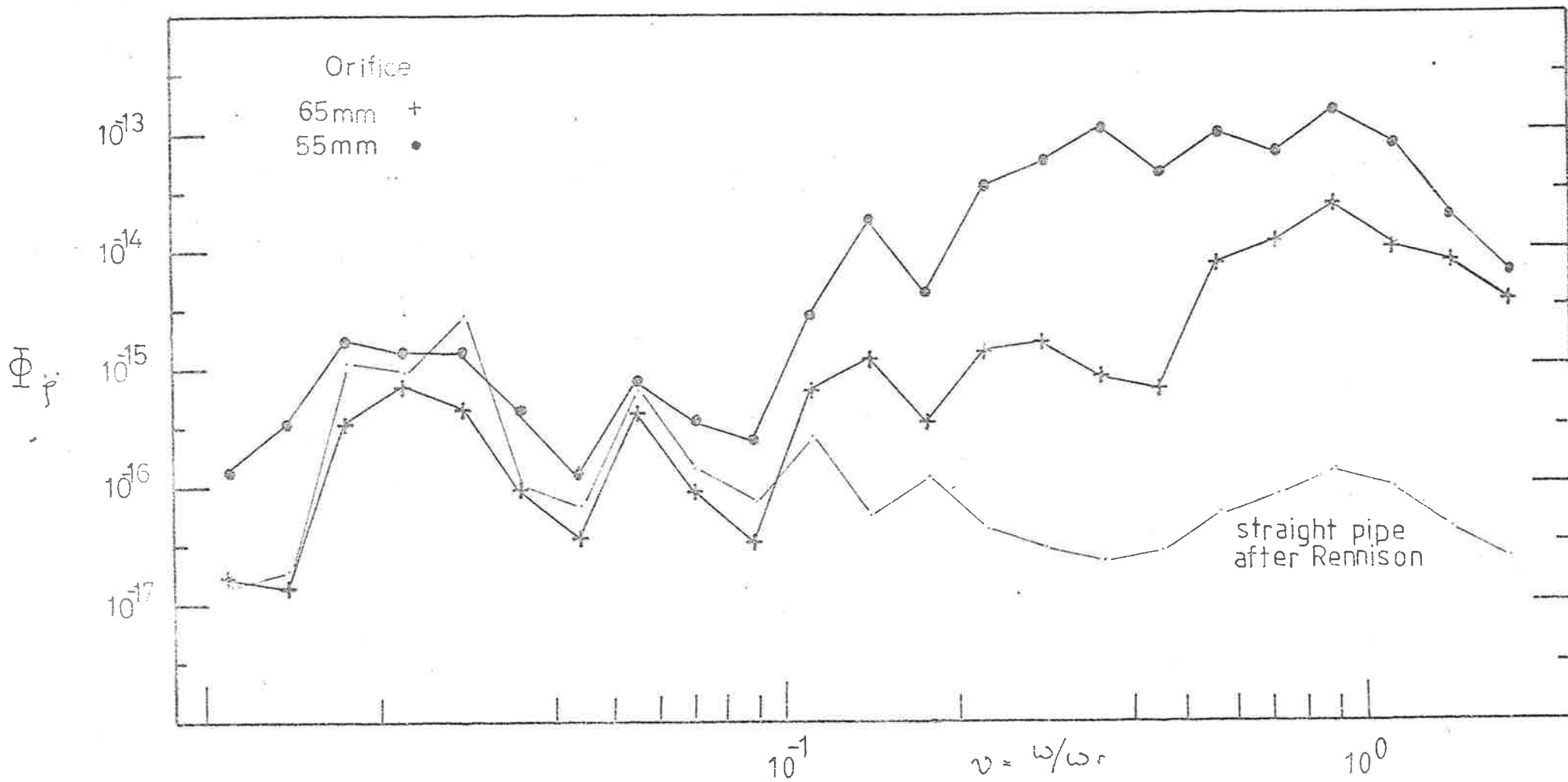


FIG C-19 NON-DIMENSIONAL ACCELERATION SPECTRA

at mid point of test section

thin walled pipe 0.89mm.

M nominal = 0.5

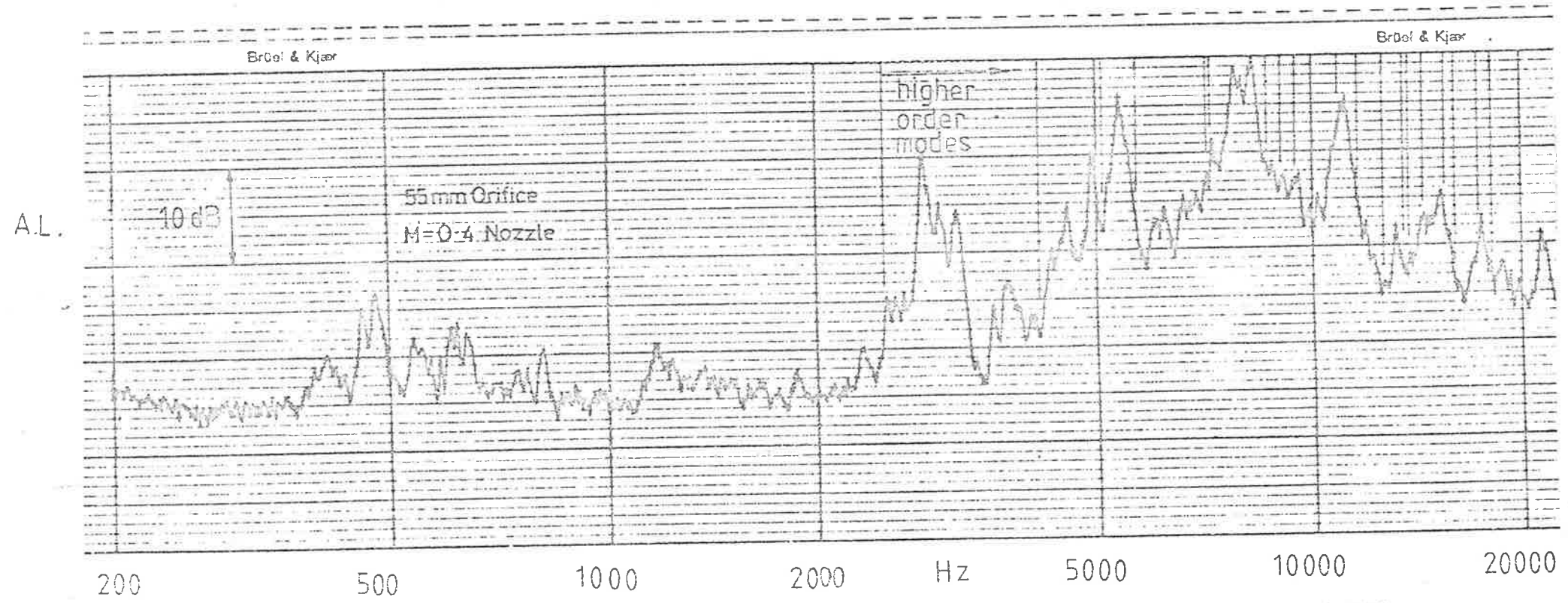


FIG C-20 NARROW BAND ANALYSIS of ACCELERATION SPECTRA
 $X/D = 50$

A.L.

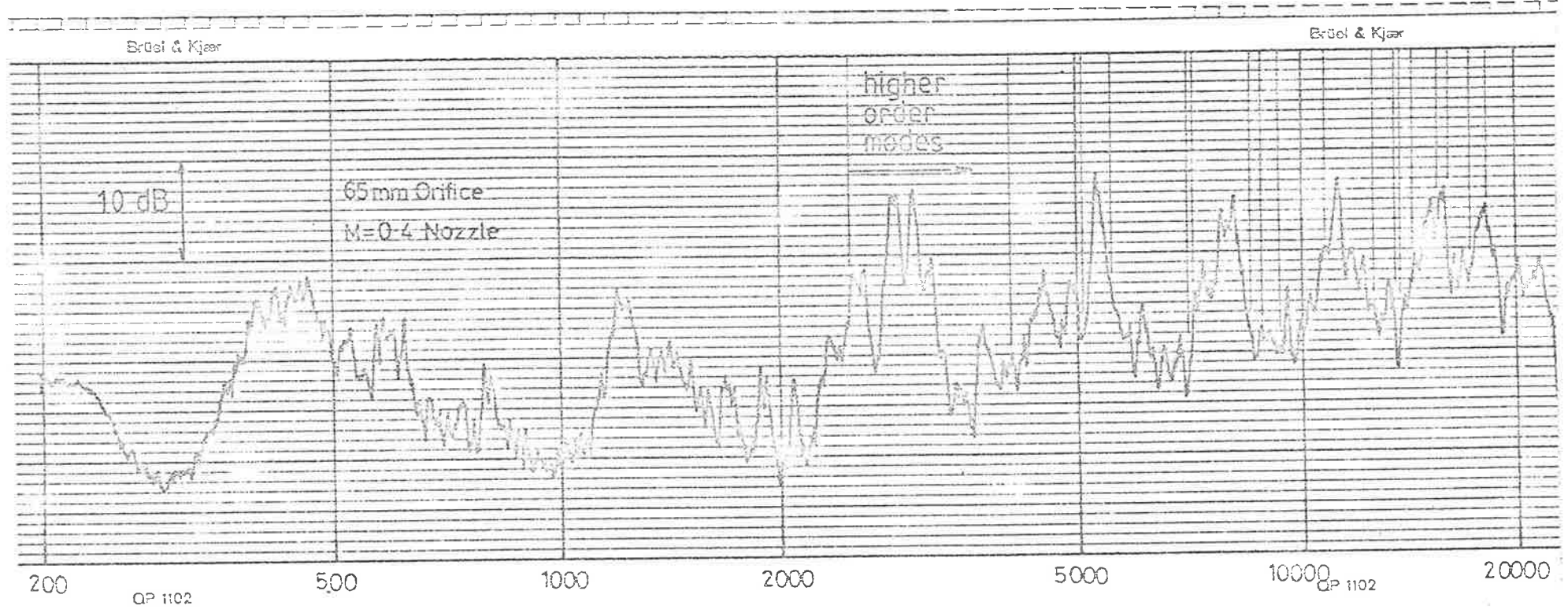


FIG C-21

NARROW BAND ANALYSIS of ACCELERATION SPECTRA

$X/D = 50$

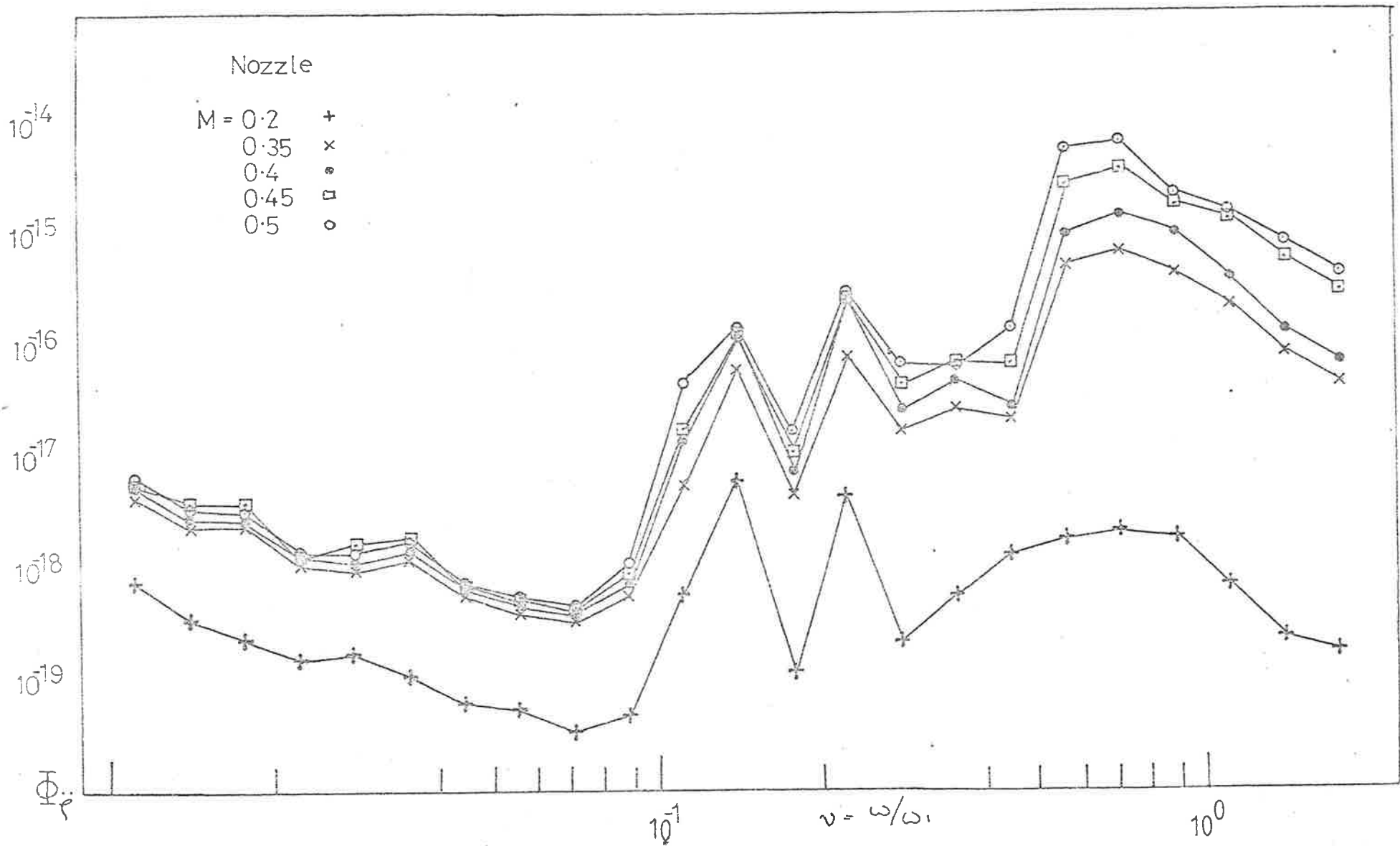


FIG C-22 NON-DIMENSIONAL ACCELERATION SPECTRA

at mid point of test section

thick walled pipe $X/D=50$

55 mm Orifice

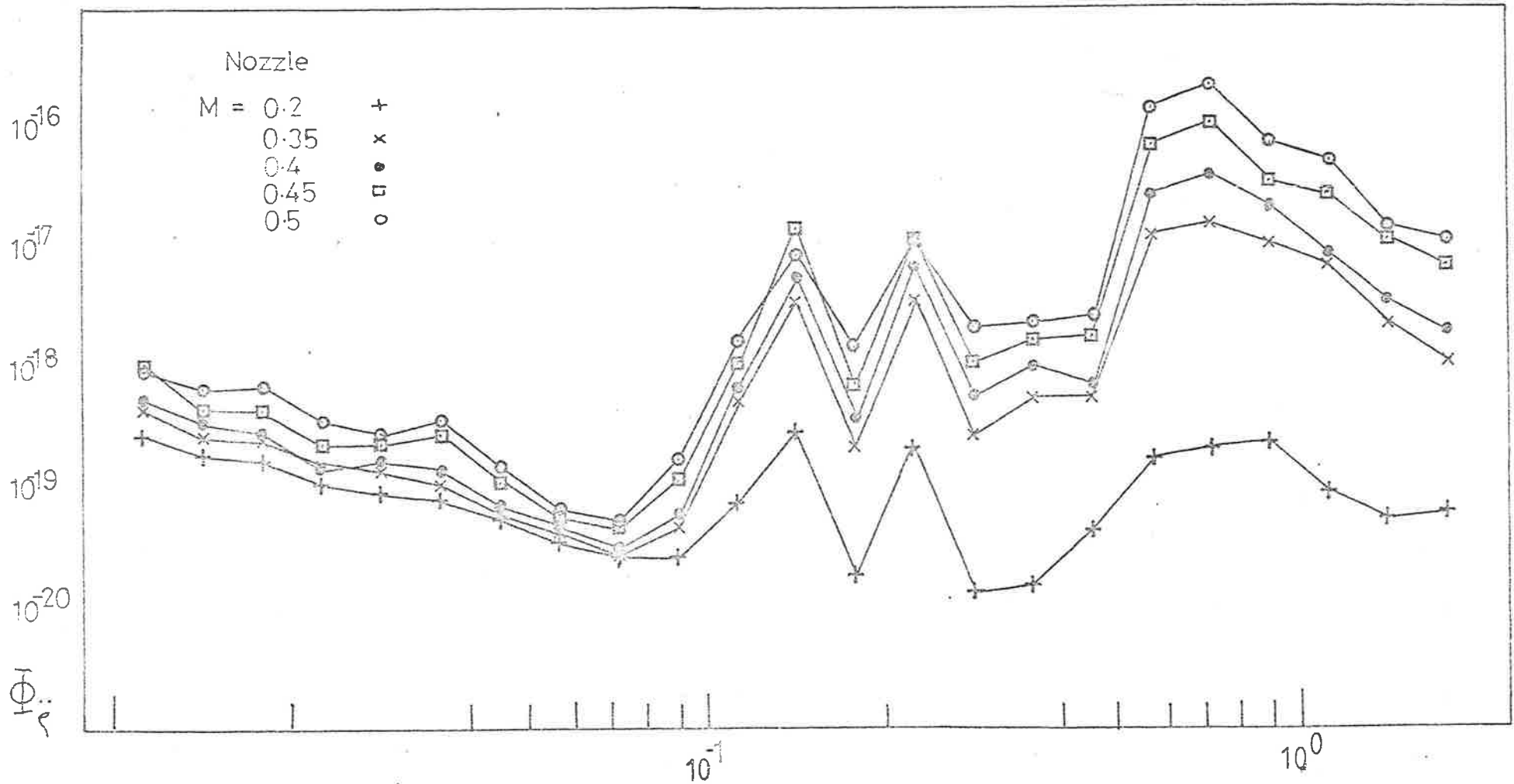


FIG C-23 NON-DIMENSIONAL ACCELERATION SPECTRA

at mid point of test section thick walled pipe X/D = 50

65 mm Orifice

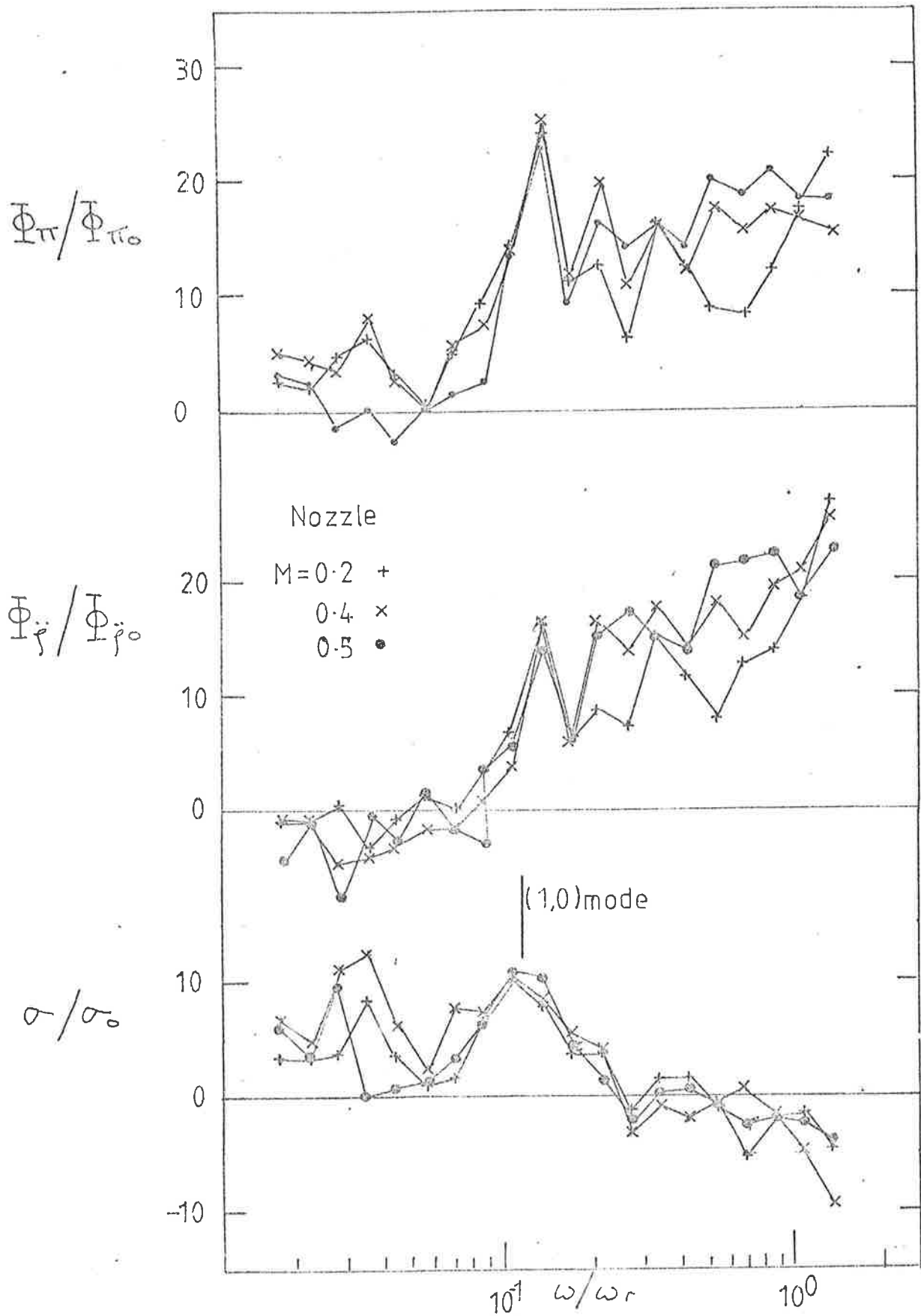
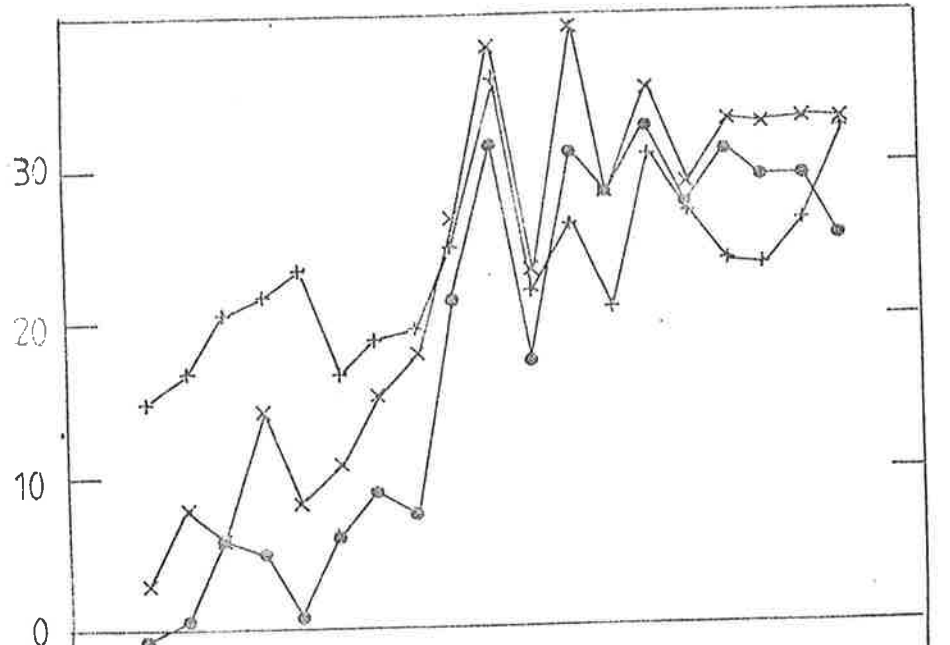
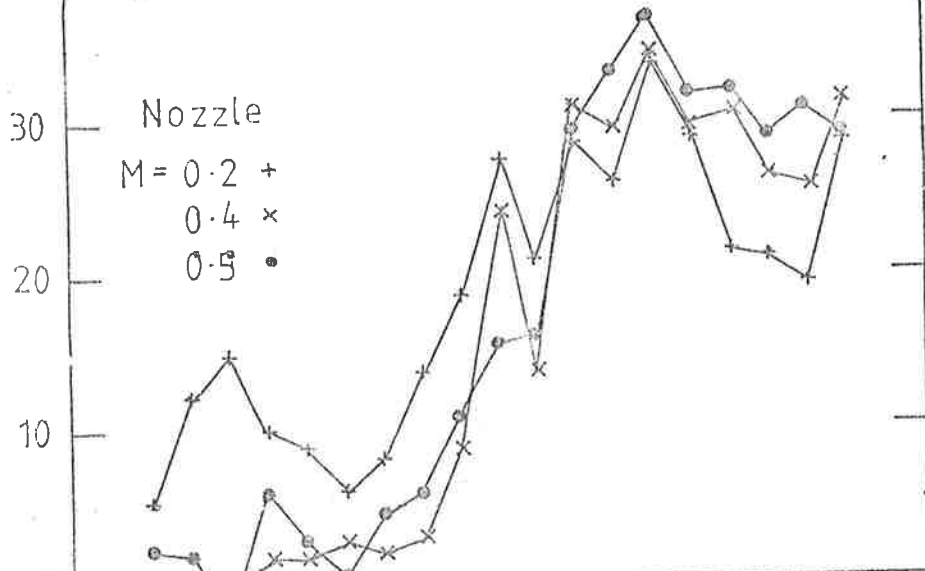


FIG C-24 SPECTRAL DENSITIES of WALL ACCELERATION
ACOUSTIC RADIATION & RADIATION RATIOS for
65mm ORFICE RELATIVE to STRAIGHT PIPE FLOW

$$\Phi_n / \Phi_{\pi_0}$$



$$\Phi_{\ddot{r}} / \Phi_{\ddot{r}_0}$$



$$a/r_0$$

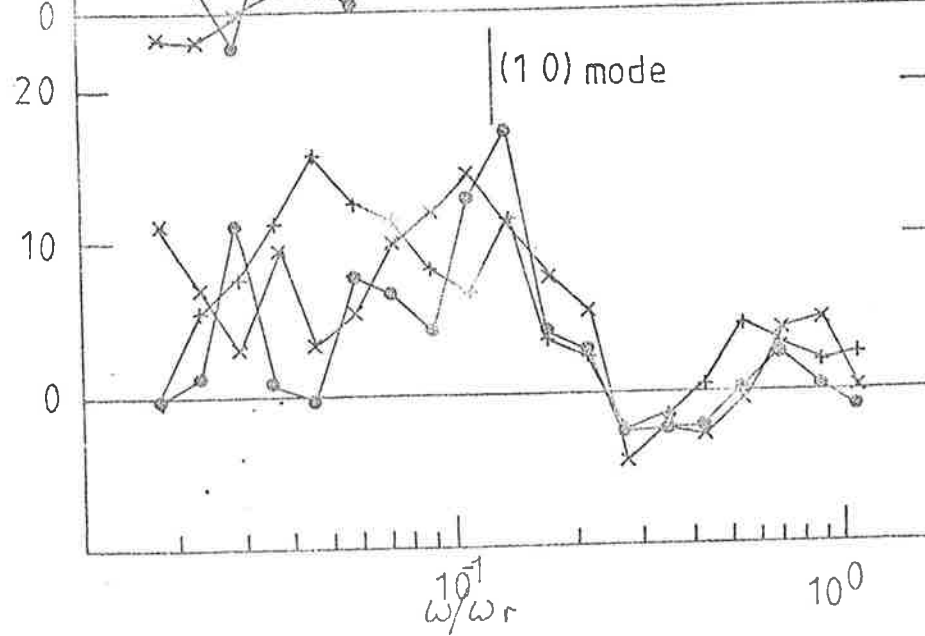


FIG C-25 SPECTRAL DENSITIES OF WALL ACCELERATION ACOUSTIC RADIATION & RADIATION RATIOS for 55mm ORIFICE RELATIVE TO STRAIGHT PIPE FLOW